EFFECT OF SECONDARY INTERACTIONS ON THE FUNDAMENTAL PROPERTIES OF SMALL MOLECULE MODELS OF THE DIIRON HYDROGENASE ACTIVE SITE

A Dissertation

by

MICHAEL LEE SINGLETON

Submitted to the Office of Graduate Studies of
Texas A&M University
in partial fulfillment of the requirements for the degree of

DOCTOR OF PHILOSOPHY

December 2010

Major Subject: Chemistry

Effect of Secondary Interactions on the Fundamental Properties of Small Molecule Models of the Diiron Hydrogenase Active Site

EFFECT OF SECONDARY INTERACTIONS ON THE FUNDAMENTAL PROPERTIES OF SMALL MOLECULE MODELS OF THE DIIRON HYDROGENASE ACTIVE SITE

A Dissertation

by

MICHAEL LEE SINGLETON

Submitted to the Office of Graduate Studies of
Texas A&M University
in partial fulfillment of the requirements for the degree of

DOCTOR OF PHILOSOPHY

Approved by:

Chair of Committee,	Marcetta Y. Darensbourg
Committee Members,	John A. Gladysz
	Michael B. Hall
	James C. Hu
Head of Department,	David H. Russell

December 2010

Major Subject: Chemistry

ABSTRACT

Effect of Secondary Interactions on the Fundamental Properties of Small Molecule Models of the Diiron Hydrogenase Active Site. (December 2010)

Michael Lee Singleton, B.S., Texas A&M University

Chair of Advisory Committee: Dr. Marcetta Y. Darensbourg

The unique active site of [FeFe]-hydrogenase has inspired over 300 small molecule models derived from the classical organometallic complex, (μ-SRS-)$[Fe(CO)_3]_2$. However, no model complex has yet reproduced the hydrogen production capabilities of the enzyme. One reason for this is that the model complexes are not subject to the large number of second coordination sphere interactions that are present in the active site. This work represents two approaches to explore the importance of non-covalent interactions on the properties of small molecule models, (μ-SRS)$[Fe(CO)_3]_2$ and (μ-SRS$[Fe(CO)_2L]_2$, of the enzyme active site.

First, a series of diiron models with additional steric bulk built into the dithiolate linker that connects the two irons were synthesized. While the electron donating ability of the dithiolate is not drastically altered, as evidenced by infrared spectroscopy, variable temperature - NMR studies show that the energy barrier for certain intramolecular dynamic processes, important in modeling the enzyme active site, is significantly lowered. Electrochemical studies on the all-CO derivatives showed no significant differences in the redox properties of the sterically bulky complexes compared to

complexes without added steric bulk. For substituted complexes in which CO is replaced by strong donor ligands greater electrochemical changes were observed, with some events being more accessible by up to 230 mV. One electron oxidation of the disubstituted complexes has produced a series of rare mixed-valent $Fe^{I}Fe^{II}$ complexes. An X-ray crystal structure of one of these complexes, $(\mu\text{-}SCH_2C(CH_3)_2CH_2S\text{-})[Fe(CO)_2PMe_3]_2PF_6$ shows both a semi-bridging carbonyl and an open site similar to the 2-Fe subsite in the H_{ox} state of the enzyme active site.

Another method for studying secondary interactions on the model complexes used a host-guest approach to provide an artificial protein environment. Reaction of an aryl sulfonate-containing diiron complex with natural β-cyclodextrin results in encapsulation of the model. The X-ray crystal structure of the inclusion complex, $Na^{+}(\mu\text{-}SCH_2N(C_6H_4SO_3^{-})CH_2S\text{-})[Fe(CO)_3]_2\cdot 2$ β-cyclodextrin shows complete enclosure of the diiron model within two cyclodextrin units. Solution studies support the formation of an inclusion complex and show that the cyclodextrin is capable of producing significant redox changes to the model complex in H_2O. This work has provided a new highly modifiable method for affecting change in the properties of model complexes through intermolecular interactions.

DEDICATION

This dissertation and all the work herein, is dedicated to my wife Aurore, whose constant love and support has given me direction; my children, Lily and Abby, whose smiles have always brightened my way; and my family and friends, for their encouragement and company along my path.

ACKNOWLEDGEMENTS

My thanks go out to my research advisor, Marcetta Y. Darensbourg for all of the opportunities that she has provided. I am grateful for her constant guidance and encouragement. Your passion for chemistry continues to inspire me. I acknowledge my committee members, Prof. John A. Gladysz, Prof. Michael B. Hall and Prof. James C. Hu for any and all advice they have given me. Special thanks to Prof. Michael B. Hall and Dr. Lisa M. Perez for all of their advice regarding the theoretical work I have done. I also thank Dr. Joseph H. Reibenspies and Dr. Nattamai Bhuvanesh for all of their help and patience in the X-ray Diffraction Laboratory. Thank you to all of the MYD and DJD group members past and present. Steve, the work herein has required a great deal of synthetic technique and the skills that you taught me when I was starting to do research have been invaluable. Leo, while your research has enriched both my own work and that of the rest of the field, I consider our friendship the most important thing to come out of our time in the lab. Roxanne and Tiffany, thank you for your friendship and for helping me keep a cheerful attitude. I must also acknowledge the efforts of numerous talented undergraduates in the work presented herin, Megan, Cory, Lauren, Tim, Michael, and Philip, thank you all.

No amount of thanks can begin to express my gratitude to my family. Mom, Dad, Jenny, and Eric, I know that I can count on you for anything. Mom, thank you for always encouraging me in everything I did and for all you do for the girls. Lily and Abby chase after bugs and frogs, they love to read, and they are smart and caring. I often think,

“They act like their grandma.” This makes me happy. Dad, one of the things I enjoy about doing chemistry is that I get to follow in your footsteps and I do feel a sense of pride when people recognize the name. I have enjoyed our tennis games, even if I have rarely been able to win, for the time it has let us spend together. I am proud to be your son.

To my wife, Aurore, I do not know where I would be today if I had not met you, but I know that I would not be as happy as I am with you. You, Lily, and Abby are everything to me and the most important part of the last five years. Thank you for all that you have done and all that you are.

To all of you, I would like to express my sincerest gratitude; you have helped make me who I am today and are an important part of who I am and what I have done.

NOMENCLATURE

H_2ase	Hydrogenase
eas	Enzyme Active Site
edt	Ethanedithiolate
pdt	Propanedithiolate
o-xdt	O*rtho*-xylyl-α,α'-dithiolate
adt	2-Aza-1,3-propanedithiolate
odt	2-Oxa-1,3-propanedithiolate
dmpdt	2,2-Dimethylpropanedithiolate
depdt	2,2-Diethylpropanedithiolate
bepdt	2-Butyl-2-ethylpropanedithiolate
IMe	1,3-Dimethylimidazole-2-ylidene
IMe·HCl	1,3-Dimethylimidazolium Chloride
IMes	1,3-Bis(2,4,6-trimethylphenyl)imidazole-2-ylidene
IMesHCl	1,3-Bis(2,4,6-trimethylphenyl)imidazolium Chloride
PPN	Bis(triphenylphosphine)iminium
PTA	1,3,5-triaza-7-phosphaadamantane
Fc	Ferrocene
Fc^+	Ferrocenium
CyD	Cyclodextrin
NHC	N-Heterocyclic Carbene

Complex **III-1**	(μ-dmpdt)$[Fe(CO)_3]_2$
Complex **III-2**	(μ-depdt)$[Fe(CO)_3]_2$
Complex **III-3**	(μ-bepdt)$[Fe(CO)_3]_2$
Complex **III-4**	(μ-dmpdt)$[Fe(CO)_3][Fe(CO)_2$IMes]
Complex **III-5**	(μ-depdt)$[Fe(CO)_3][Fe(CO)_2$IMes]
Complex **III-6**	(μ-depdt)$[Fe(CO)_3][Fe(CO)_2$IMe]
Complex **III-7**	(μ-dmpdt)$[Fe(CO)_3][Fe(CO)_2PPh_3]$
Complex **III-8**	(μ-depdt)$[Fe(CO)_3][Fe(CO)_2$PTA]
Complex **IV-1**	(μ-pdt)$[Fe(CO)_2PMe_3][Fe(CO)_2$IMes]
Complex **IV-1$_{ox}$**	(μ-pdt)$[Fe(CO)_2PMe_3][Fe(CO)_2$IMes]PF_6
Complex **IV-1***	(μ-dmpdt)$[Fe(CO)_2PMe_3][Fe(CO)_2$IMes]
Complex **IV-1$_{ox}$***	(μ-dmpdt)$[Fe(CO)_2PMe_3][Fe(CO)_2$IMes]PF_6
Complex **IV-2***	(μ-dmpdt)$[Fe(CO)_2PMe_3]_2$
Complex **IV-2$_{ox}$***	(μ-dmpdt)$[Fe(CO)_2PMe_3]_2PF_6$
Complex **IV-2**	(μ-pdt)$[Fe(CO)_2PMe_3]_2$
Complex **IV-2$_{ox}$**	(μ-pdt)$[Fe(CO)_2PMe_3]_2PF_6$
Complex **IV-3***	(μ-dmpdt)$[Fe(CO)_2P(OMe)_3]_2$
Complex **IV-3*$_{ox}$**	(μ-dmpdt)$[Fe(CO)_2P(OMe)_3]_2BF_4$
Complex **V-Na$^+$1**	Na(μ-$SCH_2N(C_6H_4SO_3)CH_2S$-)$[Fe(CO)_3]_2$
Complex **V-Et$_4$N$^+$1**	Et_4N(μ-$SCH_2N(C_6H_4SO_3)CH_2S$-)$[Fe(CO)_3]_2$
Complex **V-1-Cyd**	Na(μ-$SCH_2N(C_6H_4SO_3)CH_2S$-)$[Fe(CO)_3]_2$·2CyD
Complex **V-Na$^+$2**	Na(μ-$SCH_2N(C_6H_4SO_3)CH_2S$-)$[Fe(CO)_3][Fe(CO)_2P(OMe)_3]$

Complex **V-Et_4N^+2** $Et_4N(\mu\text{-}SCH_2N(C_6H_4SO_3)CH_2S)[Fe(CO)_3][Fe(CO)_2P(OMe)_3]$

Complex **V-Na^+3** $Na(\mu\text{-}SCH_2N(C_6H_4SO_3)CH_2S\text{-})[Fe(CO)_2PMe_3]_2$

Complex **V-Et_4N^+3** $Et_4N(\mu\text{-}SCH_2N(C_6H_4SO_3)CH_2S\text{-})[Fe(CO)_2PMe_3]_2$

TABLE OF CONTENTS

CHAPTER Page

LIST OF FIGURES

FIGURE Page

FIGURE Page

FIGURE Page

FIGURE Page

FIGURE Page

FIGURE Page

LIST OF TABLES

CHAPTER I

INTRODUCTION

Simplicity

"Look deep into nature, and then you will understand everything better."

-Albert Einstein

The coupling of two protons and two electrons to form dihydrogen is perhaps the most deceptively simple reaction in chemistry and highlights a key insufficiency in the synthetic ability of the chemical community. By way of organic and inorganic transformations chemists have been able to synthesize complex natural products, enormous metal clusters, and polymers hundreds of thousands of units in length and yet practical energy efficient methods for performing the reactions shown below remain

$$\begin{aligned} 2H^+ + 2e^- &\rightleftharpoons H_2 \\ O_2 + 4H^+ + 4e^- &\rightleftharpoons 2H_2O \end{aligned} \qquad (1)$$

elusive. However, these reactions are becoming of increasing importance for their relevance to both hydrogen fuel cells and solar cells for hydrogen production.[1-5] Currently most fuel cell catalysts for these reactions utilize platinum, and while this is arguably the best catalyst currently available, its cost and limited supply prevent it from being an economically viable solution for long term energy production.[6-7] Even with

---

This dissertation follows the style of *Journal of the American Chemical Society*.

current techniques for decreasing the amount of platinum required in fuel cells, it is difficult to escape the truth that platinum, like the fossil fuels it would be helping to replace, is a non-sustainable resource.[8] Thus, the imminent need for fuel cell catalysts derived from inexpensive and abundant metals has turned many chemists looking to nature for inspiration.

Long before fuel cells, nature had developed its own catalysts, enzymes capable of selectively performing the above reactions as part of the complex metabolic pathways found in living organisms.[9] Not only does nature perform these reactions at cellular pH under ambient temperatures and pressures, but most importantly it does not utilize rare transition metals such as platinum.[10] Instead, through eons of evolutionary fine tuning, it has found ways to efficiently use abundant metals such as Ni, Cu and most importantly Fe as molecular catalysts.

FeS Clusters and the Hydrogenases

The abundance of iron and sulfur in the prebiotic landscape of earth has led to the proposal that small metal chalcogen clusters served as catalysts in abiotic metabolic cycles that produced the small molecules necessary for the formation of life.[11] While *in vitro* experiments have shown that this is certainly plausible, the iron sulfur theory for the origin of life remains a widely debated topic.[12] Regardless, the fact that iron sulfur clusters have been harnessed by nature for a variety of roles essential for life cannot be debated. These clusters, ubiquitous to all forms of life, serve an assortment of functions ranging from electron transport, as with the ferredoxins,[13] to serving as the catalytic active site of enzymes such as nitrogenases,[14] hydrogenases,[15] and even some

oxygenases.[16] The efficiency of these enzymes in catalyzing important basic reactions has led scientists to seek out ways to exploit their reactivity for every day applications.[17] In the case of the hydrogenases, their ability to reversibly catalyze the reduction of protons to give hydrogen has commanded global attention for the possible use of these enzymes as fuel cell catalysts.[3,7,18-21]

The family of hydrogenases can be divided into three main categories based on the composition of their active sites: [NiFe]-, [FeFe]- and mono-Fe hydrogenases.[22-26] (Figure I-1) While there are a number of similar features between the structures of all three active sites including diatomic ligands (CO or CN^-) and low spin Fe, each of the

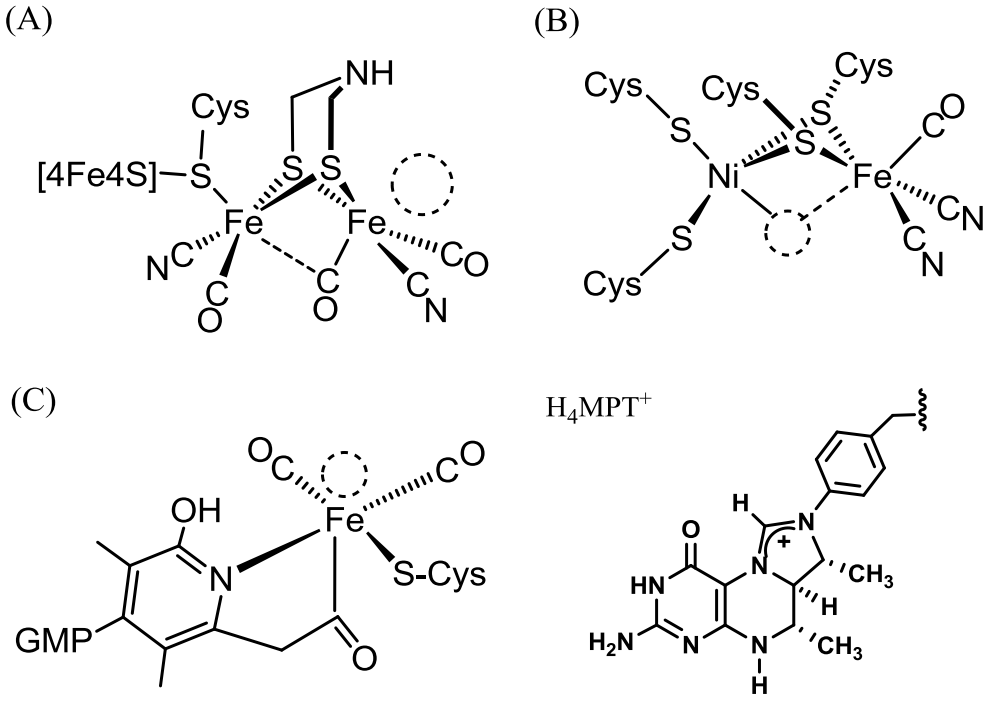

Figure I-1. Active sites of A) [FeFe]-Hydrogenase, B) [NiFe]-Hydrogenase, and C) mono-[Fe] hydrogenase with its H_4MPT^+ cofactor shown to the right.

hydrogenases has a different primary function.[27] The [NiFe] and [FeFe]-hydrogenases can both oxidize H_2 and reduce H^+, however they differ in their ability to push the reaction in one direction or the other with the [NiFe] mainly responsible for H_2 oxidation and [FeFe] primarily responsible for H_2 production. The mono-[Fe] hydrogenase has a more specialized function, and serves to heterolytically cleave hydrogen in a concerted fashion with a proton being transferred to a nearby basic site and the hydride being transferred to the H_4MPT^+ cofactor shown in Figure I-1C resulting in it being responsible for hydride transfer.[22]

While the body of work on all three classes is expansive, the similarity of the core structure of [FeFe]-hydrogenase to the classic organometallic complex (μ-pdt)$[Fe(CO)_3]_2$ [28-30] has made it a promising target for synthetic chemists looking to replicate the activity of the enzyme active site with small molecule models. The biosynthesis of the active site occurs via a series of so called Hyd proteins.[31] Recent discoveries in this area have proposed that an initial 2Fe2S cluster is held by a scaffold protein, HydF.[32] Two accessory proteins, HydG and HydE, are then responsible for the synthesis of the diatomic ligands and the dithiolate linker via proposed radical S-adenosylmethionine pathways and the addition of these components to the 2Fe2S cluster on HydF.[33-36] The assignment of each addition as by either HydG or HydE is, at this time, still a topic of some debate, though HydG has been shown to be capable of forming both CN^- and CO.[34-35] The assembled pre-active site cluster is then transferred from HydF to its final location in HydA.[37] The specific geometry and oxidation states of this diiron dithiolate species immediately before this transfer are still in 2010 uncertain.

Prior to the publication of the crystal structure of the [FeFe]-H_2ase enzyme, IR studies proved invaluable to identifying the presence of the diatomic ligands in the active site.[38] Detailed IR spectra of the enzyme showed several bands in the $\nu(CO/CN^-)$ region with 5 total in the 1750 – 2150 cm^{-1} region.[39-41] This information not only helped refine the X-ray structure of the enzyme, but through spectroelectrochemical studies and EPR measurements has identified four important states for the active site, $H_{inac,}$ $H_{trans,}$ H_{ox}, and $H_{red.}$[42] A fifth state also been reported upon addition of extrinsic CO which is referred to as the CO inhibited state or H_{ox}-CO.[43] Table I-1 shows the $\nu(CO/CN^-)$ IR stretching frequencies of the various states and the corresponding EPR parameters. Through this work and comparison to a variety of model complexes, a catalytic pathway which cycles through Fe^I and Fe^{II} was postulated rather than Fe^{II} and Fe^{III} pathway proposed by early Mössbauer work. This low oxidation state pathway, supported by theoretical work, is now widely accepted as the actual pathway.

Table I-1. IR and EPR data for different states of the H-cluster of [FeFe]-hydrogenase.

Enzyme State	$\nu(CO/CN^-)$ cm^{-1}	EPR g-tensors
H_{inac}[42]	2106, 2087, 2007, 1983,1834	2.02, 2.00
H_{trans}[42]	2100, 2075, 1983, 1977, 1836	2.06, 1.96, 1.89
H_{ox}[42]	2093, 2079, 1965, 1940, 1802	2.10, 2.04, 1.99
H_{red}[42]	2079, 2041, 1965, 1916, 1894	EPR silent
H_{ox}-CO[42]	2096, 2088, 2016, 1971, 1963, 1810	2.06, 2.00, 2.00

The structure of the active site in the holo-enzyme is well established for the H_{red} and H_{ox} states.[44-45] Attached to the rest of the protein through a cysteine that connects them to a 4Fe4S cluster, the irons of the 2Fe cluster in the H_{ox} state are isolated in a mixed-valent $Fe^{I}Fe^{II}$ resting state and are bridged by a non-protein dithiolate linker. While the identity of the central atom in the chain connecting the two sulfurs was long in dispute, ample evidence has now been provided to indicate that it is in fact a N.[46] Each of the iron atoms is bound to two terminal diatomic ligands, a CO and a CN. A third CO is located in a semi-bridging position between the two irons giving the complex an overall structure best described as two edge-bridged square pyramids with one being inverted relative to the other. This "rotated" geometry around the iron centers results in an open site trans to the semi-bridging CO that allows for the formation of a reactive terminal hydride. This unique geometry is enforced through a combination of hydrogen bonding, dipole/dipole and steric effects from nearby amino acid residues.[47] These are pictured in Figure I-2 with the residues color coded to indicate the specific effect they impart.

The surrounding protein also contains several features which play a vital role in H_2 production/oxidation.[25] In addition to the 4Fe4S cluster connected to the active site, three additional 4Fe4S clusters are spaced throughout the enzyme allowing for electron transport to and from the hydrogen producing cluster. Also, both a hydrophobic tunnel and a series of protophilic amino acids, aimed at the rotated Fe, provide a pathway for substrate to be transported to/from the active site.[48] All of these features have evolved over time to facilitate the proposed catalytic cycle shown in Figure I-3,[49] where the

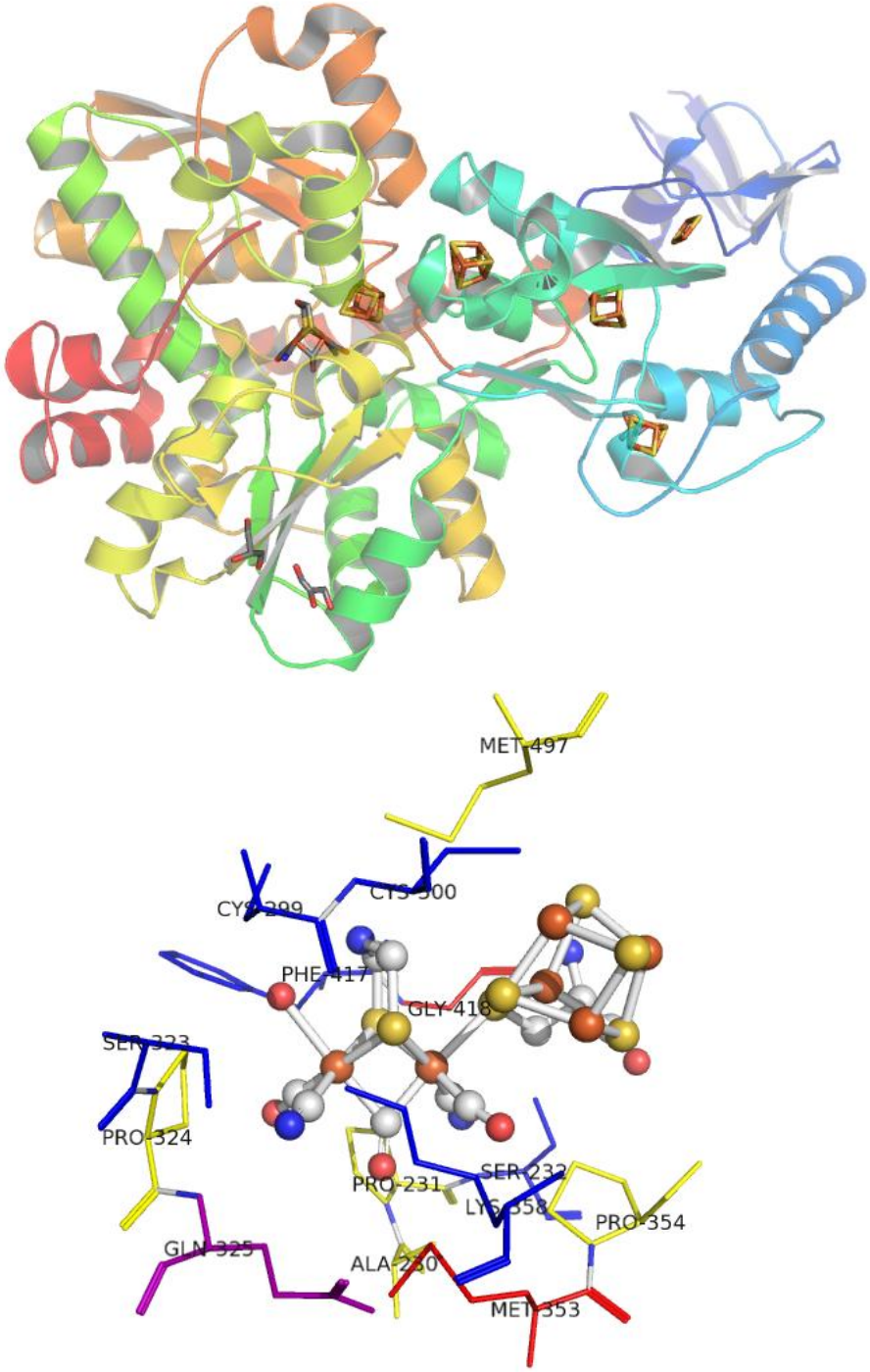

Figure I-2. Structures of top) [FeFe]-Hydrogenase isolated from *C. pasterurianum* and bottom) the 2Fe2S active site with important residues. (Blue – hydrogen bonding and dipole/dipole; yellow – steric; red – non-specific dipole).

active site undergoes a one electron reduction to the active $Fe^{I}Fe^{I}$ state. The Fe site distal to the 4Fe4S cluster then reduces a proton to give a terminal hydride on an $Fe^{II}Fe^{II}$ site that can react with a second proton to form dihydrogen. This is followed by one e^- reduction and release of dihydrogen to return to the $Fe^{I}Fe^{II}$ resting state. Throughout the redox changes required for the catalytic cycle the core structure, with the CO ligand located between the two iron atoms, remains fixed as result of the surrounding peptide.

Despite its high level of reactivity, the direct use of the enzyme as a catalyst in fuel cells has only been sporadically reported[3,50-51] and its wide spread application

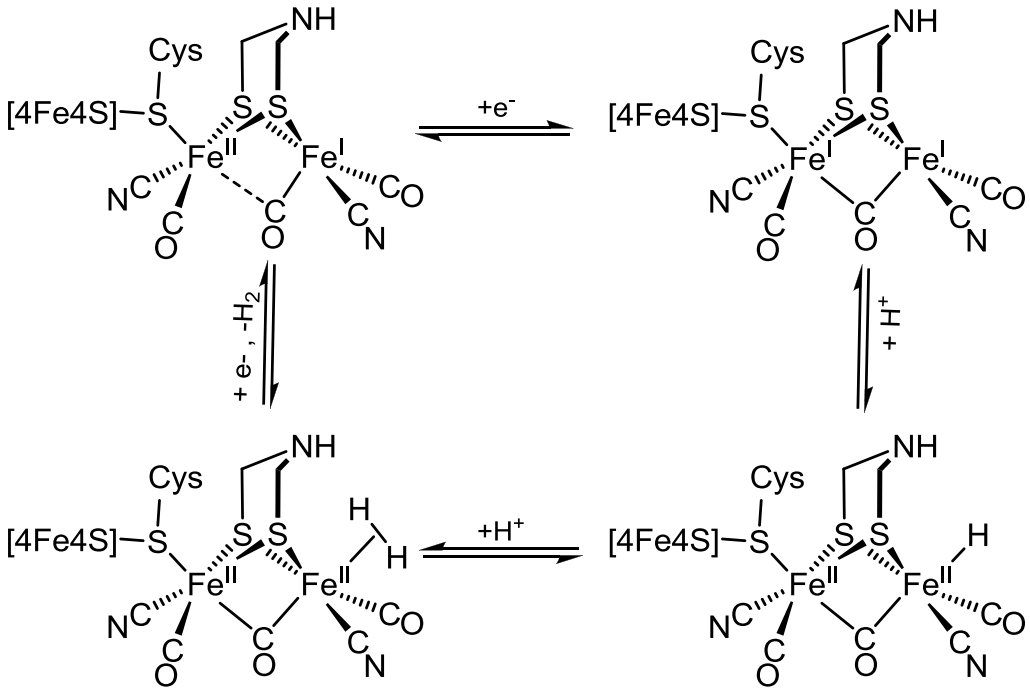

Figure I-3. Simplified mechanism for hydrogen production by [FeFe]-hydrogenase.

limited due difficulties associated with large scale production and long term instability resulting from both oxygen and light sensitivity.[43] It is with the development of functional and robust biomimetics in mind, that synthetic chemists have set out to develop small iron sulfur clusters to model both the structure and function of [FeFe]-hydrogenase.

Synthetic FeS Clusters as Models of the [FeFe]-Hydrogenase Active Site

Since the first reported synthesis of the classical organometallic complex $(\mu\text{-SMe})_2[Fe(CO)_3]_2$ over half a century ago,[52] chemists have painstakingly studied this "simple" complex and its derivatives for their spectroscopic properties and chemical reactivity. Over the decades, this research has continued to turn up new and interesting results concerning both metal- and sulfur-based reactivity.[53-57] Readers are encouraged to visit the works of Dietmar Seyferth for classical examples of this reactivity.[58-61] Most recently, because of its similarity to the hydrogen producing cluster of the diiron hydrogenase, [FeFe]-H_2ase, it has become the generic template from which over 300 small molecule models of the enzyme active site have been synthesized.[62] The complexes of this library differ from one another in the type of substituent ligands they contain, the degree of ligand substitution and the composition of the dithiolate linkers used, yet they all have one thing in common; none of the model complexes have yet been able to replicate the activity of the enzyme active site.[63] This has not however, stopped chemists from continuing to synthesize complexes with new combinations of dithiolate and substituent ligands.

The last five years have seen one major goal in modeling the enzyme active site reached; the first model complexes to replicate the rotated geometry, complete with a semi-bridging CO, and the mixed-valent $Fe^{I}Fe^{II}$ oxidation state of the H_{ox} state of the enzyme active site were reported.[64-65] This rotated geometry is important to the catalytic cycle in the enzyme active site, as described above, but in the model complexes it is also reported to be a key feature in several different processes. Thus the factors that control the formation of the rotated geometry also play a role in controlling the reactivity of the model complexes and further the pursuit of functional biomimetics.

The review below provides a cursory discussion on the synthetic methodologies and variety of model complexes produced by these methods. However, the main focus will be on several processes where the rotated geometry is reported to be a contributing factor: ligand substitution, protonation, and intramolecular ligand site exchange. Additionally, structural aspects of the model complexes that stabilize or control the rotated geometry will also be discussed.

Synthesis and the Dithiolate Linker

The synthesis of the model complexes is typically accomplished through one of the two reaction schemes shown in Figure I-4. The main difference between these two routes is the point at which the dithiolate linker is added. In the top reaction the dithiolate is reacted directly with an iron carbonyl source, typically $Fe_3(CO)_{12}$, at elevated temperatures to give the diiron complex. While this route, simplifies the number of steps required to reach the product, it typically produces low yields (30-60 %) and requires synthesis of the dithiolate when a more complex linker is desired.

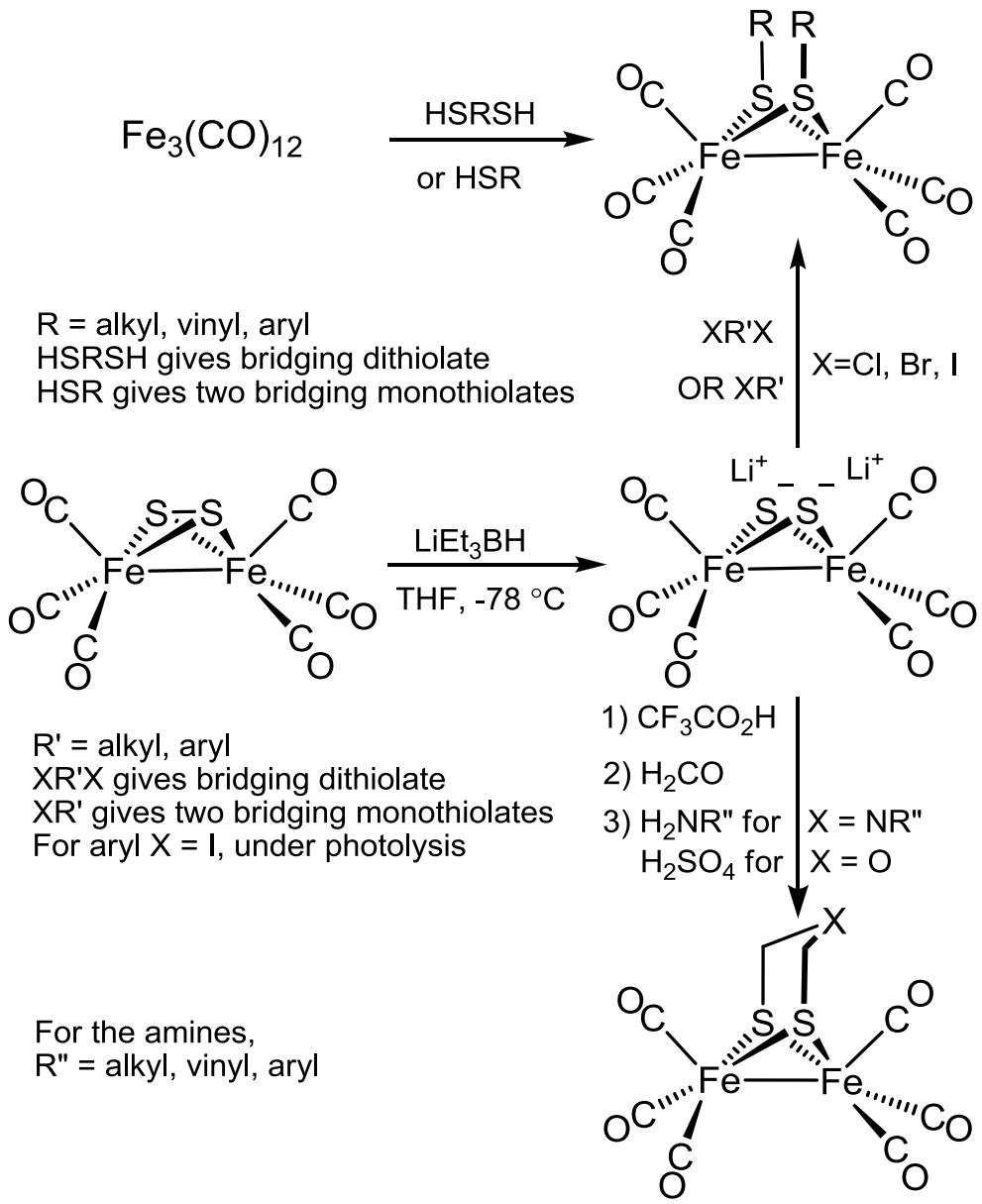

Figure I-4. Most common methods for the synthesis of hexacarbonyl diiron complexes.

The second route uses $Fe(CO)_5$ and Na_2S to form a bridging disulfide complex that serves as a precursor to many model complexes.[66] Through reduction of the disulfide and alkylation of the resulting sulfido dianion, a wide range of thiolate linkers can be accessed. The overall yield for this route is typically low due to the initial yield of the disulfide precursor (< 30%), but because of the scalability of the disulfide (following the reported procedure produces ~30 g of product on average) this approach still provides an effective route for the synthesis of new model complexes and is the only reported route used for obtaining the oxodithiolate or biologically relevent azadithiolate linkers. These two methods have been used to synthesize practically every diiron hexacarbonyl system reported within the last ten years. The notable exception is the method reported by the Rauchfuss group which reacts Rieke Fe (or $FeCl_2$ in the presence of zinc metal), with a dithiol under a CO atmosphere to give $(\mu\text{-SRS})[Fe(CO)_3]_2$ complexes.[67] This reaction is proposed to proceed through the initial formation of a ferrous dithiolate species followed by reduction and CO binding. While numerous complexes have been synthesized via these methods, the use of post-synthetic modifications is truly what has given rise to the variety of model complexes that exist.

The stability of these hexacarbonyl derivatives has allowed a wide range of reactions to be used to modify functionalized dithiolate linkers. The simplest example of direct modification of the dithiolate is through the protonation or methylation of the N atom in the azadithiolate linkers as reported by Rauchfuss and coworkers.[68] The protonation of this N atom has significant relevance to the mechanistic studies of proton reduction by the model complexes.[69] Another common method for modification is

through the initial incorporation of an ester or protected carboxylate functionality in the dithiolate linker.[70] Through deprotection and amide bond formation this has allowed the attachment of model complexes to a wide variety of supports and reactive molecules including: electrode surfaces,[71] modified polystyrene beads,[72] and photosensitizing agents.[73-75] For this last application, a large number of more elaborate modifications have been performed by the Sun and Song groups in China and have used a variety of palladium catalyzed C-C coupling reactions to attach the model complexes to Zn porphyrin or $Ru(Bipy)_3^{2+}$ photosensitizing agents.[76-77]

Methods of incorporating exogenous metal complexes are not solely limited to molecular transformations, heteroatom containing dithiolates have been used as ligands to bind other metal centers. In an effort to model both the 2Fe2S and 4Fe4S clusters found in the active site, Picket and co-workers used a trithiolate linker to attach a 4Fe4S cubane leading them to a complex that almost exactly modeled the first coordination sphere of the enzyme.[78] Despite the interesting complexes it has produced, the incorporation of highly complex groups into the dithiolate is not widely reported. Instead, the most common post-synthetic method for modifying the basic hexacarbonyl complexes is through substitution of carbon monoxide for better donor ligands.

The Substituent Ligands

The substituent ligands, as defined for this work, are the ligands that comprise the first coordination sphere, excluding the dithiolate linker. In the most general case, the susbstitution of CO for a new substituent ligand simply involves the addition of one to two equivalents of the new ligand to a solution of the diiron hexacarbonyl parent

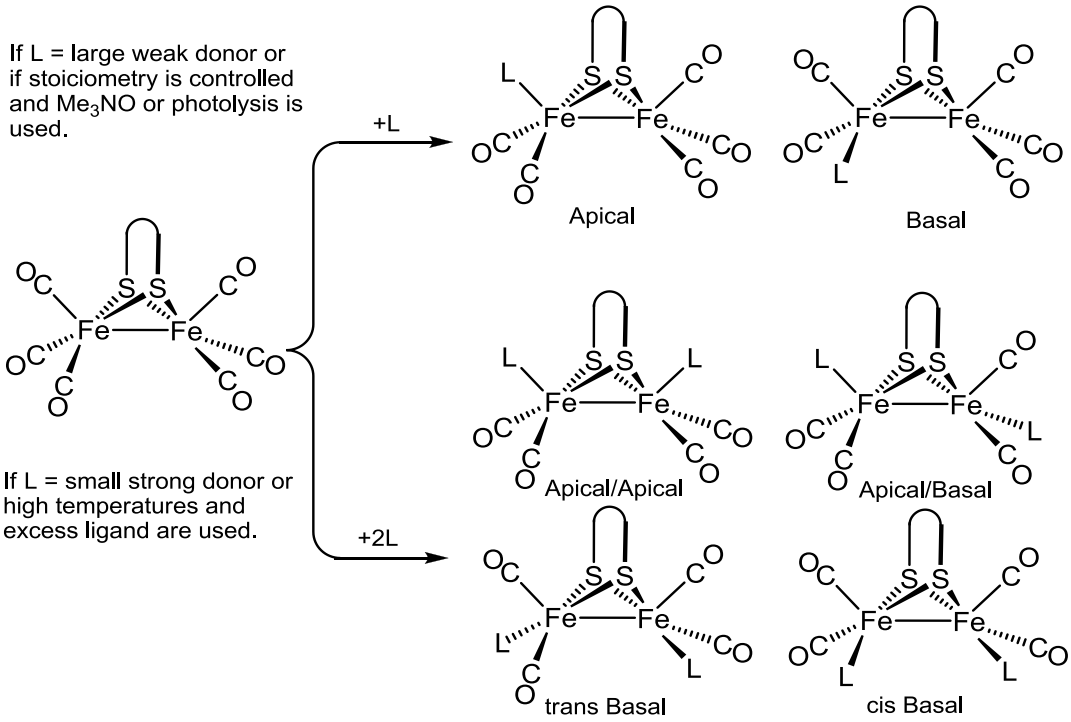

Figure I-5. Reaction showing the conditions for obtaining mono- or disubstituted complexes. Possible conformational isomers that may exist are indicated.

complex at room temperature. However, to facilitate substitution or cleanly obtain monosubstituted complexes, elevated temperatures, photolysis or CO labilizing agents such as trimethylamine N-oxide are commonly used. The exact method depends on the donating ability and size of the incoming ligand. (Figure I-5) For complexes with degrees of substitution higher than two, photolysis of a disubstituted complex in the presence of excess ligand is generally required,[79] though the facile exchange of two or more CO ligands for better donors has been noted for some Fe(II)Fe(II) model complexes.[80] Figure I-6 illustrates the diversity of complexes that can be obtained from

the substitution process. The most commonly introduced ligands are monodentate phosphines, though cyanide, amines, carbenes, and sulfur donor containing ligands have also been reported.

Bidentate ligands have also been used and have led to a number of different substitution patterns that are dependent on the length and rigidity of the group connecting the donor atoms. Long non-rigid groups tend to give 4Fe products where the ligand is spanning two diiron complexes.[81] Shorter non-rigid chains allow for single substitution on both $Fe(CO)_3$ units with the ligand spanning both irons on the same molecule.[82] Finally, short rigid linkers have allowed the synthesis of complexes where two substitutions occur on a single iron.[83] This last example is unique for the bidentate ligands. In fact, an important observation in these substituted systems is the absence of complexes where two CO's on the same iron have been replaced by monodentate ligands leaving one untouched $Fe(CO)_3$ unit. In fact, the only examples of this are reported by the Rauchfuss group where, reaction of a singly substituted complex with NO^+ results in addition to the already substituted Fe.[84] However, this pattern results from the increased electron density of the substituted iron facilitating reduction of the NO^+, and is not

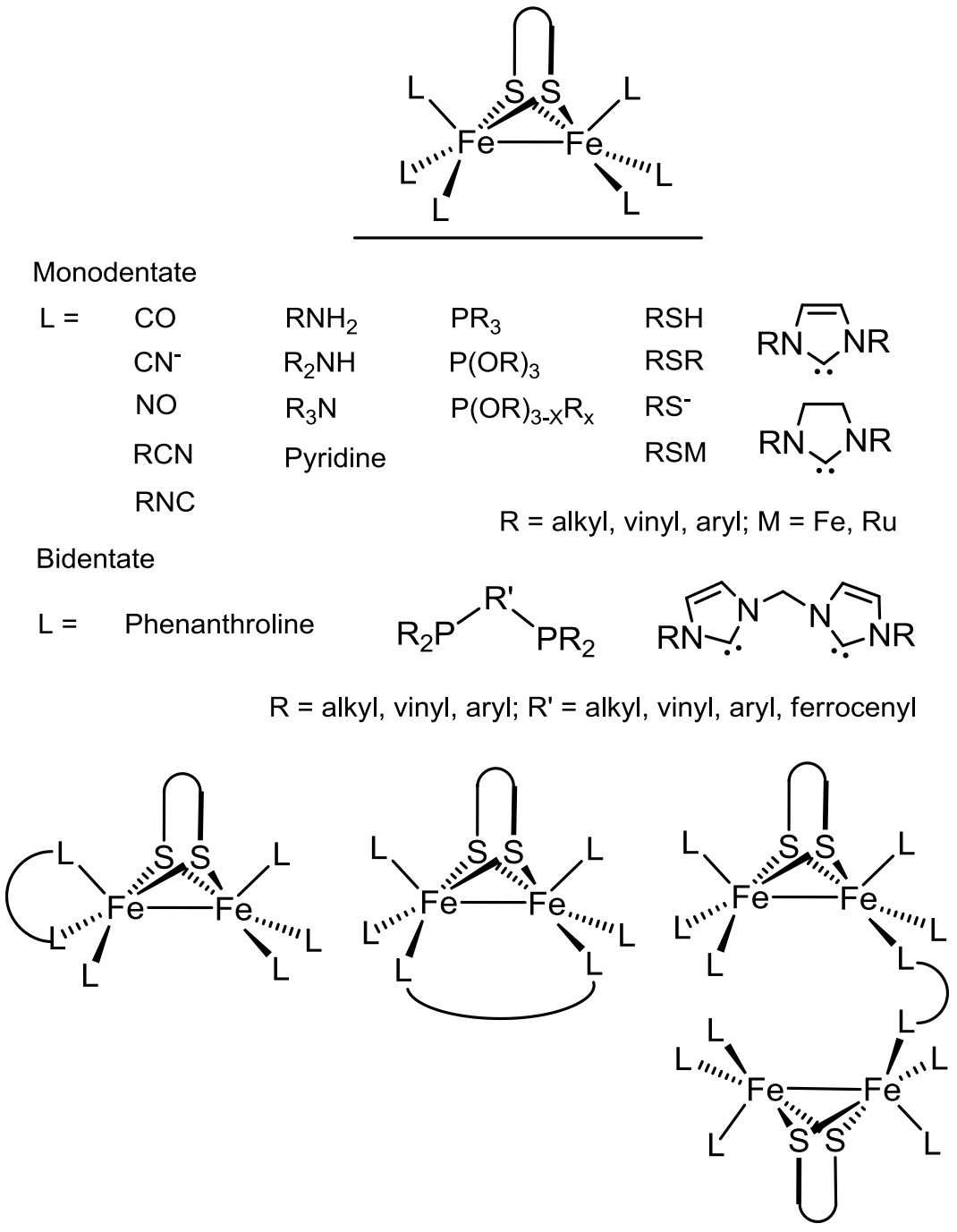

Figure I-6. Examples of ligand diversity in model complexes and possible products obtainable from bidentate ligands.

representative of the pathway proposed for normal ligand substitution.

Mechanism of Ligand Substitution

Ligand substitution on the diiron systems is proposed to occur through an associative mechanism.[85-86] (Figure I-7A) As the ligand approaches the iron, the $Fe(CO)_3$ unit rotates, giving a proposed intermediate with a carbonyl located between the two irons.[85] Transfer of this CO to the second iron and loss of a CO results in the final monosubstituted species. The separate addition of a second ligand presumably occurs through this same process starting with the remaining $Fe(CO)_3$ unit, however for the concomitant addition of two ligands in the same reaction another possibility has been reported and will be discussed later. Kinetics studies by the Darensbourg group focusing on the substitution of CO for CN^- found that enthalpic barrier for the substitution of CO was low and the entropic barrier was negative, supporting the associative pathway.[85] Also, the DFT calculated energy barriers for the steps proposed in this pathway were calculated to be sufficiently low for it to be a plausible mechanism.[87] Another study published at this same time by the Pickett group showed the first experimental evidence for the migration of CO from one iron to the other in the substitution process.[86] (Figure I-7B) Using a model complex where one CO had been substituted for a thioether group from a modified dithiolate, they monitored the addition of CN^- using stopped-flow IR. The results showed that the CN^- ligand was added to the $Fe(CO)_3$ unit and the thioether group was displaced by CO. This result confirmed that CO could in fact exchange

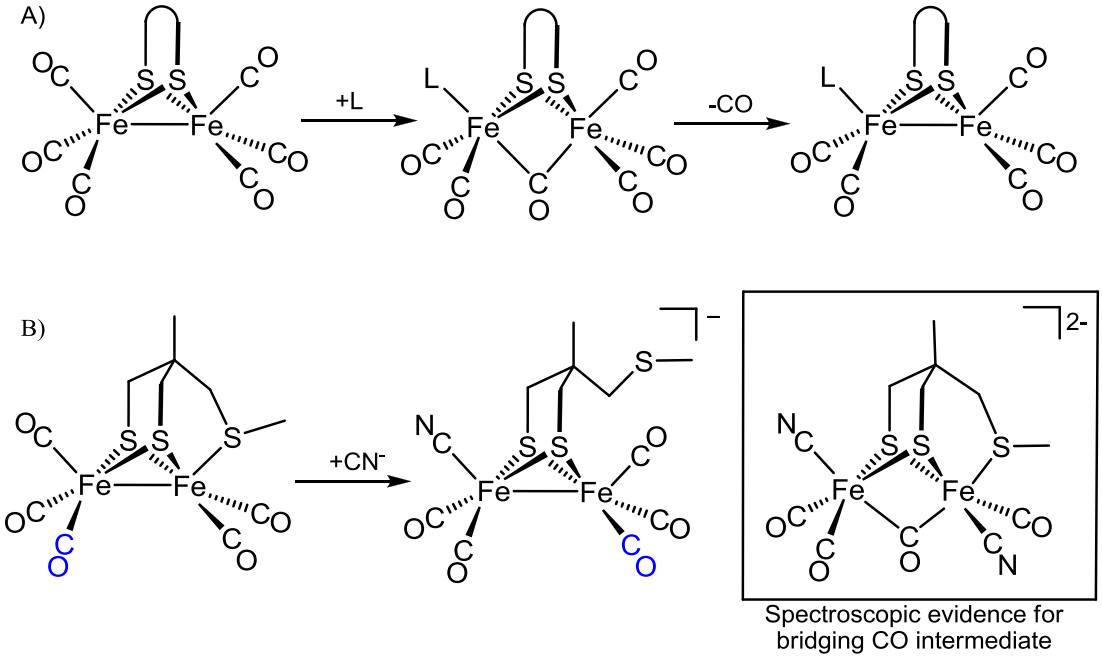

Figure I-7. A) Proposed associative pathway for ligand substitution. B) Complex from the Pickett group that showed evidence of CO migration between irons. Structure in box is a proposed stable intermediate observed to have a bridging CO by IR spectroscopy.

between irons during the substitution process. The presence of this exchange step is important in explaining differences in rates of the first and second ligand substitutions from what might be expected based on Lewis acid/base theory and metal carbonyl reactivity.

The reaction of two equivalents of CN^- with the complex (μ-pdt)$[Fe(CO)_3]_2$ occurs rapidly at room temperature, resulting in formation of the disubstituted complex without a significant build up of the monosubstituted species.[85] Even with the use of only one equivalent of cyanide the disubstituted species is primarily observed.[88] While one might expect that the decreased electrophlicity of the complex and increased π-backbonding resulting from the first substitution would make the second substitution the

rate limiting step, this reactivity suggests this is not the case. [85] The kinetic study by the Darensbourg group mentioned above, determined the rates of substitution on the monocyanide complex $Na^+(\mu\text{-}S(CH_2)_3S\text{-})[Fe(CO)_3][Fe(CO)_2CN]^-$, obtained from conversion of a single CO to CN^- by $Na^+[N(SiMe_3)_2^-]$, and directly compared it to the reaction of two equivalents of Et_4NCN with a hexacarbonyl complex. Their findings indicated that the activation barrier for substitution of the monosubstituted complex was lower than that of the hexacarbonyl derivative.

There is some debate on these findings however, as a similar study done by the Rauchfuss group reported that the Et_4N^+ salt of the monocyanide derivatives reacted slower with both PMe_3 and CN^- than the hexacarbonyl species.[88] These contradicting reports on the reactivity of $(\mu\text{-pdt})[Fe(CO)_3][Fe(CO)_2CN]^-$ could be explained by the possibility of an ion pair interaction in the Na^+ complex that is absent in the Et_4N^+ salt. Ion pair interactions have been reported for other iron cyanide complexes, such as $Na^+[Fe(CO)_4CN^-]$.[89] Also, because the two compounds would be otherwise identical the presence of such an interaction in this system is supported by difference in the IR spectra and the drastically different stabilities of the two complexes. [88] The Na^+ salt decomposes over the course of several hours at room temperature while the Et_4N^+ version is stable for days. The interaction of Na^+ with cyanide or another electronegative site in the diiron complex could result in stabilization of a different conformational isomer (i.e. CN^- in an apical versus basal position) than in the Et_4N^+ complex. Theoretical studies have shown that a strong donor in the apical position is ideally placed to stabilize the formation of

both a semi-bridging CO, as in the transition state for substitution, and a bridging CO, as in the proposed intermediate.[90]

This ion pair interaction does not explain the slower rate of reaction between $Et_4N^+(\mu\text{-pdt})[Fe(CO)_3][Fe(CO)_2CN]^-$ and CN^- compared to that of $(\mu\text{-pdt})[Fe(CO)_3]_2$ with 2 Et_4NCN which implies that an $Et_4N^+(\mu\text{-pdt})[Fe(CO)_3][Fe(CO)_2CN]^-$ intermediate pathway is not the lowest energy route for the addition of two cyanide ligands. The Rauchfuss group has instead proposed that after addition of the first CN^-, the speculated bridging CO intermediate pictured in Figure I-7A acts as the reactive species. [88] No such intermediate has been observed in the systems just described, however Pickett and co-workers have shown IR evidence of a bridging carbonyl containing species after the addition of two cyanides.[86] This intermediate slowly converts to the all terminal product at room temperature. Its stability arises from the strong donor character of the two cyanide ligands and a thioether ligand that is tethered to the dithiolate linker hindering rotation of one of the iron units. Except for one cyanide ligand these stabilizing factors would be absent in the intermediate proposed by Rauchfuss and conversion to the all terminal species would be expected to occur more readily. Thus for the purposes of reconciling the work of Darensbourg and Rauchfuss, the following mechanism that incorporates both pathways is proposed. (Figure I-8) At lower temperatures the contribution of the bridging CO intermediate to product formation (upper pathway) would remain significant while at higher temperatures conversion to the all terminal intermediate would be the preferred pathway. The rate of product formation by the lower pathway could be dependent on the preference for the first cyanide to adopt

an apical versus basal position. As the only observed species in this system are shown in blue, it is also possible that the intermediates in black differ in the conformational nature of the CN^- ligands, though rapid exchange of CN^- between apical and basal sites is observed at room temperature which makes this unlikely. Competition between these two pathways could result in an overestimate of activation barriers due to the rate constants at higher temperature reflecting greater participation of the presumably slower lower pathway.

This would also explain the exceptionally high energy barrier reported for disubstitution on the propane dithiolate complex.[85] While this mechanism fits with the experimental results described above and helps to explain the differences in reported

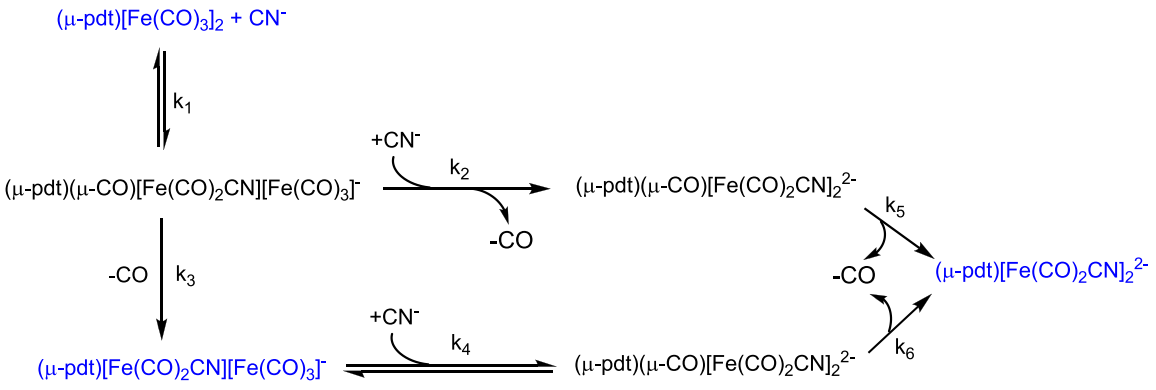

Figure I-8. Simplified mechanism for ligand substitution based on experimental data from both the Darensbourg and Rauchfuss studies. Species in blue have been confirmed experimentally.

reactivities, without the proper experiments it remains purely conjecture. What is evident though is that by either pathway the stabilization of a bridging or semi-bridging CO has the potential to greatly increase the reactivity of the diiron complex for substitution. This same stabilization is also reported to play an important role in the ability of the model complexes to react with a proton source.[91]

Protonation of the Model Complexes

Direct protonation at iron in the $Fe^{I}Fe^{I}$ model complexes is limited to multiply substituted complexes that have strong donation into the iron. For example, bistrimethyl phosphine complexes readily react with strong acids while the bistrimethylphosphite derivatives do not. The hexacarbonyl, or monosubstituted complexes actually exhibit a remarkable resilience under acidic conditions and neither protonation nor rapid decomposition are observed in most cases. The exceptions to this are, as described above, those complexes containing a basic site in the dithiolate or substituent ligands.[92]

The thermodynamic product of protonation at the one of the irons is an Fe(II)Fe(II) species with a bridging hydride.[93] Similarly reaction with MeS^{+} sources also leads to the bridging product.[94] The exclusive isolation of these species in early studies led to the proposal that the reaction of electrophiles with the irons occurred directly at the FeFe bond. This suggested a significantly different reactivity from both the enzyme active site and from the reactive pathways for ligand substitution. In 2005, Rauchfuss and co-workers reported the reaction of the diferrous complex (μ-edt)(μ-CO)[Fe(MeCN)$(PMe_3)_2$][Fe(CO)$(PMe_3)_2$]$^{2+}$ with $LiAlH_4$. [91] At room temperature the

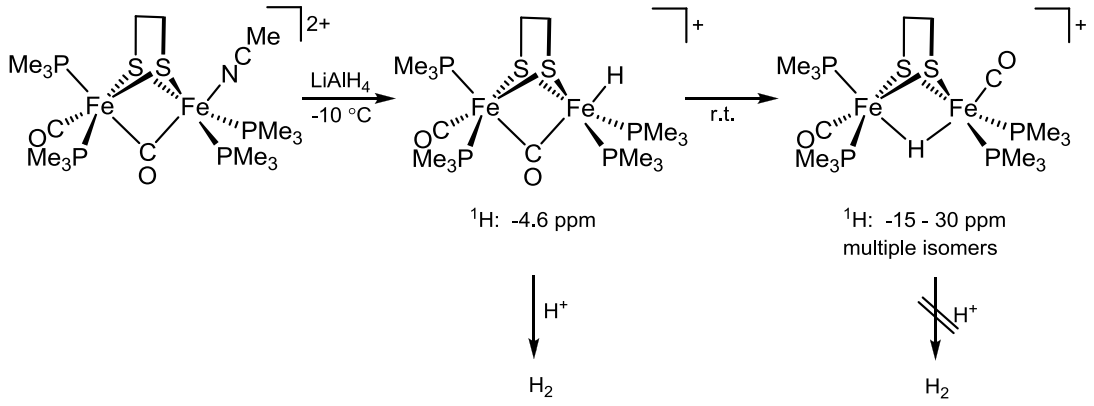

Figure I-9. Reaction of a model complex with a hydride source. This series was the first evidence of terminal hydride formation in the model complexes.

product that was observed was the bridging hydride species (μ-edt)(μ-H)[Fe(CO)$(PMe_3)_2$][Fe(CO)$(PMe_3)_2$]$^+$. The ^{1}H NMR spectra of this product showed a signal in a range characteristic of a bridging hydride (-15 - -30 ppm), (Figure I-9). However, low temperature ^{1}H NMR studies showed a signal at -4.6 ppm that was found to couple to only two phosphines. The new species was structurally characterized as the terminal hydride containing (μ-pdt)(μ-CO)[FeH$(PMe_3)_2$][Fe(CO)$(PMe_3)_2$]$^+$ and was shown to isomerize to the bridging isomer at higher temperatures. This work had two significant implications: 1) That the terminal hydride species could also be the kinetic product of protonation and 2) that this isomer could be identified at low temperatures by ^{1}H NMR studies. These possibilities were supported in a series of papers by Schollhammer, Capon, and co-workers in 2007, where they showed that upon protonation of complexes of the type (μ-S$(CH_2)_n$S-)[Fe$(CO)_3$][Fe$(CO)L_2$] (n=2 or 3; L_2

is a bidentate ligand) at -90 °C, there was ^{1}H NMR evidence of a new hydride species which, even at low temperature converted to the bridging isomer they observed at room temperature.[95-97] Since the publication of these papers, several model complexes have been reported where the researchers were able to observe a terminal hydride upon protonation of $Fe^{I}Fe^{I}$ complexes.[69,98]

The importance of the terminal hydride is also expressed in these studies. In the 2005 Rauchfuss study, the terminal hydride isomer was found to react with protons to produce hydrogen while the bridging hydride was unreactive, Figure I-9.[91] A follow up study by the same group studied the low temperature electrochemical behavior of the bridging and terminal isomers.[91] They found that the terminal hydride was reduced at a potential 200 mV less negative than the bridging isomer in CH_2Cl_2. This reduction step is important in the electrocatalytic cycle and was shown to increase the hydridic character of the terminal hydride by several pKa units. It should be noted that increased hydridic character was also observed in the more polar solvent acetonitrile.

The above systems have either more than two strong donors or have used chelating ligands on one iron. Both of these systems would be predicted to stabilize the μ-CO and slow rearrangement to the bridging hydride. In contrast, the more symmetric complexes with fewer donors such as (μ-pdt)$[Fe(CO)_2PMe_3]_2$, would be expected to convert to the terminal hydride rapidly at ambient temperatures. So it is not unexpected that, in recent studies on this complex by Pickett and co-workers, no terminal hydride was observed upon protonation at 10 °C.[99-100] These studies did indicate that the initial conformational isomers of the bridging hydride are not static in nature and conversion to

the thermodynamically stable trans-basal isomer occurs over time. This finding is significant to the fact that the complexes can exchange conformations at a reasonably low barrier despite being octahedral. The bridging hydride would be expected to be more stable than the bridging CO due to its spherically symmetric S orbital allowing better overlap with the inward directed metal orbitals. This would also explain why the initial terminal hydride, if it forms, isomerizes significantly faster than the conformational isomers once the bridging hydride forms. The exact mechanism by which these exchanges occur is, however still unknown.

Implications of Mechanistic Studies

Despite over 50 years of work on the diiron complexes, there is a significant amount of information on the basic reactivities of these compounds that has remained uncertain. This is evidenced by the continued publication of studies on the reaction pathways of these complexes for substitution, protonation or electrochemical proton reduction. The work done in the last decade on the reactivity of the model complexes has highlighted several important facts about these unique complexes and the goals that must be met to enhance their ability to electrocatalytically produce hydrogen. An important aspect present in almost all of the studies on ligand substitution and protonation is the presence of a transition state or intermediate that contains a bridging or semi-bridging CO reminiscent of the [FeFe]-hydrogenase enzyme active site. Stabilizing these μ-CO species should greatly enhance the reactivity of the model complexes. As the formation and exchange of this feature directly relates to the fluxional character of the model

complexes an understanding of the basic intramolecular dynamic processes in the model systems and the factors that control them is important.

Intramolecular Fluxional Processes

As mentioned the model systems have not been able to match the geometry of active [$Fe^{I}Fe^{I}$] form of the enzyme active site. This is in no small part due to the intramolecular dynamic processes present in the small molecule models, but absent in the active site. These processes, in addition to allowing exchange between structural isomers, also show a strong correlation with substitution rates and changes in redox properties.[85] Hence, even 50 years after the proposed thiolate bridged diiron structure of $(\mu\text{-}SR)_2[Fe(CO)_3]_2$ (or 35 years after the initial report of CO site exchange in these complexes), an examination of these fluxional processes and their relation to fundamental reactivity and electrochemical properties remains pertinent in relation to biomimetic models of the [FeFe]-H_2ase enzyme active site.

Early ^{13}C NMR studies on the $(\mu\text{-}SMe)_2[Fe(CO)_3]_2$ complex showed only a single resonance for the CO ligands at room temperature, indicating a high degree of mobility.[101] In fact, ^{1}H and ^{13}C variable temperature nmr studies of the generic complex, $(\mu\text{-pdt})[Fe(CO)_3]_2$, found two fluxional processes that defined the flexibility of the complex: 1) Boat/Chair interconversion in the Fe(-$S(CH_2)_3$S-) six member ring; and 2) apical/basal exchange (rotation) between the CO ligands of the $Fe(CO)_3$ units.[85] (Figure I-10 A&B) This latter process seemingly interconverts the CO ligands on each $Fe(CO)_3$ unit separately and does not exchange CO groups between the two irons. (Figure I-9C)

The flip in the dithiolate linker has not been as widely explored as the apical/basal exchange of the substituent ligands. The studies that have looked at this process have found it to be similar to related conformational changes in cycloalkanes. In hexacarbonyl complexes where the dithiolate is linked by three methylene groups, the estimated barrier for this exchange in the Fe(-S(CH_2)$_3$S-) six member ring (~9.3 kcal/mol) is similar to that of cyclohexane (~10.3 kcal/mol).[85] The calculated transition state is also similar to cyclohexane with the flip occurring through a half chair conformation.[87] Modification of the dithiolate results in very different behavior. Desymmetrization of either the dithiolate or substituent ligand composition on the irons makes the two conformations of the three carbon linker inequivalent and is reported to increase the barrier for the flip in some cases. The seven membered ring formed with the (-S$CH_2C_6H_4CH_2$S-) linker also has a higher barrier and remains fixed even up to 75 °C. This is attributed to the decreased flexibility afforded by the arene ring. In these systems where the ring flip is prohibited, an effect of the dithiolate orientation on the CO exchange process can be observed. This interaction is discussed more below and in Chapters III and IV.

According to DFT calculations, the exchange of the apical and basal CO ligands proceeds through a transition state similar to that proposed for ligand substitution, Figure 1-9A, where one of the basal CO's has moved down between the two iron atoms and the apical CO has taken its place in the square plane. This transition state bears a unique significance for the diiron complexes as it not only mirrors the geometry of the [FeFe]-

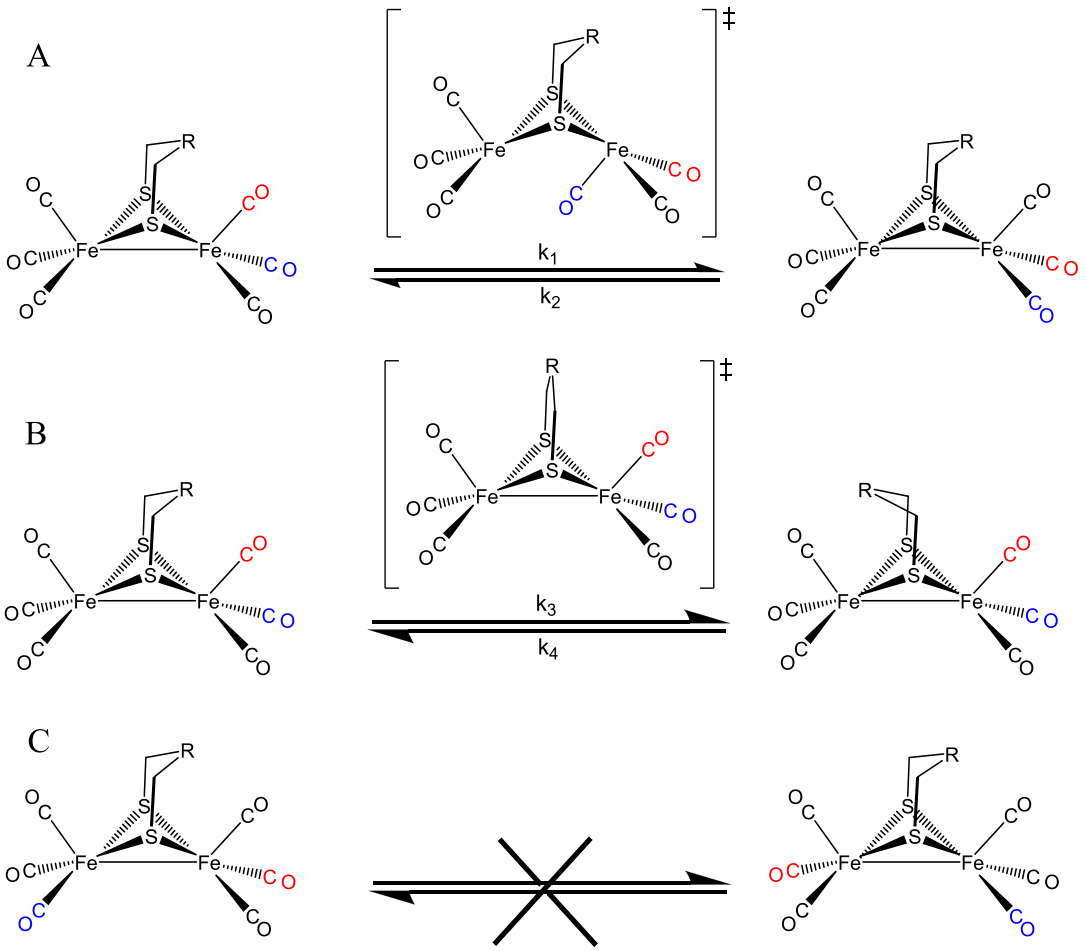

Figure I-10. Diagram of a basic $(\mu\text{-SR})_2[Fe(CO)_3]_2$ complex showing A) exchange of apical and basal CO ligands, B) ring flip of the dithiolate backbone, C) exchange of CO ligands between Fe units.

hydrogenase enzyme active site, but also is a postulated transition state/intermediate conformation in CO/ligand substitution reactions and it is the same conformation adopted by some one e^- oxidized diiron complexes.[102] By understanding how synthetic modifications can stabilize/destabilize this rotated conformation relative to the unrotated form, a higher degree of control over the substitution and redox properties of $(\mu\text{-}SR)_2[Fe(CO)_3]_2$ model complexes can be achieved.

Factors Affecting Intramolecular Ligand Exchange

While the energy barrier for these processes is typically relatively low (7-15 kcal/mol depending on the nature of the dithiolate and substituent ligands), it remains significantly higher than the estimated energy barrier for axial/equatorial exchange in the five coordinate $Fe(CO)_5$ (<3 kcal/mol) which occurs via a Berry pseudorotation. The reason for this stark difference can be explained by the presence of the FeFe bond in $(\mu\text{-}SR)_2[Fe(CO)_3]_2$ complexes which takes up a sixth coordination site resulting in a pseudo-octahedral geometry at each iron.[57] Thus for the CO exchange processes shown in Figure I-9 to occur there must be a disruption of this FeFe bond.

DFT calculations looking at this rotation indeed found that while in the unrotated ground state the highest occupied molecular orbital constitutes the FeFe bond, the rotated transition state has an occupied orbital located in a terminal position, i.e., directed away from the second Fe.[85,87,103] Important to this finding was the observation that the lowest occupied molecular orbital is FeFe antibonding and that consequently, any modifications to the complexes that push electron density in the FeFe bond should weaken it.[103] This theory is supported by the increased FeFe bond length in substituted

complexes relative to the parent hexacarbonyl species. Further calculations showed a strong dependence of the energy barrier both on the degree of substitution and the donor strength of the ligands.[94] While the stabilization of the rotated transition state varied with the orientation of the strong donors, all of the calculations done by our group have agreed on one fact; relative to the hexacarbonyl parent complexes, substituted derivatives are better able to stabilize the rotated transition state, (Figure I-11).

An equally important, and only more recently studied, contribution to the energy barrier for rotation comes from the dithiolate linker that bridges the two iron units. In contrast to (μ-pdt)$[Fe(CO)_3]_2$, where the barrier for ring flip of the dithiolate was similarly as low as the barrier for CO exchange, complexes such as (μ-*o*-$SCH_2(C_6H_4)CH_2S$-)$[Fe(CO)_3]_2$ which possesses a much higher ring flip barrier due to the seven membered ring, have allowed disambiguation of the $Fe(CO)_3$ rotation both under the steric influence of the S-to-S linker and without it.[85] The NMR studies of this complex showed that the $Fe(CO)_3$ rotor on the opposite side of the aryl ring had a barrier similar to the (μ-edt)$[Fe(CO)_3]_2$ complex, but surprisingly the rotor on the same side showed a lower barrier indicating that the positioning of the dithiolate linker could be as important as the substituent ligands. The similarity of the ν(CO) stretches of these compounds indicate that rather than being a result of increased donation by the dithiolates, this change in the barrier is best described as the result of steric repulsion between the apical carbonyl units and the closest contacts on the dithiolate linker. This places torque on the apical carbonyl and acts directly against the restoring force derived

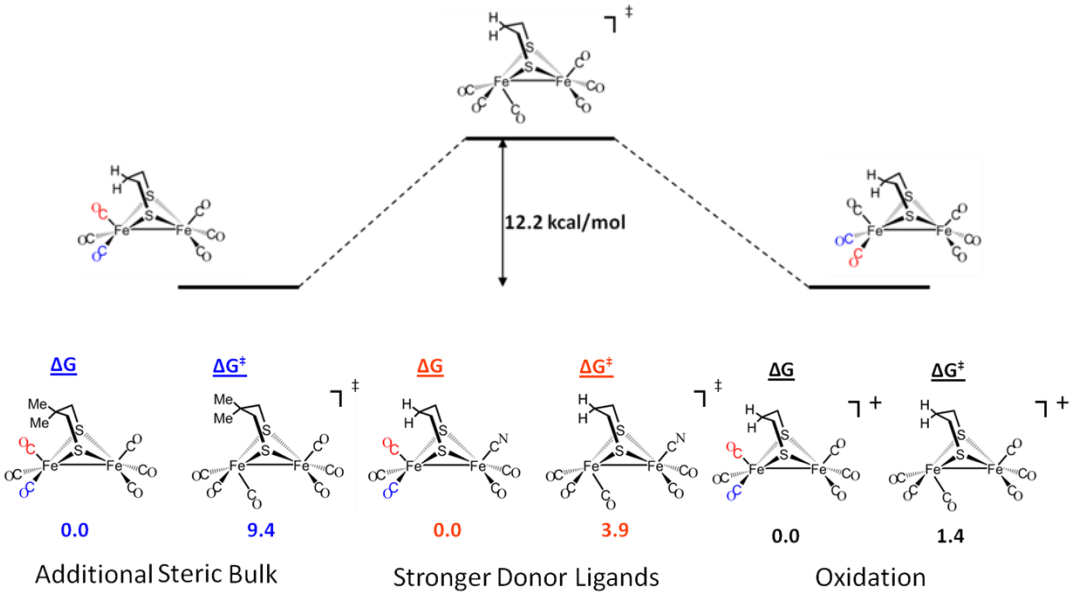

Figure I-10. Diagram of the changes in the energy barrier for intramolecular CO exchange upon modification of the model complex.

from maintaining the FeFe bond.

Theoretical work that focused on the effect of the dithiolate linker found several synthetic modifications that could produce significant changes in the barrier for rotation. Primary to the effects described above was that an increase in the steric bulk of the dithiolate linker would result in a lower barrier for rotation as long as the steric bulk was directed towards the carbonyls.[103] If the propylene linker is increased to a pentlyene linker there is a 5 kcal/mol decrease in the barrier as long as the central CH_2 group is directed towards one of the apical CO groups but if it is pointed away the significant decrease in the barrier drops to only 1 kcal/mol less than in the propylene linker. This

steric requirement can also be met through modification of the substituents on the central C of the propane dithiolate linker, and was found to similarly decrease the barrier for $Fe(CO)_3$ rotation as the size of the substituent was increased from –H to $-CH_3$ to $-C(CH_3)_3$. This theoretical study was the inspiration for the work described in Chapters III and IV of my dissertation.

Another important finding from the theoretical work, and one more closely related to the [FeFe]-H_2ase enzyme active site is that changing the central group in the propyl chain from $–CH_2-$ to –NH- to –O- has little effect on the stabilization of the rotated structure relative to the unrotated form.[103] The exception to this being that the same series in the five atom linker showed a more dramatic change when the methylene group was changed to an amine group. For the rotated and unrotated conformers the difference in energy was only 0.1 kcal/mol, with the rotated form being the more stable. While this difference is within a range that makes determining whether the rotated or unrotated form is in reality more stable impossible without further work, it does show the largest stabilization of any of the synthetic modifications and results from the N being able to directly interact with the rotated iron site. A similar effect was observed when the amine was added in a pendant fashion, i.e. $(–SCH_2CH(NH_2)CH_2S-)$, again allowing it to more directly interact with the open site created on the rotated iron thus greatly stabilizing the transition state. This effect is not only observed when Lewis basic groups are added, the addition of a Lewis acidic pendant $–BH_2$ group also lowers the energy barrier by interacting with the rotated iron. This last result shows the ambiphilic nature of the open site created on the rotated Fe and emphasizes the importance of these

fluxional properties for both nucleophilic ligand substitution reactions and processes where the iron acts as the nucleophile such as protonation.

In Figure I-11, the final way to change the energy difference between the rotated and unrotated forms of the model complexes is through reduction or oxidation. As decribed above, the calculated HOMO and LUMO for model complexes are typically the bonding and antibonding FeFe interactions respectively. Thus the addition or removal of one electron should serve to decrease the FeFe bond order to one half.[103] For the (μ-pdt)$[Fe(CO)_3]_2$ complex reduction to Fe^IFe^0 not only lowers the energy of the rotated form to only 8.0 kcal/mol higher than the unrotated form but rather than being a transition state the reduced species is a minimum on the potential energy surface. The same is true upon oxidation, with the rotated form being 1.4 kcal/mol higher in energy than the unrotated form. Further oxidation to the $Fe^{II}Fe^{II}$ state, effectively reducing the FeFe bond order to 0, results in the rotated form with a bridging carbonyl being significantly more stable (by 8.8 kcal/mol) than the unrotated form.

Thus from the wealth of computational studies the use of strong donor ligands and sufficient steric bulk should greatly stabilize the rotated geometry, as should oxidation or reduction. The work presented herein seeks to further explore the application of steric bulk to modify the fluxional properties of the model complexes and show its ability to stabilize the rotated geometry (Chapters III & IV). Additionally, through the use of cyclodextrins as supramolecular hosts, the effect of intermolecular interactions on the basic properties and reactivity of the model complex was explored and is discussed in Chapter V.

CHAPTER II

GENERAL EXPERIMENTAL DETAILS

General Procedures

All syntheses and manipulations were performed using standard Schlenk-line and syringe/rubber septa techniques under N_2 or in an Ar atmosphere glovebox. Solvents were purified according to published procedures, and freshly distilled under N_2 prior to use or purified and degassed via a Bruker solvent system. Reagents were purchased from commercial sources and used as received. The dithiolate ligands depdt, dmpdt, bepdt,[104] IMe[105], (μ-pdt)[Fe(CO)$_2$PMe$_3$]$_2$,[106] as well as the $CDFCl_2$ used for low temperature NMR measurements,[107]were synthesized according to the literature procedures. The synthesis of the (μ-S_2)[Fe(CO)$_3$]$_2$ starting material and incorporation of an amine group into the dithiolate linker were accomplished as reported.[92] Elemental analyses were performed by Atlantic Microlab, inc., Norcross, Georgia, United States. Infrared spectra were recorded on a Matteson Galaxy Series 6021 FTIR spectrometer or a Bruker Tensor 37 spectrometer in CaF_2 solution cells of 0.1 mm path length. ^{1}H and ^{13}C NMR spectra were recorded on an Inova 500 MHz superconducting NMR instrument operating at 500.6, and 125.9 MHz respectively. All variable temperature NMR spectra were recorded on a Unity+ 500 MHz superconducting NMR instrument operating at 125.9 MHz.

Experimental Details for Chapter III

Preparation of (μ-dmpdt)[Fe(CO)$_3$]$_2$, (III-1). To a 50 mL Schlenk flask containing 2,2-dimethyl-1,3-propanedithiol (1.5 g, 0.011 mol), toluene (15 mL) was

added. This light yellow solution was transferred via cannula to a 200 mL Schlenk flask containing $Fe_3(CO)_{12}$ (5.56 g, 0.011 mol) in 100 mL of toluene. The resultant blue-green solution was stirred at 60°C and monitored by IR spectroscopy. After approximately 3 h the reaction was cooled to room temperature. At this point silica gel (~2 g) was added to the flask and the solvent removed by rotary evaporation. The resulting solid containing the product and silica gel was loaded onto a 4 cm diameter column packed with 20 cm of silica gel. The product, which appeared as a bright red band, was eluted with hexanes. Upon removal of solvent by rotary evaporation, pure microcrystalline **III-1**. (Yield: 1.56 g, 3.76 mmol, 34.1%). Crystals of X-ray quality were obtained by placing concentrated solutions of (μ-dmpdt)$[Fe(CO)_3]_2$ in hexanes in the freezer overnight. IR(Hexanes) ν(CO), See Table in Figure III - 3; Elem. Anal. Calculated (found) $C_{11}H_{10}O_6S_2Fe_2$: C, 31.89 (31.93); H, 2.44 (2.44). ^{1}H NMR ($CDCl_3$): 0.99 (s, 6H), 2.08 (s, 4H) ppm. ^{13}C NMR ($CDCl_3$): 30.5, 31.8, 33.5, 207.9 ppm. Mp: 138-141°C.

Preparation of (μ-depdt)$[Fe(CO)_3]_2$, (III-2). Complex **III-2** was prepared in a manner analogous to **III-1** using 2,2-diethyl-1,3-propanedithiol (2.0 g, 0.012 mol) and $Fe_3(CO)_{12}$ (6.14 g, 0.012 mol). (Yield: 1.180 g, 2.66 mmol, 21.9%). IR(Hexanes) ν(CO), See Table in Figure III-3; Elem. Anal. Calculated (found) $C_{13}H_{14}O_6S_2Fe_2$: C, 35.30 (35.39); H, 3.19 (3.16); ^{1}H NMR ($CDCl_3$): 0.74 (t, J = 7.1 Hz, 6H), 1.35 (q, J = 7.37 Hz, 4H), 2.08 (s, 4H) ppm. ^{13}C NMR (CD_2Cl_2): 7.6, 29.4, 30.1, 38.5, 207.8 ppm. Mp: 123.8-125.5 °C.

Preparation of (μ-bepdt)$[Fe(CO)_3]_2$, (III-3). Complex **III-3** was prepared in a manner analogous to **III-1** using 2-butyl-2-ethyl-1,3-propanedithiol (2.0g, 0.010mol)

and $Fe_3(CO)_{12}$ (5.25g, 0.010 mol). (Yield: 0.95 g, 2.02 mmol, 19.4%). Elem. Anal. Calculated (found) $C_{15}H_{18}O_6S_2Fe_2$: C, 38.30 (38.20); H, 3.86 (3.84); ^{1}H NMR ($CDCl_3$): 0.73 (t, J = 6.9 Hz, 3H); 0.89 (t, J = 6.9 Hz, 3H); 1.04 (m, 2H); 1.27 (m, 4H); 1.36 (q, J = 7.39 Hz, 2H); 2.08 (s, 4H) ^{13}C NMR ($CDCl_3$): 7.6, 14.3, 23.2, 25.4, 29.8, 30.5, 37.5, 38.4, 207.8, 207.8 ppm.; Mp: 80.4-82.8 °C.

Preparation of (μ-dmpdt)[($Fe(CO)_3$)($Fe(CO)_2$IMes)], (III-4). To a 200 mL Schlenk flask containing **III-1** (0.500g 1.21mmol), IMes·HCl (0.411 g 1.21 mmol) and K^+[t-BuO]$^-$ (0.162 g, 1.45 mmol), 100 mL of dry THF was added. The reaction was stirred at 50 °C and monitored by infrared spectroscopy. After approximately 2.5 hours the dark red/purple solution was cooled to room temperature. At this point silica gel (2 g) was added to the flask and the solvent was removed by rotary evaporation. The resulting solid was loaded onto a 4 cm diameter column packed with 20 cm of silica gel. Excess **III-1** was first eluted using hexanes, and the product, which appeared as a purple-red band, was then eluted with diethyl ether. The ether was removed by rotary evaporation, leaving a dark purple-red solid. (Yield: 0.307 g, 0.645 mmol, 36.8%). Crystals of X-ray quality were obtained by slow evaporation of solvent from a concentrated solution of (μ-dmpdt)[($Fe(CO)_3$)($Fe(CO)_2$IMes)] in ether at room temperature. ν(CO) IR(THF): 2030 m, 1971 s, 1947 m sh, 1913 w cm^{-1}; Elem. Anal. Calculated (found) $C_{31}H_{34}N_2O_5S_2Fe_2$: C, 53.91 (54.20); H, 4.97 (4.98). ^{1}H NMR ($CDCl_3$): 0.77 (s, 3H); 1.58 (s, 3H); 2.18 (s, 14H); 2.35 (s, 8H); 6.94 (s, 2H); 6.99 (s, 4H) ppm; ^{13}C NMR ($CDCl_3$): 29.4, 31.2, 32.6, 34.0, 124.1, 129.1, 136.6, 137.9, 139.2, 187.2, 211.7, 215.4 ppm.

Preparation of (μ-depdt)[(Fe(CO)$_3$)(Fe(CO)$_2$IMes)], (III-5). Complex **III-5** was prepared in a manner analogous to **III-4** using (μ-depdt)[(Fe(CO)$_3$)]$_2$ (0.500 g 1.13 mmol), IMes·HCl (0.385 g, 1.13 mmol) and K^+[t-BuO]$^-$ (0.152 g 1.36 mmol) Yield: (0.358 g, 0.499 mmol, 44.1%). ν(CO) IR(THF) 2025 m, 1971 s, 1946 m sh, 1911 w cm^{-1}; Elem. Anal. Calculated (found) $C_{33}H_{38}N_2O_5S_2Fe_2$ + 1 $(C_2H_5)_2O$: C, 56.05 (55.99); H, 6.11 (5.65). ^{1}H NMR ($CDCl_3$): 0.57 (m, 6H); 1.09 (q, J = 7.2 Hz, 2H); 1.25 (q, J = 7 Hz, 2H); 2.18 (s, 14H); 2.35 (s, 8H); 6.94 (s, 2H); 7.0 (s, 4H) ppm; ^{13}C NMR ($CDCl_3$): 7.1, 7.3, 18.7, 21.2, 27.6, 31.2, 32.2, 37.7, 125.1, 129.0, 136.6, 137.8, 139.1, 188.2, 211.7, 215.4 ppm.

Preparation of (μ-depdt)[(Fe(CO)$_3$)(Fe(CO)$_2$IMe)], **(III-6)**. Complex **III-6** was prepared in a manner analogous to **III-5** using (μ-depdt)[(Fe(CO)$_3$)]$_2$ (0.500 g, 1.13 mmol), IMe·HCl (0.149 g, 1.13 mmol) and K^+[t-BuO]$^-$ (0.152 g, 1.36 mmol). (Yield: 0.086 g, 0.169 mmol, 14.9%). ν(CO) IR(THF) 2025 m, 1971 s, 1946 m sh, 1911 w cm^{-1}; Elem. Anal. Calculated (found) $C_{17}H_{22}N_2O_5S_2Fe_2$: C, 40.00 (40.46); H, 4.35 (4.45). ^{1}H NMR ($CDCl_3$): 0.42 (t, J = 7.0 Hz, 3H); 0.67 (t, J = 7.0 Hz, 3H); 1.15 (q, J = 6.9 Hz, 2H); 1.22 (q, J = 6.9 Hz, 2H); 1.58 (d, J = 12.5 Hz, 2H); 1.82 (d, J = 12.5 Hz, 2H); 4.03 (s, 6H); 7.0 (s, 2H) ppm; ^{13}C NMR ($CDCl_3$): 7.6, 7.9, 26.3, 30.4, 33.2, 37.8, 39.9, 123.7, 191.5, 211.2, 215.2 ppm.

Preparation of (μ-dmpdt)[(Fe(CO)$_3$)(Fe(CO)$_2$PPh$_3$)], (**III-7**). To a 50 mL round bottom flask containing trimethylamine-N-oxide (20 mg, 0.266 mmol), was added 20 mL of CH_3CN. The resulting solution was transferred via cannula to a 100 mL Schlenk flask containing (μ-dmpdt)[Fe(CO)$_3$]$_2$ (100 mg, 0.242 mmol) dissolved in 30

mL of CH_3CN. After the reaction had stirred for 30 min, a solution of PPh_3 (70 mg, 0.266 mmol) in 10 mL of CH_3CN was added and the reaction progress monitored by IR spectroscopy. Upon completion of the reaction, approximately 30 min, solvent was removed under vacuum. The resulting solid was dissolved in a minimal amount of ether and loaded onto a 4 cm diameter column containing 20 cm of silica gel. The product, which appeared as a dark red band, was eluted with ether. Upon removal of solvent by rotary evaporation pure product was obtained. (Yield: 24 mg, 0.037 mmol, 15.3%). ν(CO) IR(THF) 2045 ms, 1981 s, 1961 m sh, 1927 w cm^{-1}; Elem. Anal. Calculated (found) $C_{28}H_{25}O_5PS_2Fe_2$: C, 51.9 (51.71); H, 3.89 (3.83). ^{1}H NMR ($CDCl_3$): 0.93 (s, 3H); 1.16 (d, J = 12.9 Hz, 2H); 1.26 (s, 3H); 1.80 (d, J = 13.4 Hz, 2H); 7.44 (m, 3H); 7.51 (m, 6H); 7.71 (m, 6H) ppm; ^{13}C NMR ($CDCl_3$): 28.7, 29.9, 31.3, 32.8, 128.7(J_{C-P} = 12.7 Hz) 128.7(J_{C-P} = 9.8 Hz), 132.3(J_{C-P} = 10.8 Hz), 133.7(J_{C-P} = 10.9 Hz), 209.6, 214.2(J_{C-P} =12.8 Hz) ppm.

Preparation of (μ-depdt)[(Fe(CO)$_3$)(Fe(CO)$_2$PTA)], (**III-8**). Complex **III-8** was prepared in a manner analogous to **III-7**. To a 50 mL round bottom flask containing trimethylamine-N-oxide (19 mg, 0.253 mmol), was added 20 mL of CH_3CN. The resulting solution was transferred via cannula to a 100 mL Schlenk flask containing (μ-depdt)$[Fe(CO)_3]_2$ (100 mg, 0.226 mmol) dissolved in 30 mL of CH_3CN. After the reaction had stirred for 30 min, a solution of PTA (35 mg, 0.223 mmol) in 10 mL of CH_3CN was added and the reaction progress monitored by IR spectroscopy. Upon completion of the reaction, approximately 30 min, a small amount of silica gel was added to the solution and solvent was removed under vacuum. The resulting solid was

loaded onto the top of a 4 cm diameter column containing 20 cm of silica gel. Unreacted starting material was eluted with hexanes. The product, which appeared as a dark red band, was eluted with THF. Upon removal of solvent by rotary evaporation pure product was obtained. (Yield: 72 mg, 0.126 mmol, 59%). ν(CO) IR(CH_3CN) 2039 ms, 1983 s, 1963 m sh, 1925 w cm^{-1}; Elem. Anal. Calculated (found) $C_{18}H_{26}O_5PN_3S_2Fe_2$: C, 37.8 (37.6); H, 4.59 (4.56); N, 7.36 (7.47).

Variable Temperature NMR Measurements. All samples used for variable temperature NMR measurements were isotopically enriched using a 275W GE ultraviolet Sunlamp for the photolysis of the complexes in hexanes solution under a ^{13}CO atmosphere. The hexanes solutions were passed through a plug of silica gel and the solvent was removed. The resulting solids were used without further purification.

Electrochemical Studies. Cyclic voltammograms were recorded on a BAS-100A electrochemical analyzer using a three-electrode cell: a glassy carbon disk (0.071 cm^2), the working electrode; reference electrode, $Ag/AgNO_3$; and a coiled platinum wire, the counter electrode. Solutions were deaerated by an Ar purge for 5-10 min and a blanket of Ar was maintained over the solution while performing the measurements. All experiments were performed in CH_3CN solutions containing 0.1 M $^nBu_4NPF_6$ at room temperature. Ferrocene, Fc, served as the internal reference and all potentials are reported versus Fc/Fc^+ as a standard ($E_{1/2}$ = 0.00 V vs $Ag/AgNO_3$ in CH_3CN). Comparisons to earlier work in CH_3CN may be accomplished by adding 0.40 V to the potential presented herein. Glacial acetic acid was added in molar equivalent increments via microsyringe.

X-ray Structure Analysis. Low temperature (110 K) X-ray diffraction data were collected on a BRUKER SMART 1000 CCD-based diffractometer (Mo-Kα radiation, λ = 0.71073 Å) for the (μ-dmpdt)[$Fe(CO)_3]_2$, (μ -depdt)[$Fe(CO)_3]_2$, (μ -bepdt)[$Fe(CO)_3]_2$, ,(μ -depdt)[$(Fe(CO)_3)(Fe(CO)_2$IMes)], (μ -depdt)[$(Fe(CO)_3)(Fe(CO)_2$IMe)], complexes. For the (μ -dmpdt)[$(Fe(CO)_3)(Fe(CO)_2$IMes)], (μ -dmpdt)[$(Fe(CO)_3)(Fe(CO)_2PPh_3)$] and ($\mu$ -depdt)[$(Fe(CO)_3)(Fe(CO)_2$PTA)] complexes, data were obtained on a Bruker-AXS APEXII three-circle X-ray Diffractometer (Mo-Kα radiation, λ = 0.71073 Å), also operating at 110 K.

The structures were solved by direct methods. Hydrogen atoms were added at idealized positions and refined with fixed isotropic displacement parameters equal to 1.2 times the isotropic displacement parameters of the atoms to which they were attached. Anisotropic displacement parameters were determined for all non-hydrogen atoms. Programs used for data collection and cell refinement, SMART and APEX2;[108] data reduction, SAINT;[109] absorption correction, SADABS;[110] structure solution, SHELXS-97 (Sheldrick);[111] structure refinement, SHELXL-97 (Sheldrick).[111] Molecular graphics and preparation of material for publication used SHELXTL-PLUS, version 5.1 or later (Bruker).[111] X-seed was employed for the final data presentation and structure plots.[112]

Experimental Details for Chapter IV

Synthesis of (μ-dmpdt)[$(Fe(CO)_2PMe_3]_2$, (IV-2*). To a 200 mL Schlenk flask equipped with a reflux condenser and containing (μ-dmpdt)[$(Fe(CO)_3]_2$, (0.500 g, 1.21

mmol), was added 100 mL of dry toluene. PMe_3 (0.5 mL) was added and the solution was heated to 100 °C. The reaction was monitored by IR and showed complete reaction after 48 hours. Solvent was removed in vacuo and the resulting solid recrystallized from MeOH to give a dark red microcrystalline solid. (Yield: 0.451 g, 0.884 mmol, 73%). Crystals of X-ray quality were obtained from a concentrated MeOH solution stored at -4 $^{\circ}$C for 24 h. IR (CH_2Cl_2) (v(CO) 1980, 1940, 1905, 1899 cm^{-1}) Elem. Anal. Calculated (found) $C_{15}H_{28}O_4P_2S_2Fe_2$: C, 35.3 (35.4); H, 5.53 (5.49) ^{1}H NMR (CD_2Cl_2): 0.96 (s, 6H), 1.490 (d, J(^{31}P) = 9.1 Hz, 18H), 2.012 (s, 4H) ppm. ^{13}C NMR (CD_2Cl_2): 19.80 (J(^{31}P)=28.36 Hz) 30.90, 33.86, 34.85, 217.03 (J(^{31}P)=22 Hz).

Synthesis of (μ-dmpdt)[(Fe(CO)$_2$PMe$_3$]$_2$PF$_6$, (IV-2*$_{ox}$). A solution of **IV-2*** (0.051 g, 0.100 mmol) in 10ml of dichloromethane and cooled to -78 ºC, was added to a pre-cooled test tube containing solid Ferrocenium hexafluorophosphate. (0.033 g, 0.100 mmol). The reaction was allowed to stir for 10 minutes then warmed up to -42 ºC. Addition of 20 mL of pre-cooled hexane (-78 ºC) gave the product as a purple-red precipitate. The supernatant was cannulated off and the product was washed with two (20 mL) portions of -78 ºC hexane to remove impurities. (Yield 0.049 g, 0.075 mmol, 87% yield). X-ray quality crystals were obtained by transferring the CH_2Cl_2 reaction solution to a 12 mm diameter glass tube capped with a rubber septum. This was then stored in a Dewar flask filled halfway with ethylene glycol/ $CO_{2(s)}$ and the rest of the way with crushed $CO_{2(s)}$. After 14 days, suitable crystals had formed.

Synthesis of (μ-dmpdt)[(Fe(CO)$_2$P(OMe)$_3$]$_2$, (**IV-3***). To a 200 mL Schlenk flask equipped with a reflux condenser and containing (μ-dmpdt)[(Fe(CO)$_3$]$_2$, (0.500g 1.21 mmol), was added 100 mL of dry toluene. P(OMe)$_3$ (0.5 mL) was added and the solution was heated to 100°C. The reaction was monitored by IR and showed complete reaction after 6 hours. Solvent was removed in vacuo and the resulting solid recrystallized from MeOH to give a light red microcrystalline solid. (Yield: 0.47 g, 0.078 mmol, 81%). IR (CH_2Cl_2) (ν(CO) 2004, 1963, 1936, 1919 cm^{-1}) Elem. Anal. Calculated (found) $C_{15}H_{28}O_{10}P_2S_2Fe_2$: C, 29.72 (29.94); H, 4.66 (4.86). Crystals of X-ray quality were obtained from a concentrated MeOH solution of the (μ-depdt) derivative stored at -4 °C for 24 h. (μ-depdt)[(Fe(CO)$_2$P(OMe)$_3$]$_2$ was synthesized in a manner analogous to the (μ-dmpdt) complex using (μ-depdt)[(Fe(CO)$_3$]$_2$ (0.100 g 0.26 mmol) and 0.1 mL P(OMe)$_3$. (Yield: 0.044 g, 0.069 mmol, 40 %). IR (CH_2Cl_2) (ν(CO) 2004, 1962, 1936, 1920 cm^{-1})

Synthesis of (μ-dmpdt)[(Fe(CO)$_2$PMe$_3$][(Fe(CO)$_2$IMes], (**IV-4***). To a 50 mL Schlenk flask containing (μ-dmpdt)[(Fe(CO)$_3$][Fe(CO)$_2$IMes], (0.100g 0.15 mmol), was added 20 mL of dry toluene. PMe$_3$ (0.018 mL, 0.19 mmol) was added and the solution was slowly heated to 100 °C. The reaction was monitored by IR and stopped prior to completion, ~2.5 h, to prevent formation of **IV-2***. Solvent was removed in vacuo and the resulting solid recrystallized from MeOH to give a dark red microcrystalline solid. (Yield: 0.037 g, 0.050, 32%). IR (CH_2Cl_2) (ν(CO) 1972, 1932, 1894 cm^{-1})

Electrochemical Studies. Cyclic voltammograms were recorded on a BAS-100A electrochemical analyzer using a three-electrode cell: a glassy carbon disk (0.071

cm^2), the working electrode; reference electrode, $Ag/AgNO_3$; and a coiled platinum wire, the counter electrode. Solutions were deaerated by an Ar purge for 5-10 min and a blanket of Ar was maintained over the solution while performing the measurements. All experiments were performed in CH_2Cl_2 solutions containing 0.1 M $^nBu_4NPF_6$ at room temperature. All potentials are reported versus Fc/Fc^+ ($E_{1/2}$ = 0.00 V vs $Ag/AgNO_3$ in CH_2Cl_2).

X-ray Structure Analysis. Low-temperature (110 K) X-ray diffraction data for **IV-2*** and IV-**3*** were collected on a Bruker SMART 1000 CCD based diffractometer (Mo KR radiation, λ) 0.710 73 Å).[108] Low-temperature (110 K) X-ray diffraction data for **IV-1*** was collected on a Bruker Apex-II CCD based diffractometer (Mo sealed X-ray tube, Kα = 0.71073 Å).[108] The structures were solved by direct methods. Hydrogen atoms were added at idealized positions and refined with fixed isotropic displacement parameters equal to 1.2 times the isotropic displacement parameters of the atoms to which they were attached. Anisotropic displacement parameters were determined for all non-hydrogen atoms. Programs used for data collection and cell refinement, SMART and APEX2;[108] data reduction, SAINT;[109] absorption correction, SADABS;[110] structure solution, SHELXS-97 (Sheldrick);[111] structure refinement, SHELXL-97 (Sheldrick).[111] Molecular graphics and preparation of material for publication used SHELXTL-PLUS, version 5.1 or later (Bruker).[111] X-seed was employed for the final data presentation and structure plots.[112]

For (μ-dmpdt)[$(Fe(CO)_3)(Fe(CO)_2PMe_3)]_2PF_6$, **IV-2*$_{ox}$**, data was obtained on a BRUKER D8 GADDS general-purpose three-circle X-ray diffractometer (Cu-Kα

radiation, λ = 1.54184 Å), also operating at 110 K. Integrated intensity information for each reflection was obtained by reduction of the data frames with the program SAINT. The integration method employs a three dimensional profiling algorithm and all data were corrected for Lorentz and polarization factors. Finally the data was scaled to produce a suitable data set. The absorption correction program SADABS[110] was employed to correct the data for absorption and other systematic errors. The structure was solved using SHELXTL.[111] All non-hydrogen atoms were refined with anisotropic thermal parameters. The hydrogen atoms bound to carbon were placed in idealized positions, as generated in XSHELL [C–H = 0.96 Å, $U_{iso}(H) = 1.5 \times U_{iso}(C)$]. The final structure was refined (weighted least squares refinement on F^2) to convergence.[111] X-seed was employed for the structure plots.[112]

EPR. EPR spectra were obtained with a Bruker ESP 300 equipped with an Oxford ER910 cryostat operating at 10 K. Samples were ~0.5 mM in analyte in 50:50 CH_2Cl_2:Toluene and frozen in liquid N_2 prior to recording the EPR spectra at 10 K. The *g* values reported were as simulated using the *WinEPR Simfonia* program.[113]

Computations. DFT calculations, including geometry optimization and NBO analysis, were performed using a hybrid functional (the three-parameter exchange functional of Becke (B3)[114] and the correlation functional of Lee, Yang, and Parr (LYP)[115] (B3LYP) as implemented in *Gaussian 03*.[116] The effective core potentials and associated basis set of Hay and Wadt (LANL2DZ)[117-118] were used on iron sulfur and phosphorus atoms. For iron, the two outermost p functions were replaced by the reoptimized 4p functions as suggested by Couty and Hall.[119] For sulfur and phosphorus,

the basis set was augmented by the d polarization function of Höllwarth et al.[120] All carbon and hydrogen atoms were represented using Dunning's double zeta valence basis set (D95). [121-122]

Experimental Details for Chapter V

Synthesis of $Na(\mu\text{-}SCH_2N(C_6H_4SO_3)CH_2S\text{-})[Fe(CO)_3]_2$, (V-$Na^+$1). To a red solution of 2.00 g (5.81 mmol) of $(\mu\text{-}S_2)[Fe(CO)_3]_2$ in THF (30 mL) and cooled to -78 °C was added 12 mL of a 1.0 M $LiEt_3BH$ (12 mmol). The resulting green solution was allowed to stir for 30 minutes, after which time trifluoroacetic acid (1 mL) was added dropwise resulting in a color change back to dark red, and the reaction was allowed to warm to room temperature. A 1 mL portion of a 36 % formalin solution (12.0 mmol) was then added. After one hour, solid sulfanilic acid (1.01 g, 5.83 mmol) was added and the reaction was heated at 60 °C overnight. The following day a light red precipitate had crashed out resulting in a slurry and ν(CO) bands indicative of the product were observed in the IR spectra. Solvent was concentrated to ~10 mL in vacuo, and 50 mL of hexanes was added to precipitate the crude product. The solid was filtered in air, washed with hexanes and then collected and sonicated in 100 mL of water to form a slurry. Concentrated HCl, (10 mL) was added and the precipitate was collected and slurried in another 100 mL of water and sonicated to break apart any large clumps. Solid $NaHCO_3$ was then added slowly to the slurry until gas formation ceased. The light pink precipitate was first collected by vacuum filtration then dissolved in THF and added to the top of a silica column (4 cm x 20 cm). The dark red product was eluted with MeOH and solvent was removed with a rotary evaporator to the give solid **V-Na^+1**. (Yield: 1.6 g, 2.84

mmol, 48.7 %). The product can be recrystallized in water to yield an analytically pure microcrystalline sample. IR (THF) ν(CO): 1998 s, 2037 s, 2073 m, cm^{-1}; IR (H_2O) ν(CO): 2002 s, 2041 s, 2077 m, cm^{-1}; ^1H NMR (D_2O): 4.53 (s, 4H); 6.98 (d, J = 10.1 Hz, 2H); 7.73 (d, J=8.7 Hz, 2H) ppm; ^{13}C NMR (D_2O): 48.4, 114.9, 127.0, 139.5, 206.9; Absorption spectrum (H_2O): λ_{max} (ε, M^{-1} cm^{-1}) 489 (1259), 330 (9325), 303 (14206), 229 (15125), ESI-MS (neg) (THF): *m/z* = 541 (**V-Na^+1 – Na^+)**; Elemental anal. Calcd (found) for **V-Na^+1**·3 H_2O ($Fe_2S_3O_{12}NC_{14}H_{14}Na$) (MW = 619 g/mol): C, 27.16 (26.80); N, 2.26 (2.18); H, 2.28 (2.22).

Synthesis of Et_4N(μ-$SCH_2N(C_6H_4SO_3)CH_2S$-)[$Fe(CO)_3$]$_2$, (V-Et_4N^+1). To a slurry of **V-Na^+1** in 50 mL of DCM was added excess Et_4NCl and the reaction was allowed to stir overnight. The resulting red solution was filtered through celite and the solvent was concentrated in vacuo and the product precipitated out with hexanes. The solid was filtered and washed with copious amounts of water and ether. Crystals of X-ray quality were grown by layering a DMF solution of **V-Et_4N^+ 1** with ether and storing at -4 °C for several days. Elemental anal. Calcd (found) for $Fe_2S_3O_9N_2C_{22}H_{28}$ ·H_2O : C, 38.3 (37.8); N, 4.06 (3.92); H, 4.38 (3.92).

Synthesis of Na(μ-$SCH_2N(C_6H_4SO_3)CH_2S$-)[$Fe(CO)_3$]$_2$(β–cyclodextrin)$_2$ clathrate, **(V-1-CyD)**. To 10 mL of a saturated aqueous solution of ß-cyclodextrin, **V-Na^+1** (0.010 g, mol) was added and the resulting slurry was sonicated for 10 minutes. Afterwards the solution was centrifuged for 20 minutes and decanted to remove any remaining solid. The solution was then added to a test tube and layered with a dilute aqueous solution of PPNCl. This mixture was stored at 4 C for two weeks, during which

time microcrystalline needles formed at the interface and crystals of X-ray quality of the sodium salt of **V-1-CyD** grew further down in the solution.

Synthesis of Na(μ-SCH$_2$N(C$_6$H$_4$SO$_3$)CH$_2$S-)[Fe(CO)$_3$][Fe(CO)$_2$P(OMe)$_3$], (V-Na$^+$2). To a slurry of (μ-S$_2$)[Fe(CO)$_3$]$_2$, (0.50 g 0.89 mmol) in THF (30 mL) was added P(OMe)$_3$, (0.50 mL, 4.2 mmol). The solution was then heated to 60 °C and the solution was monitored by IR spectroscopy. After the IR bands indicative of the starting material were not visible, (~4 h), the solvent was removed in vacuo. The resulting solid was completely dissolved in THF and loaded onto the top of a silica column (4cm x 20cm). The dark red product was eluted with MeOH and solvent was removed with a rotary evaporator to yield 0.327 g (0.495 mmol, 56 %) of the pure product. IR (THF) ν(CO): 1940 w, 1971 s, 1996 s, 2048 m cm^{-1}. Crystals of X-ray quality were obtained by slow diffusion of ether into a CH_2Cl_2 solution of the EtN^+ salt. The increased solubility of V-Na$^+$3 in CH_2Cl_2 makes the separation of the cation exchanged product difficult. Instead the Et_4N^+ salt is best obtained by direct synthesis starting with **V-Et$_4$N$^+$1**. Crystals of X-ray quality were obtained by slow diffusion of ether into a CH_2Cl_2 solution of the Et_4N^+ salt. The Et_4N^+ salt can be obtained through counterion exchange in a similar fashion as described above or by direct synthesis starting with **V-Et$_4$N$^+$1**.

Synthesis of Na(μ-SCH$_2$N(C$_6$H$_4$SO$_3$)CH$_2$S-)[Fe(CO)$_2$PMe$_3$]$_2$, (V-Na$^+$3). To a slurry of (μ-S$_2$)[Fe(CO)$_3$]$_2$, (0.50 g 0.89 mmol) in THF (30 mL) was added PMe$_3$, (0.2 mL, 1.9 mmol). The solution was then heated to 60 °C and the solution was monitored by IR spectroscopy. After the IR bands indicative of the starting material were not visible, (~4 h), the solvent was removed in vacuo to yield the air sensitive, **V-Na$^+$3**. The

complex can be recrystallized in MeOH or THF to yield 0.325 g (0.492 mmol, 56 %) of the pure product. IR (THF) ν(CO): 1982 s, 1950 s, 1903 m, cm^{-1}. Crystals of X-ray quality were obtained by slow diffusion of ether into a concentrated CH_2Cl_2 solution of the Et_4N^+ salt. The increased solubility of **V-Na$^+$3** in CH_2Cl_2 makes the separation of the Et_4N^+ cation exchanged product difficult. Instead the Et_4N^+ salt is best obtained by direct synthesis starting with **V-EtN$^+$1**.

X-ray structure determination. All low-temperature (110 K) X-ray data were obtained on a Bruker Apex-II CCD based diffractometer (Texas A&M University) (Mo sealed X-ray tube, Kα = 0.71073 Å).[108] Space groups were determined on the basis of systematic absences and intensity statistics and structures were solved by direct methods and refined by full-matrix least squares on F^2.

For complex **V-Et$_4$N$^+$1**, intensity measurements indicated that structure was twinned. Unit cell investigation indicated a twofold twin along the *c* axis. (twin law : -1 0 0 0 -1 0 0.5 0 1). Cell_now[111] was employed to determine the orientation matrices and SAINT[109] was used to integrate and merge the twin components. R_{int} for all reflections was 0.07 and for I>3σ(I) reflections it was 0.047. 12794 corrected reflections were then merged according to the point group *2/m* and written to the data file in the HKLF 5 format. Min/Max transmission factors were 0.638/0.745. A second data set was written in the HKLF 4 format that contained only one component of the twinned data set. This data was employed to solve the structure and refine it to an R value of 0.14. The two component twinned data set was then employed (with the HKLF 5 command) to refine the data set to convergence (R = 0.041) (refined BASF of 0.416.) H atoms were placed

at idealized positions and refined with fixed isotropic displacement parameters and anisotropic displacement parameters were employed for all non-hydrogen atoms. The following programs were used: data collection, data reduction, APEX2;[108] absorption correction, *SADABS*;[110] cell refinement *SHELXTL*;[111] structure solutions, *SHELXS-97* (Sheldrick);[111] and structure refinement, *SHELXL-97* (Sheldrick).[111]

The structure of **V-1-CyD** was solved with SHELXD[111] employing FIND 145 and PLOP 190 (atoms) and the number of tries of 2000 and refined with SHELXL[111]. At completion SHELXD[111] solved the structure for roughly 90 % of the total atoms. After several cycles of refinement the remaining atoms and the solvent atoms (water) were identified and included in the refinement. Several solvent molecules were found to be partially occupied and their occupation factors were refined to convergence. The sodium cation was found to be disordered between two positions as was one terminal hydroxyl group. The site occupation factors of these disordered atoms were refined to convergence. All non-hydrogen atoms were refined with anisotropic thermal parameters. Hydrogen atoms for all non-solvent atoms were added in ideal positions and refined with a riding model. Hydrogen atoms for the waters were not added to the model; however they were tabulated in the formula. The final structure was refined (weighted least squares refinement on F^2) to convergence. The final data presentation and structure plots were generated in X-Seed Version 1.5.[112]

The structures of **V-Et_4N^+2** and **V-Et_4N^+3** were solved by direct methods. Hydrogen atoms were added at idealized positions and refined with fixed isotropic displacement parameters equal to 1.2 times the isotropic displacement parameters of the

atoms to which they were attached. Anisotropic displacement parameters were determined for all non-hydrogen atoms. Programs used for data collection and cell refinement, SMART and APEX2;[108] data reduction, SAINT;[109] absorption correction, SADABS;[110] structure solution, SHELXS-97 (Sheldrick);[111] structure refinement, SHELXL-97 (Sheldrick).[111] Molecular graphics and preparation of material for publication used SHELXTL-PLUS, version 5.1 or later (Bruker).[111] X-seed was employed for the final data presentation and structure plots.[112]

Computational studies. Single point calculations used to obtain the electrostatic potential maps were performed using the coordinates from the crystographically determined structures with the iron sulfur clusters removed as the input geometries. For the [FeFe]-H_2ase enzyme cavity, the protein structure was truncated to a sphere with a diameter of ~22 angstroms with the active site at the center. For the **1-CyD** structure, all atoms from the crystal structure were used except for those of the diiron complex. The positions of added protons for both structures were optimized through multiple minimizations and simulated annealing cycles using the Cerius^2 UFF and package of programs.[123]All Density Functional Theory calculations were performed with the Gaussian 03 suite of programs[116], using the Becke three-parameter exchange functional[114] (B3) and the Lee-Yang-Parr correlation functional[115] (LYP) (B3LYP). All atoms were represented using the split valence double- ζ basis set of Pople and coworkers (6-31g).[124-125]

Nuclear magnetic resonance studies. ^{1}H-and ^{13}C-NMR spectra were acquired on an Inova 500 spectrometer operating at 500 and 125 MHz respectively. All samples were prepared in D_2O. ^{1}H chemical shifts are reported in parts per million relative to the H_2O resonance (4.79 ppm). For ^{13}C, 1 μL of tetrahydrafuran was added to the sample to serve as a reference and all chemical shifts are reported relative to the CH_2O resonance (68.68 ppm). Samples for ^{13}C NMR spectra were partially enriched with ^{13}CO by mild photolysis (General Electric 275W Sunlamp) of a concentrated CH_3OH solution of **Na^{+}1** under 1 atm of ^{13}CO gas for ~4 hours. The solution was then filtered through silica and solvent was removed under vacuum.

Electrochemistry. All electrochemical analysis was done using Bioanalytical System (BAS) 100 electrochemical workstation with a glassy carbon working electrode, a platinum wire auxillary electrode. All voltammograms were obtained using a standard three electrode cell under an argon atmosphere at room temperature. For aqueous work, a saturated KCl Ag/AgCl reference electrode was used and the supporting electrolyte solution was 0.01 M NaCl; Samples were run at a concentration of 0.11 mM due to the low solubility of the sulfonated diiron complexes in the NaCl buffer solution. Between each scan the glassy carbon electrode was removed and polished using 1 μm polycrystalline diamond suspension and rinsed with both acetone and deionized water to remove any adsorbed material. All aqueous potentials are reported relative to the Ag/AgCl couple as 0.00 V. For work done in MeCN, a saturated $Ag/AgNO_3$ reference electrode was used and the supporting electrolyte solution was 0.1 M Et_4NPF_6. All

samples in MeCN were run at a concentration of 2 mM and potentials are reported relative to the Fc/Fc^+ couple as 0.00 V.

CHAPTER III

MODELS OF THE DIIRON HYDROGENASE ENZYME ACTIVE SITE WITH BUILT IN STERIC BULK*

Introduction

The notable similarity of a simple organometallic, (μ-pdt)$[Fe(CO)_3]_2$ (pdt = μ-$S(CH_2)_3S$), with the 2Fe subsite of the 6Fe6S hydrogen-producing or H-cluster of [FeFe]-hydrogenase, [FeFe]H_2ase, has led to an explosion of research aimed towards modifications which would better match the structure and ultimately the function of the enzyme's active site (*eas*). It is expected that the unusual square pyramid/inverted square pyramid structure is fixed in the metalloprotein by second coordination sphere interactions. As electron/proton processes relating to the mechanistic cycle that defines enzyme activity ($H_2 \leftrightarrows 2\ H^+ + 2\ e^-$) require an open site for both H_2 binding and for proton reduction, we have hypothesized that the stabilization of such a rotated or square pyramid/inverted square pyramid is key to the design of a synthetic electrocatalyst that operates at mild potentials.[21] Critical to this goal are the intrinsic properties that relate to the flexibility features of the (μ-SRS)$[Fe(CO)_3]_2$ model complexes.[85]

---

*Reproduced in part with permission from: Singleton, M. L.; Jenkins, R. M.; Klemashevich, C. L.; Darensbourg, M. Y. *C. R. Chimie*. **2008**, *11*, 861-874. Copyright **2008** Académie des sciences.[126]

The evidence for the formation of a semi-bridging CO or terminal open site in the initial steps of both protonation and ligand substitution show the ability of the model complexes to adopt this geometry. In fact, two groups have now been successful in the replication of the rotated structure in a handful of mixed valent $Fe^{I}Fe^{II}$ model complexes.[64-65]However, without the supramolecular control of the protein matrix which exists in the enzyme active site the rotation is not maintained in the small organometallic models which, upon reduction, relax to the optimal $Fe^{I}Fe^{I}$ level unrotated geometry. Hence the challenge of isolating a rotated reduced diiron complex remains.

As part of the apical/basal CO site exchange resulting from rotation of the $Fe(CO)_3$ units in the square pyramidal $S_2Fe(CO)_3$, computational studies have suggested the transition state shown in Figure III-1, a structure which bears obvious similarity to the active site of the enzyme.[87]As discussed in Chapter I, computational (DFT) analysis of this process found that both asymmetric substitution and a sterically bulky dithiolate ligand were capable of stabilizing this rotated transition state. The ability of better electron-donor ligands to effect change in the rotational energy barriers has been experimentally verified in our group. Such a result was indicated for the (μ-pdt)$[Fe(CO)_3][Fe(CO)_2$IMes] complex; i.e., solution studies found the barrier to intramolecular CO site exchange in the $[Fe(CO)_3]$ unit to be lowered, a stable rotated form in the solid state was not realized.[127]

In an attempt to obtain a stable rotated structure and test the DFT based hypothesis that "the combination of a sterically demanding S-to-S linker and asymmetric substitution of the CO ligands is predicted to be a particularly effective synthetic

target"[103]we have prepared a series of (μ-S($CH_2CR_2CH_2$)S)[$Fe(CO)_3$]$_2$, complexes and several derivatives in which a CO ligand is replaced by an N-heterocyclic carbene or phosphine ligand. While a stable Fe^IFe^I species in the rotated geometry was not observed, analysis of the variable temperature NMR spectra delineate the effect of linker and substituents on the intramolecular site exchange processes, finding further corroboration of the computational results. This study which identifies methods to stabilize the rotated structure, is preliminary to a study of oxidized disubstituted analogues, (μ-S($CH_2CR_2CH_2$)S)[$Fe(CO)_2PMe_3$]$_2^+$, i.e., mixed valent Fe^IFe^{II} species which do show evidence of stable rotated structures.[128]

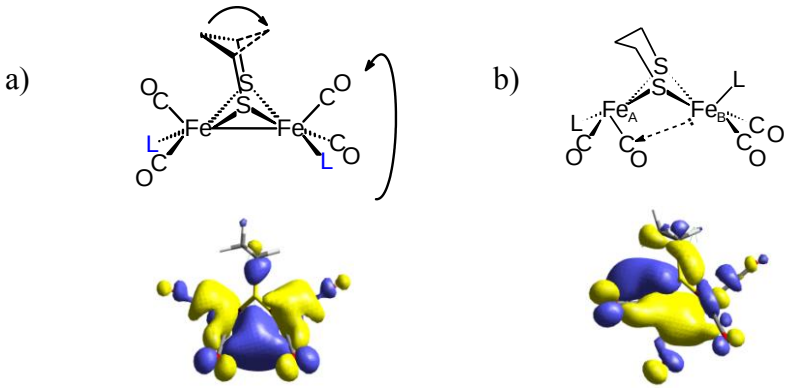

Figure III-1. Depiction of **a**) the fluxional processes of (μ-pdt)[$Fe(CO)_2L$)]$_2$ (L = CO or phosphine substituents, with the HOMO of the ground state structure of the all-CO complex below; **b**) optimized structure of the transition state for rotation or intramolecular CO_{ap}/CO_{ba} site exchange with HOMO of the all-CO complex below.[3]

Synthesis and Characterization of All Carbonyl (μ-$SCH_2CR_2CH_2S$)$[Fe(CO)_3]_2$ Complexes

Simple addition of the dithiols listed in Figure III-2 to solutions of $Fe_3(CO)_{12}$ in toluene produced the series of thermally and air stable, red-orange crystalline products of the form (μ-$S(CH_2CR_2CH_2)S)[Fe(CO)_3]_2$ (R = Me, Et, Bu) in isolated yields of 19-34

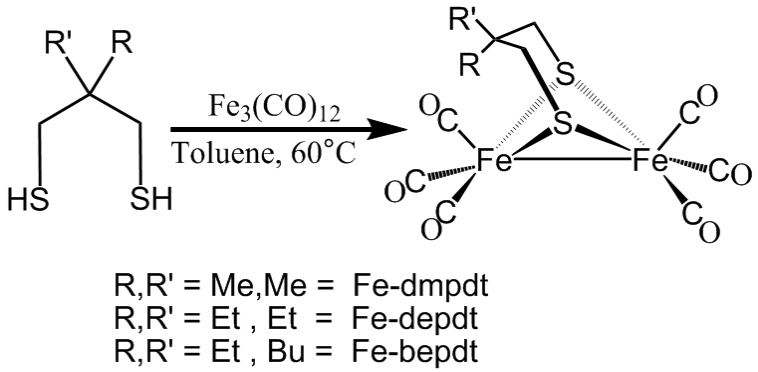

Figure III-2. Synthesis of model complexes with added steric bulk on the dithiolate linker.

%. Their infrared spectral signatures in the ν(CO) stretching region are nearly identical to each other and to the parent (μ-pdt)$[Fe(CO)_3]_2$ complex, Figure III-3, indicating that the addition of alkyl groups to the bridgehead position does not drastically change the thiolate donor ability.

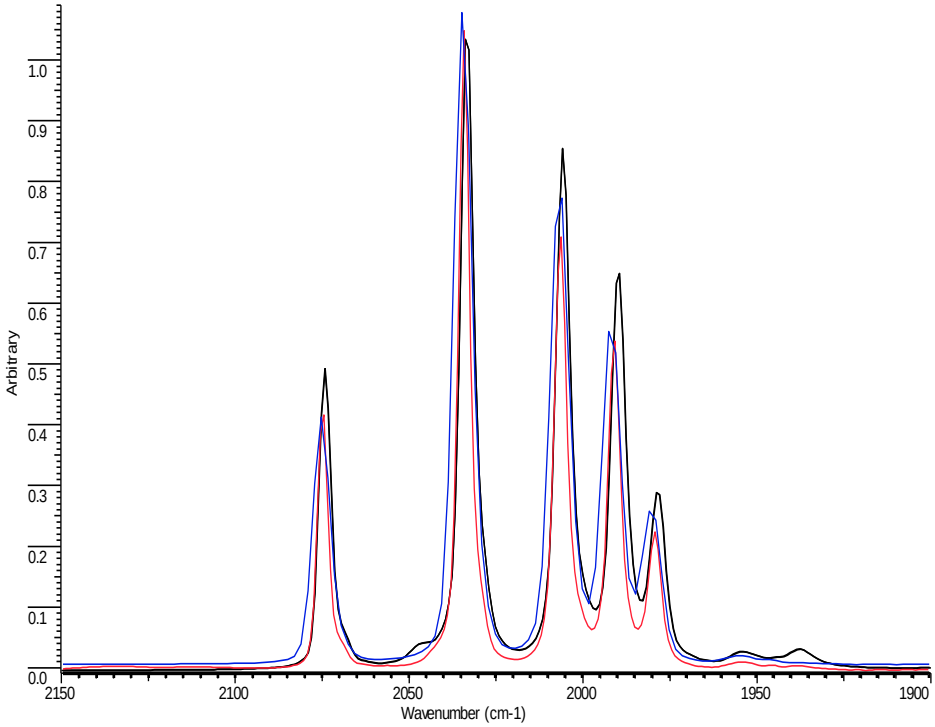

Compound	ν(CO), cm^{-1} m s s ms mw
(μ-dmpdt)[Fe(CO)$_3$]$_2$	2075, 2034, 2005, 1992, 1980
(μ-depdt)[Fe(CO)$_3$]$_2$	2073, 2031, 2005, 1990, 1979
(μ-bepdt)[Fe(CO)$_3$]$_2$	2074, 2032, 2005, 1990, 1979
(μ-pdt)[Fe(CO)$_3$]$_2$	2076, 2035, 2005, 1992, 1981

Figure III-3. Overlay of ν(CO) IR spectra of (μ-Rdt)[Fe(CO)$_3$]$_2$ recorded in hexanes solution (Blue: Rdt = dmpdt; red: Rdt = depdt; black, Rdt = bepdt) with a table listing the values and intensities for the bands.

As derived from X-ray difraction studies, ball and stick drawings of the molecular structures of the three diiron hexacarbonyl derivatives and (μ-pdt)[Fe(CO)$_3$]$_2$[29], are shown in Table III-1 along with selected metric data. Consistent

with the similar spectral properties of (μ-pdt)[Fe(CO)$_3$]$_2$ and the three analogues as found in solution, there are only minor solid state structural differences. The most significant deviation from the μ-pdt complex is evident in the torsion angle defined by the apical CO groups across the Fe-Fe bond vector. As shown in Figure III-4 the steric bulk of the bridgehead substituent induces a slight staggering of the apical CO unit, with the greatest distortion seen in the diethyl derivative. In all cases the basal CO's eclipse each other similar to the μ-pdt complex. As seen in the μ-depdt derivative, positioning

Table III-1. Comparison of structures of (μ-pdt)[Fe(CO)$_3$]$_2$ with (μ-dmpdt)-, (μ-depdt)-, (μ-bepdt)[Fe(CO)$_3$]$_2$

Name	Structure	Fe-Fe, Å	C1-Fe1-Fe2-C6, °	Flap Angle, °†	$\overline{C_{CO}\text{-FeSS}}$, °‡
(μ-pdt)[Fe(CO)$_3$]$_2$	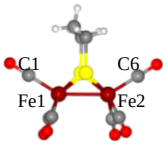	2.510(1)	0.0	137.1	107.6/ 107.6
(μ-dmpdt)[Fe (CO)$_3$]$_2$	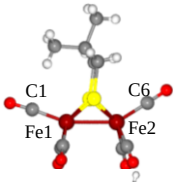	2.494(6)	5.7	134.8	118.0/ 105.7
(μ-depdt)[Fe(CO)$_3$]$_2$	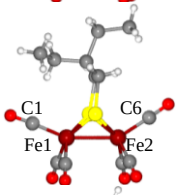	2.501(4)	15.8	136.7	115.6/ 105.2
(μ-bepdt)[Fe (CO)$_3$]$_2$	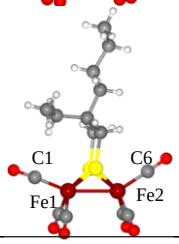	2.500(1)	6.2	137.7	116.2/ 105.1

†Refers to angle between plane made from bridgehead carbons-elbow carbons and the plane made from the elbow carbons-sulfurs.
‡Refers to angle between apical carbonyl and the adjacent Fe-S-S plane.
Bridgehead side (left side as shown)/Nonbridgehead side (right side as shown)

of the ethyl group over C1 is observed in the asymmetrically substituted bridgehead complex, (μ-bepdt)[$Fe(CO)_3$]$_2$, leaving the butyl group oriented away from the Fe_2S_2 core. In the extended packing diagram, a portion of which is shown in Figure III-5, this configuration allows the hydrophobic butyl groups of nearby complexes to be stacked, decreasing interaction of the butyl group with the nearby CO and thus the apical C-Fe-Fe-C torsion angle relative to the depdt derivative. For all of the sterically bulky complexes the substituents at the bridgehead carbon of the S-to-S linker do not cause major distortions in the $Fe(CO)_3$ units, nor are the parameters which define the $Fe_2S_2C_3$ cyclohexane like ring different.

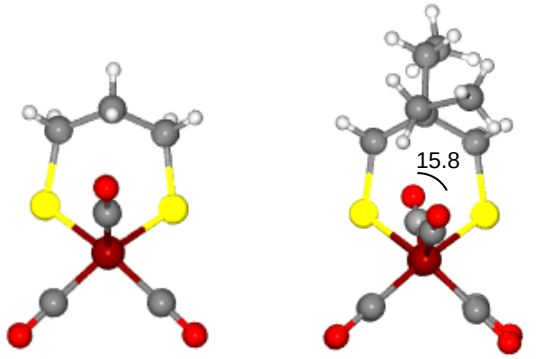

Figure III-4. Ball and stick diagram of the μ-pdt and μ-depdt derivatives showing the eclipse of (C_1O_1) and (C_6O_6) in (μ-pdt)[$Fe(CO)_3$]$_2$ and the slight stagger of the (C_1O_1) and (C_6O_6) in the (μ-depdt)[$Fe(CO)_3$]$_2$ complex.

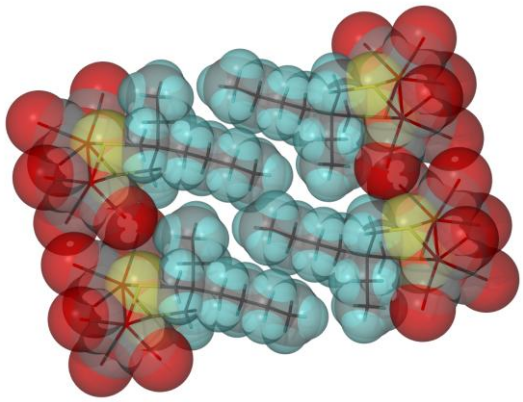

Figure III-5. Space-filling, close-packing diagram of (μ-bepdt)$[Fe(CO)_3]_2$ from the solid state structure showing the orientation of the hydrophobic butyl groups on the propane dithiolate linker.

Synthesis and Characterization of Mono-substituted (μ-$SCH_2CR_2CH_2S$)$[Fe(CO)_3]$-$[Fe(CO)_2L]$ Complexes

The products of direct CO/L exchange, or oxidatively induced ligand exchange are displayed in Figure III-6, in the form of line-drawing structures, along with the conditions required for the syntheses. The particular orientations of the FeS_2C_3 bridgehead carbon and its substituents, as well as the isomeric form of the $Fe(CO)_2L$ unit are represented as found in the solid state molecular structures, described below. Upon

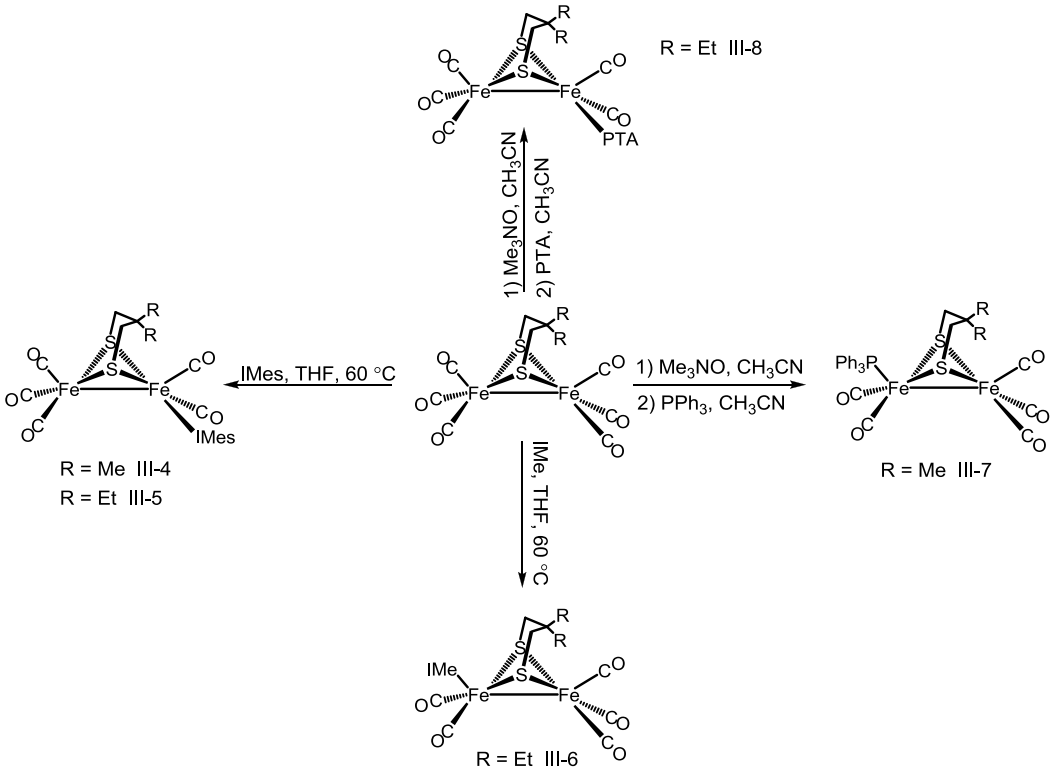

Figure III-6. Synthesis of monosubstituted derivatives of sterically bulky model complexes.

substitution for L, two distinct changes can be seen in the NMR spectra. In the ^{1}H spectra the resonance corresponding to the protons on the carbon α to the thiolates splits into two doublets. This is consistent with the loss of the plane of symmetry perpendicular to the FeFe bond. Additionally, the ^{13}C NMR now show two separate signals of different intensities for the CO ligands indicating that substitution on one of the Fe units has occurred. Infrared spectra show a ν(CO) shift, ca 30-40 cm^{-1}, of the highest energy band to lower wave numbers supporting that CO has been replaced by a better donor (Table III-2). Vibrational spectroscopy results are also consistent with the poorer electron-donating ability of PPh_3 relative to the imidazole NHC ligands. For

example, Figure III-7 is an overlay of the ν(CO) IR spectra of (μ-dmpdt)[Fe(CO)$_3$][Fe(CO)$_2$PPh$_3$] and (μ-dmpdt)[Fe(CO)$_3$][Fe(CO)$_2$IMes]. The IR bands for the former range from 12 to 23 cm^{-1} higher than those of the latter.

Table III-2. ν(CO) stretching frequencies for the monosubstituted sterically bulky complexes

Complex	ν(CO) in CH_3CN (cm^{-1})
(μ-dmpdt)[Fe(CO)$_3$][Fe(CO)$_2$IMes]	2030, 1969, 1952, 1908
(μ-depdt)[Fe(CO)$_3$][Fe(CO)$_2$IMes]	2029, 1969, 1951, 1906
(μ-depdt)[Fe(CO)$_3$][Fe(CO)$_2$IMe]	2034, 1971, 1954, 1913
(μ-dmpdt)[Fe(CO)$_3$][Fe(CO)$_2$PPh$_3$]	2046, 1983, 1929
(μ-depdt)[Fe(CO)$_3$][Fe(CO)$_2$PTA]	2039, 1983, 1963, 1925

Chemdraw figures based on the X-ray diffraction studies of the mono-substituted diiron complexes are given in Table III-3 along with selected metric data. While the overall structural features are the same as in the all-CO diiron complexes, comparison of the (μ- pdt)[Fe(CO)$_3$][Fe(CO)$_2$IMes] structure to those with steric bulk in the S to S linker finds differences in certain parameters. The IMes ligand in the μ-dmpdt and μ-depdt derivatives occupies the basal rather than apical position as was found for the μ-pdt complex.[127] Nevertheless, the bridgehead C of the FeS_2C_3 ring of both substituted derivatives is oriented towards the Fe(CO)$_2$IMes unit as it is in the μ-pdt complex. This

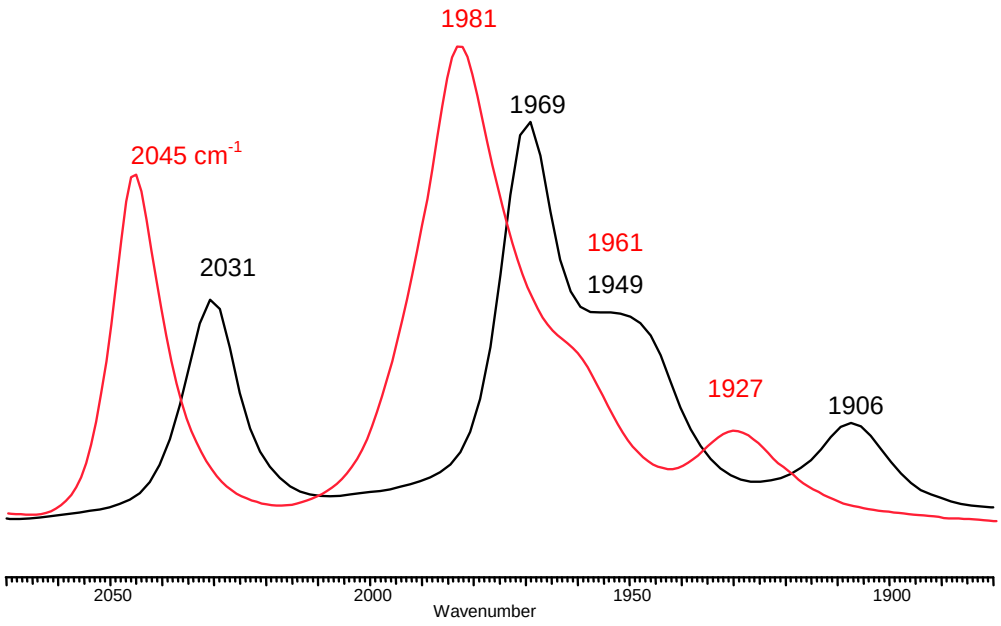

Figure III-7. Overlay of ν(CO) IR spectra of (μ-dmpdt)[Fe(CO)$_3$][Fe(CO)$_2$L] in CH_3CN solution (Black: L=IMes; Red: L=PPh_3) showing the weaker donating ability of PPh_3 versus IMes.

orientation of the bridgehead is also seen for (μ-depdt)[Fe(CO)$_3$][Fe(CO)$_2$IMe]. In contrast, the substituted bridgehead C is oriented away from the Fe(CO)$_2$$PPh_3$ and towards the Fe(CO)$_3$ unit in the (μ-dmpdt)[Fe(CO)$_3$][Fe(CO)$_2$$PPh_3$]. This results in a different conformation from (μ-pdt)[Fe(CO)$_3$][Fe(CO)$_2$$PPh_3$] where the bridgehead is oriented towards the Fe(CO)$_2$$PPh_3$ unit.[129]However, in both the IMe and PPh_3 complexes the ligands assume the apical position consistent with their respective pdt analogs.[127,129] Of the complexes the PTA derivative is the only one that adopts an identical conformation as its μ-pdt analogue, a fact that likely deals with the ligands in both cases being in a basal position and less influenced by the dithiolate.[130] These results show the

importance of steric bulk in the ligands as well as in the bridgehead carbon of the S to S linker.

The torsion angle, C_{ap}-Fe-Fe-L_{ap}, between the $Fe(CO)_3$ and $Fe(CO)_2L_{ap}$ units on the complexes with added steric bulk largely remains unchanged from that of the respective μ-pdt derivative with the exception of (μ-dmpdt)[$Fe(CO)_3$][$Fe(CO)_2$IMes] which is twisted by >36° relative to (μ-pdt)[$Fe(CO)_3$][$Fe(CO)_2$IMes]. The structure of (μ-dmpdt)[$Fe(CO)_3$][$Fe(CO)_2$IMes], Figure III-8, readily shows displacement of the apical CO while the ligands in the basal planes of each iron center remain eclipsed. This degree of distortion is however not seen for the μ-depdt derivative; the reason for this is presumed to be that the $–CH_3$ unit of the ethyl groups in (μ-depdt)[$Fe(CO)_3$][$Fe(CO)_2$IMes] inhibits the approach of the mesityl group of the IMes ligand towards the apical CO, thus decreasing the amount of steric influence from the aryl methyl groups. In the μ-dmpdt derivative both the methyl group on the S to S linker as well as on the mesityl groups assist in the deflection of the CO group.

Interestingly, the dimesitylimidazolium substituted diiron complexes induces a lengthening of the Fe-Fe bond distance by ca. 0.05 to 0.07 Å relative to their respective all-carbonyl parent compound and ca 0.03 to 0.05 Å relative to (μ-pdt)[$Fe(CO)_3$][$Fe(CO)_2$IMes]. The Fe-Fe bond length of 2.572 Å for the **III-4** complex

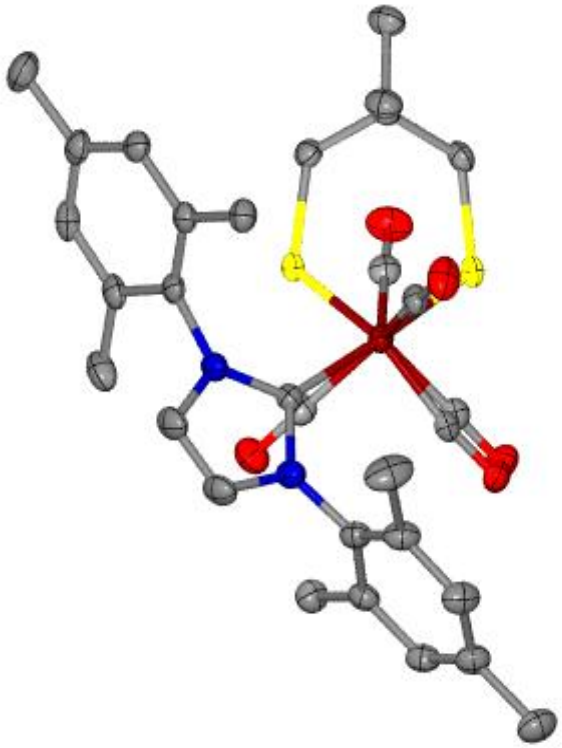

Figure III-8. Thermal elipsoid plot (50% probability) of (μ-dmpdt)[$Fe(CO)_3$] [$Fe(CO)_2$IMes] showing the staggering of the apical CO units.

Table III-3. Structural comparison of sterically bulky monosubstituted complexes with (μ-pdt) analogues.

Name	Structure	Fe-Fe, Å	L_{ap}-Fe1-Fe2-L_{ap}, °	Flap Angle°	L_{ap}-FeSS°
(μ-pdt)[Fe(CO)$_3$] [Fe(CO)$_2$IMes][127]	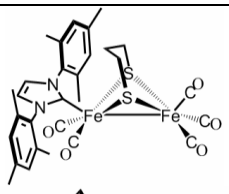	2.525	4.26	124.1	117.2/ 109.3
(μ-pdt)[Fe(CO)$_3$] [Fe(CO)$_2$PPh$_3$][129]	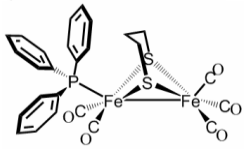	2.5247(6)	9.31	133.8	116.3/ 106.1
(μ-pdt)[Fe(CO)$_3$] [Fe(CO)$_2$IMe][131]	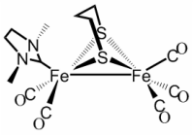	2.5333(7)	5.29	126.9	108.2/ 106.8
(μ-pdt)[Fe(CO)$_3$] [Fe(CO)$_2$PTA]	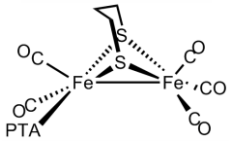	2.542(2)	5.67	123.7	113.7/ 104.7
(μ-dmpdt)[Fe(CO)$_3$] [Fe(CO)$_2$IMes]	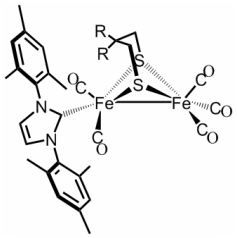	R = Me 2.572(4)	40.7	136.9	116.5/ 101.8
(μ-depdt)[Fe(CO)$_3$] [Fe(CO)$_2$IMes]		R = Et 2.552(2)	27.8	136.1	117.7/ 102.8
(μ-depdt)[Fe(CO)$_3$] [Fe(CO)$_2$IMe]	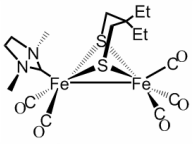	2.512(1)	18.3	133.6	117.3/ 105.9
(μ-dmpdt)[Fe(CO)$_3$] [Fe(CO)$_2$PPh$_3$]	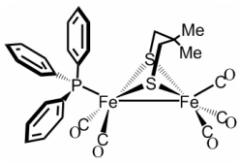	2.498(1)	9.76	138.7	117.2/ 113.4
(μ-depdt)[Fe(CO)$_3$] [Fe(CO)$_2$PTA]	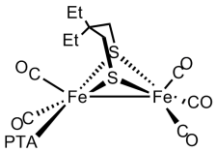	2.508(2)	10.9	135.4	119.0/ 104.7

[†]Configurations drawn as in the solid state X-ray structure. L_{ap} = adjacent ligand in the apical position FeSS=Plane made from Fe and both sulfurs.

is one of the longest reported for any mono substituted or all-carbonyl μ-dithiolate diiron complex in the Cambridge crystal database of >150 hits for $(\mu\text{-SR})_2$ or $(\mu\text{-SRS})[Fe(CO)_3]_2$. This extended bond distance is consistent with greater partial occupancy of the LUMO which is anti-bonding with respect to the Fe-Fe bond.[87]

Electrochemical Studies of Sterically Bulky Complexes

Cyclic voltammograms of complexes **III-1 – III-3** (Figure III-9 and Table III-4) in CH_3CN solution display similar events to each other as well as the $(\mu\text{-pdt})[Fe(CO)_3]_2$ derivative, with an irreversible oxidative wave in the range of +0.73 to +0.82 V and two reduction events; a quasi-reversible reduction at ca. -1.6 V and an irreversible reduction at ca. -2.4 V (vs Fc). Based on previously reported $(\mu\text{-pdt})[Fe(CO)_3]_2$ derivatives, the quasi-reversible reduction event can be assigned to the $Fe^IFe^I \rightarrow Fe^IFe^0$ reduction and the second irreversible reduction event is assumed to be $Fe^IFe^0 \rightarrow Fe^0Fe^0$.[132] These assignments represent a simplistic scheme for the electrochemical processes of these systems, and the actual behavior of these models has been reported to be more complex.[133] Reported potentials are referenced to $Fc/Fc^+ = 0.00$ V in CH_3CN. In an

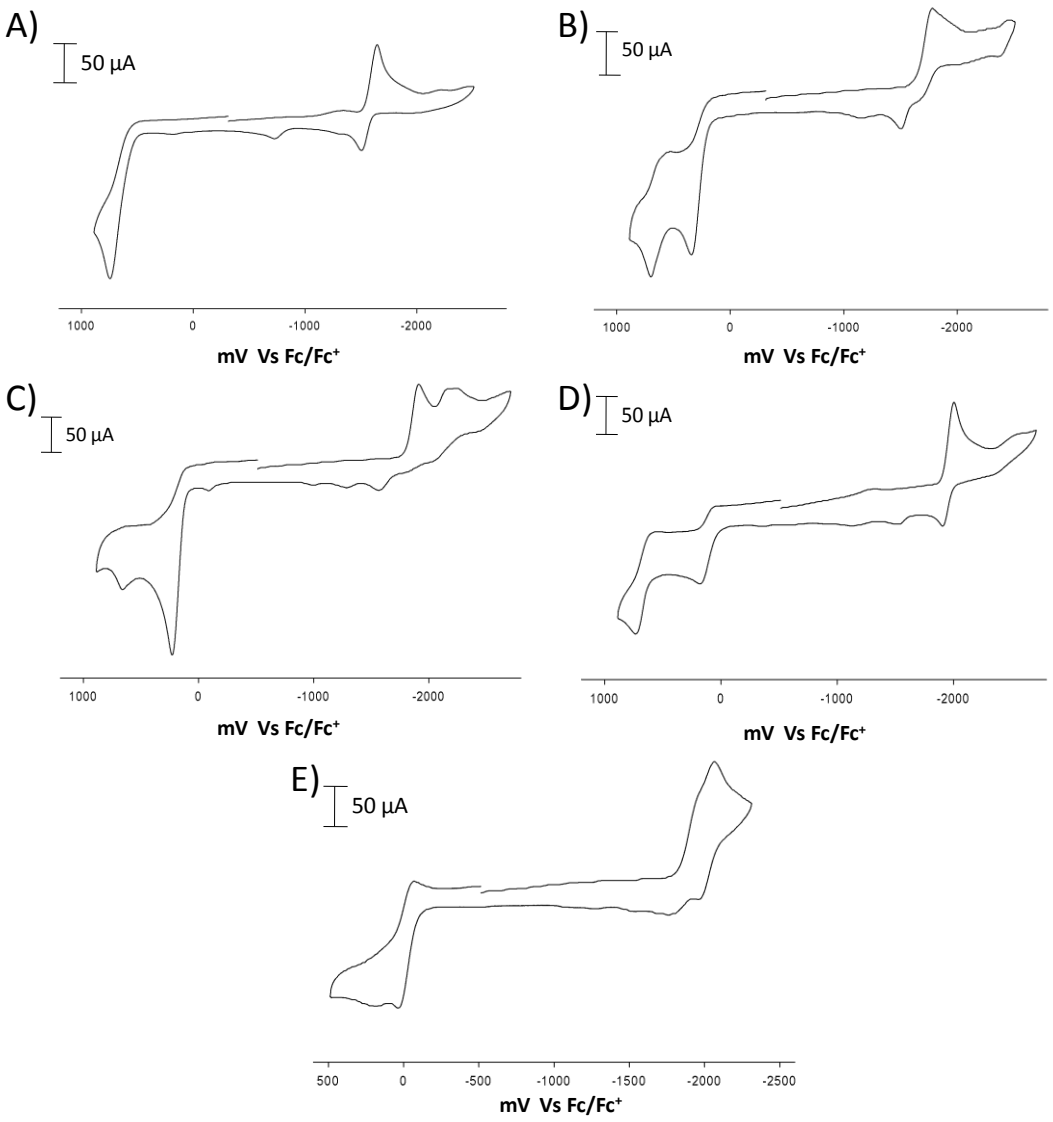

Figure III-9. Cyclic voltammograms of (µ-dRpdt)[$Fe(CO)_3$][$Fe(CO)_2$L) (A) L = CO, R = Me; B) L = PPh_3, R = Me; C) L = PTA, R = Et; D) L = IMe, R = Et and E) L = IMes, R = Me) (2mM) 0.1 M $^nBu_4NBF_4$ in MeCN solution at a scan rate of 200 mV/s.

earlier study of the electrocatalytic H_2 producing ability of the $(\mu\text{-pdt})[Fe(CO)_3]_2$ complex, NHE was used as a reference; direct comparison may be made by subtracting 0.40 V from the original values reported. The fact that the redox events remain relatively constant in this series of complexes, supports the conclusion from infrared data that the addition of alkyl substituents at the bridgehead carbon have little influence on the S-donor ability of the bridging dithiolate and hence, the electron density about the iron centers. This is in contrast to $(\mu\text{-}SC_6H_4S)[Fe(CO)_3]_2$ where an aryl group is built into the linker causing the Fe^IFe^I/Fe^IFe^0 reduction potential to shift by ca. 400 mV more positive.[134]

Electrochemical data for the NHC substituted complexes, **III-4** and **III-6**, (Figure III-9 and Table III-4) show ca. 300 mV cathodic shifts for the quasi-reversible Fe^IFe^I/Fe^0Fe^I reduction as compared to the all-CO complexes, consistent with the fact that CO has been exchanged for a more electron donating ligand. As expected, due to the poorer donor ability PPh_3, in complex **III-7** a shift of this magnitude is not seen, (Figure III-9 and Table III-4). The oxidation event presumed to be $Fe^IFe^I/Fe^{II}Fe^I$ for complexes **III -4, 6, 7** and **8** has become more accessible by ca. 600 mV for the NHC derivatives and ca. 300 mV for phosphine derivatives as compared to the all-CO complexes. In addition to an anodic shift, this first oxidation wave has become partially

Table III-4. Electrochemical Potentials (vs ferrocene) of monosubstituted derivatives

Complex	Ep_a (V) Fe^IFe^I/Fe^IFe^{II}	Ep_c (V) Fe^IFe^I/Fe^IFe^0
(μ-dmpdt)$[Fe(CO)_3]_2$ (III-**1**)[a]	+0.73	-1.61
(μ-depdt)$[Fe(CO)_3]_2$ (III-**2**)[a]	+0.82	-1.67
(μ-bepdt)$[Fe(CO)_3]_2$ (III-**3**)[a]	+0.78	-1.64
(μ-dmpdt)$[Fe(CO)_3][Fe(CO)_2$IMes$]$[a](III-**4**)	+0.05	-2.01
(μ-depdt)$[Fe(CO)_3][Fe(CO)_2$IMe$]$ [a] (III-**6**)	+0.16	-2.02
(μ-dmpdt)$[Fe(CO)_3][Fe(CO)_2PPh_3]$[a] (III-**7**)	+0.35	-1.79
(μ-depdt)$[Fe(CO)_3][Fe(CO)_2$PTA$]$[a] (III-**8**)	+0.31	-1.86
(μ-pdt)$[Fe(CO)_3]_2$[29]	+0.74[c]	-1.74 [c]
(μ-pdt)$[Fe(CO)_3][Fe(CO)_2$IMe$]$[131]	+0.17	-2.08
(μ-pdt)$[Fe(CO)_3][Fe(CO)_2$IMes$]$[127]	+0.11[c]	-2.11[c]
(μ-pdt)$[Fe(CO)_3][Fe(CO)_2$PTA$]$[130]	+0.34	-1.94

[a]Ar deaerated CH_3CN solution (0.1 M $^nBu_4NBF_4$) All experiments were recorded using a glassy carbon working electrode (A = 0.071 cm^2) referenced to Cp_2Fe/Cp_2Fe^+ as an internal standard and a Pt counter electrode at a scan rate of 200 mV/s. [c]0.40 V were subtracted from originally reported values for comparison.

reversible in the two NHC substituted complexes but remains irreversible for both the PPh_3 and PTA complexes. For all of the mono-substituted complexes with added steric bulk, the events observed are similar to those to their respective μ-pdt analogs.[29,129-130]

The electrocatalytic proton reduction activity of sterically bulky complexes was also tested. This is accomplished by studying the effect of added increments of HOAc on the cyclic voltammograms. If a complex acts as a catalyst for proton reduction, an increase in the current at the potential where the catalyst is reduced should be observed.

This occurs because the oxidative addition of a proton results in a potential inversion wherein the newly formed hydride species has a less negative reduction potential than the initial catalyst. Thus, the increase in the current then comes from the extra electrons required for the catalytic cycle. As acetic acid is reduced by glassy carbon at -2.4 mV vs Fc/Fc^{+} in CH_3CN, it is ideal for the catalysts to show the increase in current at less negative potentials than this.

Of the sterically bulky complexes, only the PTA and NHC derivatives show a increase in current at the first reduction, (Figure III-10), while the hexacarbonyl and PPh_3 complexes show an increase at more negative potentials (1.91 and 2.19 mV respectively) that is quickly surpassed by the reduction of HOAc on glassy carbon. The more negative reduction is presumed to be the $Fe^{I}Fe^{0}$/ $Fe^{0}Fe^{0}$ reduction, meaning the $Fe^{0}Fe^{0}$ species (assuming this redox level for the more negative reduction event) is active toward electrocatalytic H_2 production, whereas the $Fe^{0}Fe^{I}$ species is not. This behavior is common for the all-CO complexes and not unexpected for the triphenylphosphine derivative as the weak donor does not render the iron sufficiently electron rich to accommodate the oxidative addition of a proton. Interestingly, the complexes that do show a response at the first reduction, have less well defined electrochemical events than the corresponding (μ-pdt) derivatives. Additionally, the response (increase in current) appears to be less than that of the less sterically bulky complexes as well.[29,127,130-131] This could arise from the fact that the studies of the sterically bulky complexes were performed under an Ar atmosphere while those on the less sterically bulky complexes were performed under a CO atmosphere thus preventing

some of the resulting products proposed by Pickett and Best.[133] Alternatively, the steric bulk could also be limiting access to an open site on the irons or otherwise hindering an important process in the electrochemistry.

Variable Temperature NMR Spectra of (μ-$CH_2CR_2CH_2S$)[$Fe(CO)_3$][$Fe(CO)_2L$] (L=CO or IMes) Complexes

At 0 °C both the μ-dmpdt and μ-depdt derivatives show a single resonance in the CO region at δ 208.3 and 207.8 ppm, respectively. These signals respond to temperature changes in a completely reversible way. As shown in Figure III-11, upon cooling the (μ-depdt)$[Fe(CO)_3]_2$ to -110 °C the CO resonance splits into two singlets of differing intensities at δ = 208.2 and 206.1 with the intensity of the former roughly twice that of the latter. The δ = 208.3 ppm resonance is assigned to the basal CO's and the δ = 206.1 ppm resonance to the apical CO's in the regime where CO site exchange has ceased but the boat/chair interconversion of the FeS_2C_3 ring is still occuring. The spectra for the (μ-dmpdt)$[Fe(CO)_3]_2$ complex show a nearly identical trend.

The energy barrier for CO site exchange can be estimated using the peak separation (Δv) and coalescence temperature (T) with the equations $\Delta G^{\ddagger} = -(RT)\ln[k_t h/k_b T]$ and $k_t = (\pi\ \Delta v)/2^{0.5}$.[135] Using these formulae, $\Delta G^{\ddagger}$ of CO site exchange on the μ-depdt derivative is ca 8.4 kcal/mol. This value is lower than the μ-pdt and μ-edt derivatives which have $\Delta G^{\ddagger}$ = 10.4 kcal/mol and 12.1 kcal/mol, respectively.[85] A reasonable conclusion is that the addition of steric bulk to the bridgehead carbons has decreased the energy barrier for CO site exchange.

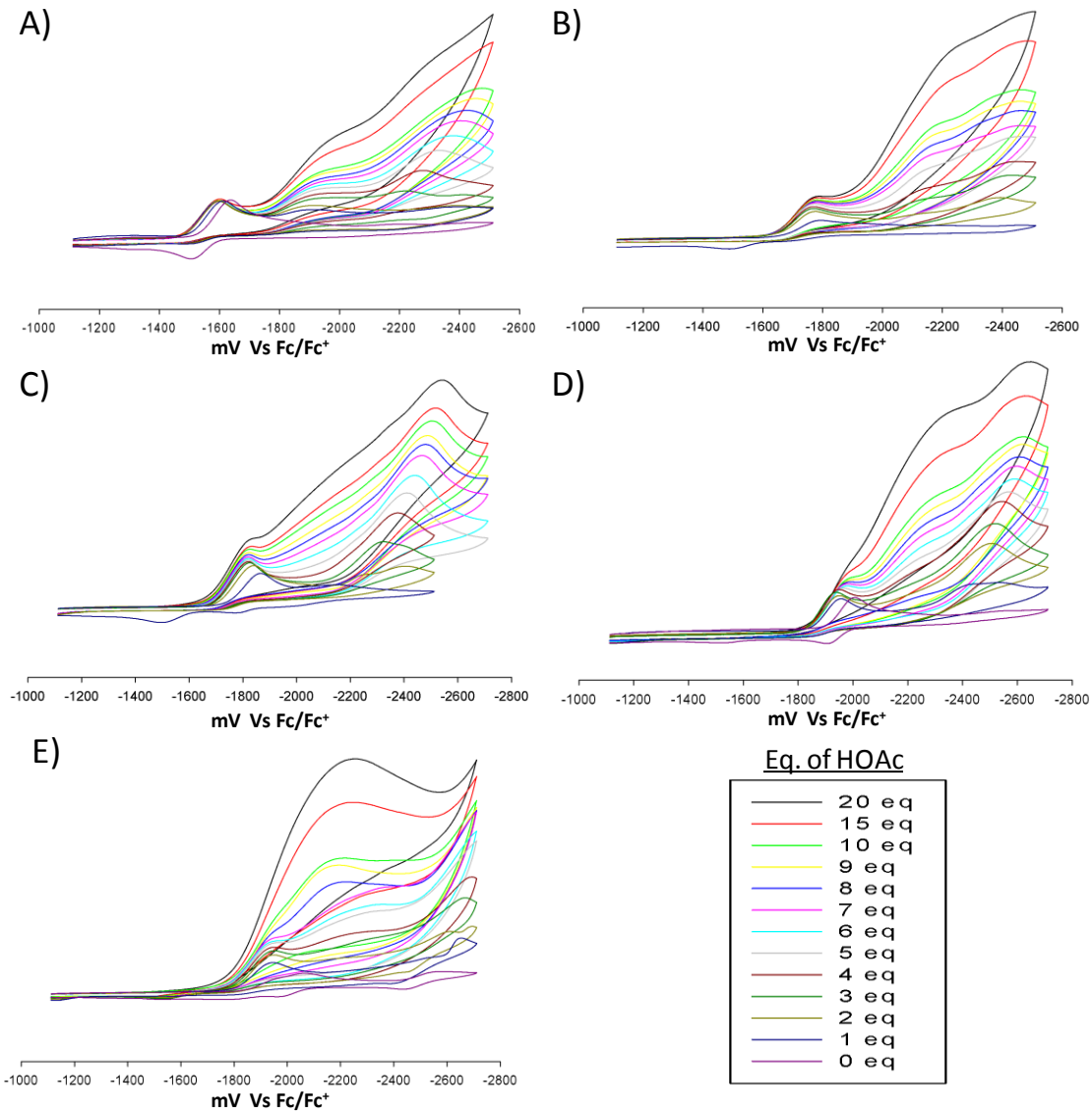

Figure III-10. Cyclic voltammograms of (μ-dRpdt)[Fe(CO)$_3$][Fe(CO)$_2$L) (A) L = CO, R = Me; B) L = PPh$_3$, R = Me; C) L = PTA, R = Et; D) L = IMe, R = Et and E) L = IMes, R = Me) with increments of HOAc in a MeCN solution (0.1 M ^{n}Bu$_4$NBF$_4$) using a glassy carbon electrode at a scan rate of 200 mV/s.

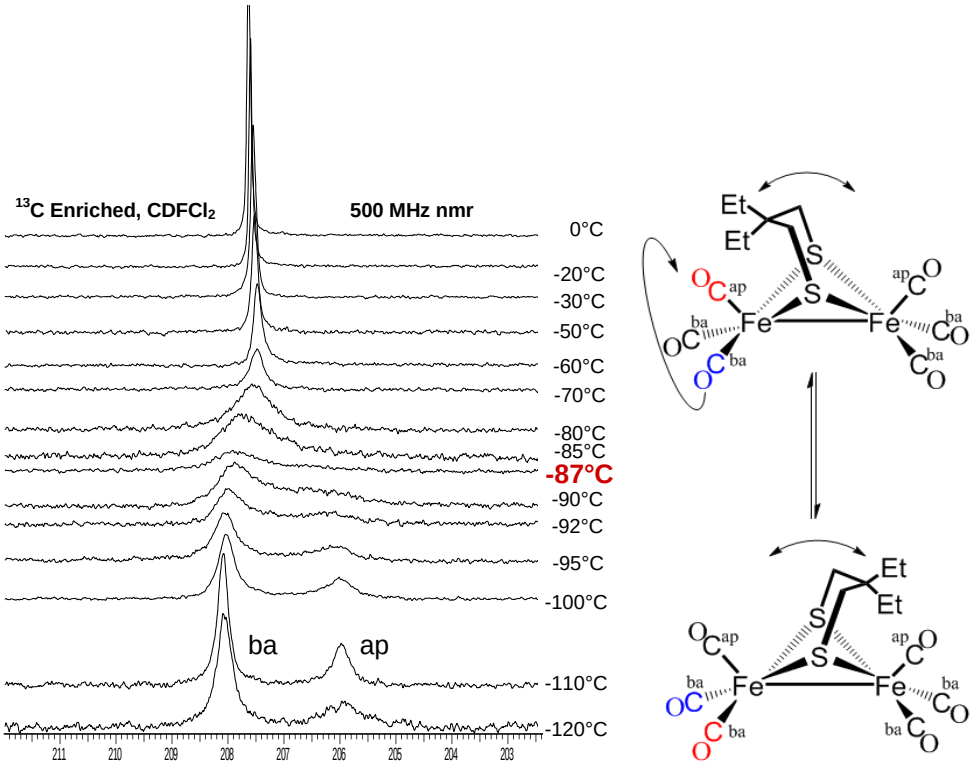

Figure III-11. ^{13}C VT-NMR of (μ-depdt)$[Fe(CO)_3]_2$ showing separate resonances for the apical CO and basal CO's at low temperature. Coalescence temperature indicated in red.

In contrast to the all-CO complexes which show only one ^{13}C resonance for the CO ligands at 0°C, the NHC substituted complex (μ-depdt)$[Fe(CO)_3][Fe(CO)_2IMes]$ shows two resonances at δ = 215.8 and 212.1, assigned to the CO's on the $[Fe(CO)_2IMes]$ and the $[Fe(CO)_3]$ units, respectively. As shown in the ^{13}C VT NMR spectra of (μ-depdt)$[Fe(CO)_3][Fe(CO)_2IMes]$ (Figure III-12) resolution of the CO's on the $[Fe(CO)_2IMes]$ unit is obtained on cooling to -40 °C. This indicates, as expected, a significantly higher energy barrier for site exchange on the bulky IMes substituted side

as compared to the all-CO complexes. For the [$Fe(CO)_3$] unit, three separate resonances at 214.7, 213.7, and 208.6 ppm appear upon cooling to -100 °C. Because of the greater range in chemical shift for the resonances at -100 °C a larger rate constant is required to obtain coalescence. Since the temperature range between coalescence and resolution is similar to that of the all-CO complex this likely indicates a lower energy barrier for site exchange on the IMes derivative. Using the difference between the midpoint of the two peaks assigned to the basal CO's and the resonance assigned to the apical CO for Δv and a coalescence temperature of ~ -85 °C, a $\Delta G^{\ddagger} = 8.0$ kcal/mol is obtained. Due to line broadening at low temperatures a full line shape analysis was not possible for these complexes, meaning that the error associated with the calculated values could make the difference between the substituted and unsubstituted complexes insignificant. The lower energy barrier observed here is supported in part by the spectral observations as well as earlier DFT studies which explored the effect of ligand substitution on transition state energies.[87] Nevertheless, these values can only be used as a rough estimate of $\Delta G^{\ddagger}$. Table III-5 lists the experimental energy barriers for apical/basal exchange of the CO ligands on the $Fe(CO)_3$ unit of several sterically bulky model complexes and their μ-pdt analogues. Interestingly the donor ligands have an almost identical effect on the fluxional processes in the complexes with the sterically bulky dithiolate as they do in the less sterically bulky derivatives, however all of the energy barriers are ~2 kcal/mol lower in energy.

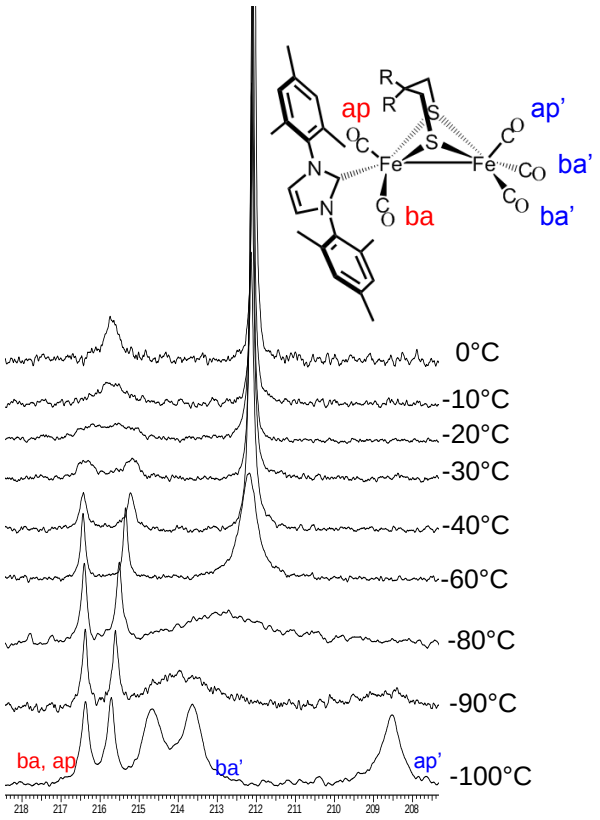

Figure III-12. ^{13}C VT-NMR of (μ-depdt)[Fe(CO)$_3$][Fe(CO)$_2$IMes]. Bands for the IMes substituted side are labeled in red and those of the unsubstituted side are labeled in blue.

Table III-5. Experimentally determined energy barriers for sterically bulky monosubstituted derivatives and the corresponding μ-pdt analogues

L=	$\Delta G^{\ddagger}$ (kcal/mol)[b]	
	(μ-dRpdt)	(μ-pdt)
CO	**8.3**	**10.4**[29]
PPh3	**7.5**[a]	**n/a**
PTA	**7.0**[a]	**9.4**[130]
IMes	**8.0**	**10.1**[127]

a) Peak seperation was not observed. Δν is estimated based on an average value for the seperation observed in other monosubstituted complexes of ~630 hz.
b) $\Delta G^{\ddagger}$ is for site exchange on the $Fe(CO)_3$ unit.

Concluding Comments

Overall, the addition of steric bulk to the μ-S to S linker of the all CO complexes has not caused large changes in the electronic properties of the $Fe(CO)_3$ units nor significantly altered the solid state structure of these compounds relative to the μ-pdt analogue, and at no time was a rotated $Fe^{I}Fe^{I}$ form observed. However, VT NMR studies of these complexes have shown that the $\Delta G^{\ddagger}$ for CO site exchange has been decreased by ca. 2 kcal/mol, indicating that the transition state, hypothesized to resemble the rotated form seen in the *eas*,[26]has been stabilized as compared to the μ-pdt complex resulting in more rapid exchange of the CO groups. Interestingly the added alkyl groups on the S to S linker also increases the rate at which the FeS_2C_3 ring flip occurs. Because of the rapid boat/chair interconversion, the interaction of the alkyl groups with the CO's may be lessened, however further exploration of the possibility of ring flip cessation

would be required to determine the full extent to which this process affects CO site exchange.

Upon addition of the sterically bulky IMes ligand to the μ-dmpdt and μ-depdt complexes more substantial changes in the solid state structure are observed. The most striking difference is the preferential positioning of IMes at a basal site of the substituted $S_2Fe(CO)_2NHC$ square pyramid. In addition to variation of the coordination site, the Fe-Fe bond distances of these complexes are lengthened by 0.05-0.07 Å giving values closer to that seen for the enzyme active site, typically 2.55-2.62 Å.[26]Also the C_{ap}-Fe-Fe-C_{ap} torsion angle has increased, with the μ-dmpdt[$Fe(CO)_3$][$Fe(CO)_2$IMes] showing a distortion from eclipsed by ca 41°. This degree of staggering is not seen for μ-dRpdt[$Fe(CO)_3$][$Fe(CO)_2$L], where R= Me or Et and L = PPh_3 or IMe. The greater changes upon addition of the more sterically bulky ligands implies that the steric bulk of the ligand as well as the S to S linker are important properties in the design of electocatalysts for H_2 production/uptake based on [FeFe] H_2ase.

CHAPTER IV

MIXED-VALENT $Fe^{I}Fe^{II}$ COMPLEXES THAT ACT AS STRUCTURAL AND SPECTROSCOPIC MODELS OF THE H_{OX} STATE OF THE ACTIVE SITE*

Introduction

The first structurally characterized model complexes to match the geometry of the enzyme active site were reported by the Darensbourg and Rauchfuss groups in 2007. These models (Figure IV-1) contained substituent ligands that were both sterically bulky and strong donors. Cyclic voltammetry studies on these complexes showed readily accessible and reversible one-electron oxidations indicating that an $Fe^{I}Fe^{II}$ complex might be obtainable. Infrared monitoring of the reaction of these complexes with one equivalent of $FcPF_6$ showed a large positive shift for most of the ν(CO) bands consistant with oxidation of the irons. However, a new lower energy band was also observed for these complexes in a range indicative of a semi-bridging CO. This initial spectroscopic evidence of the rotated structure was confirmed in the X-ray crystal structure of the two complexes, which showed a CO located between the two irons and an open site. By obtaining the rotated structure in the $Fe^{I}Fe^{II}$ model complexes, both Darensbourg and

---

*Reproduced in part, with permission, from: Singleton, M. L.; Bhuvanesh, N.; Reibenspies, J. H.; Darensbourg, M. Y. *Angew. Chem., Int. Ed.* **2008**, *47*, 9492. Copyright **2008** WILEY-VCH Verlag GmbH & Co. KGaA, Weinheim.[128]

Rauchfuss showed that the geometry referred to as the entatic state of enzyme, was in fact only an entatic state in the $Fe^{I}Fe^{I}$ oxidation state and was the ground state in the $Fe^{I}Fe^{II}$ resting form.

Since the publication of these structures, several mixed-valent diiron complexes have been reported. However, only a handful of these have been structurally characterized. This has left analysis of the v(CO) stretches and EPR spectra of the remaining models as the means for obtaining structural insight. The two initial complexes described above proved to be excellent spectroscopic models. In addition to matching important features of the v(CO) band patterns of the active site, the complexes also had EPR g-tensors nearly identical to the H_{ox} state of enzyme active

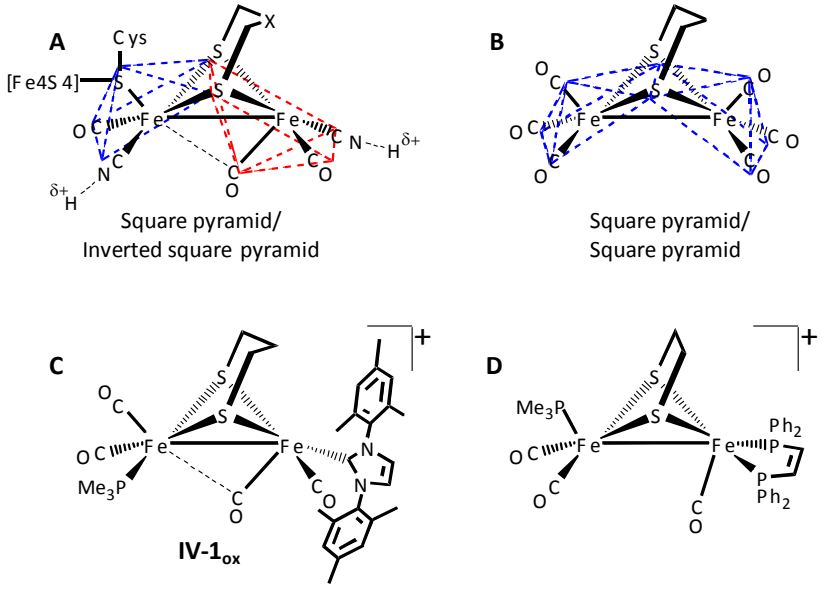

Figure IV-1. ***A)*** Structure of the enzyme active site of [FeFe]-hydrogenase showing the unique geometry. **B**) Structure of the parent model complex, (μ-pdt)$[Fe(CO)_3]_2$.[29] **C** & **D**) Recently reported model complexes that have geometries similar to the active site.[64-65]

site. For the more recent mixed-valent complexes the spectroscopic similarity to the active site is not as readily apparent. Two subsequent models produced by the Darensbourg group used less sterically bulky N-heterocyclic carbenes.[102] Upon oxidation the lowest ν(CO) band for these complexes appeared at significantly higher wavenumbers than in the more sterically bulky IMes derivative (1929 vs 1886 cm^{-1}). Additionally, the EPR signal of these complexes was significantly broadened and appeared more axial than the initial complexes reported by Darensbourg and Rauchfuss. This broadness could be the result of multiple conformational isomers. While the paramagnetic nature of the mixed valent complexes prevents studying of the conformational preferences by NMR, low temperature NMR studies of the diamagnetic (μ-pdt)[$Fe^{I}(CO)_2$IMe][$Fe^{I}(CO)_2PMe_3$] indicated multiple isomers at -80 °C.

Rauchfuss and co-workers also observed multiple isomers in their complexes, evidenced by the simulation of their EPR spectra requiring at least three different species.[136] The differentiation of the two irons in their system (Figure IV-1 D) by the presence of a single phosphine on one side versus a chelating bisphosphine on the other also allowed them to identify the rotated side as containing the Fe^{I} by the superhyperfine coupling in the EPR to the two ^{31}P nuclei from the bisphosphine lignd. This led to the interesting observation that even in similar systems, the localization of the unpaired electron could be changed soley by modifying the steric bulk of the substituent ligands or through increasing the size of the dithiolate linker from an ethylene to a propylene chain. While interesting, these results by Darensbourg and Rauchfuss raise several questions.

-Can the steric bulk of the substituent ligands instead be replaced by a sterically bulky dithiolate?

-Can a symmetrically substituted complex achieve similar results upon oxidation?

-What is the nature of the interplay between donating ability and steric bulk regarding the mixed valent complexes?

The addition of a sterically buky dithiolate ligand in the hexacarbonyl and monosubstituted complexes proved to be insufficient to the goal of isolating the rotated geometry in the $Fe^{I}Fe^{I}$ oxidation state.[126] However, the lowering of the energy barrier for rotation of the $Fe(CO)_3$ units indicated that the added steric bulk does decrease the energy difference between the unrotated ground state and the rotated transition state as compared to less bulky derivatives. This added stability should assist in the synthesis and isolation of a mixed-valent $Fe^{I}Fe^{II}$ complex with a rotated geometry. In a continuation of the work presented in Chapter III, and to test the efficacy of steric bulk in stabilizing the rotated geometry in the $Fe^{I}Fe^{II}$ oxidation state, we have prepared the disubstituted complex (μ-dmpdt)$[Fe(CO)_2PMe_3]_2$ and compared its electrochemical properties to the less sterically bulky (μ-pdt)$[Fe(CO)_2PMe_3]_2$.

Synthesis and Characterization of (μ-dmpdt)$[Fe(CO)_2PMe_3]_2$

Following a similar procedure to the one reported for (μ-pdt)$[Fe(CO)_2PMe_3]_2$, the reaction of (μ-dmpdt)$[Fe(CO)_3]_2$,[126] with PMe_3 in toluene at 100 °C yields (μ-dmpdt)$[Fe(CO)_2PMe_3]_2$ as dark red crystals in 60-70% yield (Figure IV-2). Unlike the reaction with (μ-pdt)$[Fe(CO)_3]_2$ which completely converts to the bis-PMe_3 over the

course of ~4 hours, the more sterically bulky complex requires up to two days to reach completion. As the substitution reactions are known to proceed through an associative pathway, this is attributed to the added steric bulk inhibiting the approach of the incoming ligand. Regardless of the time required, the two bisphosphine complexes have similar spectroscopic properties, notably the υ(CO) IR values of (μ-dmpdt)$[Fe(CO)_2PMe_3]_2$ are nearly identical to those of (μ-pdt)$[Fe(CO)_2PMe_3]_2$, indicating that the difference in electron donating ability resulting from the bridgehead carbon substitution is nil.[132]

Variable temperature NMR studies focused on the mobility of the $Fe(CO)_2PMe_3$ units found the barrier to intramolecular CO site exchange to be similar to the hexacarbonyl parent complex with exchange occurring down to -90 °C. The NMR studies did not show evidence for the ceasing of the ring flip in the S to S linker of (μ-dmpdt)$[Fe(CO)_2PMe_3]_2$ consistent with previous findings that the added steric bulk decreases the energy barrier for the ring flip. In contrast, (μ-pdt)$[Fe(CO)_2PMe_3]_2$ showed both cessation of the ring flip and site exchange well above -90 °C.

The molecular structure of (μ-dmpdt)$[Fe(CO)_2PMe_3]_2$ determined by X-ray diffraction (Figure IV-3 inset) is largely typical of (μ-SRS)$[Fe(CO)_2L]_2$ complexes but shows a staggering of the $Fe(CO)_2PMe_3$ units resulting in a C_{ap}-Fe-Fe'-C'_{ap} torsion angle of ~30° (~ 20° greater than for (μ-pdt)$[Fe(CO)_2PMe_3]_2$).[132] This difference is substantially more than what was observed between the hexacarbonyl parent complexes. As discussed in Chapter I, the effect of the steric bulk arises from the destabilization of

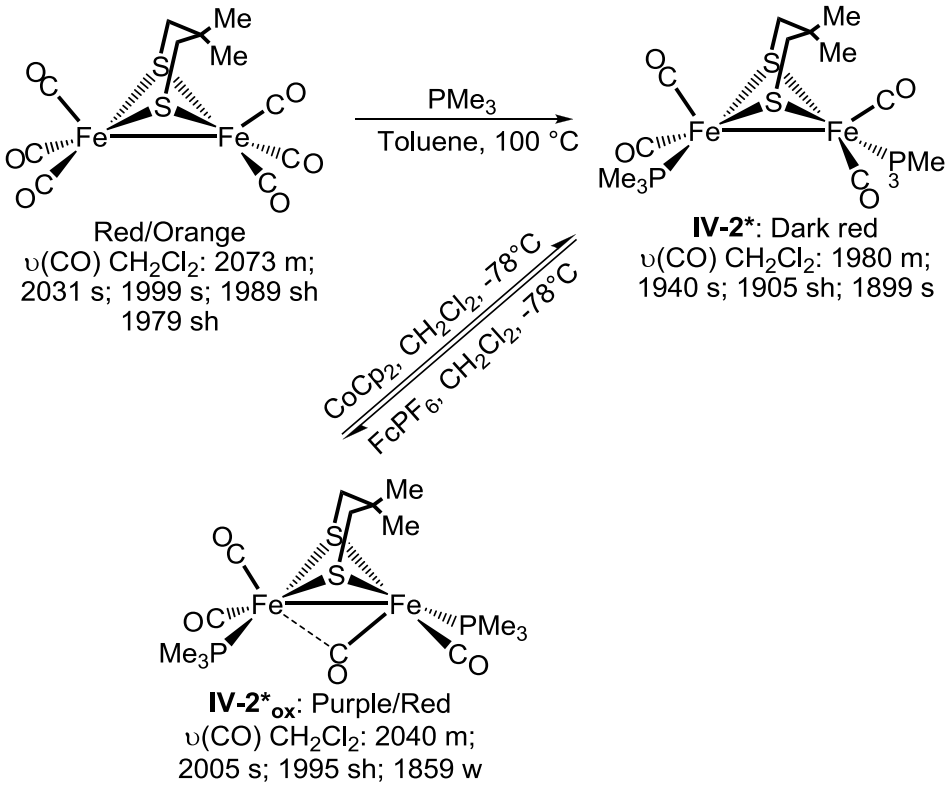

Figure IV-2. Synthesis of complexes **IV-2*** and **IV-2*$_{ox}$**

the totally eclipsed ground state (C_{ap}-Fe-Fe'-C'_{ap} torsion angle = 0°) which is enforced by the FeFe bond. Addition of the strong donors in this system weakens the FeFe bond as evidenced by the longer bond distances in the substituted complexes, and decreases the restoring force acting against the torque imposed by the added steric bulk. The destabilization of the FeFe bond is the proposed reason for the dramatic differences in the electrochemistry of the (μ-pdt)$[Fe(CO)_2PMe_3]_2$ and (μ-dmpdt)$[Fe(CO)_2PMe_3]_2$.

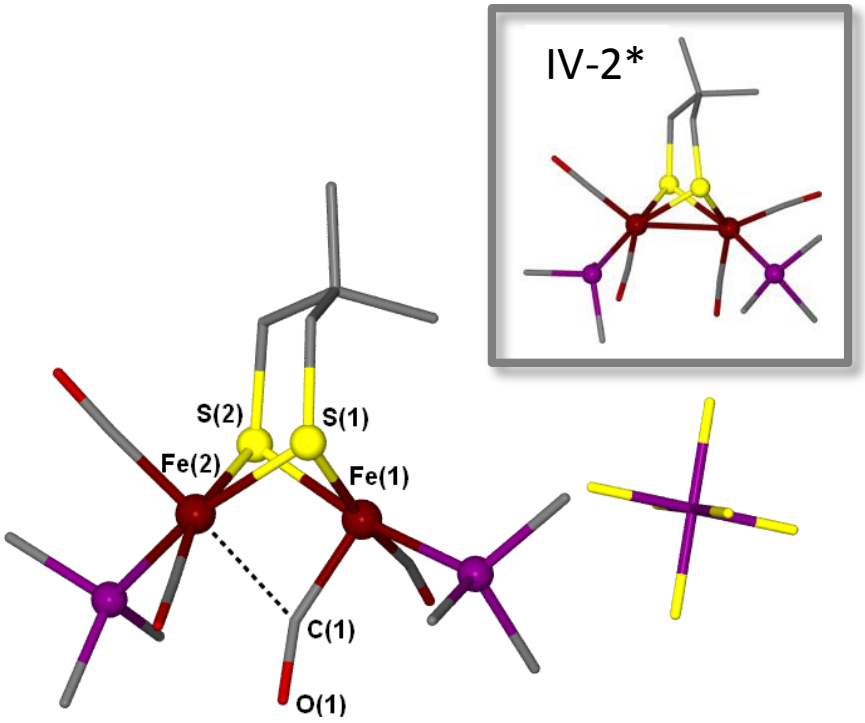

Figure IV-3. Ball and stick drawing of the molecular structure of **IV-2*$_{ox}$** cation with the **IV-2*** precursor structure in inset. Significant metric parameters of **IV-2*$_{ox}$** [**IV-2***]**:** Fe(1)-Fe(2): 2.532(2) Å; [2.569(1)º] Fe(1)-C(1) 1.814(6); Fe(2)-C(1): 2.204(6) Fe(1)-C(1) -O(1): 146 (4)º; Fe(2)-C(1)-O(1): 133(3) Flap ∠ = 123° [141°] The "flap" angle refers to the intersection of the best planes comprised of the $(CH_2)_3$ and the $S_2(CH_2)_2$ units. A full listing of metric parameters is given in appendix A.

Figure IV-4a displays the cyclic voltammograms of (μ-pdt)[Fe(CO)$_2$PMe$_3$]$_2$ (**IV-2**), (μ-dmpdt)[Fe(CO)$_2$PMe$_3$]$_2$ (**IV-2***), and (μ-pdt)[Fe(CO)$_2$IMes][Fe(CO)$_2$PMe$_3$] (**IV-1**). The Fe^IFe^I/Fe^IFe^0 oxidation of both bisphosphine complexes show up at more positive potentials than **IV-1** consistent with the weaker donor ability of PMe$_3$ relative to IMes. While the two bisphosphine complexes would be expected to have similar redox properties, the bridgehead bulk results in an anodic shift of the $Fe^IFe^I/Fe^{II}Fe^I$ oxidation wave of ~240 mV in (μ-dmpdt)[Fe(CO)$_2$PMe$_3$]$_2$ as compared to (μ-pdt)[Fe(CO)$_2$PMe$_3$]$_2$.[132] This quasi-reversible oxidation event in (μ-pdt)[Fe(CO)$_2$PMe$_3$]$_2$ also becomes fully reversible in (μ-dmpdt)[Fe(CO)$_2$PMe$_3$]$_2$. As the (μ-dmpdt) and (μ-pdt) ligands have similar electron donating abilities,[126] the observed electrochemical differences are due solely to the influence of the steric effect provided by the added *gem*-dimethyl groups on (μ-dmpdt)[Fe(CO)$_2$PMe$_3$]$_2$. Most importantly, the fully reversible redox event at -0.335 V, Figure IV-4a, suggests the possibility of bulk chemical oxidation and isolation of the oxidized Fe^IFe^{II} complex (μ-dmpdt)[Fe(CO)$_2$PMe$_3$]$_2^+$, accomplished according to Scheme 1.

Synthesis and Characterization of (μ-dmpdt)[Fe(CO)$_2$PMe$_3$]$_2^+$PF$_6^-$

Reaction of (μ-dmpdt)[Fe(CO)$_2$PMe$_3$]$_2$ with one equivalent of $Fc^+PF_6^-$, results in a minor change in the color of the solution from dark red to dark red-purple. More importantly, dramatic changes in the IR spectrum are observed. The ν(CO) IR spectral changes accompanying oxidation of (μ-dmpdt)[Fe(CO)$_2$PMe$_3$]$_2$ include a weak band at 1859 cm^{-1} indicative of a bridging or semi-bridging CO, Figure IV-4b, similar to that observed for (μ-pdt)[Fe(CO)$_2$IMes][Fe(CO)$_2$PMe$_3$]PF$_6$ by Liu and Darensbourg.[64] X-ray

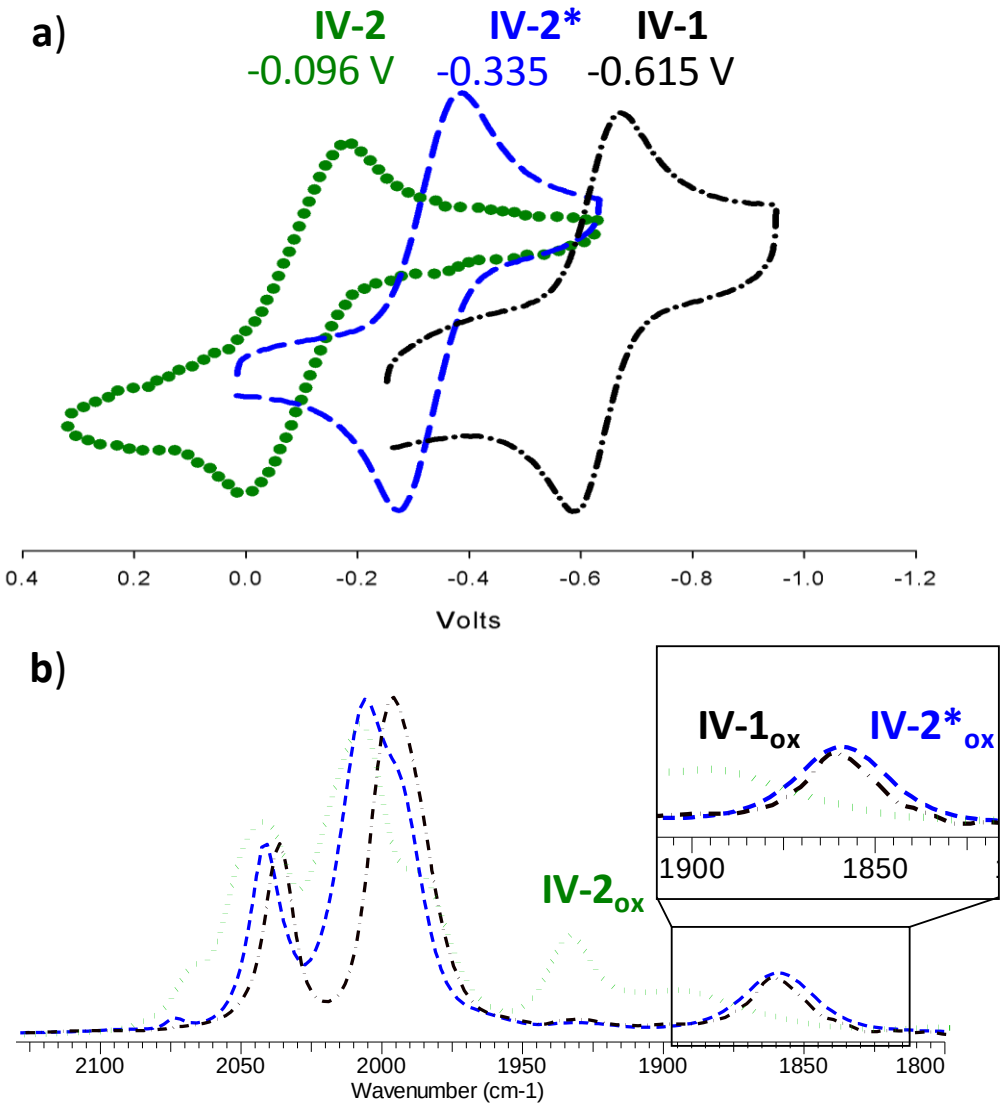

Figure IV-4. a) Cyclic voltammetry of the $Fe^{I}Fe^{I}/Fe^{II}Fe^{I}$ redox events of **IV-1**, **IV-2**, and **IV-2***. Concentrations were 2 mM in CH_2Cl_2 with 0.1 M $^{n}Bu_4NBF_4$ as an electrolyte. Scan rate:200 mV/s. b) Comparison of the infrared spectra of **IV-1$_{ox}$ (- • - •), IV-2$_{ox}$** (• • •)and **IV-2*$_{ox}$** (- - -) in the ν(CO) region.

crystallographic studies of (μ-dmpdt)$[Fe(CO)_2PMe_3]_2^+PF_6^-$ confirm the presence of this feature, Figure IV-3. Crystals of (μ-dmpdt)$[Fe(CO)_2PMe_3]_2^+PF_6^-$ were obtained from a concentrated CH_2Cl_2 solution placed in a Dewar flask with a thermal gradient from -15°C to -78°C. From X-ray diffraction analysis, the structure was determined and prominent metric parameters are given in Figure IV-3. Notable is the square pyramidal Fe(1) with a non-linear Fe(1)C(1)O(1) = 146(3)° in the apical position. Asymmetric Fe-C distances also indicate the semi-bridging character of the C(1)O(1), which leads to a pseudo 6-coordinate, octahedral geometry at Fe(2). The Fe-Fe distance of 2.532 (2) Å in the (μ-dmpdt)$[Fe(CO)_2PMe_3]_2^+PF_6^-$ cation is slightly shorter than that of the neutral (μ-dmpdt)$[Fe(CO)_2PMe_3]_2$. The dithiolate linker of the oxidized complex has a more acute "flap" angle than the Fe^IFe^I neutral precursor. The change in flap angle of 30° differs from that of (μ-pdt)$[Fe(CO)_2IMes][Fe(CO)_2PMe_3]$ vs. (μ-pdt)$[Fe(CO)_2IMes][Fe(CO)_2PMe_3]PF_6$ in which there is none (123.03° vs. 122.97°). There are no apparent intermolecular interactions that would influence the position of the bridgehead methyl substituents in (μ-dmpdt)$[Fe(CO)_2PMe_3]_2^+PF_6^-$ whereas the steric hindrance from apical CO groups in the neutral precursor accounts for the greater flap angle of (μ-dmpdt)$[Fe(CO)_2PMe_3]_2$.

Figure IV-5 presents results from DFT calculations on (μ-dmpdt)$[Fe(CO)_2PMe_3]_2^+PF_6^-$. The overlay of the DFT optimized structure of the cation with that from the X-ray diffraction study shows a precise match of the Fe_2S_2 core and the semi-bridging CO. As with (μ-pdt)$[Fe(CO)_2IMes][Fe(CO)_2PMe_3]PF_6$, the spin

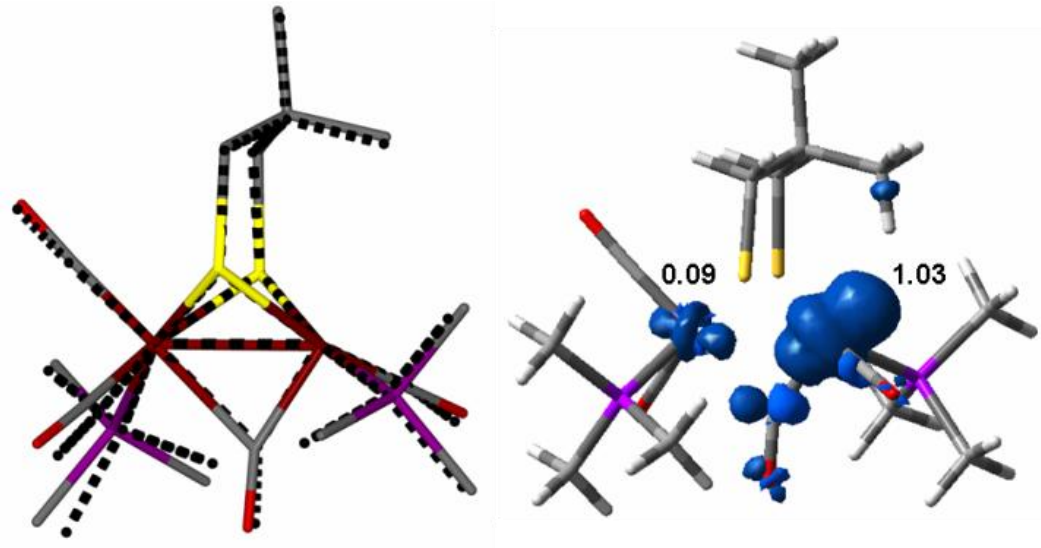

Figure IV-5. Left: Overlay of calculated structure (solid bonds) and the X-ray structure of **IV-2*$_{ox}$**. (dashed bonds) Right: Calculated spin density plot (right) showing the majority of the unpaired spin density on the rotated side of the complex. Mulliken atomic spin densities are indicated. The isodensity value for the spin density contour plot is 0.004.

density plot clearly shows the unpaired spin density that predicts the d^7 Fe^I resides in the rotated side of the (μ-dmpdt)$[Fe(CO)_2PMe_3]_2^+PF_6^-$.

The oxidized complex, (μ-dmpdt)$[Fe(CO)_2PMe_3]_2^+PF_6^-$, is EPR active and shows a rhombic signal that is simulated as a single species with hyperfine coupling to a single ^{31}P nucleus as noted in Figure IV-6. G values of 2.086, 2.025, and 2.007 are similar to those reported for both the *eas* and previously reported models, Figure 1, **C** (**IV-1$_{ox}$**) and **D**).[5,6,18,19] Hyperfine coupling (a = ca. 25) to only one of the PMe_3 ligands does not unambiguously identify the location of the unpaired electron in the (μ-dmpdt)$[Fe(CO)_2PMe_3]_2^+PF_6^-$ complex. It does however provide further evidence that the rotated iron in (μ-pdt)$[Fe(CO)_2IMes][Fe(CO)_2PMe_3]PF_6$, i.e., the one bearing the IMes ligand, is in fact Fe^I since no ^{31}P hyperfine coupling is seen in its EPR spectrum.[64] This

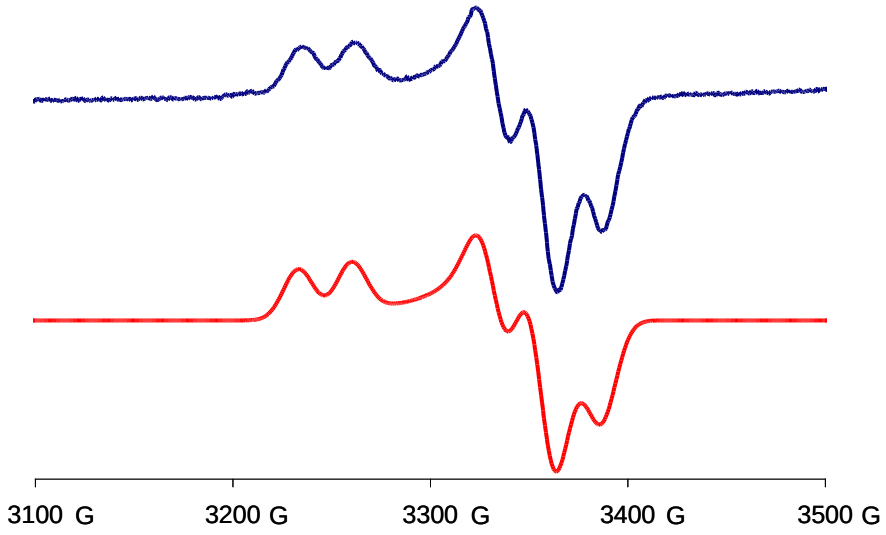

Figure IV-6. EPR spectrum of **IV-2*ox** (top) and Simfonia simulation (bottom).g-values with ^{31}P super hyperfine coupling parameters: $g_1 = 2.086$, a = 27.0 ; $g_2 = 2.025$, a = 25; $g_3 = 2.007$; a = 25.

result is also consistent with the computational studies of both (μ-pdt)[Fe(CO)$_2$IMes][Fe(CO)$_2$PMe$_3$]PF$_6$ and (μ-dmpdt)[Fe(CO)$_2$PMe$_3$]$_2^+$PF$_6^-$.[49]

Oxidation of (μ-pdt)[Fe(CO)$_2$PMe$_3$]$_2$

Despite not having a clearly reversible $Fe^IFe^I/Fe^{II}Fe^I$ redox couple at 22 ºC, the sterically unhindered (μ-pdt)[Fe(CO)$_2$PMe$_3$]$_2$ complex, reacts with FcPF$_6$ at -78 °C to produce a highly unstable one-electron oxidized species, (μ-pdt)[Fe(CO)$_2$PMe$_3$]$_2$PF$_6$, that is EPR active. Best efforts in obtaining a spectrum for this complex show an axial signal with g-values of 2.001 and 1.999. (Figure IV-7) The disparity between these values and those obtained for (μ-dmpdt)[Fe(CO)$_2$PMe$_3$]$_2^+$PF$_6^-$ indicate a difference in the

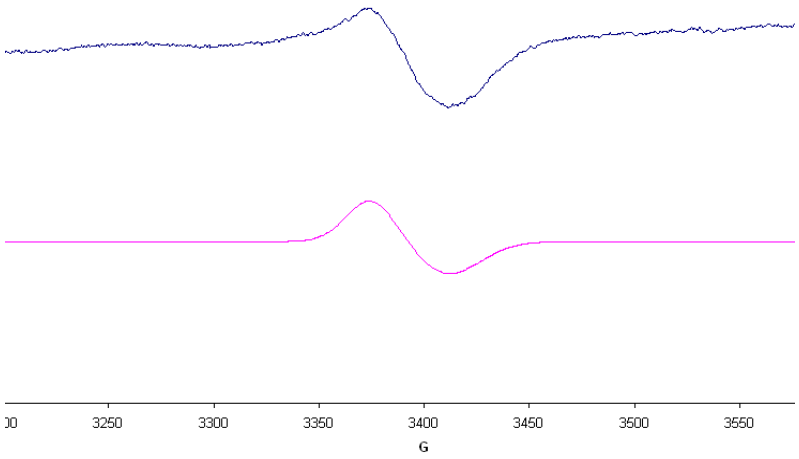

Figure IV-7. X-band EPR spectrum of ~500 μM IV-2_{ox} in 50:50 CH_2Cl_2:Toluene at 10 K (top) and Simfonia simulation (bottom).G values: 2.001,1.99,1.99.

electronic environment around the unpaired electron. A structural difference is also implied from the IR spectrum, Figure IV-4b, which shows noabsorption band indicative of a semi-bridging CO. Such sensitivity to the seemingly minor change in the dithiolate linker is evocative of the delicate balance of steric effects from the NHC ligands shown to determine rotation or not in a series of (μ-pdt)$[Fe(CO)_2PMe_3][Fe(CO)_2NHC]^+$ complex cations.[102,137]It should be noted that from studies on the mixed valent complexes produced by Rauchfuss and co-workers, the use of the counterion $B(C_6F_5)_4^-$ dramatically increased the stability of their mixed-valent complexes. They have attributed the instability of the PF_6^- and BF_4^- salts to reactions that occur between the counterion and the radical Fe at higher temperatures. Presumably the added steric bulk in

(μ-dmpdt)[$Fe(CO)_2PMe_3]_2^+PF_6^-$ hinders this reaction and prevents the rapid decomposition observed for complexes with less sterically bulky dithiolates.

Sterically Bulky Mixed-valent Complexes with Weaker and Stronger Donors

As a means to further study the role of the steric bulk in the stabilization of the mixed-valent complexes, two additional disubstituted complexes that utilized the sterically bulky dithiolate were synthesized. The reaction of $P(OMe)_3$ with (μ-dmpdt)[$Fe(CO)_3]_2$ as described in Chapter II yields (μ-dmpdt)[$Fe(CO)_2P(OMe)_3]_2$. The ν(CO) bands for this complex are on average 20 cm^{-1} higher than the PMe_3 derivative. (Figure IV-8) This is expected as the weaker donor strength of the ligands result in less electron density around the irons. The IR spectra of the complex also indicated a structural difference as compared to the PMe_3 derivatives. An additional band is observed at 1919 cm^{-1} and overlaps with the band at 1936 cm^{-1}. In the PMe_3 complexes, no extra band is observed, however the band at 1899 appears to have a shoulder. The structural difference was confirmed by X-ray diffraction studies on the related (μ-depdt)[$Fe(CO)_2P(OMe)_3]_2$ derivative (Figure IV-9) which showed that instead of the trans-basal orientation observed for the PMe_3 ligands, the $P(OMe)_3$ ligands adopt a apical/basal configuration with the sterically bulky bridgehead oriented away from the apical ligand.

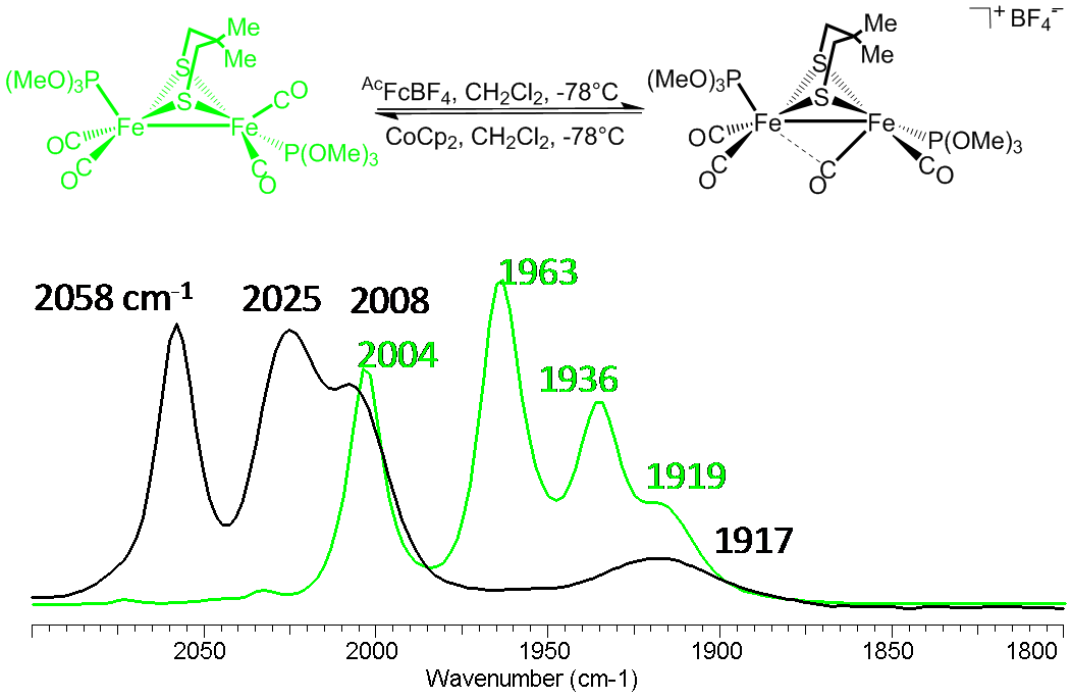

Figure IV-8. Reaction scheme for the oxidation of top) (μ-dmpdt)[$Fe(CO)_2P(OMe)_3$]$_2$ and the corresponding IR ν(CO) spectra. Spectra color match the corresponding complex in the reaction scheme.

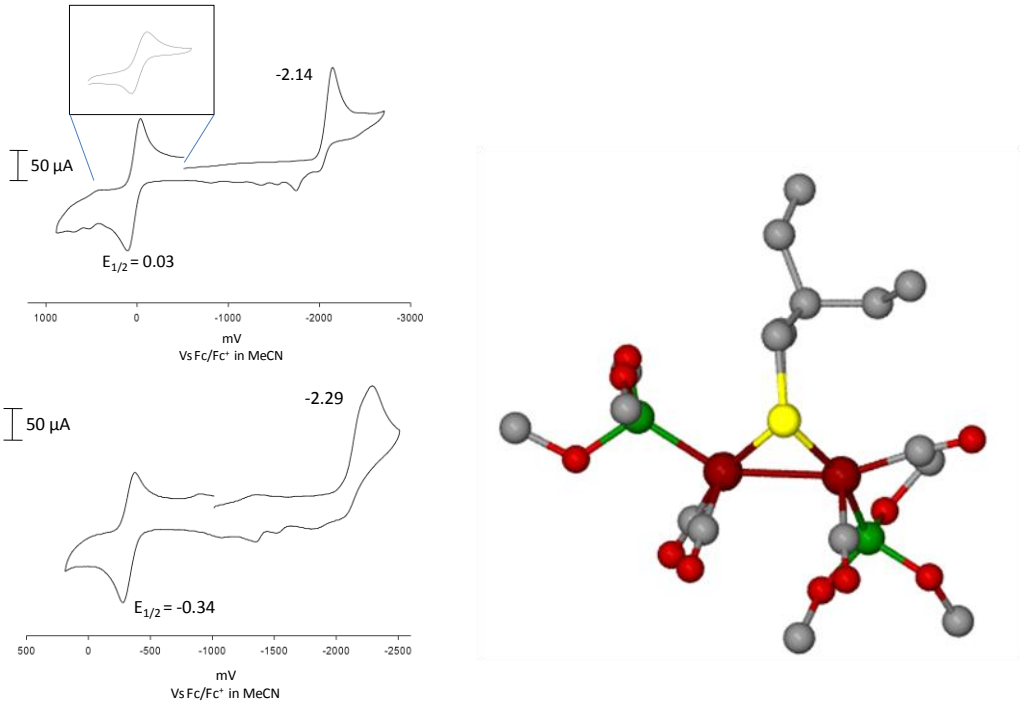

Figure IV-9. Left) Comparison of the cyclic voltammograms of (µ-dmpdt)[Fe(CO)$_2$P(OMe)$_3$]$_2$ (top) and (µ-dmpdt)[Fe(CO)$_2$PMe$_3$]$_2$ (bottom) in CH$_3$CN at 200 mV/s. Right) X-ray crystal structure of (µ-depdt)[Fe(CO)$_2$P(OMe)$_3$]$_2$ showing the apical/basal ligand conformation

Cyclic voltammetry studies supported the decreased electron density and show that the Fe^IFe^I/Fe^IFe^{II} oxidation potential for the complex in CH_3CN is ~370 mV more positive than (µ-dmpdt)[Fe(CO)$_2$PMe$_3$]$_2$ (Figure IV-9) and ~100 mV more positive than (µ-pdt)[Fe(CO)$_2$PMe$_3$]$_2$. However, similar to the observed differences in the PMe$_3$ derivatives, the oxidation of (µ-dmpdt)[Fe(CO)$_2$P(OMe)$_3$]$_2$ occurs ~90 mV more negative than in the µ-pdt analogue.[137] The most important observation however, was that (µ-dmpdt)[Fe(CO)$_2$P(OMe)$_3$]$_2$ had a reversible oxidation meaning that the one-electron oxidized species might be isolated. Because of its positive oxidation potential, (µ-dmpdt)[Fe(CO)$_2$P(OMe)$_3$]$_2$ was found to be unreactive towards FcPF$_6$ and instead

required a stronger oxidizing agent, acetylferrocenium, to reach the mixed-valent $Fe^{I}Fe^{II}$ oxidation state.

Addition of one equivalent of the oxidizing agent to (μ-dmpdt)$[Fe(CO)_2P(OMe)_3]_2$ results in a similar change in the ν(CO) region of the infrared spectra, with most of the bands shifting to higher wavenumbers consistent with shifts observed for all other reported mixed-valent complexes. However, the low energy band, that at 1859 cm^{-1} in the PMe_3 derivative indicates a bridging CO, instead appears at 1917 cm^{-1} making its assignment as a semi-bridging CO questionable. Another interesting feature observed in ν(CO) region is the difference in the band pattern for the remaining CO ligands as compared to the PMe_3 derivative. Similar to the $Fe^{I}Fe^{I}$ species, an extra band is observed as a shoulder on the higher intensity band at 2025 cm^{-1}, indicating that the structure of the mixed-valent complex may also have one of the $P(OMe)_3$ ligands in an apical position. As this would necessarily have to be on the unrotated iron in a complex with a presumably rotated geometry, the apical donor might disfavour the formation of a semi-bridging CO. This result would be consistent with the observation of the more linear Fe-C-O angle (and a lowest energy ν(CO) band at 1883 cm^{-1})in the mixed-valent complexes by the Rauchfuss group which have a PR_3 donor ligand in an apical position.[136] Additionally, theoretical work on a series of NHC complexes by Liu, Thomas, Hall and Darensbourg also showed that the energy for the ν(CO) band of the rotated CO shifted to higher wave numbers if there was a better donor than CO in the apical position.[102]

While no structure of the (μ-dmpdt)[Fe(CO)$_2$P(OMe)$_3$]$_2$BF$_4$ complex has been obtained yet, its properties make it of interest for further study. Similar to (μ-dmpdt)[Fe(CO)$_2$PMe$_3$]$_2^+$PF$_6^-$, the P(OMe)$_3$ derivative is moderately stable at room temperature. This makes it useful for comparison to the more electron rich PMe$_3$ complex in O_2 reactivity studies which are currently underway. Additionally, because (μ-dmpdt)[Fe(CO)$_2$P(OMe)$_3$]$_2$BF$_4$ shows higher stability than (μ-pdt)[Fe(CO)$_2$PMe$_3$]$_2^+$PF$_6^-$, despite being less electron rich, it supports the proposal that the steric bulk helps prevent decomposition at higher temperatures.

Interesting results were also observed when IMes is used in combination with the sterically bulky dithiolate. The complex (μ-dmpdt)[Fe(CO)$_2$PMe$_3$][Fe(CO)$_2$IMes] can be obtained upon reaction of (μ-dmpdt)[Fe(CO)$_3$][Fe(CO)$_2$IMes] with PMe$_3$, however if a large excess of phosphine is used or the reaction is allowed to go on for too long, a mixture of the desired product and (μ-dmpdt)[Fe(CO)$_2$PMe$_3$]$_2$ is obtained. This reactivity differs from that of the μ-pdt analogue where the IMes remains bound to the diiron complex even after reaction overnight.[64] The ν(CO) band pattern of (μ-dmpdt)[Fe(CO)$_2$PMe$_3$][Fe(CO)$_2$IMes] is very similar to that of the bis-PMe$_3$ analogue, but is slightly shifted to lower wavenumbers consistent with the trans-basal configuration and the stronger donating ability of IMes versus PMe$_3$ (Figure IV-10). The solid state structure of (μ-dmpdt)[Fe(CO)$_2$PMe$_3$][Fe(CO)$_2$IMes] also supports the structural assignment from the IR spectra showing both ligands in a basal position. Similar to observed differences in the structure of the monosubstituted IMes

complexes,[126] the preference of the IMes ligand for the basal position differs from the μ-pdt analogue where it adopts an apical position. (Figure IV-11)[64]

Cyclic voltammetry studies show a reversible oxidation at -620 mV in CH_2Cl_2; a value that is significantly more negative than (μ-dmpdt)[$Fe(CO)_2PMe_3$]$_2$ but nearly identical to (μ-pdt)[$Fe(CO)_2PMe_3$][$Fe(CO)_2$IMes], (-615 mV).[64] (Figure IV-11 and Figure IV-4) The small differences between these complexes is consistent with the proposal that the steric bulk on the IMes ligand is significant enough to minimize the contribution from the sterically bulky dithiolate. Similar to the other complexes discussed in this chapter, the reversible oxidation suggests chemical oxidation to obtain the mixed-valent $Fe^{I}Fe^{II}$ form is feasible. Upon reaction of (μ-dmpdt)[$Fe(CO)_2PMe_3$][$Fe(CO)_2$IMes] with one equivalent of $FcPF_6$, a similar change in IR spectra as in (μ-dmpdt)[$Fe(CO)_2PMe_3$]$_2$ is observed, (Figure IV-10). The higher energy bands are observed at 2034 and 1992 cm^{-1}, ~10 wavenumbers lower than the PMe_3 analogue. The band indicative of the semi-bridging CO is observed at 1845 cm^{-1}, a value lower than that observed for both (μ-dmpdt)[$Fe(CO)_2PMe_3$] and (μ-pdt)[$Fe(CO)_2PMe_3$][$Fe(CO)_2$IMes], where the CO is known to be in a semi-bridging configuration.[64] Unfortunately the structure for this complex has not yet been obtained.

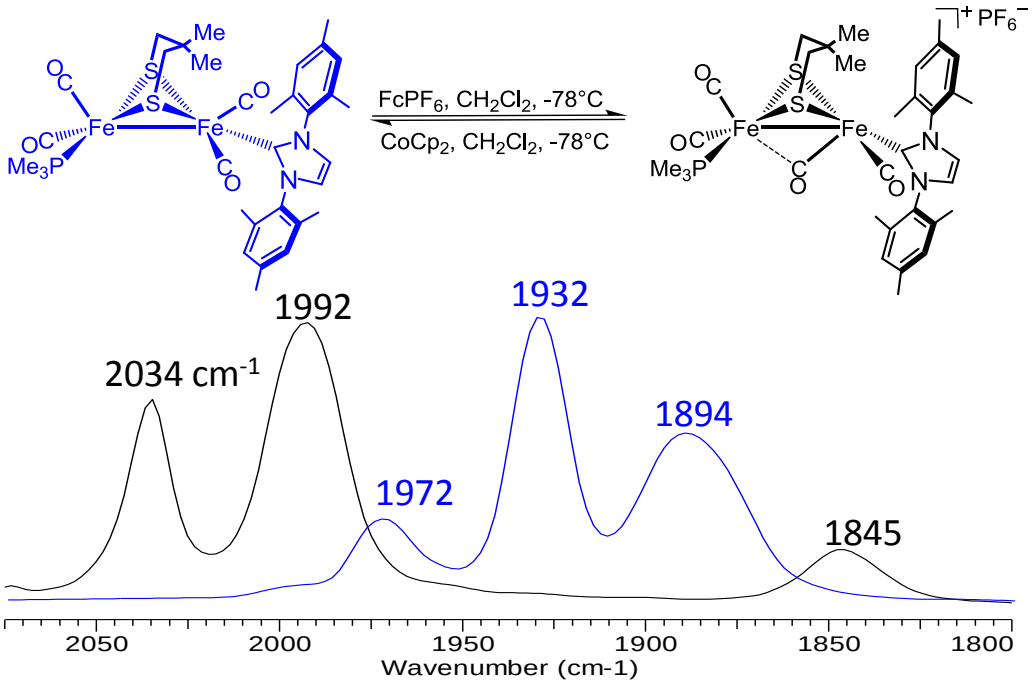

Figure IV-10. Reaction scheme for the oxidation of top) (μ-dmpdt)[$Fe(CO)_2PMe_3$][$Fe(CO)_2$IMes] and the corresponding IR ν(CO) spectra. Spectra color match the corresponding complex in the reaction scheme.

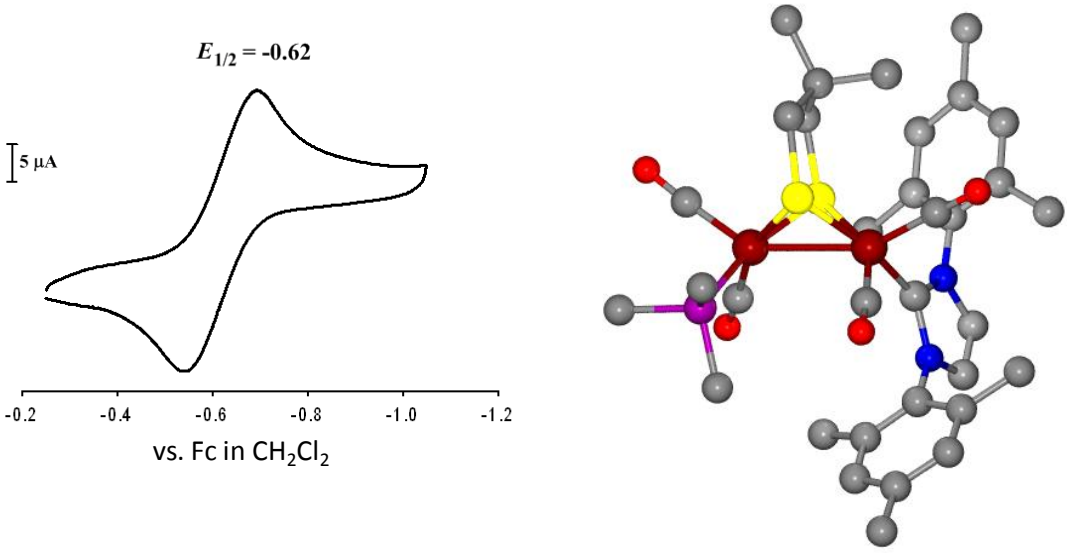

Figure IV-11. Left) Reversible $Fe^{I}Fe^{I}/Fe^{I}Fe^{II}$ oxidation of (μ-dmpdt)[$Fe(CO)_2PMe_3$][$Fe(CO)_2$IMes] as observed by cyclic voltammetric studies. Right) X-ray crystal structure of (μ-dmpdt)[$Fe(CO)_2PMe_3$][$Fe(CO)_2$IMes] showing the trans-basal ligand conformation

The mixed-valent nature of (μ-dmpdt)[$Fe(CO)_2PMe_3$][$Fe(CO)_2$IMes]PF_6 was also probed by EPR spectroscopy. The preliminary EPR data found g-tensors of 2.08, 2.03 and 2.01 which are closer to those found for (μ-dmpdt)[$Fe(CO)_2PMe_3$]PF_6 than the more closely related (μ-pdt)[$Fe(CO)_2PMe_3$][$Fe(CO)_2$IMes]PF_6,[64] indicating an electronic environment similar in nature to the bis-PMe_3 analogue, Figure IV-12. However, there is no indication that the PMe_3 containing iron has rotated in (μ-dmpdt)[$Fe(CO)_2PMe_3$][$Fe(CO)_2$IMes]PF_6, as super hyperfine coupling to the ^{31}P nucleus is not observed. Instead this may result from the proximity of the iron to the bridgehead methyl groups allowing them to influence its electronic environment. Through ongoing

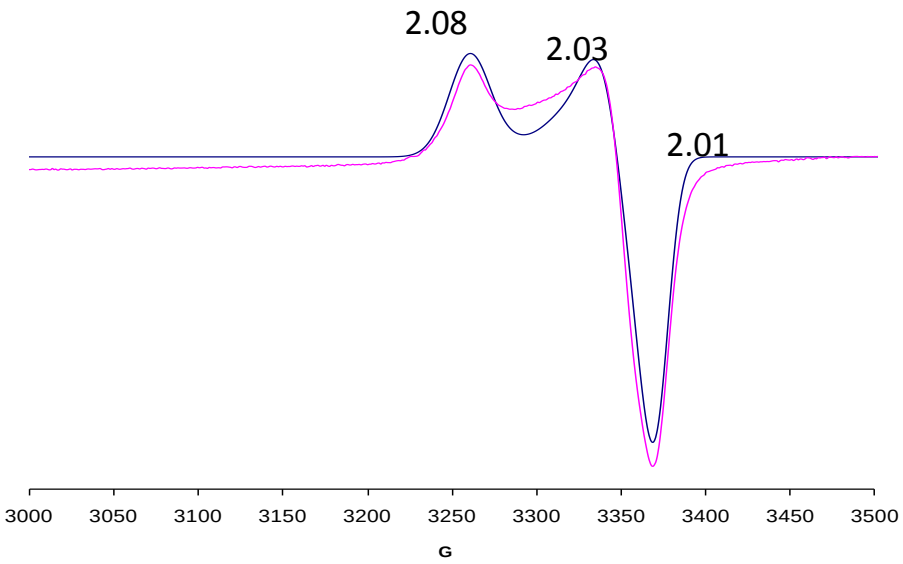

Figure IV-12. EPR spectra of (μ-dmpdt)[Fe(CO)$_2$PMe$_3$][Fe(CO)$_2$IMes] at 10 K and 10 dB. Experimental spectrum is shown in pink with the simulation overlayed in blue. G-tensors are indicated above the specra.

work studying the spectral properties of the closely related (μ-depdt) derivative, evidence to support this proposed influence might be obtained.

Concluding Comments

In summary, as predicted by de novo design[103] the addition of steric bulk to the S to S linker in these diiron model complexes is sufficient to enforce a significant twist in the solid state structure of (μ-dmpdt)[Fe(CO)$_2$PMe$_3$]$_2$. It facilitates the Fe^IFe^I/Fe^IFe^{II} oxidation leading to the first structurally characterized [FeFe]-H$_2$ase enzyme active site model complex that has a bridging CO and does not require sterically bulky ligands. Additionally, this work shows that asymmetric donation into the irons is not a requirement for the isolation of these rotated species. EPR results and DFT calculations

of (μ-dmpdt)$[Fe(CO)_2PMe_3]_2^+PF_6^-$, indicate that, similar to the Rauchfuss complexes, the rotated side of this complex contains the d^7, Fe^I, while the unrotated side is d^6, Fe^{II}.

The complex (μ-pdt)$[Fe(CO)_2PMe_3]_2$, lacking steric hindrance in substituent ligands or dithiolate linker, shows no evidence of a bridging CO upon oxidation and shows an axial signal in its EPR spectrum indicating a substantially different electronic environment around the unpaired electron. Additionally, the instability of (μ-pdt)$[Fe(CO)_2PMe_3]_2^+PF_6^-$, highlights the ability of the steric bulk to provide a moderate degree of stability to the rotated structure in (μ-dmpdt)$[Fe(CO)_2PMe_3]_2^+PF_6^-$, a conclusion also supported by work on the less electron rich (μ-dmpdt)$[Fe(CO)_2P(OMe)_3]_2^+BF_4^-$. Thus, the necessity of steric bulk to stabilize the rotated form in the Fe^IFe^{II} oxidation state can be met by two structural motifs in the model complexes: appropriate bulk in the substituent ligands or in the dithiolate linker. To maintain this rotated structure throughout the redox levels required in the catalytic cycle of hydrogen production (Fe^IFe^I), or uptake ($Fe^{II}Fe^{II}$), remains a formidable challenge.

CHAPTER V

CYCLODEXTRIN AS AN ARTIFICIAL SECOND COORDINATION SPHERE FOR ACTIVE SITE MODELS*

Introduction

The naturally engineered pockets that bind the catalytic centers of metalloenzymes impart stability to unusual molecular structures that are poised to facilitate molecular transformations. This is readily seen in the protein environment that surrounds the active site of diiron hydrogenase, [FeFe]-H_2ase, Figure V-1, an enzyme that produces H_2 at an efficiency comparable to that of the noble metal platinum in fuel cells.[26-27,138]

While strong donation into the [FeFe] unit by the CN^- and thiolate ligands contributes to the reactivity of the active site, a number of secondary interactions[47] stabilize a unique geometry in the organoiron motif that allows formation of a reactive terminal hydride.[98] In addition to an appropriately-sized, largely hydrophobic cavity, dipole/hydrogen bonding interactions between nearby peptide residues and the cyanides

---

*Reproduced in part, with permission from: Singleton, M. L.; Reibenspies, J. H.; Darensbourg, M. Y. *J. Am. Chem. Soc.* **2010**, *132*, 8870. Copyright **2010** American Chemical Society.[139]

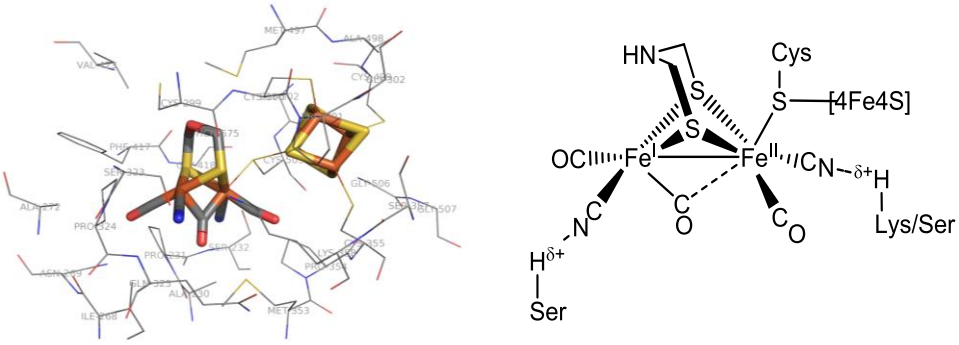

Figure V-1. Structure of the hydrogen producing H-cluster of [FeFe]-H_2ase in the protein environment (left) and as a Chemdraw figure (right) showing the important first and second coordination sphere interactions.

and semi-bridging carbonyl, result in the conservation of an open site in both the $Fe^{I}Fe^{II}$ and $Fe^{I}Fe^{I}$ states.[45] This important feature has been obtained in mixed valent $Fe^{I}Fe^{II}$ synthetic analogues of the oxidized enzyme active site; however, reduction back to $Fe^{I}Fe^{I}$ results in rearrangement to the all terminal CO conformation and loss of the open site.[64-65,102,128,136] Thus a major goal for modeling the active site should be to identify and evaluate supramolecular constructs that might enforce constraints mimicking the natural binding cavity of the [FeFe]-H_2ase active site. While there are several reports of the direct attachment of the diiron complexes to solid supports, such as electrode surfaces and resin beads, there are very few reported approaches to the application of a macromolecule as a support for models of the enzyme active site.

The Ott, Sun, and Song groups have for the last several years worked to develop photodriven systems, based on the direct attachment of a model complex to a supramolecular photosensitizer. These complexes are more directly aimed at mimicking the electron shuttle that is present in the enzyme than at modeling the specific second

coordination sphere surrounding the diiron active site. Because they have to use the hexcarbonyl derivatives for optimal electron transfer from the photosensitizer, they also suffer from the low reactivity of these complexes. These systems use zinc porphyrins,[74] ruthenium (II) trisbipyridenes, [140] or even C_{60} as their supramolecular supports.[75-76] Prior to the excitation of the photosensitizer, these complexes have not been shown to have a large effect on the properties of the model complexes.

In 2007, Jones and co-workers reported the attachment of a diiron complex to a 36 residue artificial peptide.[141] The diiron moiety was directly attached to the protein through two cystienes in the peptide. The secondary structure of the peptide was probed using circular dichroism and indicated that the ability of the peptide to maintain the α-helical structure after attachment of the model complex was dependent on the number of amino acids located between the two cystiene residues. While it provides one of the best direct models of the amino acid environment surrounding the peptide, no evidence of different structure or reactivity was reported for the bound complex versus the unbound species. Furthermore, the actual environment around the model complex was not investigated beyond the fact that it was attached to the peptide.

Based on inferences from the structure of the enzyme active site and the second coordination sphere effects that have been reported, the ideal host molecule would have the following properties: 1) It would provide site isolation, preventing interaction with neighboring molecules and dissuading ligand dissociation; 2) It would be small enough to provide steric constraints on the model complexes; 3) It would have a largely hydrophobic cavity similar to the active site cavity; and 4) It would have functional

groups capable of providing hydrogen bonding and dipole-dipole interactions. While a number of host molecules that could provide these effects have been reported, the commercial availability and extensive literature on their reactivity makes cyclodextrins an appealing candidate. Cyclodextrins are cyclic oligomers of glucose that result from the enzymatic degradation of starch.[142] The most common cyclodextrins are classified by the number of glucose units they contain with α having 6, β having 7 and γ having 8 units. (Figure V-2A) The intramolecular interactions between neighboring hydroxyl groups on the cyclodextrin provide a degree of rigidity to a structure that is best described as a conical frustum. The interior cavity ranges in diameter from 4.5 – 9.5 Å depending on the class of cyclodextrin but all three listed above are ~8 Å in height. It is this interior cavity that has made the cyclodextrins valuable as host molecules, allowing them to encapsulate a wide range of guests.

Cyclodextrins have properties long recognized as ideal for biomimetics.[142] Their hydrophobic cavities have in fact been demonstrated to serve as hosts for organometallics[143] and the hydrophilic hydroxyl rims provide hydrogen bonding sites. A classic example is the inclusion of ferrocene in α-, β-, and γ- cyclodextrin, the adducts of which have all been structurally characterized.[144] (Figure V-2B) Modficiation of the cyclopentadienyl rings with functional groups capable of acting as hydrogen bond acceptors have been shown to enhance the stability of the inclusion complex. A beautiful

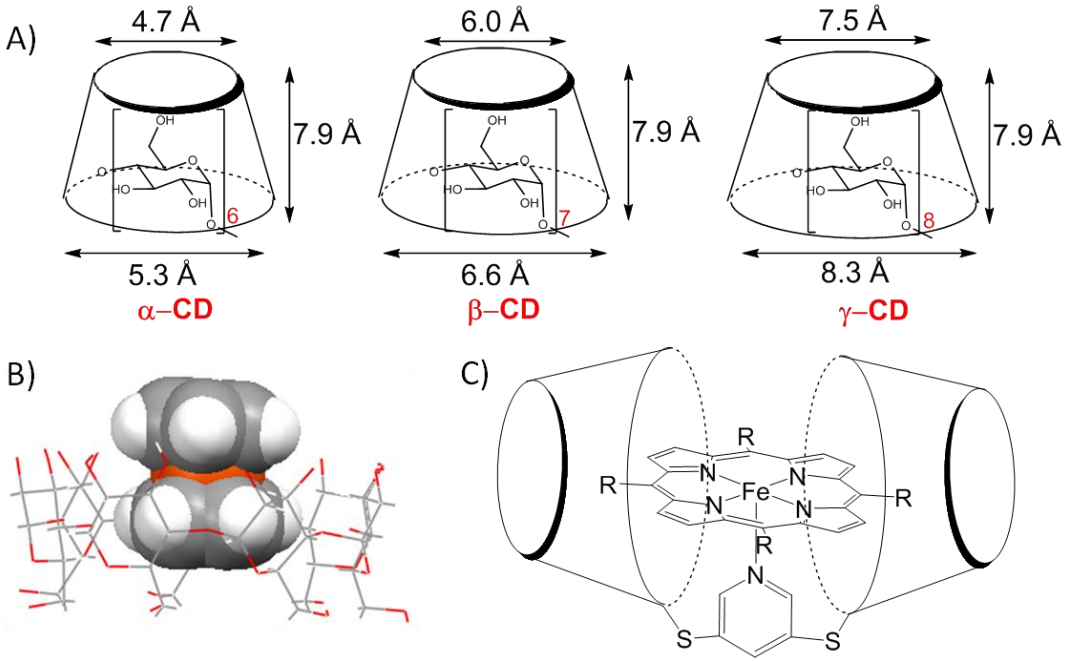

Figure V-2. A) Diagram of α-, β-, and γ-cyclodextrins B) Crystal structure of ferrocene in β-cyclodextrin C) Cartoon diagram of the biomimetic cyclodextrin system developed by Kano and co-workers. R = -*p*-$C_6H_4SO_3^-$.

example of the application of cyclodextrins in a biomimetic metal based systems was reported by Kano and co-workers. (Figure V-2C)[145] Using a dimeric cyclodextrin system, where the two cyclodextrins were connected at the 2 position via a pyridine linker, they were able to strongly bind an iron tetrakis(4-sulfonatophenyl)porphyrin. The cyclodextrin super structure provided a high degree of site isolation and allowed the iron porphyrin to bind oxygen in water without forming any μ-oxo species. The same group also showed that the O_2 binding capabilities of the porphyrin cyclodextrin adduct exceeded that of both hemoglobin and myoglobin. While highly successful cyclodextrin containing biomimetic models such as this are not common, the inherent inclusion properties of cyclodextrins and the extensive literature on methods to modify them make

them ideally suited for studying the effects of inclusion in a cavity on models of [FeFe]-hydrogenase.

In this chapter, the approach to the inclusion of a small molecule model of the [FeFe]-H_2ase active site, (μ-$SCH_2N(C_6H_4SO_3^-)CH_2S)[Fe^I(CO)_3]_2$, within β-CyD, and the X-ray crystal structure of the sodium salt of the $Na^+(\mu$-$SCH_2N(C_6H_4SO_3^-)CH_2S)[Fe^I(CO)_3]_2 \cdot 2$ β-CyD$\cdot 28$ H_2O clathrate is described.

Synthesis of Water Soluble $Na^+(\mu$-$SCH_2N(C_6H_4SO_3^-)CH_2S)[Fe^I(CO)_3]_2$, V-1

An inherent difficulty associated with the encapsulation of the model complexes in cyclodextrin is the drastically differing solubilities of the host and guest molecules. The diiron models are typically insoluble in aqueous solutions, and very few examples of water soluble systems have been reported. In contrast, natural cyclodextrins are only soluble in highly polar media such as water, DMSO, or DMF. Based on the success of the porphyrin system reported by Kano, for the diiron guest in our system, an aryl sulfonate group was incorporated into the dithiolate linker via the condenstation pathway reported by Rauchfuss and co-workers, Figure V-3.[92] The product $Na^+(\mu$-$SCH_2N(C_6H_4SO_3^-)CH_2S)[Fe^I(CO)_3]_2$, was a bright orange-red solid that was sparingly water soluble. Solubility tests indicated that a maximum concentration of ~1.1 mM $Na^+(\mu$-$SCH_2N(C_6H_4SO_3^-)CH_2S)[Fe^I(CO)_3]_2$ could be obtained in pure water, but addition of a salt (NaCl, Et_4NCl, or Ph_3PNPPh_3Cl) resulted in salting out of the iron complex. While the nitrogen of the azadithiolate in non-analinic dithiolates reacts with both protons and methylating agents, the nitrogen of **V-Na^+1** reacted with neither triflic

acid nor methyl triflate. In fact, the only product observed from reaction with methyl triflate showed methylation of the sulfonate, (Figure V-4).

X-ray diffraction quality crystals of the tetraethylammonium salt $Et_4N^+(\mu\text{-}SCH_2N(C_6H_4SO_3^-)CH_2S)[Fe^I(CO)_3]_2$ were obtained from diffusion of ether into a concentrated solution of $Et_4N^+(\mu\text{-}SCH_2N(C_6H_4SO_3^-)CH_2S)[Fe^I(CO)_3]_2$ in DMF. The structure of $Et_4N^+(\mu\text{-}SCH_2N(C_6H_4SO_3^-)CH_2S)[Fe^I(CO)_3]_2$ (Figure V-5) is overall very similar to the related complex $(\mu\text{-}SCH_2N(C_6H_5)CH_2S)[Fe^I(CO)_3]_2$, with the sulfonate group showing no significant effects on the structure. Molecular modeling studies predicted a similar structure for $(\mu\text{-}SCH_2N(C_6H_4SO_3^-)CH_2S)[Fe^I(CO)_3]_2$ and were used to examine which cyclodextrin, α- β- or γ-, would best interact with the diiron complex.

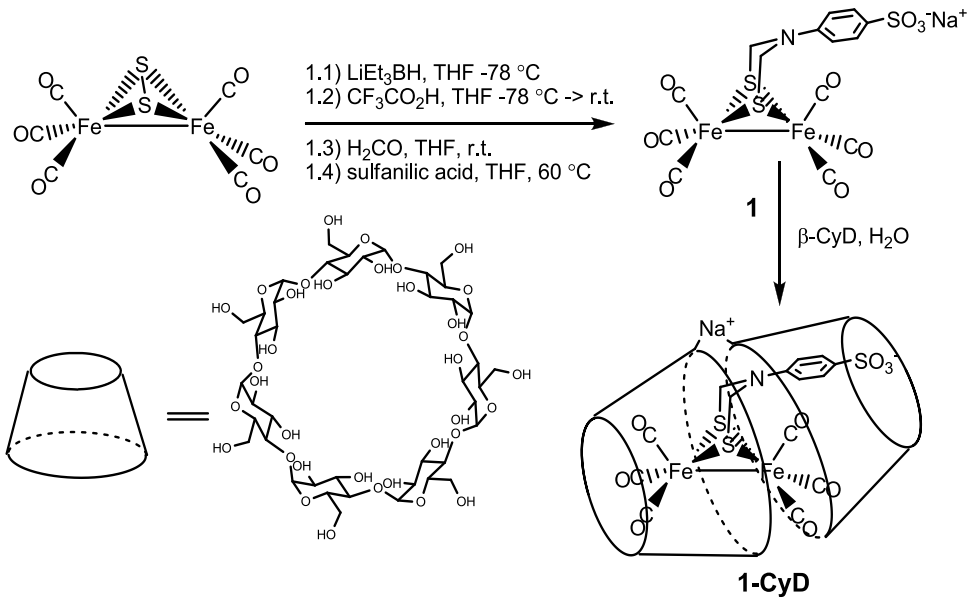

Figure V-3. Synthetic route to inclusion of a model complex in β-cyclodextrin

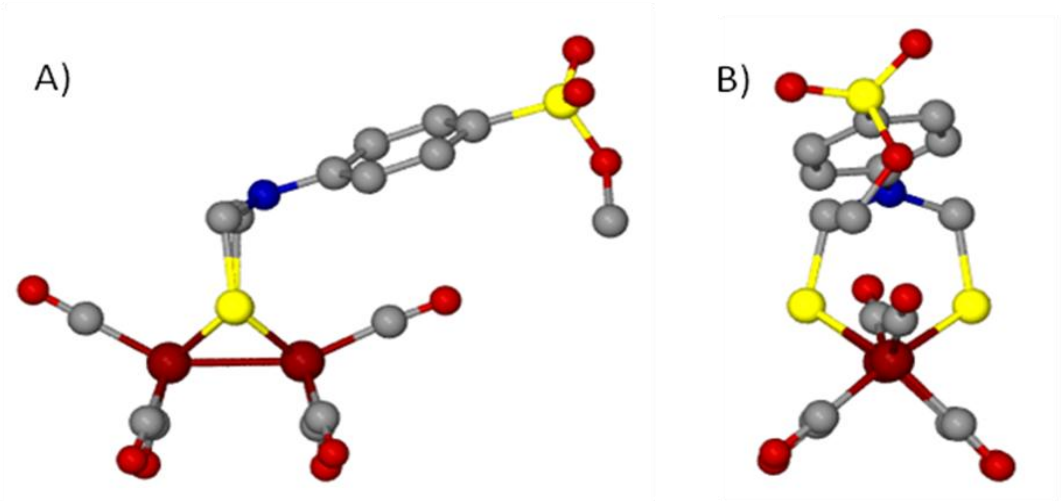

Figure V-4. Ball and stick representation of the X-ray determined structure of the methylated (μ-$SCH_2N(C_6H_4SO_3^-)CH_2S)[Fe^I(CO)_3]_2$ as viewed A) perpendicular to the FeFe bond vector, and B) along the FeFe bond vector.

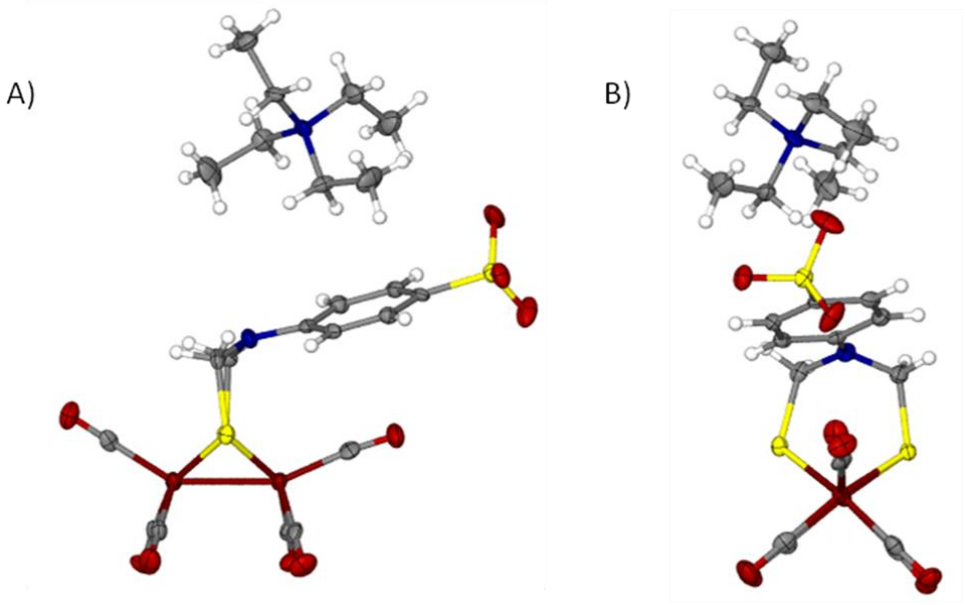

Figure V-5. Thermal ellipsoid plot of **V-1** at 50% probability viewed A) perpendicular to the FeFe bond vector, and B) along the FeFe bond vector.

From these studies β-cyclodextrin was found to be large enough to allow adequate penetration by the aryl sulfonate group while still being small enough to provide interactions with the diiron moiety.

Interaction with β-Cyclodextrin

On addition of β-CyD to an aqueous slurry of $Na^{+}(\mu\text{-}SCH_2N(C_6H_4SO_3^{-})CH_2S)[Fe^{I}(CO)_3]_2$, the latter completely dissolved. ESI mass spectral data indicated a peak bundle at m/z = 1671 representative of a 1:1 adduct in this solution. Infrared spectral monitoring also found a shift in the ν(CO) bands of **V-Na^{+}1** to higher wave numbers, as the β-CyD ratio was increased, Figure V-6.

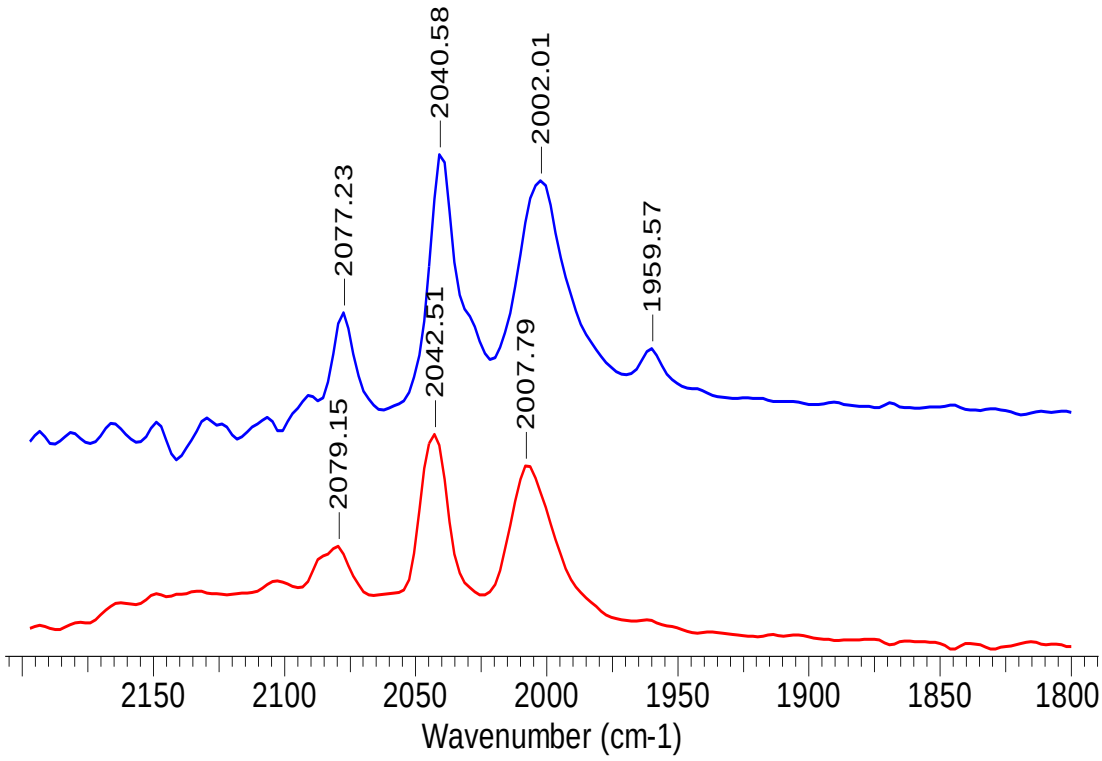

Figure V-6. Comparison of the ν(CO) IR spectra in H_2O of **V-Na$^+$1** in the absence (top) and presence (bottom) of 10 equivalents of β-cyclodextrin

Crystals of X-ray diffraction quality were obtained by carefully layering a concentrated aqueous solution of **V-1-CyD** with a dilute aqueous solution of $[Ph_3P{=}N{=}PPh_3]^+Cl^-$. While the latter was necessary for crystal growth, the red needles that resulted on standing for two weeks were of the Na^+ salt only. The structure of **V-1-CyD** shows two β-CyD molecules serve as hosts to one [FeFe]-model complex guest, Figure V-7. As anticipated, the aryl group of **1** is entirely encapsulated and the sulfonate projects through the primary hydroxyl rim of the β-CyD. The apical CO ligand of the $Fe(CO)_3$ unit on the same side is also enclosed within the cyclodextrin cavity while the basal CO's are close to the secondary hydroxyl rim. The $Fe(CO)_3$ group distal to the aryl

sulfonate is encapsulated by the second β-CyD. The two β-CyD units interact with one another through hydrogen bonds that form between the secondary hydroxyl groups on the rim and also through ion-dipole interactions with the Na^+ counterion. This Na^+ links the two β-CyD's together and also interacts with neighboring units in the extended 2-dimensional crystalline array, Figure V-7. A total of 28 water molecules per Na^+ **V-1**·2 β-CyD unit are also in the crystal lattice, with four located near, or closing off, the end of the cyclodextrin nanocapsule opposite the sulfonate. No water molecules are located in the inner part of the cyclodextrin construct. The hydrophobic character of the 2 β-CyD cavity is emphasized by comparison of the electrostatic potential plots of **V-1-CyD** and

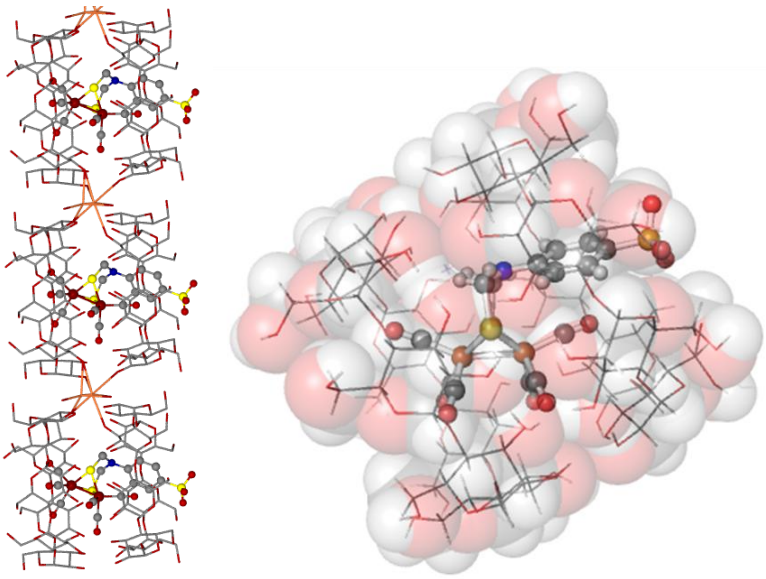

Figure V-7. Extended structure (left) and unit cell (right) of **V-1-CyD**. Protons and water molecules have been removed for clarity

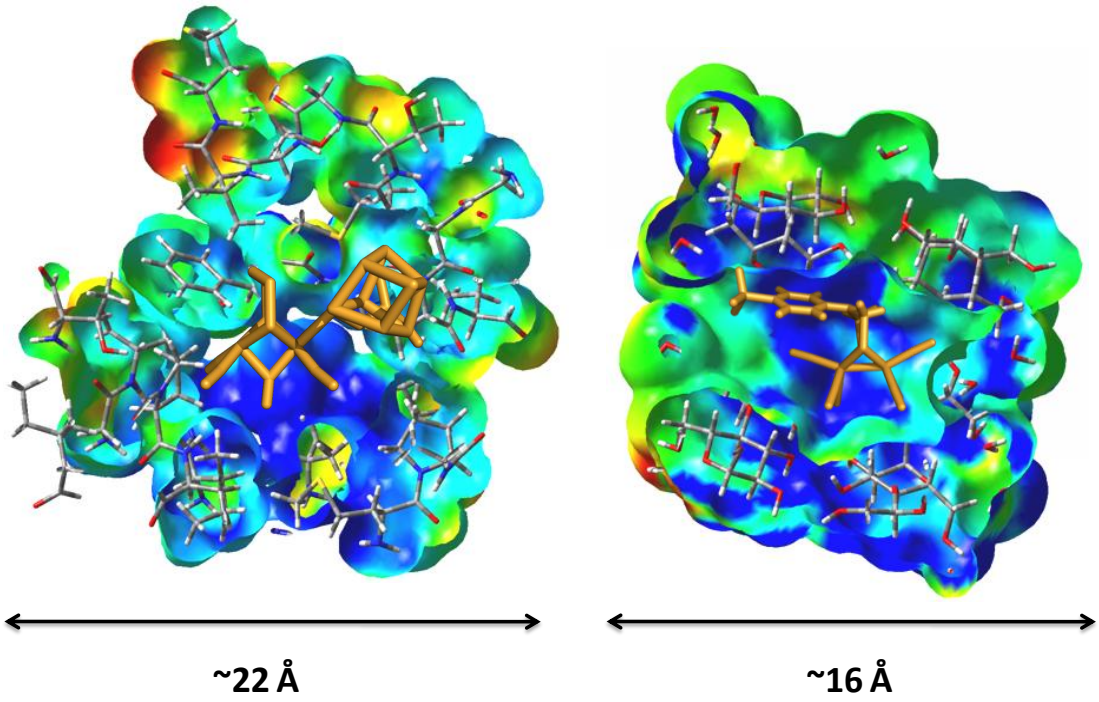

Figure V-8. Comparison of the electrostatic potential maps of the enzyme active site cavity(left) and the cyclodextrin cavity of **V-1-CyD** (right). Stick models of the diiron components are overlayed to show the orientation of the cavities.

that of the FeFe-H_2ase active site cavity which includes a ~22 Å amino acid sphere, Figure V-8.While the Fe-Fe bond distance of the included complex is not significantly altered from that of the free complex, 2.502(2) vs 2.499(1) Å, respectively, there are some minor structural differences between the structures of $Na^+(\mu\text{-}SCH_2N(C_6H_4SO_3^-)CH_2S)[Fe^I(CO)_3]_2$ and of $(\mu\text{-}SCH_2N(C_6H_4SO_3^-)CH_2S)[Fe^I(CO)_3]_2$ as found in the cyclodextrin clathrate. Most important is a ca. 20° increase in the torsion angle between

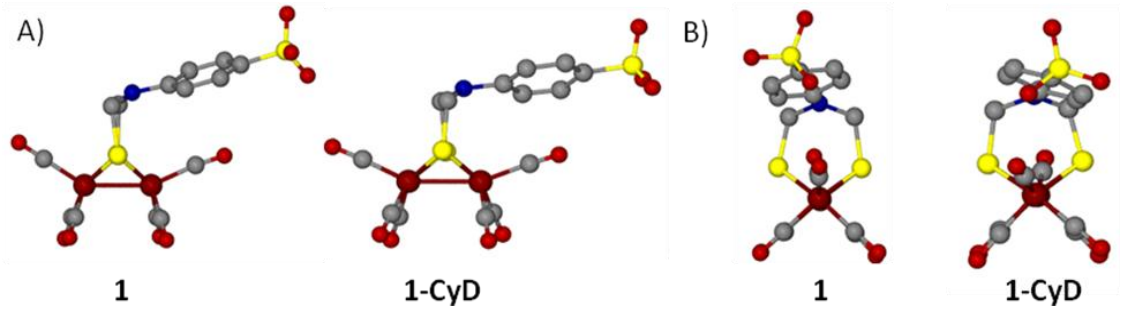

Figure V-9. Comparison of the ball and stick models of the free and encapsulated guest molecules as viewed from A) perpendicular to the FeFe bond vector and B) along the FeFe bond vector. The cyclodextrins are omitted for **V-1-CyD** and the protons and counterions for both complexes are omitted for clarity.

the apical CO groups of the $Fe(CO)_3$ sub-units in $Na^+(\mu\text{-}SCH_2NH(C_6H_4SO_3)CH_2S)[Fe^I(CO)_3]_2$ vs. $Na^+(\mu\text{-}SCH_2N(C_6H_4SO_3^-)CH_2S)[Fe^I(CO)_3]_2\cdot\beta$-cyclodextrin indicating destabilization of the more eclipsed conformation (Figure V-9).

NMR studies of inclusion in β-cyclodextrin

Evidence for inclusion complex formation in solution comes from the ^1H NMR studies in D_2O. As the mole fraction of β-CyD is increased there is a significant upfield shift in the aromatic protons of **1**, with a concomitant downfield shift for the methylene protons in the dithiolate linker. Similarly, ^{13}C NMR spectra show an ~1.0 ppm shift in the single CO resonance at 206.9 ppm. In the cyclodextrin range, the ^1H NMR spectra exhibit only minor shifts with variation in **[V-Na^+1]** ($\Delta\delta$ of ±0.02) for most of the ^1H resonances. (Figure V-10) However the C3 and C5 protons shift by 0.10 and 0.19 ppm respectively. The large change for these intracavity protons is reported to be indicative

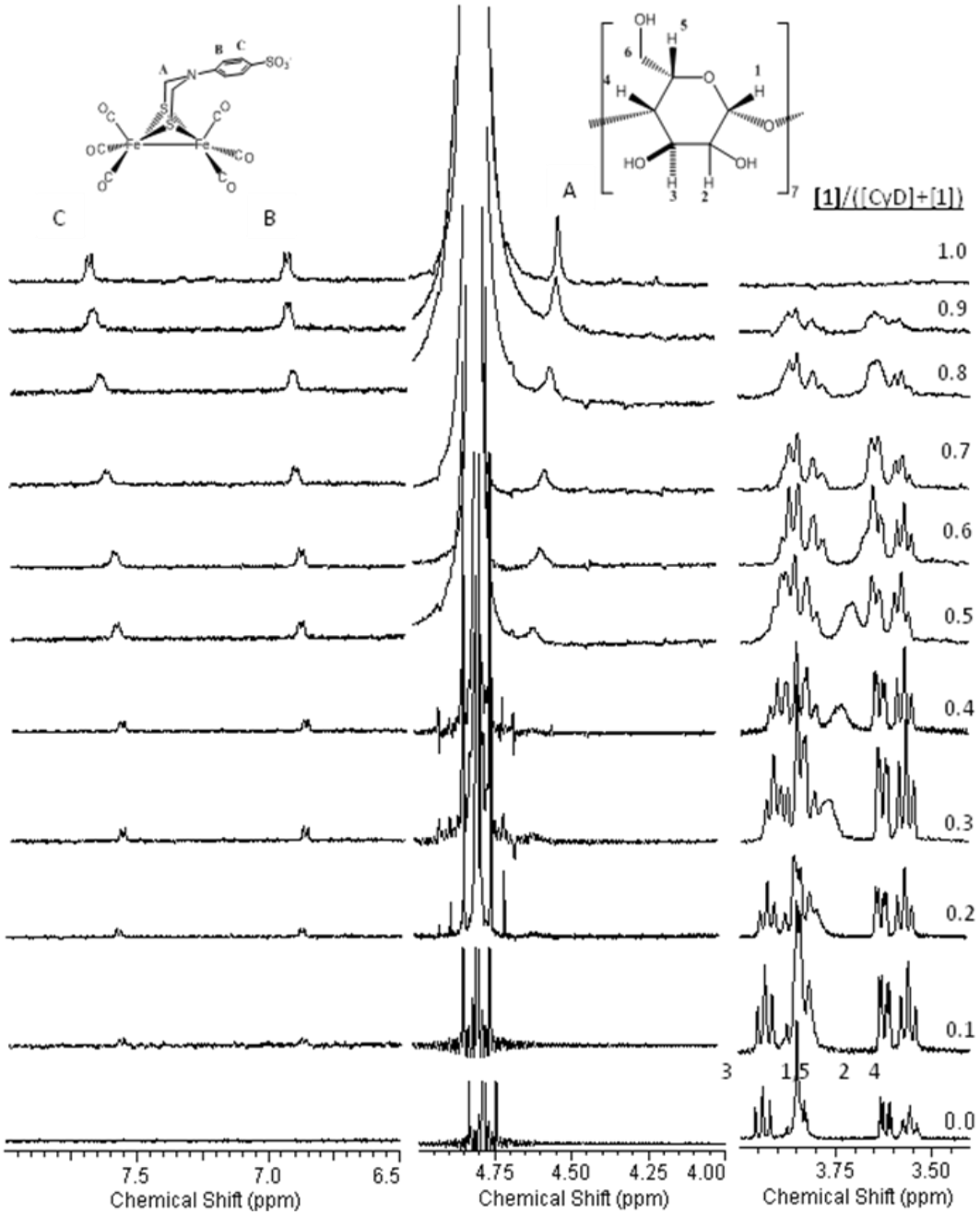

Figure V-10. Effect on the ^{1}H NMR spectra of **V-Na^{+}1** as the ratio [Guest]/([Guest]+[Host]) is varied from 0 (bottom most spectrum) to 1 (top).

of inclusion within the β-CyD cavity.[146] Averaged Job plots based on these changes have maxima near 0.5 indicating a 1:1 β-CyD:[**V-Na$^+$1**] ratio in solution, Figure V-11.[16] [N.B.: The accuracy of Job plots can be highly dependent on the nature of the binding constant of the first and second β-CyD units, making this assignment tentative.

While the changes in the chemical shift provide good evidence that the inclusion complex is forming in solution, at no point were separate signals observed for the free and encapsulated **V-Na$^+$1** indicating that the rate of exchange in and out of the cyclodextrin cavity is faster than can be observed by NMR. Even upon cooling to 5 °C in the presence of 10 equivalents of cyclodextrin only a single broad signal in the ^{13}C NMR

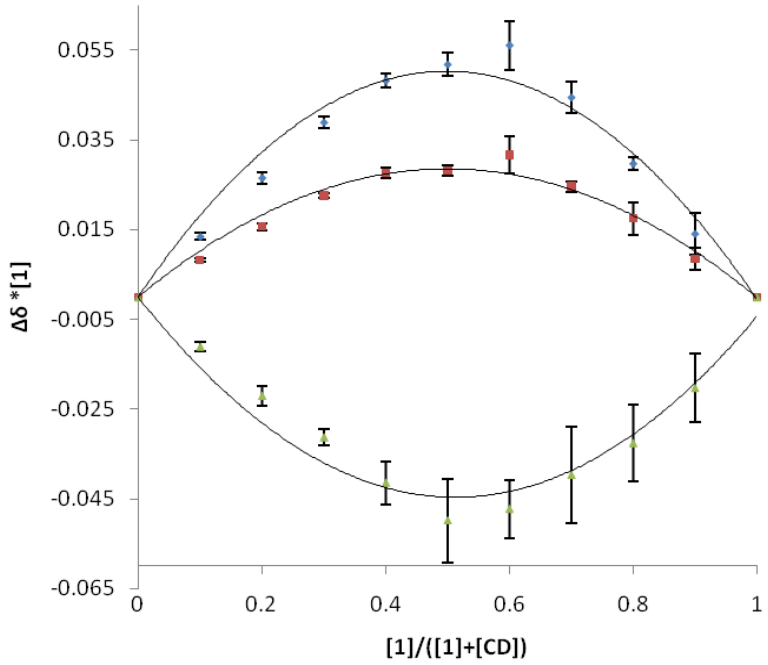

Figure V-11. A Job plot based off of the average data collected from three NMR studies using the continuous variation method and data given in Figure V-10. Changes are recorded for the: Square: Aromatic proton signal at 6.68 ppm; Diamond: Aromatic proton signal at 7.73 ppm; Triangle: Methylene protons of **Na$^+$1** at 4.53 ppm.

spectrum is observed for all six CO ligands. (Figure V-12) These results are not only consistent with the fact that the complex is exchanging rapidly in and out of the cyclodextrin but also, and likely due to this exchange, that the cyclodextrin architecture does not prevent the well studied intramolecular dynamic processes observed in similar diiron systems.[85]

Effect of Cyclodextrin on the Electrochemical Properties of Na^+(μ-$SCH_2NH(C_6H_4SO_3^-)CH_2S)[Fe^I(CO)_3]_2$

Despite the apparent instability of **V-1-CyD**, the formation of the inclusion complex still produces interesting changes in the electrochemical properties of **V-Na^+1**. Because no electrochemical studies on the myriad Fe^IFe^I model complexes have been performed in pure water, the free guest Na^+(μ-$SCH_2N(C_6H_4SO_3^-)CH_2S)[Fe^I(CO)_3]_2$ was first studied in CH_3CN for direct comparison to other model complexes. Similar to most (μ-SRS)$[Fe(CO)_3]_2$ models, Na^+(μ-$SCH_2N(C_6H_4SO_3^-)CH_2S)[Fe^I(CO)_3]_2$ shows both a mostly irreversible reduction near -1600 mV and and an irreversible oxidation at 640 mV versus the ferrocene/ferrocenium couple. The complex also has an electrocatalytic response to HOAc (presumably H_2 production) and in CH_3CN solution has very similar redox properties as (μ-$S(CH_2)_3S)[Fe(CO)_3]_2$,[137] showing a response (increase in current) to added increments of HOAc at a potential more negative than the Fe^IFe^I/Fe^IFe^0, presumably its Fe^0Fe^0 redox level. (Figure V-13) From these studies it is obvious that the addition of the sulfonate has not dramatically changed the redox properties of the model complex. In 10 mM aqueous NaCl solution, **V-Na^+1** shows an irreversible

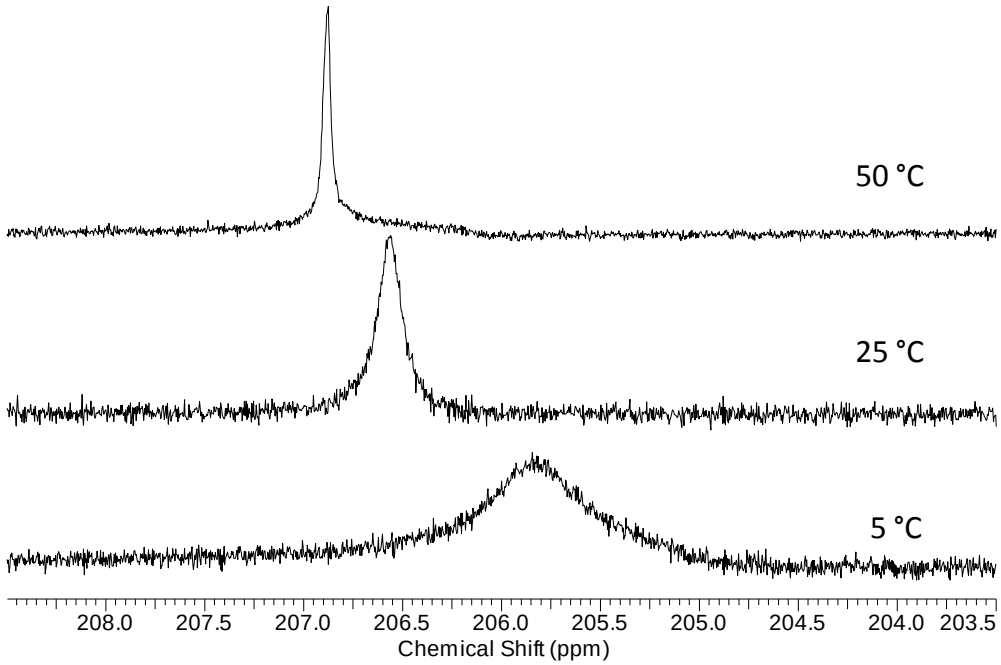

Figure V-12. Effect of temperature on the ^{13}C CO-carbon linewidth of **Na^+1** in the presence of 10 equivalents of cyclodextrin.

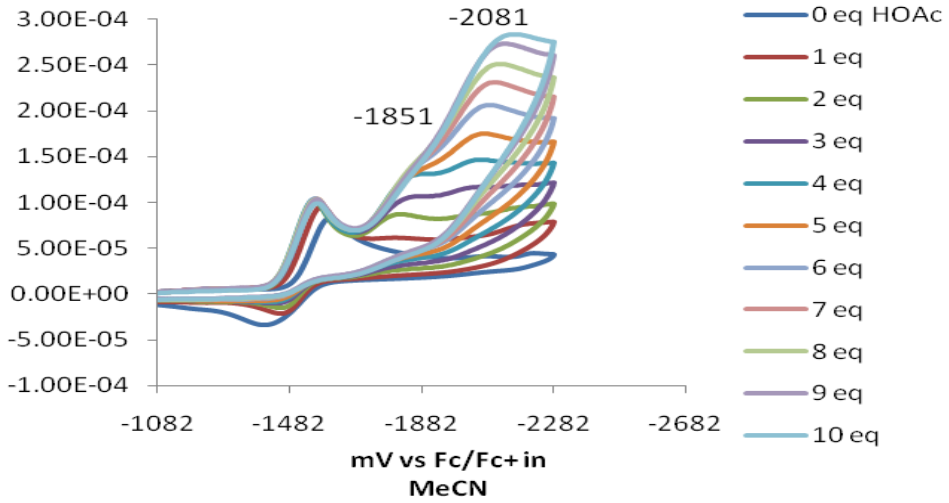

Figure V-13. Cyclic voltammograms (Bottom) showing the effect of incremental additions of HOAc to **Na^+1** in MeCN with 0.100 M Et_4NBF_4 as electrolyte. Cyclic voltammograms were run at a scan rate of 200 mV/sec. Marked potentials are relative to the Fc/Fc^+ couple as 0.00 V.

reduction at -1.15 mV and irreversible oxidation at 830 mV versus Ag/AgCl. Addition of 10 equivalents of β-cyclodextrin to the solution does not affect the potential at which oxidation occurs, but results in an ~80 mV shift of the $Fe^{I}Fe^{I}/Fe^{I}Fe^{0}$ reduction to a more negative potential. (Figure V-14) A decreased current response is also observed for both the reduction and oxidation. In other cyclodextrin systems this has been reported to be the result of a smaller diffusion coefficient for the supramolecular system, relative to the free guest. The addition of cyclodextrin also has a pronounced effect on the proton

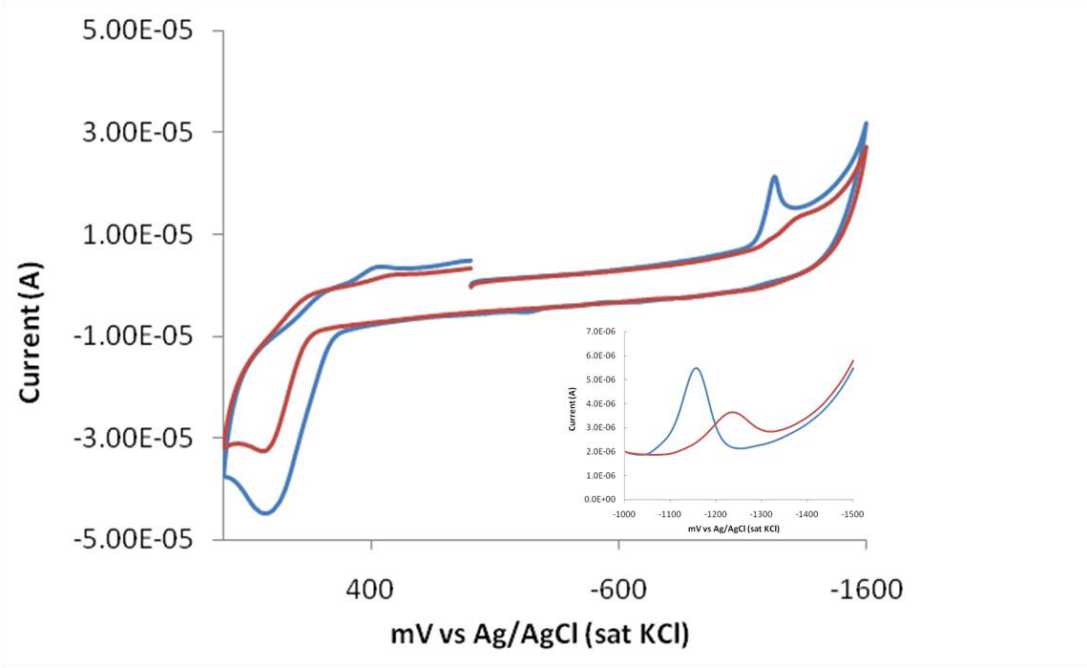

Figure V-14. Cyclic voltammogram of **V-Na^{+}1** before the addition of cyclodextrin (blue) and after the addition of 10 equivalents of β-cyclodextrin (red) in 0.01 M aqueous NaCl electrolyte solution at a scan rate of 200 mV/sec. Inset shows differential pulse voltammogram from -1000 mV to -1500 mV for **V-Na^{+}1** before the addition of cyclodextrin (blue) and after the addition of 10 equivalents of β-cyclodextrin (red). Marked potentials are relative to the Ag/AgCl (sat. KCl) couple as 0.00 V.

reduction capabilities of the model complex.

In the 10 mM NaCl buffer solution, HOAc can be reduced by glassy carbon at ~-1200 mV versus Ag/AgCl, however the response is weak (5.5 μA / mM HOAc). In the presence of free **V-Na$^+$1** the potential for proton first reduction is at -1180 mV and overlaps significantly with the reduction of HOAc on glassy carbon. (Figure V-15) Despite this, the participation of the diiron complex in proton reduction is observed by an increase in the current response that is three times larger (16.6 μA / mM HOAc) than that of glassy carbon. This response is also greater than that observed for the reduction of HOAc by free **V-Na$^+$1**. Once scaled to take into account the amount of catalyst present in both solutions ([Na^+(μ-$SCH_2N(C_6H_4SO_3^-)CH_2S$)[$Fe^I(CO)_3]_2$] = 0.11 mM in water and 2.0 mM in CH_3CN) and the current from reduction on glassy carbon is subtracted, there is an almost 10-fold increase in the catalytic response in water. While impressive, this is entirely due to the increased rate of proton transfer and the significantly lower pK_a of HOAC in water. It does however show that the efforts by the Darensbourg and Weigand groups for developing water soluble catalysts are valuable and should be further pursued.[130,147]

In the presence of cyclodextrin two reductive events are seen within the same window. The first, at -1200 mV, is attributed to the reduction of HOAc by glassy carbon and is consistent with control experiments with cyclodextrin but in the absence of any iron complex. The second event is attributed to reduction of protons by the diiron complex. This event has a greater electrocatalytic current response to added HOAc as compared to glassy carbon and occurs at more negative potential (-1.4 V). (Figure V-15)

This represents an over 200 mV negative shift in the potential for proton reduction by $Na^{+}(\mu\text{-}SCH_2N(C_6H_4SO_3^{-})CH_2S)[Fe^{I}(CO)_3]_2$ in the presence of cyclodextrin as compared to without it. Additionally this event occurs 170 mV more negative than the potential observed for the $Fe^{I}Fe^{I}/Fe^{I}Fe^{0}$ reduction in the presence of cyclodextrin. The negative

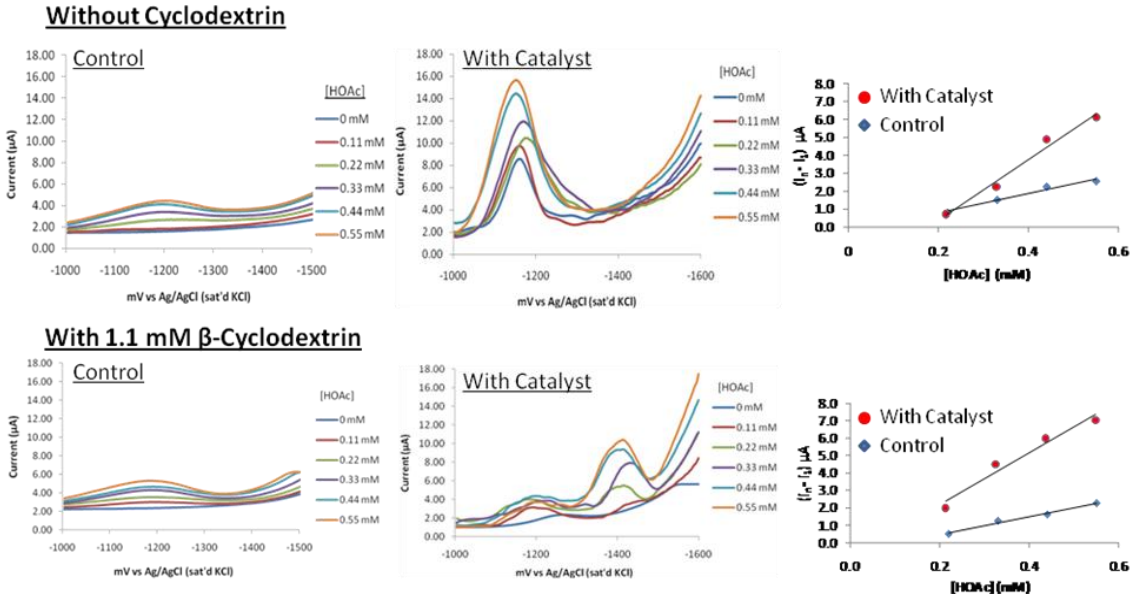

Figure V-15. Differential pulse voltammograms showing the effect of HOAc to top) 0.11 mM **V-Na^{+}1** in H_2O with 0.01 M NaCl electrolyte and bottom) 0.11 mM **V-Na^{+}1** in H_2O with 0.01 M NaCl electrolyte containing 1.1 mM β-CyD. Marked potentials are relative to the Ag/AgCl (sat. KCl) couple as 0.00 V.

shift has been attributed to the more hydrophobic nature of the cyclodextrin cavity resulting in reactivity similar to to that observed in CH_3CN where proton reduction occurs at a more negative potential than the first reduction. However, another reason exists that could also explain the large shift. The cyclodextrin may be slowing down a crucial fluxional process necessary for low potential proton reduction by the model complexex. Evans and co-workers have shown electrochemical evidence that such a

fluxional process exists in other hexacarbonyl systems.[137] Upon one electron reduction this fluxional process occurs allows the complex to take up another electron at a more positive potential. At slow scan rates this is observed as the initial reduction becoming a two electron process, while at fast scan rates it remains a one electron process. This could drastically affect the potential at which proton reduction occurs. Because the differential pulse voltammetry used to study the electrocatalytic proton reduction in the cyclodextrin system was run at a slow rate, this is unlikely to be the cause of the large negative shift, but it should not be ruled out until further electrochemical studies are conducted.

Ligand Substituted Complexes for Inclusion in Cyclodextrins

The changes in the electrochemical properties as described above resulted from the simplest combination of model complex and cyclodextrin, a hexacarbonyl model complex and an unmodified cyclodextrin. More complex systems that use ligand substituted derivatives of the sulfonate complexes and modified cyclodextrins should produce even more interesting results.

Two phosphine derivatives of $Na^{+}(\mu\text{-}SCH_2N(C_6H_4SO_3^{-})CH_2S)[Fe^{I}(CO)_3]_2$ have been synthesized following the reaction schemes shown in Figure V-16. The addition of PMe_3 to $Na^{+}(\mu\text{-}SCH_2N(C_6H_4SO_3^{-})CH_2S)[Fe^{I}(CO)_3]_2$ readily leads to the formation of the bis-PMe_3 product $Na^{+}(\mu\text{-}SCH_2N(C_6H_4SO_3^{-})CH_2S)[Fe^{I}(CO)_2PMe_3]_2$, however reaction with even an 20-fold excess of $P(OMe)_3$ only leads to the mono-substituted derivative, $Na^{+}(\mu\text{-}SCH_2N(C_6H_4SO_3^{-})CH_2S)[Fe^{I}(CO)_3][Fe^{I}(CO)_2P(OMe)_3]$. The position of the

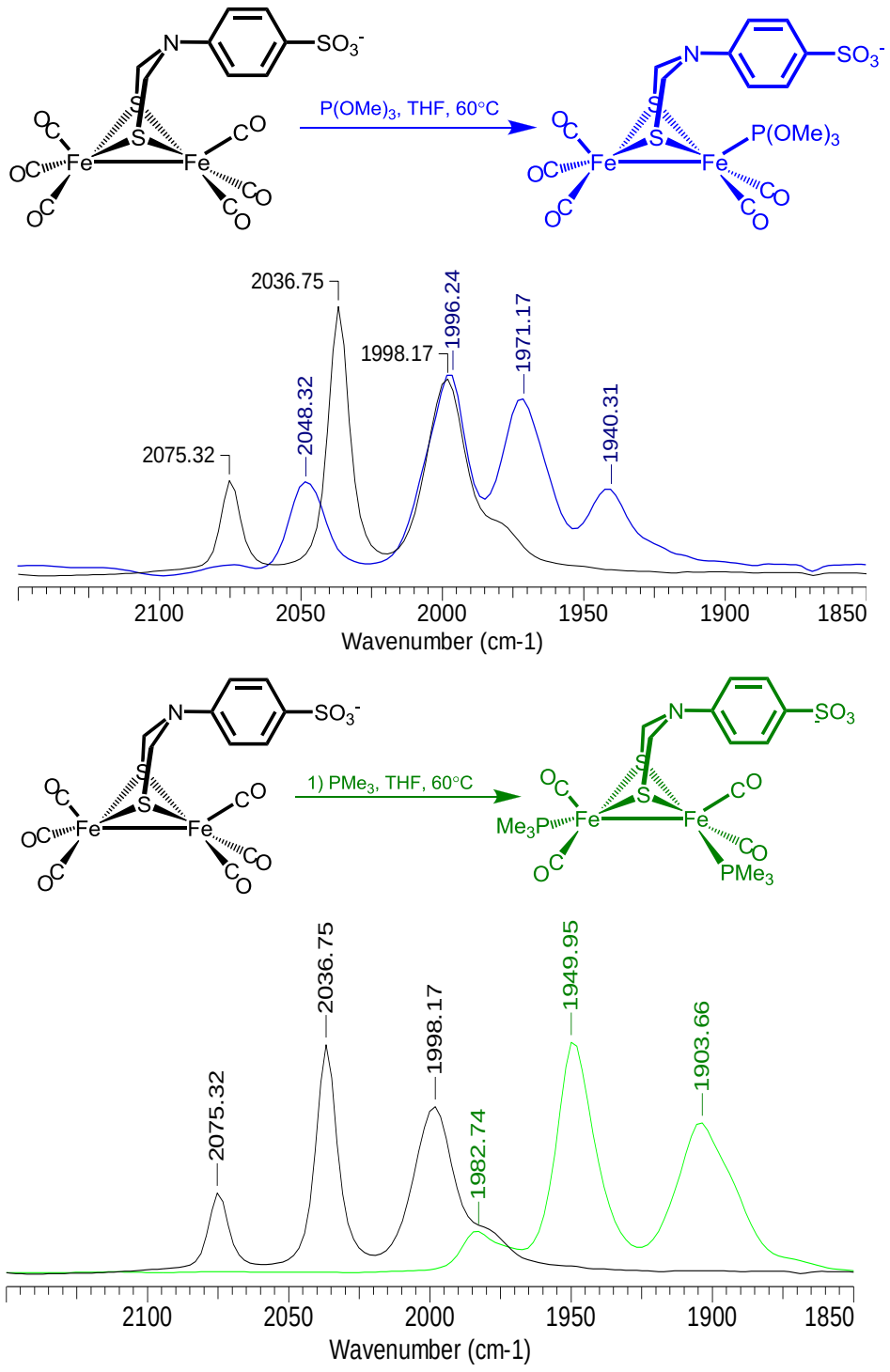

Figure V-16. Reaction scheme for the synthesis of top) $Na^{+}(\mu\text{-}SCH_2N(C_6H_4SO_3^{-})CH_2S)[Fe^{I}(CO)_3][Fe^{I}(CO)_2P(OMe)_3]$ and bottom) $Na^{+}(\mu\text{-}SCH_2N(C_6H_4SO_3^{-})CH_2S)[Fe^{I}(CO)_2PMe_3]_2$ the corresponding IR ν(CO) spectra. Spectra color match the corresponding complex in the reaction scheme.

v(CO) bands in the IR spectra are consistent with these degrees of substitutions, with the v(CO) bands of the $P(OMe)_3$ derivatives appearing in a range similar to the monosubstituted complexes described in Chapter III and the PMe_3 complex's v(CO) bands are at wavenumbers similar to the disubstituted complexes in Chapter IV, (Figure V-16). As with the hexacarbonyl complex, both derivatives are moderately water soluble.

The X-ray crystal structures of the tetraethylammonium salts of the phosphine substituted complexes (Figure V-17) were obtained from slow diffusion of ether into a CH_2Cl_2 solution of the respective complexes. In the $P(OMe)_3$ derivative, the phosphine ligand adopts an apical position on the iron opposite to the aryl sulfonate group. Apart from the new ligand, the core geometry and overall structure is identical to that of $Na^+(\mu\text{-}SCH_2N(C_6H_4SO_3^-)CH_2S)[Fe^I(CO)_3]_2$. This is not the case for the disubstituted, $Na^+(\mu\text{-}SCH_2N(C_6H_4SO_3^-)CH_2S)[Fe^I(CO)_2PMe_3]_2$ where the FeFe bond is elongated to ~ (2.599 (1) Å), representing an approximately 0.1 Å increase over the hexacarbonyl derivative and consistent with the reports described earlier where increased electron donation into the irons weakens the FeFe bond. The PMe_3 ligands adopt a trans-basal configuration similar to the bis-PMe_3 derivatives discussed in Chapter IV. However,

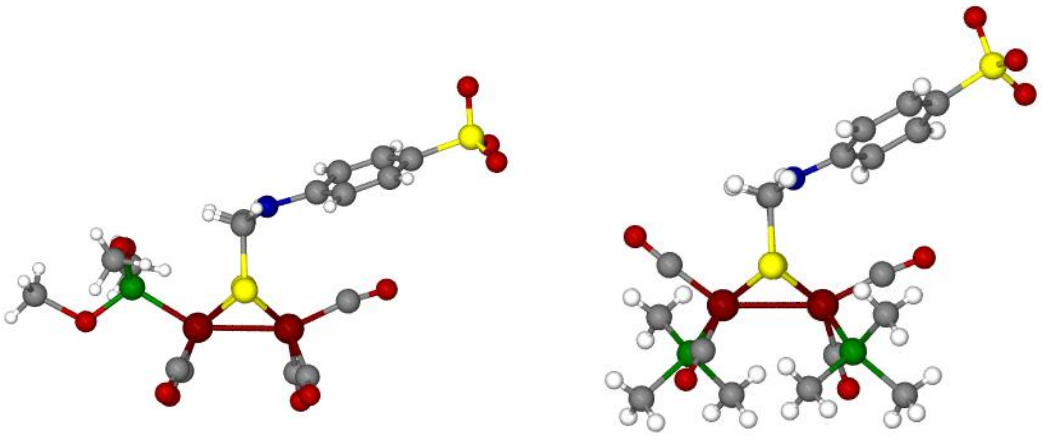

Figure V-17. Ball and stick representations of the solid state structures of left) $Na^{+}(\mu\text{-}SCH_2N(C_6H_4SO_3^{-})CH_2S)[Fe^{I}(CO)_3][Fe^{I}(CO)_2P(OMe)_3]$ and right) $Na^{+}(\mu\text{-}SCH_2N(C_6H_4SO_3^{-})CH_2S)[Fe^{I}(CO)_2PMe_3]_2$.

despite a similar configuration to the complexes in Chapter IV, no indication of a reversible oxidation was observed in the electrochemical studies.

The initial goal of using the substituted complexes was to obtain a complex that could be readily oxidized and encapsulated in the cyclodextrins. However, the cyclic voltammograms of $Na^{+}(\mu\text{-}SCH_2N(C_6H_4SO_3^{-})CH_2S)[Fe^{I}(CO)_2PMe_3]_2$ and $Na^{+}(\mu\text{-}SCH_2N(C_6H_4SO_3^{-})CH_2S)[Fe^{I}(CO)_3][Fe^{I}(CO)_2P(OMe)_3]$ show only irreversible electrochemical events, (Figure V-18), with changes in the potentials for oxidation and reduction behaving as expected upon increased donation into the irons. As the primary difference between $Na^{+}(\mu\text{-}SCH_2N(C_6H_4SO_3^{-})CH_2S)[Fe^{I}(CO)_2PMe_3]_2$ and the PMe_3 complexes discussed in Chapter IV is the dithiolate linker, the irreversibility is attributed to a process involving the sulfanilate moiety. However, the exact nature of this process remains unknown.

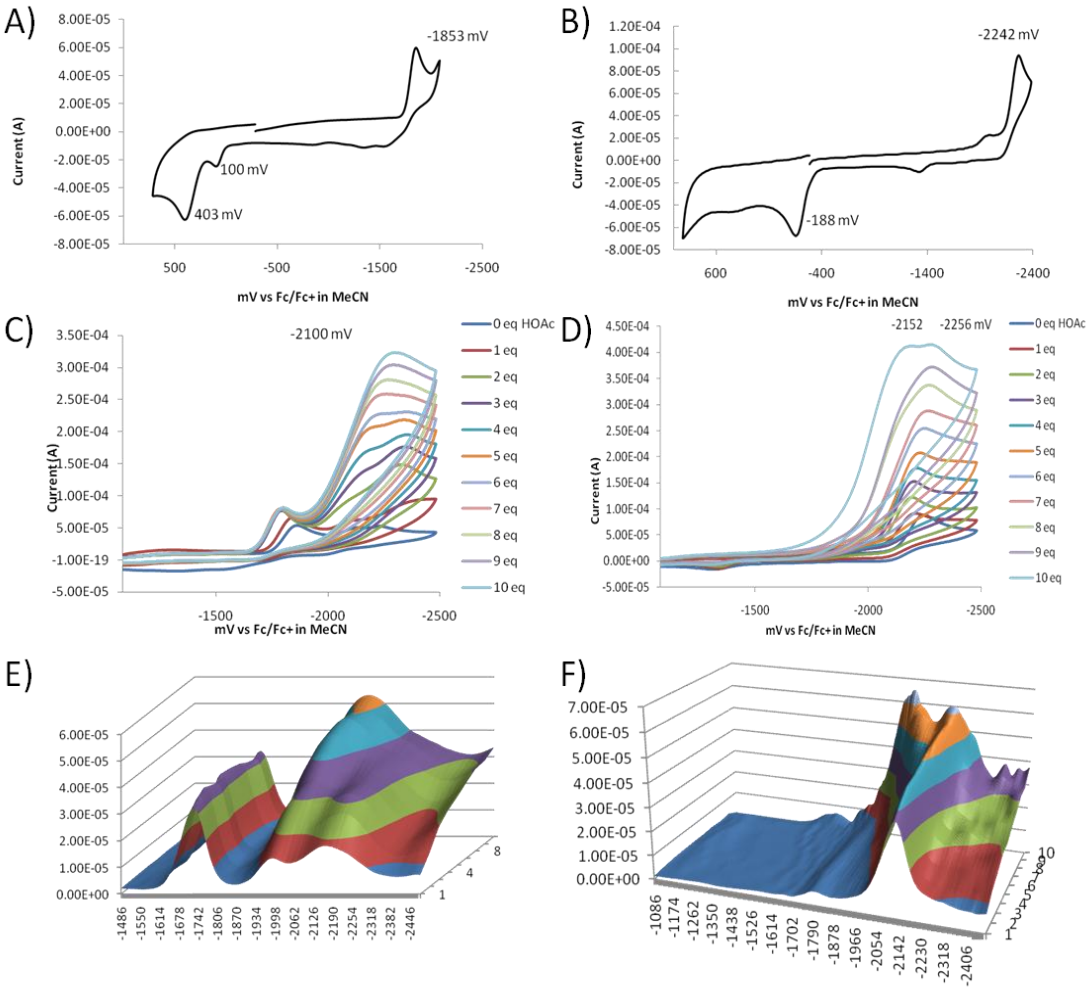

Figure V-18. Cyclic voltammograms of A) $Na^+(\mu\text{-}SCH_2N(C_6H_4SO_3^-)CH_2S)[Fe^I(CO)_3][Fe^I(CO)_2P(OMe)_3]$ (2mM) and B) $Na^+(\mu\text{-}SCH_2N(C_6H_4SO_3^-)CH_2S)[Fe^I(CO)_2PMe_3]_2$ (2mM) at 200 mV/s. Cyclic voltammograms showing the effect of incremental additions of HOAc to C) $Na^+(\mu\text{-}SCH_2N(C_6H_4SO_3^-)CH_2S)[Fe^I(CO)_3][Fe^I(CO)_2P(OMe)_3]$ and to D) $Na^+(\mu\text{-}SCH_2N(C_6H_4SO_3^-)CH_2S)[Fe^I(CO)_2PMe_3]_2$. Differential pulse voltammograms showing the effect of incremental additions of HOAc to E) $Na^+(\mu\text{-}SCH_2N(C_6H_4SO_3^-)CH_2S)[Fe^I(CO)_3][Fe^I(CO)_2P(OMe)_3]$ and to F) $Na^+(\mu\text{-}SCH_2N(C_6H_4SO_3^-)CH_2S)[Fe^I(CO)_2PMe_3]_2$. All voltammetric studies were run in MeCN with 0.100 M Et_4NBF_4 as electrolyte. All potentials are referenced to Fc/Fc^+ in CH_3CN.

Both of the substituted derivatives act as electrocatalysts for hydrogen production in CH_3CN as shown in Figure V-19. The phosphite derivative, $Na^+(\mu\text{-}SCH_2N(C_6H_4SO_3^-)CH_2S)[Fe^I(CO)_3][Fe^I(CO)_2P(OMe)_3]$, shows an increase in current intensity at c.a. -2.1 V upon incremental addition of HOAc. Differential pulse voltammetry also indicates a second event at a slightly more negative potential that has a weaker current response. As both of these events occur more than 200 mV more negative than the initial Fe^IFe^I/Fe^IFe^0 reduction the nature of the catalytic species is unknown. An increase in the current at the first reduction is observed for $Na^+(\mu\text{-}SCH_2N(C_6H_4SO_3^-)CH_2S)[Fe^I(CO)_2PMe_3]_2$ upon addition of HOAc. Unlike other reported bis-PMe_3 model complexes,[132] the event attributed to proton reduction by $Na^+(\mu\text{-}SCH_2N(C_6H_4SO_3^-)CH_2S)[Fe^I(CO)_2PMe_3]_2$ splits into two different events, that are separated by ~ 100 mV after the addition of 10 equivalents of HOAc. While the identity of these two electrochemically active species is unknown, the possibility that it could be two different conformations resulting in different potentials for proton reduction is intriguing and plausible based on the above-mentioned study by Evans and co-workers.[137] The use of spectroelectrochemical methods to monitor the changes in the complex during the catalytic cycle could help elucidate the nature of these species.

In water, $Na^+(\mu\text{-}SCH_2N(C_6H_4SO_3^-)CH_2S)[Fe^I(CO)_3][Fe^I(CO)_2P(OMe)_3]$ was not observed to acts as an electrocatalyst in the potential range studied. Even after 10 equivalents of HOAc, no increase in current at the Fe^IFe^I/Fe^IFe^0 reduction is observed. The use of differential pulse voltammetry for studying changes upon addition of HOAc, should prove useful in the ongoing work with this system, as the increased current may

not be significant enough to be observed due to the proximity of the reductive event to the solvent window. The reasons behind this lack of reactivity are still being studied. In contrast to the $P(OMe)_3$ derivative, $Na^+(\mu\text{-}SCH_2N(C_6H_4SO_3^-)CH_2S)[Fe^I(CO)_2PMe_3]_2$ is significantly more reactive. In the limited solvent window afforded in the 0.01 M NaCl solution, no Fe^IFe^I/Fe^IFe^0 reduction is observed. However, upon addition of increments of HOAc, a new reductive feature is observed. This event is attributed to the $Fe^{II}Fe^{II}/Fe^{II}Fe^I$ reduction of a hydride containing diiron complex. The potential for this event is observed to be dependent on the concentration of acid that is added, and gradually shifts from -1200 mV to ~ -1350 mV as ten equivalents of acid are added (Figure V-19). As the number of equivalents is increased the changes in the potential also become smaller appearing to reach a minimum for the reduction potential close to -1350 mV. This results from the concentration of the species being reduced being dependent on the concentration of the acid.

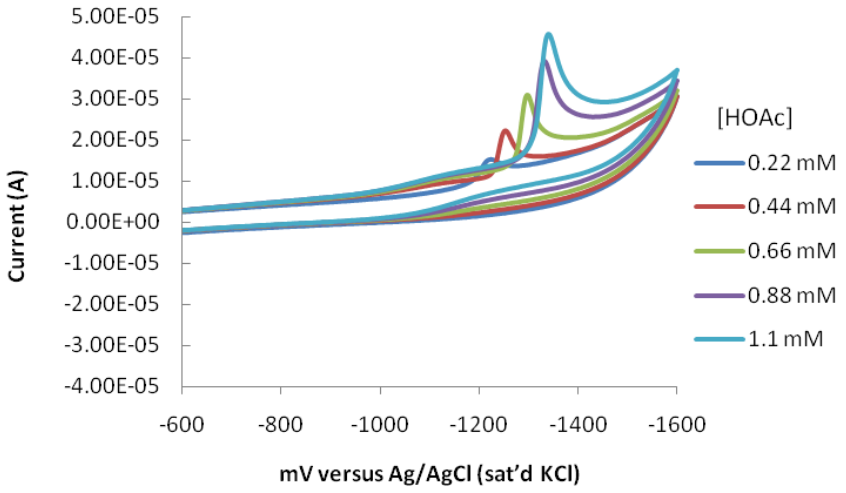

Figure V-19. Cyclic voltammograms of $Na^{+}(\mu\text{-}SCH_2N(C_6H_4SO_3^{-})CH_2S)[Fe^{I}(CO)_2PMe_3]_2$ showing effect of incremental additions of HOAc in 0.01 M aqueous NaCl solution. Potentials are referenced to Ag/AgCl (sat'd KCl).

Initial Inclusion Studies on the Substituted Derivatives

Similar to the hexacarbonyl complex, the addition of cyclodextrin to an aquesous slurry of $Na^{+}(\mu\text{-}SCH_2N(C_6H_4SO_3^{-})CH_2S)[Fe^{I}(CO)_3][Fe^{I}(CO)_2P(OMe)_3]$ immediately solubilizes the diiron complex. NMR studies, using similar methods as in the hexacarbonyl system, showed a upfield shift in the aromatic protons on the diiron complex as the mole fraction of β-cyclodextrin is increased. Additionally the upfield shift of the C3 and C5 protons on the cyclodextrin that is indicative of inclusion is also observed. (Figure V-20) A Job plot based on this data indicates that, similar to the hexacarbonyl system, a 1:1 inclusion complex is formed when the $P(OMe)_3$ derivative is used. On going NMR studies of interaction of the PMe_3 substituted complex with

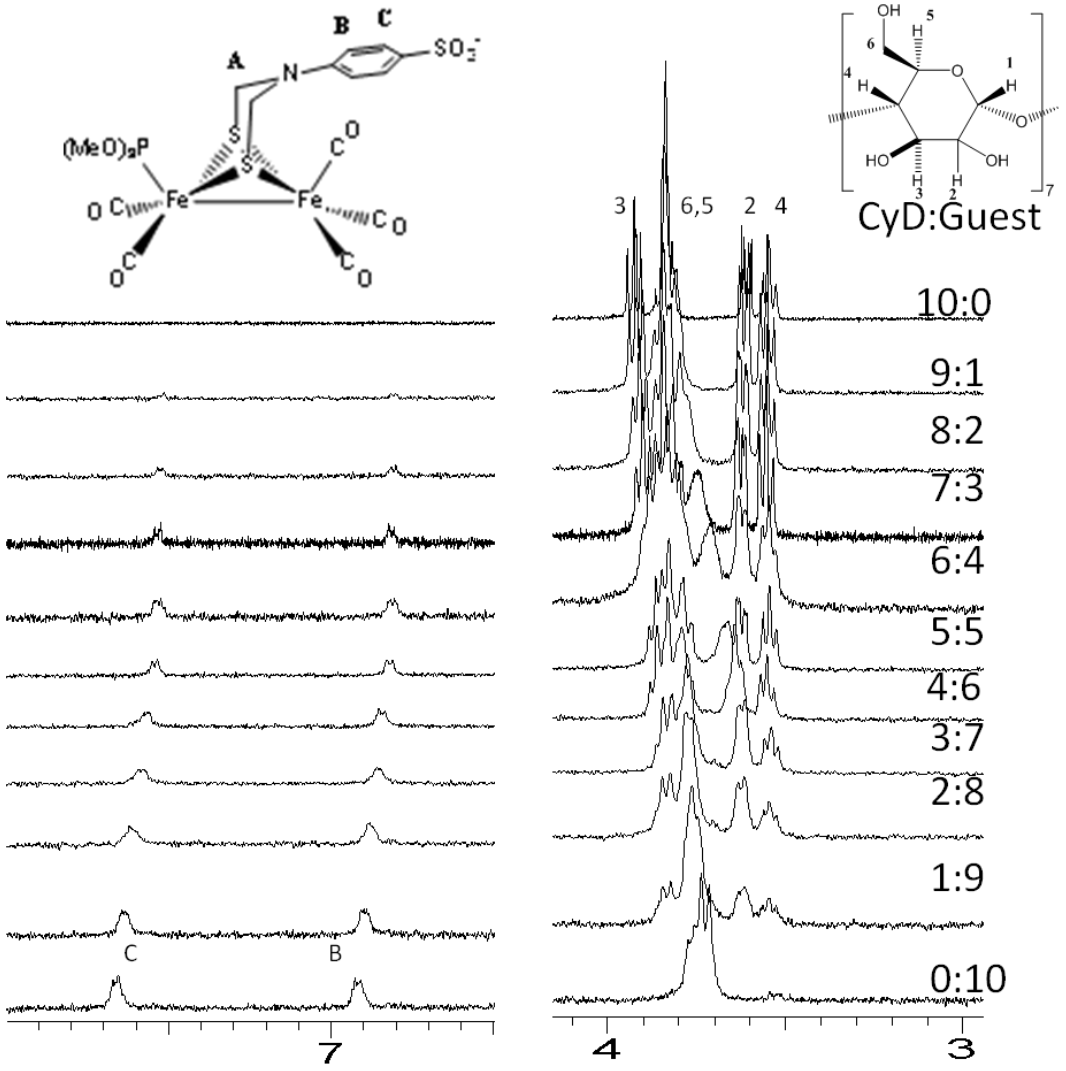

Figure V-20. Effect on the ^{1}H NMR spectra of $Na^{+}(\mu\text{-}SCH_2N(C_6H_4SO_3^{-})CH_2S)[Fe^{I}(CO)_3][Fe^{I}(CO)_2P(OMe)_3]$ as the Complex:CyD ratio is varied from 0:10 (bottom most spectrum) to 10:0 (top).

cyclodextrin have proven less conclusive. While an upfield shift is observed for the resonances of the aromatic protons on the diiron complex and the C5 cyclodextrin proton, no significant change is noted for the signal of the C3 proton indicating that if inclusion is occurring it may be in a different fashion than in the hexacarbonyl or $P(OMe)_3$ derivatives.

Electrochemical studies of both complexes proved inconclusive. Upon addition of cyclodextrin to the substituted derivatives in water, a decrease in the current intensities of the redox events is observed in the cyclic voltammograms (Figure V-21). This result is similar to what was observed in the hexacarbonyl parent complex except that no shift in the potentials for the redox events of the ligand substituted derivatives was observed. For the PMe_3 derivative this is not unexpected as the only observed events are oxidative in nature and in the hexacarbonyl system no significant change in potential was observed for the initial oxidation. Further electrochemical studies using mercury electrodes would allow a larger potential range to be explored as the reduction of water by mercury is more negative than for glassy carbon.[148] Additionally, the use of different sized cyclodextrins or modified cyclodextrins could result in more pronounced changes.

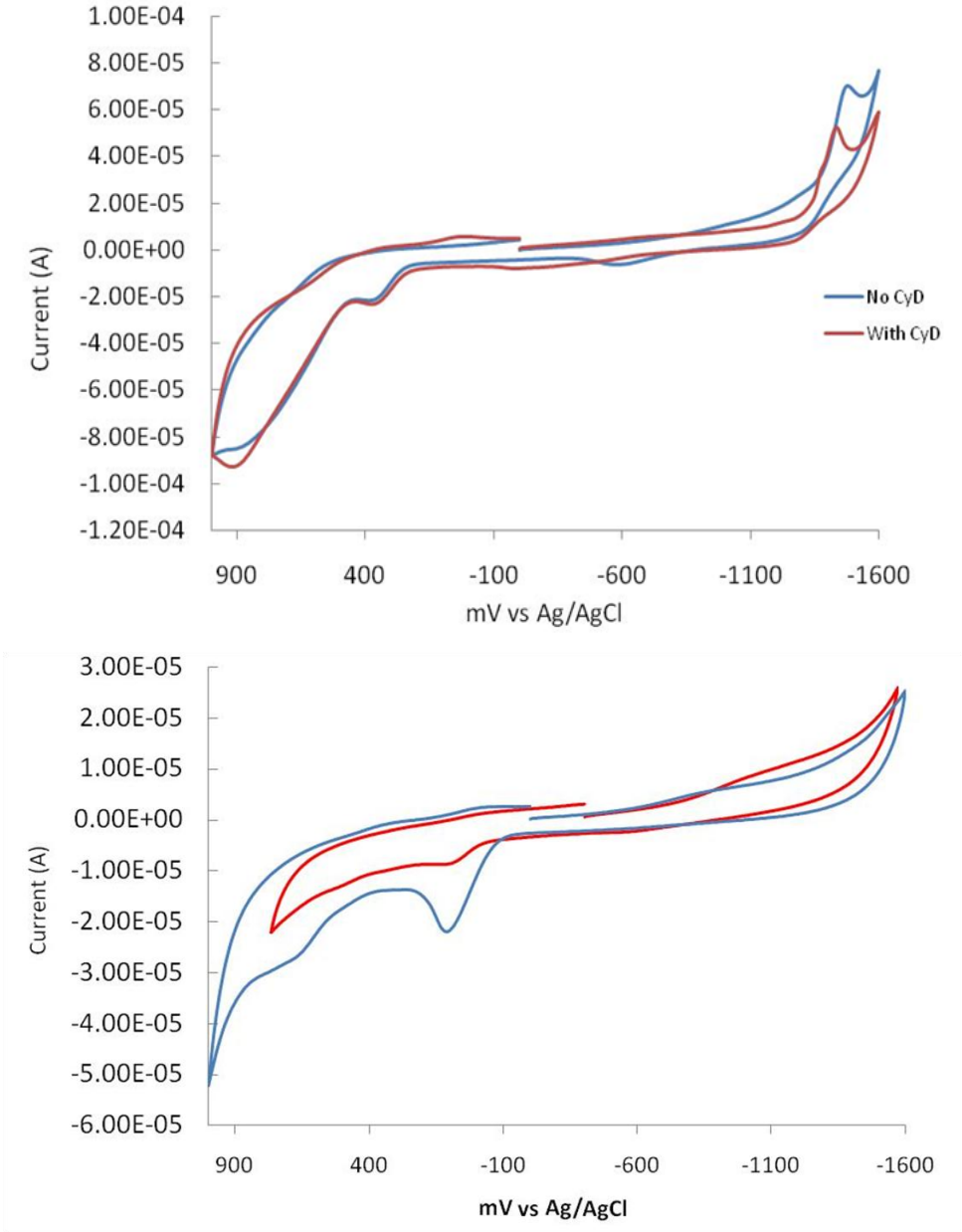

Figure V-21. Cyclic voltammograms of $Na^{+}(\mu\text{-}SCH_2N(C_6H_4SO_3^{-})CH_2S)[Fe^{I}(CO)_3][Fe^{I}(CO)_2P(OMe)_3]$ (top) and $Na^{+}(\mu\text{-}SCH_2N(C_6H_4SO_3^{-})CH_2S)[Fe^{I}(CO)_2PMe_3]_2$ (bottom) in 0.01 M aqueous NaCl solution, showing the effect of 10 equivalents of β-cyclodextrin. Scan rate = 200 mV/s

Summary and Concluding Remarks

In summary, we have used β-CyD to provide a first generation artificial protein environment for a small molecule model of the [FeFe]-hydrogenase enzyme active site and have shown evidence for inclusion both in the solid state and in solution. Inclusion in the cyclodextrin not only produces structural distortions in the diiron motif, as observed in the X-ray structure of the clathrate, but also effects change in the redox and electrocatalytic properties of $Na^{+}(\mu\text{-}SCH_2NH(C_6H_4SO_3^{-})CH_2S)[Fe^{I}(CO)_3]_2$. Specifically this work supports the fact that the protein environment around the enzyme active site could have a large contribution to both the rate of hydrogen production and the potential at which hydrogen is produced. Though no evidence of a direct interaction through hydrogen bonding was observed the natural β-cyclodextrin was still able to modulate properties of the model complexes. If modifications to the cyclodextrin host that either enhance the rate or that shift proton reduction to more favorable potentials can be found, the use of cyclodextrins as an additive in mediated electron transfer based cells could prove valuable. Additionally, modifications to the guest molecule that stabilize the clathrate and lower the rate constant for dissociation would provide a means to better directly study the host's effect on the intramolecular fluxional properties of the model complex without complications from intermolecular dynamic processes. However, even in this case, where both a generic host and model complex were used, the ability of an artificial second coordination sphere to control properties in the model complexes establishes a novel approach for modeling the active site of [FeFe]-hydrogenase based on the well established inclusion properties of cyclodextrins.

CHAPTER VI

CONCLUSIONS

Summary and Perspectives

"Nature does nothing uselessly."

- Aristotle

In the pursuit of biomimetic catalysts, we draw our inspiration from Nature and base our design principles on the efforts from a wide range of disciplines including biology, biochemistry, and biophysics. As their research delves into the intricacies of the natural system, we develop a deeper understanding of the way nature has taken base metals and turned them into highly active and efficient catalysts. In the synthesis of small molecule biomimetics of metalloenzyme active sites, many synthetic approaches aim for simple metal clusters devoid of complex synthetic components with the hope that they remain capable of replicating both the form and function of the enzyme active sites. This simple approach seeks to show that through the correct interpretation of only the first coordination sphere around the metal we can compete with the natural system. However, this approach also stems from a desire for simplicity in complex design and ignores crucial aspects of the biological systems.

It is difficult to move away from the concept that the protein environment that surrounds the metal component plays an equally important role in the high levels of reactivity observed in metalloenzymes. In fact, the protein's contribution is made even

more obvious by the majority of enzymes that do not directly require metals to perform complex reactions.

The structures and reactivity of biological metal centers are influenced by numerous interactions, not just between the protein and the active site but throughout the protein, with non-covalent interactions influencing the position of nearly every amino acid in the protein. In this respect there can be thought to be a continuum of coordination sphere layers radiating from the active site, similar to the layers of an onion, which contribute to the overall structure and play an important role in the catalytic ability of the enzyme. Because of this, there has been increasing effort in modeling the active sites of enzymes to look beyond the first coordination sphere and this has met with some success. This approach does not require the exact replication of the second coordination sphere effects, but rather the incorporation of what these effects do into the design principles used to develop synthetic analogs. Through the use of direct modification of the model complexes and non-covalent interactions from either intra- or intermolecular components, the synthetic chemist can study those effects that greatly affect either form or function. In essence, this route builds layer upon layer around the model complex in hopes to meet the biologists who start from the outside somewhere in the middle of the onion and show that these secondary interactions are of primary importance in model complexes.

Efforts to model the enzyme active site of [FeFe]-hydrogenase have utilized hundreds of combinations of substituent ligands and dithiolates. The irons have been replaced by Ru, the bridging thiolates have been replaced by other donors, and a variety

of redox levels have been explored. The first coordination sphere ligand set has been reproduced and models have been attached to 4Fe4S clusters but still no model has been able to directly replicate the active $Fe^{I}Fe^{I}$ geometry or the high rates of reactivity of the enzyme. As discussed in the previous chapters the rotated geometry and the reactive terminal hydride species that form are thought to be held in place by a number of interactions with the surrounding protein. While the largest contributions are expected to come from hydrogen bonding or dipole-dipole interactions, the steric effects imparted by the surrounding enzyme likely play an important role as well.

My graduate research at Texas A&M University has focused on understanding the role that non-covalent interactions can play in the structure and reactivity of the model complexes. Specifically a large portion of this work has been aimed at understanding the interplay between electron donation from the ligands surrounding the diiron complex and the steric effects they impose on the molecule. The work discussed in Chapters III, IV, and V has shown that the balance between these effects is such that even seemingly small or inconstant modifications to the model complexes can result in changes in their fundamental properties and reactivity.

The addition of the steric bulk to the central carbon of the propanedithiolate linker of the hexacarbonyl complexes, as discussed in Chapter III, does not drastically alter the electron density at the irons as evidence by both IR and electrochemical studies. This indicates that the observed decrease in the barrier for intramolecular CO exchange indicated by the VT-NMR studies was likely a result of a steric interaction between the carbonyl ligands and the methyl groups on the dithiolate linker. This effect also

manifests itself in the apparent decrease in the barrier to the ring flip for the dithiolate linker, with the carbonyls pushing the bridgehead carbon towards the half-chair conformation required for the ring flip to occur. In addition to the NMR evidence, the crystal structure also shows minor distortion resulting from the added steric bulk. The apical CO ligand on the same side as the bridgehead is found to be twisted away from the eclipsed conformation with the apical CO on the other iron. This structural change is an indication that the lowering of the energy barrier by steric bulk comes from a destabilization of the unrotated ground state. Such an effect is complementary to the effect provided by strong donor ligands where the lowered energy barrier arises from the stabilization of the rotated transition state.[87] This was seen in the sterically bulky systems when CO was exchanged for stronger donor ligands. The substitution with IMes resulted in a further decrease of the barrier for CO exchange. This is consistent with the results observed for the (μ-pdt) analogs and reinforces the findings from the Darensbourg group that showed differences in the energy barrier for $Fe(CO)_3$ rotation between the (μ-edt) and (μ-pdt) complexes.[85] Additionally, it supports the design principles proposed by collaborative theoretical studies by Hall and Darensbourg.[103]

The lowered barrier for rotation, caused by added steric bulk, can be thought of as resulting from a torque applied on the $Fe(CO)_3$ rotor by the dithiolate linker. A restorative force provided by the FeFe bond acts directly against this torque to maintain the unrotated geometry. In the diiron hexacarbonyl system, the contribution of ligand substitution and dithiolate modification to these forces is easy to distinguish. Because there is no evidence of any direct change to the restorative force (same electron density

at the irons), the lowered barrier results from increased torque (added steric bulk). In the substituted systems, the interplay between steric bulk and electron donation becomes much more complicated.

The new ligands can provide both steric and electronic effects, and these effects are dependent on the preference of the ligand to be in an apical or basal position. The theoretical work described in Chapter I indicated that ligands in the apical position are ideally suited for stabilizing the transition state for rotation by increasing the interaction with the semi-bridging CO. Additionally, the extra donation into the irons weakens the FeFe bond and thus the restorative force. This allows the steric bulk to have a greater effect on the model complexes. The ability of ligands to influence the positional preference of the bridgehead carbon on the dithiolate linker can also change the extent of the steric effect provided by the dithiolate by forcing it to remain on one side thus increasing its interaction with the apical ligand. As indicated by the structures of the complexes in Chapter III, this can work both ways with the dithiolate influencing the apical/basal preference of the ligands resulting in a change in the donation into the iron. While all of these interactions between the structural features make the separation of the steric and electronic effects difficult, the conclusion that strong donation and steric bulk are important design features for stabilizing the rotated geometry is shown to remain valid.

As discussed, steric bulk and strong donor ligands have proven exceptionally useful in the isolation of mixed-valent models of the [FeFe]-H_2ase active site with the rotated geometry. Unlike the $Fe^{I}Fe^{II}$ models reported by both Darensbourg and

Rauchfuss,[64-65] the complexes in Chapter IV used relatively small substituent ligands and relied on the steric bulk provided by the bridgehead to stabilize the rotated structure. Direct comparison of the ν(CO) stretching frequencies of the μ-dmpdt and μ-pdt $Fe^{I}Fe^{I}$ derivatives again showed very similar values indicating that in the substituted complexes the electron density around the irons was similar for the sterically bulky system and the complex without added steric bulk. The ~200 mv stabilization of the $Fe^{I}Fe^{II}$ oxidation state observed in the sterically bulky complexes likely results then from a steric interaction. This conclusion is also supported by the studies on the sterically bulky $P(OMe)_3$ derivative. Despite being significantly less electron rich than the (μ-pdt)$[Fe(CO)_2PMe_3]_2$ species, this complex proved more stable at room temperature, indicating that the stability of (μ-dmpdt)$[Fe(CO)_2PMe_3]_2PF_6$ resulted from the steric effect rather than greater electron density around the irons.

The ability of added steric bulk to modifiy the redox properties of the complexes was shown to have a limit. In the IMes substituted complex, (μ-dmpdt)$[Fe(CO)_2PMe_3]$ $[Fe(CO)_2IMes]$, there is no significant change in the oxidation potential relative to the (μ-pdt)$[Fe(CO)_2PMe_3][Fe(CO)_2IMes]$. This is likely due to the steric bulk on the NHC ligand overwhelming the effect of the *gem*-dimethyl groups on the dithiolate. The steric bulk does however shift the ν(CO) band for the semi-bridging CO to lower wavenumbers indicating that it may be more bridging than in the complex with less steric bulk. However in the series of mixed-valent complexes by Rauchfuss the value for the semi-bridging ν(CO) stretch is not always correlated with the Fe-C-O bond angle, so this conclusion should be cautiously viewed.[136]

An important goal in the continued studies of these complexes is the crystallization of the other mixed-valent complexes so that the structures of the complexes can be used for comparison to the spectroscopic features. As a number of these complexes act as spectroscopic models of the enzyme active site, the ability to compare the properties of well-characterized "model" complexes, even those that do not match the active site, to those of the enzyme active site should prove useful to people studying the biological system. A Mössbauer study on the mixed-valent complexes and the role of the steric bulk is currently underway in collaboration with Dr. Codrina Popescu at Ursinus College. This work should further assist interpretation of the spectroscopic data of the enzyme through the synthetic analogues.

Despite their spectroscopic importance the model complexes are largely unreactive to protons and have only been shown to react with hydrogen under high pressure. The low reactivity regarding H_2 uptake in the models is consistent with the fact that the open site on these complexes is Fe^{I}.[149] Regarding their reactivity with protons, an important observation for the mixed-valent complexes is that the rotated geometry and active site are not maintained upon reduction to the $Fe^{I}Fe^{I}$ oxidation state. As this is the proposed active oxidation state in the enzyme active site, maintaining the rotated structure in this state is desirable for developing highly active catalysts. While the work discussed in Chapters III and IV help define the necessary design principles for obtaining the rotated structure in the $Fe^{I}Fe^{II}$ oxidation state, the direct modifications to the complex through the addition of steric bulk or ligand substitution proved unable to maintain the active conformation. Thus, while steric bulk is important for obtaining the

rotated structure, the current focus on the model complexes needs to be on methods for maintaining the rotated structure at least for the duration of the catalytic cycle. A first generation approach to this was discussed in Chapter V.

The reaction of the sulfonated model complex **Na^+1** with natural β-cyclodextrin produced the first model complex shown to be encapsulated inside a supramolecular structure. The inclusion of this complex in solution by the cyclodextrin, as evidenced by NMR, produced several interesting effects on the properties of the model complex. Through non-covalent interactions the cyclodextrins proved effective in modifying the redox properties of the model complex by ~80 mV and the electrocatalytic proton reduction capabilities by ~200 mV despite the fact that the inclusion was not static in solution. The reasoning for the significantly larger difference in proton reduction potential versus the difference in the Fe^IFe^I/Fe^IFe^0 reduction potential upon addition of cyclodextrin is not fully understood and will be investigated in the ongoing studies discussed as part of Chapter V. An interesting proposal for this is that the cyclodextrin inhibits the fluxional character of the model complex important to catalytic activity. If this is the case, then it is also possible that the cyclodextrins could hinder the reorganization that occurs in the mixed-valent complexes upon one e^- reduction. The extreme broadening observed in both the ^{13}C NMR signals for the CO ligands and the ^1H signals for the methylene protons could result from the slowing of the fluxional processes that equate these atoms as well as dynamic exchange in and out of the cyclodextrin cavity. The ideal system to test this theory would have the diiron complex

held static in the cyclodextrin cavity either through covalent attachment or stronger intermolecular interactions.

Another important aspect of the work presented in Chapter V is the applicability of water as a solvent for hydrogen production catalysts. The enhanced rate of proton transfer as well as the lowered pKa of HOAc led to a strong response by the free model complex for electrocatalytic proton reduction. This is not unexpected as both the Darensbourg and Sun groups have shown the ability of water to increase the electrocatalytic capability of model complexes, but this is the first system where the electrochemisty was studied in water without any organic co-solvents. This achievement, resulting from the incorporation of the sulfonate group, is expected to be an important consideration in the design of functional biomimetics.

By combining the results from Chapters III and IV with the work in V, more interesting results are expected. The substituted complexes, discussed as part of the ongoing work should allow the cyclodextrin to have a greater impact on both the structure and properties of the model complexes. Additionally, because of the water solubility, the phosphine complexes are expected to be important in the study of electrocatalytic proton reduction in water and in obtaining hydride containing model complexes. While the inclusion of steric bulk, strong donors, water solubility and intermolecular interactions increases the complexity of the model compounds, it appears to be the required direction for modeling both form and function of the [FeFe]-Hydrogenase enzyme active site.

REFERENCES

(1) Eberle, U.; Felderhoff, M.; Schueth, F. *Angew. Chem., Int. Ed.* **2009**, *48*, 6608.

(2) Gasteiger, H. A.; Markovic, N. M. *Science (Washington, DC, US)* **2009**, *324*, 48.

(3) Hambourger, M.; Kodis, G.; Vaughn, M. D.; Moore, G. F.; Gust, D.; Moore, A. L.; Moore, T. A. *Dalton Trans.* **2009**, 9979.

(4) Peters, R. *Handb. Heterog. Catal. (2nd Ed.)* **2008**, *6*, 3045.

(5) Tollefson, J. *Nature (London, UK)* **2010**, *464*, 1262.

(6) Jacques, P.-A.; Artero, V.; Pecaut, J.; Fontecave, M. *Proc. Natl. Acad. Sci. USA* **2009**, *106*, 20627.

(7) Le Goff, A.; Artero, V.; Jousselme, B.; Tran, P. D.; Guillet, N.; Metaye, R.; Fihri, A.; Palacin, S.; Fontecave, M. *Science (Washington, DC, US)* **2009**, *326*, 1384.

(8) Gordon, R. B.; Bertram, M.; Graedel, T. E. *Proc. Natl. Acad. Sci. USA* **2006**, *103*, 1209.

(9) Vignais, P. M.; Billoud, B. *Chem. Rev. (Washington, DC, US)* **2007**, *107*, 4206.

(10) Broderick, J. B. *Compr. Coord. Chem. II* **2004**, *8*, 739.

(11) Wachtershauser, G. *Prog. Biophys. Mol. Biol.* **1992**, *58*, 85.

(12) Huber, C.; Eisenreich, W.; Hecht, S.; Wachtershauser, G. *Science (Washington, DC, US)* **2003**, *301*, 938.

(13) Chevallet, M.; Dupuis, A.; Issartel, J.-P.; Lunardi, J.; van Belzen, R.; Albracht, S. P. J. *Biochim. Biophys. Acta, Bioenerg.* **2003**, *1557*, 51.

(14) Peters, J. W.; Fisher, K.; Dean, D. R. *Annu. Rev. Microbiol.* **1995**, *49*, 335.

(15) Peters, J. W.; Lanzilotta, W. N.; Lemon, B. J.; Seefeldt, L. C. *Science (Washington, DC, US)* **1998**, *282*, 1853.

(16) Broderick, J. B. *Essays Biochem.* **1999**, *34*, 173.

(17) Pickett, C. J.; Ibrahim, S. K.; Hughes, D. L. *Faraday Discuss.* **2000**, *116*, 235.

(18) Armstrong, F. A.; Albracht, S. P. J. *Philos. Trans. R. Soc. London, Ser. A* **2005**, *363*, 937.

(19) Lojou, E.; Luo, X.; Brugna, M.; Candoni, N.; Dementin, S.; Giudici-Orticoni, M. T. *J. Biol. Inorg. Chem.* **2008**, *13*, 1157.

(20) Ruediger, O.; Gutierrez-Sanchez, C.; Olea, D.; Pereira, I. A. C.; Velez, M.; Fernandez, V. M.; De Lacey, A. L. *Electroanalysis* **2010**, *22*, 776.

(21) Tye, J. W.; Hall, M. B.; Darensbourg, M. Y. *Proc. Natl. Acad. Sci. USA* **2005**, *102*, 16911.

(22) Hiromoto, T.; Warkentin, E.; Moll, J.; Ermler, U.; Shima, S. *Angew. Chem., Int. Ed.* **2009**, *48*, 6457.

(23) Shima, S.; Thauer, R. K. *Chem. Rev. (Washington, DC, US)* **2007**, *7*, 37.

(24) Fontecilla-Camps, J. C. *JBIC, J. Biol. Inorg. Chem.* **1996**, *1*, 91.

(25) Fontecilla-Camps Juan, C.; Volbeda, A.; Cavazza, C.; Nicolet, Y. *Chem. Rev. (Washington, DC, US)* **2007**, *107*, 4273.

(26) Nicolet, Y.; Lemon, B. J.; Fontecilla-Camps, J. C.; Peters, J. W. *Trends Biochem. Sci.* **2000**, *25*, 138.

(27) Fontecilla-Camps, J. C.; Volbeda, A.; Cavazza, C.; Nicolet, Y. *Chem. Rev. (Washington, DC, US)* **2007**, *107*, 4273.

(28) Le Cloirec, A.; Davies, S. C.; Evans, D. J.; Hughes, D. L.; Pickett, C. J.; Best, S. P.; Borg, S. *Chem. Commun. (Cambridge, UK)* **1999**, 2285.

(29) Lyon, E. J.; Georgakaki, I. P.; Reibenspies, J. H.; Darensbourg, M. Y. *Angew. Chem., Int. Ed.* **1999**, *38*, 3178.

(30) Schmidt, M.; Contakes, S. M.; Rauchfuss, T. B. *J. Am. Chem. Soc.* **1999**, *121*, 9736.

(31) McGlynn, S. E.; Ruebush, S. S.; Naumov, A.; Nagy, L. E.; Dubini, A.; King, P. W.; Broderick, J. B.; Posewitz, M. C.; Peters, J. W. *JBIC, J. Biol. Inorg. Chem.* **2007**, *12*, 443.

(32) McGlynn, S. E.; Shepard, E. M.; Winslow, M. A.; Naumov, A. V.; Duschene, K. S.; Posewitz, M. C.; Broderick, W. E.; Broderick, J. B.; Peters, J. W. *FEBS Lett.* **2008**, *582*, 2183.

(33) Pilet, E.; Nicolet, Y.; Mathevon, C.; Douki, T.; Fontecilla-Camps, J. C.; Fontecave, M. *FEBS Lett.* **2009**, *583*, 506.

(34) Driesener, R. C.; Challand, M. R.; McGlynn, S. E.; Shepard, E. M.; Boyd, E. S.; Broderick, J. B.; Peters, J. W.; Roach, P. L. *Angew. Chem., Int. Ed.* **2010**, *49*, 1687.

(35) Shepard, E. M.; Duffus, B. R.; George, S. J.; McGlynn, S. E.; Challand, M. R.; Swanson, K. D.; Roach, P. L.; Cramer, S. P.; Peters, J. W.; Broderick, J. B. *J. Am. Chem. Soc.* **2010**, *132*, 9247.

(36) Shepard, E. M.; McGlynn, S. E.; Bueling, A. L.; Grady-Smith, C. S.; George, S. J.; Winslow, M. A.; Cramer, S. P.; Peters, J. W.; Broderick, J. B. *Proc. Natl. Acad. Sci. USA* **2010**, *107*, 10448.

(37) Mulder, D. W.; Boyd, E. S.; Sarma, R.; Lange, R. K.; Endrizzi, J. A.; Broderick, J. B.; Peters, J. W. *Nature (London, UK)* **2010**, *465*, 248.

(38) van der Spek, T. M.; Arendsen, A. F.; Happe, R. P.; Yun, S.; Bagley, K. A.; Stufkens, D. J.; Hagen, W. R.; Albracht, S. P. J. *Eur. J. Biochem.* **1996**, *237*, 629.

(39) Pierik, A. J.; Hulstein, M.; Hagen, W. R.; Albracht, S. P. J. *Eur. J. Biochem.* **1998**, *258*, 572.

(40) Albracht, S. P. J.; Bertrand, P.; Bleijlevens, B.; Dole, F.; Guigliarelli, B.; Hagen, W. R.; Happe, R. P.; Lubitz, W.; Maroney, M. J.; Massanz, C.; Moura, J. J. G.; Pereira, A. S.; Pierik, A. J.; Sorgenfrei, O.; Stein, M.; Tavares, P. *Hydrogen Fuel* **2001**, 110.

(41) Roseboom, W.; Lacey, A. L.; Fernandez, V. M.; Hatchikian, E. C.; Albracht, S. P. J. *JBIC, J. Biol. Inorg. Chem.* **2006**, *11*, 102.

(42) De Lacey, A. L.; Fernandez, V. M.; Rousset, M.; Cammack, R. *Chem. Rev. (Washington, DC, US)* **2007**, *107*, 4304.

(43) Chen, Z.; Lemon, B. J.; Huang, S.; Swartz, D. J.; Peters, J. W.; Bagley, K. A. *Biochemistry* **2002**, *41*, 2036.

(44) Peters, J. W.; Lanzilotta, W. N.; Lemon, B. J.; Seefeldt, L. C. *Science (Washington, DC, US)* **1999**, *283*, 35.

(45) Nicolet, Y.; de Lacey, A. L.; Vernede, X.; Fernandez, V. M.; Hatchikian, E. C.; Fontecilla-Camps, J. C. *J. Am. Chem. Soc.* **2001**, *123*, 1596.

(46) Silakov, A.; Wenk, B.; Reijerse, E.; Lubitz, W. *Phys. Chem. Chem. Phys.* **2009**, *11*, 6592.

(47) Pandey, A. S.; Harris, T. V.; Giles, L. J.; Peters, J. W.; Szilagyi, R. K. *J. Am. Chem. Soc.* **2008**, *130*, 4533.

(48) Goldet, G.; Brandmayr, C.; Stripp, S. T.; Happe, T.; Cavazza, C.; Fontecilla-Camps, J. C.; Armstrong, F. A. *J. Am. Chem. Soc.* **2009**, *131*, 14979.

(49) Thomas, C. M.; Darensbourg, M. Y.; Hall, M. B. *J. Inorg. Biochem.* **2007**, *101*, 1752.

(50) Barton, S. C. *Handb. Fuel Cells* **2009**, *5*, 112.

(51) Woolerton, T. W.; Vincent, K. A. *Electrochim. Acta* **2009**, *54*, 5011.

(52) King, R. B. *J. Am. Chem. Soc.* **1962**, *84*, 2460.

(53) Seyferth, D.; Henderson, R. S.; Song, L. C. *Organometallics (Washington, DC, US)* **1982**, *1*, 125.

(54) Seyferth, D.; Henderson, R. S. *J. Organomet. Chem.* **1981**, *218*, C34.

(55) Seyferth, D.; Henderson, R. S.; Song, L.-C. *J. Organomet. Chem.* **1980**, *192*, C1.

(56) De Beer, J. A.; Haines, R. J.; Greatrex, R.; Greenwood, N. N. *J. Chem. Soc. A* **1971**, 3271.

(57) Wei, C. H.; Dahl, L. F. *Inorg. Chem.***1965**, *4*, 1.

(58) Seyferth, D.; Brewer, K. S.; Wood, T. G.; Cowie, M.; Hilts, R. W. *Organometallics* **1992**, *11*, 2570.

(59) Seyferth, D.; Womack, G. B.; Archer, C. M.; Dewan, J. C. *Organometallics* **1989**, *8*, 430.

(60) Seyferth, D.; Womack, G. B.; Gallagher, M. K.; Cowie, M.; Hames, B. W.; Fackler, J. P., Jr.; Mazany, A. M. *Organometallics* **1987**, *6*, 283.

(61) Seyferth, D.; Womack, G. G.; Song, L. C. *Organometallics* **1983**, *2*, 776.

(62) Tard, C.; Pickett, C. J. *Chem. Rev. (Washington, DC, US)* **2009**, *109*, 2245.

(63) Felton, G. A. N.; Vannucci, A. K.; Chen, J.; Lockett, L. T.; Okumura, N.; Petro, B. J.; Zakai, U. I.; Evans, D. H.; Glass, R. S.; Lichtenberger, D. L. *J. Am. Chem. Soc.* **2007**, *129*, 12521.

(64) Liu, T.; Darensbourg, M. Y. *J. Am. Chem. Soc.* **2007**, *129*, 7008.

(65) Justice, A. K.; Rauchfuss, T. B.; Wilson, S. R. *Angew. Chem., Int. Ed.* **2007**, *46*, 6152.

(66) Stanley, J. L.; Heiden, Z. M.; Rauchfuss, T. B.; Wilson, S. R.; De Gioia, L.; Zampella, G. *Organometallics* **2008**, *27*, 119.

(67) Volkers, P. I.; Boyke, C. A.; Chen, J.; Rauchfuss, T. B.; Whaley, C. M.; Wilson, S. R.; Yao, H. *Inorg. Chem.* **2008**, *47*, 7002.

(68) Lawrence, J. D.; Li, H.; Rauchfuss, T. B.; Benard, M.; Rohmer, M.-M. *Angew. Chem., Int. Ed.* **2001**, *40*, 1768.

(69) Barton, B. E.; Olsen, M. T.; Rauchfuss, T. B. *J. Am. Chem. Soc.* **2008**, *130*, 16834.

(70) Song, L.-C.; Li, C.-G.; Gao, J.; Yin, B.-S.; Luo, X.; Zhang, X.-G.; Bao, H.-L.; Hu, Q.-M. *Inorg. Chem.***2008**, *47*, 4545.

(71) Thomas, C. M.; Ruediger, O.; Liu, T.; Carson, C. E.; Hall, M. B.; Darensbourg, M. Y. *Organometallics* **2007**, *26*, 3976.

(72) Lemon, B. J.; Nocek, B.; Peters, J. W. *Chemtracts* **2002**, *15*, 42.

(73) Boyer, J. L.; Rauchfuss, T. B.; Wilson, S. R. *C. R. Chim.* **2008**, *11*, 922.

(74) Li, X.; Wang, M.; Zhang, S.; Pan, J.; Na, Y.; Liu, J.; Aakermark, B.; Sun, L. *J. Phys. Chem. B* **2008**, *112*, 8198.

(75) Song, L.-C.; Wang, L.-X.; Tang, M.-Y.; Li, C.-G.; Song, H.-B.; Hu, Q.-M. *Organometallics* **2009**, *28*, 3834.

(76) Song, L.-C.; Tang, M.-Y.; Mei, S.-Z.; Huang, J.-H.; Hu, Q.-M. *Organometallics* **2007**, *26*, 1575.

(77) Sun, L.; Aakermark, B.; Ott, S. *Coord. Chem. Rev. (Washington, DC, US)* **2005**, *249*, 1653.

(78) Tard, C.; Liu, X.; Ibrahim, S. K.; Bruschi, M.; De Gioia, L.; Davies, S. C.; Yang, X.; Wang, L.-S.; Sawers, G.; Pickett, C. J. *Nature (London, UK)* **2005**, *433*, 610.

(79) Justice, A. K.; Zampella, G.; De Gioia, L.; Rauchfuss, T. B. *Chem. Commun. (Cambridge, UK)* **2007**, 2019.

(80) Boyke, C. A.; van der Vlugt, J. I.; Rauchfuss, T. B.; Wilson, S. R.; Zampella, G.; De Gioia, L. *J. Am. Chem. Soc.* **2005**, *127*, 11010.

(81) Adam, F. I.; Hogarth, G.; Richards, I. *J. Organomet. Chem.* **2007**, *692*, 3957.

(82) Justice, A. K.; Zampella, G.; De Gioia, L.; Rauchfuss, T. B.; van der Vlugt, J. I.; Wilson, S. R. *Inorg. Chem.* **2007**, *46*, 1655.

(83) Adam, F. I.; Hogarth, G.; Kabir, S. E.; Richards, I. *C. R. Chim.* **2008**, *11*, 890.

(84) Olsen, M. T.; Justice, A. K.; Gloaguen, F.; Rauchfuss, T. B.; Wilson, S. R. *Inorg. Chem.***2008**, *47*, 11816.

(85) Lyon, E. J.; Georgakaki, I. P.; Reibenspies, J. H.; Darensbourg, M. Y. *J. Am. Chem. Soc.* **2001**, *123*, 3268.

(86) George, S. J.; Cui, Z.; Razavet, M.; Pickett, C. J. *Chem.--Eur. J.* **2002**, *8*, 4037.

(87) Georgakaki, I. P.; Thomson, L. M.; Lyon, E. J.; Hall, M. B.; Darensbourg, M. Y. *Coord. Chem. Rev.* **2003**, *238-239*, 255.

(88) Gloaguen, F.; Lawrence, J. D.; Schmidt, M.; Wilson, S. R.; Rauchfuss, T. B. *J. Am. Chem. Soc.* **2001**, *123*, 12518.

(89) Darensbourg, M. Y.; Barros, H. L. C. *Inorg. Chem.* **1979**, *18*, 3286.

(90) Darensbourg, M. Y.; Lyon, E. J.; Zhao, X.; Georgakaki, I. P. *Proc. Natl. Acad. Sci. USA* **2003**, *100*, 3683.

(91) van der Vlugt, J. I.; Rauchfuss, T. B.; Whaley, C. M.; Wilson, S. R. *J. Am. Chem. Soc.* **2005**, *127*, 16012.

(92) Li, H.; Rauchfuss, T. B. *J. Am. Chem. Soc.* **2002**, *124*, 726.

(93) Zhao, X.; Georgakaki, I. P.; Miller, M. L.; Mejia-Rodriguez, R.; Chiang, C.-Y.; Darensbourg, M. Y. *Inorg. Chem.* **2002**, *41*, 3917.

(94) Georgakaki, I. P.; Miller, M. L.; Darensbourg, M. Y. *Inorg. Chem.* **2003**, *42*, 2489.

(95) Ezzaher, S.; Capon, J.-F.; Gloaguen, F.; Petillon, F. Y.; Schollhammer, P.; Talarmin, J.; Pichon, R.; Kervarec, N. *Inorg. Chem.***2007**, *46*, 3426.

(96) Morvan, D.; Capon, J.-F.; Gloaguen, F.; Le Goff, A.; Marchivie, M.; Michaud, F.; Schollhammer, P.; Talarmin, J.; Yaouanc, J.-J.; Pichon, R.; Kervarec, N. *Organometallics* **2007**, *26*, 2042.

(97) Orain, P.-Y.; Capon, J.-F.; Kervarec, N.; Gloaguen, F.; Petillon, F.; Pichon, R.; Schollhammer, P.; Talarmin, J. *Dalton Trans.* **2007**, 3754.

(98) Barton, B. E.; Rauchfuss, T. B. *Inorg. Chem.***2008**, *47*, 2261.

(99) Wright, J. A.; Pickett, C. J. *Chem. Commun. (Cambridge, UK)* **2009**, 5719.

(100) Jablonskyte, A.; Wright, J. A.; Pickett, C. J. *Dalton Trans.* **2010**, *39*, 3026.

(101) Ellgen, P. C.; Gerlach, J. N. *Inorg. Chem.* **1973**, *12*, 2526.

(102) Thomas, C. M.; Liu, T.; Hall, M. B.; Darensbourg, M. Y. *Inorg. Chem.***2008**, *47*, 7009.

(103) Tye, J. W.; Darensbourg, M. Y.; Hall, M. B. *Inorg. Chem.* **2006**, *45*, 1552.

(104) Aggarwal, V. K.; Davies, I. W.; Franklin, R.; Maddock, J.; Mahon, M. F.; Molloy, K. C. *J. Chem. Soc., Perkin Trans. 1* **1994**, 2363.

(105) Arduengo, A. J., III; Dias, H. V. R.; Harlow, R. L.; Kline, M. *J. Am. Chem. Soc.* **1992**, *114*, 5530.

(106) Zhao, X.; Georgakaki, I. P.; Miller, M. L.; Yarbrough, J. C.; Darensbourg, M. Y. *J. Am. Chem. Soc.* **2001**, *123*, 9710.

(107) Siegel, J. S.; Anet, F. A. L. *J. Org. Chem.* **1988**, *53*, 2629.

(108) Bruker Inc. *SMART and APEX2*, Bruker AXS Inc., Madison, WI, **2007**.

(109) Bruker Inc. *SAINT*, Bruker AXS Inc., Madison, WI, **2007**.

(110) Bruker Inc. *SADABS, "Program for Absorption Correction of Area Detector Frames"*, Bruker AXS Inc., Madison, WI, **2001**

(111) Sheldrick, G. M. *Acta Crystallogr., Sect. A Found. Crystallogr.* **2008**, *A64*, 112.

(112) Barbour, L. J. *J. Supramol. Chem.* **2003**, *1*, 189.

(113) Bruker Inc., *WinEPR Simfonia, version 1.25*, Bruker Analytische Messtechnik GmbH, **1996**.

(114) Becke, A. D. *J. Chem. Phys.* **1993**, *98*, 5648.

(115) Lee, C.; Yang, W.; Parr, R. G. *Phys. Rev. B Condens. Matter* **1988**, *37*, 785.

(116) Frisch, M. J.; Trucks, G. W.; Schlegel, H. B.; Scuseria, G. E.; Robb, M. A.; Cheeseman, J. R.; Montgomery Jr., J.A.; Vreven, T.; Kudin, K.N.; Burant, J.C.; Millam, J.M.; Lyengar, S.S.; Tomasi, J.; Barone, V.; Mennucci, B.; Cossi, M.; Scalmani, G.; Rega, N.; Petersson, G.A.; Nakatsuji, H.; Hada, M.; Ehara, M.; Toyota, K.; Fukuda, R.; Hasegawa, J.; Ishida, M.; Nakajima, T.; Honda, Y.; Kitao, O.; Nakai, H.; Klene, M.; Li, X.; Knox, J.E.; Hratchian, H.P.; Cross, J.B.; Bakken, V.; Adamo, C.; Jaramillo, J.; Gomperts, R.; Stratmann, R.E.; Yazyev, O.; Austin, A.J.; Cammi, R.; Pomelli, C.; Ochterski, J.W.; Ayala, P.Y.; Morokuma, K.; Voth, G.A.; Salvador, P.; Dannenberg, J.J.; Zakrzewski, V.G.; Dapprich, S.; Daniels, A.D.; Strain, M.C.; Farkas, O.; Malick, D.K.; Rabuck, A.D.; Raghavachari, K.; Foresman, J.B.; Ortiz, J.V.; Cui, Q.; Baboul, A.G.; Clifford, S.; Cioslowski, J.; Stefanov, B.B.; Liu, G.; Liashenko, A.; Piskorz, P.; Komaromi, I.; Martin, R.L.; Fox, D.J.; Keith, T.; Al-Laham, M.A.; Peng, C.Y.; Nanayakkara, A.; Challacombe, M.; Gill, P.M.W.; Johnson, B.; Chen, W.; Wong, M.W.; Gonzalez, C.; Pople, J.A. *Gaussian 03, Revision B.04*, Gaussian, Inc., Wallingford, CT, USA, **2004**.

(117) Hay, P. J.; Wadt, W. R. *J. Chem. Phys.* **1985**, *82*, 299.

(118) Wadt, W. R.; Hay, P. J. *J. Chem. Phys.* **1985**, *82*, 284.

(119) Couty, M.; Hall, M. B. *J. Comput. Chem.* **1996**, *17*, 1359.

(120) Höllwarth, A. B., M.; Dapprich, S.; Ehlers, A.W.; Gobbi, A.; Jonas, V.; Köhler, K.F.; Stegmann, R.; Veldkamp, A.; Frenking, G. *Chem. Phys. Lett.* **1993**, *208*, 237.

(121) Dunning, T. H., Jr. *J. Chem. Phys.* **1970**, *53*, 2823.

(122) Dunning, T. H., Jr.; Hay, P. J. *Mod. Theor. Chem.* **1977**, *3*, 1.

(123) Accelrys Software Inc. *Cerius*^{2}, *Version 4.10*, Accelrys Software Inc., San Diego, CA, **2007**.

(124) Hehre, W. J.; Ditchfield, R.; Pople, J. A. *J. Chem. Phys.* **1972**, *56*, 2257.

(125) Hariharan, P. C.; Pople, J. A. *Theor. Chim. Acta* **1973**, *28*, 213.

(126) Singleton, M. L.; Jenkins, R. M.; Klemashevich, C. L.; Darensbourg, M. Y. *C. R. Chim.* **2008**, *11*, 861.

(127) Tye, J. W.; Lee, J.; Wang, H.-W.; Mejia-Rodriguez, R.; Reibenspies, J. H.; Hall, M. B.; Darensbourg, M. Y. *Inorg. Chem.* **2005**, *44*, 5550.

(128) Singleton, M. L.; Bhuvanesh, N.; Reibenspies, J. H.; Darensbourg, M. Y. *Angew. Chem., Int. Ed.* **2008**, *47*, 9492.

(129) Li, P.; Wang, M.; He, C.; Li, G.; Liu, X.; Chen, C.; Akermark, B.; Sun, L. *Eur. J. Inorg. Chem.* **2005**, 2506.

(130) Mejia-Rodriguez, R.; Chong, D.; Reibenspies, J. H.; Soriaga, M. P.; Darensbourg, M. Y. *J. Am. Chem. Soc.* **2004**, *126*, 12004.

(131) Capon, J.-F.; El Hassnaoui, S.; Gloaguen, F.; Schollhammer, P.; Talarmin, J. *Organometallics* **2005**, *24*, 2020.

(132) Chong, D.; Georgakaki, I. P.; Mejia-Rodriguez, R.; Sanabria-Chinchilla, J.; Soriaga, M. P.; Darensbourg, M. Y. *Dalton Trans.* **2003**, 4158.

(133) Borg, S. J.; Behrsing, T.; Best, S. P.; Razavet, M.; Liu, X.; Pickett, C. J. *J. Am. Chem. Soc.* **2004**, *126*, 16988.

(134) Gloaguen, F.; Morvan, D.; Capon, J.-F.; Schollhammer, P.; Talarmin, J. *J. Electroanal. Chem.* **2007**, *603*, 15.

(135) Kessler, H. *Angew. Chem., Int. Ed. Engl.* **1970**, *9*, 219.

(136) Justice, A. K.; De Gioia, L.; Nilges, M. J.; Rauchfuss, T. B.; Wilson, S. R.; Zampella, G. *Inorg. Chem.***2008**, *47*, 7405.

(137) Felton, G. A. N.; Mebi, C. A.; Petro, B. J.; Vannucci, A. K.; Evans, D. H.; Glass, R. S.; Lichtenberger, D. L. *J. Organomet. Chem.* **2009**, *694*, 2681.

(138) Hambourger, M.; Gervaldo, M.; Svedruzic, D.; King, P. W.; Gust, D.; Ghirardi, M.; Moore, A. L.; Moore, T. A. *J. Am. Chem. Soc.* **2008**, *130*, 2015.

(139) Singleton, M. L.; Reibenspies, J. H.; Darensbourg, M. Y. *J. Am. Chem. Soc.* **2010**, *132*, 8870.

(140) Na, Y.; Pan, J.; Wang, M.; Sun, L. *Inorg. Chem.***2007**, *46*, 3813.

(141) Jones, A. K.; Lichtenstein, B. R.; Dutta, A.; Gordon, G.; Dutton, P. L. *J. Am. Chem. Soc.* **2007**, *129*, 14844.

(142) Breslow, R.; Dong, S. D. *Chem. Rev. (Washington, DC, US)* **1998**, *98*, 1997.

(143) Harwani, S.; Telford, J. R. *Chemtracts* **2005**, *18*, 437.

(144) Hapiot, F.; Tilloy, S.; Monflier, E. *Chem. Rev. (Washington, DC, US)* **2006**, *106*, 767.

(145) Kano, K. *Colloid Polym. Sci.* **2008**, *286*, 79.

(146) Schneider, H.-J.; Hacket, F.; Ruediger, V.; Ikeda, H. *Chem. Rev. (Washington, DC, US)* **1998**, *98*, 1755.

(147) Apfel, U.-P.; Halpin, Y.; Gottschaldt, M.; Goerls, H.; Vos, J. G.; Weigand, W. *Eur. J. Inorg. Chem.* **2008**, 5112.

(148) Felton, G. A. N.; Glass, R. S.; Lichtenberger, D. L.; Evans, D. H. *Inorg. Chem.* **2006**, *45*, 9181.

(149) Kubas, G. J. *Chem. Rev. (Washington, DC, US)* **2007**, *107*, 4152.

APPENDIX A

CRYSTALLOGRAPHIC DATA FOR STRUCTURES

Table A-1. Crystal data and structure refinement for Complex III-**1**.

Identification code	Fedmpdt(CO)6	
Empirical formula	C11 H10 Fe2 O6 S2	
Formula weight	414.01	
Temperature	106(2) K	
Wavelength	0.71073 Å	
Crystal system	Monoclinic	
Space group	P2(1)/c	
Unit cell dimensions	a = 8.9501(12) Å	α= 90°.
	b = 14.6721(19) Å	β= 95.806(2)°.
	c = 11.5055(15) Å	γ = 90°.
Volume	1503.1(3) $Å^3$	
Z	4	
Density (calculated)	1.829 Mg/m^3	
Absorption coefficient	2.228 mm^{-1}	
F(000)	832	
Crystal size	0.305 x 0.08 x 0.08 mm^3	
Theta range for data collection	2.26 to 28.25°.	
Index ranges	-11<=h<=11, -19<=k<=19, -14<=l<=15	
Reflections collected	14563	
Independent reflections	3631 [R(int) = 0.0954]	
Completeness to theta = 28.25°	97.7 %	
Absorption correction	None	
Refinement method	Full-matrix least-squares on F^2	
Data / restraints / parameters	3631 / 0 / 192	
Goodness-of-fit on F^2	1.005	
Final R indices [I>2sigma(I)]	R1 = 0.0286, wR2 = 0.0687	
R indices (all data)	R1 = 0.0350, wR2 = 0.0710	
Largest diff. peak and hole	0.560 and -0.504 e.$Å^{-3}$	

Table A-2. Atomic coordinates (x 10^4) and equivalent isotropic displacement parameters ($Å^2$x 10^3) for III-1. U(eq) is defined as one third of the trace of the orthogonalized U^{ij} tensor.

	x	y	z	U(eq)
Fe(1)	7621(1)	313(1)	1963(1)	14(1)
Fe(2)	5552(1)	938(1)	3025(1)	13(1)
S(1)	7629(1)	274(1)	3934(1)	14(1)
S(2)	7223(1)	1825(1)	2209(1)	15(1)
O(4)	3734(2)	-692(1)	3341(1)	28(1)
O(1)	10648(2)	-145(1)	1344(2)	33(1)
O(5)	3245(2)	1438(1)	1135(1)	27(1)
O(3)	6276(2)	661(1)	-431(1)	25(1)
O(2)	6593(2)	-1583(1)	2015(2)	32(1)
C(5)	4149(2)	1265(1)	1874(2)	18(1)
C(1)	9497(2)	62(1)	1609(2)	21(1)
O(6)	4667(2)	2093(1)	4935(1)	33(1)
C(3)	6812(2)	504(1)	491(2)	18(1)
C(7)	8766(2)	1131(1)	4783(2)	18(1)
C(6)	4997(2)	1651(1)	4191(2)	20(1)
C(2)	7001(2)	-852(2)	1978(2)	21(1)
C(11)	10171(2)	2565(2)	5135(2)	24(1)
C(4)	4458(2)	-61(1)	3255(2)	18(1)
C(10)	10881(2)	1545(2)	3564(2)	23(1)
C(8)	8444(2)	2429(1)	3327(2)	19(1)
C(9)	9549(2)	1894(1)	4176(2)	16(1)

Table A-3. Bond lengths [Å] and angles [°] for III-1.

Fe(1)-C(3)	1.795(2)
Fe(1)-C(2)	1.798(2)
Fe(1)-C(1)	1.805(2)
Fe(1)-S(1)	2.2680(6)
Fe(1)-S(2)	2.2691(6)
Fe(1)-Fe(2)	2.4939(4)
Fe(2)-C(5)	1.796(2)
Fe(2)-C(4)	1.797(2)
Fe(2)-C(6)	1.810(2)
Fe(2)-S(2)	2.2568(5)
Fe(2)-S(1)	2.2594(6)
S(1)-C(7)	1.835(2)
S(2)-C(8)	1.830(2)
O(4)-C(4)	1.141(2)
O(1)-C(1)	1.145(2)
O(5)-C(5)	1.142(2)
O(3)-C(3)	1.143(2)
O(2)-C(2)	1.135(3)
O(6)-C(6)	1.136(2)
C(7)-C(9)	1.527(3)
C(7)-H(7A)	0.9900
C(7)-H(7B)	0.9900
C(11)-C(9)	1.540(3)
C(11)-H(11A)	0.9800
C(11)-H(11B)	0.9800
C(11)-H(11C)	0.9800
C(10)-C(9)	1.532(3)
C(10)-H(10A)	0.9800
C(10)-H(10B)	0.9800
C(10)-H(10C)	0.9800
C(8)-C(9)	1.535(3)
C(8)-H(8A)	0.9900

C(8)-H(8B)	0.9900
C(3)-Fe(1)-C(2)	93.53(9)
C(3)-Fe(1)-C(1)	96.57(9)
C(2)-Fe(1)-C(1)	95.93(9)
C(3)-Fe(1)-S(1)	155.16(6)
C(2)-Fe(1)-S(1)	86.35(7)
C(1)-Fe(1)-S(1)	108.15(7)
C(3)-Fe(1)-S(2)	84.96(6)
C(2)-Fe(1)-S(2)	151.13(7)
C(1)-Fe(1)-S(2)	112.90(7)
S(1)-Fe(1)-S(2)	83.360(19)
C(3)-Fe(1)-Fe(2)	98.99(6)
C(2)-Fe(1)-Fe(2)	95.72(6)
C(1)-Fe(1)-Fe(2)	159.90(7)
S(1)-Fe(1)-Fe(2)	56.411(15)
S(2)-Fe(1)-Fe(2)	56.327(14)
C(5)-Fe(2)-C(4)	88.59(9)
C(5)-Fe(2)-C(6)	99.70(9)
C(4)-Fe(2)-C(6)	99.68(9)
C(5)-Fe(2)-S(2)	89.00(6)
C(4)-Fe(2)-S(2)	157.70(7)
C(6)-Fe(2)-S(2)	102.59(7)
C(5)-Fe(2)-S(1)	159.69(7)
C(4)-Fe(2)-S(1)	90.88(6)
C(6)-Fe(2)-S(1)	100.40(6)
S(2)-Fe(2)-S(1)	83.83(2)
C(5)-Fe(2)-Fe(1)	103.61(6)
C(4)-Fe(2)-Fe(1)	102.40(6)
C(6)-Fe(2)-Fe(1)	148.07(6)
S(2)-Fe(2)-Fe(1)	56.799(17)
S(1)-Fe(2)-Fe(1)	56.739(17)
C(7)-S(1)-Fe(2)	109.68(7)
C(7)-S(1)-Fe(1)	117.42(7)
Fe(2)-S(1)-Fe(1)	66.850(17)

C(8)-S(2)-Fe(2)	111.16(7)
C(8)-S(2)-Fe(1)	118.10(7)
Fe(2)-S(2)-Fe(1)	66.873(17)
O(5)-C(5)-Fe(2)	177.34(18)
O(1)-C(1)-Fe(1)	175.53(19)
O(3)-C(3)-Fe(1)	177.04(18)
C(9)-C(7)-S(1)	120.94(14)
C(9)-C(7)-H(7A)	107.1
S(1)-C(7)-H(7A)	107.1
C(9)-C(7)-H(7B)	107.1
S(1)-C(7)-H(7B)	107.1
H(7A)-C(7)-H(7B)	106.8
O(6)-C(6)-Fe(2)	178.89(19)
O(2)-C(2)-Fe(1)	178.2(2)
C(9)-C(11)-H(11A)	109.5
C(9)-C(11)-H(11B)	109.5
H(11A)-C(11)-H(11B)	109.5
C(9)-C(11)-H(11C)	109.5
H(11A)-C(11)-H(11C)	109.5
H(11B)-C(11)-H(11C)	109.5
O(4)-C(4)-Fe(2)	176.43(18)
C(9)-C(10)-H(10A)	109.5
C(9)-C(10)-H(10B)	109.5
H(10A)-C(10)-H(10B)	109.5
C(9)-C(10)-H(10C)	109.5
H(10A)-C(10)-H(10C)	109.5
H(10B)-C(10)-H(10C)	109.5
C(9)-C(8)-S(2)	120.02(14)
C(9)-C(8)-H(8A)	107.3
S(2)-C(8)-H(8A)	107.3
C(9)-C(8)-H(8B)	107.3
S(2)-C(8)-H(8B)	107.3
H(8A)-C(8)-H(8B)	106.9
C(7)-C(9)-C(10)	112.33(16)

C(7)-C(9)-C(8)	111.73(15)
C(10)-C(9)-C(8)	111.07(17)
C(7)-C(9)-C(11)	106.88(16)
C(10)-C(9)-C(11)	107.52(15)
C(8)-C(9)-C(11)	106.96(16)

Symmetry transformations used to generate equivalent atoms:

Table A-4. Anisotropic displacement parameters ($Å^2 x\ 10^3$) for III-1. The anisotropic displacement factor exponent takes the form: $-2\pi^2[\ h^2\ a^{*2}U^{11} + ...\ + 2\ h\ k\ a^*\ b^*\ U^{12}\ ]$

	U^{11}	U^{22}	U^{33}	U^{23}	U^{13}	U^{12}
Fe(1)	15(1)	14(1)	12(1)	-2(1)	2(1)	0(1)
Fe(2)	13(1)	14(1)	12(1)	1(1)	1(1)	0(1)
S(1)	16(1)	15(1)	12(1)	2(1)	0(1)	0(1)
S(2)	17(1)	14(1)	14(1)	2(1)	1(1)	-1(1)
O(4)	30(1)	28(1)	27(1)	5(1)	6(1)	-10(1)
O(1)	22(1)	40(1)	38(1)	-12(1)	7(1)	3(1)
O(5)	22(1)	32(1)	26(1)	10(1)	-6(1)	0(1)
O(3)	27(1)	34(1)	14(1)	0(1)	1(1)	-1(1)
O(2)	39(1)	18(1)	38(1)	-6(1)	7(1)	-6(1)
C(5)	18(1)	16(1)	20(1)	4(1)	5(1)	-1(1)
C(1)	22(1)	19(1)	20(1)	-4(1)	1(1)	-1(1)
O(6)	36(1)	38(1)	24(1)	-11(1)	0(1)	12(1)
C(3)	18(1)	17(1)	21(1)	-4(1)	5(1)	-2(1)
C(7)	19(1)	22(1)	11(1)	0(1)	-1(1)	-1(1)
C(6)	17(1)	24(1)	19(1)	0(1)	-2(1)	5(1)
C(2)	21(1)	24(1)	18(1)	-3(1)	3(1)	2(1)
C(11)	23(1)	28(1)	20(1)	-7(1)	0(1)	-7(1)
C(4)	19(1)	23(1)	12(1)	1(1)	2(1)	3(1)
C(10)	15(1)	30(1)	24(1)	-5(1)	3(1)	-4(1)
C(8)	22(1)	14(1)	19(1)	-2(1)	0(1)	-2(1)
C(9)	17(1)	18(1)	14(1)	-2(1)	2(1)	-2(1)

Table A-5. Hydrogen coordinates (x 10^4) and isotropic displacement parameters ($Å^2$x 10^{-3}) for III-1.

	x	y	z	U(eq)
H(7A)	8107	1424	5315	21
H(7B)	9551	798	5282	21
H(11A)	10640	3083	4776	36
H(11B)	10919	2255	5677	36
H(11C)	9348	2784	5562	36
H(10A)	10508	1204	2862	34
H(10B)	11504	1145	4096	34
H(10C)	11483	2063	3344	34
H(8A)	9037	2874	2919	22
H(8B)	7788	2784	3802	22

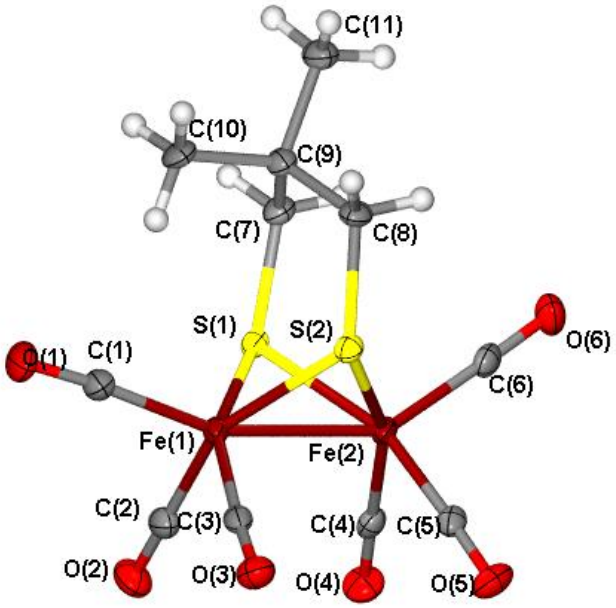
C(11)
C(10)
C(9)
C(7)
C(8)
S(1)
S(2)
O(1)
C(1)
O(6)
C(6)
Fe(1)
Fe(2)
C(2)
C(3)
C(4)
C(5)
O(2)
O(3)
O(4)
O(5)

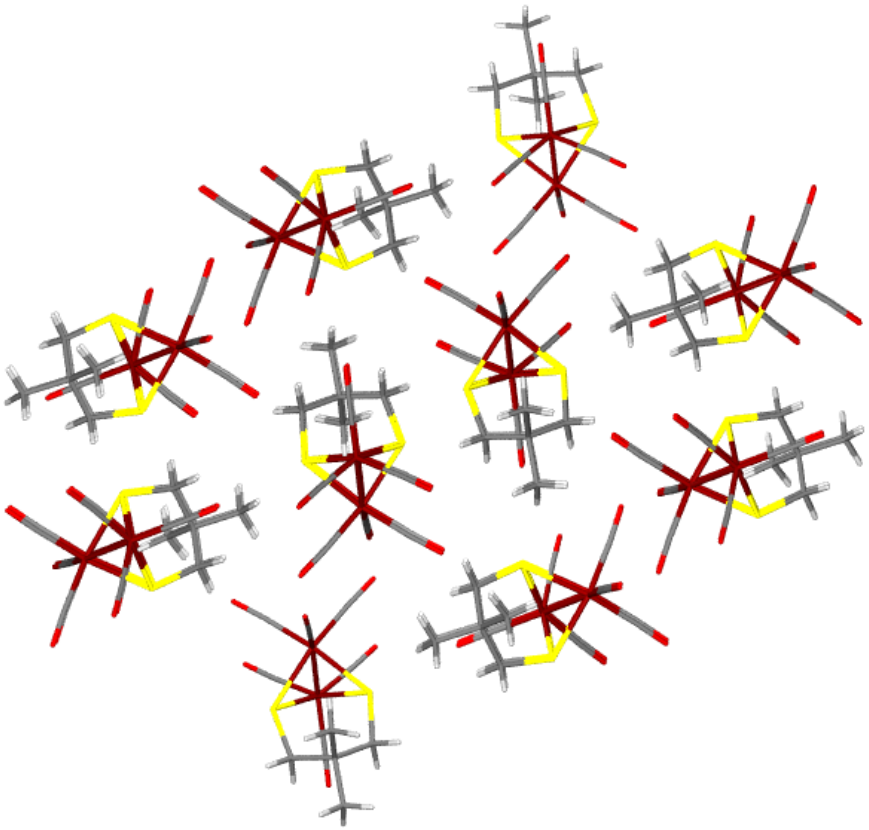

Table A-6. Crystal data and structure refinement for Complex **III-2**.

Identification code	fedepdt	
Empirical formula	C13 H14 Fe2 O6 S2	
Formula weight	442.06	
Temperature	110(2) K	
Wavelength	0.71073 Å	
Crystal system	Monoclinic	
Space group	P2(1)/n	
Unit cell dimensions	a = 7.6180(10) Å	α= 90°.
	b = 18.886(2) Å	β= 102.902(2)°.
	c = 12.0799(15) Å	γ = 90°.
Volume	1694.1(4) $Å^3$	
Z	4	
Density (calculated)	1.733 Mg/m^3	
Absorption coefficient	1.983 mm^{-1}	
F(000)	896	
Crystal size	0.75 x 0.57 x 0.21 mm^3	
Theta range for data collection	2.04 to 28.28°.	
Index ranges	-10<=h<=10, -24<=k<=24, -16<=l<=15	
Reflections collected	16449	
Independent reflections	4120 [R(int) = 0.0893]	
Completeness to theta = 28.28°	98.0 %	
Absorption correction	None	
Max. and min. transmission	0.6809 and 0.3179	
Refinement method	Full-matrix least-squares on F^2	
Data / restraints / parameters	4120 / 0 / 210	
Goodness-of-fit on F^2	1.011	
Final R indices [I>2sigma(I)]	R1 = 0.0281, wR2 = 0.0716	
R indices (all data)	R1 = 0.0343, wR2 = 0.0742	
Largest diff. peak and hole	0.609 and -0.597 $e.Å^{-3}$	

Table A-7. Atomic coordinates (x 10^4) and equivalent isotropic displacement parameters ($Å^2$x 10^3) for III-2. U(eq) is defined as one third of the trace of the orthogonalized U^{ij} tensor.

	x	y	z	U(eq)
Fe(1)	7102(1)	8492(1)	10196(1)	14(1)
Fe(2)	9568(1)	8413(1)	9138(1)	14(1)
S(3)	9661(1)	7863(1)	10799(1)	14(1)
S(4)	6878(1)	7848(1)	8601(1)	15(1)
O(1)	12436(2)	7768(1)	8190(1)	26(1)
O(6)	4408(2)	7726(1)	11142(1)	29(1)
O(4)	4691(2)	9526(1)	8795(1)	30(1)
O(5)	8588(2)	9501(1)	12025(1)	29(1)
O(3)	11877(2)	9492(1)	10487(1)	30(1)
C(6)	5466(2)	8033(1)	10801(1)	20(1)
O(2)	8123(2)	9405(1)	7280(1)	31(1)
C(4)	5627(2)	9133(1)	9353(1)	20(1)
C(3)	10990(3)	9075(1)	9949(1)	20(1)
C(1)	11287(2)	7998(1)	8547(1)	18(1)
C(5)	7975(2)	9116(1)	11315(1)	20(1)
C(2)	8713(3)	9022(1)	7997(1)	21(1)
C(9)	8394(2)	6528(1)	9637(1)	15(1)
C(7)	9181(2)	6914(1)	10752(1)	16(1)
C(8)	6726(2)	6908(1)	8948(1)	17(1)
C(10)	9733(2)	6424(1)	8859(1)	19(1)
C(11)	11671(3)	6254(1)	9445(2)	26(1)
C(12)	7806(2)	5780(1)	9956(1)	20(1)
C(13)	6608(3)	5730(1)	10813(2)	24(1)

Table A-8. Bond lengths [Å] and angles [°] for III-2.

Fe(1)-C(6)	1.8009(18)
Fe(1)-C(5)	1.8040(18)
Fe(1)-C(4)	1.8044(18)
Fe(1)-S(4)	2.2527(5)
Fe(1)-S(3)	2.2606(5)
Fe(1)-Fe(2)	2.5014(4)
Fe(2)-C(3)	1.7951(18)
Fe(2)-C(2)	1.8032(18)
Fe(2)-C(1)	1.8044(17)
Fe(2)-S(3)	2.2461(5)
Fe(2)-S(4)	2.2724(5)
S(3)-C(7)	1.8261(16)
S(4)-C(8)	1.8336(16)
O(1)-C(1)	1.144(2)
O(6)-C(6)	1.142(2)
O(4)-C(4)	1.140(2)
O(5)-C(5)	1.142(2)
O(3)-C(3)	1.142(2)
O(2)-C(2)	1.141(2)
C(9)-C(7)	1.531(2)
C(9)-C(8)	1.533(2)
C(9)-C(10)	1.546(2)
C(9)-C(12)	1.557(2)
C(7)-H(7A)	0.9900
C(7)-H(7B)	0.9900
C(8)-H(8A)	0.9900
C(8)-H(8B)	0.9900
C(10)-C(11)	1.522(2)
C(10)-H(10A)	0.9900
C(10)-H(10B)	0.9900
C(11)-H(11A)	0.9800
C(11)-H(11B)	0.9800

C(11)-H(11C)	0.9800
C(12)-C(13)	1.529(2)
C(12)-H(12A)	0.9900
C(12)-H(12B)	0.9900
C(13)-H(13A)	0.9800
C(13)-H(13B)	0.9800
C(13)-H(13C)	0.9800
C(6)-Fe(1)-C(5)	100.57(8)
C(6)-Fe(1)-C(4)	98.77(8)
C(5)-Fe(1)-C(4)	93.65(8)
C(6)-Fe(1)-S(4)	99.23(5)
C(5)-Fe(1)-S(4)	159.70(6)
C(4)-Fe(1)-S(4)	87.71(5)
C(6)-Fe(1)-S(3)	103.97(6)
C(5)-Fe(1)-S(3)	87.41(6)
C(4)-Fe(1)-S(3)	156.65(6)
S(4)-Fe(1)-S(3)	83.510(17)
C(6)-Fe(1)-Fe(2)	147.67(6)
C(5)-Fe(1)-Fe(2)	103.18(6)
C(4)-Fe(1)-Fe(2)	101.26(6)
S(4)-Fe(1)-Fe(2)	56.818(13)
S(3)-Fe(1)-Fe(2)	56.011(14)
C(3)-Fe(2)-C(2)	92.50(8)
C(3)-Fe(2)-C(1)	96.60(8)
C(2)-Fe(2)-C(1)	98.26(8)
C(3)-Fe(2)-S(3)	86.55(5)
C(2)-Fe(2)-S(3)	155.87(6)
C(1)-Fe(2)-S(3)	105.80(5)
C(3)-Fe(2)-S(4)	151.48(6)
C(2)-Fe(2)-S(4)	86.13(6)
C(1)-Fe(2)-S(4)	111.80(6)
S(3)-Fe(2)-S(4)	83.390(16)
C(3)-Fe(2)-Fe(1)	96.34(6)
C(2)-Fe(2)-Fe(1)	99.71(6)

C(1)-Fe(2)-Fe(1)	157.31(5)
S(3)-Fe(2)-Fe(1)	56.562(13)
S(4)-Fe(2)-Fe(1)	56.066(14)
C(7)-S(3)-Fe(2)	117.35(5)
C(7)-S(3)-Fe(1)	110.70(6)
Fe(2)-S(3)-Fe(1)	67.427(14)
C(8)-S(4)-Fe(1)	108.87(5)
C(8)-S(4)-Fe(2)	119.17(6)
Fe(1)-S(4)-Fe(2)	67.116(14)
O(6)-C(6)-Fe(1)	177.06(15)
O(4)-C(4)-Fe(1)	178.17(15)
O(3)-C(3)-Fe(2)	178.31(15)
O(1)-C(1)-Fe(2)	176.18(15)
O(5)-C(5)-Fe(1)	177.57(16)
O(2)-C(2)-Fe(2)	177.98(17)
C(7)-C(9)-C(8)	111.63(13)
C(7)-C(9)-C(10)	114.40(14)
C(8)-C(9)-C(10)	108.00(12)
C(7)-C(9)-C(12)	107.03(12)
C(8)-C(9)-C(12)	108.07(13)
C(10)-C(9)-C(12)	107.47(13)
C(9)-C(7)-S(3)	122.08(11)
C(9)-C(7)-H(7A)	106.8
S(3)-C(7)-H(7A)	106.8
C(9)-C(7)-H(7B)	106.8
S(3)-C(7)-H(7B)	106.8
H(7A)-C(7)-H(7B)	106.7
C(9)-C(8)-S(4)	119.40(11)
C(9)-C(8)-H(8A)	107.5
S(4)-C(8)-H(8A)	107.5
C(9)-C(8)-H(8B)	107.5
S(4)-C(8)-H(8B)	107.5
H(8A)-C(8)-H(8B)	107.0
C(11)-C(10)-C(9)	116.59(14)

C(11)-C(10)-H(10A)	108.1
C(9)-C(10)-H(10A)	108.1
C(11)-C(10)-H(10B)	108.1
C(9)-C(10)-H(10B)	108.1
H(10A)-C(10)-H(10B)	107.3
C(10)-C(11)-H(11A)	109.5
C(10)-C(11)-H(11B)	109.5
H(11A)-C(11)-H(11B)	109.5
C(10)-C(11)-H(11C)	109.5
H(11A)-C(11)-H(11C)	109.5
H(11B)-C(11)-H(11C)	109.5
C(13)-C(12)-C(9)	118.17(13)
C(13)-C(12)-H(12A)	107.8
C(9)-C(12)-H(12A)	107.8
C(13)-C(12)-H(12B)	107.8
C(9)-C(12)-H(12B)	107.8
H(12A)-C(12)-H(12B)	107.1
C(12)-C(13)-H(13A)	109.5
C(12)-C(13)-H(13B)	109.5
H(13A)-C(13)-H(13B)	109.5
C(12)-C(13)-H(13C)	109.5
H(13A)-C(13)-H(13C)	109.5
H(13B)-C(13)-H(13C)	109.5

Symmetry transformations used to generate equivalent atoms:

Table A-9. Anisotropic displacement parameters ($Å^2 x\ 10^3$) for III-2. The anisotropic displacement factor exponent takes the form: $-2\pi^2[\ h^2\ a^{*2}U^{11} + ... + 2\ h\ k\ a^*\ b^*\ U^{12}\ ]$

	U^{11}	U^{22}	U^{33}	U^{23}	U^{13}	U^{12}
Fe(1)	18(1)	13(1)	12(1)	-1(1)	4(1)	1(1)
Fe(2)	19(1)	14(1)	11(1)	0(1)	4(1)	-2(1)
S(3)	18(1)	13(1)	10(1)	-1(1)	3(1)	0(1)
S(4)	19(1)	14(1)	10(1)	0(1)	3(1)	-1(1)
O(1)	24(1)	32(1)	25(1)	-3(1)	12(1)	-2(1)
O(6)	27(1)	37(1)	23(1)	2(1)	9(1)	-6(1)
O(4)	33(1)	26(1)	28(1)	4(1)	2(1)	10(1)
O(5)	36(1)	26(1)	25(1)	-10(1)	4(1)	2(1)
O(3)	36(1)	25(1)	29(1)	-6(1)	6(1)	-11(1)
C(6)	23(1)	24(1)	11(1)	-2(1)	3(1)	3(1)
O(2)	39(1)	28(1)	23(1)	11(1)	3(1)	-2(1)
C(4)	23(1)	19(1)	19(1)	-4(1)	6(1)	2(1)
C(3)	26(1)	17(1)	19(1)	1(1)	9(1)	-3(1)
C(1)	21(1)	20(1)	14(1)	1(1)	3(1)	-3(1)
C(5)	24(1)	19(1)	20(1)	0(1)	7(1)	6(1)
C(2)	25(1)	20(1)	20(1)	-2(1)	7(1)	-5(1)
C(9)	20(1)	14(1)	13(1)	-1(1)	5(1)	-1(1)
C(7)	25(1)	12(1)	12(1)	0(1)	4(1)	0(1)
C(8)	21(1)	14(1)	14(1)	0(1)	3(1)	-3(1)
C(10)	28(1)	16(1)	17(1)	-3(1)	9(1)	0(1)
C(11)	26(1)	23(1)	31(1)	1(1)	12(1)	4(1)
C(12)	27(1)	15(1)	18(1)	0(1)	6(1)	-1(1)
C(13)	30(1)	20(1)	22(1)	3(1)	8(1)	-4(1)

Table A-10. Hydrogen coordinates (x 10^4) and isotropic displacement parameters ($Å^2$x 10^3) for III-2.

	x	y	z	U(eq)
H(7A)	10323	6672	11101	20
H(7B)	8347	6830	11260	20
H(8A)	5757	6859	9369	20
H(8B)	6329	6648	8224	20
H(10A)	9276	6037	8319	23
H(10B)	9736	6861	8408	23
H(11A)	12202	6659	9906	39
H(11B)	12366	6153	8871	39
H(11C)	11692	5838	9934	39
H(12A)	7167	5545	9247	24
H(12B)	8911	5501	10257	24
H(13A)	7293	5878	11563	35
H(13B)	6203	5240	10852	35
H(13C)	5559	6039	10573	35

Table A-11. Torsion angles [°] for III-2.

C(6)-Fe(1)-Fe(2)-C(3)	-140.22(11)
C(5)-Fe(1)-Fe(2)-C(3)	-3.97(8)
C(4)-Fe(1)-Fe(2)-C(3)	92.54(8)
S(4)-Fe(1)-Fe(2)-C(3)	172.24(6)
S(3)-Fe(1)-Fe(2)-C(3)	-81.62(6)
C(6)-Fe(1)-Fe(2)-C(2)	126.15(11)
C(5)-Fe(1)-Fe(2)-C(2)	-97.61(8)
C(4)-Fe(1)-Fe(2)-C(2)	-1.10(8)
S(4)-Fe(1)-Fe(2)-C(2)	78.60(6)
S(3)-Fe(1)-Fe(2)-C(2)	-175.26(6)
C(6)-Fe(1)-Fe(2)-C(1)	-15.78(18)
C(5)-Fe(1)-Fe(2)-C(1)	120.46(15)
C(4)-Fe(1)-Fe(2)-C(1)	-143.03(15)
S(4)-Fe(1)-Fe(2)-C(1)	-63.33(14)
S(3)-Fe(1)-Fe(2)-C(1)	42.81(14)
C(6)-Fe(1)-Fe(2)-S(3)	-58.60(10)
C(5)-Fe(1)-Fe(2)-S(3)	77.65(6)
C(4)-Fe(1)-Fe(2)-S(3)	174.15(6)
S(4)-Fe(1)-Fe(2)-S(3)	-106.14(2)
C(6)-Fe(1)-Fe(2)-S(4)	47.54(10)
C(5)-Fe(1)-Fe(2)-S(4)	-176.21(6)
C(4)-Fe(1)-Fe(2)-S(4)	-79.70(6)
S(3)-Fe(1)-Fe(2)-S(4)	106.14(2)
C(3)-Fe(2)-S(3)-C(7)	-157.61(9)
C(2)-Fe(2)-S(3)-C(7)	113.97(15)
C(1)-Fe(2)-S(3)-C(7)	-61.72(9)
S(4)-Fe(2)-S(3)-C(7)	49.12(7)
Fe(1)-Fe(2)-S(3)-C(7)	102.47(7)
C(3)-Fe(2)-S(3)-Fe(1)	99.92(6)
C(2)-Fe(2)-S(3)-Fe(1)	11.51(14)
C(1)-Fe(2)-S(3)-Fe(1)	-164.19(6)
S(4)-Fe(2)-S(3)-Fe(1)	-53.350(16)

C(6)-Fe(1)-S(3)-C(7)	39.93(7)
C(5)-Fe(1)-S(3)-C(7)	140.19(8)
C(4)-Fe(1)-S(3)-C(7)	-126.61(15)
S(4)-Fe(1)-S(3)-C(7)	-58.00(5)
Fe(2)-Fe(1)-S(3)-C(7)	-112.01(5)
C(6)-Fe(1)-S(3)-Fe(2)	151.94(5)
C(5)-Fe(1)-S(3)-Fe(2)	-107.80(6)
C(4)-Fe(1)-S(3)-Fe(2)	-14.60(14)
S(4)-Fe(1)-S(3)-Fe(2)	54.010(16)
C(6)-Fe(1)-S(4)-C(8)	-41.93(8)
C(5)-Fe(1)-S(4)-C(8)	125.21(17)
C(4)-Fe(1)-S(4)-C(8)	-140.44(8)
S(3)-Fe(1)-S(4)-C(8)	61.23(6)
Fe(2)-Fe(1)-S(4)-C(8)	114.51(6)
C(6)-Fe(1)-S(4)-Fe(2)	-156.44(6)
C(5)-Fe(1)-S(4)-Fe(2)	10.69(16)
C(4)-Fe(1)-S(4)-Fe(2)	105.04(6)
S(3)-Fe(1)-S(4)-Fe(2)	-53.282(16)
C(3)-Fe(2)-S(4)-C(8)	-115.90(13)
C(2)-Fe(2)-S(4)-C(8)	155.99(8)
C(1)-Fe(2)-S(4)-C(8)	58.63(8)
S(3)-Fe(2)-S(4)-C(8)	-45.78(6)
Fe(1)-Fe(2)-S(4)-C(8)	-99.58(6)
C(3)-Fe(2)-S(4)-Fe(1)	-16.32(12)
C(2)-Fe(2)-S(4)-Fe(1)	-104.43(6)
C(1)-Fe(2)-S(4)-Fe(1)	158.21(6)
S(3)-Fe(2)-S(4)-Fe(1)	53.798(16)
C(5)-Fe(1)-C(6)-O(6)	176(100)
C(4)-Fe(1)-C(6)-O(6)	81(3)
S(4)-Fe(1)-C(6)-O(6)	-8(3)
S(3)-Fe(1)-C(6)-O(6)	-94(3)
Fe(2)-Fe(1)-C(6)-O(6)	-47(3)
C(6)-Fe(1)-C(4)-O(4)	-94(5)
C(5)-Fe(1)-C(4)-O(4)	165(5)

S(4)-Fe(1)-C(4)-O(4)	5(5)
S(3)-Fe(1)-C(4)-O(4)	73(5)
Fe(2)-Fe(1)-C(4)-O(4)	60(5)
C(2)-Fe(2)-C(3)-O(3)	127(6)
C(1)-Fe(2)-C(3)-O(3)	-134(6)
S(3)-Fe(2)-C(3)-O(3)	-29(6)
S(4)-Fe(2)-C(3)-O(3)	41(6)
Fe(1)-Fe(2)-C(3)-O(3)	27(6)
C(3)-Fe(2)-C(1)-O(1)	-15(2)
C(2)-Fe(2)-C(1)-O(1)	79(2)
S(3)-Fe(2)-C(1)-O(1)	-103(2)
S(4)-Fe(2)-C(1)-O(1)	168(2)
Fe(1)-Fe(2)-C(1)-O(1)	-139(2)
C(6)-Fe(1)-C(5)-O(5)	121(4)
C(4)-Fe(1)-C(5)-O(5)	-139(4)
S(4)-Fe(1)-C(5)-O(5)	-46(4)
S(3)-Fe(1)-C(5)-O(5)	17(4)
Fe(2)-Fe(1)-C(5)-O(5)	-37(4)
C(3)-Fe(2)-C(2)-O(2)	-119(4)
C(1)-Fe(2)-C(2)-O(2)	144(4)
S(3)-Fe(2)-C(2)-O(2)	-31(5)
S(4)-Fe(2)-C(2)-O(2)	33(4)
Fe(1)-Fe(2)-C(2)-O(2)	-22(4)
C(8)-C(9)-C(7)-S(3)	-50.38(18)
C(10)-C(9)-C(7)-S(3)	72.64(17)
C(12)-C(9)-C(7)-S(3)	-168.43(12)
Fe(2)-S(3)-C(7)-C(9)	-11.61(16)
Fe(1)-S(3)-C(7)-C(9)	62.93(14)
C(7)-C(9)-C(8)-S(4)	54.24(17)
C(10)-C(9)-C(8)-S(4)	-72.34(15)
C(12)-C(9)-C(8)-S(4)	171.67(10)
Fe(1)-S(4)-C(8)-C(9)	-71.20(12)
Fe(2)-S(4)-C(8)-C(9)	2.55(14)
C(7)-C(9)-C(10)-C(11)	38.0(2)

C(8)-C(9)-C(10)-C(11)	162.99(14)
C(12)-C(9)-C(10)-C(11)	-80.64(17)
C(7)-C(9)-C(12)-C(13)	51.16(19)
C(8)-C(9)-C(12)-C(13)	-69.20(18)
C(10)-C(9)-C(12)-C(13)	174.48(15)

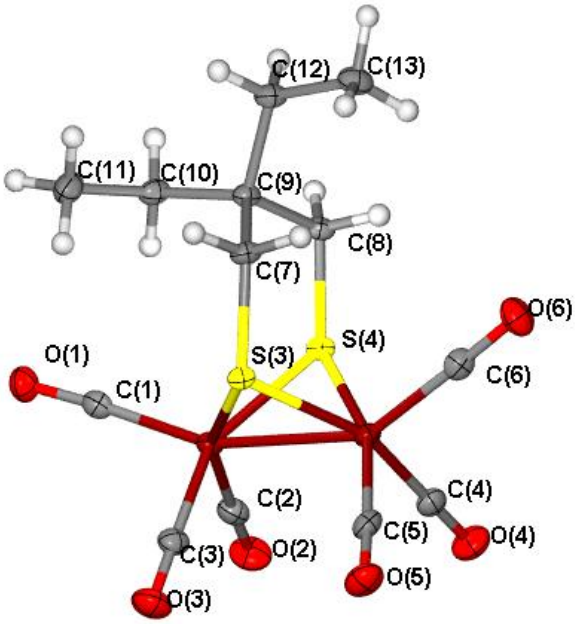

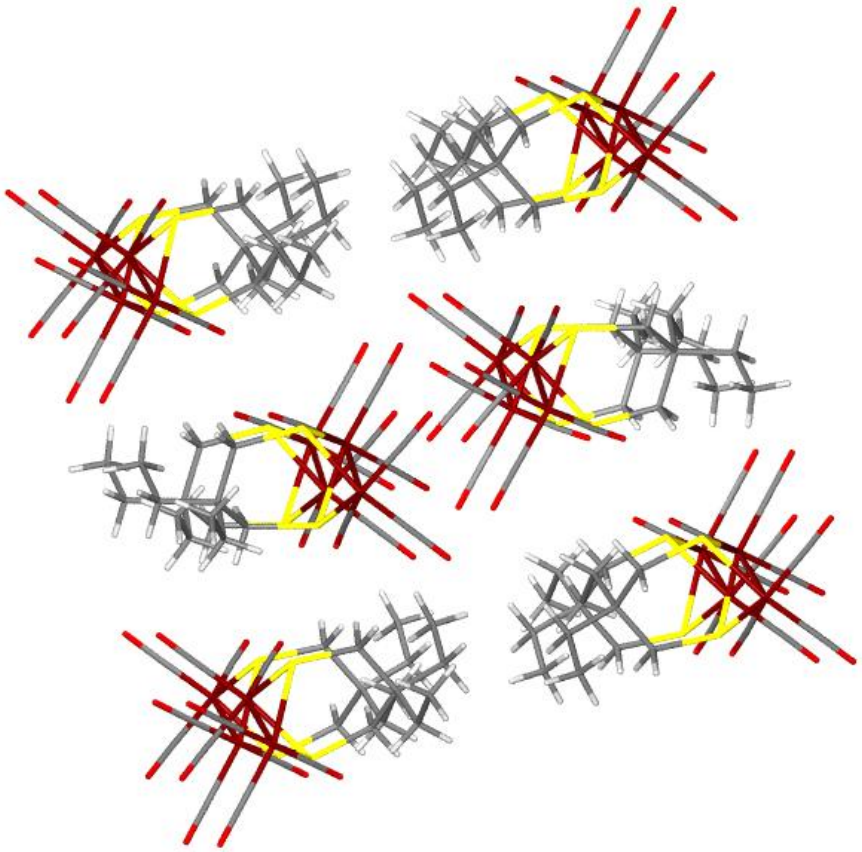

Table A-12. Crystal data and structure refinement for Complex III-**3**.

Identification code	Febepdt	
Empirical formula	C15 H18 Fe2 O6 S2	
Formula weight	470.11	
Temperature	110(2) K	
Wavelength	0.71073 Å	
Crystal system	Triclinic	
Space group	P-1	
Unit cell dimensions	a = 7.622(3) Å	α= 101.484(5)°.
	b = 11.026(4) Å	β= 91.528(6)°.
	c = 11.585(4) Å	γ = 101.247(5)°.
Volume	933.6(5) $Å^3$	
Z	2	
Density (calculated)	1.672 Mg/m^3	
Absorption coefficient	1.804 mm^{-1}	
F(000)	480	
Crystal size	0.31 x 0.13 x 0.08 mm^3	
Theta range for data collection	1.80 to 28.33°.	
Index ranges	-9<=h<=9, -14<=k<=14, -14<=l<=14	
Reflections collected	8834	
Independent reflections	4203 [R(int) = 0.0572]	
Completeness to theta = 28.33°	90.3 %	
Absorption correction	None	
Max. and min. transmission	0.8751 and 0.6082	
Refinement method	Full-matrix least-squares on F^2	
Data / restraints / parameters	4203 / 0 / 228	
Goodness-of-fit on F^2	0.999	
Final R indices [I>2sigma(I)]	R1 = 0.0560, wR2 = 0.1264	
R indices (all data)	R1 = 0.0865, wR2 = 0.1416	
Largest diff. peak and hole	2.008 and -0.477 e.$Å^{-3}$	

Table A-13. Atomic coordinates (x 10^4) and equivalent isotropic displacement parameters ($Å^2$x 10^3) for III-3. U(eq) is defined as one third of the trace of the orthogonalized U^{ij} tensor.

	x	y	z	U(eq)
Fe(1)	4047(1)	7060(1)	3991(1)	20(1)
Fe(2)	1252(1)	7654(1)	3299(1)	21(1)
S(3)	3174(2)	6837(1)	2064(1)	21(1)
S(4)	1262(1)	5933(1)	4072(1)	20(1)
C(13)	-563(6)	1861(4)	1357(4)	21(1)
O(4)	6788(4)	5550(3)	4128(3)	32(1)
O(6)	3907(4)	7880(3)	6558(3)	34(1)
O(3)	-230(5)	8683(3)	5511(3)	34(1)
C(6)	3977(6)	7575(4)	5564(4)	26(1)
C(3)	363(6)	8318(4)	4648(4)	23(1)
O(2)	2663(4)	10134(3)	2733(3)	34(1)
O(5)	6545(5)	9410(3)	3844(3)	38(1)
C(5)	5578(6)	8489(4)	3885(4)	26(1)
O(1)	-2108(4)	6838(3)	1803(3)	33(1)
C(2)	2098(6)	9178(4)	2953(4)	24(1)
C(7)	497(6)	4465(4)	2979(4)	22(1)
C(4)	5706(6)	6103(4)	4048(4)	24(1)
C(12)	312(6)	3090(4)	976(4)	24(1)
C(1)	-794(6)	7170(4)	2387(4)	24(1)
C(9)	1991(6)	5265(4)	1275(4)	23(1)
C(11)	3225(6)	3672(4)	2244(4)	25(1)
C(10)	4707(6)	3683(4)	1375(4)	33(1)
C(8)	1566(6)	4135(4)	1896(4)	21(1)
C(14)	-1833(6)	979(4)	393(4)	31(1)
C(15)	-2825(7)	-199(4)	779(5)	41(1)

Table A-14. Bond lengths [Å] and angles [°] for III-3.

Fe(1)-C(5)	1.796(5)
Fe(1)-C(6)	1.803(5)
Fe(1)-C(4)	1.805(5)
Fe(1)-S(4)	2.2557(14)
Fe(1)-S(3)	2.2634(14)
Fe(1)-Fe(2)	2.5046(11)
Fe(2)-C(1)	1.788(5)
Fe(2)-C(3)	1.797(5)
Fe(2)-C(2)	1.805(4)
Fe(2)-S(4)	2.2550(13)
Fe(2)-S(3)	2.2630(13)
S(3)-C(9)	1.835(4)
S(4)-C(7)	1.827(4)
C(13)-C(14)	1.508(6)
C(13)-C(12)	1.542(5)
C(13)-H(13A)	0.9900
C(13)-H(13B)	0.9900
O(4)-C(4)	1.130(5)
O(6)-C(6)	1.139(5)
O(3)-C(3)	1.141(5)
O(2)-C(2)	1.140(5)
O(5)-C(5)	1.143(5)
O(1)-C(1)	1.147(5)
C(7)-C(8)	1.535(6)
C(7)-H(7A)	0.9900
C(7)-H(7B)	0.9900
C(12)-C(8)	1.551(6)
C(12)-H(12A)	0.9900
C(12)-H(12B)	0.9900
C(9)-C(8)	1.545(6)
C(9)-H(9A)	0.9900
C(9)-H(9B)	0.9900

C(11)-C(8)	1.526(6)
C(11)-C(10)	1.533(6)
C(11)-H(11A)	0.9900
C(11)-H(11B)	0.9900
C(10)-H(10A)	0.9800
C(10)-H(10B)	0.9800
C(10)-H(10C)	0.9800
C(14)-C(15)	1.524(6)
C(14)-H(14A)	0.9900
C(14)-H(14B)	0.9900
C(15)-H(15A)	0.9800
C(15)-H(15B)	0.9800
C(15)-H(15C)	0.9800
C(5)-Fe(1)-C(6)	92.1(2)
C(5)-Fe(1)-C(4)	96.9(2)
C(6)-Fe(1)-C(4)	96.7(2)
C(5)-Fe(1)-S(4)	152.11(15)
C(6)-Fe(1)-S(4)	85.13(14)
C(4)-Fe(1)-S(4)	111.00(14)
C(5)-Fe(1)-S(3)	88.17(15)
C(6)-Fe(1)-S(3)	156.04(15)
C(4)-Fe(1)-S(3)	107.02(14)
S(4)-Fe(1)-S(3)	83.55(4)
C(5)-Fe(1)-Fe(2)	97.21(14)
C(6)-Fe(1)-Fe(2)	99.88(14)
C(4)-Fe(1)-Fe(2)	157.72(14)
S(4)-Fe(1)-Fe(2)	56.26(4)
S(3)-Fe(1)-Fe(2)	56.40(3)
C(1)-Fe(2)-C(3)	98.39(19)
C(1)-Fe(2)-C(2)	100.52(19)
C(3)-Fe(2)-C(2)	93.60(19)
C(1)-Fe(2)-S(4)	101.24(13)
C(3)-Fe(2)-S(4)	86.77(13)
C(2)-Fe(2)-S(4)	157.94(14)

C(1)-Fe(2)-S(3)	101.00(14)
C(3)-Fe(2)-S(3)	159.69(14)
C(2)-Fe(2)-S(3)	88.80(15)
S(4)-Fe(2)-S(3)	83.58(4)
C(1)-Fe(2)-Fe(1)	146.99(13)
C(3)-Fe(2)-Fe(1)	103.47(14)
C(2)-Fe(2)-Fe(1)	102.45(14)
S(4)-Fe(2)-Fe(1)	56.28(3)
S(3)-Fe(2)-Fe(1)	56.41(4)
C(9)-S(3)-Fe(2)	107.22(15)
C(9)-S(3)-Fe(1)	117.42(14)
Fe(2)-S(3)-Fe(1)	67.19(4)
C(7)-S(4)-Fe(2)	112.02(14)
C(7)-S(4)-Fe(1)	118.46(15)
Fe(2)-S(4)-Fe(1)	67.46(4)
C(14)-C(13)-C(12)	111.8(3)
C(14)-C(13)-H(13A)	109.3
C(12)-C(13)-H(13A)	109.3
C(14)-C(13)-H(13B)	109.3
C(12)-C(13)-H(13B)	109.3
H(13A)-C(13)-H(13B)	107.9
O(6)-C(6)-Fe(1)	178.7(4)
O(3)-C(3)-Fe(2)	176.8(4)
O(5)-C(5)-Fe(1)	178.4(4)
O(2)-C(2)-Fe(2)	178.7(4)
C(8)-C(7)-S(4)	120.7(3)
C(8)-C(7)-H(7A)	107.2
S(4)-C(7)-H(7A)	107.2
C(8)-C(7)-H(7B)	107.2
S(4)-C(7)-H(7B)	107.2
H(7A)-C(7)-H(7B)	106.8
O(4)-C(4)-Fe(1)	176.6(4)
C(13)-C(12)-C(8)	118.2(3)
C(13)-C(12)-H(12A)	107.7

C(8)-C(12)-H(12A)	107.8
C(13)-C(12)-H(12B)	107.7
C(8)-C(12)-H(12B)	107.7
H(12A)-C(12)-H(12B)	107.1
O(1)-C(1)-Fe(2)	178.9(4)
C(8)-C(9)-S(3)	121.9(3)
C(8)-C(9)-H(9A)	106.9
S(3)-C(9)-H(9A)	106.9
C(8)-C(9)-H(9B)	106.9
S(3)-C(9)-H(9B)	106.9
H(9A)-C(9)-H(9B)	106.7
C(8)-C(11)-C(10)	116.5(4)
C(8)-C(11)-H(11A)	108.2
C(10)-C(11)-H(11A)	108.2
C(8)-C(11)-H(11B)	108.2
C(10)-C(11)-H(11B)	108.2
H(11A)-C(11)-H(11B)	107.3
C(11)-C(10)-H(10A)	109.5
C(11)-C(10)-H(10B)	109.5
H(10A)-C(10)-H(10B)	109.5
C(11)-C(10)-H(10C)	109.5
H(10A)-C(10)-H(10C)	109.5
H(10B)-C(10)-H(10C)	109.5
C(11)-C(8)-C(7)	110.4(3)
C(11)-C(8)-C(9)	113.6(4)
C(7)-C(8)-C(9)	110.3(3)
C(11)-C(8)-C(12)	110.6(3)
C(7)-C(8)-C(12)	107.6(3)
C(9)-C(8)-C(12)	104.1(3)
C(13)-C(14)-C(15)	112.9(4)
C(13)-C(14)-H(14A)	109.0
C(15)-C(14)-H(14A)	109.0
C(13)-C(14)-H(14B)	109.0
C(15)-C(14)-H(14B)	109.0

H(14A)-C(14)-H(14B)	107.8
C(14)-C(15)-H(15A)	109.5
C(14)-C(15)-H(15B)	109.5
H(15A)-C(15)-H(15B)	109.5
C(14)-C(15)-H(15C)	109.5
H(15A)-C(15)-H(15C)	109.5
H(15B)-C(15)-H(15C)	109.5

Symmetry transformations used to generate equivalent atoms:

Table A-15. Anisotropic displacement parameters ($Å^2 x\ 10^3$) for III-3. The anisotropic displacement factor exponent takes the form: $-2\pi^2[\ h^2\ a^{*2}U^{11} + ...\ + 2\ h\ k\ a^*\ b^*\ U^{12}\ ]$

	U^{11}	U^{22}	U^{33}	U^{23}	U^{13}	U^{12}
Fe(1)	18(1)	22(1)	22(1)	6(1)	2(1)	5(1)
Fe(2)	20(1)	21(1)	22(1)	6(1)	3(1)	6(1)
S(3)	22(1)	22(1)	21(1)	6(1)	5(1)	5(1)
S(4)	20(1)	21(1)	20(1)	5(1)	4(1)	4(1)
C(13)	23(2)	18(2)	23(2)	5(2)	-1(2)	1(2)
O(4)	22(2)	38(2)	42(2)	17(2)	3(2)	12(2)
O(6)	34(2)	40(2)	26(2)	6(2)	4(2)	7(2)
O(3)	38(2)	35(2)	32(2)	6(1)	12(2)	14(2)
C(6)	16(2)	25(2)	35(3)	7(2)	1(2)	1(2)
C(3)	21(2)	20(2)	29(2)	9(2)	-1(2)	2(2)
O(2)	37(2)	28(2)	41(2)	13(2)	9(2)	7(2)
O(5)	35(2)	32(2)	44(2)	11(2)	-4(2)	-1(2)
C(5)	23(2)	25(2)	33(3)	10(2)	0(2)	6(2)
O(1)	23(2)	46(2)	28(2)	8(2)	-3(2)	1(2)
C(2)	18(2)	25(2)	29(2)	5(2)	2(2)	5(2)
C(7)	22(2)	17(2)	25(2)	3(2)	2(2)	0(2)
C(4)	21(2)	27(2)	24(2)	9(2)	1(2)	1(2)
C(12)	25(2)	24(2)	23(2)	6(2)	3(2)	2(2)
C(1)	29(3)	25(2)	24(2)	11(2)	14(2)	11(2)
C(9)	27(2)	20(2)	22(2)	3(2)	3(2)	5(2)
C(11)	25(2)	23(2)	28(2)	6(2)	3(2)	7(2)
C(10)	23(3)	36(3)	38(3)	4(2)	8(2)	10(2)
C(8)	19(2)	21(2)	23(2)	7(2)	4(2)	5(2)
C(14)	27(3)	27(2)	38(3)	6(2)	1(2)	6(2)
C(15)	35(3)	29(3)	54(3)	2(2)	2(3)	-2(2)

Table A-16. Hydrogen coordinates (x 10^4) and isotropic displacement parameters ($Å^2$x 10^3) for III-3.

	x	y	z	U(eq)
H(13A)	385	1429	1568	26
H(13B)	-1227	2073	2068	26
H(7A)	398	3761	3403	26
H(7B)	-732	4468	2682	26
H(12A)	-662	3464	702	29
H(12B)	1009	2857	287	29
H(9A)	835	5370	941	28
H(9B)	2698	5007	598	28
H(11A)	2836	2796	2360	30
H(11B)	3748	4202	3015	30
H(10A)	4203	3196	594	49
H(10B)	5654	3303	1653	49
H(10C)	5210	4557	1320	49
H(14A)	-1148	718	-295	37
H(14B)	-2720	1437	139	37
H(15A)	-1955	-662	1024	62
H(15B)	-3617	-742	119	62
H(15C)	-3540	51	1442	62

Table A-17. Torsion angles [°] for III-3.

C(5)-Fe(1)-Fe(2)-C(1)	136.0(3)
C(6)-Fe(1)-Fe(2)-C(1)	-130.7(3)
C(4)-Fe(1)-Fe(2)-C(1)	7.0(5)
S(4)-Fe(1)-Fe(2)-C(1)	-53.4(3)
S(3)-Fe(1)-Fe(2)-C(1)	53.0(3)
C(5)-Fe(1)-Fe(2)-C(3)	-94.0(2)
C(6)-Fe(1)-Fe(2)-C(3)	-0.56(18)
C(4)-Fe(1)-Fe(2)-C(3)	137.1(4)
S(4)-Fe(1)-Fe(2)-C(3)	76.73(14)
S(3)-Fe(1)-Fe(2)-C(3)	-176.90(14)
C(5)-Fe(1)-Fe(2)-C(2)	2.9(2)
C(6)-Fe(1)-Fe(2)-C(2)	96.3(2)
C(4)-Fe(1)-Fe(2)-C(2)	-126.0(4)
S(4)-Fe(1)-Fe(2)-C(2)	173.57(15)
S(3)-Fe(1)-Fe(2)-C(2)	-80.07(15)
C(5)-Fe(1)-Fe(2)-S(4)	-170.69(16)
C(6)-Fe(1)-Fe(2)-S(4)	-77.29(14)
C(4)-Fe(1)-Fe(2)-S(4)	60.4(4)
S(3)-Fe(1)-Fe(2)-S(4)	106.37(5)
C(5)-Fe(1)-Fe(2)-S(3)	82.94(16)
C(6)-Fe(1)-Fe(2)-S(3)	176.34(14)
C(4)-Fe(1)-Fe(2)-S(3)	-46.0(4)
S(4)-Fe(1)-Fe(2)-S(3)	-106.37(5)
C(1)-Fe(2)-S(3)-C(9)	-40.6(2)
C(3)-Fe(2)-S(3)-C(9)	121.8(4)
C(2)-Fe(2)-S(3)-C(9)	-141.0(2)
S(4)-Fe(2)-S(3)-C(9)	59.69(15)
Fe(1)-Fe(2)-S(3)-C(9)	113.13(15)
C(1)-Fe(2)-S(3)-Fe(1)	-153.69(14)
C(3)-Fe(2)-S(3)-Fe(1)	8.7(4)
C(2)-Fe(2)-S(3)-Fe(1)	105.83(14)
S(4)-Fe(2)-S(3)-Fe(1)	-53.43(4)

C(5)-Fe(1)-S(3)-C(9)	161.8(2)
C(6)-Fe(1)-S(3)-C(9)	-107.2(4)
C(4)-Fe(1)-S(3)-C(9)	65.2(2)
S(4)-Fe(1)-S(3)-C(9)	-44.84(17)
Fe(2)-Fe(1)-S(3)-C(9)	-98.25(17)
C(5)-Fe(1)-S(3)-Fe(2)	-99.91(15)
C(6)-Fe(1)-S(3)-Fe(2)	-8.9(3)
C(4)-Fe(1)-S(3)-Fe(2)	163.44(14)
S(4)-Fe(1)-S(3)-Fe(2)	53.41(4)
C(1)-Fe(2)-S(4)-C(7)	40.7(2)
C(3)-Fe(2)-S(4)-C(7)	138.6(2)
C(2)-Fe(2)-S(4)-C(7)	-129.8(4)
S(3)-Fe(2)-S(4)-C(7)	-59.33(16)
Fe(1)-Fe(2)-S(4)-C(7)	-112.88(16)
C(1)-Fe(2)-S(4)-Fe(1)	153.53(14)
C(3)-Fe(2)-S(4)-Fe(1)	-108.55(14)
C(2)-Fe(2)-S(4)-Fe(1)	-16.9(4)
S(3)-Fe(2)-S(4)-Fe(1)	53.55(4)
C(5)-Fe(1)-S(4)-C(7)	123.8(4)
C(6)-Fe(1)-S(4)-C(7)	-151.0(2)
C(4)-Fe(1)-S(4)-C(7)	-55.6(2)
S(3)-Fe(1)-S(4)-C(7)	50.16(16)
Fe(2)-Fe(1)-S(4)-C(7)	103.70(17)
C(5)-Fe(1)-S(4)-Fe(2)	20.1(3)
C(6)-Fe(1)-S(4)-Fe(2)	105.31(14)
C(4)-Fe(1)-S(4)-Fe(2)	-159.33(15)
S(3)-Fe(1)-S(4)-Fe(2)	-53.54(4)
C(5)-Fe(1)-C(6)-O(6)	175(100)
C(4)-Fe(1)-C(6)-O(6)	-88(18)
S(4)-Fe(1)-C(6)-O(6)	23(18)
S(3)-Fe(1)-C(6)-O(6)	85(19)
Fe(2)-Fe(1)-C(6)-O(6)	77(18)
C(1)-Fe(2)-C(3)-O(3)	77(7)
C(2)-Fe(2)-C(3)-O(3)	178(100)

S(4)-Fe(2)-C(3)-O(3)	-24(7)
S(3)-Fe(2)-C(3)-O(3)	-85(7)
Fe(1)-Fe(2)-C(3)-O(3)	-78(7)
C(6)-Fe(1)-C(5)-O(5)	-10(15)
C(4)-Fe(1)-C(5)-O(5)	-107(15)
S(4)-Fe(1)-C(5)-O(5)	73(15)
S(3)-Fe(1)-C(5)-O(5)	146(15)
Fe(2)-Fe(1)-C(5)-O(5)	90(15)
C(1)-Fe(2)-C(2)-O(2)	-138(18)
C(3)-Fe(2)-C(2)-O(2)	123(18)
S(4)-Fe(2)-C(2)-O(2)	33(18)
S(3)-Fe(2)-C(2)-O(2)	-37(18)
Fe(1)-Fe(2)-C(2)-O(2)	19(18)
Fe(2)-S(4)-C(7)-C(8)	63.9(4)
Fe(1)-S(4)-C(7)-C(8)	-11.5(4)
C(5)-Fe(1)-C(4)-O(4)	51(7)
C(6)-Fe(1)-C(4)-O(4)	-42(7)
S(4)-Fe(1)-C(4)-O(4)	-129(7)
S(3)-Fe(1)-C(4)-O(4)	141(7)
Fe(2)-Fe(1)-C(4)-O(4)	180(100)
C(14)-C(13)-C(12)-C(8)	176.3(4)
C(3)-Fe(2)-C(1)-O(1)	-104(21)
C(2)-Fe(2)-C(1)-O(1)	161(21)
S(4)-Fe(2)-C(1)-O(1)	-15(21)
S(3)-Fe(2)-C(1)-O(1)	70(21)
Fe(1)-Fe(2)-C(1)-O(1)	28(21)
Fe(2)-S(3)-C(9)-C(8)	-71.6(4)
Fe(1)-S(3)-C(9)-C(8)	1.2(4)
C(10)-C(11)-C(8)-C(7)	-162.3(4)
C(10)-C(11)-C(8)-C(9)	-37.8(5)
C(10)-C(11)-C(8)-C(12)	78.8(5)
S(4)-C(7)-C(8)-C(11)	76.5(4)
S(4)-C(7)-C(8)-C(9)	-49.9(5)
S(4)-C(7)-C(8)-C(12)	-162.8(3)

S(3)-C(9)-C(8)-C(11)	-68.7(5)
S(3)-C(9)-C(8)-C(7)	55.8(5)
S(3)-C(9)-C(8)-C(12)	171.0(3)
C(13)-C(12)-C(8)-C(11)	64.7(5)
C(13)-C(12)-C(8)-C(7)	-56.0(5)
C(13)-C(12)-C(8)-C(9)	-173.0(4)
C(12)-C(13)-C(14)-C(15)	-175.6(4)

Symmetry transformations used to generate equivalent atoms:

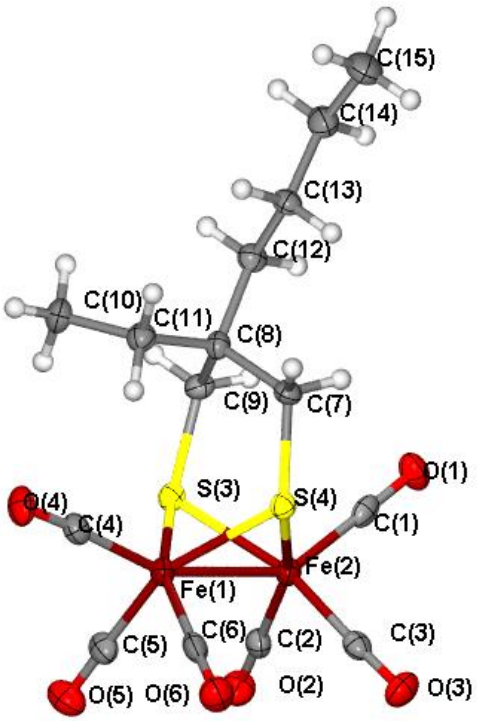

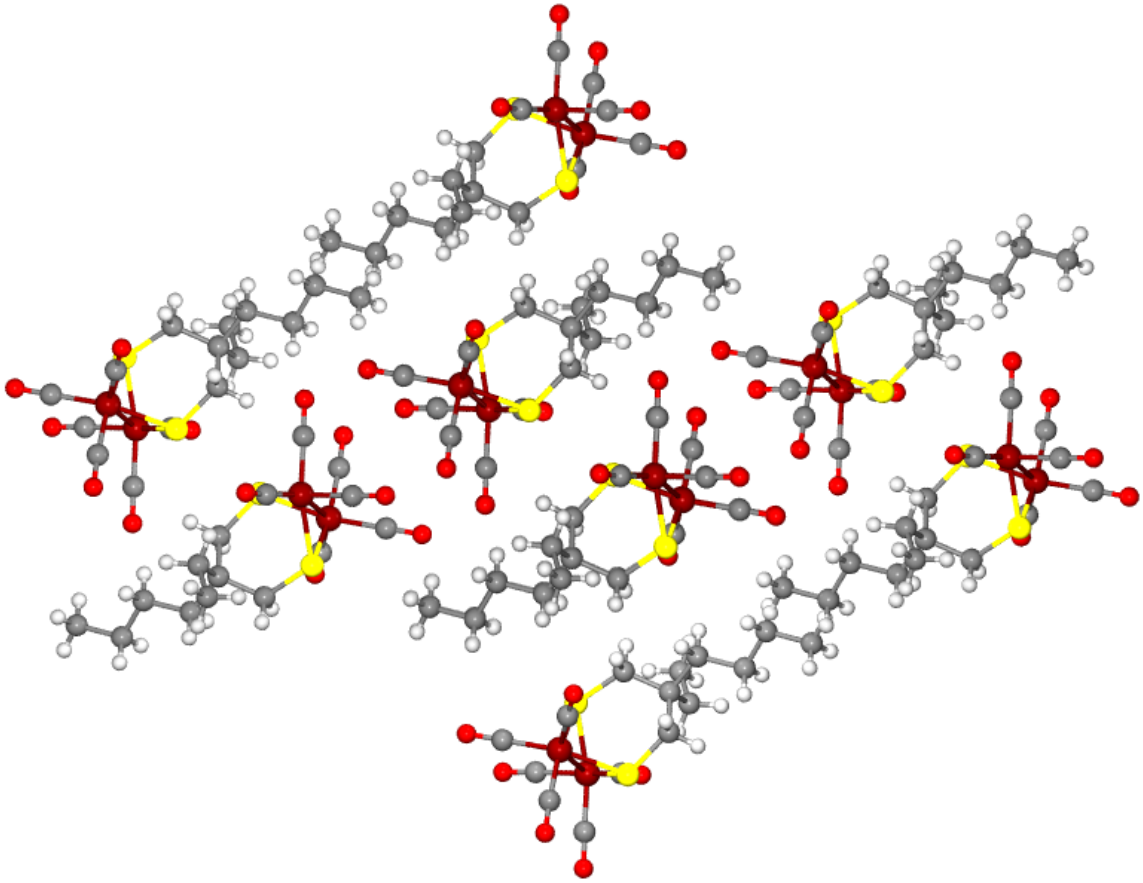

Table A-18. Crystal data and structure refinement for III-4.

Identification code	dmpdtimes	
Empirical formula	C31 H34 Fe2 N2 O5 S2	
Formula weight	690.42	
Temperature	110(2) K	
Wavelength	0.71073 Å	
Crystal system	Monoclinic	
Space group	P2(1)/c	
Unit cell dimensions	a = 11.2947(11) Å	α= 90°.
	b = 14.4543(14) Å	β= 98.0860(10)°.
	c = 19.4463(19) Å	γ = 90°.
Volume	3143.2(5) $Å^3$	
Z	4	
Density (calculated)	1.459 Mg/m^3	
Absorption coefficient	1.097 mm^{-1}	
F(000)	1432	
Crystal size	0.39 x 0.19 x 0.13 mm^3	
Theta range for data collection	1.76 to 28.70°.	
Index ranges	-15<=h<=14, -19<=k<=19, -26<=l<=25	
Reflections collected	35691	
Independent reflections	7577 [R(int) = 0.0492]	
Completeness to theta = 28.70°	93.1 %	
Absorption correction	None	
Max. and min. transmission	0.8723 and 0.6748	
Refinement method	Full-matrix least-squares on F^2	
Data / restraints / parameters	7577 / 0 / 387	
Goodness-of-fit on F^2	1.003	
Final R indices [I>2sigma(I)]	R1 = 0.0281, wR2 = 0.0867	
R indices (all data)	R1 = 0.0349, wR2 = 0.0971	
Largest diff. peak and hole	0.391 and -0.357 $e.Å^{-3}$	

Table A-19. Atomic coordinates (x 10^4) and equivalent isotropic displacement parameters ($Å^2$x 10^3) for III-4. U(eq) is defined as one third of the trace of the orthogonalized U^{ij} tensor.

	x	y	z	U(eq)
O(3)	1112(1)	2042(1)	3756(1)	42(1)
N(2)	3877(1)	4694(1)	1531(1)	26(1)
Fe(1)	3150(1)	2807(1)	2055(1)	20(1)
Fe(2)	990(1)	2732(1)	2330(1)	22(1)
S(3)	1533(1)	3341(1)	1359(1)	22(1)
O(2)	3858(1)	2245(1)	3493(1)	32(1)
C(1)	4393(2)	2314(1)	1737(1)	28(1)
C(14)	4732(1)	4215(1)	3797(1)	27(1)
O(1)	5212(1)	1941(1)	1576(1)	42(1)
O(4)	-1390(1)	2033(1)	1771(1)	48(1)
C(6)	3922(1)	4054(1)	2056(1)	23(1)
O(5)	478(1)	4599(1)	2798(1)	45(1)
C(24)	4704(2)	3732(1)	366(1)	29(1)
C(3)	1078(2)	2305(1)	3198(1)	30(1)
C(15)	3174(1)	4742(1)	849(1)	25(1)
C(5)	683(2)	3877(1)	2612(1)	30(1)
N(1)	4778(1)	4417(1)	2552(1)	27(1)
C(9)	5286(2)	4038(1)	3215(1)	27(1)
C(20)	2197(2)	5343(1)	765(1)	30(1)
C(18)	1982(2)	5058(1)	-476(1)	33(1)
C(2)	3610(2)	2527(1)	2938(1)	26(1)
C(4)	-480(2)	2325(1)	1995(1)	30(1)
C(16)	3587(1)	4312(1)	291(1)	24(1)
C(17)	2953(2)	4467(1)	-370(1)	29(1)
C(11)	6903(2)	3281(1)	3910(1)	36(1)
C(12)	6368(2)	3417(1)	4503(1)	33(1)
C(13)	5290(2)	3896(1)	4435(1)	30(1)
C(10)	6385(2)	3593(1)	3259(1)	33(1)
C(7)	4668(2)	5417(1)	1707(1)	34(1)

C(8)	5229(2)	5247(1)	2341(1)	34(1)
C(23)	3556(2)	4720(1)	3735(1)	33(1)
C(19)	1608(2)	5486(1)	103(1)	35(1)
C(26)	1804(2)	5828(1)	1385(1)	41(1)
C(22)	6968(2)	3068(2)	5195(1)	41(1)
C(25)	1362(2)	5265(2)	-1198(1)	47(1)
C(21)	7033(2)	3464(2)	2639(1)	49(1)
C(27)	1379(2)	1660(1)	527(1)	28(1)
C(28)	912(2)	2640(1)	613(1)	27(1)
C(29)	1356(2)	1074(1)	1182(1)	29(1)
C(30)	2621(2)	1681(1)	308(1)	37(1)
C(31)	527(2)	1197(1)	-64(1)	40(1)
S(1)	2031(1)	1500(1)	2033(1)	24(1)

Table A-20. Bond lengths [Å] and angles [°] for III-4.

O(3)-C(3)	1.145(2)
N(2)-C(6)	1.373(2)
N(2)-C(7)	1.386(2)
N(2)-C(15)	1.448(2)
Fe(1)-C(1)	1.7623(18)
Fe(1)-C(2)	1.7708(17)
Fe(1)-C(6)	2.0015(16)
Fe(1)-S(3)	2.2512(5)
Fe(1)-S(1)	2.2713(5)
Fe(1)-Fe(2)	2.5728(4)
Fe(2)-C(3)	1.7862(18)
Fe(2)-C(5)	1.7932(18)
Fe(2)-C(4)	1.7950(18)
Fe(2)-S(3)	2.2460(5)
Fe(2)-S(1)	2.2531(5)
S(3)-C(28)	1.8272(17)
O(2)-C(2)	1.151(2)
C(1)-O(1)	1.151(2)
C(14)-C(13)	1.388(2)
C(14)-C(9)	1.392(2)
C(14)-C(23)	1.506(2)
O(4)-C(4)	1.139(2)
C(6)-N(1)	1.371(2)
O(5)-C(5)	1.138(2)
C(24)-C(16)	1.505(2)
C(24)-H(24A)	0.9800
C(24)-H(24B)	0.9800
C(24)-H(24C)	0.9800
C(15)-C(16)	1.387(2)
C(15)-C(20)	1.396(2)
N(1)-C(8)	1.388(2)
N(1)-C(9)	1.442(2)

C(9)-C(10)	1.390(2)
C(20)-C(19)	1.380(3)
C(20)-C(26)	1.514(3)
C(18)-C(17)	1.383(3)
C(18)-C(19)	1.400(3)
C(18)-C(25)	1.508(3)
C(16)-C(17)	1.397(2)
C(17)-H(17)	0.9500
C(11)-C(12)	1.389(3)
C(11)-C(10)	1.391(3)
C(11)-H(11)	0.9500
C(12)-C(13)	1.391(3)
C(12)-C(22)	1.506(3)
C(13)-H(13)	0.9500
C(10)-C(21)	1.509(3)
C(7)-C(8)	1.328(3)
C(7)-H(7)	0.9500
C(8)-H(8)	0.9500
C(23)-H(23A)	0.9800
C(23)-H(23B)	0.9800
C(23)-H(23C)	0.9800
C(19)-H(19)	0.9500
C(26)-H(26A)	0.9800
C(26)-H(26B)	0.9800
C(26)-H(26C)	0.9800
C(22)-H(22A)	0.9800
C(22)-H(22B)	0.9800
C(22)-H(22C)	0.9800
C(25)-H(25A)	0.9800
C(25)-H(25B)	0.9800
C(25)-H(25C)	0.9800
C(21)-H(21A)	0.9800
C(21)-H(21B)	0.9800
C(21)-H(21C)	0.9800

C(27)-C(30)	1.523(3)
C(27)-C(28)	1.527(2)
C(27)-C(29)	1.532(2)
C(27)-C(31)	1.544(2)
C(28)-H(28A)	0.9900
C(28)-H(28B)	0.9900
C(29)-S(1)	1.8289(18)
C(29)-H(29A)	0.9900
C(29)-H(29B)	0.9900
C(30)-H(30A)	0.9800
C(30)-H(30B)	0.9800
C(30)-H(30C)	0.9800
C(31)-H(31A)	0.9800
C(31)-H(31B)	0.9800
C(31)-H(31C)	0.9800
C(6)-N(2)-C(7)	111.67(14)
C(6)-N(2)-C(15)	132.15(13)
C(7)-N(2)-C(15)	116.17(14)
C(1)-Fe(1)-C(2)	96.18(8)
C(1)-Fe(1)-C(6)	89.77(7)
C(2)-Fe(1)-C(6)	97.87(7)
C(1)-Fe(1)-S(3)	123.17(6)
C(2)-Fe(1)-S(3)	139.85(6)
C(6)-Fe(1)-S(3)	90.52(5)
C(1)-Fe(1)-S(1)	97.24(6)
C(2)-Fe(1)-S(1)	85.05(5)
C(6)-Fe(1)-S(1)	172.10(5)
S(3)-Fe(1)-S(1)	82.607(17)
C(1)-Fe(1)-Fe(2)	151.83(6)
C(2)-Fe(1)-Fe(2)	86.89(5)
C(6)-Fe(1)-Fe(2)	117.64(5)
S(3)-Fe(1)-Fe(2)	55.010(13)
S(1)-Fe(1)-Fe(2)	55.013(12)
C(3)-Fe(2)-C(5)	91.00(8)

C(3)-Fe(2)-C(4)	98.95(8)
C(5)-Fe(2)-C(4)	101.79(8)
C(3)-Fe(2)-S(3)	160.82(6)
C(5)-Fe(2)-S(3)	89.03(6)
C(4)-Fe(2)-S(3)	99.82(6)
C(3)-Fe(2)-S(1)	90.42(6)
C(5)-Fe(2)-S(1)	159.80(6)
C(4)-Fe(2)-S(1)	97.89(6)
S(3)-Fe(2)-S(1)	83.130(17)
C(3)-Fe(2)-Fe(1)	106.46(6)
C(5)-Fe(2)-Fe(1)	104.75(6)
C(4)-Fe(2)-Fe(1)	142.55(6)
S(3)-Fe(2)-Fe(1)	55.199(12)
S(1)-Fe(2)-Fe(1)	55.677(13)
C(28)-S(3)-Fe(2)	109.33(6)
C(28)-S(3)-Fe(1)	118.40(6)
Fe(2)-S(3)-Fe(1)	69.791(15)
O(1)-C(1)-Fe(1)	174.23(15)
C(13)-C(14)-C(9)	117.82(16)
C(13)-C(14)-C(23)	121.12(15)
C(9)-C(14)-C(23)	121.05(16)
N(1)-C(6)-N(2)	102.38(13)
N(1)-C(6)-Fe(1)	127.54(12)
N(2)-C(6)-Fe(1)	129.42(12)
C(16)-C(24)-H(24A)	109.5
C(16)-C(24)-H(24B)	109.5
H(24A)-C(24)-H(24B)	109.5
C(16)-C(24)-H(24C)	109.5
H(24A)-C(24)-H(24C)	109.5
H(24B)-C(24)-H(24C)	109.5
O(3)-C(3)-Fe(2)	178.47(17)
C(16)-C(15)-C(20)	122.31(15)
C(16)-C(15)-N(2)	119.60(14)
C(20)-C(15)-N(2)	117.34(15)

O(5)-C(5)-Fe(2)	179.10(18)
C(6)-N(1)-C(8)	111.95(14)
C(6)-N(1)-C(9)	129.49(14)
C(8)-N(1)-C(9)	118.47(14)
C(10)-C(9)-C(14)	122.23(16)
C(10)-C(9)-N(1)	118.08(15)
C(14)-C(9)-N(1)	119.31(15)
C(19)-C(20)-C(15)	118.13(16)
C(19)-C(20)-C(26)	121.14(17)
C(15)-C(20)-C(26)	120.73(17)
C(17)-C(18)-C(19)	118.31(16)
C(17)-C(18)-C(25)	121.12(18)
C(19)-C(18)-C(25)	120.55(17)
O(2)-C(2)-Fe(1)	172.18(15)
O(4)-C(4)-Fe(2)	176.93(17)
C(15)-C(16)-C(17)	117.53(15)
C(15)-C(16)-C(24)	122.90(15)
C(17)-C(16)-C(24)	119.51(15)
C(18)-C(17)-C(16)	122.01(16)
C(18)-C(17)-H(17)	119.0
C(16)-C(17)-H(17)	119.0
C(12)-C(11)-C(10)	122.14(17)
C(12)-C(11)-H(11)	118.9
C(10)-C(11)-H(11)	118.9
C(11)-C(12)-C(13)	118.01(17)
C(11)-C(12)-C(22)	120.08(17)
C(13)-C(12)-C(22)	121.90(17)
C(14)-C(13)-C(12)	122.04(16)
C(14)-C(13)-H(13)	119.0
C(12)-C(13)-H(13)	119.0
C(9)-C(10)-C(11)	117.68(16)
C(9)-C(10)-C(21)	122.46(17)
C(11)-C(10)-C(21)	119.83(17)
C(8)-C(7)-N(2)	107.23(16)

C(8)-C(7)-H(7)	126.4
N(2)-C(7)-H(7)	126.4
C(7)-C(8)-N(1)	106.76(15)
C(7)-C(8)-H(8)	126.6
N(1)-C(8)-H(8)	126.6
C(14)-C(23)-H(23A)	109.5
C(14)-C(23)-H(23B)	109.5
H(23A)-C(23)-H(23B)	109.5
C(14)-C(23)-H(23C)	109.5
H(23A)-C(23)-H(23C)	109.5
H(23B)-C(23)-H(23C)	109.5
C(20)-C(19)-C(18)	121.65(16)
C(20)-C(19)-H(19)	119.2
C(18)-C(19)-H(19)	119.2
C(20)-C(26)-H(26A)	109.5
C(20)-C(26)-H(26B)	109.5
H(26A)-C(26)-H(26B)	109.5
C(20)-C(26)-H(26C)	109.5
H(26A)-C(26)-H(26C)	109.5
H(26B)-C(26)-H(26C)	109.5
C(12)-C(22)-H(22A)	109.5
C(12)-C(22)-H(22B)	109.5
H(22A)-C(22)-H(22B)	109.5
C(12)-C(22)-H(22C)	109.5
H(22A)-C(22)-H(22C)	109.5
H(22B)-C(22)-H(22C)	109.5
C(18)-C(25)-H(25A)	109.5
C(18)-C(25)-H(25B)	109.5
H(25A)-C(25)-H(25B)	109.5
C(18)-C(25)-H(25C)	109.5
H(25A)-C(25)-H(25C)	109.5
H(25B)-C(25)-H(25C)	109.5
C(10)-C(21)-H(21A)	109.5
C(10)-C(21)-H(21B)	109.5

H(21A)-C(21)-H(21B)	109.5
C(10)-C(21)-H(21C)	109.5
H(21A)-C(21)-H(21C)	109.5
H(21B)-C(21)-H(21C)	109.5
C(30)-C(27)-C(28)	110.95(14)
C(30)-C(27)-C(29)	111.58(16)
C(28)-C(27)-C(29)	112.07(14)
C(30)-C(27)-C(31)	107.55(15)
C(28)-C(27)-C(31)	107.10(15)
C(29)-C(27)-C(31)	107.31(14)
C(27)-C(28)-S(3)	120.03(12)
C(27)-C(28)-H(28A)	107.3
S(3)-C(28)-H(28A)	107.3
C(27)-C(28)-H(28B)	107.3
S(3)-C(28)-H(28B)	107.3
H(28A)-C(28)-H(28B)	106.9
C(27)-C(29)-S(1)	120.83(12)
C(27)-C(29)-H(29A)	107.1
S(1)-C(29)-H(29A)	107.1
C(27)-C(29)-H(29B)	107.1
S(1)-C(29)-H(29B)	107.1
H(29A)-C(29)-H(29B)	106.8
C(27)-C(30)-H(30A)	109.5
C(27)-C(30)-H(30B)	109.5
H(30A)-C(30)-H(30B)	109.5
C(27)-C(30)-H(30C)	109.5
H(30A)-C(30)-H(30C)	109.5
H(30B)-C(30)-H(30C)	109.5
C(27)-C(31)-H(31A)	109.5
C(27)-C(31)-H(31B)	109.5
H(31A)-C(31)-H(31B)	109.5
C(27)-C(31)-H(31C)	109.5
H(31A)-C(31)-H(31C)	109.5
H(31B)-C(31)-H(31C)	109.5

C(29)-S(1)-Fe(2)	109.38(6)
C(29)-S(1)-Fe(1)	117.16(6)
Fe(2)-S(1)-Fe(1)	69.311(15)

Symmetry transformations used to generate equivalent atoms:

Table A-21. Anisotropic displacement parameters ($Å^2 x\ 10^3$) for III-4. The anisotropic displacement factor exponent takes the form: $-2\pi^2[\ h^2\ a^{*2}U^{11} + ...\ + 2\ h\ k\ a^*\ b^*\ U^{12}\ ]$

	U^{11}	U^{22}	U^{33}	U^{23}	U^{13}	U^{12}
O(3)	51(1)	49(1)	28(1)	8(1)	12(1)	2(1)
N(2)	30(1)	23(1)	26(1)	0(1)	6(1)	-7(1)
Fe(1)	19(1)	19(1)	23(1)	2(1)	5(1)	0(1)
Fe(2)	20(1)	23(1)	23(1)	2(1)	5(1)	1(1)
S(3)	23(1)	19(1)	24(1)	2(1)	4(1)	-1(1)
O(2)	35(1)	31(1)	28(1)	6(1)	1(1)	0(1)
C(1)	30(1)	25(1)	29(1)	4(1)	8(1)	0(1)
C(14)	24(1)	28(1)	30(1)	-6(1)	6(1)	-5(1)
O(1)	38(1)	42(1)	49(1)	8(1)	21(1)	14(1)
O(4)	28(1)	66(1)	51(1)	-17(1)	5(1)	-8(1)
C(6)	22(1)	24(1)	23(1)	-1(1)	7(1)	-1(1)
O(5)	55(1)	36(1)	45(1)	-7(1)	9(1)	12(1)
C(24)	27(1)	29(1)	32(1)	3(1)	7(1)	-1(1)
C(3)	26(1)	31(1)	32(1)	0(1)	8(1)	1(1)
C(15)	28(1)	20(1)	27(1)	5(1)	5(1)	-4(1)
C(5)	29(1)	33(1)	27(1)	1(1)	5(1)	3(1)
N(1)	27(1)	29(1)	25(1)	-2(1)	6(1)	-7(1)
C(9)	25(1)	32(1)	25(1)	-4(1)	3(1)	-5(1)
C(20)	35(1)	20(1)	37(1)	5(1)	12(1)	-1(1)
C(18)	34(1)	29(1)	34(1)	10(1)	2(1)	-5(1)
C(2)	24(1)	21(1)	32(1)	1(1)	6(1)	0(1)
C(4)	27(1)	36(1)	29(1)	-3(1)	9(1)	2(1)
C(16)	25(1)	21(1)	29(1)	4(1)	6(1)	-3(1)
C(17)	34(1)	27(1)	28(1)	4(1)	6(1)	-5(1)
C(11)	23(1)	48(1)	37(1)	-8(1)	4(1)	5(1)
C(12)	26(1)	40(1)	31(1)	-4(1)	0(1)	-3(1)
C(13)	28(1)	37(1)	26(1)	-7(1)	8(1)	-5(1)
C(10)	25(1)	43(1)	30(1)	-8(1)	6(1)	-2(1)
C(7)	41(1)	27(1)	37(1)	-1(1)	10(1)	-14(1)

C(8)	38(1)	31(1)	35(1)	-5(1)	8(1)	-16(1)
C(23)	30(1)	36(1)	34(1)	-3(1)	8(1)	4(1)
C(19)	32(1)	26(1)	47(1)	12(1)	7(1)	5(1)
C(26)	49(1)	28(1)	50(1)	1(1)	21(1)	5(1)
C(22)	33(1)	56(1)	32(1)	-1(1)	-1(1)	3(1)
C(25)	49(1)	46(1)	42(1)	15(1)	-5(1)	1(1)
C(21)	34(1)	78(2)	38(1)	-7(1)	14(1)	8(1)
C(27)	31(1)	26(1)	29(1)	-5(1)	6(1)	-5(1)
C(28)	29(1)	29(1)	24(1)	1(1)	3(1)	-3(1)
C(29)	33(1)	20(1)	35(1)	-2(1)	6(1)	-5(1)
C(30)	37(1)	42(1)	33(1)	-9(1)	12(1)	-5(1)
C(31)	44(1)	40(1)	35(1)	-9(1)	5(1)	-13(1)
S(1)	24(1)	19(1)	29(1)	4(1)	6(1)	0(1)

Table A-22. Hydrogen coordinates (x 10^4) and isotropic displacement parameters ($Å^2$x 10^3) for III-4.

	x	y	z	U(eq)
H(24A)	5065	3718	854	43
H(24B)	5273	3999	84	43
H(24C)	4502	3100	207	43
H(17)	3197	4156	-757	35
H(11)	7647	2965	3949	43
H(13)	4924	4009	4838	36
H(7)	4787	5937	1426	41
H(8)	5824	5621	2600	41
H(23A)	2921	4323	3499	49
H(23B)	3605	5289	3467	49
H(23C)	3375	4876	4200	49
H(19)	932	5884	37	42
H(26A)	1081	6191	1233	62
H(26B)	2442	6241	1595	62
H(26C)	1633	5367	1727	62
H(22A)	7676	3446	5350	61
H(22B)	7210	2423	5149	61
H(22C)	6409	3109	5536	61
H(25A)	1535	5903	-1323	70
H(25B)	497	5187	-1212	70
H(25C)	1651	4838	-1530	70
H(21A)	6456	3307	2231	73
H(21B)	7618	2963	2732	73
H(21C)	7447	4038	2550	73
H(28A)	39	2593	620	33
H(28B)	1023	2990	189	33
H(29A)	1746	477	1104	35
H(29B)	507	936	1214	35

H(30A)	2568	1929	-165	55
H(30B)	2948	1053	319	55
H(30C)	3146	2077	627	55
H(31A)	472	1581	-483	60
H(31B)	-268	1132	77	60
H(31C)	838	585	-162	60

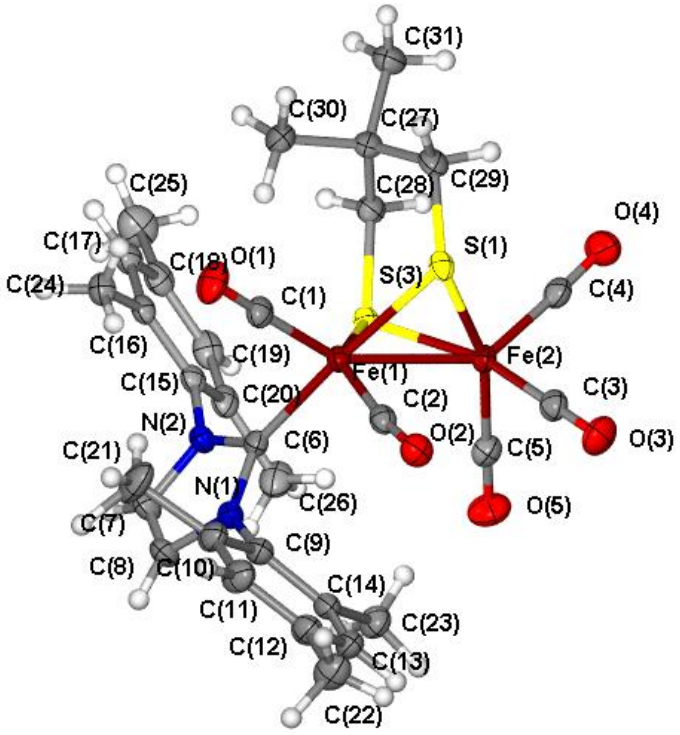

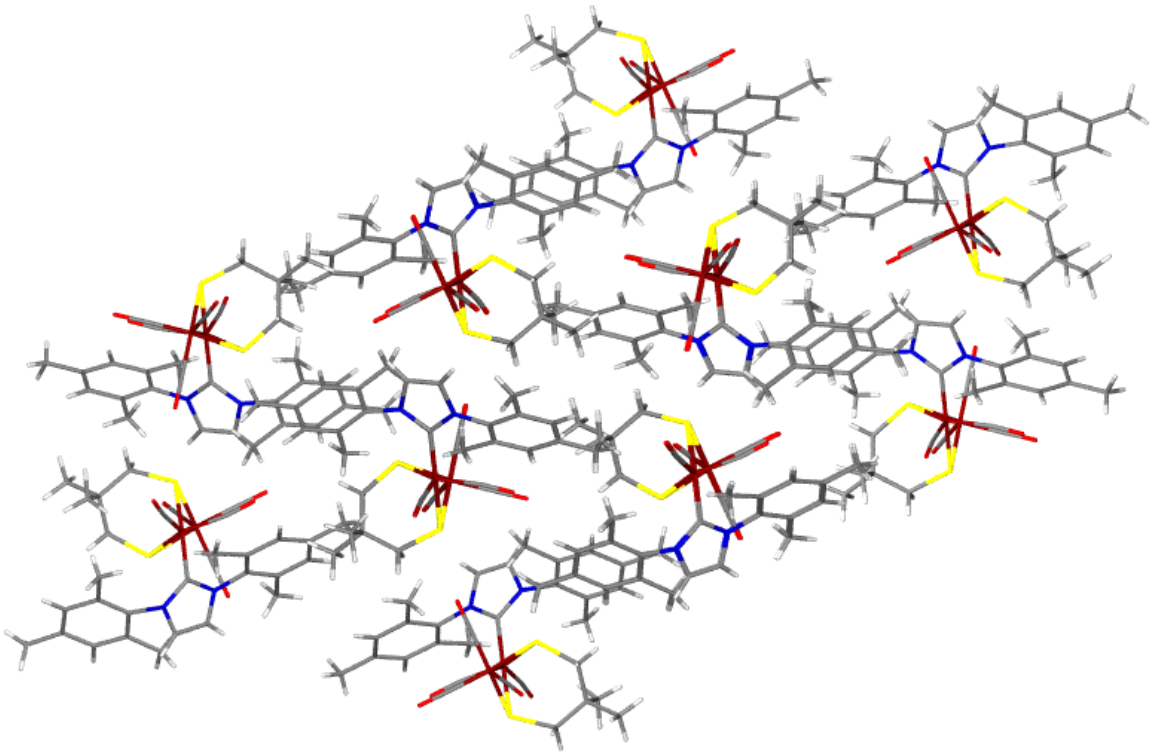

Table A-23. Crystal data and structure refinement for III-5.

Identification code	DepdtIMes	
Empirical formula	C33 H38 Fe2 N2 O5 S2	
Formula weight	718.47	
Temperature	106(2) K	
Wavelength	0.71073 Å	
Crystal system	Orthorhombic	
Space group	P2(1)2(1)2(1)	
Unit cell dimensions	a = 9.791(3) Å	α= 90°.
	b = 14.616(4) Å	β= 90°.
	c = 46.348(16) Å	γ = 90°.
Volume	6633(3) $Å^3$	
Z	8	
Density (calculated)	1.439 Mg/m^3	
Absorption coefficient	1.043 mm^{-1}	
F(000)	2992	
Crystal size	0.39 x 0.19 x 0.13 mm^3	
Theta range for data collection	1.76 to 28.21°.	
Index ranges	-12<=h<=12, -18<=k<=18, -58<=l<=58	
Reflections collected	46446	
Independent reflections	14061 [R(int) = 0.1467]	
Completeness to theta = 28.21°	91.0 %	
Absorption correction	None	
Max. and min. transmission	0.8780 and 0.6871	
Refinement method	Full-matrix least-squares on F^2	
Data / restraints / parameters	14061 / 0 / 809	
Goodness-of-fit on F^2	1.061	
Final R indices [I>2sigma(I)]	R1 = 0.0899, wR2 = 0.1902	
R indices (all data)	R1 = 0.1346, wR2 = 0.2115	
Absolute structure parameter	0.08(3)	
Largest diff. peak and hole	0.755 and -0.827 $e.Å^{-3}$	

Table A-24. Atomic coordinates (x 10^4) and equivalent isotropic displacement parameters ($Å^2$x 10^3) for III-5. U(eq) is defined as one third of the trace of the orthogonalized U^{ij} tensor.

	x	y	z	U(eq)
Fe(1)	4363(2)	1461(1)	1958(1)	25(1)
Fe(4)	6255(1)	2630(1)	1866(1)	28(1)
S(5)	6489(3)	1363(2)	2149(1)	30(1)
S(8)	4441(3)	2874(2)	2152(1)	28(1)
O(7)	5641(7)	165(4)	1558(1)	34(2)
C(1)	1296(9)	2655(6)	2137(2)	30(2)
N(3)	1581(8)	2337(5)	1846(2)	30(2)
C(2)	3595(9)	596(6)	2154(2)	27(2)
O(9)	7628(8)	1800(5)	1371(1)	41(2)
C(3)	5567(10)	2204(6)	2687(2)	27(2)
C(4)	6204(12)	2585(7)	2967(2)	39(3)
O(10)	8279(8)	3844(5)	2129(2)	40(2)
C(5)	4973(11)	3026(6)	2522(2)	29(2)
O(6)	3151(8)	-50(4)	2277(1)	38(2)
C(6)	4617(10)	773(7)	899(2)	28(2)
C(7)	5518(10)	3486(7)	1646(2)	32(2)
N(4)	2291(8)	1621(5)	1469(1)	29(2)
O(8)	5008(8)	4079(5)	1523(1)	39(2)
C(8)	3024(9)	1015(6)	1273(2)	22(2)
C(9)	7494(11)	3322(7)	2030(2)	32(2)
C(10)	888(12)	3240(8)	2692(2)	45(3)
C(11)	4362(10)	-194(6)	917(2)	25(2)
C(12)	381(11)	1077(7)	2262(2)	41(3)
C(13)	2691(10)	1822(6)	1748(2)	25(2)
C(14)	4199(12)	2380(7)	1047(2)	41(3)
C(15)	609(11)	2327(8)	2618(2)	37(2)
C(16)	4349(11)	1561(6)	2768(2)	32(2)
C(17)	612(10)	2445(6)	1631(2)	29(2)
C(18)	835(10)	2012(6)	2334(2)	28(2)

C(19)	5017(10)	701(6)	1700(2)	27(2)
C(20)	1506(10)	3580(6)	2202(2)	31(2)
C(21)	3893(10)	1375(6)	1078(2)	25(2)
C(22)	6699(10)	1735(7)	2525(2)	33(2)
C(23)	3346(11)	-497(7)	1104(2)	33(2)
C(24)	1056(11)	1991(7)	1396(2)	40(3)
C(25)	1815(12)	4277(7)	1970(2)	44(3)
C(26)	1674(10)	-288(7)	1503(2)	33(2)
C(27)	2672(11)	78(6)	1287(2)	29(2)
C(28)	1298(11)	3855(7)	2484(2)	43(3)
C(29)	5379(13)	3192(7)	3165(2)	51(3)
C(30)	5104(12)	-833(7)	721(2)	40(3)
C(31)	7096(10)	2106(7)	1574(2)	34(2)
C(32)	735(16)	3564(10)	2999(2)	70(4)
C(33)	4697(13)	637(7)	2896(2)	53(3)
Fe(2)	4117(1)	5552(1)	226(1)	24(1)
Fe(3)	2580(1)	4157(1)	310(1)	27(1)
S(6)	1923(2)	5624(2)	383(1)	26(1)
S(7)	4314(3)	4568(2)	598(1)	27(1)
O(2)	2721(7)	6080(5)	-304(1)	38(2)
N(1)	7073(8)	4891(5)	229(1)	29(2)
C(34)	3387(10)	5839(7)	-104(2)	30(2)
C(35)	1606(10)	5790(7)	772(2)	30(2)
O(5)	745(8)	3337(4)	740(1)	45(2)
O(4)	1167(8)	4107(5)	-247(1)	42(2)
O(3)	4186(8)	2548(5)	155(2)	45(2)
N(2)	6296(8)	4982(5)	-203(1)	26(2)
C(36)	7435(11)	4165(7)	694(2)	39(2)
C(37)	5567(10)	5277(6)	-457(2)	30(2)
C(38)	1459(11)	3645(7)	556(2)	33(2)
C(39)	2812(9)	5756(6)	987(2)	25(2)
C(40)	7667(11)	4681(6)	-232(2)	37(2)
C(41)	5020(10)	6435(7)	-797(2)	32(2)
C(42)	3700(11)	6625(6)	962(2)	31(2)

C(43)	4193(11)	5853(7)	-952(2)	37(2)
C(44)	5919(11)	5116(6)	78(2)	30(2)
C(45)	4656(9)	6677(6)	270(2)	25(2)
C(46)	7767(9)	5810(6)	648(2)	29(2)
C(47)	4111(12)	4936(7)	-857(2)	38(3)
C(48)	3644(10)	4871(6)	946(2)	24(2)
C(49)	7234(12)	3247(7)	556(2)	46(3)
C(50)	1380(10)	6552(6)	1395(2)	32(2)
C(51)	7928(12)	6640(7)	460(2)	47(3)
C(52)	6628(11)	6840(6)	-396(2)	34(2)
C(53)	8135(11)	4639(7)	39(2)	38(3)
C(54)	3378(13)	6167(8)	-1201(2)	55(3)
C(55)	2164(11)	5694(7)	1294(2)	36(2)
C(56)	5751(10)	6181(6)	-553(2)	28(2)
C(57)	4716(14)	3667(7)	-511(2)	54(4)
C(58)	7758(11)	4262(8)	988(2)	45(3)
C(59)	7969(11)	5074(8)	1115(2)	39(3)
C(60)	1717(10)	4145(6)	-22(2)	31(2)
C(61)	8020(11)	5872(8)	943(2)	45(3)
C(62)	8217(13)	5156(9)	1441(2)	62(4)
C(63)	4816(11)	4629(6)	-609(2)	35(3)
C(64)	4800(11)	6736(8)	1193(2)	43(3)
C(65)	7374(11)	4956(7)	529(2)	36(2)
C(66)	3508(11)	3198(6)	214(2)	33(2)
O(1)	4937(7)	7458(4)	284(1)	39(2)

Table A-25. Bond lengths [Å] and angles [°] for III-4.

Fe(1)-C(2)	1.728(10)
Fe(1)-C(19)	1.754(10)
Fe(1)-C(13)	1.976(9)
Fe(1)-S(8)	2.252(3)
Fe(1)-S(5)	2.266(3)
Fe(1)-Fe(4)	2.5563(19)
Fe(4)-C(9)	1.753(11)
Fe(4)-C(31)	1.759(10)
Fe(4)-C(7)	1.770(10)
Fe(4)-S(8)	2.243(3)
Fe(4)-S(5)	2.279(3)
S(5)-C(22)	1.838(9)
S(8)-C(5)	1.806(9)
O(7)-C(19)	1.191(11)
C(1)-C(18)	1.386(13)
C(1)-C(20)	1.400(13)
C(1)-N(3)	1.456(11)
N(3)-C(17)	1.383(11)
N(3)-C(13)	1.397(11)
C(2)-O(6)	1.185(11)
O(9)-C(31)	1.166(11)
C(3)-C(22)	1.504(13)
C(3)-C(5)	1.539(12)
C(3)-C(4)	1.544(12)
C(3)-C(16)	1.563(13)
C(4)-C(29)	1.511(14)
C(4)-H(4A)	0.9900
C(4)-H(4B)	0.9900
O(10)-C(9)	1.174(11)
C(5)-H(5A)	0.9900
C(5)-H(5B)	0.9900
C(6)-C(21)	1.401(12)

C(6)-C(11)	1.439(13)
C(6)-H(6)	0.9500
C(7)-O(8)	1.150(11)
N(4)-C(24)	1.368(13)
N(4)-C(13)	1.383(10)
N(4)-C(8)	1.458(11)
C(8)-C(21)	1.349(11)
C(8)-C(27)	1.415(12)
C(10)-C(28)	1.377(15)
C(10)-C(15)	1.404(15)
C(10)-C(32)	1.509(13)
C(11)-C(23)	1.391(13)
C(11)-C(30)	1.492(12)
C(12)-C(18)	1.475(13)
C(12)-H(12A)	0.9800
C(12)-H(12B)	0.9800
C(12)-H(12C)	0.9800
C(14)-C(21)	1.504(12)
C(14)-H(14A)	0.9800
C(14)-H(14B)	0.9800
C(14)-H(14C)	0.9800
C(15)-C(18)	1.412(11)
C(15)-H(15)	0.9500
C(16)-C(33)	1.515(13)
C(16)-H(16A)	0.9900
C(16)-H(16B)	0.9900
C(17)-C(24)	1.347(13)
C(17)-H(17)	0.9500
C(20)-C(28)	1.383(12)
C(20)-C(25)	1.512(13)
C(22)-H(22A)	0.9900
C(22)-H(22B)	0.9900
C(23)-C(27)	1.366(12)
C(23)-H(23)	0.9500

C(24)-H(24)	0.9500
C(25)-H(25A)	0.9800
C(25)-H(25B)	0.9800
C(25)-H(25C)	0.9800
C(26)-C(27)	1.497(13)
C(26)-H(26A)	0.9800
C(26)-H(26B)	0.9800
C(26)-H(26C)	0.9800
C(28)-H(28)	0.9500
C(29)-H(29A)	0.9800
C(29)-H(29B)	0.9800
C(29)-H(29C)	0.9800
C(30)-H(30A)	0.9800
C(30)-H(30B)	0.9800
C(30)-H(30C)	0.9800
C(32)-H(32A)	0.9800
C(32)-H(32B)	0.9800
C(32)-H(32C)	0.9800
C(33)-H(33A)	0.9800
C(33)-H(33B)	0.9800
C(33)-H(33C)	0.9800
Fe(2)-C(34)	1.739(9)
Fe(2)-C(45)	1.739(9)
Fe(2)-C(44)	1.997(11)
Fe(2)-S(7)	2.253(2)
Fe(2)-S(6)	2.271(3)
Fe(2)-Fe(3)	2.5640(19)
Fe(3)-C(66)	1.729(10)
Fe(3)-C(38)	1.752(10)
Fe(3)-C(60)	1.754(10)
Fe(3)-S(7)	2.242(3)
Fe(3)-S(6)	2.263(3)
S(6)-C(35)	1.845(8)
S(7)-C(48)	1.799(8)

O(2)-C(34)	1.184(10)
N(1)-C(44)	1.369(12)
N(1)-C(53)	1.411(11)
N(1)-C(65)	1.426(10)
C(35)-C(39)	1.548(12)
C(35)-H(35A)	0.9900
C(35)-H(35B)	0.9900
O(5)-C(38)	1.190(11)
O(4)-C(60)	1.176(11)
O(3)-C(66)	1.190(11)
N(2)-C(44)	1.365(11)
N(2)-C(40)	1.419(13)
N(2)-C(37)	1.444(11)
C(36)-C(65)	1.386(13)
C(36)-C(58)	1.406(14)
C(36)-C(49)	1.499(14)
C(37)-C(63)	1.393(13)
C(37)-C(56)	1.406(12)
C(39)-C(48)	1.541(12)
C(39)-C(42)	1.545(12)
C(39)-C(55)	1.560(12)
C(40)-C(53)	1.338(13)
C(40)-H(40)	0.9500
C(41)-C(43)	1.376(13)
C(41)-C(56)	1.388(13)
C(41)-H(41)	0.9500
C(42)-C(64)	1.530(13)
C(42)-H(42A)	0.9900
C(42)-H(42B)	0.9900
C(43)-C(47)	1.412(14)
C(43)-C(54)	1.476(14)
C(45)-O(1)	1.177(10)
C(46)-C(61)	1.391(12)
C(46)-C(65)	1.417(13)

C(46)-C(51)	1.502(13)
C(47)-C(63)	1.415(14)
C(47)-H(47)	0.9500
C(48)-H(48A)	0.9900
C(48)-H(48B)	0.9900
C(49)-H(49A)	0.9800
C(49)-H(49B)	0.9800
C(49)-H(49C)	0.9800
C(50)-C(55)	1.542(12)
C(50)-H(50A)	0.9800
C(50)-H(50B)	0.9800
C(50)-H(50C)	0.9800
C(51)-H(51A)	0.9800
C(51)-H(51B)	0.9800
C(51)-H(51C)	0.9800
C(52)-C(56)	1.480(13)
C(52)-H(52A)	0.9800
C(52)-H(52B)	0.9800
C(52)-H(52C)	0.9800
C(53)-H(53)	0.9500
C(54)-H(54A)	0.9800
C(54)-H(54B)	0.9800
C(54)-H(54C)	0.9800
C(55)-H(55A)	0.9900
C(55)-H(55B)	0.9900
C(57)-C(63)	1.481(13)
C(57)-H(57A)	0.9800
C(57)-H(57B)	0.9800
C(57)-H(57C)	0.9800
C(58)-C(59)	1.341(15)
C(58)-H(58)	0.9500
C(59)-C(61)	1.415(15)
C(59)-C(62)	1.534(13)
C(61)-H(61)	0.9500

C(62)-H(62A)	0.9800
C(62)-H(62B)	0.9800
C(62)-H(62C)	0.9800
C(64)-H(64A)	0.9800
C(64)-H(64B)	0.9800
C(64)-H(64C)	0.9800

C(2)-Fe(1)-C(19)	93.1(4)
C(2)-Fe(1)-C(13)	95.4(4)
C(19)-Fe(1)-C(13)	97.8(4)
C(2)-Fe(1)-S(8)	118.4(3)
C(19)-Fe(1)-S(8)	147.1(3)
C(13)-Fe(1)-S(8)	88.8(3)
C(2)-Fe(1)-S(5)	98.5(3)
C(19)-Fe(1)-S(5)	83.7(3)
C(13)-Fe(1)-S(5)	165.9(3)
S(8)-Fe(1)-S(5)	82.62(10)
C(2)-Fe(1)-Fe(4)	153.1(3)
C(19)-Fe(1)-Fe(4)	92.6(3)
C(13)-Fe(1)-Fe(4)	109.9(3)
S(8)-Fe(1)-Fe(4)	55.16(8)
S(5)-Fe(1)-Fe(4)	56.03(8)
C(9)-Fe(4)-C(31)	105.1(4)
C(9)-Fe(4)-C(7)	97.1(4)
C(31)-Fe(4)-C(7)	93.1(4)
C(9)-Fe(4)-S(8)	101.6(3)
C(31)-Fe(4)-S(8)	153.3(3)
C(7)-Fe(4)-S(8)	84.6(3)
C(9)-Fe(4)-S(5)	98.7(3)
C(31)-Fe(4)-S(5)	92.4(3)
C(7)-Fe(4)-S(5)	161.3(3)
S(8)-Fe(4)-S(5)	82.53(9)
C(9)-Fe(4)-Fe(1)	144.6(3)
C(31)-Fe(4)-Fe(1)	100.2(3)

C(7)-Fe(4)-Fe(1)	105.9(3)
S(8)-Fe(4)-Fe(1)	55.52(7)
S(5)-Fe(4)-Fe(1)	55.53(8)
C(22)-S(5)-Fe(1)	117.0(3)
C(22)-S(5)-Fe(4)	108.4(3)
Fe(1)-S(5)-Fe(4)	68.45(8)
C(5)-S(8)-Fe(4)	110.5(4)
C(5)-S(8)-Fe(1)	120.0(3)
Fe(4)-S(8)-Fe(1)	69.32(8)
C(18)-C(1)-C(20)	124.2(8)
C(18)-C(1)-N(3)	117.1(8)
C(20)-C(1)-N(3)	118.7(8)
C(17)-N(3)-C(13)	111.2(7)
C(17)-N(3)-C(1)	120.0(8)
C(13)-N(3)-C(1)	128.4(7)
O(6)-C(2)-Fe(1)	174.0(8)
C(22)-C(3)-C(5)	112.7(8)
C(22)-C(3)-C(4)	106.6(8)
C(5)-C(3)-C(4)	106.9(8)
C(22)-C(3)-C(16)	114.1(8)
C(5)-C(3)-C(16)	107.5(8)
C(4)-C(3)-C(16)	108.8(7)
C(29)-C(4)-C(3)	120.4(9)
C(29)-C(4)-H(4A)	107.2
C(3)-C(4)-H(4A)	107.2
C(29)-C(4)-H(4B)	107.2
C(3)-C(4)-H(4B)	107.2
H(4A)-C(4)-H(4B)	106.9
C(3)-C(5)-S(8)	119.1(6)
C(3)-C(5)-H(5A)	107.5
S(8)-C(5)-H(5A)	107.5
C(3)-C(5)-H(5B)	107.5
S(8)-C(5)-H(5B)	107.5
H(5A)-C(5)-H(5B)	107.0

C(21)-C(6)-C(11)	119.7(8)
C(21)-C(6)-H(6)	120.1
C(11)-C(6)-H(6)	120.1
O(8)-C(7)-Fe(4)	174.2(9)
C(24)-N(4)-C(13)	113.5(8)
C(24)-N(4)-C(8)	121.4(7)
C(13)-N(4)-C(8)	125.0(8)
C(21)-C(8)-C(27)	124.2(8)
C(21)-C(8)-N(4)	119.5(8)
C(27)-C(8)-N(4)	116.0(7)
O(10)-C(9)-Fe(4)	174.7(9)
C(28)-C(10)-C(15)	120.5(9)
C(28)-C(10)-C(32)	118.9(10)
C(15)-C(10)-C(32)	120.6(10)
C(23)-C(11)-C(6)	118.2(8)
C(23)-C(11)-C(30)	121.9(8)
C(6)-C(11)-C(30)	119.7(8)
C(18)-C(12)-H(12A)	109.5
C(18)-C(12)-H(12B)	109.5
H(12A)-C(12)-H(12B)	109.5
C(18)-C(12)-H(12C)	109.5
H(12A)-C(12)-H(12C)	109.5
H(12B)-C(12)-H(12C)	109.5
N(4)-C(13)-N(3)	101.3(7)
N(4)-C(13)-Fe(1)	129.7(7)
N(3)-C(13)-Fe(1)	129.0(6)
C(21)-C(14)-H(14A)	109.5
C(21)-C(14)-H(14B)	109.5
H(14A)-C(14)-H(14B)	109.5
C(21)-C(14)-H(14C)	109.5
H(14A)-C(14)-H(14C)	109.5
H(14B)-C(14)-H(14C)	109.5
C(10)-C(15)-C(18)	120.4(9)
C(10)-C(15)-H(15)	119.8

C(18)-C(15)-H(15)	119.8
C(33)-C(16)-C(3)	117.3(9)
C(33)-C(16)-H(16A)	108.0
C(3)-C(16)-H(16A)	108.0
C(33)-C(16)-H(16B)	108.0
C(3)-C(16)-H(16B)	108.0
H(16A)-C(16)-H(16B)	107.2
C(24)-C(17)-N(3)	107.7(9)
C(24)-C(17)-H(17)	126.1
N(3)-C(17)-H(17)	126.1
C(1)-C(18)-C(15)	116.3(9)
C(1)-C(18)-C(12)	125.4(8)
C(15)-C(18)-C(12)	117.7(9)
O(7)-C(19)-Fe(1)	168.7(8)
C(28)-C(20)-C(1)	117.5(9)
C(28)-C(20)-C(25)	120.4(9)
C(1)-C(20)-C(25)	121.8(8)
C(8)-C(21)-C(6)	118.1(8)
C(8)-C(21)-C(14)	124.7(8)
C(6)-C(21)-C(14)	117.2(8)
C(3)-C(22)-S(5)	121.7(6)
C(3)-C(22)-H(22A)	106.9
S(5)-C(22)-H(22A)	106.9
C(3)-C(22)-H(22B)	106.9
S(5)-C(22)-H(22B)	106.9
H(22A)-C(22)-H(22B)	106.7
C(27)-C(23)-C(11)	122.5(9)
C(27)-C(23)-H(23)	118.8
C(11)-C(23)-H(23)	118.7
C(17)-C(24)-N(4)	106.2(9)
C(17)-C(24)-H(24)	126.9
N(4)-C(24)-H(24)	126.9
C(20)-C(25)-H(25A)	109.5
C(20)-C(25)-H(25B)	109.5

H(25A)-C(25)-H(25B)	109.5
C(20)-C(25)-H(25C)	109.5
H(25A)-C(25)-H(25C)	109.5
H(25B)-C(25)-H(25C)	109.5
C(27)-C(26)-H(26A)	109.5
C(27)-C(26)-H(26B)	109.5
H(26A)-C(26)-H(26B)	109.5
C(27)-C(26)-H(26C)	109.5
H(26A)-C(26)-H(26C)	109.5
H(26B)-C(26)-H(26C)	109.5
C(23)-C(27)-C(8)	116.7(9)
C(23)-C(27)-C(26)	120.8(9)
C(8)-C(27)-C(26)	122.4(8)
C(10)-C(28)-C(20)	120.9(10)
C(10)-C(28)-H(28)	119.5
C(20)-C(28)-H(28)	119.5
C(4)-C(29)-H(29A)	109.5
C(4)-C(29)-H(29B)	109.5
H(29A)-C(29)-H(29B)	109.5
C(4)-C(29)-H(29C)	109.5
H(29A)-C(29)-H(29C)	109.5
H(29B)-C(29)-H(29C)	109.5
C(11)-C(30)-H(30A)	109.5
C(11)-C(30)-H(30B)	109.5
H(30A)-C(30)-H(30B)	109.5
C(11)-C(30)-H(30C)	109.5
H(30A)-C(30)-H(30C)	109.5
H(30B)-C(30)-H(30C)	109.5
O(9)-C(31)-Fe(4)	176.1(9)
C(10)-C(32)-H(32A)	109.5
C(10)-C(32)-H(32B)	109.5
H(32A)-C(32)-H(32B)	109.5
C(10)-C(32)-H(32C)	109.5
H(32A)-C(32)-H(32C)	109.5

H(32B)-C(32)-H(32C)	109.5
C(16)-C(33)-H(33A)	109.5
C(16)-C(33)-H(33B)	109.5
H(33A)-C(33)-H(33B)	109.5
C(16)-C(33)-H(33C)	109.5
H(33A)-C(33)-H(33C)	109.5
H(33B)-C(33)-H(33C)	109.5
C(34)-Fe(2)-C(45)	90.0(4)
C(34)-Fe(2)-C(44)	98.0(4)
C(45)-Fe(2)-C(44)	94.3(4)
C(34)-Fe(2)-S(7)	149.5(3)
C(45)-Fe(2)-S(7)	119.1(3)
C(44)-Fe(2)-S(7)	89.0(2)
C(34)-Fe(2)-S(6)	83.2(3)
C(45)-Fe(2)-S(6)	101.8(3)
C(44)-Fe(2)-S(6)	163.9(3)
S(7)-Fe(2)-S(6)	82.22(9)
C(34)-Fe(2)-Fe(3)	94.8(3)
C(45)-Fe(2)-Fe(3)	155.8(3)
C(44)-Fe(2)-Fe(3)	108.5(3)
S(7)-Fe(2)-Fe(3)	55.01(7)
S(6)-Fe(2)-Fe(3)	55.42(7)
C(66)-Fe(3)-C(38)	98.7(4)
C(66)-Fe(3)-C(60)	91.2(4)
C(38)-Fe(3)-C(60)	105.4(4)
C(66)-Fe(3)-S(7)	88.4(3)
C(38)-Fe(3)-S(7)	101.6(3)
C(60)-Fe(3)-S(7)	152.8(3)
C(66)-Fe(3)-S(6)	162.9(3)
C(38)-Fe(3)-S(6)	97.4(3)
C(60)-Fe(3)-S(6)	90.2(3)
S(7)-Fe(3)-S(6)	82.65(9)
C(66)-Fe(3)-Fe(2)	107.3(3)
C(38)-Fe(3)-Fe(2)	143.8(3)

C(60)-Fe(3)-Fe(2)	99.1(3)
S(7)-Fe(3)-Fe(2)	55.44(7)
S(6)-Fe(3)-Fe(2)	55.70(7)
C(35)-S(6)-Fe(3)	108.6(3)
C(35)-S(6)-Fe(2)	118.6(3)
Fe(3)-S(6)-Fe(2)	68.88(8)
C(48)-S(7)-Fe(3)	108.9(3)
C(48)-S(7)-Fe(2)	120.0(3)
Fe(3)-S(7)-Fe(2)	69.56(8)
C(44)-N(1)-C(53)	110.6(7)
C(44)-N(1)-C(65)	130.9(8)
C(53)-N(1)-C(65)	118.3(8)
O(2)-C(34)-Fe(2)	169.7(8)
C(39)-C(35)-S(6)	119.9(6)
C(39)-C(35)-H(35A)	107.4
S(6)-C(35)-H(35A)	107.4
C(39)-C(35)-H(35B)	107.4
S(6)-C(35)-H(35B)	107.4
H(35A)-C(35)-H(35B)	106.9
C(44)-N(2)-C(40)	113.0(8)
C(44)-N(2)-C(37)	126.9(8)
C(40)-N(2)-C(37)	118.8(7)
C(65)-C(36)-C(58)	117.4(10)
C(65)-C(36)-C(49)	120.4(8)
C(58)-C(36)-C(49)	122.2(9)
C(63)-C(37)-C(56)	123.1(9)
C(63)-C(37)-N(2)	118.1(8)
C(56)-C(37)-N(2)	118.5(9)
O(5)-C(38)-Fe(3)	175.0(8)
C(48)-C(39)-C(42)	112.5(8)
C(48)-C(39)-C(35)	110.6(7)
C(42)-C(39)-C(35)	110.6(7)
C(48)-C(39)-C(55)	106.2(6)
C(42)-C(39)-C(55)	110.3(7)

C(35)-C(39)-C(55)	106.3(8)
C(53)-C(40)-N(2)	104.4(8)
C(53)-C(40)-H(40)	127.8
N(2)-C(40)-H(40)	127.8
C(43)-C(41)-C(56)	124.3(9)
C(43)-C(41)-H(41)	117.8
C(56)-C(41)-H(41)	117.8
C(64)-C(42)-C(39)	115.4(8)
C(64)-C(42)-H(42A)	108.4
C(39)-C(42)-H(42A)	108.4
C(64)-C(42)-H(42B)	108.4
C(39)-C(42)-H(42B)	108.4
H(42A)-C(42)-H(42B)	107.5
C(41)-C(43)-C(47)	117.2(9)
C(41)-C(43)-C(54)	122.3(9)
C(47)-C(43)-C(54)	120.4(10)
N(2)-C(44)-N(1)	103.3(8)
N(2)-C(44)-Fe(2)	127.7(7)
N(1)-C(44)-Fe(2)	129.1(6)
O(1)-C(45)-Fe(2)	174.4(8)
C(61)-C(46)-C(65)	119.1(9)
C(61)-C(46)-C(51)	120.0(9)
C(65)-C(46)-C(51)	121.0(8)
C(43)-C(47)-C(63)	121.7(9)
C(43)-C(47)-H(47)	119.1
C(63)-C(47)-H(47)	119.1
C(39)-C(48)-S(7)	120.7(6)
C(39)-C(48)-H(48A)	107.2
S(7)-C(48)-H(48A)	107.2
C(39)-C(48)-H(48B)	107.2
S(7)-C(48)-H(48B)	107.2
H(48A)-C(48)-H(48B)	106.8
C(36)-C(49)-H(49A)	109.5
C(36)-C(49)-H(49B)	109.5

H(49A)-C(49)-H(49B)	109.5
C(36)-C(49)-H(49C)	109.5
H(49A)-C(49)-H(49C)	109.5
H(49B)-C(49)-H(49C)	109.5
C(55)-C(50)-H(50A)	109.5
C(55)-C(50)-H(50B)	109.5
H(50A)-C(50)-H(50B)	109.5
C(55)-C(50)-H(50C)	109.5
H(50A)-C(50)-H(50C)	109.5
H(50B)-C(50)-H(50C)	109.5
C(46)-C(51)-H(51A)	109.5
C(46)-C(51)-H(51B)	109.5
H(51A)-C(51)-H(51B)	109.5
C(46)-C(51)-H(51C)	109.5
H(51A)-C(51)-H(51C)	109.5
H(51B)-C(51)-H(51C)	109.5
C(56)-C(52)-H(52A)	109.5
C(56)-C(52)-H(52B)	109.5
H(52A)-C(52)-H(52B)	109.5
C(56)-C(52)-H(52C)	109.5
H(52A)-C(52)-H(52C)	109.5
H(52B)-C(52)-H(52C)	109.5
C(40)-C(53)-N(1)	108.7(9)
C(40)-C(53)-H(53)	125.6
N(1)-C(53)-H(53)	125.6
C(43)-C(54)-H(54A)	109.5
C(43)-C(54)-H(54B)	109.5
H(54A)-C(54)-H(54B)	109.5
C(43)-C(54)-H(54C)	109.5
H(54A)-C(54)-H(54C)	109.5
H(54B)-C(54)-H(54C)	109.5
C(50)-C(55)-C(39)	115.5(7)
C(50)-C(55)-H(55A)	108.4
C(39)-C(55)-H(55A)	108.4

C(50)-C(55)-H(55B)	108.4
C(39)-C(55)-H(55B)	108.4
H(55A)-C(55)-H(55B)	107.5
C(41)-C(56)-C(37)	116.3(9)
C(41)-C(56)-C(52)	121.7(8)
C(37)-C(56)-C(52)	122.0(8)
C(63)-C(57)-H(57A)	109.5
C(63)-C(57)-H(57B)	109.5
H(57A)-C(57)-H(57B)	109.5
C(63)-C(57)-H(57C)	109.5
H(57A)-C(57)-H(57C)	109.5
H(57B)-C(57)-H(57C)	109.5
C(59)-C(58)-C(36)	123.3(10)
C(59)-C(58)-H(58)	118.4
C(36)-C(58)-H(58)	118.4
C(58)-C(59)-C(61)	119.1(9)
C(58)-C(59)-C(62)	121.7(10)
C(61)-C(59)-C(62)	119.1(10)
O(4)-C(60)-Fe(3)	177.4(9)
C(46)-C(61)-C(59)	119.7(10)
C(46)-C(61)-H(61)	120.2
C(59)-C(61)-H(61)	120.2
C(59)-C(62)-H(62A)	109.5
C(59)-C(62)-H(62B)	109.5
H(62A)-C(62)-H(62B)	109.5
C(59)-C(62)-H(62C)	109.5
H(62A)-C(62)-H(62C)	109.5
H(62B)-C(62)-H(62C)	109.5
C(37)-C(63)-C(47)	117.0(8)
C(37)-C(63)-C(57)	121.7(10)
C(47)-C(63)-C(57)	121.3(10)
C(42)-C(64)-H(64A)	109.5
C(42)-C(64)-H(64B)	109.5
H(64A)-C(64)-H(64B)	109.5

C(42)-C(64)-H(64C)	109.5
H(64A)-C(64)-H(64C)	109.5
H(64B)-C(64)-H(64C)	109.5
C(36)-C(65)-C(46)	120.6(8)
C(36)-C(65)-N(1)	119.4(9)
C(46)-C(65)-N(1)	119.6(8)
O(3)-C(66)-Fe(3)	177.5(9)

Symmetry transformations used to generate equivalent atoms:

Table A-26. Anisotropic displacement parameters ($Å^2 x\ 10^3$) for III-4. The anisotropic displacement factor exponent takes the form: $-2\pi^2[\ h^2\ a^{*2}U^{11} + ... + 2\ h\ k\ a^*\ b^*\ U^{12}\ ]$

	U^{11}	U^{22}	U^{33}	U^{23}	U^{13}	U^{12}
Fe(1)	28(1)	28(1)	21(1)	1(1)	0(1)	1(1)
Fe(4)	28(1)	32(1)	24(1)	-1(1)	1(1)	-1(1)
S(5)	32(2)	34(1)	23(1)	-4(1)	-2(1)	2(1)
S(8)	35(1)	29(1)	19(1)	-1(1)	0(1)	1(1)
O(7)	34(4)	39(4)	30(3)	-5(3)	2(3)	5(3)
C(1)	18(5)	40(5)	31(4)	-6(4)	4(4)	3(4)
N(3)	25(5)	35(4)	30(4)	2(4)	-4(3)	-3(4)
C(2)	26(5)	30(5)	24(4)	-11(4)	-4(4)	3(4)
O(9)	36(4)	50(4)	38(4)	-8(3)	17(3)	-4(4)
C(3)	17(5)	37(5)	27(4)	2(4)	-10(4)	10(4)
C(4)	59(8)	41(6)	18(4)	4(4)	-5(4)	6(6)
O(10)	36(4)	41(4)	44(4)	-9(3)	-6(3)	-4(3)
C(5)	32(6)	32(5)	25(4)	0(4)	-5(4)	13(4)
O(6)	45(5)	31(4)	39(4)	1(3)	-3(3)	-6(3)
C(6)	29(6)	49(6)	7(3)	-3(4)	-2(3)	-1(5)
C(7)	17(5)	44(6)	35(5)	6(5)	-1(4)	-10(5)
N(4)	29(5)	39(4)	20(3)	-5(3)	-4(3)	1(4)
O(8)	59(5)	31(4)	26(3)	6(3)	-3(3)	1(4)
C(8)	15(5)	40(5)	11(4)	0(4)	1(3)	5(4)
C(9)	31(6)	39(6)	25(4)	-12(4)	9(4)	9(5)
C(10)	37(7)	59(7)	38(5)	-4(5)	9(5)	11(6)
C(11)	29(5)	24(4)	22(4)	-5(4)	4(4)	2(4)
C(12)	35(7)	38(6)	50(6)	-1(5)	7(5)	-11(5)
C(13)	30(6)	28(5)	16(4)	-3(3)	5(4)	-3(4)
C(14)	49(7)	47(6)	28(5)	14(5)	4(5)	3(6)
C(15)	29(6)	62(7)	20(4)	4(5)	6(4)	8(6)
C(16)	40(6)	27(5)	30(4)	0(4)	5(4)	-5(5)
C(17)	23(5)	33(5)	32(4)	-5(4)	0(4)	7(4)
C(18)	22(5)	37(5)	26(4)	-4(4)	0(4)	7(4)

C(19)	24(5)	20(5)	38(5)	3(4)	-11(4)	-3(4)
C(20)	36(6)	28(5)	30(5)	4(4)	1(4)	10(4)
C(21)	29(6)	30(5)	18(4)	0(4)	2(4)	-3(4)
C(22)	19(5)	49(6)	32(5)	-1(4)	-12(4)	-2(5)
C(23)	44(7)	37(5)	18(4)	-9(4)	-7(4)	0(5)
C(24)	36(7)	45(6)	41(5)	8(5)	4(5)	14(5)
C(25)	52(7)	39(6)	41(5)	-2(5)	-1(5)	7(5)
C(26)	31(6)	39(6)	29(5)	-4(4)	2(4)	2(5)
C(27)	34(6)	33(5)	19(4)	-3(4)	0(4)	5(4)
C(28)	42(7)	45(6)	42(6)	-20(5)	-2(5)	14(5)
C(29)	70(9)	54(7)	30(5)	-17(5)	-16(6)	-7(6)
C(30)	58(7)	41(6)	20(4)	-8(4)	7(4)	13(6)
C(31)	26(6)	33(5)	42(5)	-8(5)	-3(4)	6(4)
C(32)	77(10)	94(10)	40(6)	-19(7)	7(7)	0(9)
C(33)	76(10)	48(7)	35(5)	21(5)	-11(6)	-14(6)
Fe(2)	26(1)	24(1)	23(1)	0(1)	0(1)	-1(1)
Fe(3)	29(1)	28(1)	25(1)	0(1)	1(1)	-2(1)
S(6)	26(1)	27(1)	24(1)	1(1)	0(1)	1(1)
S(7)	29(1)	28(1)	24(1)	1(1)	2(1)	0(1)
O(2)	30(4)	54(4)	31(3)	-2(3)	0(3)	1(3)
N(1)	42(5)	28(4)	16(3)	1(3)	2(3)	9(4)
C(34)	29(6)	37(5)	24(4)	-1(4)	-4(4)	12(5)
C(35)	29(6)	38(6)	23(4)	10(4)	3(4)	6(5)
O(5)	56(5)	34(4)	44(4)	-2(3)	15(4)	-6(4)
O(4)	55(5)	42(4)	30(3)	8(3)	-15(3)	-4(4)
O(3)	40(5)	38(4)	59(4)	-4(4)	-5(4)	14(4)
N(2)	27(5)	30(4)	21(3)	3(3)	3(3)	4(3)
C(36)	29(6)	50(6)	38(5)	27(5)	7(4)	6(5)
C(37)	24(6)	35(5)	32(5)	-4(4)	-3(4)	6(4)
C(38)	39(6)	36(5)	25(4)	-1(4)	-4(4)	8(5)
C(39)	29(6)	22(5)	24(4)	6(4)	-3(4)	0(4)
C(40)	37(6)	34(5)	39(5)	-3(4)	12(5)	13(5)
C(41)	39(6)	32(5)	25(4)	-3(4)	5(4)	-10(5)
C(42)	37(6)	24(5)	32(5)	-7(4)	8(4)	-6(4)

C(43)	45(7)	43(6)	24(4)	-7(4)	7(4)	-15(6)
C(44)	38(7)	28(5)	23(4)	6(4)	-9(4)	-3(4)
C(45)	11(5)	37(5)	27(4)	1(4)	3(3)	-4(4)
C(46)	23(5)	39(5)	26(4)	3(4)	-6(4)	-6(4)
C(47)	54(8)	38(6)	23(4)	-15(4)	4(5)	-14(5)
C(48)	29(6)	25(4)	18(4)	-1(4)	-7(4)	2(4)
C(49)	46(8)	40(6)	50(6)	26(5)	4(5)	19(5)
C(50)	29(6)	34(5)	33(5)	-6(4)	8(4)	0(5)
C(51)	32(7)	38(6)	70(7)	22(6)	-11(5)	-11(5)
C(52)	53(7)	18(4)	32(5)	1(4)	-5(5)	6(4)
C(53)	36(6)	47(6)	30(5)	-1(5)	14(4)	15(5)
C(54)	51(8)	72(9)	43(6)	-3(6)	-3(6)	2(7)
C(55)	41(7)	34(6)	34(5)	0(4)	7(4)	5(5)
C(56)	23(5)	32(5)	28(4)	2(4)	10(4)	-4(4)
C(57)	80(10)	35(6)	48(6)	-10(5)	20(6)	-27(6)
C(58)	31(7)	62(8)	42(6)	24(6)	7(5)	-3(6)
C(59)	25(6)	64(7)	29(5)	3(5)	4(4)	-10(5)
C(60)	35(6)	16(4)	43(5)	8(4)	1(5)	0(4)
C(61)	28(6)	57(7)	49(6)	-2(6)	-1(5)	-2(6)
C(62)	48(8)	110(11)	27(5)	23(6)	-19(5)	-39(8)
C(63)	51(7)	26(5)	29(5)	0(4)	19(5)	-2(5)
C(64)	41(7)	61(7)	25(5)	-10(5)	0(4)	-12(6)
C(65)	33(6)	58(7)	16(4)	13(4)	-6(4)	-4(5)
C(66)	41(6)	28(5)	29(5)	9(4)	5(4)	-5(5)
O(1)	49(5)	35(4)	32(3)	-12(3)	10(3)	-10(3)

Table A-27. Hydrogen coordinates (x 10^4) and isotropic displacement parameters ($Å^2$x 10^3) for III-4.

	x	y	z	U(eq)
H(4A)	6515	2054	3083	47
H(4B)	7032	2931	2911	47
H(5A)	5667	3518	2525	35
H(5B)	4174	3251	2632	35
H(6)	5274	1003	767	34
H(12A)	-610	1075	2233	62
H(12B)	612	663	2421	62
H(12C)	838	872	2086	62
H(14A)	4790	2477	879	62
H(14B)	4662	2598	1221	62
H(14C)	3344	2718	1021	62
H(15)	267	1918	2760	44
H(16A)	3761	1891	2907	38
H(16B)	3799	1457	2592	38
H(17)	-217	2778	1647	35
H(22A)	6953	1186	2638	40
H(22B)	7496	2151	2530	40
H(23)	3113	-1128	1103	40
H(24)	603	1940	1216	48
H(25A)	2617	4080	1860	66
H(25B)	2000	4872	2060	66
H(25C)	1028	4332	1841	66
H(26A)	1393	-906	1447	50
H(26B)	872	112	1510	50
H(26C)	2106	-309	1694	50
H(28)	1440	4477	2536	52
H(29A)	5314	3807	3082	77
H(29B)	5827	3227	3354	77

H(29C)	4460	2937	3188	77
H(30A)	6020	-950	797	60
H(30B)	5177	-559	528	60
H(30C)	4601	-1412	708	60
H(32A)	1641	3661	3084	105
H(32B)	242	3102	3112	105
H(32C)	224	4141	3002	105
H(33A)	5280	297	2762	80
H(33B)	3854	292	2931	80
H(33C)	5181	723	3079	80
H(35A)	1156	6393	795	36
H(35B)	936	5321	832	36
H(40)	8144	4540	-405	44
H(41)	5095	7050	-861	38
H(42A)	4151	6622	770	37
H(42B)	3092	7166	968	37
H(47)	3569	4515	-963	46
H(48A)	3061	4356	1011	29
H(48B)	4427	4900	1081	29
H(49A)	6300	3202	481	68
H(49B)	7386	2766	700	68
H(49C)	7884	3174	397	68
H(50A)	1979	7088	1381	48
H(50B)	1086	6470	1595	48
H(50C)	579	6643	1271	48
H(51A)	7586	7180	562	70
H(51B)	7408	6555	281	70
H(51C)	8896	6726	413	70
H(52A)	6800	7374	-519	51
H(52B)	7497	6546	-347	51
H(52C)	6166	7035	-219	51
H(53)	9034	4469	94	46
H(54A)	2584	6511	-1132	83
H(54B)	3069	5636	-1312	83

H(54C)	3940	6562	-1324	83
H(55A)	1529	5167	1298	44
H(55B)	2900	5567	1435	44
H(57A)	5627	3442	-459	81
H(57B)	4336	3290	-666	81
H(57C)	4118	3634	-341	81
H(58)	7830	3724	1102	54
H(61)	8225	6447	1028	53
H(62A)	7439	4895	1545	93
H(62B)	8319	5802	1493	93
H(62C)	9050	4823	1492	93
H(64A)	4376	6709	1385	64
H(64B)	5256	7328	1169	64
H(64C)	5472	6243	1175	64

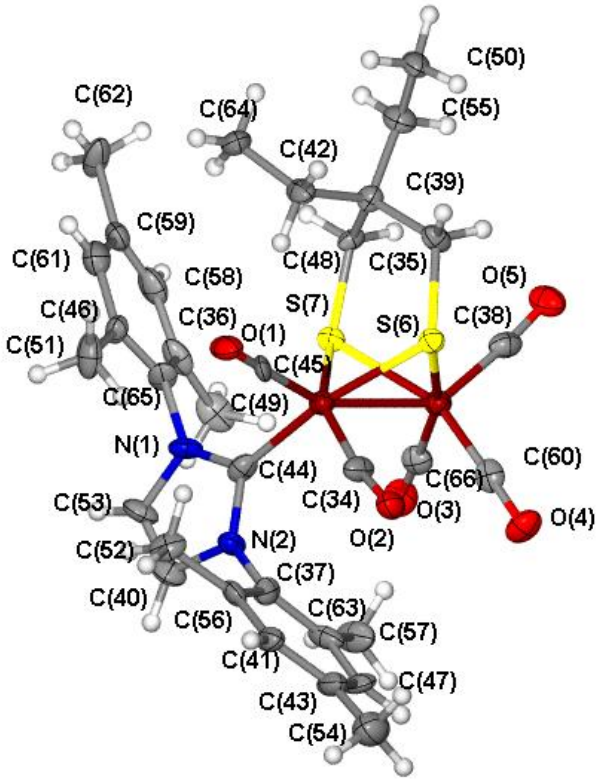
C(50)
C(62)
C(64)
C(55)
C(42)
C(39)
C(59)
C(61)
C(48)
C(35)
O(5)
C(58)
S(7)
C(46)
C(36)
S(6)
C(38)
O(1)
C(51)
C(45)
C(65)
C(49)
N(1)
C(44)
C(60)
C(66)
C(53)
C(34)
O(3)
O(4)
C(52)
N(2)
O(2)
C(37)
C(40)
C(63)
C(56)
C(57)
C(41)
C(47)
C(43)
C(54)

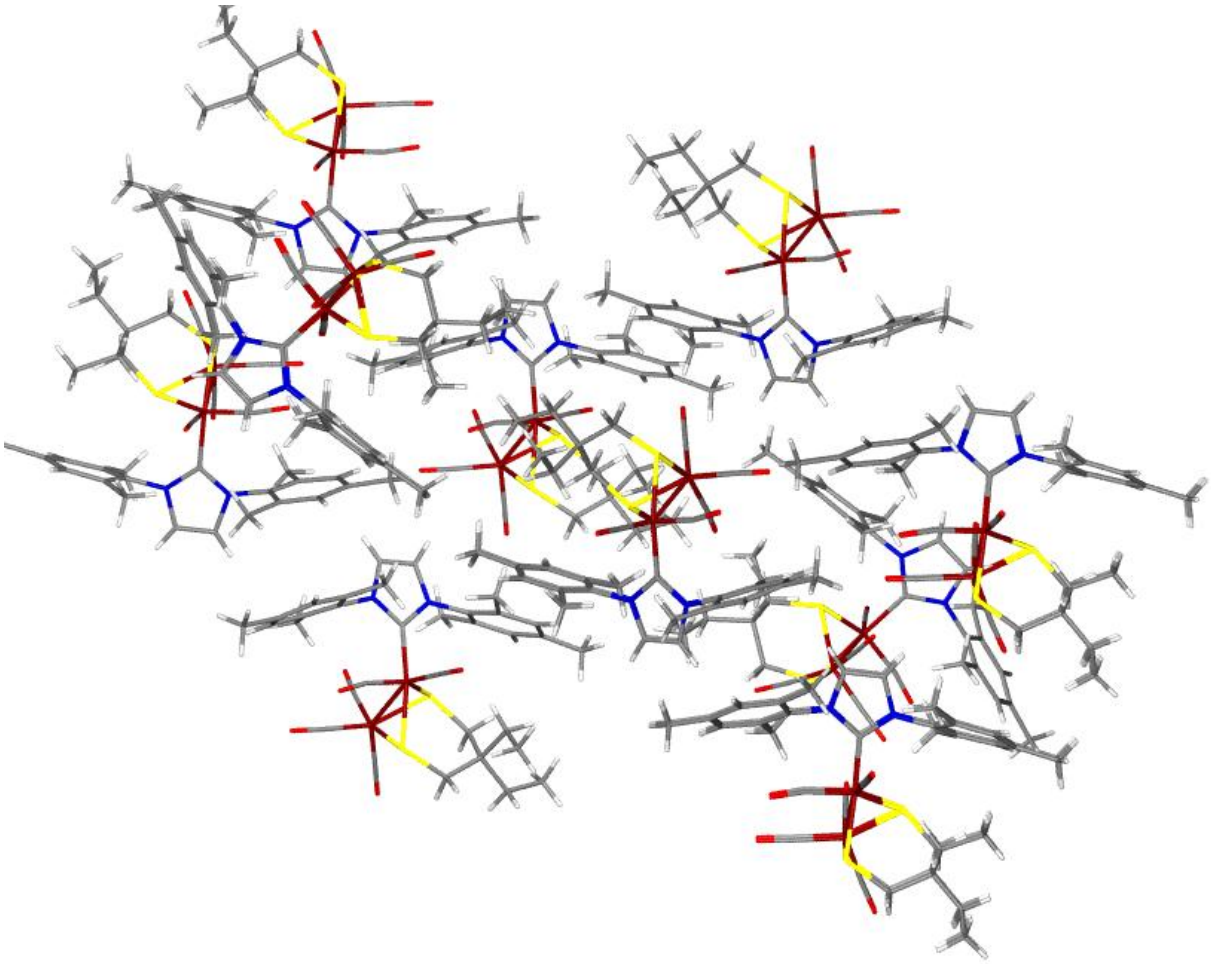

Table A-28. Crystal data and structure refinement for Complex III-6.

Identification code	depdtime	
Empirical formula	C17 H22 Fe2 N2 O5 S2	
Formula weight	510.19	
Temperature	110(2) K	
Wavelength	0.71073 Å	
Crystal system	Monoclinic	
Space group	P2(1)/c	
Unit cell dimensions	a = 12.507(4) Å	α= 90°.
	b = 11.645(4) Å	β= 93.409(5)°.
	c = 14.070(5) Å	γ = 90°.
Volume	2045.6(12) $Å^3$	
Z	4	
Density (calculated)	1.657 Mg/m^3	
Absorption coefficient	1.653 mm^{-1}	
F(000)	1048	
Crystal size	0.51 x 0.44 x 0.03 mm^3	
Theta range for data collection	1.63 to 28.34°.	
Index ranges	-16<=h<=16, -15<=k<=15, -18<=l<=18	
Reflections collected	19311	
Independent reflections	4990 [R(int) = 0.2927]	
Completeness to theta = 28.34°	97.7 %	
Absorption correction	None	
Max. and min. transmission	0.9475 and 0.4878	
Refinement method	Full-matrix least-squares on F^2	
Data / restraints / parameters	4990 / 0 / 257	
Goodness-of-fit on F^2	1.015	
Final R indices [I>2sigma(I)]	R1 = 0.0586, wR2 = 0.1769	
R indices (all data)	R1 = 0.0652, wR2 = 0.1867	
Largest diff. peak and hole	1.302 and -1.475 $e.Å^{-3}$	

Table A-29. Atomic coordinates (x 10^4) and equivalent isotropic displacement parameters ($Å^2$x 10^3) for III-6. U(eq) is defined as one third of the trace of the orthogonalized U^{ij} tensor.

	x	y	z	U(eq)
Fe(1)	7798(1)	-603(1)	1298(1)	15(1)
Fe(2)	7434(1)	1511(1)	1133(1)	14(1)
S(3)	8738(1)	573(1)	377(1)	14(1)
S(4)	6370(1)	149(1)	417(1)	15(1)
O(2)	9073(2)	2434(2)	2493(2)	27(1)
O(1)	5793(2)	2016(2)	2468(2)	28(1)
O(3)	9487(2)	-216(2)	2806(2)	28(1)
O(4)	6200(2)	-1150(2)	2668(2)	26(1)
N(1)	7860(2)	3614(2)	-49(2)	20(1)
C(4)	6832(2)	-955(3)	2140(2)	19(1)
C(11)	8428(2)	485(3)	-907(2)	15(1)
C(3)	8832(2)	-382(3)	2213(2)	20(1)
C(1)	6437(2)	1819(3)	1939(2)	18(1)
O(5)	8455(2)	-2965(2)	837(2)	34(1)
C(13)	6433(2)	232(3)	-882(2)	16(1)
C(5)	8179(3)	-2045(3)	975(2)	24(1)
C(2)	8425(2)	2104(3)	1938(2)	19(1)
N(2)	6172(2)	3255(2)	-63(2)	18(1)
C(7)	5113(2)	2787(3)	110(2)	25(1)
C(17)	6436(3)	-331(3)	-3011(2)	25(1)
C(16)	7378(2)	158(3)	-2398(2)	19(1)
C(6)	7146(2)	2846(3)	297(2)	17(1)
C(15)	8597(3)	-2033(3)	-1442(2)	27(1)
C(9)	7352(3)	4458(3)	-581(2)	23(1)
C(12)	7455(2)	-187(3)	-1324(2)	16(1)
C(8)	6291(3)	4238(3)	-598(2)	22(1)
C(10)	9021(3)	3584(3)	129(2)	26(1)
C(14)	7530(2)	-1492(3)	-1223(2)	18(1)

Table A-30. Bond lengths [Å] and angles [°] for III-6.

Fe(1)-C(3)	1.788(3)
Fe(1)-C(4)	1.789(3)
Fe(1)-C(5)	1.811(4)
Fe(1)-S(3)	2.2622(9)
Fe(1)-S(4)	2.2872(10)
Fe(1)-Fe(2)	2.5121(10)
Fe(2)-C(2)	1.769(3)
Fe(2)-C(1)	1.772(3)
Fe(2)-C(6)	1.969(3)
Fe(2)-S(4)	2.2681(10)
Fe(2)-S(3)	2.2780(9)
S(3)-C(11)	1.827(3)
S(4)-C(13)	1.837(3)
O(2)-C(2)	1.156(4)
O(1)-C(1)	1.151(4)
O(3)-C(3)	1.149(4)
O(4)-C(4)	1.140(3)
N(1)-C(9)	1.368(4)
N(1)-C(6)	1.374(4)
N(1)-C(10)	1.459(4)
C(11)-C(12)	1.534(4)
C(11)-H(11A)	0.9900
C(11)-H(11B)	0.9900
O(5)-C(5)	1.146(4)
C(13)-C(12)	1.535(4)
C(13)-H(13A)	0.9900
C(13)-H(13B)	0.9900
N(2)-C(6)	1.376(4)
N(2)-C(8)	1.382(4)
N(2)-C(7)	1.467(4)
C(7)-H(7A)	0.9800
C(7)-H(7B)	0.9800

C(7)-H(7C)	0.9800
C(17)-C(16)	1.529(4)
C(17)-H(17A)	0.9800
C(17)-H(17B)	0.9800
C(17)-H(17C)	0.9800
C(16)-C(12)	1.561(4)
C(16)-H(16A)	0.9900
C(16)-H(16B)	0.9900
C(15)-C(14)	1.524(4)
C(15)-H(15A)	0.9800
C(15)-H(15B)	0.9800
C(15)-H(15C)	0.9800
C(9)-C(8)	1.351(5)
C(9)-H(9)	0.9500
C(12)-C(14)	1.528(4)
C(8)-H(8)	0.9500
C(10)-H(10A)	0.9800
C(10)-H(10B)	0.9800
C(10)-H(10C)	0.9800
C(14)-H(14A)	0.9900
C(14)-H(14B)	0.9900

C(3)-Fe(1)-C(4)	92.55(14)
C(3)-Fe(1)-C(5)	97.13(15)
C(4)-Fe(1)-C(5)	98.75(14)
C(3)-Fe(1)-S(3)	87.00(10)
C(4)-Fe(1)-S(3)	155.79(11)
C(5)-Fe(1)-S(3)	105.33(10)
C(3)-Fe(1)-S(4)	147.49(11)
C(4)-Fe(1)-S(4)	84.83(10)
C(5)-Fe(1)-S(4)	115.31(11)
S(3)-Fe(1)-S(4)	82.70(4)
C(3)-Fe(1)-Fe(2)	92.58(11)
C(4)-Fe(1)-Fe(2)	99.17(11)

C(5)-Fe(1)-Fe(2)	159.17(10)
S(3)-Fe(1)-Fe(2)	56.71(3)
S(4)-Fe(1)-Fe(2)	56.17(2)
C(2)-Fe(2)-C(1)	90.24(14)
C(2)-Fe(2)-C(6)	99.83(14)
C(1)-Fe(2)-C(6)	96.43(13)
C(2)-Fe(2)-S(4)	158.10(11)
C(1)-Fe(2)-S(4)	90.52(11)
C(6)-Fe(2)-S(4)	101.83(9)
C(2)-Fe(2)-S(3)	89.59(10)
C(1)-Fe(2)-S(3)	161.19(10)
C(6)-Fe(2)-S(3)	102.13(8)
S(4)-Fe(2)-S(3)	82.77(4)
C(2)-Fe(2)-Fe(1)	101.95(11)
C(1)-Fe(2)-Fe(1)	105.64(10)
C(6)-Fe(2)-Fe(1)	148.70(8)
S(4)-Fe(2)-Fe(1)	56.90(3)
S(3)-Fe(2)-Fe(1)	56.11(2)
C(11)-S(3)-Fe(1)	116.46(10)
C(11)-S(3)-Fe(2)	111.89(10)
Fe(1)-S(3)-Fe(2)	67.19(3)
C(13)-S(4)-Fe(2)	110.27(10)
C(13)-S(4)-Fe(1)	118.81(10)
Fe(2)-S(4)-Fe(1)	66.93(3)
C(9)-N(1)-C(6)	111.8(3)
C(9)-N(1)-C(10)	122.5(3)
C(6)-N(1)-C(10)	125.7(3)
O(4)-C(4)-Fe(1)	178.0(3)
C(12)-C(11)-S(3)	121.61(19)
C(12)-C(11)-H(11A)	106.9
S(3)-C(11)-H(11A)	106.9
C(12)-C(11)-H(11B)	106.9
S(3)-C(11)-H(11B)	106.9
H(11A)-C(11)-H(11B)	106.7

O(3)-C(3)-Fe(1)	178.4(3)
O(1)-C(1)-Fe(2)	179.5(3)
C(12)-C(13)-S(4)	118.2(2)
C(12)-C(13)-H(13A)	107.8
S(4)-C(13)-H(13A)	107.8
C(12)-C(13)-H(13B)	107.8
S(4)-C(13)-H(13B)	107.8
H(13A)-C(13)-H(13B)	107.1
O(5)-C(5)-Fe(1)	175.0(3)
O(2)-C(2)-Fe(2)	176.1(3)
C(6)-N(2)-C(8)	111.5(3)
C(6)-N(2)-C(7)	126.7(3)
C(8)-N(2)-C(7)	121.7(3)
N(2)-C(7)-H(7A)	109.5
N(2)-C(7)-H(7B)	109.5
H(7A)-C(7)-H(7B)	109.5
N(2)-C(7)-H(7C)	109.5
H(7A)-C(7)-H(7C)	109.5
H(7B)-C(7)-H(7C)	109.5
C(16)-C(17)-H(17A)	109.5
C(16)-C(17)-H(17B)	109.5
H(17A)-C(17)-H(17B)	109.5
C(16)-C(17)-H(17C)	109.5
H(17A)-C(17)-H(17C)	109.5
H(17B)-C(17)-H(17C)	109.5
C(17)-C(16)-C(12)	116.8(3)
C(17)-C(16)-H(16A)	108.1
C(12)-C(16)-H(16A)	108.1
C(17)-C(16)-H(16B)	108.1
C(12)-C(16)-H(16B)	108.1
H(16A)-C(16)-H(16B)	107.3
N(1)-C(6)-N(2)	102.9(3)
N(1)-C(6)-Fe(2)	128.8(2)
N(2)-C(6)-Fe(2)	128.3(2)

C(14)-C(15)-H(15A)	109.5
C(14)-C(15)-H(15B)	109.5
H(15A)-C(15)-H(15B)	109.5
C(14)-C(15)-H(15C)	109.5
H(15A)-C(15)-H(15C)	109.5
H(15B)-C(15)-H(15C)	109.5
C(8)-C(9)-N(1)	107.3(3)
C(8)-C(9)-H(9)	126.4
N(1)-C(9)-H(9)	126.4
C(14)-C(12)-C(11)	115.4(2)
C(14)-C(12)-C(13)	109.1(2)
C(11)-C(12)-C(13)	110.0(2)
C(14)-C(12)-C(16)	110.3(3)
C(11)-C(12)-C(16)	103.9(2)
C(13)-C(12)-C(16)	107.8(2)
C(9)-C(8)-N(2)	106.5(3)
C(9)-C(8)-H(8)	126.7
N(2)-C(8)-H(8)	126.7
N(1)-C(10)-H(10A)	109.5
N(1)-C(10)-H(10B)	109.5
H(10A)-C(10)-H(10B)	109.5
N(1)-C(10)-H(10C)	109.5
H(10A)-C(10)-H(10C)	109.5
H(10B)-C(10)-H(10C)	109.5
C(15)-C(14)-C(12)	116.2(3)
C(15)-C(14)-H(14A)	108.2
C(12)-C(14)-H(14A)	108.2
C(15)-C(14)-H(14B)	108.2
C(12)-C(14)-H(14B)	108.2
H(14A)-C(14)-H(14B)	107.4

Symmetry transformations used to generate equivalent atoms:

Table A-31. Anisotropic displacement parameters ($Å^2 x\ 10^3$) for III-6. The anisotropic displacement factor exponent takes the form: $-2\pi^2[\ h^2\ a^{*2}U^{11} + ...\ + 2\ h\ k\ a^*\ b^*\ U^{12}\ ]$

	U^{11}	U^{22}	U^{33}	U^{23}	U^{13}	U^{12}
Fe(1)	17(1)	14(1)	14(1)	2(1)	4(1)	1(1)
Fe(2)	15(1)	13(1)	13(1)	0(1)	3(1)	1(1)
S(3)	14(1)	15(1)	14(1)	0(1)	3(1)	0(1)
S(4)	14(1)	15(1)	15(1)	1(1)	4(1)	0(1)
O(2)	24(1)	30(1)	27(1)	-10(1)	-3(1)	4(1)
O(1)	29(1)	30(1)	25(1)	1(1)	12(1)	6(1)
O(3)	27(1)	31(1)	26(1)	6(1)	-3(1)	-1(1)
O(4)	27(1)	24(1)	26(1)	4(1)	9(1)	0(1)
N(1)	23(1)	20(1)	17(1)	1(1)	0(1)	-2(1)
C(4)	25(1)	15(2)	18(1)	3(1)	2(1)	1(1)
C(11)	15(1)	19(2)	11(1)	-1(1)	3(1)	-3(1)
C(3)	23(1)	19(2)	19(1)	6(1)	7(1)	2(1)
C(1)	23(1)	15(2)	17(1)	5(1)	-1(1)	3(1)
O(5)	52(2)	22(1)	30(1)	-1(1)	6(1)	13(1)
C(13)	19(1)	18(2)	12(1)	1(1)	2(1)	0(1)
C(5)	30(2)	23(2)	18(1)	4(1)	4(1)	5(1)
C(2)	24(1)	18(2)	16(1)	0(1)	4(1)	6(1)
N(2)	20(1)	17(1)	17(1)	0(1)	1(1)	0(1)
C(7)	20(1)	22(2)	33(2)	4(1)	3(1)	3(1)
C(17)	27(2)	30(2)	16(1)	0(1)	-3(1)	-7(1)
C(16)	19(1)	22(2)	15(1)	1(1)	2(1)	-4(1)
C(6)	20(1)	17(2)	14(1)	-3(1)	4(1)	-2(1)
C(15)	30(2)	21(2)	29(2)	-6(1)	3(1)	10(1)
C(9)	29(2)	19(2)	20(1)	4(1)	1(1)	-4(1)
C(12)	17(1)	17(2)	14(1)	0(1)	5(1)	-1(1)
C(8)	30(2)	18(2)	18(1)	4(1)	1(1)	3(1)
C(10)	20(1)	25(2)	32(2)	5(1)	1(1)	-6(1)
C(14)	21(1)	13(2)	19(1)	0(1)	0(1)	3(1)

Table A-32. Hydrogen coordinates (x 10^4) and isotropic displacement parameters ($Å^2$x 10^3) for III-6.

	x	y	z	U(eq)
H(11A)	8351	1283	-1144	18
H(11B)	9067	160	-1190	18
H(13A)	5824	-214	-1173	20
H(13B)	6319	1044	-1072	20
H(7A)	5136	1947	77	37
H(7B)	4585	3078	-373	37
H(7C)	4909	3023	743	37
H(17A)	6450	-1172	-2977	37
H(17B)	6490	-88	-3673	37
H(17C)	5762	-48	-2776	37
H(16A)	7343	1007	-2437	22
H(16B)	8049	-83	-2681	22
H(15A)	8758	-1851	-2098	40
H(15B)	8554	-2868	-1366	40
H(15C)	9165	-1728	-1003	40
H(9)	7685	5083	-882	27
H(8)	5736	4673	-915	26
H(10A)	9362	3983	-386	38
H(10B)	9264	2784	158	38
H(10C)	9216	3964	736	38
H(14A)	7376	-1696	-562	21
H(14B)	6962	-1840	-1650	21

Table A-33. Torsion angles [°] for III-6.

C(3)-Fe(1)-Fe(2)-C(2)	3.39(13)
C(4)-Fe(1)-Fe(2)-C(2)	96.39(14)
C(5)-Fe(1)-Fe(2)-C(2)	-114.5(3)
S(3)-Fe(1)-Fe(2)-C(2)	-81.32(10)
S(4)-Fe(1)-Fe(2)-C(2)	173.79(9)
C(3)-Fe(1)-Fe(2)-C(1)	-90.26(14)
C(4)-Fe(1)-Fe(2)-C(1)	2.74(14)
C(5)-Fe(1)-Fe(2)-C(1)	151.8(3)
S(3)-Fe(1)-Fe(2)-C(1)	-174.97(11)
S(4)-Fe(1)-Fe(2)-C(1)	80.14(11)
C(3)-Fe(1)-Fe(2)-C(6)	136.55(19)
C(4)-Fe(1)-Fe(2)-C(6)	-130.45(19)
C(5)-Fe(1)-Fe(2)-C(6)	18.6(4)
S(3)-Fe(1)-Fe(2)-C(6)	51.85(16)
S(4)-Fe(1)-Fe(2)-C(6)	-53.05(16)
C(3)-Fe(1)-Fe(2)-S(4)	-170.40(10)
C(4)-Fe(1)-Fe(2)-S(4)	-77.40(10)
C(5)-Fe(1)-Fe(2)-S(4)	71.7(3)
S(3)-Fe(1)-Fe(2)-S(4)	104.89(4)
C(3)-Fe(1)-Fe(2)-S(3)	84.70(10)
C(4)-Fe(1)-Fe(2)-S(3)	177.71(10)
C(5)-Fe(1)-Fe(2)-S(3)	-33.2(3)
S(4)-Fe(1)-Fe(2)-S(3)	-104.89(4)
C(3)-Fe(1)-S(3)-C(11)	160.90(15)
C(4)-Fe(1)-S(3)-C(11)	-109.6(3)
C(5)-Fe(1)-S(3)-C(11)	64.32(15)
S(4)-Fe(1)-S(3)-C(11)	-50.00(11)
Fe(2)-Fe(1)-S(3)-C(11)	-104.03(11)
C(3)-Fe(1)-S(3)-Fe(2)	-95.07(11)
C(4)-Fe(1)-S(3)-Fe(2)	-5.5(2)
C(5)-Fe(1)-S(3)-Fe(2)	168.35(11)
S(4)-Fe(1)-S(3)-Fe(2)	54.03(3)

C(2)-Fe(2)-S(3)-C(11)	-144.66(15)
C(1)-Fe(2)-S(3)-C(11)	125.8(3)
C(6)-Fe(2)-S(3)-C(11)	-44.69(14)
S(4)-Fe(2)-S(3)-C(11)	55.92(11)
Fe(1)-Fe(2)-S(3)-C(11)	110.61(11)
C(2)-Fe(2)-S(3)-Fe(1)	104.73(10)
C(1)-Fe(2)-S(3)-Fe(1)	15.2(3)
C(6)-Fe(2)-S(3)-Fe(1)	-155.30(9)
S(4)-Fe(2)-S(3)-Fe(1)	-54.69(3)
C(2)-Fe(2)-S(4)-C(13)	-130.1(3)
C(1)-Fe(2)-S(4)-C(13)	137.94(14)
C(6)-Fe(2)-S(4)-C(13)	41.26(13)
S(3)-Fe(2)-S(4)-C(13)	-59.68(11)
Fe(1)-Fe(2)-S(4)-C(13)	-113.64(11)
C(2)-Fe(2)-S(4)-Fe(1)	-16.5(2)
C(1)-Fe(2)-S(4)-Fe(1)	-108.42(10)
C(6)-Fe(2)-S(4)-Fe(1)	154.90(8)
S(3)-Fe(2)-S(4)-Fe(1)	53.96(3)
C(3)-Fe(1)-S(4)-C(13)	119.3(2)
C(4)-Fe(1)-S(4)-C(13)	-154.05(16)
C(5)-Fe(1)-S(4)-C(13)	-56.80(16)
S(3)-Fe(1)-S(4)-C(13)	46.74(12)
Fe(2)-Fe(1)-S(4)-C(13)	101.27(12)
C(3)-Fe(1)-S(4)-Fe(2)	18.05(18)
C(4)-Fe(1)-S(4)-Fe(2)	104.68(11)
C(5)-Fe(1)-S(4)-Fe(2)	-158.07(11)
S(3)-Fe(1)-S(4)-Fe(2)	-54.53(3)
C(3)-Fe(1)-C(4)-O(4)	114(9)
C(5)-Fe(1)-C(4)-O(4)	-148(9)
S(3)-Fe(1)-C(4)-O(4)	26(9)
S(4)-Fe(1)-C(4)-O(4)	-33(9)
Fe(2)-Fe(1)-C(4)-O(4)	21(9)
Fe(1)-S(3)-C(11)-C(12)	10.4(3)
Fe(2)-S(3)-C(11)-C(12)	-64.1(3)

C(4)-Fe(1)-C(3)-O(3)	-78(10)
C(5)-Fe(1)-C(3)-O(3)	-177(100)
S(3)-Fe(1)-C(3)-O(3)	78(10)
S(4)-Fe(1)-C(3)-O(3)	7(10)
Fe(2)-Fe(1)-C(3)-O(3)	22(10)
C(2)-Fe(2)-C(1)-O(1)	-42(43)
C(6)-Fe(2)-C(1)-O(1)	-142(43)
S(4)-Fe(2)-C(1)-O(1)	116(43)
S(3)-Fe(2)-C(1)-O(1)	47(43)
Fe(1)-Fe(2)-C(1)-O(1)	60(43)
Fe(2)-S(4)-C(13)-C(12)	73.0(3)
Fe(1)-S(4)-C(13)-C(12)	-1.1(3)
C(3)-Fe(1)-C(5)-O(5)	25(4)
C(4)-Fe(1)-C(5)-O(5)	-69(4)
S(3)-Fe(1)-C(5)-O(5)	114(3)
S(4)-Fe(1)-C(5)-O(5)	-157(3)
Fe(2)-Fe(1)-C(5)-O(5)	142(3)
C(1)-Fe(2)-C(2)-O(2)	80(4)
C(6)-Fe(2)-C(2)-O(2)	177(4)
S(4)-Fe(2)-C(2)-O(2)	-12(4)
S(3)-Fe(2)-C(2)-O(2)	-81(4)
Fe(1)-Fe(2)-C(2)-O(2)	-26(4)
C(9)-N(1)-C(6)-N(2)	0.9(3)
C(10)-N(1)-C(6)-N(2)	179.4(3)
C(9)-N(1)-C(6)-Fe(2)	-177.6(2)
C(10)-N(1)-C(6)-Fe(2)	0.9(4)
C(8)-N(2)-C(6)-N(1)	-0.6(3)
C(7)-N(2)-C(6)-N(1)	-177.6(3)
C(8)-N(2)-C(6)-Fe(2)	177.9(2)
C(7)-N(2)-C(6)-Fe(2)	0.9(4)
C(2)-Fe(2)-C(6)-N(1)	41.1(3)
C(1)-Fe(2)-C(6)-N(1)	132.4(3)
S(4)-Fe(2)-C(6)-N(1)	-135.7(3)
S(3)-Fe(2)-C(6)-N(1)	-50.7(3)

Fe(1)-Fe(2)-C(6)-N(1)	-92.5(3)
C(2)-Fe(2)-C(6)-N(2)	-137.0(3)
C(1)-Fe(2)-C(6)-N(2)	-45.7(3)
S(4)-Fe(2)-C(6)-N(2)	46.2(3)
S(3)-Fe(2)-C(6)-N(2)	131.3(2)
Fe(1)-Fe(2)-C(6)-N(2)	89.4(3)
C(6)-N(1)-C(9)-C(8)	-0.8(4)
C(10)-N(1)-C(9)-C(8)	-179.4(3)
S(3)-C(11)-C(12)-C(14)	-69.5(3)
S(3)-C(11)-C(12)-C(13)	54.5(3)
S(3)-C(11)-C(12)-C(16)	169.6(2)
S(4)-C(13)-C(12)-C(14)	69.3(3)
S(4)-C(13)-C(12)-C(11)	-58.2(3)
S(4)-C(13)-C(12)-C(16)	-170.9(2)
C(17)-C(16)-C(12)-C(14)	58.9(3)
C(17)-C(16)-C(12)-C(11)	-176.9(3)
C(17)-C(16)-C(12)-C(13)	-60.1(4)
N(1)-C(9)-C(8)-N(2)	0.4(4)
C(6)-N(2)-C(8)-C(9)	0.1(4)
C(7)-N(2)-C(8)-C(9)	177.2(3)
C(11)-C(12)-C(14)-C(15)	-43.9(4)
C(13)-C(12)-C(14)-C(15)	-168.3(2)
C(16)-C(12)-C(14)-C(15)	73.5(3)

Symmetry transformations used to generate equivalent atoms:

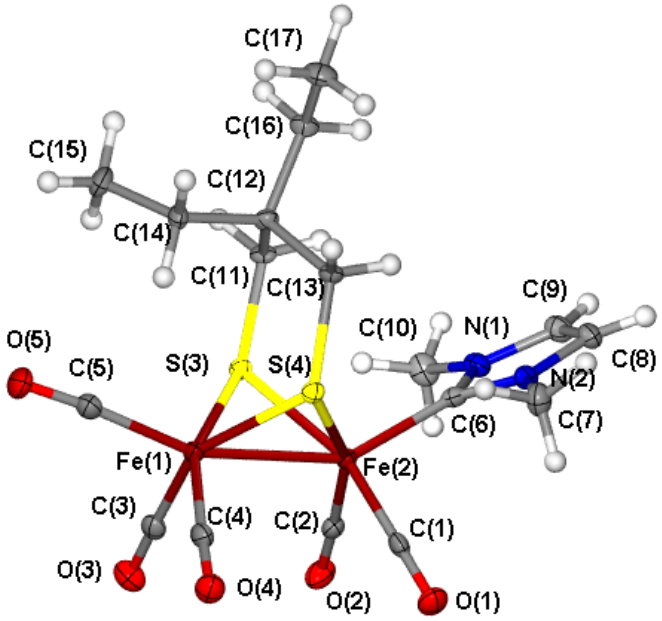
C(17)
C(16)
C(15)
C(12)
C(14)
C(11)
C(13)
C(9)
C(10)
N(1)
C(8)
O(5)
C(5)
S(3)
S(4)
N(2)
C(6)
C(7)
Fe(1)
Fe(2)
C(3)
C(4)
C(2)
C(1)
O(3)
O(4)
O(2)
O(1)

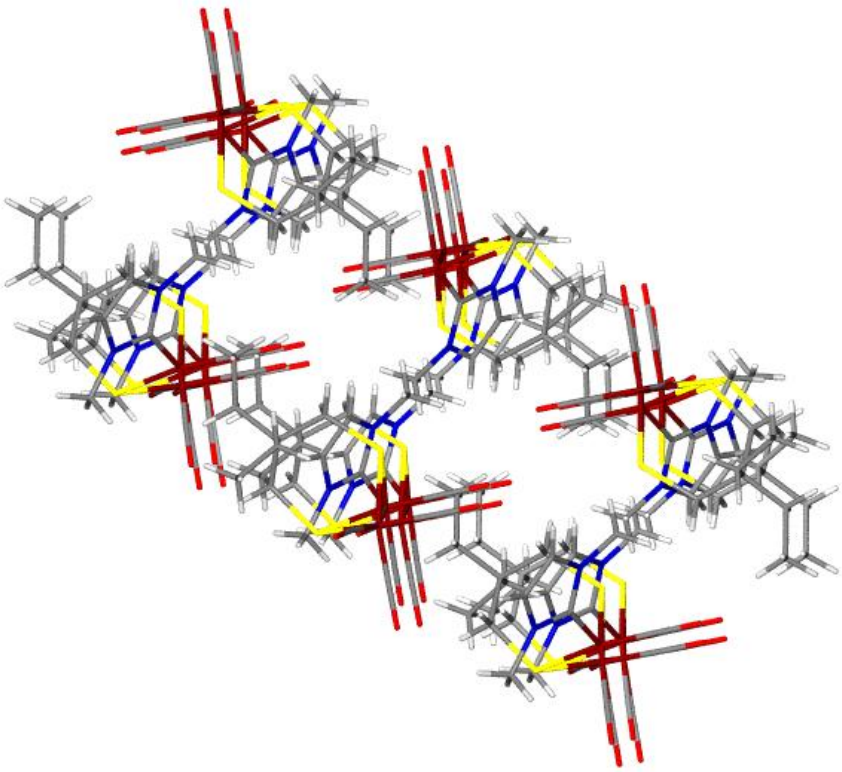

Table A-34. Crystal data and structure refinement for Complex III-7.

Identification code	Fedmpdt(CO)5PPh3	
Empirical formula	C28 H25 Fe2 O5 P S2	
Formula weight	648.27	
Temperature	106(2) K	
Wavelength	0.71073 Å	
Crystal system	Triclinic	
Space group	P-1	
Unit cell dimensions	a = 9.492(4) Å	α= 96.580(5)°.
	b = 10.481(4) Å	β= 99.330(5)°.
	c = 14.968(6) Å	γ = 104.946(5)°.
Volume	1400.5(9) $Å^3$	
Z	2	
Density (calculated)	1.537 Mg/m^3	
Absorption coefficient	1.279 mm^{-1}	
F(000)	664	
Crystal size	0.35 x 0.13 x 0.07 mm^3	
Theta range for data collection	2.04 to 28.58°.	
Index ranges	-12<=h<=12, -13<=k<=14, -20<=l<=19	
Reflections collected	16198	
Independent reflections	6522 [R(int) = 0.1139]	
Completeness to theta = 28.58°	91.2 %	
Absorption correction	None	
Max. and min. transmission	0.9158 and 0.6631	
Refinement method	Full-matrix least-squares on F^2	
Data / restraints / parameters	6522 / 0 / 345	
Goodness-of-fit on F^2	1.004	
Final R indices [I>2sigma(I)]	R1 = 0.0469, wR2 = 0.0720	
R indices (all data)	R1 = 0.1475, wR2 = 0.1045	
Largest diff. peak and hole	0.451 and -0.383 $e.Å^{-3}$	

Table A-35. Atomic coordinates (x 10^4) and equivalent isotropic displacement parameters ($Å^2$x 10^3) for III-7. U(eq) is defined as one third of the trace of the orthogonalized U^{ij} tensor.

	x	y	z	U(eq)
Fe(1)	8058(1)	3174(1)	2183(1)	22(1)
Fe(2)	8536(1)	1199(1)	1313(1)	27(1)
P(1)	6751(2)	4267(1)	2925(1)	23(1)
S(2)	6355(2)	1718(1)	1034(1)	24(1)
S(1)	8110(2)	1279(1)	2762(1)	25(1)
O(4)	10782(4)	4428(4)	3534(3)	40(1)
O(5)	8824(4)	5078(4)	939(3)	41(1)
C(23)	7859(6)	5977(5)	3438(4)	23(1)
C(17)	6128(6)	3468(5)	3869(3)	25(1)
C(5)	8503(6)	4336(5)	1433(4)	26(1)
C(11)	5132(6)	4608(5)	2299(3)	23(1)
C(22)	4617(6)	2954(5)	3875(4)	31(1)
C(8)	4997(6)	-289(5)	2070(4)	26(1)
C(4)	9721(6)	3947(5)	2984(3)	24(1)
O(3)	9121(5)	2400(5)	-313(3)	60(1)
C(7)	4803(6)	780(5)	1478(4)	29(1)
O(2)	11696(5)	1838(4)	2111(3)	51(1)
C(28)	8440(6)	6408(5)	4361(4)	29(1)
C(18)	7167(6)	3223(5)	4545(3)	27(1)
C(3)	8911(6)	1925(7)	316(4)	40(2)
C(6)	6308(6)	266(5)	2889(3)	27(1)
C(2)	10446(7)	1581(6)	1792(4)	34(1)
C(19)	6736(6)	2492(5)	5214(4)	34(1)
C(26)	9742(6)	8564(6)	4078(4)	37(2)
C(15)	3460(6)	4517(5)	874(4)	36(2)
C(12)	4292(6)	5306(5)	2751(4)	30(1)
C(13)	3068(6)	5573(5)	2274(4)	35(2)
C(21)	4189(6)	2207(5)	4547(4)	35(2)
C(14)	2645(6)	5182(5)	1333(4)	34(1)

C(20)	5239(7)	1976(6)	5207(4)	39(2)
O(1)	8198(5)	-1545(5)	480(4)	90(2)
C(24)	8221(6)	6869(5)	2831(4)	35(2)
C(25)	9161(7)	8146(6)	3153(4)	43(2)
C(27)	9376(6)	7693(6)	4677(4)	36(2)
C(10)	3574(6)	-708(6)	2466(4)	36(2)
C(16)	4695(6)	4240(5)	1361(4)	30(1)
C(1)	8293(7)	-465(7)	821(5)	46(2)
C(9)	5158(7)	-1530(5)	1500(4)	40(2)

Table A-36. Bond lengths [Å] and angles [°] for III-7.

Fe(1)-C(4)	1.758(6)
Fe(1)-C(5)	1.768(6)
Fe(1)-P(1)	2.2306(17)
Fe(1)-S(2)	2.2632(16)
Fe(1)-S(1)	2.2645(17)
Fe(1)-Fe(2)	2.4986(13)
Fe(2)-C(1)	1.755(6)
Fe(2)-C(2)	1.761(6)
Fe(2)-C(3)	1.795(7)
Fe(2)-S(2)	2.2605(17)
Fe(2)-S(1)	2.2666(17)
P(1)-C(11)	1.806(5)
P(1)-C(17)	1.827(5)
P(1)-C(23)	1.833(5)
S(2)-C(7)	1.816(5)
S(1)-C(6)	1.818(5)
O(4)-C(4)	1.149(6)
O(5)-C(5)	1.151(6)
C(23)-C(28)	1.377(7)
C(23)-C(24)	1.395(7)
C(17)-C(18)	1.388(7)
C(17)-C(22)	1.398(7)
C(11)-C(16)	1.377(7)
C(11)-C(12)	1.412(7)
C(22)-C(21)	1.393(7)
C(22)-H(22)	0.9500
C(8)-C(9)	1.527(7)
C(8)-C(7)	1.535(7)
C(8)-C(6)	1.536(7)
C(8)-C(10)	1.544(7)
O(3)-C(3)	1.136(7)
C(7)-H(7A)	0.9900

C(7)-H(7B)	0.9900
O(2)-C(2)	1.154(6)
C(28)-C(27)	1.388(7)
C(28)-H(28)	0.9500
C(18)-C(19)	1.381(7)
C(18)-H(18)	0.9500
C(6)-H(6A)	0.9900
C(6)-H(6B)	0.9900
C(19)-C(20)	1.382(7)
C(19)-H(19)	0.9500
C(26)-C(27)	1.373(8)
C(26)-C(25)	1.380(8)
C(26)-H(26)	0.9500
C(15)-C(14)	1.377(7)
C(15)-C(16)	1.393(7)
C(15)-H(15)	0.9500
C(12)-C(13)	1.371(7)
C(12)-H(12)	0.9500
C(13)-C(14)	1.383(7)
C(13)-H(13)	0.9500
C(21)-C(20)	1.374(7)
C(21)-H(21)	0.9500
C(14)-H(14)	0.9500
C(20)-H(20)	0.9500
O(1)-C(1)	1.162(7)
C(24)-C(25)	1.385(7)
C(24)-H(24)	0.9500
C(25)-H(25)	0.9500
C(27)-H(27)	0.9500
C(10)-H(10A)	0.9800
C(10)-H(10B)	0.9800
C(10)-H(10C)	0.9800
C(16)-H(16)	0.9500
C(9)-H(9A)	0.9800

C(9)-H(9B)	0.9800
C(9)-H(9C)	0.9800
C(4)-Fe(1)-C(5)	92.5(2)
C(4)-Fe(1)-P(1)	93.04(17)
C(5)-Fe(1)-P(1)	96.11(18)
C(4)-Fe(1)-S(2)	161.26(18)
C(5)-Fe(1)-S(2)	91.02(17)
P(1)-Fe(1)-S(2)	104.89(6)
C(4)-Fe(1)-S(1)	86.17(17)
C(5)-Fe(1)-S(1)	154.01(18)
P(1)-Fe(1)-S(1)	109.88(6)
S(2)-Fe(1)-S(1)	82.68(6)
C(4)-Fe(1)-Fe(2)	104.84(17)
C(5)-Fe(1)-Fe(2)	99.09(18)
P(1)-Fe(1)-Fe(2)	155.89(5)
S(2)-Fe(1)-Fe(2)	56.42(5)
S(1)-Fe(1)-Fe(2)	56.58(5)
C(1)-Fe(2)-C(2)	97.2(3)
C(1)-Fe(2)-C(3)	96.5(3)
C(2)-Fe(2)-C(3)	92.0(3)
C(1)-Fe(2)-S(2)	110.1(2)
C(2)-Fe(2)-S(2)	152.75(19)
C(3)-Fe(2)-S(2)	85.64(19)
C(1)-Fe(2)-S(1)	109.9(2)
C(2)-Fe(2)-S(1)	87.66(18)
C(3)-Fe(2)-S(1)	153.5(2)
S(2)-Fe(2)-S(1)	82.70(5)
C(1)-Fe(2)-Fe(1)	159.8(2)
C(2)-Fe(2)-Fe(1)	97.06(19)
C(3)-Fe(2)-Fe(1)	97.4(2)
S(2)-Fe(2)-Fe(1)	56.53(4)
S(1)-Fe(2)-Fe(1)	56.49(4)
C(11)-P(1)-C(17)	105.4(2)

C(11)-P(1)-C(23)	99.9(2)
C(17)-P(1)-C(23)	106.0(2)
C(11)-P(1)-Fe(1)	119.93(18)
C(17)-P(1)-Fe(1)	112.56(17)
C(23)-P(1)-Fe(1)	111.53(17)
C(7)-S(2)-Fe(2)	118.45(18)
C(7)-S(2)-Fe(1)	110.48(18)
Fe(2)-S(2)-Fe(1)	67.05(5)
C(6)-S(1)-Fe(1)	114.63(18)
C(6)-S(1)-Fe(2)	116.19(17)
Fe(1)-S(1)-Fe(2)	66.93(5)
C(28)-C(23)-C(24)	118.3(5)
C(28)-C(23)-P(1)	124.9(4)
C(24)-C(23)-P(1)	116.6(4)
C(18)-C(17)-C(22)	118.7(5)
C(18)-C(17)-P(1)	119.4(4)
C(22)-C(17)-P(1)	121.5(4)
O(5)-C(5)-Fe(1)	178.1(5)
C(16)-C(11)-C(12)	117.3(5)
C(16)-C(11)-P(1)	121.6(4)
C(12)-C(11)-P(1)	121.1(4)
C(21)-C(22)-C(17)	119.7(5)
C(21)-C(22)-H(22)	120.2
C(17)-C(22)-H(22)	120.2
C(9)-C(8)-C(7)	111.5(4)
C(9)-C(8)-C(6)	110.9(5)
C(7)-C(8)-C(6)	111.9(4)
C(9)-C(8)-C(10)	108.1(4)
C(7)-C(8)-C(10)	107.1(4)
C(6)-C(8)-C(10)	107.0(4)
O(4)-C(4)-Fe(1)	177.2(5)
C(8)-C(7)-S(2)	120.6(4)
C(8)-C(7)-H(7A)	107.2
S(2)-C(7)-H(7A)	107.2

C(8)-C(7)-H(7B)	107.2
S(2)-C(7)-H(7B)	107.2
H(7A)-C(7)-H(7B)	106.8
C(23)-C(28)-C(27)	120.8(5)
C(23)-C(28)-H(28)	119.6
C(27)-C(28)-H(28)	119.6
C(19)-C(18)-C(17)	121.4(5)
C(19)-C(18)-H(18)	119.3
C(17)-C(18)-H(18)	119.3
O(3)-C(3)-Fe(2)	178.3(6)
C(8)-C(6)-S(1)	121.9(4)
C(8)-C(6)-H(6A)	106.8
S(1)-C(6)-H(6A)	106.8
C(8)-C(6)-H(6B)	106.8
S(1)-C(6)-H(6B)	106.8
H(6A)-C(6)-H(6B)	106.7
O(2)-C(2)-Fe(2)	179.5(6)
C(18)-C(19)-C(20)	119.5(5)
C(18)-C(19)-H(19)	120.3
C(20)-C(19)-H(19)	120.3
C(27)-C(26)-C(25)	119.0(5)
C(27)-C(26)-H(26)	120.5
C(25)-C(26)-H(26)	120.5
C(14)-C(15)-C(16)	119.7(6)
C(14)-C(15)-H(15)	120.1
C(16)-C(15)-H(15)	120.1
C(13)-C(12)-C(11)	121.0(5)
C(13)-C(12)-H(12)	119.5
C(11)-C(12)-H(12)	119.5
C(12)-C(13)-C(14)	120.6(6)
C(12)-C(13)-H(13)	119.7
C(14)-C(13)-H(13)	119.7
C(20)-C(21)-C(22)	120.6(5)
C(20)-C(21)-H(21)	119.7

C(22)-C(21)-H(21)	119.7
C(15)-C(14)-C(13)	119.6(5)
C(15)-C(14)-H(14)	120.2
C(13)-C(14)-H(14)	120.2
C(21)-C(20)-C(19)	120.2(5)
C(21)-C(20)-H(20)	119.9
C(19)-C(20)-H(20)	119.9
C(25)-C(24)-C(23)	120.5(5)
C(25)-C(24)-H(24)	119.8
C(23)-C(24)-H(24)	119.8
C(26)-C(25)-C(24)	120.6(6)
C(26)-C(25)-H(25)	119.7
C(24)-C(25)-H(25)	119.7
C(26)-C(27)-C(28)	120.8(6)
C(26)-C(27)-H(27)	119.6
C(28)-C(27)-H(27)	119.6
C(8)-C(10)-H(10A)	109.5
C(8)-C(10)-H(10B)	109.5
H(10A)-C(10)-H(10B)	109.5
C(8)-C(10)-H(10C)	109.5
H(10A)-C(10)-H(10C)	109.5
H(10B)-C(10)-H(10C)	109.5
C(11)-C(16)-C(15)	121.8(5)
C(11)-C(16)-H(16)	119.1
C(15)-C(16)-H(16)	119.1
O(1)-C(1)-Fe(2)	176.6(6)
C(8)-C(9)-H(9A)	109.5
C(8)-C(9)-H(9B)	109.5
H(9A)-C(9)-H(9B)	109.5
C(8)-C(9)-H(9C)	109.5
H(9A)-C(9)-H(9C)	109.5
H(9B)-C(9)-H(9C)	109.5

Symmetry transformations used to generate equivalent atoms:

Table A-37. Anisotropic displacement parameters ($Å^2 x\ 10^3$) for III-7. The anisotropic displacement factor exponent takes the form: $-2\pi^2[\ h^2\ a^{*2}U^{11} + ...\ + 2\ h\ k\ a^*\ b^*\ U^{12}\ ]$

	U^{11}	U^{22}	U^{33}	U^{23}	U^{13}	U^{12}
Fe(1)	21(1)	25(1)	18(1)	6(1)	3(1)	5(1)
Fe(2)	26(1)	31(1)	24(1)	3(1)	5(1)	10(1)
P(1)	23(1)	25(1)	19(1)	5(1)	3(1)	5(1)
S(2)	23(1)	28(1)	19(1)	5(1)	1(1)	7(1)
S(1)	27(1)	26(1)	21(1)	6(1)	1(1)	7(1)
O(4)	34(2)	50(3)	29(2)	11(2)	3(2)	-2(2)
O(5)	41(3)	47(3)	36(3)	24(2)	7(2)	8(2)
C(23)	27(3)	16(3)	27(3)	2(2)	3(2)	8(2)
C(17)	27(3)	24(3)	21(3)	-1(2)	4(2)	5(3)
C(5)	21(3)	31(3)	21(3)	0(3)	-3(2)	3(3)
C(11)	23(3)	22(3)	23(3)	6(2)	2(2)	6(2)
C(22)	36(4)	32(3)	28(3)	4(3)	6(3)	14(3)
C(8)	26(3)	24(3)	26(3)	6(2)	4(3)	4(3)
C(4)	30(3)	28(3)	17(3)	9(2)	8(2)	9(3)
O(3)	53(3)	107(4)	41(3)	37(3)	27(2)	36(3)
C(7)	22(3)	34(3)	28(3)	7(3)	3(2)	5(3)
O(2)	35(3)	61(3)	55(3)	3(2)	2(2)	16(2)
C(28)	34(3)	26(3)	26(3)	5(3)	4(3)	10(3)
C(18)	32(3)	30(3)	21(3)	2(2)	8(3)	9(3)
C(3)	31(4)	58(4)	35(4)	5(3)	7(3)	18(3)
C(6)	32(3)	27(3)	24(3)	8(2)	7(3)	8(3)
C(2)	41(4)	38(4)	26(3)	4(3)	9(3)	15(3)
C(19)	40(4)	38(4)	25(3)	10(3)	6(3)	14(3)
C(26)	28(3)	24(3)	50(4)	-3(3)	4(3)	0(3)
C(15)	45(4)	33(4)	29(3)	6(3)	-1(3)	12(3)
C(12)	35(3)	31(3)	27(3)	7(3)	9(3)	11(3)
C(13)	33(4)	29(3)	52(4)	20(3)	16(3)	13(3)
C(21)	34(4)	41(4)	33(3)	13(3)	14(3)	8(3)
C(14)	27(3)	28(3)	48(4)	13(3)	3(3)	9(3)

C(20)	46(4)	47(4)	31(4)	17(3)	15(3)	18(3)
O(1)	57(4)	52(3)	145(6)	-42(4)	28(4)	6(3)
C(24)	49(4)	23(3)	32(3)	2(3)	7(3)	8(3)
C(25)	59(4)	25(3)	46(4)	14(3)	14(4)	10(3)
C(27)	37(4)	28(3)	40(4)	-3(3)	-3(3)	12(3)
C(10)	35(4)	39(4)	32(3)	10(3)	11(3)	3(3)
C(16)	28(3)	31(3)	29(3)	3(3)	-2(3)	10(3)
C(1)	27(4)	47(4)	56(5)	-12(4)	6(3)	8(3)
C(9)	47(4)	33(4)	34(4)	10(3)	13(3)	-2(3)

Table A-38. Hydrogen coordinates (x 10^4) and isotropic displacement parameters ($Å^2$x 10^3) for III-7.

	x	y	z	U(eq)
H(22)	3885	3113	3422	38
H(7A)	4449	1438	1842	34
H(7B)	3990	335	944	34
H(28)	8196	5819	4785	34
H(18)	8197	3566	4546	33
H(6A)	6482	-511	3161	33
H(6B)	5966	804	3352	33
H(19)	7463	2344	5676	40
H(26)	10386	9441	4298	44
H(15)	3180	4248	227	44
H(12)	4578	5596	3396	36
H(13)	2507	6029	2592	42
H(21)	3162	1855	4549	42
H(14)	1798	5371	1005	41
H(20)	4934	1460	5660	47
H(24)	7819	6598	2193	42
H(25)	9409	8741	2732	51
H(27)	9767	7972	5316	44
H(10A)	2704	-1031	1962	54
H(10B)	3478	65	2862	54
H(10C)	3636	-1423	2826	54
H(16)	5253	3784	1038	36
H(9A)	5299	-2184	1899	59
H(9B)	6021	-1275	1209	59
H(9C)	4258	-1926	1025	59

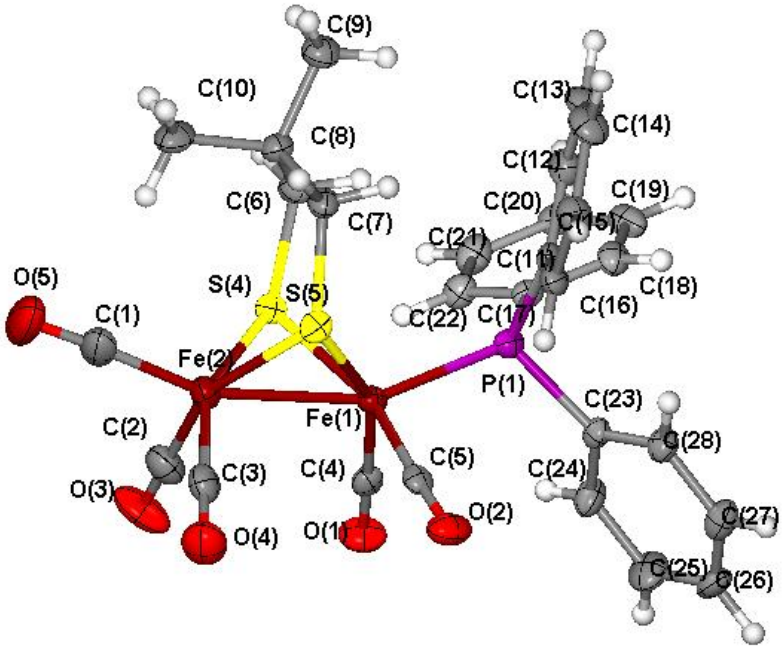
C(9)
C(10)
C(8)
C(6)
C(7)
O(5)
S(4)
S(5)
C(1)
Fe(2)
Fe(1)
C(2)
C(3)
C(4)
C(5)
O(3)
O(4)
O(1)
O(2)
C(13)
C(14)
C(12)
C(20)
C(19)
C(15)
C(21)
C(11)
C(18)
C(16)
C(22)
C(17)
P(1)
C(23)
C(28)
C(24)
C(27)
C(25)
O(26)

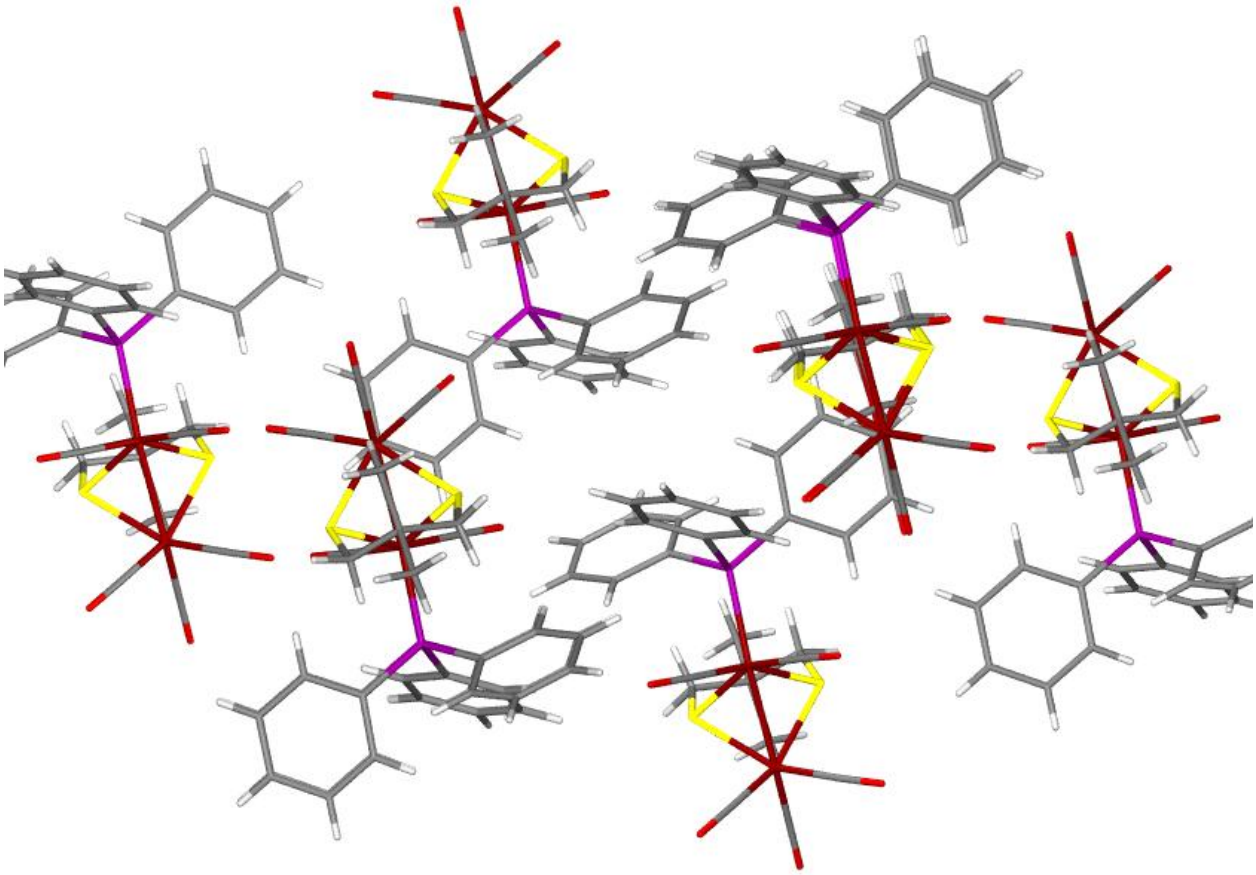

Table A-39. Crystal data and structure refinement for III-8.

Identification code	dmpdt[$Fe(CO)_3$][$Fe(CO)_2$PTA]	
Empirical formula	C18 H26 Fe2 N3 O5 P S2	
Formula weight	571.21	
Temperature	110(2) K	
Wavelength	0.71073 Å	
Crystal system	Triclinic	
Space group	P1	
Unit cell dimensions	a = 10.2360(4) Å	α= 64.561(2)°.
	b = 10.9276(5) Å	β= 77.339(2)°.
	c = 11.6299(5) Å	γ = 80.531(2)°.
Volume	1142.51(8) $Å^3$	
Z	2	
Density (calculated)	1.660 Mg/m^3	
Absorption coefficient	1.558 mm^{-1}	
F(000)	588	
Crystal size	0.31 x 0.13 x 0.10 mm^3	
Theta range for data collection	1.97 to 30.94°.	
Index ranges	-14<=h<=14, -15<=k<=15, -16<=l<=16	
Reflections collected	43511	
Independent reflections	13638 [R(int) = 0.0738]	
Completeness to theta = 30.94°	99.0 %	
Absorption correction	Semi-empirical from equivalents	
Max. and min. transmission	0.8598 and 0.6438	
Refinement method	Full-matrix least-squares on F^2	
Data / restraints / parameters	13638 / 3 / 563	
Goodness-of-fit on F^2	0.855	
Final R indices [I>2sigma(I)]	R1 = 0.0344, wR2 = 0.0740	
R indices (all data)	R1 = 0.0517, wR2 = 0.0801	
Absolute structure parameter	0.34(3)	
Largest diff. peak and hole	0.655 and -0.474 e.$Å^{-3}$	

Table A-40. Atomic coordinates (x 10^4) and equivalent isotropic displacement parameters ($Å^2$x 10^3) for III-8. U(eq) is defined as one third of the trace of the orthogonalized U^{ij} tensor.

	x	y	z	U(eq)
Fe(1)	922(1)	7168(1)	3151(1)	14(1)
Fe(3)	2765(1)	5836(1)	4417(1)	16(1)
S(6)	2217(2)	5409(2)	2845(2)	15(1)
P(8)	2047(2)	8563(2)	1325(2)	15(1)
S(10)	547(2)	5649(2)	5232(2)	19(1)
Fe(2)	7689(1)	3190(1)	457(1)	15(1)
Fe(4)	5851(1)	4518(1)	-806(1)	16(1)
S(5)	6398(2)	4946(2)	759(2)	15(1)
P(7)	6566(2)	1788(2)	2286(2)	15(1)
S(9)	8081(2)	4702(2)	-1623(2)	18(1)
C(12)	8457(8)	6837(8)	-859(7)	17(2)
C(14)	162(8)	3542(8)	4488(8)	19(2)
C(19)	1516(7)	3754(8)	3559(8)	17(2)
C(20)	7092(8)	6616(8)	35(8)	20(2)
O(1)	5261(6)	6958(6)	2746(6)	24(1)
O(2)	3336(6)	3398(7)	836(6)	27(1)
O(3)	10182(6)	2476(7)	1488(6)	26(1)
O(4)	-1603(6)	7898(7)	2116(6)	27(1)
N(5)	3639(7)	10744(7)	138(7)	18(1)
O(6)	557(7)	9254(6)	4170(6)	28(2)
O(7)	8021(7)	1103(6)	-551(7)	29(2)
N(8)	4968(7)	-364(7)	3495(7)	20(2)
O(9)	3944(8)	3137(7)	5989(6)	35(2)
N(10)	4001(7)	9049(7)	-841(7)	21(2)
N(11)	4621(7)	1281(7)	4462(7)	19(2)
O(12)	4680(7)	7209(6)	-2382(6)	30(2)
O(13)	2753(7)	7282(7)	6030(6)	32(2)
N(14)	6625(7)	-328(7)	4707(7)	21(2)
O(15)	5900(7)	3044(7)	-2431(6)	30(2)

N(16)	1950(7)	10672(7)	-1087(7)	22(2)
C(17)	8476(9)	6425(8)	-1984(8)	20(2)
C(18)	137(9)	3951(8)	5577(8)	21(2)
C(1)	5634(8)	546(8)	2204(8)	18(2)
C(2)	3984(8)	410(8)	4082(8)	20(2)
C(21)	4582(8)	9936(8)	-495(8)	22(2)
C(22)	2956(8)	9865(8)	1397(7)	17(2)
C(23)	3379(8)	7949(8)	295(8)	17(2)
C(24)	4285(8)	6536(8)	3390(8)	16(2)
C(25)	5244(8)	2438(8)	3319(8)	19(2)
C(26)	7497(8)	592(9)	3604(7)	21(2)
C(27)	-48(8)	2039(8)	5036(7)	24(2)
C(28)	4320(9)	3847(9)	219(8)	22(2)
C(29)	9235(8)	2804(8)	1077(8)	18(2)
C(30)	2663(8)	11534(8)	-723(8)	21(2)
C(31)	2749(9)	6736(9)	5398(8)	22(2)
C(32)	1090(7)	9762(8)	78(7)	21(2)
C(33)	714(8)	8442(7)	3746(7)	16(2)
C(34)	7930(8)	1916(8)	-154(8)	24(2)
C(35)	5959(8)	-1123(8)	4348(8)	23(2)
C(36)	3470(8)	4183(8)	5387(8)	19(2)
C(37)	-568(9)	7563(8)	2529(8)	21(2)
C(38)	-950(8)	4230(8)	3722(8)	30(2)
C(39)	5832(9)	3634(9)	-1790(8)	23(2)
C(40)	5128(9)	6164(9)	-1775(8)	26(2)
C(7)	2970(9)	9897(8)	-1662(8)	23(2)
C(8)	5583(9)	448(9)	5287(8)	24(2)
C(3)	831(8)	1116(8)	5935(8)	88(3)
C(4)	7760(4)	9318(4)	-2437(4)	12(1)
C(5)	10969(3)	5856(4)	-777(4)	18(1)
C(6)	-2292(10)	4458(10)	4410(10)	117(3)
C(13)	8607(8)	8415(7)	-1474(8)	22(2)
C(15)	9592(8)	6061(8)	-47(7)	19(2)

Table A-41. Bond lengths [Å] and angles [°] for III-8.

Fe(1)-C(37)	1.742(9)
Fe(1)-C(33)	1.768(7)
Fe(1)-P(8)	2.210(2)
Fe(1)-S(10)	2.261(2)
Fe(1)-S(6)	2.263(2)
Fe(1)-Fe(3)	2.5134(15)
Fe(3)-C(31)	1.794(9)
Fe(3)-C(24)	1.795(8)
Fe(3)-C(36)	1.799(8)
Fe(3)-S(10)	2.266(2)
Fe(3)-S(6)	2.268(2)
S(6)-C(19)	1.830(8)
P(8)-C(32)	1.829(8)
P(8)-C(23)	1.849(8)
P(8)-C(22)	1.862(8)
S(10)-C(18)	1.822(9)
Fe(2)-C(34)	1.778(9)
Fe(2)-C(29)	1.794(8)
Fe(2)-P(7)	2.214(2)
Fe(2)-S(9)	2.258(2)
Fe(2)-S(5)	2.258(2)
Fe(2)-Fe(4)	2.5075(15)
Fe(4)-C(39)	1.791(10)
Fe(4)-C(28)	1.794(9)
Fe(4)-C(40)	1.800(9)
Fe(4)-S(5)	2.261(2)
Fe(4)-S(9)	2.278(2)
S(5)-C(20)	1.840(8)
P(7)-C(1)	1.827(8)
P(7)-C(26)	1.863(8)
P(7)-C(25)	1.866(8)
S(9)-C(17)	1.839(8)

C(12)-C(20)	1.533(11)
C(12)-C(17)	1.552(11)
C(12)-C(15)	1.558(10)
C(12)-C(13)	1.577(10)
C(14)-C(38)	1.497(11)
C(14)-C(18)	1.508(12)
C(14)-C(27)	1.519(10)
C(14)-C(19)	1.542(10)
O(1)-C(24)	1.140(10)
O(2)-C(28)	1.146(10)
O(3)-C(29)	1.113(10)
O(4)-C(37)	1.197(10)
N(5)-C(22)	1.456(10)
N(5)-C(30)	1.470(10)
N(5)-C(21)	1.489(10)
O(6)-C(33)	1.162(9)
O(7)-C(34)	1.148(10)
N(8)-C(2)	1.453(10)
N(8)-C(35)	1.469(11)
N(8)-C(1)	1.484(10)
O(9)-C(36)	1.145(10)
N(10)-C(21)	1.444(11)
N(10)-C(23)	1.454(11)
N(10)-C(7)	1.498(11)
N(11)-C(8)	1.445(11)
N(11)-C(25)	1.491(11)
N(11)-C(2)	1.490(11)
O(12)-C(40)	1.135(10)
O(13)-C(31)	1.130(11)
N(14)-C(35)	1.422(11)
N(14)-C(26)	1.463(11)
N(14)-C(8)	1.480(11)
O(15)-C(39)	1.163(11)
N(16)-C(7)	1.464(11)

N(16)-C(32)	1.485(10)
N(16)-C(30)	1.517(11)
C(27)-C(3)	1.459(11)
C(38)-C(6)	1.471(12)
C(4)-C(13)	1.475(8)
C(5)-C(15)	1.515(8)

C(37)-Fe(1)-C(33)	98.2(4)
C(37)-Fe(1)-P(8)	93.0(3)
C(33)-Fe(1)-P(8)	88.9(2)
C(37)-Fe(1)-S(10)	108.9(3)
C(33)-Fe(1)-S(10)	87.2(2)
P(8)-Fe(1)-S(10)	158.08(9)
C(37)-Fe(1)-S(6)	113.6(3)
C(33)-Fe(1)-S(6)	148.2(2)
P(8)-Fe(1)-S(6)	88.46(8)
S(10)-Fe(1)-S(6)	83.60(8)
C(37)-Fe(1)-Fe(3)	160.9(3)
C(33)-Fe(1)-Fe(3)	93.4(2)
P(8)-Fe(1)-Fe(3)	102.39(7)
S(10)-Fe(1)-Fe(3)	56.38(7)
S(6)-Fe(1)-Fe(3)	56.40(6)
C(31)-Fe(3)-C(24)	92.2(4)
C(31)-Fe(3)-C(36)	100.9(4)
C(24)-Fe(3)-C(36)	98.6(4)
C(31)-Fe(3)-S(10)	86.1(3)
C(24)-Fe(3)-S(10)	160.0(3)
C(36)-Fe(3)-S(10)	101.2(3)
C(31)-Fe(3)-S(6)	157.5(3)
C(24)-Fe(3)-S(6)	91.0(3)
C(36)-Fe(3)-S(6)	100.6(3)
S(10)-Fe(3)-S(6)	83.37(8)
C(31)-Fe(3)-Fe(1)	101.5(3)
C(24)-Fe(3)-Fe(1)	105.0(2)

C(36)-Fe(3)-Fe(1)	146.5(3)
S(10)-Fe(3)-Fe(1)	56.17(6)
S(6)-Fe(3)-Fe(1)	56.22(6)
C(19)-S(6)-Fe(1)	118.1(3)
C(19)-S(6)-Fe(3)	109.6(3)
Fe(1)-S(6)-Fe(3)	67.39(7)
C(32)-P(8)-C(23)	98.6(4)
C(32)-P(8)-C(22)	95.9(4)
C(23)-P(8)-C(22)	99.1(4)
C(32)-P(8)-Fe(1)	118.0(2)
C(23)-P(8)-Fe(1)	122.5(3)
C(22)-P(8)-Fe(1)	117.6(3)
C(18)-S(10)-Fe(1)	118.6(3)
C(18)-S(10)-Fe(3)	109.0(3)
Fe(1)-S(10)-Fe(3)	67.44(7)
C(34)-Fe(2)-C(29)	97.7(4)
C(34)-Fe(2)-P(7)	89.6(3)
C(29)-Fe(2)-P(7)	93.8(3)
C(34)-Fe(2)-S(9)	86.6(3)
C(29)-Fe(2)-S(9)	107.7(3)
P(7)-Fe(2)-S(9)	158.54(9)
C(34)-Fe(2)-S(5)	148.9(3)
C(29)-Fe(2)-S(5)	113.4(3)
P(7)-Fe(2)-S(5)	88.68(8)
S(9)-Fe(2)-S(5)	83.84(8)
C(34)-Fe(2)-Fe(4)	93.9(3)
C(29)-Fe(2)-Fe(4)	160.1(3)
P(7)-Fe(2)-Fe(4)	102.47(7)
S(9)-Fe(2)-Fe(4)	56.83(7)
S(5)-Fe(2)-Fe(4)	56.35(6)
C(39)-Fe(4)-C(28)	92.2(4)
C(39)-Fe(4)-C(40)	99.8(4)
C(28)-Fe(4)-C(40)	97.3(4)
C(39)-Fe(4)-S(5)	158.6(3)

C(28)-Fe(4)-S(5)	90.7(3)
C(40)-Fe(4)-S(5)	100.9(3)
C(39)-Fe(4)-S(9)	87.0(3)
C(28)-Fe(4)-S(9)	160.7(3)
C(40)-Fe(4)-S(9)	101.9(3)
S(5)-Fe(4)-S(9)	83.31(8)
C(39)-Fe(4)-Fe(2)	102.6(3)
C(28)-Fe(4)-Fe(2)	105.6(3)
C(40)-Fe(4)-Fe(2)	147.1(3)
S(5)-Fe(4)-Fe(2)	56.24(6)
S(9)-Fe(4)-Fe(2)	56.06(6)
C(20)-S(5)-Fe(2)	118.4(3)
C(20)-S(5)-Fe(4)	109.4(3)
Fe(2)-S(5)-Fe(4)	67.42(7)
C(1)-P(7)-C(26)	97.9(4)
C(1)-P(7)-C(25)	99.3(4)
C(26)-P(7)-C(25)	96.4(4)
C(1)-P(7)-Fe(2)	117.5(3)
C(26)-P(7)-Fe(2)	119.5(3)
C(25)-P(7)-Fe(2)	121.4(3)
C(17)-S(9)-Fe(2)	119.1(3)
C(17)-S(9)-Fe(4)	108.4(3)
Fe(2)-S(9)-Fe(4)	67.11(7)
C(20)-C(12)-C(17)	110.6(7)
C(20)-C(12)-C(15)	109.3(6)
C(17)-C(12)-C(15)	113.3(7)
C(20)-C(12)-C(13)	106.3(6)
C(17)-C(12)-C(13)	107.1(6)
C(15)-C(12)-C(13)	110.0(7)
C(38)-C(14)-C(18)	114.2(7)
C(38)-C(14)-C(27)	104.2(7)
C(18)-C(14)-C(27)	109.5(6)
C(38)-C(14)-C(19)	109.0(7)
C(18)-C(14)-C(19)	112.5(7)

C(27)-C(14)-C(19)	106.9(6)
C(14)-C(19)-S(6)	119.9(5)
C(12)-C(20)-S(5)	120.6(6)
C(22)-N(5)-C(30)	110.5(6)
C(22)-N(5)-C(21)	111.2(6)
C(30)-N(5)-C(21)	107.3(7)
C(2)-N(8)-C(35)	109.6(7)
C(2)-N(8)-C(1)	110.6(6)
C(35)-N(8)-C(1)	110.9(6)
C(21)-N(10)-C(23)	111.6(7)
C(21)-N(10)-C(7)	107.3(7)
C(23)-N(10)-C(7)	110.0(6)
C(8)-N(11)-C(25)	111.8(7)
C(8)-N(11)-C(2)	109.2(7)
C(25)-N(11)-C(2)	112.1(7)
C(35)-N(14)-C(26)	112.0(7)
C(35)-N(14)-C(8)	107.7(7)
C(26)-N(14)-C(8)	110.5(7)
C(7)-N(16)-C(32)	111.5(7)
C(7)-N(16)-C(30)	108.2(7)
C(32)-N(16)-C(30)	109.7(7)
C(12)-C(17)-S(9)	119.6(6)
C(14)-C(18)-S(10)	120.2(6)
N(8)-C(1)-P(7)	112.3(5)
N(8)-C(2)-N(11)	112.4(7)
N(10)-C(21)-N(5)	117.1(7)
N(5)-C(22)-P(8)	113.0(5)
N(10)-C(23)-P(8)	112.9(5)
O(1)-C(24)-Fe(3)	178.8(8)
N(11)-C(25)-P(7)	110.2(5)
N(14)-C(26)-P(7)	112.7(5)
C(3)-C(27)-C(14)	116.4(7)
O(2)-C(28)-Fe(4)	177.0(8)
O(3)-C(29)-Fe(2)	175.3(8)

N(5)-C(30)-N(16)	113.5(7)
O(13)-C(31)-Fe(3)	178.7(8)
N(16)-C(32)-P(8)	113.1(5)
O(6)-C(33)-Fe(1)	178.1(7)
O(7)-C(34)-Fe(2)	176.7(7)
N(14)-C(35)-N(8)	115.5(7)
O(9)-C(36)-Fe(3)	178.6(8)
O(4)-C(37)-Fe(1)	176.3(8)
C(6)-C(38)-C(14)	118.6(7)
O(15)-C(39)-Fe(4)	176.0(8)
O(12)-C(40)-Fe(4)	179.3(9)
N(16)-C(7)-N(10)	114.9(7)
N(11)-C(8)-N(14)	114.0(7)
C(4)-C(13)-C(12)	118.6(6)
C(5)-C(15)-C(12)	117.2(6)

Symmetry transformations used to generate equivalent atoms:

Table A-42. Anisotropic displacement parameters ($Å^2 x\ 10^3$)for III-8. The anisotropic displacement factor exponent takes the form: $-2\pi^2[\ h^2 a^{*2} U^{11} + ... + 2\ h\ k\ a^*\ b^*\ U^{12}\ ]$

	U^{11}	U^{22}	U^{33}	U^{23}	U^{13}	U^{12}
Fe(1)	13(1)	15(1)	18(1)	-10(1)	0(1)	-2(1)
Fe(3)	19(1)	14(1)	15(1)	-6(1)	-3(1)	-4(1)
S(6)	16(1)	14(1)	16(1)	-8(1)	1(1)	-3(1)
P(8)	15(1)	14(1)	18(1)	-8(1)	-4(1)	-2(1)
S(10)	21(1)	20(1)	19(1)	-12(1)	4(1)	-7(1)
Fe(2)	13(1)	16(1)	19(1)	-11(1)	0(1)	-2(1)
Fe(4)	15(1)	16(1)	17(1)	-8(1)	-1(1)	-5(1)
S(5)	13(1)	15(1)	17(1)	-8(1)	1(1)	-3(1)
P(7)	11(1)	15(1)	19(1)	-9(1)	-1(1)	-1(1)
S(9)	21(1)	18(1)	18(1)	-11(1)	4(1)	-8(1)
C(12)	19(4)	22(4)	18(3)	-16(3)	-1(3)	0(3)
C(14)	18(4)	14(3)	24(4)	-7(3)	6(3)	-11(3)
C(19)	14(3)	17(4)	24(4)	-13(3)	3(3)	-3(3)
C(20)	30(4)	11(4)	18(4)	-7(3)	3(3)	-9(3)
O(1)	16(3)	27(3)	28(3)	-13(3)	0(2)	-2(2)
O(2)	22(3)	31(3)	31(3)	-13(3)	-1(3)	-11(3)
O(3)	17(3)	33(3)	34(4)	-20(3)	-8(3)	4(3)
O(4)	16(3)	33(4)	39(4)	-20(3)	-7(3)	0(3)
N(5)	17(3)	16(3)	21(4)	-9(3)	0(3)	-3(3)
O(6)	32(3)	29(4)	31(3)	-20(3)	-5(3)	0(3)
O(7)	35(4)	24(3)	41(4)	-24(3)	-17(3)	8(3)
N(8)	21(4)	14(3)	23(4)	-8(3)	-1(3)	-4(3)
O(9)	51(5)	29(4)	26(3)	-7(3)	-17(3)	-1(3)
N(10)	28(4)	16(3)	18(3)	-8(3)	1(3)	-9(3)
N(11)	17(3)	17(3)	21(4)	-8(3)	3(3)	-1(3)
O(12)	47(4)	15(3)	28(3)	-5(3)	-12(3)	1(3)
O(13)	40(4)	33(4)	33(4)	-18(3)	-9(3)	-11(3)
N(14)	26(4)	15(3)	20(3)	-4(3)	-8(3)	-2(3)
O(15)	39(4)	35(4)	25(3)	-20(3)	0(3)	-9(3)

N(16)	24(4)	21(4)	21(4)	-9(3)	-1(3)	-3(3)
C(17)	21(4)	17(4)	24(4)	-13(3)	5(3)	-5(3)
C(18)	24(4)	20(4)	19(4)	-8(3)	4(3)	-12(3)
C(1)	17(4)	13(3)	26(4)	-12(3)	-4(3)	2(3)
C(2)	19(4)	19(4)	25(4)	-12(3)	1(3)	-9(3)
C(21)	15(3)	16(4)	28(4)	-7(3)	2(3)	-1(3)
C(22)	19(4)	17(3)	18(4)	-6(3)	-3(3)	-6(3)
C(23)	15(4)	13(3)	22(4)	-11(3)	4(3)	-4(3)
C(24)	17(4)	13(3)	19(4)	-6(3)	-6(3)	-1(3)
C(25)	20(4)	19(4)	18(4)	-7(3)	-1(3)	-1(3)
C(26)	24(3)	24(3)	20(3)	-14(3)	-10(2)	8(3)
C(27)	25(4)	28(3)	17(3)	-7(2)	-3(3)	-7(3)
C(28)	25(5)	20(4)	24(4)	-11(3)	-10(4)	1(3)
C(29)	17(4)	24(4)	21(4)	-17(3)	-1(3)	-2(3)
C(30)	26(4)	13(3)	32(4)	-12(3)	-10(3)	-4(3)
C(31)	22(4)	25(4)	21(4)	-12(3)	-4(3)	-2(3)
C(32)	12(3)	18(3)	29(3)	-6(3)	-3(2)	-6(2)
C(33)	21(4)	8(3)	21(4)	-3(3)	-8(3)	-2(3)
C(34)	11(3)	37(4)	23(4)	-15(3)	1(3)	1(3)
C(35)	25(4)	18(3)	16(3)	-3(3)	3(3)	3(3)
C(36)	20(4)	18(4)	24(4)	-12(3)	-6(3)	0(3)
C(37)	22(4)	16(4)	26(4)	-14(3)	6(3)	-4(3)
C(38)	21(4)	29(4)	53(5)	-30(3)	3(3)	-8(3)
C(39)	22(4)	19(4)	23(4)	-1(3)	-3(3)	-12(3)
C(40)	37(5)	28(5)	14(4)	-8(3)	-1(3)	-14(4)
C(7)	33(4)	17(4)	19(4)	-5(3)	-5(3)	-3(3)
C(8)	28(4)	26(4)	19(4)	-12(3)	1(3)	-8(3)
C(3)	86(6)	106(6)	98(6)	-73(5)	42(5)	-64(5)
C(4)	19(2)	4(2)	6(2)	6(1)	-11(2)	4(2)
C(5)	0(1)	22(2)	28(2)	-12(2)	5(1)	4(1)
C(6)	145(8)	109(8)	102(7)	-21(6)	-64(6)	-27(6)
C(13)	20(3)	8(2)	37(4)	-12(3)	6(3)	-4(2)
C(15)	16(3)	23(3)	18(3)	-5(2)	-7(2)	-2(3)

Table A-43. Hydrogen coordinates (x 10^4) and isotropic displacement parameters ($Å^2$x 10^3) for III-8.

	x	y	z	U(eq)
H(19A)	1423	3537	2839	20
H(19B)	2192	3070	4028	20
H(20A)	6424	7288	-457	24
H(20B)	7150	6852	754	24
H(17A)	9382	6561	-2516	24
H(17B)	7836	7075	-2531	24
H(18A)	764	3293	6136	26
H(18B)	-774	3827	6099	26
H(1A)	4946	1032	1647	21
H(1B)	6259	-10	1802	21
H(2A)	3433	-225	4856	24
H(2B)	3378	992	3463	24
H(21A)	5103	10579	-1289	26
H(21B)	5226	9376	91	26
H(22A)	2306	10431	1769	21
H(22B)	3625	9399	1980	21
H(23A)	4078	7378	810	20
H(23B)	2988	7371	16	20
H(25A)	5648	2996	3611	23
H(25B)	4545	3022	2810	23
H(26A)	8210	49	3259	25
H(26B)	7936	1122	3899	25
H(27A)	-990	1911	5482	29
H(27B)	69	1770	4306	29
H(30A)	3134	12219	-1521	25
H(30B)	1984	12029	-294	25
H(32A)	589	9245	-180	25
H(32B)	426	10323	444	25

H(35A)	5499	-1819	5145	27
H(35B)	6645	-1606	3913	27
H(38A)	-665	5124	3064	36
H(38B)	-1040	3685	3253	36
H(7A)	3437	10541	-2492	28
H(7B)	2513	9294	-1856	28
H(8A)	5096	-199	6102	28
H(8B)	6030	1039	5506	28
H(3A)	1768	1310	5553	132
H(3B)	715	175	6114	132
H(3C)	602	1243	6742	132
H(4A)	8108	9245	-3262	19
H(4B)	7772	10259	-2553	19
H(4C)	6836	9050	-2135	19
H(5A)	10929	5257	-1196	26
H(5B)	11611	5441	-173	26
H(5C)	11260	6736	-1433	26
H(6A)	-2496	3649	5210	176
H(6B)	-2964	4637	3860	176
H(6C)	-2309	5241	4616	176
H(13A)	8431	8717	-761	26
H(13B)	9557	8560	-1885	26
H(15A)	9683	6558	467	23
H(15B)	9296	5155	571	23

Table A-44. Torsion angles [°] for III-8.

C(37)-Fe(1)-Fe(3)-C(31)	-120.3(9)
C(33)-Fe(1)-Fe(3)-C(31)	7.1(4)
P(8)-Fe(1)-Fe(3)-C(31)	96.8(3)
S(10)-Fe(1)-Fe(3)-C(31)	-77.2(3)
S(6)-Fe(1)-Fe(3)-C(31)	176.5(3)
C(37)-Fe(1)-Fe(3)-C(24)	144.2(9)
C(33)-Fe(1)-Fe(3)-C(24)	-88.3(4)
P(8)-Fe(1)-Fe(3)-C(24)	1.3(3)
S(10)-Fe(1)-Fe(3)-C(24)	-172.7(3)
S(6)-Fe(1)-Fe(3)-C(24)	81.0(3)
C(37)-Fe(1)-Fe(3)-C(36)	10.9(10)
C(33)-Fe(1)-Fe(3)-C(36)	138.4(5)
P(8)-Fe(1)-Fe(3)-C(36)	-132.0(5)
S(10)-Fe(1)-Fe(3)-C(36)	54.0(5)
S(6)-Fe(1)-Fe(3)-C(36)	-52.3(5)
C(37)-Fe(1)-Fe(3)-S(10)	-43.1(8)
C(33)-Fe(1)-Fe(3)-S(10)	84.3(3)
P(8)-Fe(1)-Fe(3)-S(10)	174.00(10)
S(6)-Fe(1)-Fe(3)-S(10)	-106.32(9)
C(37)-Fe(1)-Fe(3)-S(6)	63.2(8)
C(33)-Fe(1)-Fe(3)-S(6)	-169.3(3)
P(8)-Fe(1)-Fe(3)-S(6)	-79.69(9)
S(10)-Fe(1)-Fe(3)-S(6)	106.32(9)
C(37)-Fe(1)-S(6)-C(19)	-60.5(4)
C(33)-Fe(1)-S(6)-C(19)	121.4(5)
P(8)-Fe(1)-S(6)-C(19)	-153.1(3)
S(10)-Fe(1)-S(6)-C(19)	47.4(3)
Fe(3)-Fe(1)-S(6)-C(19)	100.9(3)
C(37)-Fe(1)-S(6)-Fe(3)	-161.4(3)
C(33)-Fe(1)-S(6)-Fe(3)	20.5(5)
P(8)-Fe(1)-S(6)-Fe(3)	106.00(8)
S(10)-Fe(1)-S(6)-Fe(3)	-53.54(7)

C(31)-Fe(3)-S(6)-C(19)	-122.3(8)
C(24)-Fe(3)-S(6)-C(19)	139.4(3)
C(36)-Fe(3)-S(6)-C(19)	40.5(4)
S(10)-Fe(3)-S(6)-C(19)	-59.8(3)
Fe(1)-Fe(3)-S(6)-C(19)	-113.2(3)
C(31)-Fe(3)-S(6)-Fe(1)	-9.1(7)
C(24)-Fe(3)-S(6)-Fe(1)	-107.4(3)
C(36)-Fe(3)-S(6)-Fe(1)	153.6(3)
S(10)-Fe(3)-S(6)-Fe(1)	53.38(7)
C(37)-Fe(1)-P(8)-C(32)	11.6(4)
C(33)-Fe(1)-P(8)-C(32)	-86.5(4)
S(10)-Fe(1)-P(8)-C(32)	-166.3(4)
S(6)-Fe(1)-P(8)-C(32)	125.2(3)
Fe(3)-Fe(1)-P(8)-C(32)	-179.8(3)
C(37)-Fe(1)-P(8)-C(23)	-111.1(4)
C(33)-Fe(1)-P(8)-C(23)	150.7(4)
S(10)-Fe(1)-P(8)-C(23)	71.0(4)
S(6)-Fe(1)-P(8)-C(23)	2.4(3)
Fe(3)-Fe(1)-P(8)-C(23)	57.5(3)
C(37)-Fe(1)-P(8)-C(22)	125.8(4)
C(33)-Fe(1)-P(8)-C(22)	27.6(4)
S(10)-Fe(1)-P(8)-C(22)	-52.1(4)
S(6)-Fe(1)-P(8)-C(22)	-120.6(3)
Fe(3)-Fe(1)-P(8)-C(22)	-65.6(3)
C(37)-Fe(1)-S(10)-C(18)	66.3(5)
C(33)-Fe(1)-S(10)-C(18)	164.0(4)
P(8)-Fe(1)-S(10)-C(18)	-115.9(4)
S(6)-Fe(1)-S(10)-C(18)	-46.5(3)
Fe(3)-Fe(1)-S(10)-C(18)	-100.0(4)
C(37)-Fe(1)-S(10)-Fe(3)	166.3(3)
C(33)-Fe(1)-S(10)-Fe(3)	-96.0(2)
P(8)-Fe(1)-S(10)-Fe(3)	-15.9(3)
S(6)-Fe(1)-S(10)-Fe(3)	53.55(7)
C(31)-Fe(3)-S(10)-C(18)	-139.3(4)

C(24)-Fe(3)-S(10)-C(18)	135.1(8)
C(36)-Fe(3)-S(10)-C(18)	-39.0(4)
S(6)-Fe(3)-S(10)-C(18)	60.5(3)
Fe(1)-Fe(3)-S(10)-C(18)	114.0(3)
C(31)-Fe(3)-S(10)-Fe(1)	106.7(3)
C(24)-Fe(3)-S(10)-Fe(1)	21.1(8)
C(36)-Fe(3)-S(10)-Fe(1)	-152.9(3)
S(6)-Fe(3)-S(10)-Fe(1)	-53.42(7)
C(34)-Fe(2)-Fe(4)-C(39)	-5.8(4)
C(29)-Fe(2)-Fe(4)-C(39)	119.8(8)
P(7)-Fe(2)-Fe(4)-C(39)	-96.2(3)
S(9)-Fe(2)-Fe(4)-C(39)	77.6(3)
S(5)-Fe(2)-Fe(4)-C(39)	-176.1(3)
C(34)-Fe(2)-Fe(4)-C(28)	90.1(4)
C(29)-Fe(2)-Fe(4)-C(28)	-144.3(8)
P(7)-Fe(2)-Fe(4)-C(28)	-0.3(3)
S(9)-Fe(2)-Fe(4)-C(28)	173.5(3)
S(5)-Fe(2)-Fe(4)-C(28)	-80.2(3)
C(34)-Fe(2)-Fe(4)-C(40)	-137.7(6)
C(29)-Fe(2)-Fe(4)-C(40)	-12.2(10)
P(7)-Fe(2)-Fe(4)-C(40)	131.9(5)
S(9)-Fe(2)-Fe(4)-C(40)	-54.4(5)
S(5)-Fe(2)-Fe(4)-C(40)	52.0(5)
C(34)-Fe(2)-Fe(4)-S(5)	170.3(3)
C(29)-Fe(2)-Fe(4)-S(5)	-64.1(8)
P(7)-Fe(2)-Fe(4)-S(5)	79.89(9)
S(9)-Fe(2)-Fe(4)-S(5)	-106.32(9)
C(34)-Fe(2)-Fe(4)-S(9)	-83.4(3)
C(29)-Fe(2)-Fe(4)-S(9)	42.2(8)
P(7)-Fe(2)-Fe(4)-S(9)	-173.79(10)
S(5)-Fe(2)-Fe(4)-S(9)	106.32(9)
C(34)-Fe(2)-S(5)-C(20)	-119.6(6)
C(29)-Fe(2)-S(5)-C(20)	59.9(4)
P(7)-Fe(2)-S(5)-C(20)	153.4(3)

S(9)-Fe(2)-S(5)-C(20)	-46.7(3)
Fe(4)-Fe(2)-S(5)-C(20)	-100.6(3)
C(34)-Fe(2)-S(5)-Fe(4)	-18.9(5)
C(29)-Fe(2)-S(5)-Fe(4)	160.5(3)
P(7)-Fe(2)-S(5)-Fe(4)	-105.95(8)
S(9)-Fe(2)-S(5)-Fe(4)	53.90(7)
C(39)-Fe(4)-S(5)-C(20)	124.0(8)
C(28)-Fe(4)-S(5)-C(20)	-138.2(4)
C(40)-Fe(4)-S(5)-C(20)	-40.7(4)
S(9)-Fe(4)-S(5)-C(20)	60.2(3)
Fe(2)-Fe(4)-S(5)-C(20)	113.5(3)
C(39)-Fe(4)-S(5)-Fe(2)	10.4(7)
C(28)-Fe(4)-S(5)-Fe(2)	108.3(3)
C(40)-Fe(4)-S(5)-Fe(2)	-154.2(3)
S(9)-Fe(4)-S(5)-Fe(2)	-53.29(7)
C(34)-Fe(2)-P(7)-C(1)	-30.2(4)
C(29)-Fe(2)-P(7)-C(1)	-127.9(4)
S(9)-Fe(2)-P(7)-C(1)	49.3(4)
S(5)-Fe(2)-P(7)-C(1)	118.7(3)
Fe(4)-Fe(2)-P(7)-C(1)	63.7(3)
C(34)-Fe(2)-P(7)-C(26)	88.0(4)
C(29)-Fe(2)-P(7)-C(26)	-9.7(4)
S(9)-Fe(2)-P(7)-C(26)	167.6(4)
S(5)-Fe(2)-P(7)-C(26)	-123.0(3)
Fe(4)-Fe(2)-P(7)-C(26)	-178.1(3)
C(34)-Fe(2)-P(7)-C(25)	-152.3(4)
C(29)-Fe(2)-P(7)-C(25)	110.0(4)
S(9)-Fe(2)-P(7)-C(25)	-72.8(4)
S(5)-Fe(2)-P(7)-C(25)	-3.4(3)
Fe(4)-Fe(2)-P(7)-C(25)	-58.5(3)
C(34)-Fe(2)-S(9)-C(17)	-164.0(4)
C(29)-Fe(2)-S(9)-C(17)	-67.1(4)
P(7)-Fe(2)-S(9)-C(17)	115.9(4)
S(5)-Fe(2)-S(9)-C(17)	45.6(3)

Fe(4)-Fe(2)-S(9)-C(17)	99.1(3)
C(34)-Fe(2)-S(9)-Fe(4)	96.9(3)
C(29)-Fe(2)-S(9)-Fe(4)	-166.1(3)
P(7)-Fe(2)-S(9)-Fe(4)	16.8(3)
S(5)-Fe(2)-S(9)-Fe(4)	-53.47(7)
C(39)-Fe(4)-S(9)-C(17)	138.0(4)
C(28)-Fe(4)-S(9)-C(17)	-133.9(9)
C(40)-Fe(4)-S(9)-C(17)	38.6(4)
S(5)-Fe(4)-S(9)-C(17)	-61.1(3)
Fe(2)-Fe(4)-S(9)-C(17)	-114.6(3)
C(39)-Fe(4)-S(9)-Fe(2)	-107.4(3)
C(28)-Fe(4)-S(9)-Fe(2)	-19.3(9)
C(40)-Fe(4)-S(9)-Fe(2)	153.2(3)
S(5)-Fe(4)-S(9)-Fe(2)	53.45(7)
C(38)-C(14)-C(19)-S(6)	75.0(8)
C(18)-C(14)-C(19)-S(6)	-52.7(9)
C(27)-C(14)-C(19)-S(6)	-172.9(5)
Fe(1)-S(6)-C(19)-C(14)	-8.1(7)
Fe(3)-S(6)-C(19)-C(14)	66.1(6)
C(17)-C(12)-C(20)-S(5)	54.6(9)
C(15)-C(12)-C(20)-S(5)	-70.8(8)
C(13)-C(12)-C(20)-S(5)	170.5(6)
Fe(2)-S(5)-C(20)-C(12)	5.9(7)
Fe(4)-S(5)-C(20)-C(12)	-68.3(7)
C(20)-C(12)-C(17)-S(9)	-55.8(9)
C(15)-C(12)-C(17)-S(9)	67.2(9)
C(13)-C(12)-C(17)-S(9)	-171.3(6)
Fe(2)-S(9)-C(17)-C(12)	-3.4(8)
Fe(4)-S(9)-C(17)-C(12)	70.1(7)
C(38)-C(14)-C(18)-S(10)	-70.4(9)
C(27)-C(14)-C(18)-S(10)	173.2(6)
C(19)-C(14)-C(18)-S(10)	54.5(9)
Fe(1)-S(10)-C(18)-C(14)	4.9(8)
Fe(3)-S(10)-C(18)-C(14)	-69.2(7)

C(2)-N(8)-C(1)-P(7)	62.2(8)
C(35)-N(8)-C(1)-P(7)	-59.7(8)
C(26)-P(7)-C(1)-N(8)	48.6(6)
C(25)-P(7)-C(1)-N(8)	-49.2(6)
Fe(2)-P(7)-C(1)-N(8)	177.9(4)
C(35)-N(8)-C(2)-N(11)	52.9(9)
C(1)-N(8)-C(2)-N(11)	-69.7(9)
C(8)-N(11)-C(2)-N(8)	-54.5(9)
C(25)-N(11)-C(2)-N(8)	70.0(9)
C(23)-N(10)-C(21)-N(5)	-66.1(9)
C(7)-N(10)-C(21)-N(5)	54.5(9)
C(22)-N(5)-C(21)-N(10)	65.0(9)
C(30)-N(5)-C(21)-N(10)	-56.0(9)
C(30)-N(5)-C(22)-P(8)	63.2(7)
C(21)-N(5)-C(22)-P(8)	-55.9(8)
C(32)-P(8)-C(22)-N(5)	-52.9(6)
C(23)-P(8)-C(22)-N(5)	46.8(6)
Fe(1)-P(8)-C(22)-N(5)	-178.9(4)
C(21)-N(10)-C(23)-P(8)	58.3(8)
C(7)-N(10)-C(23)-P(8)	-60.8(8)
C(32)-P(8)-C(23)-N(10)	50.1(6)
C(22)-P(8)-C(23)-N(10)	-47.3(6)
Fe(1)-P(8)-C(23)-N(10)	-178.6(4)
C(31)-Fe(3)-C(24)-O(1)	113(37)
C(36)-Fe(3)-C(24)-O(1)	12(37)
S(10)-Fe(3)-C(24)-O(1)	-162(36)
S(6)-Fe(3)-C(24)-O(1)	-89(37)
Fe(1)-Fe(3)-C(24)-O(1)	-144(37)
C(8)-N(11)-C(25)-P(7)	63.2(8)
C(2)-N(11)-C(25)-P(7)	-59.8(8)
C(1)-P(7)-C(25)-N(11)	47.6(6)
C(26)-P(7)-C(25)-N(11)	-51.5(6)
Fe(2)-P(7)-C(25)-N(11)	178.1(4)
C(35)-N(14)-C(26)-P(7)	58.7(8)

C(8)-N(14)-C(26)-P(7)	-61.4(8)
C(1)-P(7)-C(26)-N(14)	-47.9(6)
C(25)-P(7)-C(26)-N(14)	52.4(7)
Fe(2)-P(7)-C(26)-N(14)	-175.9(5)
C(38)-C(14)-C(27)-C(3)	-174.5(7)
C(18)-C(14)-C(27)-C(3)	-52.0(10)
C(19)-C(14)-C(27)-C(3)	70.2(9)
C(39)-Fe(4)-C(28)-O(2)	-10(15)
C(40)-Fe(4)-C(28)-O(2)	90(15)
S(5)-Fe(4)-C(28)-O(2)	-169(15)
S(9)-Fe(4)-C(28)-O(2)	-97(15)
Fe(2)-Fe(4)-C(28)-O(2)	-113(15)
C(34)-Fe(2)-C(29)-O(3)	-38(10)
P(7)-Fe(2)-C(29)-O(3)	52(9)
S(9)-Fe(2)-C(29)-O(3)	-127(9)
S(5)-Fe(2)-C(29)-O(3)	142(9)
Fe(4)-Fe(2)-C(29)-O(3)	-163(9)
C(22)-N(5)-C(30)-N(16)	-67.0(9)
C(21)-N(5)-C(30)-N(16)	54.4(9)
C(7)-N(16)-C(30)-N(5)	-55.8(9)
C(32)-N(16)-C(30)-N(5)	66.1(9)
C(24)-Fe(3)-C(31)-O(13)	-90(40)
C(36)-Fe(3)-C(31)-O(13)	10(40)
S(10)-Fe(3)-C(31)-O(13)	110(40)
S(6)-Fe(3)-C(31)-O(13)	172(40)
Fe(1)-Fe(3)-C(31)-O(13)	165(40)
C(7)-N(16)-C(32)-P(8)	57.8(8)
C(30)-N(16)-C(32)-P(8)	-62.1(8)
C(23)-P(8)-C(32)-N(16)	-47.6(7)
C(22)-P(8)-C(32)-N(16)	52.6(6)
Fe(1)-P(8)-C(32)-N(16)	178.2(5)
C(37)-Fe(1)-C(33)-O(6)	88(21)
P(8)-Fe(1)-C(33)-O(6)	-179(100)
S(10)-Fe(1)-C(33)-O(6)	-20(21)

S(6)-Fe(1)-C(33)-O(6)	-94(21)
Fe(3)-Fe(1)-C(33)-O(6)	-77(21)
C(29)-Fe(2)-C(34)-O(7)	164(13)
P(7)-Fe(2)-C(34)-O(7)	70(13)
S(9)-Fe(2)-C(34)-O(7)	-89(13)
S(5)-Fe(2)-C(34)-O(7)	-16(13)
Fe(4)-Fe(2)-C(34)-O(7)	-32(13)
C(26)-N(14)-C(35)-N(8)	-66.8(9)
C(8)-N(14)-C(35)-N(8)	54.9(9)
C(2)-N(8)-C(35)-N(14)	-55.4(9)
C(1)-N(8)-C(35)-N(14)	67.1(9)
C(31)-Fe(3)-C(36)-O(9)	-98(33)
C(24)-Fe(3)-C(36)-O(9)	-4(33)
S(10)-Fe(3)-C(36)-O(9)	174(100)
S(6)-Fe(3)-C(36)-O(9)	89(33)
Fe(1)-Fe(3)-C(36)-O(9)	131(33)
C(33)-Fe(1)-C(37)-O(4)	8(12)
P(8)-Fe(1)-C(37)-O(4)	-81(12)
S(10)-Fe(1)-C(37)-O(4)	98(12)
S(6)-Fe(1)-C(37)-O(4)	-171(12)
Fe(3)-Fe(1)-C(37)-O(4)	135(11)
C(18)-C(14)-C(38)-C(6)	-38.3(11)
C(27)-C(14)-C(38)-C(6)	81.1(9)
C(19)-C(14)-C(38)-C(6)	-165.1(7)
C(28)-Fe(4)-C(39)-O(15)	-140(11)
C(40)-Fe(4)-C(39)-O(15)	123(11)
S(5)-Fe(4)-C(39)-O(15)	-42(11)
S(9)-Fe(4)-C(39)-O(15)	21(11)
Fe(2)-Fe(4)-C(39)-O(15)	-33(11)
C(39)-Fe(4)-C(40)-O(12)	-150(78)
C(28)-Fe(4)-C(40)-O(12)	116(78)
S(5)-Fe(4)-C(40)-O(12)	24(78)
S(9)-Fe(4)-C(40)-O(12)	-61(78)
Fe(2)-Fe(4)-C(40)-O(12)	-18(79)

C(32)-N(16)-C(7)-N(10)	-65.6(9)
C(30)-N(16)-C(7)-N(10)	55.1(9)
C(21)-N(10)-C(7)-N(16)	-54.1(9)
C(23)-N(10)-C(7)-N(16)	67.5(10)
C(25)-N(11)-C(8)-N(14)	-68.5(10)
C(2)-N(11)-C(8)-N(14)	56.1(10)
C(35)-N(14)-C(8)-N(11)	-55.9(10)
C(26)-N(14)-C(8)-N(11)	66.7(9)
C(20)-C(12)-C(13)-C(4)	-70.9(8)
C(17)-C(12)-C(13)-C(4)	47.4(9)
C(15)-C(12)-C(13)-C(4)	170.9(6)
C(20)-C(12)-C(15)-C(5)	165.1(6)
C(17)-C(12)-C(15)-C(5)	41.3(9)
C(13)-C(12)-C(15)-C(5)	-78.5(8)

Symmetry transformations used to generate equivalent atoms:

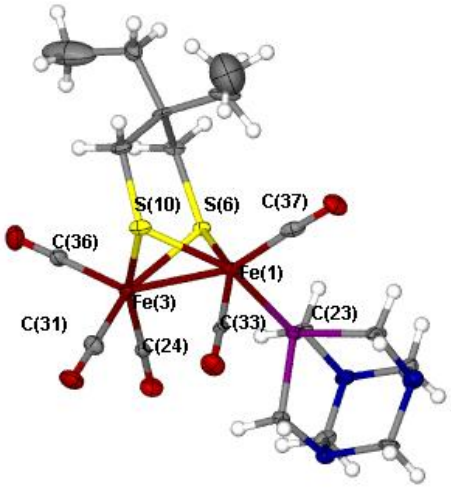
S(10)
S(6)
C(37)
C(36)
Fe(1)
Fe(3)
C(31)
C(33)
C(23)
C(24)

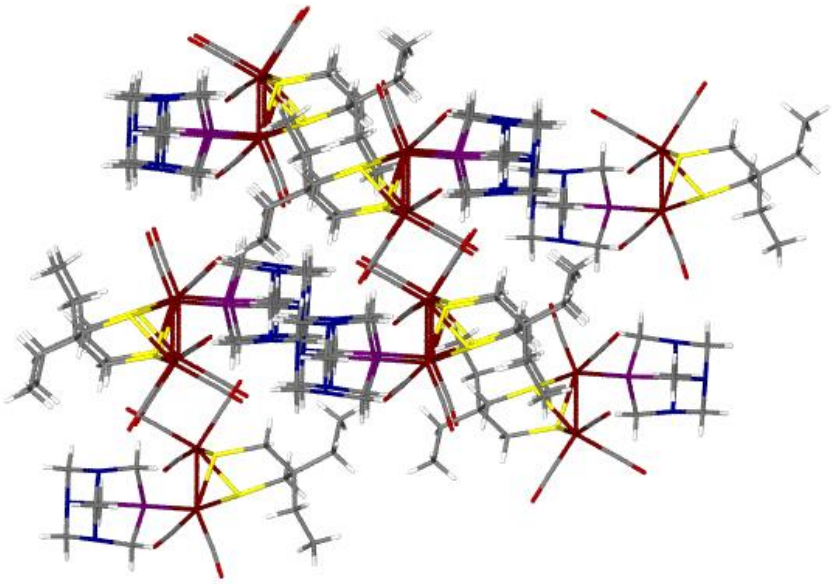

Table A-45. Crystal data and structure refinement for IV-2*.

Identification code	dmpdtbispme3	
Empirical formula	C15 H28 Fe2 O4 P2 S2	
Formula weight	510.13	
Temperature	110(2) K	
Wavelength	0.71073 Å	
Crystal system	Orthorhombic	
Space group	Pbca	
Unit cell dimensions	a = 10.8327(13) Å	α= 90°.
	b = 12.0403(15) Å	β= 90°.
	c = 34.742(4) Å	γ = 90°.
Volume	4531.4(10) $Å^3$	
Z	8	
Density (calculated)	1.496 Mg/m^3	
Absorption coefficient	1.621 mm^{-1}	
F(000)	2112	
Crystal size	0.32 x 0.11 x 0.09 mm^3	
Theta range for data collection	2.22 to 23.69°.	
Index ranges	-12<=h<=12, -13<=k<=13, -39<=l<=39	
Reflections collected	35685	
Independent reflections	3418 [R(int) = 0.0785]	
Completeness to theta = 23.69°	99.5 %	
Absorption correction	None	
Max. and min. transmission	0.8678 and 0.6250	
Refinement method	Full-matrix least-squares on F^2	
Data / restraints / parameters	3418 / 0 / 234	
Goodness-of-fit on F^2	1.015	
Final R indices [I>2sigma(I)]	R1 = 0.0318, wR2 = 0.0801	
R indices (all data)	R1 = 0.0442, wR2 = 0.0848	
Largest diff. peak and hole	0.458 and -0.318 $e.Å^{-3}$	

Table A-46. Atomic coordinates (x 10^4) and equivalent isotropic displacement parameters ($Å^2$x 10^3) for IV-2*. U(eq) is defined as one third of the trace of the orthogonalized U^{ij} tensor.

	x	y	z	U(eq)
Fe(1)	797(1)	6385(1)	4129(1)	29(1)
Fe(2)	707(1)	7273(1)	3457(1)	28(1)
S(3)	1696(1)	5673(1)	3598(1)	28(1)
S(4)	1808(1)	7938(1)	3955(1)	30(1)
P(2)	-415(1)	7355(1)	4526(1)	39(1)
P(1)	-434(1)	6289(1)	3055(1)	39(1)
O(3)	-1046(2)	4622(2)	4178(1)	53(1)
O(1)	1560(2)	8676(2)	2826(1)	53(1)
O(4)	2432(2)	5524(2)	4722(1)	61(1)
C(12)	4031(3)	6842(3)	3662(1)	34(1)
C(11)	3368(3)	5747(3)	3658(1)	43(1)
C(13)	3461(3)	7693(3)	3928(1)	39(1)
O(2)	-1400(3)	8668(3)	3622(1)	101(1)
C(4)	1775(3)	5868(3)	4490(1)	40(1)
C(1)	1270(3)	8086(3)	3073(1)	35(1)
C(3)	-319(3)	5325(3)	4144(1)	38(1)
C(5)	445(3)	5631(3)	2672(1)	51(1)
C(6)	-1574(4)	7092(4)	2785(1)	70(1)
C(2)	-556(4)	8108(4)	3568(1)	57(1)
C(14)	4083(4)	7304(3)	3245(1)	55(1)
C(15)	5364(3)	6662(3)	3790(1)	59(1)
C(7)	-1361(4)	5163(3)	3239(1)	61(1)
C(8)	-2056(3)	7283(4)	4443(1)	78(1)
C(10)	-371(4)	6823(5)	5009(1)	96(2)
C(9)	-174(5)	8825(4)	4580(2)	106(2)

Table A-47. Bond lengths [Å] and angles [°] for IV-2*.

Fe(1)-C(4)	1.757(4)
Fe(1)-C(3)	1.759(4)
Fe(1)-P(2)	2.2342(10)
Fe(1)-S(4)	2.2497(9)
Fe(1)-S(3)	2.2534(9)
Fe(1)-Fe(2)	2.5690(7)
Fe(2)-C(2)	1.741(4)
Fe(2)-C(1)	1.764(4)
Fe(2)-P(1)	2.2097(10)
Fe(2)-S(4)	2.2476(9)
Fe(2)-S(3)	2.2589(9)
S(3)-C(11)	1.825(3)
S(4)-C(13)	1.817(3)
P(2)-C(9)	1.798(4)
P(2)-C(10)	1.795(4)
P(2)-C(8)	1.803(4)
P(1)-C(7)	1.805(4)
P(1)-C(5)	1.817(4)
P(1)-C(6)	1.826(4)
O(3)-C(3)	1.162(4)
O(1)-C(1)	1.158(4)
O(4)-C(4)	1.153(4)
C(12)-C(11)	1.501(4)
C(12)-C(13)	1.513(5)
C(12)-C(15)	1.526(5)
C(12)-C(14)	1.554(5)
C(11)-H(11A)	0.9900
C(11)-H(11B)	0.9900
C(13)-H(13A)	0.9900
C(13)-H(13B)	0.9900
O(2)-C(2)	1.151(4)
C(5)-H(5A)	0.9800

C(5)-H(5B)	0.9800
C(5)-H(5C)	0.9800
C(6)-H(6A)	0.9800
C(6)-H(6B)	0.9800
C(6)-H(6C)	0.9800
C(14)-H(14A)	0.9800
C(14)-H(14B)	0.9800
C(14)-H(14C)	0.9800
C(15)-H(15A)	0.9800
C(15)-H(15B)	0.9800
C(15)-H(15C)	0.9800
C(7)-H(7A)	0.9800
C(7)-H(7B)	0.9800
C(7)-H(7C)	0.9800
C(8)-H(8A)	0.9800
C(8)-H(8B)	0.9800
C(8)-H(8C)	0.9800
C(10)-H(10A)	0.9800
C(10)-H(10B)	0.9800
C(10)-H(10C)	0.9800
C(9)-H(9A)	0.9800
C(9)-H(9B)	0.9800
C(9)-H(9C)	0.9800

C(4)-Fe(1)-C(3)	97.80(15)
C(4)-Fe(1)-P(2)	95.61(12)
C(3)-Fe(1)-P(2)	87.56(11)
C(4)-Fe(1)-S(4)	101.12(11)
C(3)-Fe(1)-S(4)	161.07(11)
P(2)-Fe(1)-S(4)	91.01(4)
C(4)-Fe(1)-S(3)	100.87(12)
C(3)-Fe(1)-S(3)	92.61(11)
P(2)-Fe(1)-S(3)	163.33(4)
S(4)-Fe(1)-S(3)	83.45(3)

C(4)-Fe(1)-Fe(2)	145.03(11)
C(3)-Fe(1)-Fe(2)	107.67(10)
P(2)-Fe(1)-Fe(2)	108.76(3)
S(4)-Fe(1)-Fe(2)	55.12(2)
S(3)-Fe(1)-Fe(2)	55.40(3)
C(2)-Fe(2)-C(1)	96.85(17)
C(2)-Fe(2)-P(1)	90.62(15)
C(1)-Fe(2)-P(1)	90.73(11)
C(2)-Fe(2)-S(4)	92.30(14)
C(1)-Fe(2)-S(4)	101.58(11)
P(1)-Fe(2)-S(4)	166.91(4)
C(2)-Fe(2)-S(3)	144.75(14)
C(1)-Fe(2)-S(3)	118.31(11)
P(1)-Fe(2)-S(3)	86.89(4)
S(4)-Fe(2)-S(3)	83.37(3)
C(2)-Fe(2)-Fe(1)	93.89(12)
C(1)-Fe(2)-Fe(1)	154.85(11)
P(1)-Fe(2)-Fe(1)	111.87(3)
S(4)-Fe(2)-Fe(1)	55.20(2)
S(3)-Fe(2)-Fe(1)	55.20(2)
C(11)-S(3)-Fe(1)	108.50(12)
C(11)-S(3)-Fe(2)	116.98(11)
Fe(1)-S(3)-Fe(2)	69.41(3)
C(13)-S(4)-Fe(2)	115.22(11)
C(13)-S(4)-Fe(1)	111.02(11)
Fe(2)-S(4)-Fe(1)	69.67(3)
C(9)-P(2)-C(10)	104.4(3)
C(9)-P(2)-C(8)	102.0(2)
C(10)-P(2)-C(8)	99.1(2)
C(9)-P(2)-Fe(1)	119.60(15)
C(10)-P(2)-Fe(1)	112.03(16)
C(8)-P(2)-Fe(1)	117.06(16)
C(7)-P(1)-C(5)	102.91(18)
C(7)-P(1)-C(6)	101.7(2)

C(5)-P(1)-C(6)	102.13(18)
C(7)-P(1)-Fe(2)	119.36(13)
C(5)-P(1)-Fe(2)	113.81(12)
C(6)-P(1)-Fe(2)	114.74(15)
C(11)-C(12)-C(13)	113.8(3)
C(11)-C(12)-C(15)	109.3(3)
C(13)-C(12)-C(15)	107.8(3)
C(11)-C(12)-C(14)	108.9(3)
C(13)-C(12)-C(14)	110.0(3)
C(15)-C(12)-C(14)	106.7(3)
C(12)-C(11)-S(3)	121.3(2)
C(12)-C(11)-H(11A)	107.0
S(3)-C(11)-H(11A)	107.0
C(12)-C(11)-H(11B)	107.0
S(3)-C(11)-H(11B)	107.0
H(11A)-C(11)-H(11B)	106.7
C(12)-C(13)-S(4)	122.9(2)
C(12)-C(13)-H(13A)	106.6
S(4)-C(13)-H(13A)	106.6
C(12)-C(13)-H(13B)	106.6
S(4)-C(13)-H(13B)	106.6
H(13A)-C(13)-H(13B)	106.6
O(4)-C(4)-Fe(1)	178.7(3)
O(1)-C(1)-Fe(2)	174.5(3)
O(3)-C(3)-Fe(1)	175.9(3)
P(1)-C(5)-H(5A)	109.5
P(1)-C(5)-H(5B)	109.5
H(5A)-C(5)-H(5B)	109.5
P(1)-C(5)-H(5C)	109.5
H(5A)-C(5)-H(5C)	109.5
H(5B)-C(5)-H(5C)	109.5
P(1)-C(6)-H(6A)	109.5
P(1)-C(6)-H(6B)	109.5
H(6A)-C(6)-H(6B)	109.5

P(1)-C(6)-H(6C)	109.5
H(6A)-C(6)-H(6C)	109.5
H(6B)-C(6)-H(6C)	109.5
O(2)-C(2)-Fe(2)	176.5(3)
C(12)-C(14)-H(14A)	109.5
C(12)-C(14)-H(14B)	109.5
H(14A)-C(14)-H(14B)	109.5
C(12)-C(14)-H(14C)	109.5
H(14A)-C(14)-H(14C)	109.5
H(14B)-C(14)-H(14C)	109.5
C(12)-C(15)-H(15A)	109.5
C(12)-C(15)-H(15B)	109.5
H(15A)-C(15)-H(15B)	109.5
C(12)-C(15)-H(15C)	109.5
H(15A)-C(15)-H(15C)	109.5
H(15B)-C(15)-H(15C)	109.5
P(1)-C(7)-H(7A)	109.5
P(1)-C(7)-H(7B)	109.5
H(7A)-C(7)-H(7B)	109.5
P(1)-C(7)-H(7C)	109.5
H(7A)-C(7)-H(7C)	109.5
H(7B)-C(7)-H(7C)	109.5
P(2)-C(8)-H(8A)	109.5
P(2)-C(8)-H(8B)	109.5
H(8A)-C(8)-H(8B)	109.5
P(2)-C(8)-H(8C)	109.5
H(8A)-C(8)-H(8C)	109.5
H(8B)-C(8)-H(8C)	109.5
P(2)-C(10)-H(10A)	109.5
P(2)-C(10)-H(10B)	109.5
H(10A)-C(10)-H(10B)	109.5
P(2)-C(10)-H(10C)	109.5
H(10A)-C(10)-H(10C)	109.5
H(10B)-C(10)-H(10C)	109.5

P(2)-C(9)-H(9A)	109.5
P(2)-C(9)-H(9B)	109.5
H(9A)-C(9)-H(9B)	109.5
P(2)-C(9)-H(9C)	109.5
H(9A)-C(9)-H(9C)	109.5
H(9B)-C(9)-H(9C)	109.5

Symmetry transformations used to generate equivalent atoms:

Table A-48. Anisotropic displacement parameters ($Å^2 x\ 10^3$) for IV-2*. The anisotropic displacement factor exponent takes the form: $-2\pi^2[\ h^2\ a^{*2}U^{11} + ... + 2\ h\ k\ a^*\ b^*\ U^{12}\ ]$

	U^{11}	U^{22}	U^{33}	U^{23}	U^{13}	U^{12}
Fe(1)	37(1)	27(1)	24(1)	2(1)	-4(1)	-4(1)
Fe(2)	32(1)	28(1)	24(1)	2(1)	-3(1)	6(1)
S(3)	30(1)	22(1)	33(1)	-4(1)	-7(1)	1(1)
S(4)	44(1)	21(1)	26(1)	-2(1)	1(1)	-1(1)
P(2)	33(1)	53(1)	32(1)	-3(1)	2(1)	-5(1)
P(1)	29(1)	56(1)	30(1)	6(1)	-8(1)	-9(1)
O(3)	55(2)	47(2)	57(2)	4(1)	3(1)	-22(1)
O(1)	73(2)	45(2)	41(2)	13(1)	4(1)	-2(1)
O(4)	57(2)	77(2)	48(2)	12(2)	-21(1)	9(2)
C(12)	33(2)	35(2)	34(2)	-2(2)	-4(2)	-4(2)
C(11)	31(2)	29(2)	70(3)	-9(2)	-9(2)	5(2)
C(13)	43(2)	32(2)	42(2)	-3(2)	-11(2)	-4(2)
O(2)	97(3)	141(3)	65(2)	7(2)	7(2)	88(3)
C(4)	42(2)	39(2)	38(2)	1(2)	1(2)	-5(2)
C(1)	45(2)	31(2)	29(2)	-2(2)	-5(2)	3(2)
C(3)	46(2)	39(2)	30(2)	5(2)	-2(2)	3(2)
C(5)	53(2)	66(3)	33(2)	-12(2)	-6(2)	-22(2)
C(6)	46(3)	111(4)	54(3)	18(3)	-21(2)	7(3)
C(2)	59(3)	75(3)	36(2)	8(2)	1(2)	30(2)
C(14)	51(3)	74(3)	39(2)	0(2)	2(2)	5(2)
C(15)	39(2)	54(3)	85(3)	-3(2)	-17(2)	-4(2)
C(7)	53(3)	82(3)	47(2)	8(2)	-8(2)	-34(2)
C(8)	42(3)	89(4)	102(4)	-19(3)	-1(2)	13(3)
C(10)	80(4)	165(5)	43(3)	7(3)	17(2)	31(4)
C(9)	118(4)	70(3)	128(5)	-59(3)	75(4)	-28(3)

Table A-49. Hydrogen coordinates (x 10^4) and isotropic displacement parameters ($Å^2$x 10^3) for IV-2*.

	x	y	z	U(eq)
H(11A)	3568	5369	3903	52
H(11B)	3739	5297	3450	52
H(13A)	3847	8415	3864	47
H(13B)	3734	7502	4192	47
H(5A)	1059	5129	2784	76
H(5B)	864	6202	2519	76
H(5C)	-115	5208	2506	76
H(6A)	-1955	6618	2589	105
H(6B)	-1168	7724	2661	105
H(6C)	-2212	7364	2962	105
H(14A)	4596	6816	3085	82
H(14B)	4440	8052	3248	82
H(14C)	3246	7336	3138	82
H(15A)	5375	6385	4055	89
H(15B)	5813	7367	3776	89
H(15C)	5759	6118	3620	89
H(7A)	-1789	4797	3025	91
H(7B)	-1970	5456	3421	91
H(7C)	-829	4625	3370	91
H(8A)	-2491	7674	4650	117
H(8B)	-2317	6503	4438	117
H(8C)	-2252	7631	4196	117
H(10A)	426	7005	5126	144
H(10B)	-478	6015	5003	144
H(10C)	-1038	7159	5159	144
H(9A)	-730	9113	4779	158
H(9B)	-344	9198	4335	158

H(9C)	684	8963	4656	158

Table A-50. Torsion angles [°] for IV-2*.

C(4)-Fe(1)-Fe(2)-C(2)	-144.2(2)
C(3)-Fe(1)-Fe(2)-C(2)	81.0(2)
P(2)-Fe(1)-Fe(2)-C(2)	-12.46(16)
S(4)-Fe(1)-Fe(2)-C(2)	-90.09(16)
S(3)-Fe(1)-Fe(2)-C(2)	161.73(16)
C(4)-Fe(1)-Fe(2)-C(1)	-29.0(3)
C(3)-Fe(1)-Fe(2)-C(1)	-163.7(3)
P(2)-Fe(1)-Fe(2)-C(1)	102.8(3)
S(4)-Fe(1)-Fe(2)-C(1)	25.1(3)
S(3)-Fe(1)-Fe(2)-C(1)	-83.0(3)
C(4)-Fe(1)-Fe(2)-P(1)	123.6(2)
C(3)-Fe(1)-Fe(2)-P(1)	-11.20(12)
P(2)-Fe(1)-Fe(2)-P(1)	-104.69(4)
S(4)-Fe(1)-Fe(2)-P(1)	177.67(4)
S(3)-Fe(1)-Fe(2)-P(1)	69.50(4)
C(4)-Fe(1)-Fe(2)-S(4)	-54.1(2)
C(3)-Fe(1)-Fe(2)-S(4)	171.13(12)
P(2)-Fe(1)-Fe(2)-S(4)	77.64(4)
S(3)-Fe(1)-Fe(2)-S(4)	-108.17(4)
C(4)-Fe(1)-Fe(2)-S(3)	54.1(2)
C(3)-Fe(1)-Fe(2)-S(3)	-80.70(12)
P(2)-Fe(1)-Fe(2)-S(3)	-174.19(4)
S(4)-Fe(1)-Fe(2)-S(3)	108.17(4)
C(4)-Fe(1)-S(3)-C(11)	-39.14(16)
C(3)-Fe(1)-S(3)-C(11)	-137.60(16)
P(2)-Fe(1)-S(3)-C(11)	132.19(17)
S(4)-Fe(1)-S(3)-C(11)	60.98(12)
Fe(2)-Fe(1)-S(3)-C(11)	112.66(12)
C(4)-Fe(1)-S(3)-Fe(2)	-151.80(11)
C(3)-Fe(1)-S(3)-Fe(2)	109.74(11)
P(2)-Fe(1)-S(3)-Fe(2)	19.53(13)
S(4)-Fe(1)-S(3)-Fe(2)	-51.68(3)

C(2)-Fe(2)-S(3)-C(11)	-133.7(3)
C(1)-Fe(2)-S(3)-C(11)	50.47(19)
P(1)-Fe(2)-S(3)-C(11)	139.62(14)
S(4)-Fe(2)-S(3)-C(11)	-49.14(14)
Fe(1)-Fe(2)-S(3)-C(11)	-100.90(14)
C(2)-Fe(2)-S(3)-Fe(1)	-32.8(3)
C(1)-Fe(2)-S(3)-Fe(1)	151.37(12)
P(1)-Fe(2)-S(3)-Fe(1)	-119.48(3)
S(4)-Fe(2)-S(3)-Fe(1)	51.76(3)
C(2)-Fe(2)-S(4)-C(13)	-162.47(19)
C(1)-Fe(2)-S(4)-C(13)	-65.00(17)
P(1)-Fe(2)-S(4)-C(13)	94.8(2)
S(3)-Fe(2)-S(4)-C(13)	52.63(13)
Fe(1)-Fe(2)-S(4)-C(13)	104.38(13)
C(2)-Fe(2)-S(4)-Fe(1)	93.14(14)
C(1)-Fe(2)-S(4)-Fe(1)	-169.38(11)
P(1)-Fe(2)-S(4)-Fe(1)	-9.58(18)
S(3)-Fe(2)-S(4)-Fe(1)	-51.76(3)
C(4)-Fe(1)-S(4)-C(13)	41.62(16)
C(3)-Fe(1)-S(4)-C(13)	-137.1(4)
P(2)-Fe(1)-S(4)-C(13)	137.53(12)
S(3)-Fe(1)-S(4)-C(13)	-58.22(12)
Fe(2)-Fe(1)-S(4)-C(13)	-110.15(12)
C(4)-Fe(1)-S(4)-Fe(2)	151.76(12)
C(3)-Fe(1)-S(4)-Fe(2)	-26.9(3)
P(2)-Fe(1)-S(4)-Fe(2)	-112.32(3)
S(3)-Fe(1)-S(4)-Fe(2)	51.92(3)
C(4)-Fe(1)-P(2)-C(9)	99.2(3)
C(3)-Fe(1)-P(2)-C(9)	-163.2(3)
S(4)-Fe(1)-P(2)-C(9)	-2.1(2)
S(3)-Fe(1)-P(2)-C(9)	-72.3(3)
Fe(2)-Fe(1)-P(2)-C(9)	-55.4(2)
C(4)-Fe(1)-P(2)-C(10)	-23.5(2)
C(3)-Fe(1)-P(2)-C(10)	74.1(2)

S(4)-Fe(1)-P(2)-C(10)	-124.7(2)
S(3)-Fe(1)-P(2)-C(10)	165.1(2)
Fe(2)-Fe(1)-P(2)-C(10)	-178.0(2)
C(4)-Fe(1)-P(2)-C(8)	-136.9(2)
C(3)-Fe(1)-P(2)-C(8)	-39.3(2)
S(4)-Fe(1)-P(2)-C(8)	121.82(19)
S(3)-Fe(1)-P(2)-C(8)	51.7(2)
Fe(2)-Fe(1)-P(2)-C(8)	68.54(19)
C(2)-Fe(2)-P(1)-C(7)	-84.2(2)
C(1)-Fe(2)-P(1)-C(7)	178.9(2)
S(4)-Fe(2)-P(1)-C(7)	18.7(3)
S(3)-Fe(2)-P(1)-C(7)	60.61(17)
Fe(1)-Fe(2)-P(1)-C(7)	10.23(18)
C(2)-Fe(2)-P(1)-C(5)	153.90(19)
C(1)-Fe(2)-P(1)-C(5)	57.04(18)
S(4)-Fe(2)-P(1)-C(5)	-103.2(2)
S(3)-Fe(2)-P(1)-C(5)	-61.28(14)
Fe(1)-Fe(2)-P(1)-C(5)	-111.66(14)
C(2)-Fe(2)-P(1)-C(6)	36.8(2)
C(1)-Fe(2)-P(1)-C(6)	-60.10(19)
S(4)-Fe(2)-P(1)-C(6)	139.7(2)
S(3)-Fe(2)-P(1)-C(6)	-178.42(16)
Fe(1)-Fe(2)-P(1)-C(6)	131.21(15)
C(13)-C(12)-C(11)-S(3)	49.0(4)
C(15)-C(12)-C(11)-S(3)	169.6(3)
C(14)-C(12)-C(11)-S(3)	-74.1(4)
Fe(1)-S(3)-C(11)-C(12)	-68.4(3)
Fe(2)-S(3)-C(11)-C(12)	7.4(3)
C(11)-C(12)-C(13)-S(4)	-44.4(4)
C(15)-C(12)-C(13)-S(4)	-165.8(3)
C(14)-C(12)-C(13)-S(4)	78.2(3)
Fe(2)-S(4)-C(13)-C(12)	-16.9(3)
Fe(1)-S(4)-C(13)-C(12)	59.7(3)
C(3)-Fe(1)-C(4)-O(4)	107(15)

P(2)-Fe(1)-C(4)-O(4)	-165(15)
S(4)-Fe(1)-C(4)-O(4)	-73(15)
S(3)-Fe(1)-C(4)-O(4)	12(15)
Fe(2)-Fe(1)-C(4)-O(4)	-30(15)
C(2)-Fe(2)-C(1)-O(1)	-2(3)
P(1)-Fe(2)-C(1)-O(1)	89(3)
S(4)-Fe(2)-C(1)-O(1)	-96(3)
S(3)-Fe(2)-C(1)-O(1)	176(100)
Fe(1)-Fe(2)-C(1)-O(1)	-116(3)
C(4)-Fe(1)-C(3)-O(3)	37(4)
P(2)-Fe(1)-C(3)-O(3)	-58(4)
S(4)-Fe(1)-C(3)-O(3)	-144(4)
S(3)-Fe(1)-C(3)-O(3)	138(4)
Fe(2)-Fe(1)-C(3)-O(3)	-167(4)
C(1)-Fe(2)-C(2)-O(2)	40(7)
P(1)-Fe(2)-C(2)-O(2)	-51(7)
S(4)-Fe(2)-C(2)-O(2)	142(7)
S(3)-Fe(2)-C(2)-O(2)	-136(7)
Fe(1)-Fe(2)-C(2)-O(2)	-163(7)

Symmetry transformations used to generate equivalent atoms:

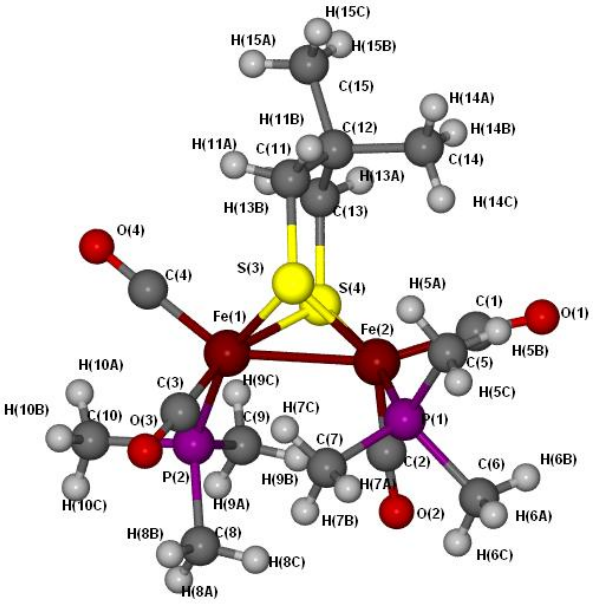
H(15C)
H(15A)
H(15B)
C(15)
H(14A)
H(11B)
C(12)
H(14B)
H(11A)
C(11)
C(14)
H(13A)
H(14C)
H(13B)
C(13)
O(4)
S(3)
C(4)
S(4)
H(5A)
C(1)
O(1)
Fe(1)
Fe(2)
H(5B)
C(5)
H(10A)
C(3)
H(9C)
H(5C)
H(10B)
H(7C)
C(10)
O(3)
C(9)
P(1)
C(7)
C(2)
C(6)
H(6B)
P(2)
H(9B)
H(7A)
H(10C)
H(9A)
O(2)
H(6A)
H(7B)
H(8B)
C(8)
H(8C)
H(6C)
H(8A)

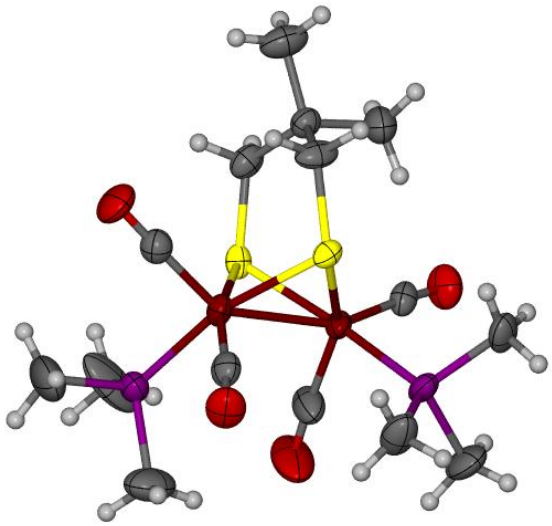

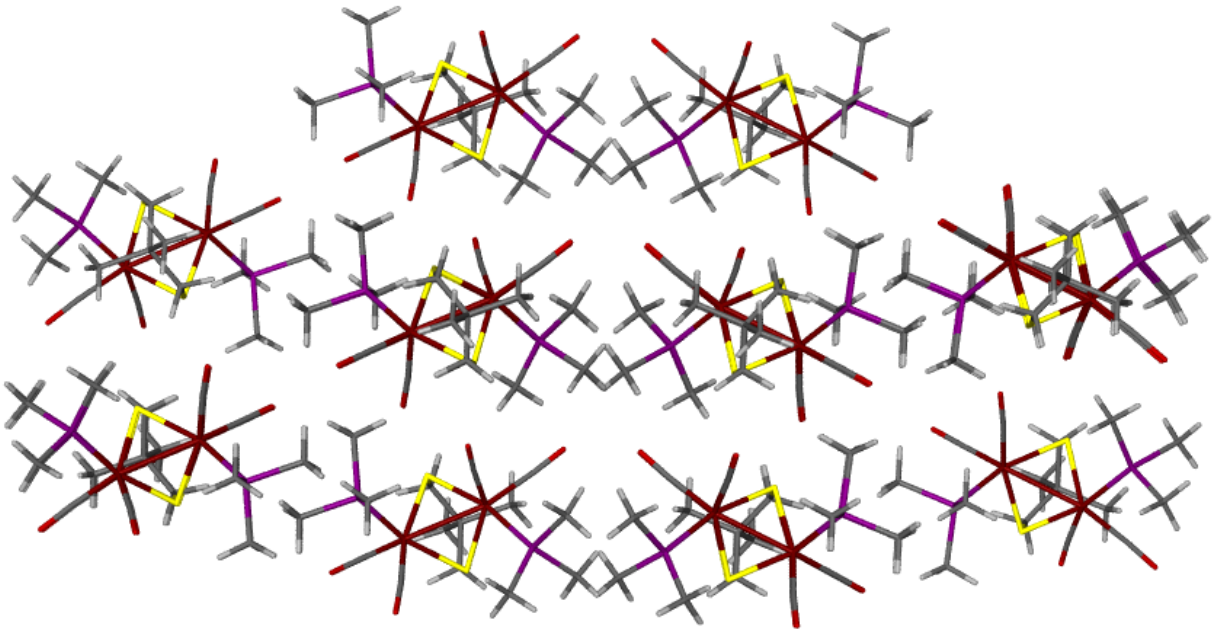

Table A-51. Crystal data and structure refinement for IV_**2*$_{ox}$**.

Identification code	mdb	
Empirical formula	C15 H28 F6 Fe2 O4 P3 S2	
Formula weight	655.10	
Temperature	110(2) K	
Wavelength	1.54178 Å	
Crystal system	C	
Space group	Monoclinic	
Unit cell dimensions	a = 20.460(2) Å	α= 90°.
	b = 10.4979(10) Å	β= 101.306(6)°.
	c = 12.3170(12) Å	γ = 90°.
Volume	2594.2(4) Å^3	
Z	4	
Density (calculated)	1.677 Mg/m^3	
Absorption coefficient	12.821 mm^{-1}	
F(000)	1332	
Crystal size	0.11 x 0.05 x 0.04 mm^3	
Theta range for data collection	4.41 to 60.55°.	
Index ranges	-23<=h<=23, -11<=k<=11, -12<=l<=13	
Reflections collected	7363	
Independent reflections	1820 [R(int) = 0.0495]	
Completeness to theta = 60.55°	93.0 %	
Absorption correction	Semi-empirical from equivalents	
Max. and min. transmission	0.6281 and 0.3329	
Refinement method	Full-matrix least-squares on F^2	
Data / restraints / parameters	1820 / 191 / 229	
Goodness-of-fit on F^2	1.002	
Final R indices [I>2sigma(I)]	R1 = 0.0386, wR2 = 0.0869	
R indices (all data)	R1 = 0.0470, wR2 = 0.0917	
Largest diff. peak and hole	0.329 and -0.289 e.Å^{-3}	

Table A-52. Atomic coordinates (x 10^4) and equivalent isotropic displacement parameters ($Å^2$x 10^3) for **IV_2*$_{ox}$**. U(eq) is defined as one third of the trace of the orthogonalized U^{ij} tensor.

	x	y	z	U(eq)
Fe(1)	577(3)	2976(6)	2044(5)	19(1)
Fe(1')	493(3)	2717(6)	2237(5)	18(1)
S(1)	406(1)	3875(1)	3714(1)	22(1)
P(1)	1434(1)	1845(1)	3110(1)	23(1)
C(1)	0	1358(6)	2500	34(1)
O(1)	10(40)	260(40)	2330(50)	29(5)
O(1')	-70(30)	270(40)	2830(40)	29(5)
C(2)	574(2)	2021(4)	884(3)	32(1)
O(2)	563(2)	1471(3)	85(2)	46(1)
C(3)	1098(4)	4264(8)	1748(6)	27(2)
O(3)	1402(3)	5107(6)	1551(5)	39(1)
C(4)	2173(2)	2821(4)	3428(3)	33(1)
C(5)	1330(2)	1257(4)	4450(3)	34(1)
C(6)	1697(2)	446(4)	2464(4)	33(1)
C(7)	225(3)	5595(10)	3414(6)	28(2)
C(7')	458(6)	5589(10)	3525(8)	30(2)
C(8)	443(3)	5970(5)	2329(5)	26(2)
C(9)	466(5)	7437(5)	2306(6)	34(2)
C(10)	1058(3)	5479(8)	1908(7)	31(2)
P(2)	2500	2500	0	63(1)
F(1)	3039(5)	2889(13)	1041(9)	85(2)
F(2)	1942(6)	2699(13)	741(11)	76(2)
F(3)	2571(7)	1036(7)	408(11)	73(2)
P(2A)	2500	2500	0	63(1)
F(1A)	2956(7)	2411(17)	1171(9)	83(3)
F(2A)	1876(8)	2910(20)	520(15)	76(3)
F(3A)	2327(10)	1023(11)	52(13)	79(3)

Table A-53. Bond lengths [Å] and angles [°] for **IV_2*$_{ox}$**.

Fe(1)-C(2)	1.744(8)
Fe(1)-C(3)	1.803(9)
Fe(1)-C(1)	2.204(6)
Fe(1)-S(1)#1	2.250(7)
Fe(1)-P(1)	2.304(7)
Fe(1)-S(1)	2.351(7)
Fe(1)-H(10C)	1.9530
Fe(1')-C(1)	1.814(6)
Fe(1')-C(2)	1.856(8)
Fe(1')-P(1)	2.211(7)
Fe(1')-S(1)	2.224(7)
Fe(1')-S(1)#1	2.321(7)
S(1)-C(7')	1.819(10)
S(1)-C(7)	1.865(9)
S(1)-Fe(1)#1	2.250(7)
S(1)-Fe(1')#1	2.321(7)
P(1)-C(6)	1.801(4)
P(1)-C(4)	1.804(4)
P(1)-C(5)	1.813(4)
C(1)-O(1')#1	1.23(4)
C(1)-Fe(1')#1	1.814(6)
C(1)-Fe(1)#1	2.204(6)
C(2)-O(2)	1.138(5)
C(3)-O(3)	1.134(9)
C(4)-H(4A)	0.9600
C(4)-H(4B)	0.9600
C(4)-H(4C)	0.9599
C(5)-H(5A)	0.9599
C(5)-H(5B)	0.9600
C(5)-H(5C)	0.9599
C(6)-H(6A)	0.9601
C(6)-H(6B)	0.9600

C(6)-H(6C)	0.9600
C(7)-C(8)	1.542(2)
C(7)-H(7A)	0.9600
C(7)-H(7B)	0.9599
C(7')-C(8)	1.522(14)
C(7')-H(7'A)	0.9599
C(7')-H(7'B)	0.9600
C(8)-C(10)	1.540(2)
C(8)-C(9)	1.541(2)
C(9)-H(9A)	0.9599
C(9)-H(9B)	0.9600
C(9)-H(9C)	0.9601
C(10)-H(10A)	0.9600
C(10)-H(10B)	0.9600
C(10)-H(10C)	0.9600
P(2)-F(1)	1.572(8)
P(2)-F(2)	1.609(9)
P(2)-F(3)	1.615(7)
C(2)-Fe(1)-C(3)	99.9(4)
C(2)-Fe(1)-C(1)	81.4(3)
C(3)-Fe(1)-C(1)	175.8(5)
C(2)-Fe(1)-S(1)#1	92.5(3)
C(3)-Fe(1)-S(1)#1	96.8(3)
C(1)-Fe(1)-S(1)#1	87.1(2)
C(2)-Fe(1)-P(1)	92.9(3)
C(3)-Fe(1)-P(1)	95.0(4)
C(1)-Fe(1)-P(1)	80.97(18)
S(1)#1-Fe(1)-P(1)	166.1(2)
C(2)-Fe(1)-S(1)	166.0(3)
C(3)-Fe(1)-S(1)	94.1(4)
C(1)-Fe(1)-S(1)	84.68(18)
S(1)#1-Fe(1)-S(1)	85.4(2)
P(1)-Fe(1)-S(1)	86.3(2)
C(1)-Fe(1')-C(2)	90.1(3)

C(1)-Fe(1')-P(1)	92.8(2)
C(2)-Fe(1')-P(1)	92.9(3)
C(1)-Fe(1')-S(1)	98.5(2)
C(2)-Fe(1')-S(1)	170.1(3)
P(1)-Fe(1')-S(1)	91.8(3)
C(1)-Fe(1')-S(1)#1	95.1(3)
C(2)-Fe(1')-S(1)#1	87.4(3)
P(1)-Fe(1')-S(1)#1	172.1(2)
S(1)-Fe(1')-S(1)#1	86.8(2)
C(7')-S(1)-Fe(1')	114.8(4)
C(7')-S(1)-Fe(1)#1	115.6(4)
Fe(1')-S(1)-Fe(1)#1	68.93(17)
C(7)-S(1)-Fe(1')#1	107.5(3)
Fe(1')-S(1)-Fe(1')#1	58.9(2)
Fe(1)#1-S(1)-Fe(1')#1	10.37(17)
C(7)-S(1)-Fe(1)	105.8(3)
Fe(1')#1-S(1)-Fe(1)	65.63(17)
C(6)-P(1)-C(4)	104.4(2)
C(6)-P(1)-C(5)	102.9(2)
C(4)-P(1)-C(5)	103.82(19)
C(6)-P(1)-Fe(1')	115.4(2)
C(4)-P(1)-Fe(1')	118.88(19)
C(5)-P(1)-Fe(1')	109.72(19)
C(6)-P(1)-Fe(1)	115.4(2)
C(4)-P(1)-Fe(1)	110.05(19)
C(5)-P(1)-Fe(1)	118.84(19)
Fe(1')-P(1)-Fe(1)	10.39(18)
O(1)-C(1)-Fe(1')	136(3)
O(1)#1-C(1)-Fe(1')	146(4)
O(1')#1-C(1)-Fe(1')	124(2)
O(1')-C(1)-Fe(1')	154(3)
Fe(1')-C(1)-Fe(1')#1	76.2(5)
O(1)-C(1)-Fe(1)	133(3)
O(1)#1-C(1)-Fe(1)	146(4)

O(1')#1-C(1)-Fe(1)	122(2)
O(1')-C(1)-Fe(1)	155(3)
Fe(1')#1-C(1)-Fe(1)	77.5(2)
O(2)-C(2)-Fe(1)	175.3(4)
O(2)-C(2)-Fe(1')	170.5(4)
O(3)-C(3)-Fe(1)	176.9(8)
P(1)-C(4)-H(4A)	109.4
P(1)-C(4)-H(4B)	109.5
H(4A)-C(4)-H(4B)	109.5
P(1)-C(4)-H(4C)	109.5
H(4A)-C(4)-H(4C)	109.5
H(4B)-C(4)-H(4C)	109.5
P(1)-C(5)-H(5A)	109.5
P(1)-C(5)-H(5B)	109.4
H(5A)-C(5)-H(5B)	109.5
P(1)-C(5)-H(5C)	109.4
H(5A)-C(5)-H(5C)	109.5
H(5B)-C(5)-H(5C)	109.5
P(1)-C(6)-H(6A)	109.5
P(1)-C(6)-H(6B)	109.4
H(6A)-C(6)-H(6B)	109.5
P(1)-C(6)-H(6C)	109.5
H(6A)-C(6)-H(6C)	109.5
H(6B)-C(6)-H(6C)	109.5
C(8)-C(7)-S(1)	109.8(6)
C(8)-C(7)-H(7A)	109.4
S(1)-C(7)-H(7A)	109.6
C(8)-C(7)-H(7B)	109.4
S(1)-C(7)-H(7B)	109.9
H(7A)-C(7)-H(7B)	108.7
C(8)-C(7)-H(7'A)	87.1
S(1)-C(7)-H(7'A)	88.7
C(8)-C(7)-H(7'B)	127.5
S(1)-C(7)-H(7'B)	122.3

C(8)-C(7')-S(1)	113.1(7)
C(8)-C(7')-H(7A)	122.6
S(1)-C(7')-H(7A)	124.1
C(8)-C(7')-H(7B)	89.3
S(1)-C(7')-H(7B)	93.2
H(7A)-C(7')-H(7B)	84.2
C(8)-C(7')-H(7'A)	107.4
S(1)-C(7')-H(7'A)	108.0
C(8)-C(7')-H(7'B)	110.3
S(1)-C(7')-H(7'B)	110.2
H(7'A)-C(7')-H(7'B)	107.6
C(7')-C(8)-C(10)	112.1(6)
C(7')-C(8)-C(9)	106.6(6)
C(10)-C(8)-C(9)	107.4(6)
C(10)-C(8)-C(7)	127.0(6)
C(9)-C(8)-C(7)	106.6(6)
C(8)-C(9)-H(9A)	104.6
C(8)-C(9)-H(9B)	111.2
H(9A)-C(9)-H(9B)	109.5
C(8)-C(9)-H(9C)	112.5
H(9A)-C(9)-H(9C)	109.5
H(9B)-C(9)-H(9C)	109.5
C(8)-C(10)-H(10A)	109.6
C(8)-C(10)-H(10B)	109.9
H(10A)-C(10)-H(10B)	109.5
C(8)-C(10)-H(10C)	108.9
H(10A)-C(10)-H(10C)	109.5
H(10B)-C(10)-H(10C)	109.5
F(1)-P(2)-F(2)	88.0(6)
F(1)-P(2)-F(3)	89.3(4)
F(2)-P(2)-F(3)	88.7(5)

Symmetry transformations used to generate equivalent atoms: #1 -x,y,-z+1/2

Table A-54. Anisotropic displacement parameters ($Å^2 x\ 10^3$) for IV_**2*$_{ox}$**. The anisotropic displacement factor exponent takes the form: $-2\pi^2[\ h^2\ a^{*2}U^{11} + ... + 2\ h\ k\ a^*\ b^*\ U^{12}\ ]$

	U^{11}	U^{22}	U^{33}	U^{23}	U^{13}	U^{12}
Fe(1)	25(2)	16(2)	14(2)	-1(1)	1(1)	2(1)
Fe(1')	22(2)	16(2)	14(2)	-2(1)	-1(1)	3(1)
S(1)	30(1)	14(1)	23(1)	-2(1)	3(1)	-3(1)
P(1)	23(1)	20(1)	24(1)	2(1)	1(1)	-1(1)
C(1)	28(3)	23(3)	50(4)	0	7(3)	0
O(1)	23(8)	16(5)	48(9)	-2(8)	5(8)	1(8)
O(1')	27(8)	14(5)	46(9)	-3(8)	6(7)	0(7)
C(2)	34(2)	26(2)	33(2)	-5(2)	-1(2)	13(2)
O(2)	60(2)	39(2)	33(2)	-16(1)	-3(1)	18(2)
C(3)	37(4)	19(4)	24(4)	2(3)	2(3)	2(4)
O(3)	46(4)	29(3)	41(3)	6(3)	8(3)	-10(3)
C(4)	30(2)	39(2)	27(2)	4(2)	3(2)	-6(2)
C(5)	35(2)	29(2)	37(2)	7(2)	8(2)	-7(2)
C(6)	31(2)	25(2)	41(2)	2(2)	3(2)	6(2)
C(7)	44(5)	13(3)	20(3)	-6(3)	-12(3)	-7(4)
C(7')	51(5)	12(3)	19(3)	-7(3)	-15(3)	-2(4)
C(8)	44(4)	11(3)	20(3)	-4(2)	-3(3)	-1(3)
C(9)	56(5)	16(4)	27(4)	2(3)	-1(4)	-2(4)
C(10)	36(3)	26(3)	30(3)	4(3)	5(3)	-2(3)
P(2)	110(2)	55(1)	31(1)	-15(1)	28(1)	-54(1)
F(1)	126(4)	75(5)	51(4)	-26(4)	9(3)	-45(4)
F(2)	122(4)	70(5)	44(5)	9(3)	37(4)	-29(3)
F(3)	105(5)	57(3)	59(5)	8(3)	23(4)	-32(3)
P(2A)	110(2)	55(1)	31(1)	-15(1)	28(1)	-54(1)
F(1A)	129(5)	77(6)	42(4)	-12(4)	15(4)	-58(5)
F(2A)	119(5)	80(6)	40(5)	6(4)	42(4)	-41(4)
F(3A)	123(6)	62(4)	53(5)	-13(4)	19(4)	-67(4)

Table A-55. Hydrogen coordinates (x 10^4) and isotropic displacement parameters ($Å^2$x 10^3) for **IV_2*$_{ox}$**.

	x	y	z	U(eq)
H(4A)	2533	2328	3840	49
H(4B)	2291	3112	2752	49
H(4C)	2089	3541	3860	49
H(5A)	1733	843	4812	50
H(5B)	1234	1957	4895	50
H(5C)	968	659	4352	50
H(6A)	2082	86	2937	49
H(6B)	1342	-168	2346	49
H(6C)	1806	674	1767	49
H(7A)	462	6103	4011	33
H(7B)	-244	5752	3344	33
H(7'A)	874	5876	3957	36
H(7'B)	108	6011	3801	36
H(9A)	889	7652	2757	51
H(9B)	446	7748	1568	51
H(9C)	116	7818	2612	51
H(10A)	1070	5855	1201	46
H(10B)	1457	5699	2425	46
H(10C)	1028	4570	1832	46

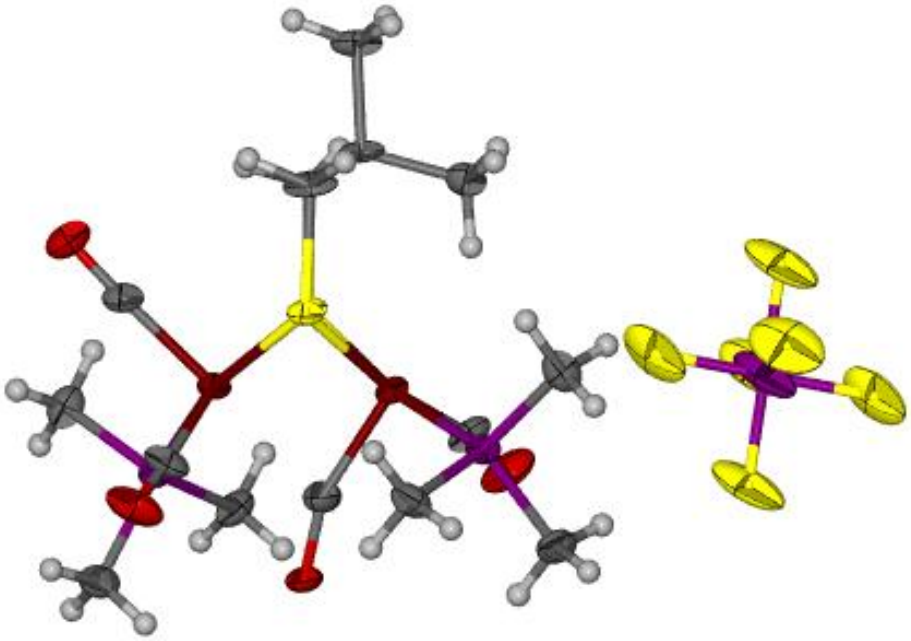

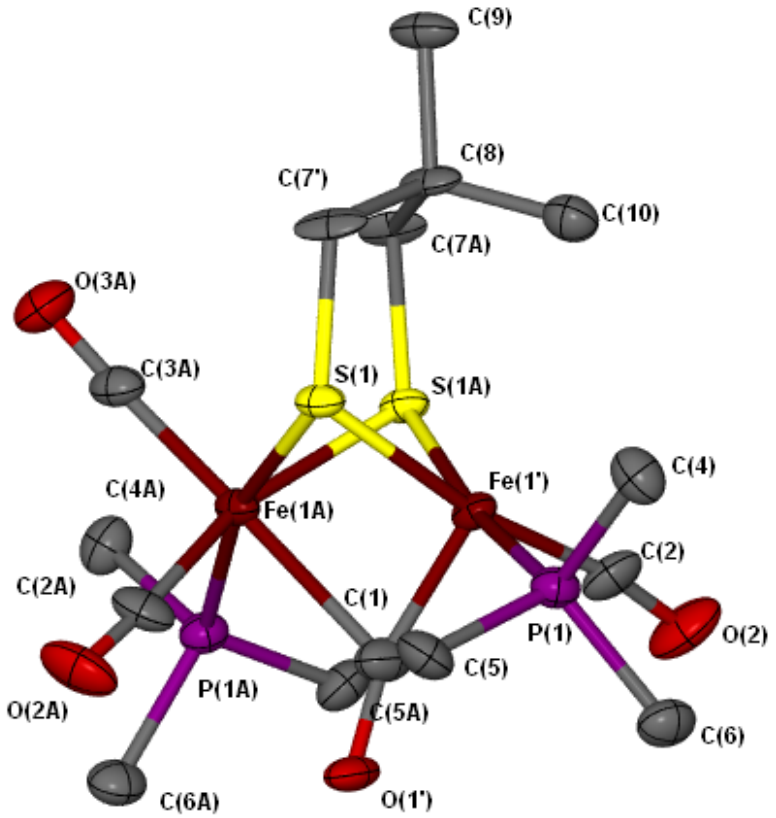
C(9)
C(8)
C(7')
C(10)
C(7A)
O(3A)
C(3A)
S(1)
S(1A)
C(4)
C(4A)
Fe(1')
Fe(1A)
C(2)
C(2A)
C(1)
P(1)
O(2)
C(5)
P(1A)
O(2A)
C(5A)
C(6)
C(6A)
O(1')

Table A-56. Crystal data and structure refinement for IV-3*:.

Identification code	(depdt)[$Fe(CO)_2P(OMe)_3$]$_2$	
Empirical formula	C17 H32 Fe2 O10 P2 S2	
Formula weight	634.19	
Temperature	110(2) K	
Wavelength	0.71073 Å	
Crystal system	Orthorhombic	
Space group	P212121	
Unit cell dimensions	a = 9.404(2) Å	α= 90°.
	b = 10.076(2) Å	β= 90°.
	c = 27.156(6) Å	γ = 90°.
Volume	2573.2(9) Å^3	
Z	4	
Density (calculated)	1.637 Mg/m^3	
Absorption coefficient	1.462 mm^{-1}	
F(000)	1312	
Crystal size	0.65 x 0.49 x 0.24 mm^3	
Theta range for data collection	1.50 to 34.97°.	
Index ranges	-15<=h<=15, -16<=k<=15, -43<=l<=43	
Reflections collected	118788	
Independent reflections	11117 [R(int) = 0.0852]	
Completeness to theta = 34.97°	98.5 %	
Absorption correction	Semi-empirical from equivalents	
Max. and min. transmission	0.7205 and 0.4500	
Refinement method	Full-matrix least-squares on F^2	
Data / restraints / parameters	11117 / 0 / 306	
Goodness-of-fit on F^2	1.025	
Final R indices [I>2sigma(I)]	R1 = 0.0233, wR2 = 0.0578	
R indices (all data)	R1 = 0.0267, wR2 = 0.0592	
Absolute structure parameter	-0.003(5)	
Largest diff. peak and hole	0.570 and -0.456 e.Å^{-3}	

Table A-57. Atomic coordinates (x 10^4) and equivalent isotropic displacement parameters ($Å^2$x 10^3) for IV-3*. U(eq) is defined as one third of the trace of the orthogonalized U^{ij} tensor.

	x	y	z	U(eq)
Fe(1)	2850(1)	385(1)	885(1)	13(1)
Fe(2)	2496(1)	-290(1)	1771(1)	13(1)
S(3)	4622(1)	319(1)	1451(1)	13(1)
P(4)	3024(1)	2521(1)	879(1)	15(1)
S(5)	2504(1)	-1743(1)	1131(1)	14(1)
P(6)	3018(1)	-1592(1)	2375(1)	14(1)
O(3)	2228(1)	-1181(1)	2876(1)	19(1)
C(5)	2445(1)	1149(1)	2149(1)	17(1)
O(6)	4643(1)	-1790(1)	2533(1)	17(1)
C(7)	4076(1)	-2812(1)	1174(1)	16(1)
O(10)	3617(1)	236(1)	-158(1)	30(1)
C(11)	622(1)	-405(1)	1814(1)	19(1)
C(12)	5582(1)	-2273(1)	1084(1)	15(1)
C(13)	2517(2)	-1943(1)	3317(1)	24(1)
C(15)	999(1)	495(1)	765(1)	20(1)
C(16)	5410(1)	-627(1)	2702(1)	21(1)
C(17)	8167(2)	-3205(2)	1189(1)	28(1)
C(19)	6580(1)	-3430(1)	1245(1)	20(1)
C(21)	5892(1)	-1072(1)	1415(1)	16(1)
C(22)	5360(2)	-2863(2)	155(1)	30(1)
C(23)	3378(1)	277(1)	258(1)	19(1)
C(26)	5860(1)	-1888(1)	546(1)	18(1)
C(28)	1293(2)	-3554(2)	2181(1)	26(1)
O(41)	2707(1)	-3152(1)	2324(1)	19(1)
O(1)	2380(1)	3414(1)	1315(1)	21(1)
O(2)	4545(1)	3226(1)	898(1)	18(1)
O(4)	2286(1)	3094(1)	392(1)	23(1)
O(5)	-598(1)	-435(1)	1847(1)	30(1)
O(8)	2340(1)	2036(1)	2409(1)	25(1)

O(7)	-197(1)	563(1)	684(1)	29(1)
C(8)	2308(2)	4505(1)	290(1)	30(1)
C(9)	5621(2)	2798(2)	554(1)	24(1)
C(10)	873(2)	3339(2)	1400(1)	28(1)

Table A-58. Bond lengths [Å] and angles [°] for IV-3*.

Fe(1)-C(15)	1.7737(14)
Fe(1)-C(23)	1.7763(12)
Fe(1)-P(4)	2.1581(6)
Fe(1)-S(3)	2.2688(5)
Fe(1)-S(5)	2.2693(5)
Fe(1)-Fe(2)	2.5226(5)
Fe(2)-C(11)	1.7701(13)
Fe(2)-C(5)	1.7783(12)
Fe(2)-P(6)	2.1573(4)
Fe(2)-S(3)	2.2638(5)
Fe(2)-S(5)	2.2718(5)
S(3)-C(21)	1.8433(12)
P(4)-O(2)	1.5980(10)
P(4)-O(4)	1.6028(10)
P(4)-O(1)	1.6053(10)
S(5)-C(7)	1.8322(12)
P(6)-O(6)	1.6002(10)
P(6)-O(3)	1.6046(9)
P(6)-O(41)	1.6049(10)
O(3)-C(13)	1.4472(15)
C(5)-O(8)	1.1431(15)
O(6)-C(16)	1.4507(15)
C(7)-C(12)	1.5363(17)
O(10)-C(23)	1.1520(15)
C(11)-O(5)	1.1511(16)
C(12)-C(21)	1.5352(16)
C(12)-C(26)	1.5359(16)
C(12)-C(19)	1.5588(17)
C(15)-O(7)	1.1481(17)
C(17)-C(19)	1.517(2)
C(22)-C(26)	1.5195(19)
C(28)-O(41)	1.4432(16)

O(1)-C(10)	1.4376(17)
O(2)-C(9)	1.4428(16)
O(4)-C(8)	1.4491(16)

C(15)-Fe(1)-C(23)	95.89(6)
C(15)-Fe(1)-P(4)	90.63(4)
C(23)-Fe(1)-P(4)	91.92(4)
C(15)-Fe(1)-S(3)	147.85(4)
C(23)-Fe(1)-S(3)	116.26(4)
P(4)-Fe(1)-S(3)	88.759(12)
C(15)-Fe(1)-S(5)	88.43(4)
C(23)-Fe(1)-S(5)	105.32(4)
P(4)-Fe(1)-S(5)	162.742(14)
S(3)-Fe(1)-S(5)	82.958(12)
C(15)-Fe(1)-Fe(2)	93.58(4)
C(23)-Fe(1)-Fe(2)	159.10(4)
P(4)-Fe(1)-Fe(2)	106.594(12)
S(3)-Fe(1)-Fe(2)	56.087(14)
S(5)-Fe(1)-Fe(2)	56.302(8)
C(11)-Fe(2)-C(5)	89.30(6)
C(11)-Fe(2)-P(6)	97.83(4)
C(5)-Fe(2)-P(6)	93.59(4)
C(11)-Fe(2)-S(3)	157.26(4)
C(5)-Fe(2)-S(3)	91.42(4)
P(6)-Fe(2)-S(3)	104.813(16)
C(11)-Fe(2)-S(5)	90.68(4)
C(5)-Fe(2)-S(5)	165.37(4)
P(6)-Fe(2)-S(5)	100.91(2)
S(3)-Fe(2)-S(5)	83.016(14)
C(11)-Fe(2)-Fe(1)	102.24(4)
C(5)-Fe(2)-Fe(1)	109.56(4)
P(6)-Fe(2)-Fe(1)	149.277(13)
S(3)-Fe(2)-Fe(1)	56.279(9)
S(5)-Fe(2)-Fe(1)	56.209(15)

C(21)-S(3)-Fe(2)	112.72(4)
C(21)-S(3)-Fe(1)	117.54(4)
Fe(2)-S(3)-Fe(1)	67.634(17)
O(2)-P(4)-O(4)	104.71(5)
O(2)-P(4)-O(1)	93.71(5)
O(4)-P(4)-O(1)	104.11(5)
O(2)-P(4)-Fe(1)	120.74(4)
O(4)-P(4)-Fe(1)	109.38(4)
O(1)-P(4)-Fe(1)	121.69(4)
C(7)-S(5)-Fe(1)	117.30(4)
C(7)-S(5)-Fe(2)	109.44(4)
Fe(1)-S(5)-Fe(2)	67.490(16)
O(6)-P(6)-O(3)	104.28(5)
O(6)-P(6)-O(41)	94.32(5)
O(3)-P(6)-O(41)	103.97(5)
O(6)-P(6)-Fe(2)	119.82(4)
O(3)-P(6)-Fe(2)	112.49(4)
O(41)-P(6)-Fe(2)	119.25(4)
C(13)-O(3)-P(6)	118.48(8)
O(8)-C(5)-Fe(2)	175.53(12)
C(16)-O(6)-P(6)	117.32(8)
C(12)-C(7)-S(5)	121.73(8)
O(5)-C(11)-Fe(2)	177.64(12)
C(21)-C(12)-C(26)	109.06(10)
C(21)-C(12)-C(7)	111.15(9)
C(26)-C(12)-C(7)	113.37(10)
C(21)-C(12)-C(19)	108.17(10)
C(26)-C(12)-C(19)	110.63(10)
C(7)-C(12)-C(19)	104.28(9)
O(7)-C(15)-Fe(1)	179.46(13)
C(17)-C(19)-C(12)	116.94(11)
C(12)-C(21)-S(3)	120.47(8)
O(10)-C(23)-Fe(1)	174.81(12)
C(22)-C(26)-C(12)	116.64(11)

C(28)-O(41)-P(6)	117.78(9)
C(10)-O(1)-P(4)	117.39(9)
C(9)-O(2)-P(4)	118.31(8)
C(8)-O(4)-P(4)	120.37(8)

Symmetry transformations used to generate equivalent atoms:

Table A-59. Anisotropic displacement parameters ($Å^2 x\ 10^3$)for IV-3*. The anisotropic displacement factor exponent takes the form: $-2\pi^2[\ h^2 a^{*2} U^{11} + ... + 2\ h\ k\ a^*\ b^*\ U^{12}\ ]$

	U^{11}	U^{22}	U^{33}	U^{23}	U^{13}	U^{12}
Fe(1)	15(1)	13(1)	11(1)	0(1)	-2(1)	0(1)
Fe(2)	13(1)	14(1)	11(1)	-1(1)	-1(1)	0(1)
S(3)	14(1)	13(1)	13(1)	-1(1)	-2(1)	-1(1)
P(4)	16(1)	14(1)	14(1)	0(1)	-3(1)	0(1)
S(5)	15(1)	14(1)	13(1)	-1(1)	-1(1)	-1(1)
P(6)	14(1)	15(1)	12(1)	-1(1)	0(1)	1(1)
O(3)	21(1)	23(1)	12(1)	1(1)	1(1)	4(1)
C(5)	15(1)	18(1)	17(1)	-1(1)	0(1)	0(1)
O(6)	14(1)	18(1)	18(1)	-1(1)	-2(1)	1(1)
C(7)	18(1)	13(1)	15(1)	-1(1)	2(1)	0(1)
O(10)	38(1)	37(1)	14(1)	-2(1)	0(1)	8(1)
C(11)	20(1)	20(1)	16(1)	-5(1)	-2(1)	1(1)
C(12)	16(1)	15(1)	14(1)	0(1)	1(1)	1(1)
C(13)	24(1)	33(1)	15(1)	4(1)	2(1)	4(1)
C(15)	24(1)	17(1)	18(1)	0(1)	-4(1)	-1(1)
C(16)	19(1)	22(1)	21(1)	-4(1)	-6(1)	0(1)
C(17)	22(1)	25(1)	36(1)	-3(1)	-2(1)	5(1)
C(19)	21(1)	17(1)	22(1)	1(1)	-1(1)	4(1)
C(21)	15(1)	16(1)	18(1)	-2(1)	-2(1)	2(1)
C(22)	45(1)	29(1)	17(1)	-5(1)	3(1)	-1(1)
C(23)	22(1)	19(1)	15(1)	0(1)	-3(1)	3(1)
C(26)	19(1)	20(1)	14(1)	2(1)	3(1)	2(1)
C(28)	25(1)	24(1)	27(1)	3(1)	-2(1)	-10(1)
O(41)	21(1)	16(1)	20(1)	1(1)	-1(1)	-2(1)
O(1)	20(1)	19(1)	24(1)	-5(1)	0(1)	1(1)
O(2)	18(1)	19(1)	17(1)	0(1)	-1(1)	-3(1)
O(4)	28(1)	16(1)	25(1)	5(1)	-12(1)	-2(1)
O(5)	17(1)	38(1)	33(1)	-12(1)	0(1)	0(1)
O(8)	26(1)	22(1)	27(1)	-9(1)	2(1)	-1(1)

O(7)	22(1)	33(1)	34(1)	0(1)	-9(1)	0(1)
C(8)	38(1)	18(1)	36(1)	9(1)	-16(1)	-3(1)
C(9)	23(1)	30(1)	21(1)	2(1)	5(1)	-4(1)
C(10)	23(1)	25(1)	35(1)	-5(1)	6(1)	5(1)

Table A-60. Hydrogen coordinates (x 10^4) and isotropic displacement parameters ($Å^2$x 10^3) for IV-3*.

	x	y	z	U(eq)
H(7A)	4071	-3206	1508	19
H(7B)	3931	-3551	939	19
H(13A)	2015	-2794	3299	36
H(13B)	2189	-1448	3606	36
H(13C)	3542	-2103	3344	36
H(16A)	5078	156	2521	31
H(16B)	6430	-750	2644	31
H(16C)	5240	-500	3055	31
H(17A)	8406	-3131	839	41
H(17B)	8684	-3955	1333	41
H(17C)	8437	-2385	1359	41
H(19A)	6384	-3632	1595	24
H(19B)	6321	-4226	1051	24
H(21A)	6816	-699	1310	20
H(21B)	6025	-1412	1754	20
H(22A)	5702	-3755	237	45
H(22B)	5736	-2597	-166	45
H(22C)	4318	-2865	144	45
H(26A)	5394	-1023	483	21
H(26B)	6896	-1756	504	21
H(28A)	1139	-3337	1833	38
H(28B)	592	-3085	2383	38
H(28C)	1188	-4513	2229	38
H(8A)	1928	4990	573	45
H(8B)	1722	4690	-1	45
H(8C)	3288	4789	227	45
H(9A)	5966	1916	649	37
H(9B)	6414	3429	558	37

H(9C)	5214	2758	223	37
H(10A)	367	3722	1118	42
H(10B)	633	3834	1699	42
H(10C)	593	2408	1440	42

Table A-61. Torsion angles [°] for IV-3*.

C(15)-Fe(1)-Fe(2)-C(11)	3.22(6)
C(23)-Fe(1)-Fe(2)-C(11)	-113.64(13)
P(4)-Fe(1)-Fe(2)-C(11)	94.95(4)
S(3)-Fe(1)-Fe(2)-C(11)	171.79(4)
S(5)-Fe(1)-Fe(2)-C(11)	-82.50(4)
C(15)-Fe(1)-Fe(2)-C(5)	-90.43(6)
C(23)-Fe(1)-Fe(2)-C(5)	152.70(13)
P(4)-Fe(1)-Fe(2)-C(5)	1.29(4)
S(3)-Fe(1)-Fe(2)-C(5)	78.14(4)
S(5)-Fe(1)-Fe(2)-C(5)	-176.15(4)
C(15)-Fe(1)-Fe(2)-P(6)	132.86(5)
C(23)-Fe(1)-Fe(2)-P(6)	15.99(12)
P(4)-Fe(1)-Fe(2)-P(6)	-135.42(2)
S(3)-Fe(1)-Fe(2)-P(6)	-58.57(3)
S(5)-Fe(1)-Fe(2)-P(6)	47.14(3)
C(15)-Fe(1)-Fe(2)-S(3)	-168.57(4)
C(23)-Fe(1)-Fe(2)-S(3)	74.57(12)
P(4)-Fe(1)-Fe(2)-S(3)	-76.846(14)
S(5)-Fe(1)-Fe(2)-S(3)	105.710(14)
C(15)-Fe(1)-Fe(2)-S(5)	85.72(4)
C(23)-Fe(1)-Fe(2)-S(5)	-31.14(12)
P(4)-Fe(1)-Fe(2)-S(5)	177.444(15)
S(3)-Fe(1)-Fe(2)-S(5)	-105.710(14)
C(11)-Fe(2)-S(3)-C(21)	-132.86(11)
C(5)-Fe(2)-S(3)-C(21)	135.58(6)
P(6)-Fe(2)-S(3)-C(21)	41.49(4)
S(5)-Fe(2)-S(3)-C(21)	-58.00(4)
Fe(1)-Fe(2)-S(3)-C(21)	-111.70(4)
C(11)-Fe(2)-S(3)-Fe(1)	-21.15(11)
C(5)-Fe(2)-S(3)-Fe(1)	-112.72(4)
P(6)-Fe(2)-S(3)-Fe(1)	153.197(13)
S(5)-Fe(2)-S(3)-Fe(1)	53.707(14)

C(15)-Fe(1)-S(3)-C(21)	126.68(9)
C(23)-Fe(1)-S(3)-C(21)	-52.59(7)
P(4)-Fe(1)-S(3)-C(21)	-144.12(5)
S(5)-Fe(1)-S(3)-C(21)	51.06(5)
Fe(2)-Fe(1)-S(3)-C(21)	104.86(5)
C(15)-Fe(1)-S(3)-Fe(2)	21.82(8)
C(23)-Fe(1)-S(3)-Fe(2)	-157.45(5)
P(4)-Fe(1)-S(3)-Fe(2)	111.025(12)
S(5)-Fe(1)-S(3)-Fe(2)	-53.802(10)
C(15)-Fe(1)-P(4)-O(2)	-171.80(6)
C(23)-Fe(1)-P(4)-O(2)	-75.89(6)
S(3)-Fe(1)-P(4)-O(2)	40.35(4)
S(5)-Fe(1)-P(4)-O(2)	101.46(6)
Fe(2)-Fe(1)-P(4)-O(2)	94.28(4)
C(15)-Fe(1)-P(4)-O(4)	-50.30(6)
C(23)-Fe(1)-P(4)-O(4)	45.61(6)
S(3)-Fe(1)-P(4)-O(4)	161.85(4)
S(5)-Fe(1)-P(4)-O(4)	-137.04(6)
Fe(2)-Fe(1)-P(4)-O(4)	-144.22(4)
C(15)-Fe(1)-P(4)-O(1)	71.10(6)
C(23)-Fe(1)-P(4)-O(1)	167.01(6)
S(3)-Fe(1)-P(4)-O(1)	-76.75(5)
S(5)-Fe(1)-P(4)-O(1)	-15.64(7)
Fe(2)-Fe(1)-P(4)-O(1)	-22.82(5)
C(15)-Fe(1)-S(5)-C(7)	163.60(6)
C(23)-Fe(1)-S(5)-C(7)	67.92(6)
P(4)-Fe(1)-S(5)-C(7)	-109.33(6)
S(3)-Fe(1)-S(5)-C(7)	-47.44(5)
Fe(2)-Fe(1)-S(5)-C(7)	-101.05(4)
C(15)-Fe(1)-S(5)-Fe(2)	-95.35(4)
C(23)-Fe(1)-S(5)-Fe(2)	168.97(4)
P(4)-Fe(1)-S(5)-Fe(2)	-8.28(5)
S(3)-Fe(1)-S(5)-Fe(2)	53.606(13)
C(11)-Fe(2)-S(5)-C(7)	-143.34(6)

C(5)-Fe(2)-S(5)-C(7)	126.83(17)
P(6)-Fe(2)-S(5)-C(7)	-45.24(4)
S(3)-Fe(2)-S(5)-C(7)	58.57(4)
Fe(1)-Fe(2)-S(5)-C(7)	112.34(4)
C(11)-Fe(2)-S(5)-Fe(1)	104.31(4)
C(5)-Fe(2)-S(5)-Fe(1)	14.49(17)
P(6)-Fe(2)-S(5)-Fe(1)	-157.582(13)
S(3)-Fe(2)-S(5)-Fe(1)	-53.771(10)
C(11)-Fe(2)-P(6)-O(6)	-175.91(6)
C(5)-Fe(2)-P(6)-O(6)	-86.13(6)
S(3)-Fe(2)-P(6)-O(6)	6.30(4)
S(5)-Fe(2)-P(6)-O(6)	91.87(4)
Fe(1)-Fe(2)-P(6)-O(6)	53.53(5)
C(11)-Fe(2)-P(6)-O(3)	-52.88(6)
C(5)-Fe(2)-P(6)-O(3)	36.91(6)
S(3)-Fe(2)-P(6)-O(3)	129.33(4)
S(5)-Fe(2)-P(6)-O(3)	-145.10(4)
Fe(1)-Fe(2)-P(6)-O(3)	176.56(4)
C(11)-Fe(2)-P(6)-O(41)	69.22(6)
C(5)-Fe(2)-P(6)-O(41)	159.00(6)
S(3)-Fe(2)-P(6)-O(41)	-108.58(4)
S(5)-Fe(2)-P(6)-O(41)	-23.00(4)
Fe(1)-Fe(2)-P(6)-O(41)	-61.34(5)
O(6)-P(6)-O(3)-C(13)	-46.62(11)
O(41)-P(6)-O(3)-C(13)	51.63(11)
Fe(2)-P(6)-O(3)-C(13)	-177.98(9)
C(11)-Fe(2)-C(5)-O(8)	36.1(15)
P(6)-Fe(2)-C(5)-O(8)	-61.7(15)
S(3)-Fe(2)-C(5)-O(8)	-166.6(15)
S(5)-Fe(2)-C(5)-O(8)	126.1(14)
Fe(1)-Fe(2)-C(5)-O(8)	138.9(15)
O(3)-P(6)-O(6)-C(16)	-65.30(9)
O(41)-P(6)-O(6)-C(16)	-170.91(9)
Fe(2)-P(6)-O(6)-C(16)	61.63(9)

Fe(1)-S(5)-C(7)-C(12)	4.40(11)
Fe(2)-S(5)-C(7)-C(12)	-69.66(10)
C(5)-Fe(2)-C(11)-O(5)	21(3)
P(6)-Fe(2)-C(11)-O(5)	114(3)
S(3)-Fe(2)-C(11)-O(5)	-71(3)
S(5)-Fe(2)-C(11)-O(5)	-145(3)
Fe(1)-Fe(2)-C(11)-O(5)	-89(3)
S(5)-C(7)-C(12)-C(21)	54.29(13)
S(5)-C(7)-C(12)-C(26)	-68.98(12)
S(5)-C(7)-C(12)-C(19)	170.61(8)
C(23)-Fe(1)-C(15)-O(7)	14(21)
P(4)-Fe(1)-C(15)-O(7)	106(54)
S(3)-Fe(1)-C(15)-O(7)	-166(100)
S(5)-Fe(1)-C(15)-O(7)	-92(21)
Fe(2)-Fe(1)-C(15)-O(7)	-148(21)
C(21)-C(12)-C(19)-C(17)	-62.82(14)
C(26)-C(12)-C(19)-C(17)	56.57(15)
C(7)-C(12)-C(19)-C(17)	178.79(11)
C(26)-C(12)-C(21)-S(3)	76.02(12)
C(7)-C(12)-C(21)-S(3)	-49.69(13)
C(19)-C(12)-C(21)-S(3)	-163.60(8)
Fe(2)-S(3)-C(21)-C(12)	63.69(10)
Fe(1)-S(3)-C(21)-C(12)	-12.01(11)
C(15)-Fe(1)-C(23)-O(10)	13.1(14)
P(4)-Fe(1)-C(23)-O(10)	-77.7(14)
S(3)-Fe(1)-C(23)-O(10)	-167.3(14)
S(5)-Fe(1)-C(23)-O(10)	103.1(14)
Fe(2)-Fe(1)-C(23)-O(10)	129.6(14)
C(21)-C(12)-C(26)-C(22)	-169.29(11)
C(7)-C(12)-C(26)-C(22)	-44.87(15)
C(19)-C(12)-C(26)-C(22)	71.86(14)
O(6)-P(6)-O(41)-C(28)	179.80(9)
O(3)-P(6)-O(41)-C(28)	73.91(10)
Fe(2)-P(6)-O(41)-C(28)	-52.32(10)

O(2)-P(4)-O(1)-C(10)	169.40(10)
O(4)-P(4)-O(1)-C(10)	63.22(11)
Fe(1)-P(4)-O(1)-C(10)	-60.66(11)
O(4)-P(4)-O(2)-C(9)	-73.39(10)
O(1)-P(4)-O(2)-C(9)	-179.03(9)
Fe(1)-P(4)-O(2)-C(9)	50.36(10)
O(2)-P(4)-O(4)-C(8)	-46.77(12)
O(1)-P(4)-O(4)-C(8)	50.99(12)
Fe(1)-P(4)-O(4)-C(8)	-177.51(10)

Symmetry transformations used to generate equivalent atoms:

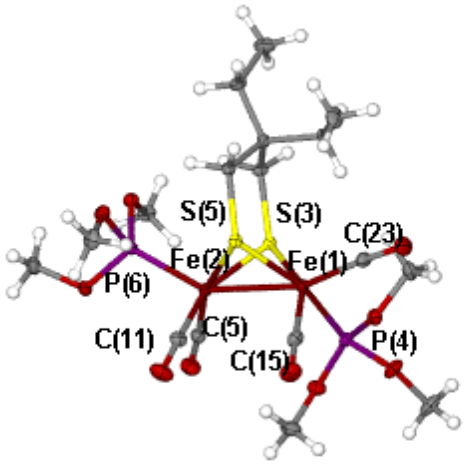

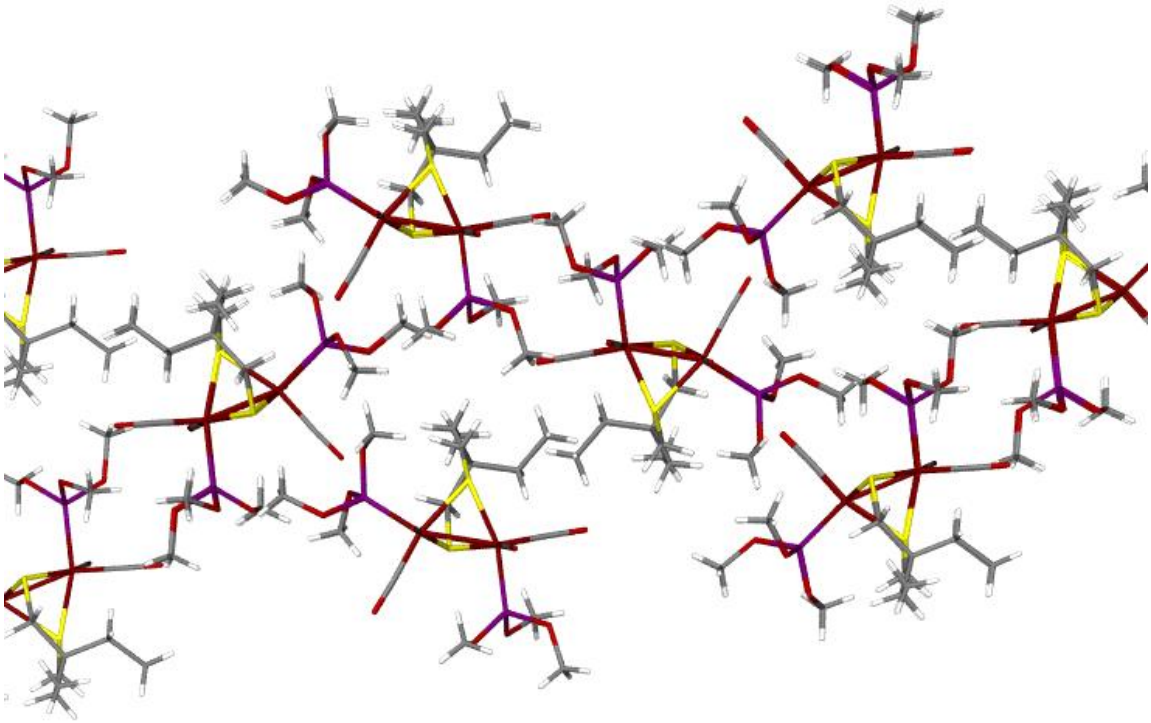

Table A-62 Crystal data and structure refinement for V-Et_4N^+1.

Identification code	md5	
Empirical formula	C22 H24 Fe2 N2 O9 S3	
Formula weight	668.31	
Temperature	110(2) K	
Wavelength	0.71073 Å	
Crystal system	Monoclinic	
Space group	P2(1)/c	
Unit cell dimensions	a = 22.1279(2) Å	α= 90°.
	b = 7.6853(5) Å	β= 99.752(2)°.
	c = 16.7425(10) Å	γ = 90°.
Volume	2806.1(2) $Å^3$	
Z	4	
Density (calculated)	1.582 Mg/m^3	
Absorption coefficient	1.308 mm^{-1}	
F(000)	1368	
Crystal size	0.10 x 0.01 x 0.01 mm^3	
Theta range for data collection	2.49 to 25.00°.	
Index ranges	-26<=h<=25, 0<=k<=9, 0<=l<=19	
Reflections collected	4854	
Independent reflections	4889 [R(int) = 0.0000]	
Completeness to theta = 25.00°	99.2 %	
Absorption correction	Semi-empirical from equivalents	
Max. and min. transmission	0.9870 and 0.8803	
Refinement method	Full-matrix least-squares on F^2	
Data / restraints / parameters	4889 / 0 / 345	
Goodness-of-fit on F^2	1.064	
Final R indices [I>2sigma(I)]	R1 = 0.0408, wR2 = 0.0888	
R indices (all data)	R1 = 0.0575, wR2 = 0.0941	
Extinction coefficient	0.0010(5)	
Largest diff. peak and hole	0.537 and -0.366 $e.Å^{-3}$	

Table A-63. Atomic coordinates (x 10^4) and equivalent isotropic displacement parameters ($Å^2$x 10^3) for V-Et_4N^+1. U(eq) is defined as one third of the trace of the orthogonalized U^{ij} tensor.

	x	y	z	U(eq)
Fe(1)	767(1)	2831(1)	3813(1)	19(1)
Fe(2)	1243(1)	-37(1)	4252(1)	18(1)
S(1)	1788(1)	2428(2)	4114(1)	21(1)
S(2)	789(1)	532(1)	2968(1)	19(1)
S(3)	3785(1)	-4838(2)	3318(1)	22(1)
O(1)	-546(2)	2253(4)	3789(2)	30(1)
O(2)	881(2)	4691(4)	5355(2)	39(1)
O(3)	792(2)	5931(5)	2798(2)	37(1)
O(4)	103(2)	-1920(5)	4326(2)	34(1)
O(5)	1534(2)	511(5)	6014(2)	36(1)
O(6)	2026(2)	-3137(4)	4235(2)	36(1)
O(7)	3470(2)	-6314(4)	3599(2)	41(1)
O(8)	4274(1)	-4181(4)	3917(2)	28(1)
O(9)	3976(2)	-5133(5)	2552(2)	44(1)
N(1)	1984(2)	1028(5)	2640(2)	21(1)
C(1)	-45(2)	2474(6)	3769(3)	23(1)
C(2)	829(2)	3961(6)	4747(3)	24(1)
C(3)	758(2)	4708(6)	3159(3)	23(1)
C(4)	558(2)	-1200(6)	4315(3)	23(1)
C(5)	1419(2)	275(6)	5327(3)	26(1)
C(6)	1742(2)	-1907(6)	4207(3)	25(1)
C(7)	2082(2)	2577(6)	3139(3)	21(1)
C(8)	1357(2)	781(6)	2273(3)	24(1)
C(9)	2391(2)	-396(6)	2833(3)	19(1)
C(10)	2885(2)	-290(6)	3464(3)	19(1)
C(11)	3305(2)	-1653(6)	3608(3)	19(1)
C(12)	3240(2)	-3127(6)	3145(3)	18(1)
C(13)	2748(2)	-3221(6)	2511(3)	21(1)
C(14)	2326(2)	-1889(6)	2351(3)	22(1)

N(1E)	3962(2)	795(5)	1198(2)	22(1)
C(1E)	3904(2)	553(7)	2086(3)	26(1)
C(2E)	4490(2)	-38(8)	2630(3)	43(2)
C(3E)	4228(2)	-799(6)	855(4)	34(1)
C(4E)	3881(3)	-2495(7)	917(4)	44(2)
C(5E)	4391(2)	2305(6)	1137(3)	22(1)
C(6E)	4431(3)	2887(7)	285(3)	36(1)
C(7E)	3338(2)	1138(7)	720(3)	28(1)
C(8E)	3030(3)	2781(7)	975(4)	46(2)

Table A-64. Bond lengths [Å] and angles [°] for V-Et_4N^+1.

Fe(1)-C(2)	1.773(5)
Fe(1)-C(1)	1.807(5)
Fe(1)-C(3)	1.809(5)
Fe(1)-S(1)	2.2508(13)
Fe(1)-S(2)	2.2691(13)
Fe(1)-Fe(2)	2.4986(9)
Fe(2)-C(4)	1.778(5)
Fe(2)-C(5)	1.793(6)
Fe(2)-C(6)	1.821(5)
Fe(2)-S(2)	2.2565(13)
Fe(2)-S(1)	2.2778(13)
S(1)-C(7)	1.860(5)
S(2)-C(8)	1.861(5)
S(3)-O(9)	1.435(4)
S(3)-O(8)	1.436(3)
S(3)-O(7)	1.450(4)
S(3)-C(12)	1.774(5)
O(1)-C(1)	1.128(5)
O(2)-C(2)	1.151(5)
O(3)-C(3)	1.127(5)
O(4)-C(4)	1.152(5)
O(5)-C(5)	1.149(6)
O(6)-C(6)	1.132(5)
N(1)-C(9)	1.420(6)
N(1)-C(8)	1.433(5)
N(1)-C(7)	1.449(6)
C(9)-C(10)	1.388(6)
C(9)-C(14)	1.396(6)
C(10)-C(11)	1.394(6)
C(11)-C(12)	1.367(6)
C(12)-C(13)	1.387(6)
C(13)-C(14)	1.381(6)

N(1E)-C(7E)	1.498(6)
N(1E)-C(5E)	1.514(6)
N(1E)-C(3E)	1.513(6)
N(1E)-C(1E)	1.525(6)
C(1E)-C(2E)	1.523(7)
C(3E)-C(4E)	1.526(7)
C(5E)-C(6E)	1.512(7)
C(7E)-C(8E)	1.530(7)

C(2)-Fe(1)-C(1)	92.2(2)
C(2)-Fe(1)-C(3)	97.7(2)
C(1)-Fe(1)-C(3)	100.8(2)
C(2)-Fe(1)-S(1)	86.87(17)
C(1)-Fe(1)-S(1)	160.33(15)
C(3)-Fe(1)-S(1)	98.76(16)
C(2)-Fe(1)-S(2)	157.60(15)
C(1)-Fe(1)-S(2)	88.99(16)
C(3)-Fe(1)-S(2)	104.06(15)
S(1)-Fe(1)-S(2)	84.60(5)
C(2)-Fe(1)-Fe(2)	101.94(15)
C(1)-Fe(1)-Fe(2)	104.17(15)
C(3)-Fe(1)-Fe(2)	147.36(16)
S(1)-Fe(1)-Fe(2)	57.03(4)
S(2)-Fe(1)-Fe(2)	56.25(4)
C(4)-Fe(2)-C(5)	92.8(2)
C(4)-Fe(2)-C(6)	97.7(2)
C(5)-Fe(2)-C(6)	96.7(2)
C(4)-Fe(2)-S(2)	84.72(15)
C(5)-Fe(2)-S(2)	156.51(16)
C(6)-Fe(2)-S(2)	106.81(17)
C(4)-Fe(2)-S(1)	153.56(16)
C(5)-Fe(2)-S(1)	87.84(15)
C(6)-Fe(2)-S(1)	108.48(14)
S(2)-Fe(2)-S(1)	84.26(5)

C(4)-Fe(2)-Fe(1)	98.07(15)
C(5)-Fe(2)-Fe(1)	100.76(15)
C(6)-Fe(2)-Fe(1)	155.80(16)
S(2)-Fe(2)-Fe(1)	56.73(4)
S(1)-Fe(2)-Fe(1)	56.00(3)
C(7)-S(1)-Fe(1)	106.41(15)
C(7)-S(1)-Fe(2)	114.23(16)
Fe(1)-S(1)-Fe(2)	66.97(4)
C(8)-S(2)-Fe(2)	112.13(15)
C(8)-S(2)-Fe(1)	113.43(16)
Fe(2)-S(2)-Fe(1)	67.02(4)
O(9)-S(3)-O(8)	112.2(2)
O(9)-S(3)-O(7)	113.3(2)
O(8)-S(3)-O(7)	113.3(2)
O(9)-S(3)-C(12)	105.4(2)
O(8)-S(3)-C(12)	105.4(2)
O(7)-S(3)-C(12)	106.5(2)
C(9)-N(1)-C(8)	121.8(4)
C(9)-N(1)-C(7)	118.4(4)
C(8)-N(1)-C(7)	113.3(4)
O(1)-C(1)-Fe(1)	176.0(5)
O(2)-C(2)-Fe(1)	178.7(5)
O(3)-C(3)-Fe(1)	174.3(4)
O(4)-C(4)-Fe(2)	177.1(4)
O(5)-C(5)-Fe(2)	178.6(4)
O(6)-C(6)-Fe(2)	173.5(4)
N(1)-C(7)-S(1)	114.4(3)
N(1)-C(8)-S(2)	116.9(3)
C(10)-C(9)-C(14)	118.6(4)
C(10)-C(9)-N(1)	121.0(4)
C(14)-C(9)-N(1)	120.2(4)
C(9)-C(10)-C(11)	120.2(4)
C(12)-C(11)-C(10)	121.5(4)
C(11)-C(12)-C(13)	118.0(4)

C(11)-C(12)-S(3)	121.2(4)
C(13)-C(12)-S(3)	120.7(4)
C(14)-C(13)-C(12)	121.8(4)
C(13)-C(14)-C(9)	119.8(4)
C(7E)-N(1E)-C(5E)	111.1(4)
C(7E)-N(1E)-C(3E)	108.8(4)
C(5E)-N(1E)-C(3E)	107.9(4)
C(7E)-N(1E)-C(1E)	108.6(4)
C(5E)-N(1E)-C(1E)	108.4(3)
C(3E)-N(1E)-C(1E)	112.0(4)
C(2E)-C(1E)-N(1E)	114.6(4)
N(1E)-C(3E)-C(4E)	115.6(4)
C(6E)-C(5E)-N(1E)	115.3(4)
N(1E)-C(7E)-C(8E)	114.3(4)

Symmetry transformations used to generate equivalent atoms:

Table A-65. Anisotropic displacement parameters ($Å^2 x\ 10^3$) for V-Et_4N^+1. The anisotropic displacement factor exponent takes the form: $-2\pi^2[\ h^2 a^{*2} U^{11} + ... + 2\ h\ k\ a^*\ b^*\ U^{12}\ ]$

	U^{11}	U^{22}	U^{33}	U^{23}	U^{13}	U^{12}
Fe(1)	23(1)	16(1)	18(1)	-2(1)	2(1)	2(1)
Fe(2)	21(1)	15(1)	18(1)	1(1)	2(1)	0(1)
S(1)	22(1)	17(1)	22(1)	0(1)	0(1)	-1(1)
S(2)	19(1)	20(1)	18(1)	-2(1)	1(1)	0(1)
S(3)	22(1)	18(1)	25(1)	0(1)	4(1)	0(1)
O(1)	25(2)	36(2)	29(2)	-8(2)	9(2)	4(2)
O(2)	62(3)	27(2)	28(2)	-6(2)	4(2)	7(2)
O(3)	42(2)	28(2)	36(2)	10(2)	-1(2)	2(2)
O(4)	29(2)	42(2)	33(2)	7(2)	8(2)	-9(2)
O(5)	47(2)	44(2)	16(2)	1(2)	-1(2)	-7(2)
O(6)	34(2)	20(2)	55(3)	7(2)	15(2)	6(2)
O(7)	27(2)	26(2)	67(3)	15(2)	0(2)	-7(2)
O(8)	21(2)	25(2)	36(2)	-3(2)	-2(2)	4(2)
O(9)	61(3)	46(2)	26(2)	0(2)	14(2)	31(2)
N(1)	21(2)	15(2)	29(2)	-1(2)	5(2)	2(2)
C(1)	31(3)	19(2)	17(3)	0(2)	-1(3)	10(2)
C(2)	27(3)	19(3)	27(3)	2(2)	5(2)	5(2)
C(3)	21(3)	27(3)	17(3)	-5(2)	-6(2)	6(2)
C(4)	32(3)	21(3)	16(3)	2(2)	1(2)	4(2)
C(5)	25(3)	17(3)	38(3)	11(2)	7(2)	1(2)
C(6)	23(3)	21(3)	32(3)	5(2)	10(2)	-8(2)
C(7)	20(2)	17(3)	27(3)	0(2)	5(2)	1(2)
C(8)	13(3)	34(3)	25(3)	-3(2)	7(2)	-2(2)
C(9)	18(2)	20(3)	23(3)	3(2)	9(2)	-1(2)
C(10)	26(3)	14(2)	20(3)	-2(2)	11(2)	-3(2)
C(11)	17(2)	21(3)	20(3)	-1(2)	3(2)	-1(2)
C(12)	18(3)	18(3)	19(2)	-3(2)	10(2)	0(2)
C(13)	27(3)	16(3)	24(3)	-2(2)	11(2)	-3(2)
C(14)	20(3)	23(3)	23(3)	0(2)	4(2)	1(2)

N(1E)	28(2)	20(2)	18(2)	-6(2)	7(2)	5(2)
C(1E)	25(3)	34(3)	20(3)	5(2)	5(2)	-6(2)
C(2E)	36(3)	60(4)	28(3)	17(3)	-4(3)	1(3)
C(3E)	43(4)	24(3)	39(3)	-6(3)	18(3)	0(3)
C(4E)	70(4)	24(3)	40(4)	1(2)	16(3)	-2(3)
C(5E)	25(3)	21(3)	22(3)	-4(2)	12(2)	-2(2)
C(6E)	50(4)	27(3)	33(3)	1(3)	15(3)	-7(3)
C(7E)	26(3)	30(3)	24(3)	0(2)	-4(2)	-2(2)
C(8E)	35(3)	60(4)	37(3)	-3(3)	-10(3)	21(3)

Table A-66. Hydrogen coordinates (x 10^4) and isotropic displacement parameters ($Å^2$x 10^3) for V-Et_4N^+1.

	x	y	z	U(eq)
H(10A)	2937	714	3799	23
H(11A)	3644	-1555	4037	23
H(13A)	2700	-4230	2179	26
H(14A)	1992	-1989	1914	26
H(1EA)	3772	1670	2295	31
H(1EB)	3578	-314	2119	31
H(2EA)	4413	-181	3185	64
H(2EB)	4811	836	2622	64
H(2EC)	4623	-1151	2433	64
H(3EA)	4655	-953	1138	41
H(3EB)	4244	-580	276	41
H(4EA)	4089	-3446	684	66
H(4EB)	3461	-2381	620	66
H(4EC)	3869	-2747	1488	66
H(5EA)	4256	3306	1435	26
H(5EB)	4807	1975	1412	26
H(6EA)	4714	3872	306	54
H(6EB)	4023	3243	8	54
H(6EC)	4580	1923	-12	54
H(7EA)	3072	127	777	33
H(7EB)	3373	1240	140	33
H(8EA)	2624	2911	640	69
H(8EB)	3282	3799	901	69
H(8EC)	2986	2687	1546	69

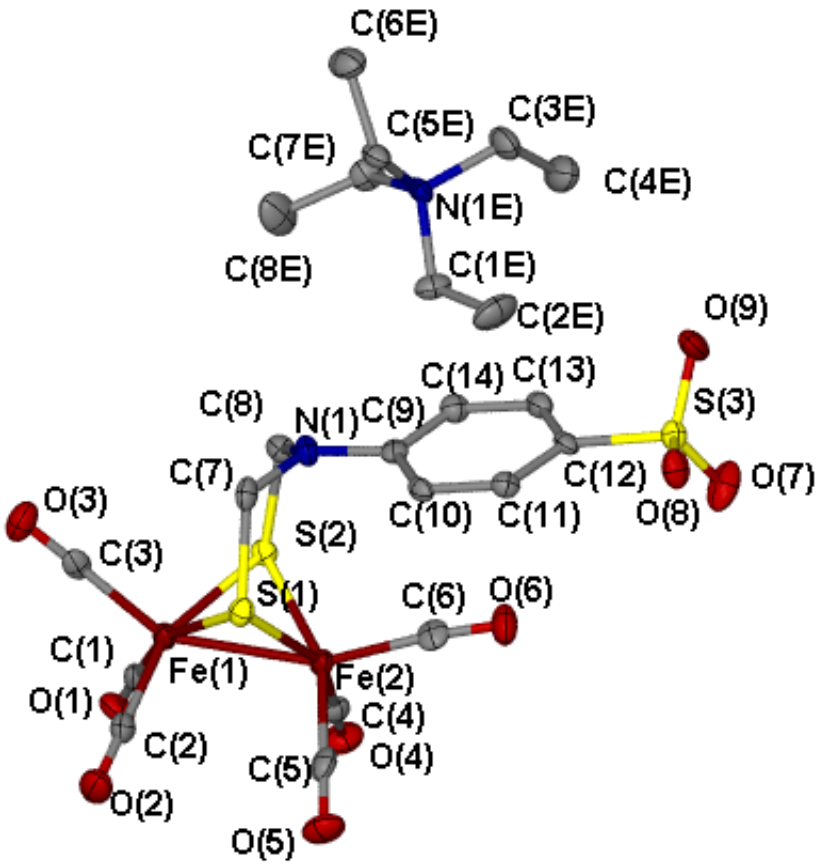
C(6E)
C(5E)
C(3E)
C(7E)
C(4E)
N(1E)
C(8E)
C(1E)
C(2E)
O(9)
C(14)
C(13)
C(8)
N(1)
C(9)
S(3)
C(7)
C(12)
O(7)
O(3)
C(10)
C(11)
O(8)
S(2)
C(3)
S(1)
C(6)
O(6)
C(1)
Fe(1)
Fe(2)
O(1)
C(4)
C(2)
C(5)
O(4)
O(2)
O(5)

Table A-67. Crystal data and structure refinement for V-Me1.

Identification code	Mesulfonate[$Fe(CO)_3]_2$	
Empirical formula	C15 H11 Fe2 N O9 S3	
Formula weight	557.13	
Temperature	110(2) K	
Wavelength	0.71073 Å	
Crystal system	Triclinic	
Space group	P1	
Unit cell dimensions	a = 8.075(4) Å	α= 75.851(9)°.
	b = 10.028(5) Å	β= 75.119(9)°.
	c = 13.486(7) Å	γ = 83.751(9)°.
Volume	1022.2(9) $Å^3$	
Z	2	
Density (calculated)	1.810 Mg/m^3	
Absorption coefficient	1.774 mm^{-1}	
F(000)	560	
Crystal size	0.30 x 0.15 x 0.11 mm^3	
Theta range for data collection	1.60 to 29.07°.	
Index ranges	-10<=h<=10, -13<=k<=12, -18<=l<=17	
Reflections collected	12096	
Independent reflections	9264 [R(int) = 0.0397]	
Completeness to theta = 29.07°	89.3 %	
Absorption correction	Semi-empirical from equivalents	
Max. and min. transmission	0.8288 and 0.6181	
Refinement method	Full-matrix least-squares on F^2	
Data / restraints / parameters	9264 / 3 / 543	
Goodness-of-fit on F^2	0.888	
Final R indices [I>2sigma(I)]	R1 = 0.0488, wR2 = 0.0801	
R indices (all data)	R1 = 0.0870, wR2 = 0.0893	
Absolute structure parameter	0.33(5)	
Largest diff. peak and hole	0.806 and -0.370 $e.Å^{-3}$	

Table A-68. Atomic coordinates (x 10^4) and equivalent isotropic displacement parameters ($Å^2$x 10^3) for V-Me1. U(eq) is defined as one third of the trace of the orthogonalized U^{ij} tensor.

	x	y	z	U(eq)
Fe(1)	9060(2)	4409(1)	4972(1)	19(1)
Fe(3)	11828(2)	5588(2)	4195(1)	23(1)
S(5)	11604(4)	3315(3)	4364(3)	21(1)
S(6)	9650(5)	5887(3)	3371(3)	28(1)
S(8)	4903(5)	-421(4)	3389(3)	38(1)
C(1)	6439(13)	1942(13)	2486(9)	27(3)
N(4)	10324(13)	3479(11)	2597(9)	23(2)
O(5)	3482(12)	156(9)	4252(7)	23(2)
O(7)	4130(14)	-155(12)	2500(8)	36(3)
O(8)	5488(15)	-1777(10)	3841(10)	43(3)
C(17)	12908(17)	5172(12)	5217(11)	37(4)
C(18)	6607(15)	698(9)	3114(8)	13(2)
C(19)	11774(17)	3103(13)	3010(10)	38(3)
C(20)	7399(18)	3406(13)	4916(11)	33(3)
O(22)	9540(18)	3009(11)	7060(9)	49(3)
O(26)	7025(16)	6659(12)	5851(9)	54(3)
C(27)	7984(15)	373(12)	3596(10)	25(3)
O(29)	13602(15)	4894(12)	5901(9)	55(4)
O(30)	6154(16)	2835(13)	4987(11)	51(3)
O(31)	15039(15)	6026(12)	2512(9)	42(3)
C(34)	9173(16)	2573(14)	2804(10)	21(2)
C(35)	7870(20)	5798(17)	5493(14)	65(5)
C(39)	7685(16)	2891(11)	2296(8)	18(3)
C(40)	9148(16)	1257(12)	3457(8)	23(3)
C(45)	9347(17)	3538(12)	6281(7)	19(2)
C(46)	10139(14)	4895(13)	2329(10)	25(3)
C(47)	13690(20)	5900(14)	3163(12)	49(4)
C(49)	3710(20)	-147(16)	5328(10)	47(4)
Fe(2)	6402(2)	7700(2)	9036(1)	25(1)

Fe(4)	9162(2)	8874(2)	8264(1)	29(1)
S(7)	13325(4)	13690(3)	9847(2)	17(1)
S(9)	6636(4)	9959(3)	8871(3)	25(1)
S(10)	8579(4)	7421(3)	9862(3)	24(1)
C(2)	11704(15)	11253(10)	10816(9)	20(3)
N(3)	7833(15)	9808(11)	10647(8)	22(2)
O(6)	14787(14)	13168(11)	8990(8)	38(3)
C(9)	7040(13)	6048(11)	8752(8)	22(3)
O(10)	14089(14)	13460(12)	10702(8)	35(3)
O(11)	12787(14)	15051(11)	9425(8)	37(3)
C(12)	11728(17)	12565(14)	10117(11)	34(3)
O(13)	4653(16)	8333(13)	7330(9)	53(3)
C(14)	10420(16)	12973(12)	9608(9)	21(3)
C(16)	6374(12)	10233(11)	10209(8)	13(2)
C(21)	5362(16)	8117(13)	7970(9)	30(3)
O(23)	7524(12)	5019(11)	8506(10)	46(3)
O(25)	8691(18)	10250(13)	6186(10)	59(4)
C(28)	10492(17)	10345(14)	10982(11)	28(3)
O(32)	3288(16)	7234(13)	10700(10)	54(3)
C(33)	10488(12)	7529(10)	7756(8)	15(2)
C(36)	9260(15)	10724(11)	10472(10)	17(2)
C(37)	8900(20)	9680(16)	7061(13)	56(4)
C(38)	8224(18)	8307(12)	10965(10)	28(3)
C(41)	10945(17)	9853(15)	8250(12)	38(3)
C(42)	9099(15)	12016(12)	9797(10)	26(3)
O(43)	12012(14)	10462(14)	8251(11)	53(3)
O(44)	11209(16)	6653(12)	7438(10)	55(3)
C(48)	4465(13)	7384(12)	10077(8)	22(3)
C(50)	14501(19)	13430(14)	7958(11)	39(4)
O(2)	10773(14)	8300(9)	4646(10)	51(3)
C(5)	11207(18)	7282(13)	4451(10)	46(4)

Table A-69. Bond lengths [Å] and angles [°] for V-Me1.

Fe(1)-C(20)	1.789(13)
Fe(1)-C(35)	1.789(18)
Fe(1)-C(45)	1.829(10)
Fe(1)-S(6)	2.269(4)
Fe(1)-S(5)	2.276(4)
Fe(1)-Fe(3)	2.502(3)
Fe(3)-C(17)	1.758(14)
Fe(3)-C(47)	1.765(16)
Fe(3)-C(5)	1.809(15)
Fe(3)-S(5)	2.257(4)
Fe(3)-S(6)	2.269(4)
S(5)-C(19)	1.858(14)
S(6)-C(46)	1.853(14)
S(8)-O(8)	1.431(11)
S(8)-O(7)	1.445(10)
S(8)-O(5)	1.583(10)
S(8)-C(18)	1.778(11)
C(1)-C(18)	1.340(17)
C(1)-C(39)	1.393(17)
N(4)-C(34)	1.302(17)
N(4)-C(46)	1.378(17)
N(4)-C(19)	1.400(17)
O(5)-C(49)	1.464(15)
C(17)-O(29)	1.161(17)
C(18)-C(27)	1.398(16)
C(20)-O(30)	1.182(18)
O(22)-C(45)	1.097(15)
O(26)-C(35)	1.162(19)
C(27)-C(40)	1.309(17)
O(31)-C(47)	1.207(18)
C(34)-C(40)	1.395(18)
C(34)-C(39)	1.499(16)

Fe(2)-C(9)	1.784(10)
Fe(2)-C(21)	1.788(11)
Fe(2)-C(48)	1.811(9)
Fe(2)-S(9)	2.245(4)
Fe(2)-S(10)	2.270(4)
Fe(2)-Fe(4)	2.493(3)
Fe(4)-C(37)	1.681(17)
Fe(4)-C(33)	1.787(9)
Fe(4)-C(41)	1.823(16)
Fe(4)-S(10)	2.254(4)
Fe(4)-S(9)	2.260(4)
S(7)-O(10)	1.402(11)
S(7)-O(11)	1.412(11)
S(7)-O(6)	1.569(11)
S(7)-C(12)	1.716(14)
S(9)-C(16)	1.846(10)
S(10)-C(38)	1.860(13)
C(2)-C(28)	1.349(17)
C(2)-C(12)	1.418(18)
N(3)-C(16)	1.430(14)
N(3)-C(38)	1.483(16)
N(3)-C(36)	1.487(15)
O(6)-C(50)	1.425(17)
C(9)-O(23)	1.158(14)
C(12)-C(14)	1.377(18)
O(13)-C(21)	1.120(16)
C(14)-C(42)	1.445(17)
O(25)-C(37)	1.22(2)
C(28)-C(36)	1.322(17)
O(32)-C(48)	1.091(14)
C(33)-O(44)	1.114(14)
C(36)-C(42)	1.404(17)
C(41)-O(43)	1.110(19)
O(2)-C(5)	1.113(17)

C(20)-Fe(1)-C(35)	102.4(7)
C(20)-Fe(1)-C(45)	98.7(7)
C(35)-Fe(1)-C(45)	90.2(7)
C(20)-Fe(1)-S(6)	104.2(5)
C(35)-Fe(1)-S(6)	87.9(6)
C(45)-Fe(1)-S(6)	156.9(4)
C(20)-Fe(1)-S(5)	107.0(4)
C(35)-Fe(1)-S(5)	150.6(5)
C(45)-Fe(1)-S(5)	85.2(4)
S(6)-Fe(1)-S(5)	85.11(14)
C(20)-Fe(1)-Fe(3)	152.6(4)
C(35)-Fe(1)-Fe(3)	96.6(5)
C(45)-Fe(1)-Fe(3)	100.8(4)
S(6)-Fe(1)-Fe(3)	56.54(11)
S(5)-Fe(1)-Fe(3)	56.14(11)
C(17)-Fe(3)-C(47)	95.7(6)
C(17)-Fe(3)-C(5)	90.9(6)
C(47)-Fe(3)-C(5)	102.3(6)
C(17)-Fe(3)-S(5)	88.7(4)
C(47)-Fe(3)-S(5)	100.7(4)
C(5)-Fe(3)-S(5)	157.0(4)
C(17)-Fe(3)-S(6)	159.7(5)
C(47)-Fe(3)-S(6)	104.5(5)
C(5)-Fe(3)-S(6)	87.0(4)
S(5)-Fe(3)-S(6)	85.55(13)
C(17)-Fe(3)-Fe(1)	104.3(4)
C(47)-Fe(3)-Fe(1)	148.8(4)
C(5)-Fe(3)-Fe(1)	101.1(4)
S(5)-Fe(3)-Fe(1)	56.86(10)
S(6)-Fe(3)-Fe(1)	56.54(11)
C(19)-S(5)-Fe(3)	105.4(4)
C(19)-S(5)-Fe(1)	110.6(5)
Fe(3)-S(5)-Fe(1)	67.00(11)

C(46)-S(6)-Fe(1)	109.2(4)
C(46)-S(6)-Fe(3)	110.4(4)
Fe(1)-S(6)-Fe(3)	66.92(12)
O(8)-S(8)-O(7)	121.7(7)
O(8)-S(8)-O(5)	109.6(6)
O(7)-S(8)-O(5)	103.3(6)
O(8)-S(8)-C(18)	108.0(6)
O(7)-S(8)-C(18)	109.8(6)
O(5)-S(8)-C(18)	102.8(5)
C(18)-C(1)-C(39)	119.0(9)
C(34)-N(4)-C(46)	129.0(10)
C(34)-N(4)-C(19)	118.4(11)
C(46)-N(4)-C(19)	109.0(10)
C(49)-O(5)-S(8)	118.3(9)
O(29)-C(17)-Fe(3)	179.1(13)
C(1)-C(18)-C(27)	120.5(10)
C(1)-C(18)-S(8)	116.6(8)
C(27)-C(18)-S(8)	122.7(8)
N(4)-C(19)-S(5)	117.5(9)
O(30)-C(20)-Fe(1)	170.3(11)
C(40)-C(27)-C(18)	121.9(10)
N(4)-C(34)-C(40)	127.4(11)
N(4)-C(34)-C(39)	119.9(11)
C(40)-C(34)-C(39)	112.7(11)
O(26)-C(35)-Fe(1)	176.4(14)
C(1)-C(39)-C(34)	121.7(10)
C(27)-C(40)-C(34)	124.2(10)
O(22)-C(45)-Fe(1)	179.0(12)
N(4)-C(46)-S(6)	119.8(9)
O(31)-C(47)-Fe(3)	174.3(13)
C(9)-Fe(2)-C(21)	89.3(5)
C(9)-Fe(2)-C(48)	103.5(5)
C(21)-Fe(2)-C(48)	96.2(6)
C(9)-Fe(2)-S(9)	155.6(4)

C(21)-Fe(2)-S(9)	89.0(4)
C(48)-Fe(2)-S(9)	100.9(4)
C(9)-Fe(2)-S(10)	87.7(3)
C(21)-Fe(2)-S(10)	158.1(4)
C(48)-Fe(2)-S(10)	105.6(4)
S(9)-Fe(2)-S(10)	84.78(14)
C(9)-Fe(2)-Fe(4)	100.1(4)
C(21)-Fe(2)-Fe(4)	103.1(4)
C(48)-Fe(2)-Fe(4)	149.6(4)
S(9)-Fe(2)-Fe(4)	56.69(11)
S(10)-Fe(2)-Fe(4)	56.26(11)
C(37)-Fe(4)-C(33)	91.7(6)
C(37)-Fe(4)-C(41)	96.9(7)
C(33)-Fe(4)-C(41)	95.0(5)
C(37)-Fe(4)-S(10)	157.4(6)
C(33)-Fe(4)-S(10)	88.7(4)
C(41)-Fe(4)-S(10)	105.6(5)
C(37)-Fe(4)-S(9)	85.3(6)
C(33)-Fe(4)-S(9)	154.8(4)
C(41)-Fe(4)-S(9)	110.3(4)
S(10)-Fe(4)-S(9)	84.78(14)
C(37)-Fe(4)-Fe(2)	100.9(6)
C(33)-Fe(4)-Fe(2)	100.2(4)
C(41)-Fe(4)-Fe(2)	156.1(5)
S(10)-Fe(4)-Fe(2)	56.85(10)
S(9)-Fe(4)-Fe(2)	56.10(11)
O(10)-S(7)-O(11)	118.3(7)
O(10)-S(7)-O(6)	102.2(6)
O(11)-S(7)-O(6)	109.1(6)
O(10)-S(7)-C(12)	109.9(7)
O(11)-S(7)-C(12)	111.8(7)
O(6)-S(7)-C(12)	104.2(6)
C(16)-S(9)-Fe(2)	107.1(4)
C(16)-S(9)-Fe(4)	113.6(3)

Fe(2)-S(9)-Fe(4)	67.21(13)
C(38)-S(10)-Fe(4)	113.1(4)
C(38)-S(10)-Fe(2)	115.4(4)
Fe(4)-S(10)-Fe(2)	66.88(12)
C(28)-C(2)-C(12)	123.3(11)
C(16)-N(3)-C(38)	117.3(10)
C(16)-N(3)-C(36)	122.8(10)
C(38)-N(3)-C(36)	116.6(10)
C(50)-O(6)-S(7)	116.4(9)
O(23)-C(9)-Fe(2)	175.5(11)
C(14)-C(12)-C(2)	119.2(12)
C(14)-C(12)-S(7)	117.1(10)
C(2)-C(12)-S(7)	123.7(10)
C(12)-C(14)-C(42)	117.8(11)
N(3)-C(16)-S(9)	114.9(7)
O(13)-C(21)-Fe(2)	176.7(13)
C(36)-C(28)-C(2)	117.4(12)
O(44)-C(33)-Fe(4)	175.0(11)
C(28)-C(36)-C(42)	124.6(11)
C(28)-C(36)-N(3)	120.8(11)
C(42)-C(36)-N(3)	114.5(10)
O(25)-C(37)-Fe(4)	179.0(15)
N(3)-C(38)-S(10)	113.0(8)
O(43)-C(41)-Fe(4)	178.9(12)
C(36)-C(42)-C(14)	117.6(11)
O(32)-C(48)-Fe(2)	177.9(12)
O(2)-C(5)-Fe(3)	177.0(12)

Symmetry transformations used to generate equivalent atoms:

Table A-70. Anisotropic displacement parameters ($Å^2 x\ 10^3$)for V-Me1. The anisotropic displacement factor exponent takes the form: $-2\pi^2[\ h^2 a^{*2} U^{11} + ... + 2\ h\ k\ a^*\ b^*\ U^{12}\ ]$

	U^{11}	U^{22}	U^{33}	U^{23}	U^{13}	U^{12}
Fe(1)	22(1)	9(1)	23(1)	-4(1)	1(1)	-5(1)
Fe(3)	17(1)	24(1)	29(1)	-6(1)	-9(1)	-4(1)
S(5)	15(2)	27(2)	24(2)	-13(1)	-7(1)	4(1)
S(6)	39(2)	24(2)	22(2)	-6(1)	-9(2)	-2(1)
S(8)	34(2)	36(2)	52(2)	-11(2)	-12(2)	-20(2)
C(1)	3(4)	62(8)	31(6)	-30(6)	-14(4)	0(5)
N(4)	11(5)	24(6)	32(6)	-3(5)	-10(4)	6(4)
O(5)	18(4)	36(5)	21(5)	-18(4)	0(4)	-4(4)
O(7)	35(6)	55(7)	26(5)	-6(5)	-22(5)	-13(5)
O(8)	41(6)	16(4)	74(8)	-9(5)	-23(6)	9(4)
C(17)	29(7)	18(5)	45(7)	2(5)	9(6)	19(5)
C(18)	18(5)	2(4)	13(5)	12(4)	-6(4)	-8(4)
C(19)	46(8)	18(6)	42(7)	-2(5)	4(6)	-16(5)
C(20)	48(8)	21(6)	36(7)	-23(5)	-1(6)	-8(5)
O(22)	84(10)	36(6)	24(6)	-6(5)	-5(6)	-5(6)
O(26)	59(7)	47(6)	58(7)	-47(6)	4(5)	22(5)
C(27)	20(5)	27(6)	30(6)	0(5)	-21(5)	16(4)
O(29)	57(7)	74(8)	43(7)	-19(6)	-40(6)	42(6)
O(30)	45(7)	55(7)	63(8)	-41(6)	-3(6)	-4(6)
O(31)	33(6)	50(6)	33(6)	-10(5)	12(5)	-6(5)
C(34)	9(4)	44(6)	19(5)	-16(4)	-15(4)	9(4)
C(35)	61(9)	64(10)	72(10)	9(8)	-36(8)	-26(7)
C(39)	31(7)	12(5)	4(4)	7(4)	-9(4)	13(4)
C(40)	28(7)	31(6)	10(5)	12(4)	-16(5)	-7(5)
C(45)	32(6)	17(5)	-1(3)	4(3)	5(3)	6(4)
C(46)	6(4)	41(7)	22(6)	5(5)	-2(4)	-7(4)
C(47)	84(10)	26(7)	65(9)	-20(6)	-57(8)	1(6)
C(49)	61(10)	83(11)	6(5)	-6(6)	-15(6)	-24(8)
Fe(2)	28(1)	24(1)	23(1)	-7(1)	-8(1)	2(1)

Fe(4)	22(1)	39(1)	28(1)	-10(1)	-8(1)	9(1)
S(7)	20(2)	25(2)	8(1)	-6(1)	-7(1)	9(1)
S(9)	29(2)	22(2)	21(2)	1(1)	-9(1)	4(1)
S(10)	15(2)	19(2)	38(2)	0(1)	-15(1)	3(1)
C(2)	34(6)	7(4)	10(4)	11(4)	-2(4)	7(4)
N(3)	33(6)	27(6)	14(5)	-9(4)	-11(5)	-10(5)
O(6)	39(6)	47(6)	23(5)	8(4)	-11(4)	-3(5)
C(9)	13(5)	36(6)	38(6)	-35(5)	-16(4)	5(4)
O(10)	29(6)	49(7)	26(5)	-10(5)	-3(4)	-10(5)
O(11)	35(6)	41(5)	39(6)	-7(4)	-14(5)	-16(4)
C(12)	22(6)	59(8)	32(7)	-31(6)	-12(5)	9(5)
O(13)	57(7)	75(8)	44(7)	-42(6)	-15(6)	4(6)
C(14)	27(5)	17(5)	17(5)	-11(4)	9(4)	-12(4)
C(16)	1(4)	32(5)	11(5)	-14(4)	-7(4)	11(4)
C(21)	30(7)	58(8)	19(5)	-28(5)	-16(5)	-6(5)
O(23)	18(4)	57(6)	72(7)	-27(5)	-13(4)	-2(4)
O(25)	64(9)	72(8)	34(7)	-4(6)	-15(6)	19(7)
C(28)	15(6)	34(7)	41(7)	-16(5)	-8(5)	-6(5)
O(32)	54(8)	61(8)	52(8)	-23(6)	-1(6)	-32(6)
C(33)	4(4)	18(5)	17(5)	-13(4)	7(3)	12(3)
C(36)	21(5)	10(4)	20(5)	-4(4)	-1(4)	-6(4)
C(37)	45(8)	43(8)	92(11)	-34(8)	-20(8)	-2(6)
C(38)	56(7)	16(5)	21(5)	-3(4)	-27(5)	0(5)
C(41)	7(5)	57(8)	39(7)	-11(6)	7(5)	14(5)
C(42)	11(6)	29(6)	46(7)	-31(5)	-6(5)	11(5)
O(43)	13(5)	61(8)	85(9)	-32(7)	6(5)	-14(5)
O(44)	49(7)	45(7)	65(7)	-2(6)	-15(6)	6(6)
C(48)	9(4)	31(6)	15(5)	1(4)	17(4)	-12(4)
C(50)	38(9)	31(7)	41(8)	-7(6)	6(6)	-10(6)
O(2)	70(7)	4(4)	90(8)	-19(4)	-36(6)	8(4)
C(5)	44(8)	28(7)	50(8)	37(5)	-19(6)	-17(6)

Table A-71. Hydrogen coordinates (x 10^4) and isotropic displacement parameters ($Å^2$x 10^3) for V-Me1.

	x	y	z	U(eq)
H(1)	5485	2173	2175	32
H(19A)	12732	3649	2530	46
H(19B)	12091	2124	3000	46
H(27)	8077	-515	4038	30
H(39)	7590	3761	1833	21
H(40)	10032	984	3824	28
H(46A)	9216	5133	1944	30
H(46B)	11214	5234	1824	30
H(49A)	3571	-1130	5645	71
H(49B)	2854	395	5746	71
H(49C)	4864	91	5314	71
H(2)	12585	11000	11187	24
H(14)	10388	13854	9147	25
H(16A)	6106	11224	10190	15
H(16B)	5378	9725	10682	15
H(28)	10523	9467	11446	34
H(38A)	7261	7890	11537	34
H(38B)	9263	8158	11247	34
H(42)	8156	12252	9477	31
H(50A)	13676	12791	7944	59
H(50B)	15587	13300	7454	59
H(50C)	14044	14379	7768	59

Table A-72. Torsion angles [°] for V-Me1.

C(20)-Fe(1)-Fe(3)-C(17)	-136.8(11)
C(35)-Fe(1)-Fe(3)-C(17)	89.4(7)
C(45)-Fe(1)-Fe(3)-C(17)	-2.1(5)
S(6)-Fe(1)-Fe(3)-C(17)	172.6(4)
S(5)-Fe(1)-Fe(3)-C(17)	-78.7(4)
C(20)-Fe(1)-Fe(3)-C(47)	-8.7(14)
C(35)-Fe(1)-Fe(3)-C(47)	-142.5(11)
C(45)-Fe(1)-Fe(3)-C(47)	126.1(10)
S(6)-Fe(1)-Fe(3)-C(47)	-59.3(9)
S(5)-Fe(1)-Fe(3)-C(47)	49.4(9)
C(20)-Fe(1)-Fe(3)-C(5)	129.4(11)
C(35)-Fe(1)-Fe(3)-C(5)	-4.4(7)
C(45)-Fe(1)-Fe(3)-C(5)	-95.9(5)
S(6)-Fe(1)-Fe(3)-C(5)	78.8(4)
S(5)-Fe(1)-Fe(3)-C(5)	-172.6(4)
C(20)-Fe(1)-Fe(3)-S(5)	-58.1(10)
C(35)-Fe(1)-Fe(3)-S(5)	168.2(6)
C(45)-Fe(1)-Fe(3)-S(5)	76.7(4)
S(6)-Fe(1)-Fe(3)-S(5)	-108.69(16)
C(20)-Fe(1)-Fe(3)-S(6)	50.6(10)
C(35)-Fe(1)-Fe(3)-S(6)	-83.2(6)
C(45)-Fe(1)-Fe(3)-S(6)	-174.7(4)
S(5)-Fe(1)-Fe(3)-S(6)	108.69(16)
C(17)-Fe(3)-S(5)-C(19)	-145.7(6)
C(47)-Fe(3)-S(5)-C(19)	-50.2(6)
C(5)-Fe(3)-S(5)-C(19)	125.2(12)
S(6)-Fe(3)-S(5)-C(19)	53.8(5)
Fe(1)-Fe(3)-S(5)-C(19)	106.2(5)
C(17)-Fe(3)-S(5)-Fe(1)	108.1(4)
C(47)-Fe(3)-S(5)-Fe(1)	-156.4(5)
C(5)-Fe(3)-S(5)-Fe(1)	19.0(11)
S(6)-Fe(3)-S(5)-Fe(1)	-52.44(13)

C(20)-Fe(1)-S(5)-C(19)	57.4(7)
C(35)-Fe(1)-S(5)-C(19)	-123.1(12)
C(45)-Fe(1)-S(5)-C(19)	155.0(6)
S(6)-Fe(1)-S(5)-C(19)	-46.1(4)
Fe(3)-Fe(1)-S(5)-C(19)	-98.5(4)
C(20)-Fe(1)-S(5)-Fe(3)	155.9(5)
C(35)-Fe(1)-S(5)-Fe(3)	-24.5(11)
C(45)-Fe(1)-S(5)-Fe(3)	-106.5(4)
S(6)-Fe(1)-S(5)-Fe(3)	52.49(12)
C(20)-Fe(1)-S(6)-C(46)	-53.9(6)
C(35)-Fe(1)-S(6)-C(46)	-156.2(6)
C(45)-Fe(1)-S(6)-C(46)	118.1(10)
S(5)-Fe(1)-S(6)-C(46)	52.5(4)
Fe(3)-Fe(1)-S(6)-C(46)	104.6(4)
C(20)-Fe(1)-S(6)-Fe(3)	-158.5(4)
C(35)-Fe(1)-S(6)-Fe(3)	99.2(5)
C(45)-Fe(1)-S(6)-Fe(3)	13.5(9)
S(5)-Fe(1)-S(6)-Fe(3)	-52.14(12)
C(17)-Fe(3)-S(6)-C(46)	-124.1(12)
C(47)-Fe(3)-S(6)-C(46)	49.7(6)
C(5)-Fe(3)-S(6)-C(46)	151.6(6)
S(5)-Fe(3)-S(6)-C(46)	-50.2(4)
Fe(1)-Fe(3)-S(6)-C(46)	-102.9(4)
C(17)-Fe(3)-S(6)-Fe(1)	-21.1(11)
C(47)-Fe(3)-S(6)-Fe(1)	152.6(5)
C(5)-Fe(3)-S(6)-Fe(1)	-105.5(4)
S(5)-Fe(3)-S(6)-Fe(1)	52.71(12)
O(8)-S(8)-O(5)-C(49)	38.9(11)
O(7)-S(8)-O(5)-C(49)	170.0(10)
C(18)-S(8)-O(5)-C(49)	-75.8(10)
C(47)-Fe(3)-C(17)-O(29)	-179(100)
C(5)-Fe(3)-C(17)-O(29)	78(72)
S(5)-Fe(3)-C(17)-O(29)	-79(72)
S(6)-Fe(3)-C(17)-O(29)	-5(73)

Fe(1)-Fe(3)-C(17)-O(29)	-23(72)
C(39)-C(1)-C(18)-C(27)	1.9(17)
C(39)-C(1)-C(18)-S(8)	176.2(9)
O(8)-S(8)-C(18)-C(1)	166.1(10)
O(7)-S(8)-C(18)-C(1)	31.3(12)
O(5)-S(8)-C(18)-C(1)	-78.1(10)
O(8)-S(8)-C(18)-C(27)	-19.8(13)
O(7)-S(8)-C(18)-C(27)	-154.6(10)
O(5)-S(8)-C(18)-C(27)	96.0(11)
C(34)-N(4)-C(19)-S(5)	-86.1(13)
C(46)-N(4)-C(19)-S(5)	74.4(12)
Fe(3)-S(5)-C(19)-N(4)	-77.4(9)
Fe(1)-S(5)-C(19)-N(4)	-6.7(10)
C(35)-Fe(1)-C(20)-O(30)	-22(8)
C(45)-Fe(1)-C(20)-O(30)	70(8)
S(6)-Fe(1)-C(20)-O(30)	-113(8)
S(5)-Fe(1)-C(20)-O(30)	158(8)
Fe(3)-Fe(1)-C(20)-O(30)	-155(8)
C(1)-C(18)-C(27)-C(40)	0.0(19)
S(8)-C(18)-C(27)-C(40)	-173.8(10)
C(46)-N(4)-C(34)-C(40)	-151.8(13)
C(19)-N(4)-C(34)-C(40)	4(2)
C(46)-N(4)-C(34)-C(39)	30(2)
C(19)-N(4)-C(34)-C(39)	-174.4(11)
C(20)-Fe(1)-C(35)-O(26)	19(25)
C(45)-Fe(1)-C(35)-O(26)	-80(25)
S(6)-Fe(1)-C(35)-O(26)	124(25)
S(5)-Fe(1)-C(35)-O(26)	-160(24)
Fe(3)-Fe(1)-C(35)-O(26)	180(100)
C(18)-C(1)-C(39)-C(34)	-2.1(17)
N(4)-C(34)-C(39)-C(1)	179.1(12)
C(40)-C(34)-C(39)-C(1)	0.4(17)
C(18)-C(27)-C(40)-C(34)	-2(2)
N(4)-C(34)-C(40)-C(27)	-177.0(14)

C(39)-C(34)-C(40)-C(27)	1.7(18)
C(20)-Fe(1)-C(45)-O(22)	109(76)
C(35)-Fe(1)-C(45)-O(22)	-148(76)
S(6)-Fe(1)-C(45)-O(22)	-63(77)
S(5)-Fe(1)-C(45)-O(22)	3(76)
Fe(3)-Fe(1)-C(45)-O(22)	-51(76)
C(34)-N(4)-C(46)-S(6)	92.1(15)
C(19)-N(4)-C(46)-S(6)	-65.6(12)
Fe(1)-S(6)-C(46)-N(4)	-8.6(10)
Fe(3)-S(6)-C(46)-N(4)	63.2(9)
C(17)-Fe(3)-C(47)-O(31)	33(12)
C(5)-Fe(3)-C(47)-O(31)	125(11)
S(5)-Fe(3)-C(47)-O(31)	-57(12)
S(6)-Fe(3)-C(47)-O(31)	-145(11)
Fe(1)-Fe(3)-C(47)-O(31)	-97(11)
C(9)-Fe(2)-Fe(4)-C(37)	95.0(6)
C(21)-Fe(2)-Fe(4)-C(37)	3.4(6)
C(48)-Fe(2)-Fe(4)-C(37)	-124.4(10)
S(9)-Fe(2)-Fe(4)-C(37)	-76.7(5)
S(10)-Fe(2)-Fe(4)-C(37)	175.4(6)
C(9)-Fe(2)-Fe(4)-C(33)	1.3(5)
C(21)-Fe(2)-Fe(4)-C(33)	-90.4(5)
C(48)-Fe(2)-Fe(4)-C(33)	141.8(9)
S(9)-Fe(2)-Fe(4)-C(33)	-170.4(4)
S(10)-Fe(2)-Fe(4)-C(33)	81.6(4)
C(9)-Fe(2)-Fe(4)-C(41)	-127.4(12)
C(21)-Fe(2)-Fe(4)-C(41)	141.0(12)
C(48)-Fe(2)-Fe(4)-C(41)	13.2(14)
S(9)-Fe(2)-Fe(4)-C(41)	60.9(11)
S(10)-Fe(2)-Fe(4)-C(41)	-47.0(11)
C(9)-Fe(2)-Fe(4)-S(10)	-80.4(4)
C(21)-Fe(2)-Fe(4)-S(10)	-172.0(4)
C(48)-Fe(2)-Fe(4)-S(10)	60.2(8)
S(9)-Fe(2)-Fe(4)-S(10)	107.94(16)

C(9)-Fe(2)-Fe(4)-S(9)	171.7(4)
C(21)-Fe(2)-Fe(4)-S(9)	80.0(4)
C(48)-Fe(2)-Fe(4)-S(9)	-47.7(8)
S(10)-Fe(2)-Fe(4)-S(9)	-107.94(16)
C(9)-Fe(2)-S(9)-C(16)	-129.1(9)
C(21)-Fe(2)-S(9)-C(16)	144.7(5)
C(48)-Fe(2)-S(9)-C(16)	48.6(5)
S(10)-Fe(2)-S(9)-C(16)	-56.3(4)
Fe(4)-Fe(2)-S(9)-C(16)	-108.9(4)
C(9)-Fe(2)-S(9)-Fe(4)	-20.1(8)
C(21)-Fe(2)-S(9)-Fe(4)	-106.3(4)
C(48)-Fe(2)-S(9)-Fe(4)	157.6(4)
S(10)-Fe(2)-S(9)-Fe(4)	52.61(13)
C(37)-Fe(4)-S(9)-C(16)	-154.0(7)
C(33)-Fe(4)-S(9)-C(16)	122.0(9)
C(41)-Fe(4)-S(9)-C(16)	-58.3(7)
S(10)-Fe(4)-S(9)-C(16)	46.3(4)
Fe(2)-Fe(4)-S(9)-C(16)	99.5(4)
C(37)-Fe(4)-S(9)-Fe(2)	106.5(5)
C(33)-Fe(4)-S(9)-Fe(2)	22.5(9)
C(41)-Fe(4)-S(9)-Fe(2)	-157.8(5)
S(10)-Fe(4)-S(9)-Fe(2)	-53.12(12)
C(37)-Fe(4)-S(10)-C(38)	-120.8(15)
C(33)-Fe(4)-S(10)-C(38)	147.9(6)
C(41)-Fe(4)-S(10)-C(38)	53.1(6)
S(9)-Fe(4)-S(10)-C(38)	-56.5(5)
Fe(2)-Fe(4)-S(10)-C(38)	-109.0(5)
C(37)-Fe(4)-S(10)-Fe(2)	-11.8(14)
C(33)-Fe(4)-S(10)-Fe(2)	-103.1(4)
C(41)-Fe(4)-S(10)-Fe(2)	162.1(4)
S(9)-Fe(4)-S(10)-Fe(2)	52.46(13)
C(9)-Fe(2)-S(10)-C(38)	-150.5(6)
C(21)-Fe(2)-S(10)-C(38)	126.9(11)
C(48)-Fe(2)-S(10)-C(38)	-47.2(6)

S(9)-Fe(2)-S(10)-C(38)	52.7(5)
Fe(4)-Fe(2)-S(10)-C(38)	105.7(5)
C(9)-Fe(2)-S(10)-Fe(4)	103.8(4)
C(21)-Fe(2)-S(10)-Fe(4)	21.2(11)
C(48)-Fe(2)-S(10)-Fe(4)	-152.8(4)
S(9)-Fe(2)-S(10)-Fe(4)	-52.98(13)
O(10)-S(7)-O(6)-C(50)	-171.9(10)
O(11)-S(7)-O(6)-C(50)	-45.9(11)
C(12)-S(7)-O(6)-C(50)	73.6(11)
C(21)-Fe(2)-C(9)-O(23)	68(11)
C(48)-Fe(2)-C(9)-O(23)	164(11)
S(9)-Fe(2)-C(9)-O(23)	-19(12)
S(10)-Fe(2)-C(9)-O(23)	-91(11)
Fe(4)-Fe(2)-C(9)-O(23)	-36(12)
C(28)-C(2)-C(12)-C(14)	2.8(19)
C(28)-C(2)-C(12)-S(7)	-176.3(11)
O(10)-S(7)-C(12)-C(14)	153.9(10)
O(11)-S(7)-C(12)-C(14)	20.4(12)
O(6)-S(7)-C(12)-C(14)	-97.3(10)
O(10)-S(7)-C(12)-C(2)	-26.9(13)
O(11)-S(7)-C(12)-C(2)	-160.4(10)
O(6)-S(7)-C(12)-C(2)	81.9(11)
C(2)-C(12)-C(14)-C(42)	-1.4(17)
S(7)-C(12)-C(14)-C(42)	177.8(8)
C(38)-N(3)-C(16)-S(9)	-71.4(12)
C(36)-N(3)-C(16)-S(9)	87.4(12)
Fe(2)-S(9)-C(16)-N(3)	75.9(9)
Fe(4)-S(9)-C(16)-N(3)	3.9(10)
C(9)-Fe(2)-C(21)-O(13)	70(19)
C(48)-Fe(2)-C(21)-O(13)	-34(19)
S(9)-Fe(2)-C(21)-O(13)	-135(19)
S(10)-Fe(2)-C(21)-O(13)	152(19)
Fe(4)-Fe(2)-C(21)-O(13)	170(19)
C(12)-C(2)-C(28)-C(36)	-1.1(19)

C(37)-Fe(4)-C(33)-O(44)	-78(12)
C(41)-Fe(4)-C(33)-O(44)	-175(12)
S(10)-Fe(4)-C(33)-O(44)	79(12)
S(9)-Fe(4)-C(33)-O(44)	5(13)
Fe(2)-Fe(4)-C(33)-O(44)	23(12)
C(2)-C(28)-C(36)-C(42)	-2(2)
C(2)-C(28)-C(36)-N(3)	-177.3(11)
C(16)-N(3)-C(36)-C(28)	172.7(11)
C(38)-N(3)-C(36)-C(28)	-28.3(17)
C(16)-N(3)-C(36)-C(42)	-3.1(16)
C(38)-N(3)-C(36)-C(42)	155.9(10)
C(33)-Fe(4)-C(37)-O(25)	71(88)
C(41)-Fe(4)-C(37)-O(25)	166(88)
S(10)-Fe(4)-C(37)-O(25)	-20(89)
S(9)-Fe(4)-C(37)-O(25)	-84(88)
Fe(2)-Fe(4)-C(37)-O(25)	-30(88)
C(16)-N(3)-C(38)-S(10)	58.2(13)
C(36)-N(3)-C(38)-S(10)	-102.1(10)
Fe(4)-S(10)-C(38)-N(3)	18.4(10)
Fe(2)-S(10)-C(38)-N(3)	-56.0(10)
C(37)-Fe(4)-C(41)-O(43)	97(84)
C(33)-Fe(4)-C(41)-O(43)	-171(100)
S(10)-Fe(4)-C(41)-O(43)	-81(84)
S(9)-Fe(4)-C(41)-O(43)	9(85)
Fe(2)-Fe(4)-C(41)-O(43)	-41(85)
C(28)-C(36)-C(42)-C(14)	3.1(18)
N(3)-C(36)-C(42)-C(14)	178.7(10)
C(12)-C(14)-C(42)-C(36)	-1.3(16)
C(9)-Fe(2)-C(48)-O(32)	-169(33)
C(21)-Fe(2)-C(48)-O(32)	-78(33)
S(9)-Fe(2)-C(48)-O(32)	12(33)
S(10)-Fe(2)-C(48)-O(32)	100(33)
Fe(4)-Fe(2)-C(48)-O(32)	51(33)
C(17)-Fe(3)-C(5)-O(2)	-76(23)

C(47)-Fe(3)-C(5)-O(2)	-172(23)
S(5)-Fe(3)-C(5)-O(2)	13(24)
S(6)-Fe(3)-C(5)-O(2)	84(23)
Fe(1)-Fe(3)-C(5)-O(2)	29(23)

Symmetry transformations used to generate equivalent atoms:

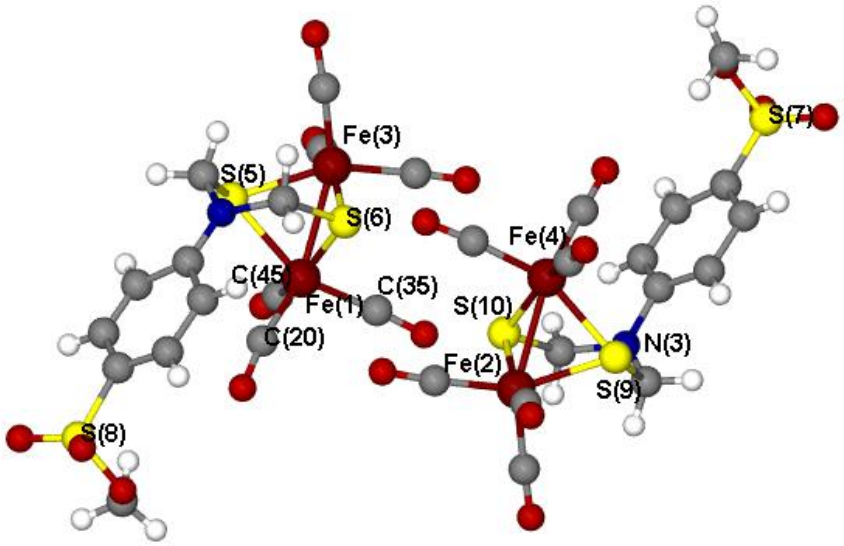

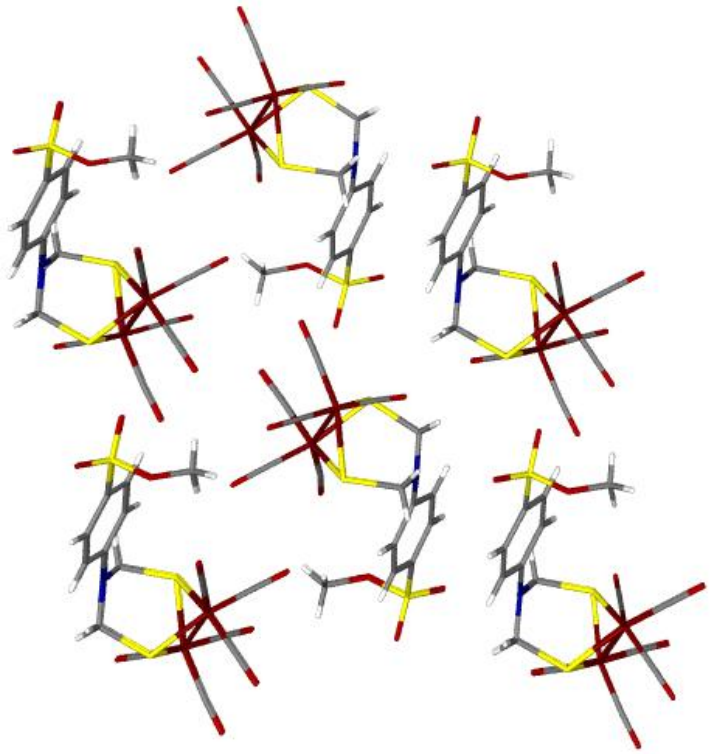

Table A-73. Crystal data and structure refinement for V-Et_4N^+2.

Identification code	ms1	
Empirical formula	C29 H47 Cl10 Fe2 N2 O11 P S3	
Formula weight	1193.04	
Temperature	213(2) K	
Wavelength	0.71073 Å	
Crystal system	Orthorhombic	
Space group	Pca2(1)	
Unit cell dimensions	a = 14.046(14) Å	α= 90°.
	b = 33.262(15) Å	β= 90°.
	c = 16.28(3) Å	γ = 90°.
Volume	7606(18) $Å^3$	
Z	4	
Density (calculated)	1.042 Mg/m^3	
Absorption coefficient	0.869 mm^{-1}	
F(000)	2432	
Crystal size	0.50 x 0.10 x 0.01 mm^3	
Theta range for data collection	2.90 to 25.00°.	
Index ranges	-16<=h<=16, -39<=k<=39, -19<=l<=19	
Reflections collected	68112	
Independent reflections	13222 [R(int) = 0.2440]	
Completeness to theta = 25.00°	98.9 %	
Absorption correction	Semi-empirical from equivalents	
Max. and min. transmission	0.9914 and 0.6705	
Refinement method	Full-matrix least-squares on F^2	
Data / restraints / parameters	13222 / 1 / 396	
Goodness-of-fit on F^2	1.001	
Final R indices [I>2sigma(I)]	R1 = 0.0740, wR2 = 0.1228	
R indices (all data)	R1 = 0.1654, wR2 = 0.1503	
Absolute structure parameter	0.0(3)	
Largest diff. peak and hole	0.352 and -0.417 $e.Å^{-3}$	

Table A-74. Atomic coordinates (x 10^4) and equivalent isotropic displacement parameters ($Å^2$x 10^3) for V-Et_4N^+2. U(eq) is defined as one third of the trace of the orthogonalized U^{ij} tensor.

	x	y	z	U(eq)
Fe(1)	-890(1)	1597(1)	3942(1)	64(1)
Fe(2)	688(1)	1727(1)	4605(1)	55(1)
S(1)	-727(1)	1803(1)	5254(1)	56(1)
S(2)	136(1)	1117(1)	4277(1)	49(1)
S(3)	-4939(1)	343(1)	5094(1)	52(1)
O(4)	-206(5)	1510(2)	2267(4)	93(2)
O(5)	-2666(4)	1166(2)	3618(4)	79(2)
O(6)	2656(3)	1828(2)	5430(3)	59(2)
O(7)	1415(4)	1631(2)	6483(3)	61(2)
O(8)	1985(3)	1120(2)	5675(3)	51(1)
O(9)	-5164(3)	133(2)	5821(3)	63(2)
O(10)	-5541(4)	651(2)	4920(4)	107(2)
O(11)	-4828(4)	52(2)	4401(3)	72(2)
N(1)	-2713(4)	-178(2)	7540(3)	31(1)
C(8)	2349(5)	904(2)	4968(4)	60(2)
P(3)	1689(1)	1588(1)	5545(1)	51(1)
O(1)	914(6)	2607(3)	4749(5)	121(3)
O(2)	2068(5)	1672(2)	3256(4)	101(2)
O(3)	-1599(8)	2423(3)	3729(6)	175(4)
C(1)	830(7)	2283(4)	4693(6)	76(3)
C(2)	1515(7)	1701(3)	3757(5)	60(2)
C(3)	-1384(5)	2121(3)	3664(6)	56(3)
C(4)	-465(6)	1543(3)	2925(6)	62(2)
C(5)	-1999(6)	1330(3)	3815(5)	66(3)
C(6)	3493(7)	1709(4)	6053(7)	131(5)
C(7)	1199(6)	2007(3)	6830(5)	84(3)
C(9)	-234(4)	832(2)	5210(5)	55(2)
N(2)	-1055(5)	993(2)	5642(4)	65(2)
C(11)	-880(6)	1382(3)	5976(5)	69(3)

C(12)	-1991(5)	848(2)	5475(4)	43(2)
C(13)	-2155(4)	462(2)	5196(4)	24(1)
C(14)	-2975(4)	313(2)	5054(3)	21(1)
C(15)	-3785(4)	540(2)	5233(4)	33(2)
C(16)	-3653(5)	926(2)	5538(4)	46(2)
C(17)	-2782(5)	1078(2)	5655(4)	38(2)
C(18)	-3306(7)	97(3)	7141(5)	90(3)
C(19)	-3975(6)	393(3)	7733(5)	69(3)
C(20)	-1905(7)	48(3)	8044(6)	94(3)
C(21)	-1413(7)	396(3)	7571(7)	98(3)
C(22)	-2181(7)	-394(3)	6859(6)	90(3)
C(23)	-1501(6)	-731(3)	7219(5)	75(3)
C(24)	-3202(10)	-473(4)	8122(7)	119(4)
C(25)	-3926(7)	-718(3)	7618(7)	102(4)

Table A-75. Bond lengths [Å] and angles [°] for V-Et_4N^+2.

Fe(1)-C(4)	1.770(10)
Fe(1)-C(5)	1.804(9)
Fe(1)-C(3)	1.931(8)
Fe(1)-S(2)	2.220(3)
Fe(1)-S(1)	2.254(5)
Fe(1)-Fe(2)	2.504(3)
Fe(2)-C(2)	1.807(10)
Fe(2)-C(1)	1.865(12)
Fe(2)-P(3)	2.128(3)
Fe(2)-S(2)	2.240(3)
Fe(2)-S(1)	2.266(3)
S(1)-C(11)	1.842(9)
S(2)-C(9)	1.864(7)
S(3)-O(10)	1.358(7)
S(3)-O(9)	1.410(6)
S(3)-O(11)	1.494(6)
S(3)-C(15)	1.762(6)
O(4)-C(4)	1.137(9)
O(5)-C(5)	1.131(8)
O(6)-P(3)	1.586(5)
O(6)-C(6)	1.603(10)
O(7)-C(7)	1.405(10)
O(7)-P(3)	1.582(6)
O(8)-C(8)	1.451(8)
O(8)-P(3)	1.625(6)
N(1)-C(18)	1.396(10)
N(1)-C(22)	1.520(10)
N(1)-C(24)	1.528(13)
N(1)-C(20)	1.588(11)
C(8)-H(8A)	0.9700
C(8)-H(8B)	0.9700
C(8)-H(8C)	0.9700

O(1)-C(1)	1.088(10)
O(2)-C(2)	1.129(9)
O(3)-C(3)	1.052(10)
C(6)-H(6A)	0.9700
C(6)-H(6B)	0.9700
C(6)-H(6C)	0.9700
C(7)-H(7A)	0.9700
C(7)-H(7B)	0.9700
C(7)-H(7C)	0.9700
C(9)-N(2)	1.452(9)
C(9)-H(9A)	0.9800
C(9)-H(9B)	0.9800
N(2)-C(11)	1.425(10)
N(2)-C(12)	1.426(9)
C(11)-H(11A)	0.9800
C(11)-H(11B)	0.9800
C(12)-C(13)	1.380(9)
C(12)-C(17)	1.381(9)
C(13)-C(14)	1.276(7)
C(13)-H(13)	0.9400
C(14)-C(15)	1.396(8)
C(14)-H(14)	0.9400
C(15)-C(16)	1.389(9)
C(16)-C(17)	1.337(9)
C(16)-H(16)	0.9400
C(17)-H(17)	0.9400
C(18)-C(19)	1.669(11)
C(18)-H(18A)	0.9800
C(18)-H(18B)	0.9800
C(19)-H(19A)	0.9700
C(19)-H(19B)	0.9700
C(19)-H(19C)	0.9700
C(20)-C(21)	1.551(13)
C(20)-H(20A)	0.9800

C(20)-H(20B)	0.9800
C(21)-H(21A)	0.9700
C(21)-H(21B)	0.9700
C(21)-H(21C)	0.9700
C(22)-C(23)	1.584(12)
C(22)-H(22A)	0.9800
C(22)-H(22B)	0.9800
C(23)-H(23A)	0.9700
C(23)-H(23B)	0.9700
C(23)-H(23C)	0.9700
C(24)-C(25)	1.540(14)
C(24)-H(24A)	0.9800
C(24)-H(24B)	0.9800
C(25)-H(25A)	0.9700
C(25)-H(25B)	0.9700
C(25)-H(25C)	0.9700
C(4)-Fe(1)-C(5)	97.7(4)
C(4)-Fe(1)-C(3)	89.6(4)
C(5)-Fe(1)-C(3)	96.1(4)
C(4)-Fe(1)-S(2)	86.4(3)
C(5)-Fe(1)-S(2)	103.6(3)
C(3)-Fe(1)-S(2)	160.3(3)
C(4)-Fe(1)-S(1)	152.0(3)
C(5)-Fe(1)-S(1)	110.2(3)
C(3)-Fe(1)-S(1)	89.1(3)
S(2)-Fe(1)-S(1)	85.46(10)
C(4)-Fe(1)-Fe(2)	97.0(3)
C(5)-Fe(1)-Fe(2)	154.0(3)
C(3)-Fe(1)-Fe(2)	105.3(3)
S(2)-Fe(1)-Fe(2)	56.21(7)
S(1)-Fe(1)-Fe(2)	56.58(7)
C(2)-Fe(2)-C(1)	92.2(4)
C(2)-Fe(2)-P(3)	96.6(3)
C(1)-Fe(2)-P(3)	95.2(3)

C(2)-Fe(2)-S(2)	89.8(3)
C(1)-Fe(2)-S(2)	162.7(3)
P(3)-Fe(2)-S(2)	101.71(11)
C(2)-Fe(2)-S(1)	157.8(3)
C(1)-Fe(2)-S(1)	87.0(3)
P(3)-Fe(2)-S(1)	105.61(15)
S(2)-Fe(2)-S(1)	84.74(9)
C(2)-Fe(2)-Fe(1)	103.4(3)
C(1)-Fe(2)-Fe(1)	107.4(3)
P(3)-Fe(2)-Fe(1)	148.98(9)
S(2)-Fe(2)-Fe(1)	55.48(6)
S(1)-Fe(2)-Fe(1)	56.15(12)
C(11)-S(1)-Fe(1)	111.2(3)
C(11)-S(1)-Fe(2)	108.3(3)
Fe(1)-S(1)-Fe(2)	67.27(10)
C(9)-S(2)-Fe(1)	112.6(2)
C(9)-S(2)-Fe(2)	111.2(3)
Fe(1)-S(2)-Fe(2)	68.30(9)
O(10)-S(3)-O(9)	114.0(4)
O(10)-S(3)-O(11)	113.3(4)
O(9)-S(3)-O(11)	109.7(3)
O(10)-S(3)-C(15)	108.6(4)
O(9)-S(3)-C(15)	106.4(3)
O(11)-S(3)-C(15)	104.0(3)
P(3)-O(6)-C(6)	115.4(5)
C(7)-O(7)-P(3)	121.4(5)
C(8)-O(8)-P(3)	117.4(5)
C(18)-N(1)-C(22)	105.3(6)
C(18)-N(1)-C(24)	116.2(7)
C(22)-N(1)-C(24)	111.6(7)
C(18)-N(1)-C(20)	110.9(7)
C(22)-N(1)-C(20)	104.5(6)
C(24)-N(1)-C(20)	107.8(7)
O(8)-C(8)-H(8A)	109.5

O(8)-C(8)-H(8B)	109.5
H(8A)-C(8)-H(8B)	109.5
O(8)-C(8)-H(8C)	109.5
H(8A)-C(8)-H(8C)	109.5
H(8B)-C(8)-H(8C)	109.5
O(7)-P(3)-O(6)	106.1(3)
O(7)-P(3)-O(8)	91.3(3)
O(6)-P(3)-O(8)	106.2(3)
O(7)-P(3)-Fe(2)	120.9(2)
O(6)-P(3)-Fe(2)	111.8(2)
O(8)-P(3)-Fe(2)	118.1(2)
O(1)-C(1)-Fe(2)	179.6(11)
O(2)-C(2)-Fe(2)	175.9(9)
O(3)-C(3)-Fe(1)	160.0(11)
O(4)-C(4)-Fe(1)	178.9(9)
O(5)-C(5)-Fe(1)	170.1(8)
O(6)-C(6)-H(6A)	109.5
O(6)-C(6)-H(6B)	109.5
H(6A)-C(6)-H(6B)	109.5
O(6)-C(6)-H(6C)	109.5
H(6A)-C(6)-H(6C)	109.5
H(6B)-C(6)-H(6C)	109.5
O(7)-C(7)-H(7A)	109.5
O(7)-C(7)-H(7B)	109.5
H(7A)-C(7)-H(7B)	109.5
O(7)-C(7)-H(7C)	109.5
H(7A)-C(7)-H(7C)	109.5
H(7B)-C(7)-H(7C)	109.5
N(2)-C(9)-S(2)	115.5(5)
N(2)-C(9)-H(9A)	108.4
S(2)-C(9)-H(9A)	108.4
N(2)-C(9)-H(9B)	108.4
S(2)-C(9)-H(9B)	108.4
H(9A)-C(9)-H(9B)	107.5

C(11)-N(2)-C(12)	122.5(7)
C(11)-N(2)-C(9)	112.4(6)
C(12)-N(2)-C(9)	121.1(7)
N(2)-C(11)-S(1)	117.9(6)
N(2)-C(11)-H(11A)	107.8
S(1)-C(11)-H(11A)	107.8
N(2)-C(11)-H(11B)	107.8
S(1)-C(11)-H(11B)	107.8
H(11A)-C(11)-H(11B)	107.2
C(13)-C(12)-C(17)	116.8(6)
C(13)-C(12)-N(2)	122.0(7)
C(17)-C(12)-N(2)	121.0(7)
C(14)-C(13)-C(12)	124.9(6)
C(14)-C(13)-H(13)	117.6
C(12)-C(13)-H(13)	117.6
C(13)-C(14)-C(15)	119.2(6)
C(13)-C(14)-H(14)	120.4
C(15)-C(14)-H(14)	120.4
C(16)-C(15)-C(14)	117.7(6)
C(16)-C(15)-S(3)	120.8(5)
C(14)-C(15)-S(3)	121.5(5)
C(17)-C(16)-C(15)	121.6(6)
C(17)-C(16)-H(16)	119.2
C(15)-C(16)-H(16)	119.2
C(16)-C(17)-C(12)	119.7(7)
C(16)-C(17)-H(17)	120.1
C(12)-C(17)-H(17)	120.1
N(1)-C(18)-C(19)	117.0(7)
N(1)-C(18)-H(18A)	108.1
C(19)-C(18)-H(18A)	108.1
N(1)-C(18)-H(18B)	108.1
C(19)-C(18)-H(18B)	108.1
H(18A)-C(18)-H(18B)	107.3
C(18)-C(19)-H(19A)	109.5

C(18)-C(19)-H(19B)	109.5
H(19A)-C(19)-H(19B)	109.5
C(18)-C(19)-H(19C)	109.5
H(19A)-C(19)-H(19C)	109.5
H(19B)-C(19)-H(19C)	109.5
C(21)-C(20)-N(1)	114.5(8)
C(21)-C(20)-H(20A)	108.6
N(1)-C(20)-H(20A)	108.6
C(21)-C(20)-H(20B)	108.6
N(1)-C(20)-H(20B)	108.6
H(20A)-C(20)-H(20B)	107.6
C(20)-C(21)-H(21A)	109.5
C(20)-C(21)-H(21B)	109.5
H(21A)-C(21)-H(21B)	109.5
C(20)-C(21)-H(21C)	109.5
H(21A)-C(21)-H(21C)	109.5
H(21B)-C(21)-H(21C)	109.5
N(1)-C(22)-C(23)	111.1(8)
N(1)-C(22)-H(22A)	109.4
C(23)-C(22)-H(22A)	109.4
N(1)-C(22)-H(22B)	109.4
C(23)-C(22)-H(22B)	109.4
H(22A)-C(22)-H(22B)	108.0
C(22)-C(23)-H(23A)	109.5
C(22)-C(23)-H(23B)	109.5
H(23A)-C(23)-H(23B)	109.5
C(22)-C(23)-H(23C)	109.5
H(23A)-C(23)-H(23C)	109.5
H(23B)-C(23)-H(23C)	109.5
N(1)-C(24)-C(25)	107.8(8)
N(1)-C(24)-H(24A)	110.1
C(25)-C(24)-H(24A)	110.1
N(1)-C(24)-H(24B)	110.1
C(25)-C(24)-H(24B)	110.1

H(24A)-C(24)-H(24B)	108.5
C(24)-C(25)-H(25A)	109.5
C(24)-C(25)-H(25B)	109.5
H(25A)-C(25)-H(25B)	109.5
C(24)-C(25)-H(25C)	109.5
H(25A)-C(25)-H(25C)	109.5
H(25B)-C(25)-H(25C)	109.5

Symmetry transformations used to generate equivalent atoms:

Table A-76. Anisotropic displacement parameters ($Å^2 x\ 10^3$)for V-Et_4N^+2. The anisotropic displacement factor exponent takes the form: $-2\pi^2[\ h^2a^{*2}U^{11} + ... + 2\ h\ k\ a^*\ b^*\ U^{12}\ ]$

	U^{11}	U^{22}	U^{33}	U^{23}	U^{13}	U^{12}
Fe(1)	36(1)	88(1)	69(1)	-12(1)	-20(1)	11(1)
Fe(2)	37(1)	75(1)	53(1)	-4(1)	-8(1)	-6(1)
S(1)	51(1)	60(1)	56(1)	-7(1)	-4(1)	-2(1)
S(2)	38(1)	61(1)	50(1)	-2(1)	-5(1)	0(1)
S(3)	31(1)	73(2)	51(1)	5(1)	-2(1)	-3(1)
O(4)	110(5)	109(6)	60(4)	-2(4)	-5(4)	-12(4)
O(5)	51(4)	111(5)	77(5)	4(4)	-16(3)	-21(4)
O(6)	38(3)	86(4)	55(3)	12(3)	-8(2)	-16(3)
O(7)	62(4)	62(4)	58(4)	-12(3)	1(3)	-2(3)
O(8)	39(3)	77(4)	37(3)	-5(3)	-5(2)	-3(3)
O(9)	50(3)	91(4)	46(4)	-16(3)	5(3)	-36(3)
O(10)	54(4)	130(6)	137(7)	6(5)	-7(4)	-8(4)
O(11)	67(4)	94(4)	55(4)	6(4)	-17(3)	-25(3)
N(1)	30(3)	59(4)	4(3)	3(3)	3(3)	13(3)
C(8)	70(5)	79(6)	30(5)	-20(4)	-8(4)	18(5)
P(3)	42(1)	70(2)	43(1)	0(1)	1(1)	-5(1)
O(1)	124(6)	107(7)	133(7)	18(6)	-1(5)	-9(6)
O(2)	93(5)	132(7)	77(5)	-29(5)	24(4)	-23(5)
O(3)	210(10)	173(10)	143(9)	-7(8)	-48(7)	41(8)
C(1)	79(7)	103(10)	47(6)	15(7)	-9(5)	20(7)
C(2)	71(6)	70(6)	38(5)	-10(5)	-10(5)	15(5)
C(3)	35(4)	37(5)	97(8)	6(5)	3(4)	12(4)
C(4)	72(6)	50(6)	63(7)	-2(5)	-2(5)	-1(5)
C(5)	42(5)	96(7)	60(6)	-5(5)	-21(5)	-1(5)
C(6)	61(6)	216(14)	115(9)	34(9)	-38(6)	-35(8)
C(7)	75(7)	127(9)	49(6)	-8(6)	-7(5)	-18(6)
C(9)	16(3)	95(6)	55(5)	31(5)	10(4)	-10(4)
N(2)	46(4)	76(5)	73(5)	-8(4)	0(4)	-3(4)
C(11)	45(5)	94(7)	68(6)	-25(6)	13(4)	-9(5)

C(12)	40(5)	59(6)	29(4)	13(4)	6(3)	-7(4)
C(13)	27(4)	24(4)	23(4)	0(3)	-2(3)	4(3)
C(14)	22(3)	38(4)	3(3)	-2(3)	-1(3)	3(3)
C(15)	15(3)	63(5)	21(4)	-1(4)	10(3)	-7(3)
C(16)	37(4)	57(5)	45(5)	-21(4)	0(4)	13(4)
C(17)	25(4)	39(5)	51(5)	-6(4)	-2(3)	-8(4)
C(18)	80(7)	137(10)	53(6)	8(6)	0(5)	8(7)
C(19)	65(6)	85(6)	57(6)	-9(5)	7(4)	20(5)
C(20)	81(8)	135(10)	65(7)	-12(7)	7(6)	29(7)
C(21)	63(6)	131(9)	99(8)	28(7)	36(6)	-3(7)
C(22)	83(8)	102(9)	86(8)	-13(7)	14(6)	-29(7)
C(23)	74(7)	71(6)	80(7)	-8(5)	-19(5)	8(6)
C(24)	158(12)	128(11)	72(8)	0(8)	3(8)	62(10)
C(25)	65(7)	118(9)	125(10)	-2(8)	1(6)	12(7)

Table A-77. Hydrogen coordinates (x 10^4) and isotropic displacement parameters ($Å^2$x 10^3) for V-Et_4N^+2.

	x	y	z	U(eq)
H(8A)	1827	839	4601	89
H(8B)	2656	658	5148	89
H(8C)	2808	1071	4681	89
H(6A)	3389	1841	6576	196
H(6B)	4100	1794	5827	196
H(6C)	3498	1420	6132	196
H(7A)	1635	2208	6616	125
H(7B)	1263	1992	7422	125
H(7C)	551	2081	6690	125
H(9A)	-374	555	5049	66
H(9B)	305	825	5592	66
H(11A)	-305	1365	6315	83
H(11B)	-1410	1448	6343	83
H(13)	-1622	297	5105	29
H(14)	-3033	54	4830	25
H(16)	-4188	1084	5664	56
H(17)	-2710	1340	5860	46
H(18A)	-3730	-54	6777	108
H(18B)	-2907	269	6794	108
H(19A)	-3863	329	8306	103
H(19B)	-4642	351	7604	103
H(19C)	-3809	672	7634	103
H(20A)	-2186	157	8548	112
H(20B)	-1420	-148	8205	112
H(21A)	-1126	291	7073	147
H(21B)	-924	515	7915	147
H(21C)	-1882	599	7430	147
H(22A)	-1803	-200	6546	109

H(22B)	-2641	-518	6483	109
H(23A)	-1001	-605	7541	112
H(23B)	-1218	-881	6772	112
H(23C)	-1865	-911	7566	112
H(24A)	-3527	-327	8563	143
H(24B)	-2730	-653	8371	143
H(25A)	-4496	-760	7942	154
H(25B)	-3650	-975	7472	154
H(25C)	-4087	-571	7122	154

Table A-78. Torsion angles [°] for V-Et_4N^+2.

C(4)-Fe(1)-Fe(2)-C(2)	-0.6(4)
C(5)-Fe(1)-Fe(2)-C(2)	123.5(7)
C(3)-Fe(1)-Fe(2)-C(2)	-92.1(4)
S(2)-Fe(1)-Fe(2)-C(2)	80.3(3)
S(1)-Fe(1)-Fe(2)-C(2)	-170.6(3)
C(4)-Fe(1)-Fe(2)-C(1)	96.0(4)
C(5)-Fe(1)-Fe(2)-C(1)	-139.8(7)
C(3)-Fe(1)-Fe(2)-C(1)	4.6(4)
S(2)-Fe(1)-Fe(2)-C(1)	176.9(3)
S(1)-Fe(1)-Fe(2)-C(1)	-73.9(3)
C(4)-Fe(1)-Fe(2)-P(3)	-129.2(3)
C(5)-Fe(1)-Fe(2)-P(3)	-5.0(7)
C(3)-Fe(1)-Fe(2)-P(3)	139.4(3)
S(2)-Fe(1)-Fe(2)-P(3)	-48.25(18)
S(1)-Fe(1)-Fe(2)-P(3)	60.86(19)
C(4)-Fe(1)-Fe(2)-S(2)	-80.9(3)
C(5)-Fe(1)-Fe(2)-S(2)	43.2(6)
C(3)-Fe(1)-Fe(2)-S(2)	-172.4(3)
S(1)-Fe(1)-Fe(2)-S(2)	109.11(11)
C(4)-Fe(1)-Fe(2)-S(1)	170.0(3)
C(5)-Fe(1)-Fe(2)-S(1)	-65.9(6)
C(3)-Fe(1)-Fe(2)-S(1)	78.5(3)
S(2)-Fe(1)-Fe(2)-S(1)	-109.11(11)
C(4)-Fe(1)-S(1)-C(11)	-123.4(7)
C(5)-Fe(1)-S(1)-C(11)	53.0(4)
C(3)-Fe(1)-S(1)-C(11)	149.2(4)
S(2)-Fe(1)-S(1)-C(11)	-49.8(3)
Fe(2)-Fe(1)-S(1)-C(11)	-101.8(3)
C(4)-Fe(1)-S(1)-Fe(2)	-21.6(6)
C(5)-Fe(1)-S(1)-Fe(2)	154.8(3)
C(3)-Fe(1)-S(1)-Fe(2)	-109.0(2)
S(2)-Fe(1)-S(1)-Fe(2)	51.98(8)

C(2)-Fe(2)-S(1)-C(11)	130.7(8)
C(1)-Fe(2)-S(1)-C(11)	-140.8(4)
P(3)-Fe(2)-S(1)-C(11)	-46.2(3)
S(2)-Fe(2)-S(1)-C(11)	54.5(3)
Fe(1)-Fe(2)-S(1)-C(11)	105.9(3)
C(2)-Fe(2)-S(1)-Fe(1)	24.9(8)
C(1)-Fe(2)-S(1)-Fe(1)	113.3(3)
P(3)-Fe(2)-S(1)-Fe(1)	-152.14(10)
S(2)-Fe(2)-S(1)-Fe(1)	-51.43(7)
C(4)-Fe(1)-S(2)-C(9)	-154.3(4)
C(5)-Fe(1)-S(2)-C(9)	-57.2(4)
C(3)-Fe(1)-S(2)-C(9)	127.0(9)
S(1)-Fe(1)-S(2)-C(9)	52.5(3)
Fe(2)-Fe(1)-S(2)-C(9)	104.8(3)
C(4)-Fe(1)-S(2)-Fe(2)	100.9(3)
C(5)-Fe(1)-S(2)-Fe(2)	-162.0(3)
C(3)-Fe(1)-S(2)-Fe(2)	22.2(9)
S(1)-Fe(1)-S(2)-Fe(2)	-52.29(7)
C(2)-Fe(2)-S(2)-C(9)	146.7(3)
C(1)-Fe(2)-S(2)-C(9)	-116.6(11)
P(3)-Fe(2)-S(2)-C(9)	50.1(3)
S(1)-Fe(2)-S(2)-C(9)	-54.8(2)
Fe(1)-Fe(2)-S(2)-C(9)	-106.8(2)
C(2)-Fe(2)-S(2)-Fe(1)	-106.5(3)
C(1)-Fe(2)-S(2)-Fe(1)	-9.8(11)
P(3)-Fe(2)-S(2)-Fe(1)	156.88(9)
S(1)-Fe(2)-S(2)-Fe(1)	52.00(12)
C(7)-O(7)-P(3)-O(6)	63.9(6)
C(7)-O(7)-P(3)-O(8)	171.2(6)
C(7)-O(7)-P(3)-Fe(2)	-64.6(6)
C(6)-O(6)-P(3)-O(7)	52.5(7)
C(6)-O(6)-P(3)-O(8)	-43.7(7)
C(6)-O(6)-P(3)-Fe(2)	-173.9(6)
C(8)-O(8)-P(3)-O(7)	-178.4(5)

C(8)-O(8)-P(3)-O(6)	-71.3(5)
C(8)-O(8)-P(3)-Fe(2)	55.1(5)
C(2)-Fe(2)-P(3)-O(7)	170.4(4)
C(1)-Fe(2)-P(3)-O(7)	77.6(4)
S(2)-Fe(2)-P(3)-O(7)	-98.5(3)
S(1)-Fe(2)-P(3)-O(7)	-10.7(3)
Fe(1)-Fe(2)-P(3)-O(7)	-59.6(3)
C(2)-Fe(2)-P(3)-O(6)	44.5(4)
C(1)-Fe(2)-P(3)-O(6)	-48.3(4)
S(2)-Fe(2)-P(3)-O(6)	135.6(2)
S(1)-Fe(2)-P(3)-O(6)	-136.6(2)
Fe(1)-Fe(2)-P(3)-O(6)	174.5(2)
C(2)-Fe(2)-P(3)-O(8)	-79.2(4)
C(1)-Fe(2)-P(3)-O(8)	-172.0(4)
S(2)-Fe(2)-P(3)-O(8)	12.0(2)
S(1)-Fe(2)-P(3)-O(8)	99.7(2)
Fe(1)-Fe(2)-P(3)-O(8)	50.8(3)
C(2)-Fe(2)-C(1)-O(1)	-121(100)
P(3)-Fe(2)-C(1)-O(1)	-25(100)
S(2)-Fe(2)-C(1)-O(1)	142(100)
S(1)-Fe(2)-C(1)-O(1)	81(100)
Fe(1)-Fe(2)-C(1)-O(1)	134(100)
C(1)-Fe(2)-C(2)-O(2)	114(13)
P(3)-Fe(2)-C(2)-O(2)	19(13)
S(2)-Fe(2)-C(2)-O(2)	-83(13)
S(1)-Fe(2)-C(2)-O(2)	-158(12)
Fe(1)-Fe(2)-C(2)-O(2)	-137(13)
C(4)-Fe(1)-C(3)-O(3)	-149(3)
C(5)-Fe(1)-C(3)-O(3)	113(3)
S(2)-Fe(1)-C(3)-O(3)	-71(3)
S(1)-Fe(1)-C(3)-O(3)	3(3)
Fe(2)-Fe(1)-C(3)-O(3)	-52(3)
C(5)-Fe(1)-C(4)-O(4)	44(47)
C(3)-Fe(1)-C(4)-O(4)	-52(47)

S(2)-Fe(1)-C(4)-O(4)	147(47)
S(1)-Fe(1)-C(4)-O(4)	-139(47)
Fe(2)-Fe(1)-C(4)-O(4)	-158(100)
C(4)-Fe(1)-C(5)-O(5)	-11(5)
C(3)-Fe(1)-C(5)-O(5)	79(5)
S(2)-Fe(1)-C(5)-O(5)	-100(5)
S(1)-Fe(1)-C(5)-O(5)	170(5)
Fe(2)-Fe(1)-C(5)-O(5)	-135(4)
Fe(1)-S(2)-C(9)-N(2)	-7.5(6)
Fe(2)-S(2)-C(9)-N(2)	67.0(6)
S(2)-C(9)-N(2)-C(11)	-64.3(8)
S(2)-C(9)-N(2)-C(12)	93.7(8)
C(12)-N(2)-C(11)-S(1)	-89.3(8)
C(9)-N(2)-C(11)-S(1)	68.4(8)
Fe(1)-S(1)-C(11)-N(2)	1.2(7)
Fe(2)-S(1)-C(11)-N(2)	-70.9(6)
C(11)-N(2)-C(12)-C(13)	-176.2(7)
C(9)-N(2)-C(12)-C(13)	28.0(10)
C(11)-N(2)-C(12)-C(17)	-2.0(11)
C(9)-N(2)-C(12)-C(17)	-157.8(7)
C(17)-C(12)-C(13)-C(14)	4.0(10)
N(2)-C(12)-C(13)-C(14)	178.3(6)
C(12)-C(13)-C(14)-C(15)	-4.2(9)
C(13)-C(14)-C(15)-C(16)	2.0(9)
C(13)-C(14)-C(15)-S(3)	-177.1(5)
O(10)-S(3)-C(15)-C(16)	30.2(7)
O(9)-S(3)-C(15)-C(16)	-93.0(6)
O(11)-S(3)-C(15)-C(16)	151.2(5)
O(10)-S(3)-C(15)-C(14)	-150.7(5)
O(9)-S(3)-C(15)-C(14)	86.1(6)
O(11)-S(3)-C(15)-C(14)	-29.7(6)
C(14)-C(15)-C(16)-C(17)	0.1(10)
S(3)-C(15)-C(16)-C(17)	179.3(6)
C(15)-C(16)-C(17)-C(12)	-0.2(11)

C(13)-C(12)-C(17)-C(16)	-1.6(10)
N(2)-C(12)-C(17)-C(16)	-176.0(7)
C(22)-N(1)-C(18)-C(19)	-178.6(7)
C(24)-N(1)-C(18)-C(19)	57.4(11)
C(20)-N(1)-C(18)-C(19)	-66.1(10)
C(18)-N(1)-C(20)-C(21)	-45.1(10)
C(22)-N(1)-C(20)-C(21)	67.9(9)
C(24)-N(1)-C(20)-C(21)	-173.3(8)
C(18)-N(1)-C(22)-C(23)	-177.9(7)
C(24)-N(1)-C(22)-C(23)	-51.0(9)
C(20)-N(1)-C(22)-C(23)	65.2(8)
C(18)-N(1)-C(24)-C(25)	59.6(10)
C(22)-N(1)-C(24)-C(25)	-61.1(9)
C(20)-N(1)-C(24)-C(25)	-175.3(7)

Symmetry transformations used to generate equivalent atoms:

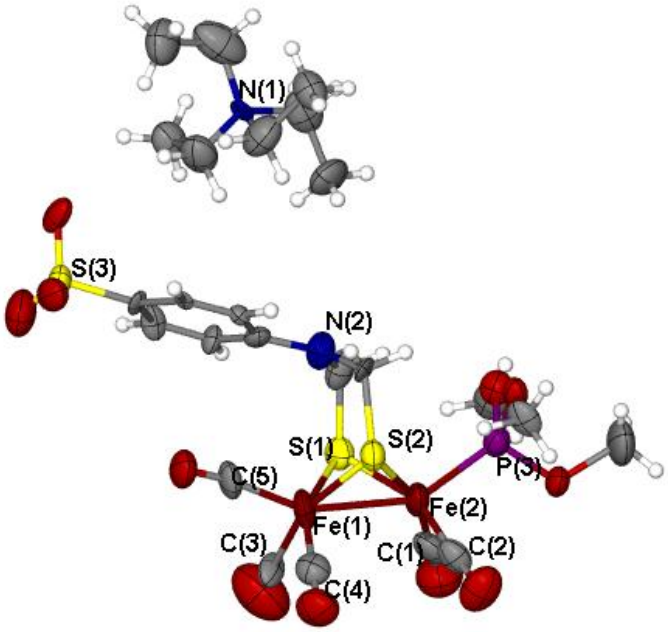
N(1)
S(3)
N(2)
S(1)
S(2)
P(3)
C(5)
Fe(1)
Fe(2)
C(3)
C(1)
C(2)
C(4)

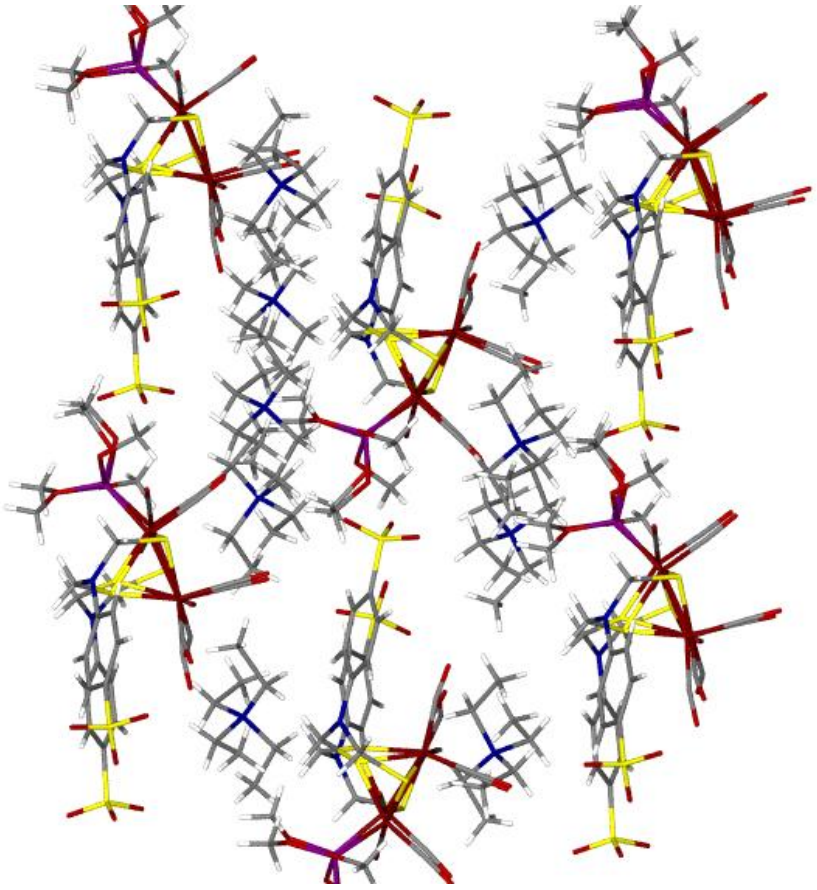

Table A-79. Crystal data and structure refinement for V-Et_4N^+3:.

Identification code	V-Et_4^+3	
Empirical formula	C27 H50 Fe2 N2 O8 P2 S3	
Formula weight	800.51	
Temperature	110(2) K	
Wavelength	0.71073 Å	
Crystal system	Monoclinic	
Space group	P21/c	
Unit cell dimensions	a = 10.311(2) Å	α= 90°.
	b = 34.159(7) Å	β= 91.713(2)°.
	c = 10.437(2) Å	γ = 90°.
Volume	3674.4(12) $Å^3$	
Z	4	
Density (calculated)	1.447 Mg/m^3	
Absorption coefficient	1.093 mm^{-1}	
F(000)	1680	
Crystal size	0.20 x 0.18 x 0.13 mm^3	
Theta range for data collection	1.98 to 20.50°.	
Index ranges	-10<=h<=10, -33<=k<=33, -10<=l<=10	
Reflections collected	22680	
Independent reflections	3676 [R(int) = 0.0646]	
Completeness to theta = 20.50°	99.5 %	
Absorption correction	Semi-empirical from equivalents	
Max. and min. transmission	0.8710 and 0.8111	
Refinement method	Full-matrix least-squares on F^2	
Data / restraints / parameters	3676 / 0 / 407	
Goodness-of-fit on F^2	1.096	
Final R indices [I>2sigma(I)]	R1 = 0.0489, wR2 = 0.1465	
R indices (all data)	R1 = 0.0622, wR2 = 0.1625	
Largest diff. peak and hole	1.914 and -0.487 e.$Å^{-3}$	

Table A-80. Atomic coordinates (x 10^4) and equivalent isotropic displacement parameters ($Å^2$x 10^3) for V-Et_4N^+3. U(eq) is defined as one third of the trace of the orthogonalized U^{ij} tensor.

	x	y	z	U(eq)
Fe(1)	553(1)	3354(1)	7736(1)	25(1)
Fe(2)	2981(1)	3149(1)	7905(1)	23(1)
S(3)	2248(2)	3772(1)	7848(2)	24(1)
S(4)	-2395(2)	4793(1)	2827(2)	24(1)
S(5)	1650(2)	3056(1)	6183(2)	23(1)
P(6)	3893(2)	3260(1)	9838(2)	32(1)
P(7)	-747(2)	2844(1)	7733(2)	36(1)
O(1)	-1628(5)	5079(1)	2160(4)	34(1)
O(2)	-3107(5)	4961(2)	3870(4)	37(1)
N(3)	1845(5)	3808(2)	5186(5)	21(1)
O(4)	5399(5)	3214(2)	6559(5)	49(2)
C(5)	-678(6)	4568(2)	4727(6)	21(2)
N(6)	-7163(5)	5026(1)	1886(5)	17(1)
O(7)	-1665(5)	3794(2)	6687(5)	40(1)
O(8)	-3205(4)	4556(1)	1959(4)	26(1)
C(9)	756(6)	4019(2)	4681(6)	18(2)
C(10)	299(6)	4348(2)	5288(6)	19(2)
O(11)	3120(5)	2309(2)	8407(5)	37(1)
C(12)	-7239(6)	4793(2)	3112(6)	24(2)
C(14)	2617(6)	3961(2)	6231(6)	24(2)
C(15)	5102(8)	3644(2)	9847(7)	46(2)
C(16)	160(6)	3911(2)	3512(6)	22(2)
C(17)	2067(7)	3405(2)	4904(6)	21(2)
C(18)	218(7)	3432(2)	9353(8)	34(2)
C(20)	-8307(7)	5614(2)	800(6)	29(2)
C(21)	-8499(7)	4527(2)	606(7)	31(2)
C(22)	-1242(6)	4465(2)	3548(6)	17(2)
C(23)	-737(8)	3623(2)	7059(7)	30(2)
C(24)	-833(6)	4133(2)	2968(6)	21(2)

C(26)	-5570(7)	5526(2)	2846(8)	41(2)
C(27)	3021(7)	2638(2)	8219(6)	28(2)
C(28)	4759(7)	2846(2)	10530(7)	40(2)
C(29)	-56(7)	2368(2)	8024(8)	43(2)
C(30)	2916(8)	3410(2)	11157(7)	44(2)
C(31)	-8267(6)	5323(2)	1895(6)	24(2)
C(32)	4463(8)	3187(2)	7121(7)	31(2)
C(34)	-1627(8)	2770(3)	6221(8)	58(2)
C(35)	-7286(7)	4765(2)	706(6)	26(2)
C(36)	-5858(6)	5234(2)	1800(7)	28(2)
C(37)	-6263(7)	4466(2)	3260(6)	31(2)
C(42)	-2100(8)	2884(2)	8794(8)	52(2)
O(5)	-82(5)	3486(2)	10404(6)	50(2)
C(3)	6200(8)	3792(2)	4072(8)	47(2)
O(3)	6744(7)	3278(4)	3301(8)	190(7)

Table A-81. Bond lengths [Å] and angles [°] for V-Et_4N^+3.

Fe(1)-C(23)	1.749(9)
Fe(1)-C(18)	1.754(9)
Fe(1)-P(7)	2.198(2)
Fe(1)-S(5)	2.2462(19)
Fe(1)-S(3)	2.257(2)
Fe(1)-Fe(2)	2.5992(14)
Fe(2)-C(32)	1.760(9)
Fe(2)-C(27)	1.778(8)
Fe(2)-P(6)	2.233(2)
Fe(2)-S(5)	2.251(2)
Fe(2)-S(3)	2.2557(19)
S(3)-C(14)	1.858(6)
S(4)-O(1)	1.448(5)
S(4)-O(2)	1.450(5)
S(4)-O(8)	1.458(5)
S(4)-C(22)	1.783(6)
S(5)-C(17)	1.849(6)
P(6)-C(30)	1.805(8)
P(6)-C(15)	1.810(8)
P(6)-C(28)	1.810(7)
P(7)-C(29)	1.797(8)
P(7)-C(42)	1.812(8)
P(7)-C(34)	1.814(8)
N(3)-C(9)	1.422(8)
N(3)-C(17)	1.428(8)
N(3)-C(14)	1.429(8)
O(4)-C(32)	1.148(8)
C(5)-C(10)	1.374(9)
C(5)-C(22)	1.390(9)
N(6)-C(12)	1.511(8)
N(6)-C(35)	1.522(8)
N(6)-C(31)	1.525(8)

N(6)-C(36)	1.525(8)
O(7)-C(23)	1.176(8)
C(9)-C(10)	1.382(9)
C(9)-C(16)	1.399(9)
O(11)-C(27)	1.144(8)
C(12)-C(37)	1.509(9)
C(16)-C(24)	1.384(9)
C(18)-O(5)	1.163(8)
C(20)-C(31)	1.514(9)
C(21)-C(35)	1.494(9)
C(22)-C(24)	1.358(9)
C(26)-C(36)	1.503(9)

C(23)-Fe(1)-C(18)	98.0(3)
C(23)-Fe(1)-P(7)	87.7(2)
C(18)-Fe(1)-P(7)	89.1(2)
C(23)-Fe(1)-S(5)	109.9(2)
C(18)-Fe(1)-S(5)	151.8(2)
P(7)-Fe(1)-S(5)	87.77(8)
C(23)-Fe(1)-S(3)	105.4(2)
C(18)-Fe(1)-S(3)	91.6(2)
P(7)-Fe(1)-S(3)	166.58(8)
S(5)-Fe(1)-S(3)	85.29(7)
C(23)-Fe(1)-Fe(2)	152.6(2)
C(18)-Fe(1)-Fe(2)	101.1(2)
P(7)-Fe(1)-Fe(2)	111.93(7)
S(5)-Fe(1)-Fe(2)	54.78(5)
S(3)-Fe(1)-Fe(2)	54.81(5)
C(32)-Fe(2)-C(27)	98.1(3)
C(32)-Fe(2)-P(6)	93.4(2)
C(27)-Fe(2)-P(6)	89.6(2)
C(32)-Fe(2)-S(5)	99.0(2)
C(27)-Fe(2)-S(5)	91.1(2)
P(6)-Fe(2)-S(5)	167.37(8)

C(32)-Fe(2)-S(3)	102.3(2)
C(27)-Fe(2)-S(3)	159.5(2)
P(6)-Fe(2)-S(3)	89.81(7)
S(5)-Fe(2)-S(3)	85.20(7)
C(32)-Fe(2)-Fe(1)	142.8(2)
C(27)-Fe(2)-Fe(1)	107.1(2)
P(6)-Fe(2)-Fe(1)	113.28(7)
S(5)-Fe(2)-Fe(1)	54.61(5)
S(3)-Fe(2)-Fe(1)	54.86(5)
C(14)-S(3)-Fe(2)	106.0(2)
C(14)-S(3)-Fe(1)	110.6(2)
Fe(2)-S(3)-Fe(1)	70.34(6)
O(1)-S(4)-O(2)	112.9(3)
O(1)-S(4)-O(8)	112.7(3)
O(2)-S(4)-O(8)	113.2(3)
O(1)-S(4)-C(22)	105.0(3)
O(2)-S(4)-C(22)	106.2(3)
O(8)-S(4)-C(22)	106.0(3)
C(17)-S(5)-Fe(1)	111.2(2)
C(17)-S(5)-Fe(2)	109.6(2)
Fe(1)-S(5)-Fe(2)	70.61(6)
C(30)-P(6)-C(15)	101.0(4)
C(30)-P(6)-C(28)	101.4(4)
C(15)-P(6)-C(28)	103.4(4)
C(30)-P(6)-Fe(2)	120.5(3)
C(15)-P(6)-Fe(2)	113.5(3)
C(28)-P(6)-Fe(2)	114.7(3)
C(29)-P(7)-C(42)	105.9(4)
C(29)-P(7)-C(34)	101.9(4)
C(42)-P(7)-C(34)	99.6(4)
C(29)-P(7)-Fe(1)	118.6(3)
C(42)-P(7)-Fe(1)	114.9(3)
C(34)-P(7)-Fe(1)	113.6(3)
C(9)-N(3)-C(17)	122.8(5)

C(9)-N(3)-C(14)	120.9(5)
C(17)-N(3)-C(14)	114.9(5)
C(10)-C(5)-C(22)	121.3(6)
C(12)-N(6)-C(35)	111.8(5)
C(12)-N(6)-C(31)	106.7(5)
C(35)-N(6)-C(31)	110.5(5)
C(12)-N(6)-C(36)	111.3(5)
C(35)-N(6)-C(36)	106.1(5)
C(31)-N(6)-C(36)	110.5(5)
C(10)-C(9)-C(16)	117.9(6)
C(10)-C(9)-N(3)	121.2(6)
C(16)-C(9)-N(3)	120.8(6)
C(5)-C(10)-C(9)	120.4(6)
C(37)-C(12)-N(6)	115.2(5)
N(3)-C(14)-S(3)	116.2(5)
C(24)-C(16)-C(9)	120.9(6)
N(3)-C(17)-S(5)	115.5(4)
O(5)-C(18)-Fe(1)	175.9(6)
C(24)-C(22)-C(5)	118.6(6)
C(24)-C(22)-S(4)	123.2(5)
C(5)-C(22)-S(4)	118.1(5)
O(7)-C(23)-Fe(1)	174.4(6)
C(22)-C(24)-C(16)	120.7(6)
O(11)-C(27)-Fe(2)	176.1(6)
C(20)-C(31)-N(6)	115.8(5)
O(4)-C(32)-Fe(2)	176.9(6)
C(21)-C(35)-N(6)	115.2(5)
C(26)-C(36)-N(6)	114.9(6)

Symmetry transformations used to generate equivalent atoms:

Table A-82. Anisotropic displacement parameters ($Å^2 x\ 10^3$)for V-Et_4N^+3. The anisotropic displacement factor exponent takes the form: $-2\pi^2[\ h^2a^{*2}U^{11} + ... + 2\ h\ k\ a^*\ b^*\ U^{12}\ ]$

	U^{11}	U^{22}	U^{33}	U^{23}	U^{13}	U^{12}
Fe(1)	25(1)	25(1)	25(1)	-1(1)	2(1)	0(1)
Fe(2)	25(1)	20(1)	26(1)	3(1)	-1(1)	1(1)
S(3)	31(1)	19(1)	22(1)	0(1)	-2(1)	0(1)
S(4)	25(1)	24(1)	21(1)	0(1)	-3(1)	7(1)
S(5)	26(1)	19(1)	26(1)	0(1)	1(1)	0(1)
P(6)	37(1)	29(1)	29(1)	4(1)	-6(1)	-1(1)
P(7)	31(1)	32(1)	45(1)	-2(1)	7(1)	-2(1)
O(1)	39(3)	29(3)	34(3)	9(2)	-12(2)	-3(2)
O(2)	37(3)	53(3)	22(3)	-9(2)	-6(2)	20(3)
N(3)	29(4)	15(3)	19(3)	-2(3)	-6(3)	1(3)
O(4)	29(3)	60(4)	57(4)	20(3)	12(3)	4(3)
C(5)	22(4)	19(4)	20(4)	-1(3)	2(3)	1(3)
N(6)	14(3)	18(3)	20(3)	-1(3)	2(2)	1(2)
O(7)	35(3)	41(3)	46(3)	3(3)	3(3)	3(3)
O(8)	22(3)	32(3)	24(3)	-1(2)	-6(2)	-2(2)
C(9)	21(4)	17(4)	17(4)	4(3)	3(3)	-3(3)
C(10)	24(4)	21(4)	13(4)	-3(3)	-3(3)	2(3)
O(11)	50(3)	18(3)	44(3)	7(3)	3(3)	2(3)
C(12)	27(4)	31(4)	14(4)	6(3)	2(3)	2(3)
C(14)	27(4)	23(4)	22(4)	2(3)	-2(3)	4(3)
C(15)	52(5)	45(5)	40(5)	5(4)	-16(4)	-11(4)
C(16)	29(4)	18(4)	19(4)	-2(3)	1(3)	1(3)
C(17)	29(4)	17(4)	17(4)	2(3)	0(3)	4(3)
C(18)	30(5)	34(5)	37(6)	1(4)	0(4)	0(4)
C(20)	33(4)	30(4)	24(4)	2(3)	-3(3)	8(4)
C(21)	40(5)	23(4)	28(4)	-6(3)	-7(4)	-6(4)
C(22)	18(4)	15(4)	18(4)	2(3)	2(3)	-1(3)
C(23)	28(5)	28(4)	33(5)	1(4)	7(4)	-1(4)
C(24)	22(4)	25(4)	16(4)	-1(3)	0(3)	-1(3)

C(26)	28(5)	31(5)	64(6)	-4(4)	-13(4)	1(4)
C(27)	30(4)	30(5)	23(4)	2(4)	-1(3)	-4(4)
C(28)	42(5)	44(5)	34(5)	7(4)	-10(4)	5(4)
C(29)	37(5)	30(5)	62(6)	1(4)	8(4)	-6(4)
C(30)	60(6)	43(5)	27(5)	-3(4)	-8(4)	13(4)
C(31)	16(4)	27(4)	29(4)	-5(3)	1(3)	4(3)
C(32)	36(5)	27(5)	29(5)	11(3)	-2(4)	-1(4)
C(34)	51(6)	58(6)	65(6)	-3(5)	-10(5)	-12(5)
C(35)	36(5)	23(4)	19(4)	-6(3)	5(3)	3(4)
C(36)	23(4)	24(4)	37(5)	3(3)	-1(3)	-1(3)
C(37)	33(5)	32(4)	28(4)	12(3)	6(3)	4(4)
C(42)	41(5)	44(6)	73(6)	7(5)	13(5)	-2(4)
O(5)	58(4)	63(4)	30(4)	-4(3)	11(3)	-1(3)
C(3)	58(6)	24(5)	62(6)	-9(4)	16(5)	15(4)
O(3)	58(5)	404(17)	104(6)	170(9)	-77(5)	-120(8)

Table A-83. Hydrogen coordinates (x 10^4) and isotropic displacement parameters ($Å^2$x 10^3) for V-Et_4N^+3.

	x	y	z	U(eq)
H(5)	-976	4796	5154	25
H(10)	664	4424	6097	23
H(12A)	-7119	4974	3846	29
H(12B)	-8121	4680	3157	29
H(14A)	2513	4249	6239	29
H(14B)	3539	3905	6067	29
H(15A)	4693	3891	9585	69
H(15B)	5782	3577	9248	69
H(15C)	5486	3671	10713	69
H(16)	442	3682	3086	26
H(17A)	2996	3371	4716	26
H(17B)	1557	3336	4118	26
H(20A)	-7512	5771	827	44
H(20B)	-9061	5786	880	44
H(20C)	-8376	5473	-17	44
H(21A)	-8516	4341	1323	46
H(21B)	-8522	4382	-205	46
H(21C)	-9255	4700	637	46
H(24)	-1234	4053	2180	25
H(26A)	-6215	5737	2801	62
H(26B)	-4702	5636	2740	62
H(26C)	-5606	5396	3681	62
H(28A)	5185	2925	11342	60
H(28B)	5414	2756	9936	60
H(28C)	4147	2633	10688	60
H(29A)	432	2369	8844	64
H(29B)	528	2302	7333	64
H(29C)	-752	2173	8054	64

H(30A)	2247	3213	11302	65
H(30B)	2502	3662	10952	65
H(30C)	3468	3438	11932	65
H(31A)	-9099	5178	1884	29
H(31B)	-8204	5471	2711	29
H(34A)	-1009	2733	5536	87
H(34B)	-2167	3000	6030	87
H(34C)	-2180	2538	6282	87
H(35A)	-7242	4932	-66	31
H(35B)	-6533	4586	705	31
H(36A)	-5163	5034	1816	34
H(36B)	-5832	5370	964	34
H(37A)	-6406	4275	2570	46
H(37B)	-6366	4337	4090	46
H(37C)	-5384	4573	3216	46
H(42A)	-2657	2653	8693	79
H(42B)	-2603	3119	8578	79
H(42C)	-1773	2901	9683	79

Table A-84. Torsion angles [°] for V-Et_4N^+3.

C(23)-Fe(1)-Fe(2)-C(32)	-11.0(7)
C(18)-Fe(1)-Fe(2)-C(32)	-144.4(5)
P(7)-Fe(1)-Fe(2)-C(32)	122.1(4)
S(5)-Fe(1)-Fe(2)-C(32)	51.7(4)
S(3)-Fe(1)-Fe(2)-C(32)	-60.3(4)
C(23)-Fe(1)-Fe(2)-C(27)	-141.5(5)
C(18)-Fe(1)-Fe(2)-C(27)	85.1(3)
P(7)-Fe(1)-Fe(2)-C(27)	-8.4(2)
S(5)-Fe(1)-Fe(2)-C(27)	-78.8(2)
S(3)-Fe(1)-Fe(2)-C(27)	169.2(2)
C(23)-Fe(1)-Fe(2)-P(6)	121.4(5)
C(18)-Fe(1)-Fe(2)-P(6)	-12.0(3)
P(7)-Fe(1)-Fe(2)-P(6)	-105.49(9)
S(5)-Fe(1)-Fe(2)-P(6)	-175.89(9)
S(3)-Fe(1)-Fe(2)-P(6)	72.10(8)
C(23)-Fe(1)-Fe(2)-S(5)	-62.7(5)
C(18)-Fe(1)-Fe(2)-S(5)	163.9(3)
P(7)-Fe(1)-Fe(2)-S(5)	70.40(9)
S(3)-Fe(1)-Fe(2)-S(5)	-112.01(8)
C(23)-Fe(1)-Fe(2)-S(3)	49.3(5)
C(18)-Fe(1)-Fe(2)-S(3)	-84.1(2)
P(7)-Fe(1)-Fe(2)-S(3)	-177.60(9)
S(5)-Fe(1)-Fe(2)-S(3)	112.01(8)
C(32)-Fe(2)-S(3)-C(14)	40.8(3)
C(27)-Fe(2)-S(3)-C(14)	-137.5(7)
P(6)-Fe(2)-S(3)-C(14)	134.3(2)
S(5)-Fe(2)-S(3)-C(14)	-57.4(2)
Fe(1)-Fe(2)-S(3)-C(14)	-106.7(2)
C(32)-Fe(2)-S(3)-Fe(1)	147.5(2)
C(27)-Fe(2)-S(3)-Fe(1)	-30.8(6)
P(6)-Fe(2)-S(3)-Fe(1)	-119.06(7)
S(5)-Fe(2)-S(3)-Fe(1)	49.33(6)

C(23)-Fe(1)-S(3)-C(14)	-58.6(3)
C(18)-Fe(1)-S(3)-C(14)	-157.3(3)
P(7)-Fe(1)-S(3)-C(14)	109.9(4)
S(5)-Fe(1)-S(3)-C(14)	50.8(2)
Fe(2)-Fe(1)-S(3)-C(14)	100.2(2)
C(23)-Fe(1)-S(3)-Fe(2)	-158.8(2)
C(18)-Fe(1)-S(3)-Fe(2)	102.5(2)
P(7)-Fe(1)-S(3)-Fe(2)	9.6(4)
S(5)-Fe(1)-S(3)-Fe(2)	-49.46(6)
C(23)-Fe(1)-S(5)-C(17)	50.0(3)
C(18)-Fe(1)-S(5)-C(17)	-139.3(6)
P(7)-Fe(1)-S(5)-C(17)	136.8(2)
S(3)-Fe(1)-S(5)-C(17)	-54.7(2)
Fe(2)-Fe(1)-S(5)-C(17)	-104.2(2)
C(23)-Fe(1)-S(5)-Fe(2)	154.2(2)
C(18)-Fe(1)-S(5)-Fe(2)	-35.1(5)
P(7)-Fe(1)-S(5)-Fe(2)	-119.01(7)
S(3)-Fe(1)-S(5)-Fe(2)	49.49(6)
C(32)-Fe(2)-S(5)-C(17)	-44.9(3)
C(27)-Fe(2)-S(5)-C(17)	-143.3(3)
P(6)-Fe(2)-S(5)-C(17)	123.9(4)
S(3)-Fe(2)-S(5)-C(17)	56.9(2)
Fe(1)-Fe(2)-S(5)-C(17)	106.4(2)
C(32)-Fe(2)-S(5)-Fe(1)	-151.3(2)
C(27)-Fe(2)-S(5)-Fe(1)	110.3(2)
P(6)-Fe(2)-S(5)-Fe(1)	17.5(4)
S(3)-Fe(2)-S(5)-Fe(1)	-49.53(6)
C(32)-Fe(2)-P(6)-C(30)	161.6(4)
C(27)-Fe(2)-P(6)-C(30)	-100.3(4)
S(5)-Fe(2)-P(6)-C(30)	-7.4(5)
S(3)-Fe(2)-P(6)-C(30)	59.2(3)
Fe(1)-Fe(2)-P(6)-C(30)	8.1(3)
C(32)-Fe(2)-P(6)-C(15)	41.8(4)
C(27)-Fe(2)-P(6)-C(15)	140.0(4)

S(5)-Fe(2)-P(6)-C(15)	-127.1(4)
S(3)-Fe(2)-P(6)-C(15)	-60.5(3)
Fe(1)-Fe(2)-P(6)-C(15)	-111.6(3)
C(32)-Fe(2)-P(6)-C(28)	-76.8(4)
C(27)-Fe(2)-P(6)-C(28)	21.3(4)
S(5)-Fe(2)-P(6)-C(28)	114.3(4)
S(3)-Fe(2)-P(6)-C(28)	-179.1(3)
Fe(1)-Fe(2)-P(6)-C(28)	129.8(3)
C(23)-Fe(1)-P(7)-C(29)	167.3(4)
C(18)-Fe(1)-P(7)-C(29)	-94.7(4)
S(5)-Fe(1)-P(7)-C(29)	57.3(3)
S(3)-Fe(1)-P(7)-C(29)	-1.6(5)
Fe(2)-Fe(1)-P(7)-C(29)	6.9(3)
C(23)-Fe(1)-P(7)-C(42)	-66.2(4)
C(18)-Fe(1)-P(7)-C(42)	31.9(4)
S(5)-Fe(1)-P(7)-C(42)	-176.1(3)
S(3)-Fe(1)-P(7)-C(42)	125.0(4)
Fe(2)-Fe(1)-P(7)-C(42)	133.5(3)
C(23)-Fe(1)-P(7)-C(34)	47.6(4)
C(18)-Fe(1)-P(7)-C(34)	145.7(4)
S(5)-Fe(1)-P(7)-C(34)	-62.3(3)
S(3)-Fe(1)-P(7)-C(34)	-121.2(5)
Fe(2)-Fe(1)-P(7)-C(34)	-112.7(3)
C(17)-N(3)-C(9)-C(10)	156.4(6)
C(14)-N(3)-C(9)-C(10)	-9.1(9)
C(17)-N(3)-C(9)-C(16)	-27.4(9)
C(14)-N(3)-C(9)-C(16)	167.1(6)
C(22)-C(5)-C(10)-C(9)	0.5(9)
C(16)-C(9)-C(10)-C(5)	-2.2(9)
N(3)-C(9)-C(10)-C(5)	174.1(6)
C(35)-N(6)-C(12)-C(37)	56.0(7)
C(31)-N(6)-C(12)-C(37)	176.9(6)
C(36)-N(6)-C(12)-C(37)	-62.4(7)
C(9)-N(3)-C(14)-S(3)	97.9(6)

C(17)-N(3)-C(14)-S(3)	-68.6(6)
Fe(2)-S(3)-C(14)-N(3)	71.9(5)
Fe(1)-S(3)-C(14)-N(3)	-2.6(5)
C(10)-C(9)-C(16)-C(24)	1.5(9)
N(3)-C(9)-C(16)-C(24)	-174.8(6)
C(9)-N(3)-C(17)-S(5)	-102.3(6)
C(14)-N(3)-C(17)-S(5)	63.9(7)
Fe(1)-S(5)-C(17)-N(3)	10.3(5)
Fe(2)-S(5)-C(17)-N(3)	-65.9(5)
C(23)-Fe(1)-C(18)-O(5)	29(9)
P(7)-Fe(1)-C(18)-O(5)	-58(9)
S(5)-Fe(1)-C(18)-O(5)	-142(9)
S(3)-Fe(1)-C(18)-O(5)	135(9)
Fe(2)-Fe(1)-C(18)-O(5)	-170(9)
C(10)-C(5)-C(22)-C(24)	2.0(9)
C(10)-C(5)-C(22)-S(4)	-174.2(5)
O(1)-S(4)-C(22)-C(24)	-91.9(6)
O(2)-S(4)-C(22)-C(24)	148.4(5)
O(8)-S(4)-C(22)-C(24)	27.7(6)
O(1)-S(4)-C(22)-C(5)	84.1(5)
O(2)-S(4)-C(22)-C(5)	-35.6(6)
O(8)-S(4)-C(22)-C(5)	-156.3(5)
C(18)-Fe(1)-C(23)-O(7)	-36(7)
P(7)-Fe(1)-C(23)-O(7)	53(7)
S(5)-Fe(1)-C(23)-O(7)	140(7)
S(3)-Fe(1)-C(23)-O(7)	-130(7)
Fe(2)-Fe(1)-C(23)-O(7)	-170(6)
C(5)-C(22)-C(24)-C(16)	-2.7(9)
S(4)-C(22)-C(24)-C(16)	173.3(5)
C(9)-C(16)-C(24)-C(22)	0.9(9)
C(32)-Fe(2)-C(27)-O(11)	16(9)
P(6)-Fe(2)-C(27)-O(11)	-77(9)
S(5)-Fe(2)-C(27)-O(11)	115(9)
S(3)-Fe(2)-C(27)-O(11)	-166(8)

Fe(1)-Fe(2)-C(27)-O(11)	168(9)
C(12)-N(6)-C(31)-C(20)	175.0(6)
C(35)-N(6)-C(31)-C(20)	-63.3(7)
C(36)-N(6)-C(31)-C(20)	53.8(7)
C(27)-Fe(2)-C(32)-O(4)	108(12)
P(6)-Fe(2)-C(32)-O(4)	-162(12)
S(5)-Fe(2)-C(32)-O(4)	16(12)
S(3)-Fe(2)-C(32)-O(4)	-71(12)
Fe(1)-Fe(2)-C(32)-O(4)	-25(13)
C(12)-N(6)-C(35)-C(21)	57.5(7)
C(31)-N(6)-C(35)-C(21)	-61.2(7)
C(36)-N(6)-C(35)-C(21)	179.0(6)
C(12)-N(6)-C(36)-C(26)	-61.4(7)
C(35)-N(6)-C(36)-C(26)	176.8(6)
C(31)-N(6)-C(36)-C(26)	57.0(7)

Symmetry transformations used to generate equivalent atoms:

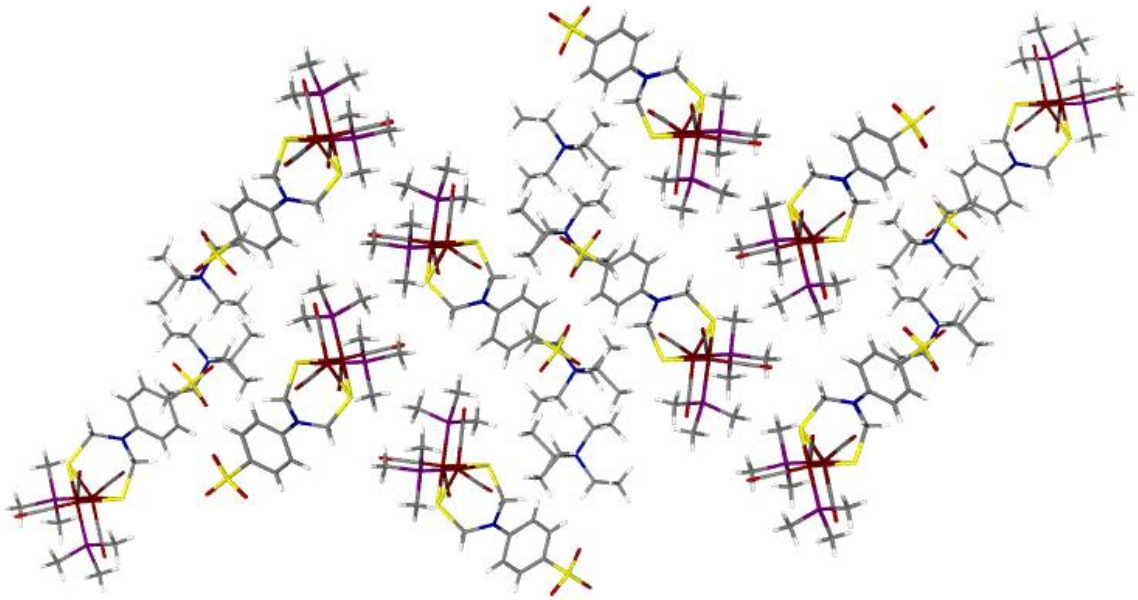

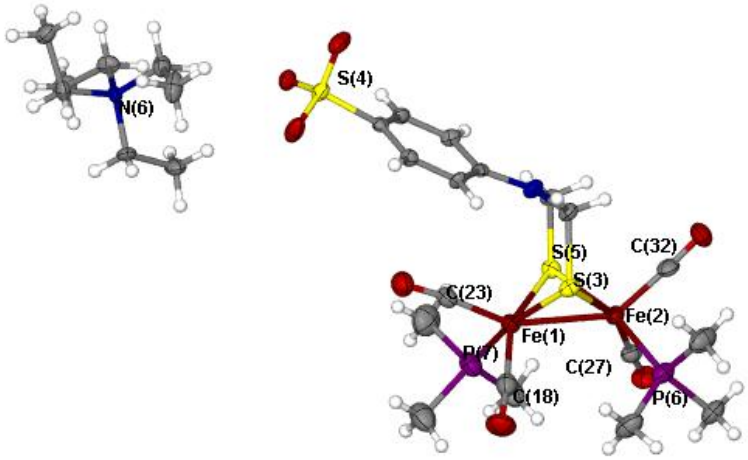
S(4)
N(6)
S(5)
S(3)
C(32)
C(23)
Fe(2)
Fe(1)
C(27)
C(18)
P(6)

Table A-85. Crystal data and structure refinement for V-**1-CyD**.

Identification code	mlsm	
Empirical formula	C98 H204 Fe2 N Na O107 S3	
Formula weight	3339.49	
Temperature	110(2) K	
Wavelength	0.71073 Å	
Crystal system	Triclinic	
Space group	P1	
Unit cell dimensions	a = 15.346(4) Å	α= 113.517(3)°.
	b = 15.422(4) Å	β= 98.507(3)°.
	c = 17.595(4) Å	γ = 103.154(3)°.
Volume	3582.9(15) $Å^3$	
Z	1	
Density (calculated)	1.548 Mg/m^3	
Absorption coefficient	0.375 mm^{-1}	
F(000)	1766	
Crystal size	0.30 x 0.10 x 0.10 mm^3	
Theta range for data collection	2.41 to 25.00°.	
Index ranges	-18<=h<=18, -18<=k<=18, -20<=l<=20	
Reflections collected	33320	
Independent reflections	24259 [R(int) = 0.0585]	
Completeness to theta = 25.00°	98.8 %	
Absorption correction	Semi-empirical from equivalents	
Max. and min. transmission	0.9634 and 0.8958	
Refinement method	Full-matrix least-squares on F^2	
Data / restraints / parameters	24259 / 53 / 1958	
Goodness-of-fit on F^2	0.999	
Final R indices [I>2sigma(I)]	R1 = 0.0832, wR2 = 0.1797	
R indices (all data)	R1 = 0.1277, wR2 = 0.2086	
Absolute structure parameter	0.02(2)	
Largest diff. peak and hole	0.843 and -0.561 $e.Å^{-3}$	

Table A-86. Atomic coordinates (x 10^4) and equivalent isotropic displacement parameters ($Å^2$x 10^3) for **V-1-CyD**. U(eq) is defined as one third of the trace of the orthogonalized U^{ij} tensor.

	x	y	z	U(eq)
Fe(1)	-4827(1)	-2073(1)	-3201(1)	30(1)
Fe(2)	-5591(1)	-3444(1)	-4691(1)	30(1)
S(1)	-6399(2)	-2824(2)	-3756(2)	33(1)
S(2)	-4768(2)	-3637(2)	-3625(2)	32(1)
S(3)	-5232(2)	-714(2)	878(2)	42(1)
Na(1)	-3056(4)	-7243(4)	-3339(5)	28(2)
Na(1')	-2837(10)	-7394(14)	-3859(18)	55(7)
O(1)	-4076(5)	-1114(5)	-1322(4)	42(2)
O(2)	-5115(5)	-323(6)	-3315(5)	50(2)
O(3)	-2988(5)	-1476(5)	-3427(4)	44(2)
O(4)	-6914(5)	-5365(6)	-5976(5)	56(2)
O(5)	-4158(5)	-3644(6)	-5608(5)	54(2)
O(6)	-6117(5)	-2406(6)	-5667(5)	49(2)
O(7)	-5528(6)	-1229(6)	1349(5)	66(2)
O(8)	-5685(5)	17(6)	901(5)	56(2)
O(9)	-4214(5)	-244(6)	1148(5)	60(2)
N(1)	-6157(5)	-3809(6)	-2756(5)	33(2)
C(1)	-4387(6)	-1484(7)	-2018(7)	36(2)
C(2)	-5022(5)	-1050(7)	-3288(5)	29(2)
C(3)	-3712(7)	-1715(7)	-3337(6)	33(2)
C(4)	-6409(7)	-4619(8)	-5455(6)	34(2)
C(5)	-4689(6)	-3574(8)	-5235(6)	37(2)
C(6)	-5918(6)	-2795(7)	-5261(7)	37(2)
C(7)	-5471(7)	-4249(7)	-3119(6)	42(2)
C(8)	-6822(7)	-3772(7)	-3388(6)	40(2)
C(9)	-5925(6)	-3071(7)	-1903(6)	33(2)

C(10)	-5326(6)	-3115(7)	-1242(6)	33(2)
C(11)	-5119(7)	-2396(7)	-402(6)	35(2)
C(12)	-5482(6)	-1611(7)	-185(6)	35(2)
C(13)	-6042(6)	-1538(7)	-850(6)	32(2)
C(14)	-6273(6)	-2264(8)	-1668(6)	37(2)
O(1A)	-5752(4)	-25(4)	-6269(3)	24(1)
O(2A)	-4693(4)	-266(4)	-5352(3)	24(1)
O(3A)	-4920(4)	1337(4)	-3934(3)	24(1)
O(4A)	-6769(4)	217(5)	-4161(4)	34(2)
O(5A)	-7606(4)	-517(4)	-7293(4)	30(1)
O(6A)	-2710(4)	-916(5)	-6116(4)	29(1)
O(7A)	-2462(4)	-1707(4)	-5258(4)	27(1)
O(8A)	-1669(4)	98(4)	-3798(4)	30(1)
O(9A)	-3273(4)	774(4)	-3853(4)	27(1)
O(10A)	-4116(5)	-2064(5)	-7657(4)	47(2)
O(11A)	-1824(4)	-3997(4)	-6176(3)	24(1)
O(12A)	-2793(4)	-4597(4)	-5456(4)	25(1)
O(13A)	-1347(4)	-3562(4)	-3934(3)	24(1)
O(14A)	-1273(4)	-1615(4)	-3788(4)	29(1)
O(15A)	-1071(4)	-2579(4)	-6775(4)	30(1)
O(16A)	-4355(4)	-7158(4)	-6694(4)	31(1)
O(17A)	-5456(4)	-6952(4)	-5917(4)	26(1)
O(18A)	-4297(4)	-6981(4)	-4556(4)	29(1)
O(19A)	-2769(4)	-5258(4)	-4196(4)	30(1)
O(20A)	-2804(5)	-6425(6)	-7298(4)	47(2)
O(21A)	-7906(4)	-8422(4)	-7092(4)	28(1)
O(22A)	-8334(4)	-7083(4)	-6237(4)	27(1)
O(23A)	-8155(4)	-7664(4)	-4912(4)	30(1)
O(24A)	-6188(4)	-7219(4)	-4633(4)	29(1)
O(25A)	-6544(4)	-9251(4)	-7783(4)	31(1)
O(26A)	-10075(4)	-6207(4)	-7135(3)	26(1)
O(27A)	-9222(4)	-4565(4)	-6163(4)	27(1)
O(28A)	-10038(4)	-4979(5)	-4887(4)	33(2)
O(29A)	-9138(4)	-6351(5)	-4874(4)	35(2)

O(30A)	-9609(5)	-7225(5)	-8622(5)	45(2)
O(31A)	-9024(4)	-2506(4)	-6755(4)	26(1)
O(32A)	-7594(3)	-1525(4)	-5759(3)	22(1)
O(33A)	-8421(4)	-1055(4)	-4438(4)	31(1)
O(34A)	-9133(4)	-2953(4)	-4604(4)	32(1)
O(35A)	-10473(4)	-4085(5)	-7893(4)	33(1)
C(1A)	-5100(5)	431(6)	-5463(5)	23(2)
C(2A)	-5573(6)	793(6)	-4749(5)	23(2)
C(3A)	-6303(6)	-96(6)	-4815(5)	25(2)
C(4A)	-6980(5)	-627(6)	-5705(5)	23(2)
C(5A)	-6511(6)	-887(7)	-6429(6)	28(2)
C(6A)	-7147(6)	-1218(6)	-7293(5)	24(2)
C(7A)	-2162(6)	-828(6)	-5352(6)	30(2)
C(8A)	-2201(5)	21(6)	-4576(5)	26(2)
C(9A)	-3206(6)	-50(7)	-4530(6)	29(2)
C(10A)	-3740(5)	-147(7)	-5383(6)	27(2)
C(11A)	-3691(6)	-1056(7)	-6125(6)	28(2)
C(12A)	-4159(7)	-1171(8)	-6990(6)	37(2)
C(13A)	-1855(5)	-4223(6)	-5484(5)	27(2)
C(14A)	-1362(6)	-3317(6)	-4653(5)	26(2)
C(15A)	-1809(6)	-2535(6)	-4553(5)	26(2)
C(16A)	-1863(6)	-2331(6)	-5336(5)	23(2)
C(17A)	-2238(5)	-3268(6)	-6180(5)	22(2)
C(18A)	-2037(6)	-3021(7)	-6911(6)	30(2)
C(19A)	-4711(5)	-7319(7)	-6039(5)	24(2)
C(20A)	-3947(6)	-6813(6)	-5210(6)	27(2)
C(21A)	-3526(6)	-5708(6)	-4947(5)	27(2)
C(22A)	-3178(5)	-5606(6)	-5667(5)	23(2)
C(23A)	-3953(6)	-6115(6)	-6480(5)	26(2)
C(24A)	-3636(7)	-6112(8)	-7253(6)	43(3)
C(25A)	-8315(6)	-8049(7)	-6413(5)	28(2)
C(26A)	-7751(6)	-7972(7)	-5596(6)	28(2)
C(27A)	-6765(5)	-7268(6)	-5358(5)	22(2)
C(28A)	-6360(5)	-7684(6)	-6132(5)	23(2)

C(29A)	-6980(5)	-7818(6)	-6955(5)	22(2)
C(30A)	-6663(6)	-8359(6)	-7735(5)	27(2)
C(31A)	-10041(6)	-5393(6)	-6379(5)	27(2)
C(32A)	-10006(6)	-5682(6)	-5643(5)	23(2)
C(33A)	-9178(6)	-6036(7)	-5537(5)	26(2)
C(34A)	-9210(5)	-6884(6)	-6350(5)	23(2)
C(35A)	-9330(6)	-6610(6)	-7108(6)	28(2)
C(36A)	-9550(7)	-7482(8)	-7934(6)	39(2)
C(37A)	-8563(5)	-1689(6)	-5958(5)	24(2)
C(38A)	-8905(6)	-1884(6)	-5243(5)	25(2)
C(39A)	-8806(5)	-2812(6)	-5259(5)	25(2)
C(40A)	-9327(6)	-3670(6)	-6125(6)	25(2)
C(41A)	-9002(6)	-3448(7)	-6838(5)	28(2)
C(42A)	-9551(6)	-4199(7)	-7722(5)	28(2)
O(1B)	-9084(4)	-1947(4)	-836(4)	26(1)
O(2B)	-8541(4)	-3201(4)	-1631(4)	24(1)
O(3B)	-9632(4)	-3409(4)	-3136(3)	25(1)
O(4B)	-8742(4)	-1521(5)	-2949(4)	32(1)
O(5B)	-8801(4)	164(4)	172(4)	31(1)
O(6B)	-8134(5)	-4994(5)	-860(4)	37(2)
O(7B)	-7057(4)	-5343(4)	-1644(4)	29(1)
O(8B)	-8465(4)	-6553(4)	-3140(4)	34(2)
O(9B)	-9170(4)	-5040(4)	-3189(4)	32(1)
O(10B)	-9265(6)	-3952(7)	-73(6)	77(3)
O(11B)	-4951(4)	-5755(4)	-748(4)	26(1)
O(12B)	-4164(4)	-4920(4)	-1426(4)	25(1)
O(13B)	-4845(4)	-6660(4)	-2982(4)	30(1)
O(14B)	-6741(4)	-6723(4)	-3143(4)	32(1)
O(15B)	-6501(4)	-6383(5)	-176(4)	37(2)
O(16B)	-1813(4)	-3145(4)	-215(4)	27(1)
O(17B)	-1896(4)	-2264(4)	-1010(4)	27(1)
O(18B)	-1546(4)	-3739(4)	-2364(3)	27(1)
O(19B)	-3195(4)	-5284(4)	-2715(4)	32(1)
O(20B)	-2605(5)	-4417(7)	474(5)	60(2)

O(21B)	-902(4)	465(4)	98(4)	26(1)
O(22B)	-2077(4)	538(4)	-867(4)	27(1)
O(23B)	-1085(4)	118(4)	-2088(4)	31(1)
O(24B)	-1296(4)	-1828(4)	-2296(4)	31(1)
O(25B)	-80(4)	-510(5)	889(4)	37(2)
O(26B)	-3186(4)	2424(5)	43(4)	32(1)
O(27B)	-4571(4)	1448(4)	-1025(3)	24(1)
O(28B)	-3851(4)	2005(4)	-2190(4)	31(1)
O(29B)	-2441(4)	1068(5)	-2217(4)	32(1)
O(30B)	-1390(6)	2754(7)	1011(6)	54(3)
O(30')	-3030(20)	1710(30)	1253(16)	54(3)
O(31B)	-6699(4)	1440(4)	-277(4)	29(1)
O(32B)	-7430(4)	-212(4)	-1311(3)	26(1)
O(33B)	-7771(4)	437(5)	-2558(4)	36(2)
O(34B)	-5819(4)	1281(4)	-2423(4)	30(1)
O(35B)	-5230(4)	3133(4)	797(4)	35(2)
C(1B)	-9269(5)	-2783(6)	-1608(5)	24(2)
C(2B)	-9396(5)	-2551(6)	-2348(5)	24(2)
C(3B)	-8561(6)	-1762(6)	-2262(6)	26(2)
C(4B)	-8326(6)	-883(6)	-1412(5)	26(2)
C(5B)	-8243(5)	-1155(6)	-665(5)	25(2)
C(6B)	-8117(6)	-306(7)	189(5)	28(2)
C(7B)	-7997(5)	-5701(6)	-1605(5)	24(2)
C(8B)	-8629(6)	-5858(6)	-2396(5)	26(2)
C(9B)	-8529(6)	-4876(6)	-2439(6)	26(2)
C(10B)	-8686(6)	-4150(6)	-1622(6)	28(2)
C(11B)	-8065(7)	-4047(7)	-832(6)	33(2)
C(12B)	-8303(8)	-3463(8)	-12(7)	46(3)
C(13B)	-4541(6)	-5846(6)	-1428(5)	25(2)
C(14B)	-5277(6)	-6529(7)	-2286(5)	29(2)
C(15B)	-6052(6)	-6081(7)	-2346(5)	29(2)
C(16B)	-6438(6)	-5913(6)	-1612(5)	24(2)
C(17B)	-5704(6)	-5335(6)	-741(6)	26(2)
C(18B)	-6091(6)	-5386(6)	-18(5)	29(2)

C(19B)	-1545(6)	-2958(6)	-867(6)	29(2)
C(20B)	-1854(6)	-3929(7)	-1707(5)	26(2)
C(21B)	-2913(6)	-4372(7)	-1956(5)	26(2)
C(22B)	-3156(6)	-4513(6)	-1200(5)	24(2)
C(23B)	-2822(6)	-3556(6)	-392(6)	28(2)
C(24B)	-2984(7)	-3664(8)	401(6)	42(3)
C(25B)	-1106(5)	655(6)	-596(5)	24(2)
C(26B)	-897(5)	-89(6)	-1376(5)	23(2)
C(27B)	-1496(6)	-1132(6)	-1602(6)	28(2)
C(28B)	-1270(6)	-1317(6)	-825(5)	23(2)
C(29B)	-1397(5)	-511(6)	-13(5)	22(2)
C(30B)	-1028(6)	-592(7)	783(6)	33(2)
C(31B)	-3760(5)	2291(6)	-724(6)	26(2)
C(32B)	-3273(6)	2110(7)	-1432(6)	35(2)
C(33B)	-2933(6)	1226(6)	-1576(5)	26(2)
C(34B)	-2343(6)	1391(7)	-731(6)	31(2)
C(35B)	-2849(7)	1607(7)	-49(6)	38(2)
C(36B)	-2225(10)	1905(10)	838(7)	66(4)
C(37B)	-7366(6)	795(6)	-1082(6)	31(2)
C(38B)	-7092(6)	1077(6)	-1759(6)	27(2)
C(39B)	-6131(5)	973(6)	-1825(5)	24(2)
C(40B)	-5450(5)	1628(6)	-965(5)	25(2)
C(41B)	-5759(5)	1393(7)	-258(5)	25(2)
C(42B)	-5189(6)	2156(7)	639(6)	34(2)
O(1W)	-7938(6)	1379(5)	-3621(5)	67(2)
O(2W)	-1939(4)	-5650(5)	-8226(4)	43(2)
O(3W)	-9457(4)	-1117(5)	-7940(4)	42(2)
O(4W)	-3613(4)	-5380(5)	1207(4)	41(2)
O(5W)	-9660(4)	-288(5)	-3708(4)	28(2)
O(6W)	-10272(4)	-719(5)	-6616(4)	44(2)
O(7W)	-8306(5)	-7220(6)	-536(5)	57(2)
O(8W)	-9475(5)	1335(6)	-2088(5)	42(2)
O(8')	-9840(30)	1390(30)	-2660(30)	42(2)
O(9W)	-8305(6)	-7847(6)	670(6)	62(2)

O(10W)	-6439(7)	-6562(6)	-8237(6)	71(3)
O(11W)	-10317(5)	-3173(5)	1032(4)	49(2)
O(12W)	-6008(5)	-4547(6)	-7241(5)	62(2)
O(13W)	-9648(6)	549(6)	-4883(5)	67(2)
O(14W)	-4362(6)	-3962(6)	-7714(5)	69(2)
O(15W)	-7348(7)	-4000(8)	-8119(7)	82(3)
O(16W)	-3096(6)	-1330(6)	1451(6)	65(2)
O(17W)	-6010(6)	-3062(7)	1273(6)	72(2)
O(18W)	-1698(7)	-99(9)	-7041(7)	91(3)
O(19W)	-3429(7)	1609(7)	-7635(6)	89(3)
O(20W)	-10160(6)	-7781(7)	-4191(7)	95(4)
O(21W)	-659(7)	-7940(8)	-2836(8)	81(4)
O(22W)	-181(14)	-5670(17)	-366(13)	100(6)
O(22')	-1860(30)	-5690(30)	20(30)	100(6)
O(22")	-1463(11)	-5558(13)	-450(13)	76(5)
O(23W)	-1062(5)	-5332(6)	-3619(6)	11(2)
O(23')	-1044(7)	-5446(8)	-3121(8)	11(2)
O(24W)	-1355(7)	-6352(10)	-2184(9)	136(5)
O(25W)	-1791(12)	-7361(10)	-4659(9)	112(8)
O(26W)	-1944(16)	1796(13)	-6405(14)	110(9)
O(27W)	-8879(11)	-5659(12)	494(11)	85(7)
O(28W)	-692(17)	3582(19)	596(16)	17(7)

Table A-87. Bond lengths [Å] and angles [°] for V-**1-CyD**.

Fe(1)-C(2)	1.731(10)
Fe(1)-C(3)	1.755(10)
Fe(1)-C(1)	1.847(12)
Fe(1)-S(2)	2.250(3)
Fe(1)-S(1)	2.291(3)
Fe(1)-Fe(2)	2.5020(18)
Fe(2)-C(6)	1.772(12)
Fe(2)-C(4)	1.785(11)
Fe(2)-C(5)	1.799(10)
Fe(2)-S(1)	2.248(3)
Fe(2)-S(2)	2.261(3)
S(1)-C(8)	1.850(10)
S(2)-C(7)	1.828(9)
S(3)-O(7)	1.413(8)
S(3)-O(8)	1.444(8)
S(3)-O(9)	1.477(7)
S(3)-C(12)	1.744(10)
Na(1)-O(24W)	2.721(12)
Na(1)-O(9A)#1	2.742(7)
Na(1)-O(19B)	2.845(8)
Na(1)-O(18A)	2.865(8)
Na(1)-O(3A)#1	2.917(8)
Na(1)-O(28B)#1	2.980(10)
Na(1')-O(18A)	2.717(16)
Na(1')-O(9A)#1	2.755(17)
Na(1')-O(24W)	3.00(2)
O(1)-C(1)	1.095(11)
O(2)-C(2)	1.181(11)
O(3)-C(3)	1.144(11)
O(4)-C(4)	1.143(11)
O(5)-C(5)	1.116(11)
O(6)-C(6)	1.151(12)

N(1)-C(9)	1.404(12)
N(1)-C(8)	1.422(12)
N(1)-C(7)	1.468(13)
C(9)-C(10)	1.405(13)
C(9)-C(14)	1.401(13)
C(10)-C(11)	1.382(13)
C(11)-C(12)	1.387(13)
C(12)-C(13)	1.403(13)
C(13)-C(14)	1.354(13)
O(1A)-C(1A)	1.403(10)
O(1A)-C(5A)	1.450(10)
O(2A)-C(1A)	1.422(9)
O(2A)-C(10A)	1.443(9)
O(3A)-C(2A)	1.414(10)
O(3A)-Na(1)#2	2.917(8)
O(4A)-C(3A)	1.424(10)
O(5A)-C(6A)	1.418(10)
O(6A)-C(7A)	1.414(10)
O(6A)-C(11A)	1.468(10)
O(7A)-C(7A)	1.413(10)
O(7A)-C(16A)	1.457(9)
O(8A)-C(8A)	1.430(9)
O(9A)-C(9A)	1.391(10)
O(9A)-Na(1)#2	2.742(7)
O(9A)-Na(1')#2	2.755(17)
O(10A)-C(12A)	1.433(11)
O(11A)-C(13A)	1.398(10)
O(11A)-C(17A)	1.414(10)
O(12A)-C(22A)	1.401(10)
O(12A)-C(13A)	1.440(9)
O(13A)-C(14A)	1.456(9)
O(14A)-C(15A)	1.455(9)
O(15A)-C(18A)	1.423(10)
O(16A)-C(19A)	1.428(10)

O(16A)-C(23A)	1.451(10)
O(17A)-C(19A)	1.395(10)
O(17A)-C(28A)	1.461(9)
O(18A)-C(20A)	1.427(10)
O(19A)-C(21A)	1.422(10)
O(20A)-C(24A)	1.465(13)
O(21A)-C(25A)	1.411(10)
O(21A)-C(29A)	1.436(10)
O(22A)-C(25A)	1.404(11)
O(22A)-C(34A)	1.447(9)
O(23A)-C(26A)	1.400(10)
O(24A)-C(27A)	1.406(10)
O(25A)-C(30A)	1.399(10)
O(26A)-C(31A)	1.401(10)
O(26A)-C(35A)	1.423(10)
O(27A)-C(40A)	1.403(10)
O(27A)-C(31A)	1.447(10)
O(28A)-C(32A)	1.356(10)
O(29A)-C(33A)	1.430(10)
O(30A)-C(36A)	1.413(11)
O(31A)-C(37A)	1.394(10)
O(31A)-C(41A)	1.411(10)
O(32A)-C(37A)	1.415(9)
O(32A)-C(4A)	1.445(9)
O(33A)-C(38A)	1.415(10)
O(34A)-C(39A)	1.396(10)
O(35A)-C(42A)	1.468(10)
C(1A)-C(2A)	1.520(11)
C(2A)-C(3A)	1.511(11)
C(3A)-C(4A)	1.520(12)
C(4A)-C(5A)	1.516(11)
C(5A)-C(6A)	1.496(12)
C(7A)-C(8A)	1.488(12)
C(8A)-C(9A)	1.537(11)

C(9A)-C(10A)	1.532(12)
C(10A)-C(11A)	1.514(12)
C(11A)-C(12A)	1.506(12)
C(13A)-C(14A)	1.491(12)
C(14A)-C(15A)	1.483(12)
C(15A)-C(16A)	1.525(11)
C(16A)-C(17A)	1.510(11)
C(17A)-C(18A)	1.534(12)
C(19A)-C(20A)	1.510(12)
C(20A)-C(21A)	1.521(12)
C(21A)-C(22A)	1.496(12)
C(22A)-C(23A)	1.501(11)
C(23A)-C(24A)	1.512(12)
C(25A)-C(26A)	1.509(12)
C(26A)-C(27A)	1.531(12)
C(27A)-C(28A)	1.544(12)
C(28A)-C(29A)	1.519(12)
C(29A)-C(30A)	1.511(12)
C(31A)-C(32A)	1.526(12)
C(32A)-C(33A)	1.510(12)
C(33A)-C(34A)	1.489(12)
C(34A)-C(35A)	1.551(12)
C(35A)-C(36A)	1.458(13)
C(37A)-C(38A)	1.542(11)
C(38A)-C(39A)	1.463(12)
C(39A)-C(40A)	1.503(12)
C(40A)-C(41A)	1.545(12)
C(41A)-C(42A)	1.484(12)
O(1B)-C(1B)	1.382(10)
O(1B)-C(5B)	1.456(9)
O(2B)-C(1B)	1.410(9)
O(2B)-C(10B)	1.435(10)
O(3B)-C(2B)	1.405(10)
O(4B)-C(3B)	1.409(10)

O(5B)-C(6B)	1.408(10)
O(6B)-C(7B)	1.413(10)
O(6B)-C(11B)	1.420(11)
O(7B)-C(7B)	1.445(10)
O(7B)-C(16B)	1.443(10)
O(8B)-C(8B)	1.423(9)
O(9B)-C(9B)	1.416(10)
O(10B)-C(12B)	1.463(13)
O(11B)-C(13B)	1.406(10)
O(11B)-C(17B)	1.446(10)
O(12B)-C(13B)	1.412(10)
O(12B)-C(22B)	1.456(9)
O(13B)-C(14B)	1.445(10)
O(14B)-C(15B)	1.429(10)
O(15B)-C(18B)	1.416(10)
O(16B)-C(19B)	1.385(10)
O(16B)-C(23B)	1.466(10)
O(17B)-C(19B)	1.392(10)
O(17B)-C(28B)	1.432(9)
O(18B)-C(20B)	1.418(9)
O(19B)-C(21B)	1.414(11)
O(20B)-C(24B)	1.452(13)
O(21B)-C(25B)	1.375(10)
O(21B)-C(29B)	1.443(10)
O(22B)-C(34B)	1.405(10)
O(22B)-C(25B)	1.441(9)
O(23B)-C(26B)	1.416(9)
O(24B)-C(27B)	1.396(10)
O(25B)-C(30B)	1.409(10)
O(26B)-C(31B)	1.410(10)
O(26B)-C(35B)	1.429(11)
O(27B)-C(31B)	1.428(10)
O(27B)-C(40B)	1.449(10)
O(28B)-C(32B)	1.416(11)

O(28B)-Na(1)#2	2.980(10)
O(29B)-C(33B)	1.419(10)
O(30B)-C(36B)	1.501(17)
O(30')-C(36B)	1.55(3)
O(31B)-C(37B)	1.424(10)
O(31B)-C(41B)	1.457(10)
O(32B)-C(37B)	1.415(10)
O(32B)-C(4B)	1.459(9)
O(33B)-C(38B)	1.424(10)
O(34B)-C(39B)	1.417(10)
O(35B)-C(42B)	1.437(11)
C(1B)-C(2B)	1.480(12)
C(2B)-C(3B)	1.494(11)
C(3B)-C(4B)	1.485(12)
C(4B)-C(5B)	1.528(12)
C(5B)-C(6B)	1.496(12)
C(7B)-C(8B)	1.470(12)
C(8B)-C(9B)	1.522(12)
C(9B)-C(10B)	1.523(12)
C(10B)-C(11B)	1.493(12)
C(11B)-C(12B)	1.516(14)
C(13B)-C(14B)	1.533(12)
C(14B)-C(15B)	1.515(12)
C(15B)-C(16B)	1.454(12)
C(16B)-C(17B)	1.534(12)
C(17B)-C(18B)	1.502(12)
C(19B)-C(20B)	1.535(12)
C(20B)-C(21B)	1.531(11)
C(21B)-C(22B)	1.516(11)
C(22B)-C(23B)	1.492(12)
C(23B)-C(24B)	1.519(12)
C(25B)-C(26B)	1.531(12)
C(26B)-C(27B)	1.516(11)
C(27B)-C(28B)	1.514(12)

C(28B)-C(29B)	1.549(11)
C(29B)-C(30B)	1.495(12)
C(31B)-C(32B)	1.510(12)
C(32B)-C(33B)	1.510(12)
C(33B)-C(34B)	1.514(12)
C(34B)-C(35B)	1.494(13)
C(35B)-C(36B)	1.532(14)
C(37B)-C(38B)	1.503(12)
C(38B)-C(39B)	1.537(12)
C(39B)-C(40B)	1.494(12)
C(40B)-C(41B)	1.536(11)
C(41B)-C(42B)	1.510(12)

C(2)-Fe(1)-C(3)	89.4(4)
C(2)-Fe(1)-C(1)	97.5(4)
C(3)-Fe(1)-C(1)	92.7(4)
C(2)-Fe(1)-S(2)	158.4(3)
C(3)-Fe(1)-S(2)	89.2(3)
C(1)-Fe(1)-S(2)	104.1(3)
C(2)-Fe(1)-S(1)	86.0(3)
C(3)-Fe(1)-S(1)	150.9(3)
C(1)-Fe(1)-S(1)	116.4(3)
S(2)-Fe(1)-S(1)	84.81(9)
C(2)-Fe(1)-Fe(2)	102.4(3)
C(3)-Fe(1)-Fe(2)	97.6(3)
C(1)-Fe(1)-Fe(2)	157.7(3)
S(2)-Fe(1)-Fe(2)	56.54(7)
S(1)-Fe(1)-Fe(2)	55.75(7)
C(6)-Fe(2)-C(4)	94.2(4)
C(6)-Fe(2)-C(5)	87.1(4)
C(4)-Fe(2)-C(5)	95.0(4)
C(6)-Fe(2)-S(1)	90.2(3)
C(4)-Fe(2)-S(1)	102.4(3)
C(5)-Fe(2)-S(1)	162.6(3)

C(6)-Fe(2)-S(2)	156.5(3)
C(4)-Fe(2)-S(2)	109.3(3)
C(5)-Fe(2)-S(2)	90.1(3)
S(1)-Fe(2)-S(2)	85.53(9)
C(6)-Fe(2)-Fe(1)	102.5(3)
C(4)-Fe(2)-Fe(1)	153.3(3)
C(5)-Fe(2)-Fe(1)	106.5(3)
S(1)-Fe(2)-Fe(1)	57.36(7)
S(2)-Fe(2)-Fe(1)	56.10(7)
C(8)-S(1)-Fe(2)	106.6(4)
C(8)-S(1)-Fe(1)	111.0(3)
Fe(2)-S(1)-Fe(1)	66.89(8)
C(7)-S(2)-Fe(1)	109.7(3)
C(7)-S(2)-Fe(2)	114.8(3)
Fe(1)-S(2)-Fe(2)	67.37(8)
O(7)-S(3)-O(8)	113.9(5)
O(7)-S(3)-O(9)	112.1(5)
O(8)-S(3)-O(9)	109.8(5)
O(7)-S(3)-C(12)	106.6(5)
O(8)-S(3)-C(12)	108.8(5)
O(9)-S(3)-C(12)	105.1(4)
O(24W)-Na(1)-O(9A)#1	102.1(4)
O(24W)-Na(1)-O(19B)	84.9(3)
O(9A)#1-Na(1)-O(19B)	167.8(4)
O(24W)-Na(1)-O(18A)	142.3(4)
O(9A)#1-Na(1)-O(18A)	110.8(2)
O(19B)-Na(1)-O(18A)	66.51(19)
O(24W)-Na(1)-O(3A)#1	148.9(5)
O(9A)#1-Na(1)-O(3A)#1	60.52(19)
O(19B)-Na(1)-O(3A)#1	108.6(3)
O(18A)-Na(1)-O(3A)#1	67.37(18)
O(24W)-Na(1)-O(28B)#1	91.3(4)
O(9A)#1-Na(1)-O(28B)#1	67.2(2)
O(19B)-Na(1)-O(28B)#1	103.0(3)

O(18A)-Na(1)-O(28B)#1	117.9(3)
O(3A)#1-Na(1)-O(28B)#1	58.8(2)
O(18A)-Na(1')-O(9A)#1	114.9(6)
O(18A)-Na(1')-O(24W)	135.0(9)
O(9A)#1-Na(1')-O(24W)	95.0(7)
C(9)-N(1)-C(8)	118.5(8)
C(9)-N(1)-C(7)	121.5(7)
C(8)-N(1)-C(7)	112.1(7)
O(1)-C(1)-Fe(1)	175.8(8)
O(2)-C(2)-Fe(1)	176.7(8)
O(3)-C(3)-Fe(1)	179.4(8)
O(4)-C(4)-Fe(2)	176.5(8)
O(5)-C(5)-Fe(2)	175.9(9)
O(6)-C(6)-Fe(2)	176.4(8)
N(1)-C(7)-S(2)	117.6(6)
N(1)-C(8)-S(1)	115.8(6)
C(10)-C(9)-N(1)	120.8(9)
C(10)-C(9)-C(14)	117.0(9)
N(1)-C(9)-C(14)	122.2(8)
C(11)-C(10)-C(9)	120.3(9)
C(10)-C(11)-C(12)	121.5(9)
C(11)-C(12)-C(13)	118.2(9)
C(11)-C(12)-S(3)	121.4(7)
C(13)-C(12)-S(3)	120.4(8)
C(14)-C(13)-C(12)	120.1(9)
C(13)-C(14)-C(9)	122.8(9)
C(1A)-O(1A)-C(5A)	116.1(6)
C(1A)-O(2A)-C(10A)	118.0(6)
C(2A)-O(3A)-Na(1)#2	132.6(5)
C(7A)-O(6A)-C(11A)	113.0(6)
C(7A)-O(7A)-C(16A)	119.0(6)
C(9A)-O(9A)-Na(1)#2	140.7(5)
C(9A)-O(9A)-Na(1')#2	120.2(8)
Na(1)#2-O(9A)-Na(1')#2	20.6(5)

C(13A)-O(11A)-C(17A)	115.1(6)
C(22A)-O(12A)-C(13A)	120.1(6)
C(19A)-O(16A)-C(23A)	114.0(6)
C(19A)-O(17A)-C(28A)	116.6(6)
C(20A)-O(18A)-Na(1')	98.4(7)
C(20A)-O(18A)-Na(1)	117.1(5)
Na(1')-O(18A)-Na(1)	20.0(5)
C(25A)-O(21A)-C(29A)	114.8(6)
C(25A)-O(22A)-C(34A)	120.6(6)
C(31A)-O(26A)-C(35A)	116.7(6)
C(40A)-O(27A)-C(31A)	119.2(6)
C(37A)-O(31A)-C(41A)	117.0(6)
C(37A)-O(32A)-C(4A)	118.8(6)
O(1A)-C(1A)-O(2A)	110.1(6)
O(1A)-C(1A)-C(2A)	110.1(6)
O(2A)-C(1A)-C(2A)	107.9(6)
O(3A)-C(2A)-C(3A)	112.9(6)
O(3A)-C(2A)-C(1A)	111.3(6)
C(3A)-C(2A)-C(1A)	108.4(6)
O(4A)-C(3A)-C(2A)	110.0(6)
O(4A)-C(3A)-C(4A)	111.2(7)
C(2A)-C(3A)-C(4A)	109.4(7)
O(32A)-C(4A)-C(5A)	109.9(6)
O(32A)-C(4A)-C(3A)	106.6(6)
C(5A)-C(4A)-C(3A)	113.5(7)
O(1A)-C(5A)-C(6A)	107.4(7)
O(1A)-C(5A)-C(4A)	109.8(7)
C(6A)-C(5A)-C(4A)	113.6(7)
O(5A)-C(6A)-C(5A)	111.9(7)
O(6A)-C(7A)-O(7A)	110.9(7)
O(6A)-C(7A)-C(8A)	111.8(7)
O(7A)-C(7A)-C(8A)	108.2(7)
O(8A)-C(8A)-C(7A)	112.2(7)
O(8A)-C(8A)-C(9A)	109.8(6)

C(7A)-C(8A)-C(9A)	111.7(7)
O(9A)-C(9A)-C(10A)	109.3(7)
O(9A)-C(9A)-C(8A)	113.3(7)
C(10A)-C(9A)-C(8A)	107.2(7)
O(2A)-C(10A)-C(11A)	109.7(7)
O(2A)-C(10A)-C(9A)	106.7(6)
C(11A)-C(10A)-C(9A)	109.9(7)
O(6A)-C(11A)-C(12A)	105.1(7)
O(6A)-C(11A)-C(10A)	107.8(7)
C(12A)-C(11A)-C(10A)	112.9(7)
O(10A)-C(12A)-C(11A)	109.8(8)
O(11A)-C(13A)-O(12A)	112.1(6)
O(11A)-C(13A)-C(14A)	110.6(7)
O(12A)-C(13A)-C(14A)	107.6(6)
O(13A)-C(14A)-C(15A)	110.9(6)
O(13A)-C(14A)-C(13A)	110.7(7)
C(15A)-C(14A)-C(13A)	110.1(7)
O(14A)-C(15A)-C(14A)	110.2(7)
O(14A)-C(15A)-C(16A)	108.8(6)
C(14A)-C(15A)-C(16A)	110.0(6)
O(7A)-C(16A)-C(17A)	110.8(7)
O(7A)-C(16A)-C(15A)	105.6(6)
C(17A)-C(16A)-C(15A)	113.2(6)
O(11A)-C(17A)-C(16A)	111.7(6)
O(11A)-C(17A)-C(18A)	108.1(6)
C(16A)-C(17A)-C(18A)	109.6(7)
O(15A)-C(18A)-C(17A)	111.9(7)
O(17A)-C(19A)-O(16A)	110.9(6)
O(17A)-C(19A)-C(20A)	109.9(7)
O(16A)-C(19A)-C(20A)	109.4(6)
O(18A)-C(20A)-C(19A)	109.6(7)
O(18A)-C(20A)-C(21A)	112.2(7)
C(19A)-C(20A)-C(21A)	111.4(7)
O(19A)-C(21A)-C(22A)	108.9(7)

O(19A)-C(21A)-C(20A)	110.6(7)
C(22A)-C(21A)-C(20A)	108.3(7)
O(12A)-C(22A)-C(21A)	110.3(7)
O(12A)-C(22A)-C(23A)	110.4(7)
C(21A)-C(22A)-C(23A)	110.2(7)
O(16A)-C(23A)-C(22A)	110.3(6)
O(16A)-C(23A)-C(24A)	105.5(7)
C(22A)-C(23A)-C(24A)	113.1(7)
O(20A)-C(24A)-C(23A)	110.6(7)
O(22A)-C(25A)-O(21A)	111.2(7)
O(22A)-C(25A)-C(26A)	106.4(7)
O(21A)-C(25A)-C(26A)	110.3(7)
O(23A)-C(26A)-C(25A)	112.9(7)
O(23A)-C(26A)-C(27A)	110.8(7)
C(25A)-C(26A)-C(27A)	109.4(7)
O(24A)-C(27A)-C(26A)	112.0(6)
O(24A)-C(27A)-C(28A)	108.5(7)
C(26A)-C(27A)-C(28A)	107.3(6)
O(17A)-C(28A)-C(29A)	109.9(6)
O(17A)-C(28A)-C(27A)	106.0(6)
C(29A)-C(28A)-C(27A)	111.5(6)
O(21A)-C(29A)-C(30A)	106.3(6)
O(21A)-C(29A)-C(28A)	109.5(6)
C(30A)-C(29A)-C(28A)	111.9(7)
O(25A)-C(30A)-C(29A)	112.3(7)
O(26A)-C(31A)-O(27A)	109.7(7)
O(26A)-C(31A)-C(32A)	109.7(7)
O(27A)-C(31A)-C(32A)	109.3(6)
O(28A)-C(32A)-C(33A)	111.9(7)
O(28A)-C(32A)-C(31A)	115.6(7)
C(33A)-C(32A)-C(31A)	109.3(7)
O(29A)-C(33A)-C(34A)	108.4(7)
O(29A)-C(33A)-C(32A)	111.1(7)
C(34A)-C(33A)-C(32A)	111.2(7)

O(22A)-C(34A)-C(33A)	107.8(6)
O(22A)-C(34A)-C(35A)	108.5(6)
C(33A)-C(34A)-C(35A)	110.5(7)
O(26A)-C(35A)-C(36A)	106.7(7)
O(26A)-C(35A)-C(34A)	110.8(7)
C(36A)-C(35A)-C(34A)	111.6(7)
O(30A)-C(36A)-C(35A)	111.7(8)
O(31A)-C(37A)-O(32A)	111.8(6)
O(31A)-C(37A)-C(38A)	109.7(6)
O(32A)-C(37A)-C(38A)	106.4(7)
O(33A)-C(38A)-C(39A)	111.7(7)
O(33A)-C(38A)-C(37A)	109.0(6)
C(39A)-C(38A)-C(37A)	111.9(7)
O(34A)-C(39A)-C(38A)	109.3(7)
O(34A)-C(39A)-C(40A)	111.2(7)
C(38A)-C(39A)-C(40A)	109.9(7)
O(27A)-C(40A)-C(39A)	110.8(7)
O(27A)-C(40A)-C(41A)	112.0(6)
C(39A)-C(40A)-C(41A)	109.7(7)
O(31A)-C(41A)-C(42A)	107.5(7)
O(31A)-C(41A)-C(40A)	112.2(7)
C(42A)-C(41A)-C(40A)	113.8(7)
O(35A)-C(42A)-C(41A)	109.4(7)
C(1B)-O(1B)-C(5B)	113.6(6)
C(1B)-O(2B)-C(10B)	119.9(6)
C(7B)-O(6B)-C(11B)	115.8(7)
C(7B)-O(7B)-C(16B)	119.0(6)
C(13B)-O(11B)-C(17B)	115.0(6)
C(13B)-O(12B)-C(22B)	117.3(6)
C(19B)-O(16B)-C(23B)	113.2(6)
C(19B)-O(17B)-C(28B)	119.3(6)
C(21B)-O(19B)-Na(1)	141.2(5)
C(25B)-O(21B)-C(29B)	116.3(6)
C(34B)-O(22B)-C(25B)	118.8(6)

C(31B)-O(26B)-C(35B)	114.0(6)
C(31B)-O(27B)-C(40B)	117.8(6)
C(32B)-O(28B)-Na(1)#2	120.9(5)
C(37B)-O(31B)-C(41B)	114.5(6)
C(37B)-O(32B)-C(4B)	117.2(6)
O(1B)-C(1B)-O(2B)	111.3(6)
O(1B)-C(1B)-C(2B)	111.7(7)
O(2B)-C(1B)-C(2B)	107.7(6)
O(3B)-C(2B)-C(1B)	111.8(7)
O(3B)-C(2B)-C(3B)	111.6(7)
C(1B)-C(2B)-C(3B)	111.2(7)
O(4B)-C(3B)-C(4B)	112.2(7)
O(4B)-C(3B)-C(2B)	108.9(7)
C(4B)-C(3B)-C(2B)	109.6(7)
O(32B)-C(4B)-C(3B)	106.8(6)
O(32B)-C(4B)-C(5B)	108.5(6)
C(3B)-C(4B)-C(5B)	112.8(7)
O(1B)-C(5B)-C(6B)	108.1(6)
O(1B)-C(5B)-C(4B)	108.6(6)
C(6B)-C(5B)-C(4B)	114.0(7)
O(5B)-C(6B)-C(5B)	112.3(7)
O(6B)-C(7B)-O(7B)	109.0(6)
O(6B)-C(7B)-C(8B)	112.1(7)
O(7B)-C(7B)-C(8B)	107.8(7)
O(8B)-C(8B)-C(7B)	111.2(7)
O(8B)-C(8B)-C(9B)	110.0(7)
C(7B)-C(8B)-C(9B)	110.6(7)
O(9B)-C(9B)-C(10B)	112.0(7)
O(9B)-C(9B)-C(8B)	109.6(7)
C(10B)-C(9B)-C(8B)	108.2(7)
O(2B)-C(10B)-C(11B)	110.6(7)
O(2B)-C(10B)-C(9B)	108.8(7)
C(11B)-C(10B)-C(9B)	111.9(7)
O(6B)-C(11B)-C(10B)	111.1(7)

O(6B)-C(11B)-C(12B)	105.3(7)
C(10B)-C(11B)-C(12B)	113.4(8)
O(10B)-C(12B)-C(11B)	109.1(8)
O(11B)-C(13B)-O(12B)	112.5(6)
O(11B)-C(13B)-C(14B)	109.3(7)
O(12B)-C(13B)-C(14B)	107.9(6)
O(13B)-C(14B)-C(15B)	112.4(7)
O(13B)-C(14B)-C(13B)	109.1(7)
C(15B)-C(14B)-C(13B)	109.0(7)
O(14B)-C(15B)-C(16B)	112.0(7)
O(14B)-C(15B)-C(14B)	108.9(7)
C(16B)-C(15B)-C(14B)	110.8(7)
O(7B)-C(16B)-C(15B)	107.2(6)
O(7B)-C(16B)-C(17B)	108.5(7)
C(15B)-C(16B)-C(17B)	113.7(7)
O(11B)-C(17B)-C(18B)	106.3(6)
O(11B)-C(17B)-C(16B)	110.6(7)
C(18B)-C(17B)-C(16B)	112.1(7)
O(15B)-C(18B)-C(17B)	111.8(7)
O(16B)-C(19B)-O(17B)	113.0(7)
O(16B)-C(19B)-C(20B)	110.2(6)
O(17B)-C(19B)-C(20B)	109.1(7)
O(18B)-C(20B)-C(21B)	111.4(6)
O(18B)-C(20B)-C(19B)	109.9(7)
C(21B)-C(20B)-C(19B)	108.9(7)
O(19B)-C(21B)-C(22B)	112.2(7)
O(19B)-C(21B)-C(20B)	108.9(7)
C(22B)-C(21B)-C(20B)	106.4(7)
O(12B)-C(22B)-C(23B)	110.1(6)
O(12B)-C(22B)-C(21B)	106.7(6)
C(23B)-C(22B)-C(21B)	111.9(7)
O(16B)-C(23B)-C(22B)	108.3(6)
O(16B)-C(23B)-C(24B)	105.6(7)
C(22B)-C(23B)-C(24B)	114.2(7)

O(20B)-C(24B)-C(23B)	109.2(8)
O(21B)-C(25B)-O(22B)	112.5(6)
O(21B)-C(25B)-C(26B)	110.3(6)
O(22B)-C(25B)-C(26B)	105.5(6)
O(23B)-C(26B)-C(27B)	109.8(7)
O(23B)-C(26B)-C(25B)	110.6(6)
C(27B)-C(26B)-C(25B)	108.7(7)
O(24B)-C(27B)-C(28B)	109.4(7)
O(24B)-C(27B)-C(26B)	109.8(7)
C(28B)-C(27B)-C(26B)	107.8(7)
O(17B)-C(28B)-C(27B)	107.8(6)
O(17B)-C(28B)-C(29B)	108.3(6)
C(27B)-C(28B)-C(29B)	111.8(7)
O(21B)-C(29B)-C(30B)	107.9(7)
O(21B)-C(29B)-C(28B)	109.4(6)
C(30B)-C(29B)-C(28B)	112.0(7)
O(25B)-C(30B)-C(29B)	109.8(7)
O(26B)-C(31B)-O(27B)	110.2(7)
O(26B)-C(31B)-C(32B)	111.8(7)
O(27B)-C(31B)-C(32B)	107.3(7)
O(28B)-C(32B)-C(31B)	111.0(7)
O(28B)-C(32B)-C(33B)	112.9(7)
C(31B)-C(32B)-C(33B)	109.8(7)
O(29B)-C(33B)-C(32B)	110.5(7)
O(29B)-C(33B)-C(34B)	112.0(7)
C(32B)-C(33B)-C(34B)	109.2(7)
O(22B)-C(34B)-C(35B)	110.8(7)
O(22B)-C(34B)-C(33B)	108.5(7)
C(35B)-C(34B)-C(33B)	111.6(7)
O(26B)-C(35B)-C(34B)	111.0(8)
O(26B)-C(35B)-C(36B)	105.9(8)
C(34B)-C(35B)-C(36B)	112.4(9)
O(30B)-C(36B)-C(35B)	107.1(10)
O(30B)-C(36B)-O(30')	137.5(16)

C(35B)-C(36B)-O(30')	96.0(14)
O(32B)-C(37B)-O(31B)	110.7(7)
O(32B)-C(37B)-C(38B)	110.3(7)
O(31B)-C(37B)-C(38B)	109.2(6)
O(33B)-C(38B)-C(37B)	108.7(7)
O(33B)-C(38B)-C(39B)	110.6(7)
C(37B)-C(38B)-C(39B)	109.4(7)
O(34B)-C(39B)-C(40B)	107.7(6)
O(34B)-C(39B)-C(38B)	111.6(7)
C(40B)-C(39B)-C(38B)	108.6(7)
O(27B)-C(40B)-C(39B)	107.4(7)
O(27B)-C(40B)-C(41B)	108.9(6)
C(39B)-C(40B)-C(41B)	111.7(7)
O(31B)-C(41B)-C(42B)	104.3(7)
O(31B)-C(41B)-C(40B)	109.0(6)
C(42B)-C(41B)-C(40B)	113.2(7)
O(35B)-C(42B)-C(41B)	110.9(7)
Na(1)-O(24W)-Na(1')	18.9(4)

Symmetry transformations used to generate equivalent atoms:

#1 x,y-1,z #2 x,y+1,z

Table A-88. Anisotropic displacement parameters ($Å^2 x\ 10^3$) for V-**1-CyD**. The anisotropic displacement factor exponent takes the form: $-2\pi^2[\ h^2\ a^{*2}U^{11} + ...\ + 2\ h\ k\ a^*\ b^*\ U^{12}\ ]$

	U^{11}	U^{22}	U^{33}	U^{23}	U^{13}	U^{12}
Fe(1)	19(1)	37(1)	36(1)	20(1)	10(1)	7(1)
Fe(2)	21(1)	34(1)	36(1)	18(1)	10(1)	6(1)
S(1)	22(1)	38(1)	38(1)	18(1)	12(1)	6(1)
S(2)	22(1)	36(1)	38(1)	19(1)	9(1)	5(1)
S(3)	35(1)	50(2)	40(2)	18(1)	13(1)	14(1)
Na(1)	21(3)	25(3)	36(4)	13(3)	2(3)	5(2)
Na(1')	31(8)	73(12)	76(17)	47(11)	18(9)	17(8)
O(1)	38(4)	55(5)	25(4)	20(3)	6(3)	-2(3)
O(2)	48(5)	44(4)	58(5)	27(4)	-2(4)	14(4)
O(3)	28(4)	54(4)	46(4)	21(4)	10(3)	9(3)
O(4)	49(5)	44(5)	51(5)	8(4)	10(4)	-1(4)
O(5)	30(4)	91(6)	59(5)	43(5)	21(4)	27(4)
O(6)	60(5)	57(5)	51(5)	38(4)	18(4)	30(4)
O(7)	91(7)	67(6)	51(5)	32(4)	26(5)	31(5)
O(8)	56(5)	67(5)	58(5)	29(4)	30(4)	34(4)
O(9)	28(4)	53(5)	72(6)	7(4)	6(4)	6(3)
N(1)	30(4)	31(4)	31(4)	15(4)	6(3)	-2(3)
C(1)	24(5)	41(6)	51(7)	26(5)	21(5)	8(4)
C(2)	7(4)	48(6)	27(5)	16(5)	5(3)	2(4)
C(3)	25(5)	36(5)	43(6)	28(5)	4(4)	1(4)
C(4)	37(6)	38(6)	33(6)	18(5)	18(5)	9(5)
C(5)	22(5)	51(6)	43(6)	25(5)	9(5)	11(5)
C(6)	20(5)	32(5)	46(6)	3(5)	19(4)	5(4)
C(7)	46(6)	35(6)	55(7)	29(5)	20(5)	10(5)
C(8)	38(6)	35(6)	38(6)	17(5)	8(5)	-3(4)
C(9)	14(4)	36(6)	44(6)	20(5)	7(4)	-4(4)
C(10)	24(5)	35(5)	40(6)	17(5)	12(4)	7(4)
C(11)	32(5)	43(6)	35(6)	22(5)	11(4)	12(5)
C(12)	24(5)	44(6)	39(6)	22(5)	12(4)	7(4)

C(13)	22(5)	33(5)	39(6)	14(5)	16(4)	3(4)
C(14)	14(4)	51(6)	38(6)	22(5)	0(4)	-6(4)
O(1A)	13(3)	30(3)	30(3)	18(3)	4(2)	2(2)
O(2A)	16(3)	24(3)	31(3)	11(3)	8(2)	6(2)
O(3A)	14(3)	27(3)	26(3)	7(3)	6(2)	5(2)
O(4A)	18(3)	47(4)	26(3)	11(3)	10(3)	-2(3)
O(5A)	19(3)	38(4)	29(3)	16(3)	1(3)	2(3)
O(6A)	21(3)	43(4)	30(3)	21(3)	10(3)	9(3)
O(7A)	20(3)	29(3)	36(3)	18(3)	9(3)	6(3)
O(8A)	17(3)	25(3)	37(4)	8(3)	5(3)	2(3)
O(9A)	24(3)	32(3)	23(3)	11(3)	3(3)	11(3)
O(10A)	40(4)	60(5)	34(4)	19(4)	13(3)	8(4)
O(11A)	23(3)	26(3)	25(3)	13(3)	9(3)	5(3)
O(12A)	15(3)	21(3)	30(3)	7(3)	6(2)	-3(2)
O(13A)	13(3)	35(3)	26(3)	19(3)	1(2)	4(2)
O(14A)	21(3)	29(3)	31(3)	11(3)	8(3)	1(3)
O(15A)	30(3)	34(3)	29(3)	20(3)	11(3)	0(3)
O(16A)	27(3)	28(3)	35(4)	15(3)	7(3)	4(3)
O(17A)	18(3)	25(3)	29(3)	11(3)	7(3)	1(3)
O(18A)	22(3)	37(4)	34(3)	23(3)	11(3)	4(3)
O(19A)	17(3)	42(4)	24(3)	14(3)	3(3)	0(3)
O(20A)	50(5)	56(5)	45(4)	25(4)	33(4)	16(4)
O(21A)	13(3)	31(3)	35(3)	12(3)	6(3)	1(2)
O(22A)	14(3)	26(3)	37(3)	10(3)	8(3)	7(2)
O(23A)	28(3)	33(3)	36(4)	19(3)	15(3)	10(3)
O(24A)	21(3)	45(4)	31(3)	21(3)	12(3)	15(3)
O(25A)	24(3)	30(3)	42(4)	19(3)	11(3)	9(3)
O(26A)	23(3)	23(3)	24(3)	6(3)	3(2)	7(3)
O(27A)	12(3)	33(3)	30(3)	10(3)	3(2)	3(3)
O(28A)	22(3)	41(4)	35(4)	15(3)	12(3)	8(3)
O(29A)	34(4)	40(4)	35(4)	17(3)	15(3)	16(3)
O(30A)	39(4)	52(4)	48(4)	22(4)	19(3)	15(4)
O(31A)	13(3)	37(4)	28(3)	17(3)	3(3)	3(3)
O(32A)	11(3)	24(3)	32(3)	14(3)	8(2)	3(2)

O(33A)	18(3)	38(4)	26(3)	8(3)	10(3)	0(3)
O(34A)	25(3)	34(4)	37(4)	18(3)	14(3)	2(3)
O(35A)	22(3)	35(4)	33(4)	9(3)	7(3)	7(3)
C(1A)	22(4)	19(4)	30(5)	13(4)	8(4)	3(4)
C(2A)	25(5)	25(5)	26(5)	17(4)	7(4)	8(4)
C(3A)	25(5)	23(5)	26(5)	7(4)	15(4)	6(4)
C(4A)	18(4)	27(5)	26(5)	14(4)	7(4)	4(4)
C(5A)	23(5)	30(5)	38(5)	20(4)	19(4)	6(4)
C(6A)	35(5)	25(5)	20(4)	13(4)	9(4)	14(4)
C(7A)	27(5)	32(5)	37(5)	18(4)	13(4)	11(4)
C(8A)	13(4)	29(5)	44(5)	25(4)	10(4)	5(4)
C(9A)	17(4)	32(5)	34(5)	12(4)	9(4)	5(4)
C(10A)	17(4)	41(5)	36(5)	27(5)	12(4)	9(4)
C(11A)	23(5)	30(5)	37(5)	20(4)	10(4)	10(4)
C(12A)	32(5)	53(6)	29(5)	14(5)	16(4)	22(5)
C(13A)	16(4)	31(5)	35(5)	16(4)	11(4)	6(4)
C(14A)	15(4)	30(5)	22(5)	7(4)	-1(4)	1(4)
C(15A)	28(5)	23(5)	24(5)	12(4)	11(4)	-1(4)
C(16A)	24(5)	20(4)	38(5)	19(4)	16(4)	14(4)
C(17A)	15(4)	31(5)	13(4)	4(4)	6(3)	5(4)
C(18A)	18(4)	32(5)	36(5)	13(4)	8(4)	5(4)
C(19A)	22(4)	30(5)	22(5)	14(4)	11(4)	5(4)
C(20A)	29(5)	23(5)	35(5)	16(4)	17(4)	8(4)
C(21A)	18(4)	26(5)	24(5)	3(4)	2(4)	-1(4)
C(22A)	18(4)	21(5)	27(5)	9(4)	6(4)	3(4)
C(23A)	21(4)	33(5)	17(4)	11(4)	1(4)	1(4)
C(24A)	41(6)	52(7)	40(6)	33(5)	6(5)	-1(5)
C(25A)	20(4)	36(5)	30(5)	14(4)	12(4)	8(4)
C(26A)	27(5)	29(5)	37(5)	18(4)	15(4)	17(4)
C(27A)	21(4)	22(4)	22(4)	12(4)	1(4)	2(4)
C(28A)	9(4)	16(4)	35(5)	12(4)	3(3)	-7(3)
C(29A)	17(4)	23(5)	30(5)	15(4)	9(4)	7(4)
C(30A)	17(4)	29(5)	31(5)	14(4)	6(4)	1(4)
C(31A)	19(4)	19(5)	25(5)	3(4)	-6(4)	-7(4)

C(32A)	17(4)	12(4)	23(5)	-1(4)	-1(3)	-3(3)
C(33A)	24(5)	30(5)	29(5)	20(4)	8(4)	6(4)
C(34A)	9(4)	36(5)	26(5)	14(4)	4(3)	12(4)
C(35A)	19(4)	24(5)	39(5)	16(4)	4(4)	6(4)
C(36A)	46(6)	53(6)	31(5)	21(5)	14(5)	30(5)
C(37A)	12(4)	23(5)	36(5)	11(4)	9(4)	8(4)
C(38A)	16(4)	27(5)	26(5)	8(4)	9(4)	1(4)
C(39A)	10(4)	38(5)	24(5)	13(4)	5(3)	1(4)
C(40A)	18(4)	15(4)	35(5)	4(4)	10(4)	5(3)
C(41A)	15(4)	34(5)	32(5)	14(4)	4(4)	7(4)
C(42A)	17(4)	36(5)	23(5)	8(4)	5(4)	5(4)
O(1B)	20(3)	26(3)	26(3)	8(3)	9(2)	3(3)
O(2B)	16(3)	26(3)	34(3)	16(3)	10(2)	8(2)
O(3B)	19(3)	20(3)	26(3)	6(3)	-1(2)	1(2)
O(4B)	32(3)	39(4)	21(3)	11(3)	5(3)	9(3)
O(5B)	37(4)	32(4)	24(3)	8(3)	13(3)	14(3)
O(6B)	44(4)	33(4)	41(4)	24(3)	15(3)	13(3)
O(7B)	18(3)	33(3)	36(3)	19(3)	7(3)	4(3)
O(8B)	26(3)	35(4)	37(4)	15(3)	8(3)	8(3)
O(9B)	25(3)	42(4)	28(3)	17(3)	2(3)	8(3)
O(10B)	66(6)	91(7)	72(6)	33(5)	44(5)	12(5)
O(11B)	23(3)	32(3)	28(3)	17(3)	12(3)	11(3)
O(12B)	19(3)	29(3)	28(3)	15(3)	8(3)	4(3)
O(13B)	27(3)	28(3)	32(3)	13(3)	14(3)	2(3)
O(14B)	18(3)	35(4)	27(3)	6(3)	4(3)	-1(3)
O(15B)	32(4)	43(4)	43(4)	28(3)	14(3)	6(3)
O(16B)	21(3)	29(3)	28(3)	12(3)	9(3)	2(3)
O(17B)	22(3)	27(3)	36(3)	18(3)	8(3)	7(3)
O(18B)	26(3)	27(3)	26(3)	9(3)	13(3)	6(3)
O(19B)	29(3)	34(4)	22(3)	9(3)	4(3)	1(3)
O(20B)	45(5)	87(6)	59(5)	53(5)	10(4)	2(4)
O(21B)	29(3)	20(3)	26(3)	9(3)	1(3)	7(3)
O(22B)	16(3)	26(3)	31(3)	8(3)	2(3)	1(3)
O(23B)	19(3)	38(4)	34(4)	17(3)	6(3)	7(3)

O(24B)	27(3)	30(3)	40(4)	19(3)	11(3)	8(3)
O(25B)	15(3)	58(4)	43(4)	26(3)	13(3)	10(3)
O(26B)	27(3)	36(4)	26(3)	7(3)	0(3)	12(3)
O(27B)	19(3)	25(3)	29(3)	12(3)	8(2)	6(2)
O(28B)	19(3)	42(4)	41(4)	27(3)	9(3)	12(3)
O(29B)	23(3)	45(4)	35(4)	20(3)	16(3)	17(3)
O(30B)	29(5)	58(6)	42(5)	-3(5)	-12(4)	18(5)
O(30')	29(5)	58(6)	42(5)	-3(5)	-12(4)	18(5)
O(31B)	23(3)	31(3)	23(3)	6(3)	10(3)	2(3)
O(32B)	15(3)	27(3)	28(3)	8(3)	6(2)	-2(2)
O(33B)	25(3)	37(4)	30(4)	12(3)	0(3)	-8(3)
O(34B)	32(3)	33(3)	18(3)	11(3)	5(3)	0(3)
O(35B)	35(4)	27(3)	30(3)	6(3)	7(3)	0(3)
C(1B)	7(4)	26(5)	35(5)	15(4)	3(3)	-1(3)
C(2B)	11(4)	26(5)	30(5)	6(4)	6(4)	7(3)
C(3B)	14(4)	33(5)	36(5)	22(4)	5(4)	3(4)
C(4B)	13(4)	29(5)	33(5)	14(4)	6(4)	0(4)
C(5B)	4(4)	34(5)	35(5)	19(4)	4(3)	0(3)
C(6B)	18(4)	34(5)	26(5)	10(4)	5(4)	2(4)
C(7B)	16(4)	21(5)	31(5)	11(4)	6(4)	1(4)
C(8B)	17(4)	31(5)	28(5)	8(4)	10(4)	10(4)
C(9B)	20(4)	24(5)	34(5)	16(4)	4(4)	3(4)
C(10B)	23(5)	33(5)	40(5)	25(5)	16(4)	10(4)
C(11B)	38(5)	35(5)	25(5)	17(4)	3(4)	4(4)
C(12B)	58(7)	37(6)	52(7)	26(5)	17(6)	17(5)
C(13B)	34(5)	23(5)	18(4)	11(4)	5(4)	8(4)
C(14B)	33(5)	26(5)	22(5)	8(4)	5(4)	6(4)
C(15B)	22(5)	35(5)	20(5)	11(4)	-2(4)	1(4)
C(16B)	23(4)	28(5)	28(5)	22(4)	3(4)	5(4)
C(17B)	22(5)	25(5)	43(5)	26(4)	14(4)	8(4)
C(18B)	33(5)	28(5)	20(4)	8(4)	3(4)	7(4)
C(19B)	25(5)	28(5)	39(5)	17(4)	11(4)	8(4)
C(20B)	19(4)	34(5)	37(5)	27(4)	11(4)	6(4)
C(21B)	16(4)	45(6)	23(5)	21(4)	14(4)	6(4)

C(22B)	25(5)	25(5)	28(5)	15(4)	17(4)	5(4)
C(23B)	19(4)	29(5)	36(5)	13(4)	12(4)	7(4)
C(24B)	38(6)	54(7)	26(5)	16(5)	15(4)	2(5)
C(25B)	8(4)	33(5)	31(5)	19(4)	-2(3)	3(4)
C(26B)	9(4)	25(5)	34(5)	17(4)	-4(4)	0(3)
C(27B)	12(4)	22(5)	37(5)	7(4)	5(4)	-4(3)
C(28B)	16(4)	27(5)	19(4)	8(4)	4(3)	-1(4)
C(29B)	11(4)	22(4)	35(5)	15(4)	8(4)	5(3)
C(30B)	27(5)	34(5)	35(5)	11(4)	13(4)	12(4)
C(31B)	21(4)	12(4)	32(5)	2(4)	0(4)	-1(4)
C(32B)	27(5)	39(6)	32(5)	11(4)	16(4)	5(4)
C(33B)	19(4)	27(5)	34(5)	15(4)	8(4)	8(4)
C(34B)	20(5)	25(5)	41(6)	12(4)	4(4)	2(4)
C(35B)	49(6)	37(6)	21(5)	8(4)	4(4)	16(5)
C(36B)	91(10)	83(9)	31(6)	16(6)	11(6)	64(9)
C(37B)	25(5)	34(5)	37(5)	20(5)	15(4)	2(4)
C(38B)	20(4)	22(5)	35(5)	12(4)	4(4)	2(4)
C(39B)	17(4)	24(5)	28(5)	11(4)	9(4)	-1(4)
C(40B)	21(4)	26(5)	27(5)	12(4)	9(4)	2(4)
C(41B)	13(4)	35(5)	30(5)	17(4)	6(4)	7(4)
C(42B)	22(5)	52(6)	34(5)	28(5)	14(4)	5(4)
O(1W)	66(5)	22(4)	83(6)	21(4)	-14(4)	-13(4)
O(2W)	31(4)	37(4)	51(4)	13(3)	14(3)	5(3)
O(3W)	33(4)	65(5)	51(4)	42(4)	20(3)	24(3)
O(4W)	34(4)	42(4)	47(4)	25(3)	14(3)	1(3)
O(5W)	6(3)	24(4)	40(4)	5(3)	3(3)	-1(3)
O(6W)	34(4)	53(4)	51(4)	26(4)	19(3)	13(3)
O(7W)	27(4)	60(5)	85(6)	36(4)	22(4)	6(3)
O(8W)	30(5)	42(5)	36(5)	8(4)	14(4)	-7(4)
O(8')	30(5)	42(5)	36(5)	8(4)	14(4)	-7(4)
O(9W)	66(5)	63(5)	100(6)	53(5)	69(5)	37(4)
O(10W)	100(7)	56(5)	82(6)	39(5)	54(6)	34(5)
O(11W)	40(4)	54(5)	44(4)	17(4)	8(3)	8(4)
O(12W)	48(5)	67(5)	64(5)	25(5)	23(4)	10(4)

O(13W)	58(5)	62(5)	67(5)	20(4)	-2(4)	23(4)
O(14W)	52(5)	68(5)	68(6)	23(5)	18(4)	0(4)
O(15W)	74(6)	108(8)	106(7)	69(6)	47(6)	53(6)
O(16W)	58(5)	76(6)	83(6)	44(5)	33(5)	35(5)
O(17W)	48(5)	84(6)	77(6)	35(5)	11(4)	14(5)
O(18W)	65(6)	130(9)	128(9)	95(8)	40(6)	41(6)
O(19W)	83(7)	77(6)	98(7)	31(6)	49(6)	8(5)
O(20W)	36(5)	46(5)	154(10)	7(6)	13(5)	3(4)
O(21W)	55(7)	64(7)	103(9)	46(6)	-14(6)	-10(5)
O(22W)	67(12)	112(15)	94(13)	38(12)	32(10)	-14(10)
O(22')	67(12)	112(15)	94(13)	38(12)	32(10)	-14(10)
O(22")	40(9)	64(11)	104(15)	27(11)	18(10)	1(8)
O(23W)	5(2)	7(3)	20(3)	6(2)	-2(3)	4(2)
O(23')	5(2)	7(3)	20(3)	6(2)	-2(3)	4(2)
O(24W)	53(7)	138(11)	141(11)	-1(8)	2(7)	26(7)
O(25W)	131(14)	64(9)	88(11)	4(7)	-62(9)	51(9)
O(26W)	125(18)	51(11)	106(16)	22(11)	-63(14)	24(11)
O(27W)	60(11)	52(10)	77(12)	-35(9)	54(10)	-7(8)
O(28W)	16(8)	13(8)	22(9)	5(5)	-1(5)	13(5)

Table A-89. Hydrogen coordinates (x 10^4) and isotropic displacement parameters ($Å^2$x 10^3) for V-**1-CyD**.

	x	y	z	U(eq)
H(7B)	-5396	-4832	-3092	50
H(8B)	-7352	-3645	-3152	48
H(8C)	-7059	-4435	-3895	48
H(10A)	-5063	-3641	-1374	40
H(11A)	-4718	-2441	38	42
H(13A)	-6259	-980	-725	39
H(14A)	-6688	-2224	-2101	45
H(3AA)	-4452	1143	-3948	36
H(4AA)	-7282	-221	-4299	51
H(5AA)	-8059	-787	-7731	45
H(8AA)	-1340	694	-3483	45
H(9AA)	-3006	811	-3384	41
H(10B)	-4077	-1980	-8095	70
H(13B)	-800	-3505	-3712	36
H(14B)	-1635	-1371	-3518	44
H(15A)	-984	-2471	-7193	45
H(19A)	-2960	-5304	-3786	45
H(20A)	-2639	-6423	-7732	71
H(23A)	-8443	-7277	-4958	45
H(24G)	-5680	-7347	-4658	35
H(25A)	-6029	-9127	-7453	46
H(28A)	-9765	-4410	-4831	50
H(29A)	-9417	-6146	-4487	42
H(30A)	-9565	-7690	-9059	68
H(33A)	-8670	-960	-4024	37
H(34A)	-9471	-3538	-4734	38
H(35A)	-10624	-3859	-7430	49
H(1AA)	-4605	1009	-5422	28

H(2AA)	-5896	1249	-4849	28
H(3AB)	-5990	-567	-4732	30
H(4AB)	-7354	-191	-5761	28
H(5AB)	-6254	-1434	-6449	33
H(6AA)	-6784	-1313	-7724	29
H(6AB)	-7616	-1868	-7463	29
H(7AA)	-1503	-714	-5382	37
H(8AB)	-1926	648	-4618	31
H(9AB)	-3487	-662	-4469	35
H(10C)	-3477	465	-5450	32
H(11B)	-3961	-1671	-6063	33
H(12A)	-4816	-1202	-7022	45
H(12B)	-3847	-588	-7069	45
H(13C)	-1543	-4739	-5540	32
H(14C)	-707	-3056	-4662	32
H(15B)	-2451	-2766	-4500	31
H(16A)	-1229	-1948	-5309	28
H(17A)	-2925	-3545	-6289	26
H(18A)	-2274	-3640	-7461	36
H(18B)	-2371	-2558	-6958	36
H(19B)	-4928	-8052	-6217	29
H(20B)	-3446	-7128	-5307	32
H(21A)	-4010	-5370	-4835	33
H(22A)	-2684	-5932	-5760	28
H(23B)	-4444	-5782	-6398	31
H(24B)	-4139	-6571	-7784	52
H(24C)	-3498	-5434	-7213	52
H(25B)	-8962	-8502	-6566	34
H(26A)	-7708	-8648	-5713	33
H(27A)	-6788	-6586	-5247	27
H(28B)	-6279	-8336	-6207	27
H(29B)	-6988	-7152	-6908	26
H(30B)	-7128	-8506	-8260	32
H(30C)	-6068	-7921	-7713	32

H(31A)	-10608	-5192	-6470	33
H(32A)	-10570	-6270	-5830	27
H(33B)	-8600	-5473	-5376	31
H(34B)	-9733	-7488	-6478	28
H(35B)	-8742	-6106	-7035	33
H(36A)	-9065	-7808	-7931	47
H(36B)	-10150	-7965	-8021	47
H(37A)	-8687	-1079	-5957	29
H(38A)	-9579	-1944	-5340	30
H(39A)	-8134	-2759	-5156	30
H(40A)	-10002	-3733	-6210	30
H(41A)	-8344	-3446	-6781	34
H(42A)	-9227	-4105	-8144	33
H(42B)	-9614	-4878	-7782	33
H(3BA)	-9448	-3847	-3057	37
H(4BA)	-8856	-2031	-3417	49
H(5BA)	-8612	739	587	47
H(8BA)	-8975	-6952	-3489	51
H(9BA)	-9705	-5121	-3114	48
H(10D)	-9416	-3602	360	116
H(13D)	-4346	-6190	-2810	45
H(14D)	-6491	-6821	-3551	48
H(15C)	-6901	-6404	100	56
H(18C)	-1348	-4198	-2651	40
H(20C)	-2699	-4484	908	91
H(23C)	-598	491	-2096	46
H(24A)	-1178	-2324	-2257	37
H(25C)	-27	-1049	547	56
H(28C)	-4410	1788	-2203	46
H(29C)	-1886	1065	-2095	38
H(30D)	-1540	3275	1126	81
H(33C)	-7994	-123	-2577	54
H(34C)	-6167	893	-2920	45
H(35C)	-5230	3449	1311	52

H(1BA)	-9852	-3290	-1677	28
H(2BA)	-9928	-2278	-2341	29
H(3BB)	-8026	-2032	-2297	32
H(4BB)	-8808	-542	-1403	32
H(5BB)	-7701	-1409	-632	30
H(6BA)	-8142	-556	626	34
H(6BB)	-7497	189	362	34
H(7BA)	-8096	-6348	-1575	29
H(8BB)	-9281	-6135	-2386	32
H(9BB)	-7884	-4601	-2467	31
H(10E)	-9346	-4407	-1621	34
H(11C)	-7409	-3709	-790	40
H(12C)	-7880	-3432	488	55
H(12D)	-8226	-2773	72	55
H(13E)	-4036	-6149	-1382	30
H(14E)	-5540	-7193	-2301	35
H(15D)	-5788	-5424	-2343	34
H(16B)	-6801	-6570	-1663	29
H(17B)	-5453	-4622	-621	31
H(18D)	-5586	-5039	523	35
H(18E)	-6563	-5037	55	35
H(19C)	-852	-2689	-701	35
H(20D)	-1570	-4412	-1611	31
H(21B)	-3206	-3898	-2057	31
H(22B)	-2874	-5001	-1111	29
H(23D)	-3124	-3076	-471	33
H(24E)	-2678	-3019	920	50
H(24F)	-3658	-3860	355	50
H(25D)	-726	1348	-449	29
H(26B)	-227	-41	-1227	28
H(27B)	-2167	-1188	-1753	33
H(28D)	-616	-1332	-714	27
H(29D)	-2072	-583	-87	26
H(30E)	-1106	-55	1289	39

H(30F)	-1380	-1241	740	39
H(31B)	-3951	2900	-611	32
H(32B)	-2716	2709	-1232	42
H(33D)	-3485	621	-1782	32
H(34D)	-1771	1972	-540	38
H(35D)	-3386	1002	-207	45
H(36C)	-2562	2111	1284	79
H(36D)	-2033	1335	840	79
H(37B)	-7986	879	-1035	37
H(38B)	-7068	1783	-1597	33
H(39B)	-6155	265	-2000	29
H(40B)	-5376	2343	-818	30
H(41B)	-5740	715	-353	30
H(42C)	-5428	1972	1065	40
H(42D)	-4536	2162	709	40

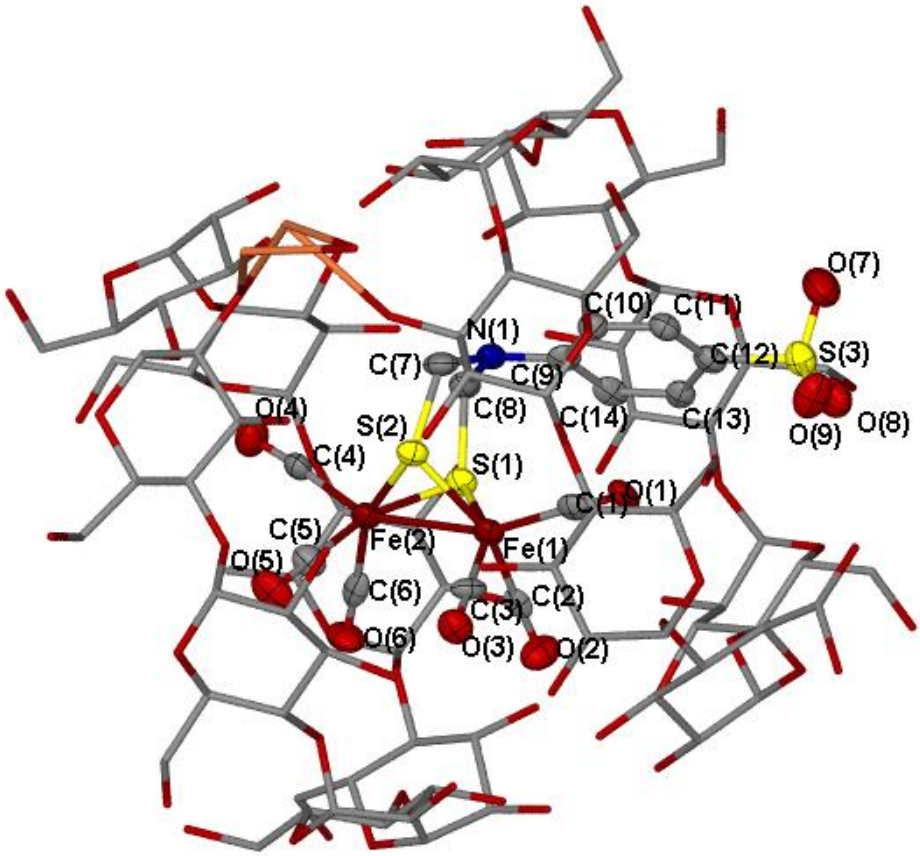
O(7)
C(10)
C(11)
N(1)
C(12)
S(3)
C(7)
C(9)
O(4)
C(8)
C(14)
C(13)
O(9)
O(8)
S(2)
C(4)
S(1)
O(1)
C(1)
C(5)
Fe(2)
Fe(1)
O(5)
C(6)
C(3)
C(2)
O(6)
O(3)
O(2)

VITA

Name: Michael Lee Singleton

Address: Department of Chemistry, Texas A&M University
Mail Stop 3255, College Station, TX 77843-3255

Email Address: msingleton@mail.chem.tamu.edu

Education: B.S., Chemistry, Texas A&M University, 2005
Ph.D., Chemistry, Texas A&M University, 2010

Publications as of July 2010:

1. Singleton, M. L.; Reibenspies, J. H; Darensbourg, M. Y. "A Cyclodextrin Host-Guest Approach to a Hydrogenase Active Site Biomimetic Cavity" *J. Am. Chem. Soc.* **2010**, 132(26) 8870-8871.

2. Jenkins, R. M.; Singleton, M. L.; Leamer, L. A.; Reibenspies, J. H.; Darensbourg, M. Y. "The Orientation and Stereodynamic Paths of Planar Monodentate Ligands in Square Planar Nickel N_2S Complexes" *Inorg. Chem.* **2010**, 49, 5503-5514.

3. Li, B.; Liu, T.; Singleton, M. L.; Darensbourg, M. Y. "Influence of Sulf-Oxygenation on CO/L Substitution and $Fe(CO)_3$ Rotation in Thiolate-Bridged Diiron Complexes" *Inorg. Chem.* **2009**, 48, 8393-8403.

4. Jenkins, R. M.; Singleton, M. L.; Almaraz, E; Reipenspies, J.; Darensbourg, M. Y. "Imidazole-Containing $Ni(N_3S)$ Complexes Relating to Nickel Containing Biomolecules" *Inorg. Chem.* **2009**, 48, 7280-7293.

5. Liu, T.; Li, B.; Singleton, M. L.; Hall, M. B.; Darensbourg, M. Y. "Sulfur Oxygenates of Biomimetics of the Diiron Subsite of the [FeFe]-Hydrogenase Active Site: Properties and Oxygen Damage Repair Possibilities" *J. Am. Chem. Soc.* **2009**, 131, 8296-8307.

6. Singleton, M. L.; Bhuvanesh, N.; Reibenspies, J. H; Darensbourg, M. Y. "Synthetic Support of Denovo Design: Sterically Bulky [FeFe]-Hydrogenase Models" *Angew. Chem. Int. ed.* **2008**, 47, 9492-9495.

7. Singleton, M. L.; Jenkins, R. M.; Klemashevich, C. L.; Darensbourg, M. Y. "The Effect of Bridgehead Steric Bulk on the Ground State and Intramolecular Exchange Processes of (μ-$SCH_2CR_2CH_2S$-)$[Fe(CO)_3[Fe(CO)_2L]$ complexes" *C. R. Chimie*. **2008**, *11*, 861-874.

8. Jeffery, S. P.; Singleton, M. L.; Reibenspies, J. H.; Darensbourg, M. Y. "Control of S Based Aggregation: Designed Synthesis of NiM_2 and Ni_2M Trinuclear Complexes" *Inorg. Chem.* **2007**, *46*, 179-185.